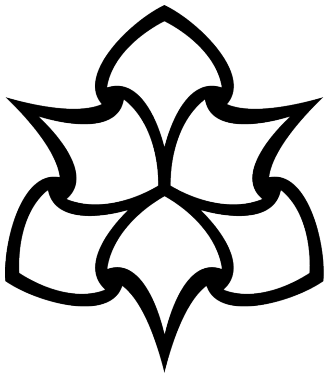

HiPIMS plasma diagnostic to study the repeatability of low temperature deposition of crystalline Titania

A thesis submitted in partial fulfilment of the requirements of Manchester Metropolitan University for the degree of Doctor of Philosophy

BRICE DELFOUR-PEYRETHON

Faculty of Science and Engineering

School of Engineering

Surface Engineering Group

2018

Declaration

This is to certify that the material contained in this thesis has been produced by the author and has not been accepted in substance for any other degree and is not currently submitted in candidature for any other academic award.

Acknowledgements

First, I would like to thank my Director of Studies, Dr. Glen West, for his continuous help throughout the project. He was here for me when I needed him and our conversations always ended in a better comprehension of magnetron sputtering, a better vision on the project, and more ideas (and work) to look into. He was here to guide me and help me focusing on the right things. He has also been of great help when it came to correct and revise my writing. He took the time to comment and discuss each point. Without him, this project could not be what it is today.

I would also like to thank Prof. Peter Kelly, Head of Surface Engineering research team for his great advices and the quality of his answers to any of the questions I could ask him. He is the great man behind a research team happy to work together and he deserves to be thanked for that.

I am grateful to Prof. James Bradley from the University of Liverpool for letting me use the thermal probe. This probe was essential to this project.

I also want to thank all my colleagues in the Surface Engineering group for their support, their guidance and their experience. I have been glad to work in such a research team, where everyone has a different background but work perfectly together. A special thank for Marina and David for being here when I needed it.

Now comes the time when I need to thank every person I have met during these three years in Manchester. First comes the Cavendish crew, my international friends. A group where everyone is unique and in which I have made amazing friends. The kind of friendship that lasts no matter the distance and time. Listing all of them would take too long but I want each one of them to know they have made my new life a dream; especially Alejandro, Berk, Chloé, Éva, Jane, Ken, Laura, Maxwell, Noelia, Paulina, Rafael, Ryan, Stijn and Tristan. Every person I have lived with during these three years needs to be acknowledged, really. I know it is not an easy thing. Of course, I cannot ignore the MMU

Swim Team for accepting me as one of them and offering me a place where I could empty my mind and make great memories. To all of you, thank you for the laughs, the drinks, and every single moment we spent together.

I want to thank Ellie for bringing me what the others could not. She has been here to take care of me and make me happy during the most difficult year of my PhD.

Je ne peux pas oublier mes amis français. Ces amis dont il a été si difficile de se séparer au début et qui m'ont pourtant prouvé que l'amitié, la véritable, supporte la distance. Je veux les remercier pour toutes ces années où ils ont rendu ma vie plus belle. Nos souvenirs ne s'effaceront jamais et ils étaient là quand j'en avais le plus besoin, dans les mauvais moments comme dans les bons. Je suis certain que cette amitié durera encore longtemps. Ils savent ce qu'ils représentent pour moi, mais je me dois de les citer. Les Piapiapia, vous savez que je parle de vous. Un merci encore plus spécial à Amandine, Berend, Charles, Estelle, Flora, Hélène, Marien, Morgan, Sandra et Solène. Les autres, vous savez que je n'en pense pas moins de vous, bien sûr. Une pensée à tous mes amis étudiants qui ont été avec moi dans les salles de cours et dans les bars, au cours de ces années étudiantes françaises. Vous avez fait de ma vie étudiante un plaisir et je me suis fait de véritables amis en chemin, que ce soit à Clermont-Ferrand, Tours ou Nantes.

Je me dois de remercier tous les enseignants qui ont accompagné mon parcours étudiant, du plus jeune âge jusqu'à maintenant. Ceux qui croyaient en moi m'ont donné l'envie et la force de parvenir où j'en suis maintenant et ce qui ne croyaient pas en moi m'ont donné cette même envie et cette même force, de leur prouver qu'ils avaient tort et que je pouvais atteindre mon rêve à ma manière.

Je tiens à remercier mon frère Rémi pour m'avoir montré la voie à plusieurs reprises, jusqu'au doctorat. Merci à lui et Océane pour le petit Hector, qui me rappelle à quel point la famille est importante à chaque fois que je le vois. J'aurais aimé être plus présent à ses côtés.

Finalement, mes derniers remerciements vont à mes parents. C'est grâce à eux que j'ai la chance de vivre ma vie telle qu'elle est. Ils ont fait de moi un homme dont j'espère qu'ils sont fiers. Si j'ai fait cette thèse, c'est pour qu'ils puissent être fiers de moi.

Abstract

In the last few decades, Titanium dioxide (also called Titania or TiO_2) has experienced significant scientific interest due to its range of properties and possibility for further developments in a range of applications, including photocatalysis. Initially, the material was widely used in this application in powder form for water decontamination applications. It was later developed as a thin film coating onto glasses and metals (industrial, construction scale) for its self-cleaning properties. Indeed, the scientific community realised that TiO_2 coatings could present both antimicrobial properties (via degradation of cell walls) and a strong hydrophilic behaviour. Recently, thin films technologies, and more particularly magnetron sputtering processes, have undergone a new expansion: the HiPIMS (High Power Impulse Magnetron Sputtering) process. The HiPIMS process is 15 years old and its principal aim is to provide a more ionized deposition flux (by an order of magnitude), easing the control of the deposited film properties (density, structure, composition, targeted areas on the substrate, etc…). It has also been shown to facilitate low substrate temperatures during operation. The combination of both characteristics should lead to the possible deposition of crystalline films at low temperature.

The first aim in this work is to provide the reader with a deep understanding of the HiPIMS discharge and how it can influence the deposition process. To do so, plasma diagnostics have been carried out on different coating systems (rigs) and using different power supplies to show how both of these aspects can drastically change the processes occurring within the discharge. For the rig used for deposition of the films, thermal and deposition rates measurements have also been carried out. This leads to the establishment of a process envelope, suitable for the deposition of crystalline titanium dioxide films. Subsequently, TiO_2 coatings have been deposited by HiPIMS onto various substrates and the influences of the deposition parameters studied to better understand the plasma behaviour and its consequences on the thin film properties, in order to

optimize the latter's crystallography. The final aim of this project is to deposit a crystalline photo-active (i.e. photocatalytic, hydrophilic) film onto a polymeric substrate at low temperature.

This project implies the use of a large range of characterisation techniques. The structural, mechanical, chemical and crystallographic properties have been studied by using a large array of techniques including X-Ray Diffraction (XRD), Scanning Electron Microscopy (SEM), Raman spectroscopy, etc... The photocatalytic activity was assessed using dye degradation tests under UV light, and the hydrophilicity by contact angle measurements.

In this project, it has been shown that a modification of the deposition rig can bring drastic changes to the plasma. These changes are even more important when it comes to the reactive plasma. Each rig has its own process envelope and transferring from a laboratory scaled rig to an industrial rig is not a simple task. Parameters influences on the plasma can also vary from one configuration to another and optimized deposition conditions are not necessarily repeatable from one rig to another. Mainly, it seems that the oxidation process is greatly modified by the rig configuration. This thesis presents plasma diagnostic conducted using only an oscilloscope, to show that this is a simple and cheap way for industrials to deposit in reactive atmosphere. Here, the author has optimized deposition conditions on a given apparatus, where crystalline Anatase (TiO_2) has been deposited at low temperature, typically, below 60 °C. These films have also been deposited onto polymeric substrates with no destruction of the latter. The oxygen content during deposition appears to be the more important point to control during deposition. For the rig used here, films have been deposited in the poisoned mode, at low pressure, high frequency and short pulse width as it seemed to provide the more ionized discharge, facilitating the films crystallization.

Contents

Table of Figures

Table of Tables

Table of Equations

Chapter I. Literature review

This chapter is here to provide the knowledge necessary to the discussions given in this report. It relies on a deep study of the literature currently existing on the different subjects presented. First, a complete review is given on the High Power Impulse Magnetron Sputtering (HiPIMS) process.

The review starts with an introduction to vacuum technology: definitions, and descriptions of gauges and pumps are given. Then, the plasma used for Physical Vapour Deposition (PVD) is described in more details. The fundamental physic behind the plasma is explained as well as the different processes taking place during deposition (i.e. sputtering, transportation and deposition). In the continuity, a historical review is given on the evolution of sputtering processes until the HiPIMS process. The discharge of the latter is described in more details right after. Finally, the existing knowledge on parameters influences on films deposition is summarized. Once the HiPIMS process has been fully presented and understood, the report focuses on titanium dioxide. Again, a brief historical overview is given and followed by the presentation of the material's characteristics and properties.

I.1. The High Power Impulse Magnetron Sputtering process

I.1.1. Vacuum

I.1.1.1. Definition

The term *Vacuum* concerns every gaseous system of which the pressure is below that of the surrounding atmosphere. In the gaseous mode, the particles are energetic (more than in the solid and liquid states) and that is why they collide with each other but also with the boundary walls of the chamber. The pressure is then determined as the force delivered by the gas particles to the boundary walls. The units are directly proportional to $N.m^{-2}$ (Force/Area).

There are several units used when it comes to pressure such as Pa, bar, Torr, at, atm, psi, etc... In vacuum studies, mbar and mTorr are the commonly used units but Pa is the S.I. unit: it should be used in papers. It corresponds to a 1 N force applied on a 1 m^2 surface. Historically, the Torr has been defined as being the pressure generated by a 1 mm high column of mercury and is exactly equal to 1/750 of the standard atmosphere. The bar, itself, is defined as being exactly the atmospheric pressure at sea level on Earth. However, in sciences, and especially in vacuum technologies, the mTorr and mbar units are preferred to bar and Torr. The conversions between these different units are as follows:

	mbar	**mTorr**	**Pascal**
mbar		750	100
mTorr	$1.33\ 10^{-3}$		0.133
Pascal	10^{-2}	7.5	

Table 1. Equivalence factors between major pressure units

The range of vacuum pressures accessible in the early 21st century goes from 1.10^3 to 1.10^{-10} mbar. This very large range logically induces changes in the kinetics of the gases; and therefore, changes the way of measuring their pressures. There are four different

processes responsible for an increase of the pressure in a vacuumed chamber: vaporization, desorption, diffusion and permeation. The first, the *vaporization* process, describes the case when the boundary wall itself starts to lose particles which are directly going in the vacuum chamber. *Desorption* is very similar but concerns atoms previously deposited in the wall by adsorption. Those two phenomena originate from the kinetic energy transferred by the gaseous particles reaching the surface. It is therefore expected to see their occurring rates increased when the temperature is raised: i.e. the particles within the chamber are more energetic. Another phenomenon is called *diffusion*. This process follows the adsorption of certain particles. It corresponds to the moment when the atoms contained inside the wall material diffuse across the material to its surface and are then released into the chamber. Finally, the fourth and last phenomenon, the so-called *permeation,* is the combination of the absorption of an atom on the atmospheric side of the wall and the diffusion of this atom to the inside of the vacuum chamber. In addition to these four phenomena corresponding to perfect systems, the gaseous leaks should not be forgotten. Indeed, the systems are not perfectly hermetic and there are always some physical holes in the chamber walls. There is always a need to create an aperture in the chamber walls -even if it is just a door to be able to insert substrates in the chamber- and it can be at the origin of minor defects in the hermetic envelope. Indeed, some minor defects can appear at the interface between the chamber wall and the connected device (e.g. door, gauges, sensor, pump, etc.)

As stated previously, the vacuum technologies range is very large and therefore needs different types of gauges to measure its pressure because the physical behaviours are different for every pressure range. They are categorised into three different types: mechanical gauges, transport gauges and ionization gauges. The first category includes U-tube manometer, capsule dial gauges, strain gauges, capacitance manometer, and McLeod gauge. The second category is for the spinning rotor, Pirani and thermocouple gauges. Finally, the cold and hot cathode ionization gauges (or Penning gauge and ion gauge, respectively) constitute the third class. In the work presented in this report, the only gauges used are the capacitance manometer, the Pirani gauge and the Penning gauge.

I.1.1.2. Gauges

The capacitance manometer gauge principle relies on the fact that a capacitance between one (or two) electrode(s) and a diaphragm is modified if the position of the diaphragm changes. The device is thus composed of a diaphragm positioned in a way that one of its side is exposed to the vacuum chamber pressure and the other one is exposed to a volume sealed at a given pressure. Atoms coming from the chamber therefore impact on the diaphragm with more or less intensity -depending on the pressure- and modify the position of the latter. And since the capacitance measured is a function of this position, it is possible to retrieve the corresponding pressure by measuring the capacitance in a circuit.

The Pirani gauge uses the modification of the ability of a gas to conduct heat when pressure is changed. The cell consists of a thin filament (Tungsten in most cases) constantly heated (through a constant applied voltage) and exposed to the atmosphere to be measured. When the pressure is decreased, the number of collisions between the atoms from the gas and the filament diminishes and less heat is removed. The temperature of the filament therefore rises, and the resistance does the same. Since this filament is part of a Wheatstone bridge, the balance of the latter changes and it then possible to measure the difference of pressure. It should be noted that sometimes, the constant voltage is replaced by a constant current (constant temperature). Because every chemical component has a different temperature conductance, the given pressure is not the absolute pressure if the chamber gas is composed of other components than those for which the gauge has been calibrated (Nitrogen in most cases).

The Penning gauge consists in a cylindrical anode and a cathode pin separated by the studied gas and they are both *enveloped* by a magnet. This magnet generates a magnetic field which remains parallel to the electrodes and accelerate electrons along its field lines. These electrons therefore ionize the species within the gauge. Indeed, when a high voltage is applied to the cathode, the produced electrons can ionise the gaseous atoms between the electrodes. The produced ions are attracted by the cathode to generate a current. This system composed of ions and electrons then reaches an equilibrium between the production (i.e. ionization) and the collection and recombination rates. The value of this stable current is then reflecting the quantity of atoms present in the cell (i.e. the pressure). However, because of the different possible

ionization degrees for different gaseous species, the measure is subject to an error going from -50% to +100%.

I.1.1.3. Pumps

The rig used for this project is composed of two pumps: a rotary vane pump and a turbomolecular pump. The first is used constantly (from atmospheric pressure to below) but the turbo pump is only switched on when a pressure of ~10^{-3} mbar has been reached. The need for different pumps comes from the fact that a gas dynamics is function of its pressure. Between the atmospheric pressure and the mTorr scale, the gas is considered as being viscous. It means that the gas is considered as a fluid where the particles are continuously moving and interact with each other. It is dense enough to be considered as one unique system. The major difference between the viscous and the molecular flows is the mean free path of the atoms. Indeed, the molecular flow describes the gases at pressures lower than roughly 1 mTorr. In this case, the mean free path of the particles is a few centimetres long and is thus longer than the dimension of the pumping chamber. For such systems, the atoms are considered as being independent one from another since there are practically no collisions.

The rotary pump principle of functioning relies on the fact that air behaves as a fluid when the pressure is close to the atmospheric conditions. It is the most generally used pumping system. The pressures reached are commonly as low as $10^{-2}/10^{-3}$ mbar. It is composed of an empty cylindrical stator in which is fitted a smaller cylindrical rotor. This rotor is not centred in the stator but is in barely in contact with the wall. In fact, a gap (approximately 0,025mm) remains between the two parts. To do so, the curvature of the stator is slightly modified in this area to be the same as the one of the rotor. Oil is used to complete the seal between the components (blades, rotor, stator,). The inlet and the outlet are separated by this contact region (as shown below). The rotor includes two movable (sliding within the rotor) blades diametrically opposed that always remain in contact with the stator during the rotation. During the pumping, the blades catches a certain amount of gas when the space between them is exposed to the inlet pipe. After a 180° rotation, this gas is compressed against the exhaust valve (outlet pipe) and is extracted. It can be seen on the following figure (Figure 1) that during a complete rotation, two pumping cycles are occurring:

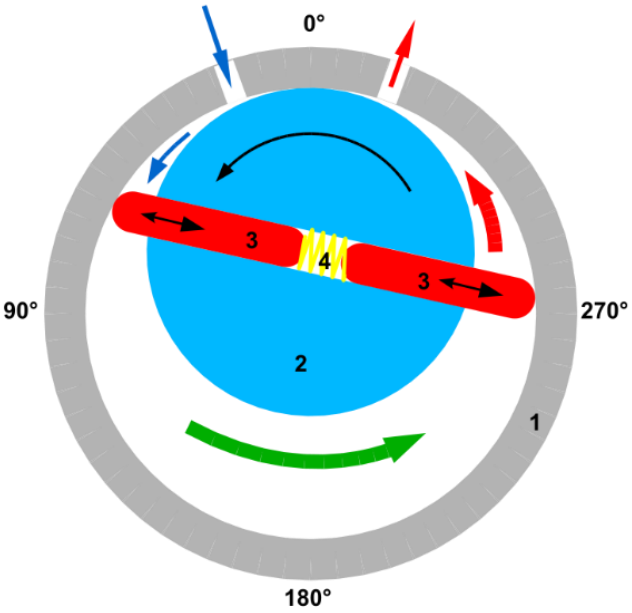

Figure 1. Schematic representation of a rotary pump

Rotary vane pumps generally rotate with speeds between 350 and 750 rev/min but some systems reach rotation speeds up to 1400 rev/min to improve their efficiency. In some cases, this system is improved by combining two of these pumps. One creating a low-pressure and cleaning the oil before the second one, which is pumping to a lower pressure. However, it should be kept in mind that this kind of pumping system is generally noisy and hot because of the friction between the components (e.g. rotors, blades, oil). The rotary pump must always be running and pump to reach a pressure of roughly 1.10^{-2} mbar pressure before operating the turbomolecular pump.

The turbomolecular pump functions via the reaction between atoms and moving surfaces (rotors). Indeed, every atom striking a moving surface receives more energy in the direction of the surface movement. The pump is composed of blades rotating (rotors) between stators so the atomic flow is transferred in a specific way: towards a rotary pump for its evacuation. To do so, the blades need to rotate at a speed which is around the atomic speed (470 m/s for Nitrogen, 1900 m/s for Hydrogen). It means that their rotating speed must be around 60 000 rev.min^{-1}. Their ability to push the atoms depends on the blade design and the rotation speed. There are two types of designs for those pumps: dual or single flow. Their principles are the same but their geometries are different. No matter their conception, all these devices need to be cooled down and this can be done either by

using air or water cooling systems. Water cooling is preferred for long functioning periods (increase of the temperature) and hot working environment. One should note that pumps with magnetically levitating rotors also exist. They present the advantages of less heating (i.e. no need to cool the pump) and they avoid vibrations and noise. They also do not need the use of any lubricants ; to avoid hydrocarbon contamination.

I.1.2. Plasma for sputtering

I.1.2.1. Introduction

The sputtering process could be succinctly defined as being the ejection of atoms and secondary electrons from a solid surface following its bombardment by energetic particles; usually ions. To do so, a plasma must be generated in a vacuum chamber, and it then provides the ions necessary to erode the target. The plasma is defined as the fourth state of matter, after solid, liquid and gaseous states. It is a gas fully or partially ionized but it also consists of electrons and atoms; molecules sometimes. In fact, the ionization rate, which is the partial proportion of ions in the plasma (i.e. $\frac{Metallic\ ions}{Metallic\ ions+atoms}$) is a very important parameter. The reasons why are explained further, along this section I.1.2. It should be noticed that both negative and positive species are present in the atmosphere and result in a quasi-neutrality of the plasma. Some atoms (or ions) may, after having undertaken an inelastic collision, be in a state of high energy, the so-called *excited* state. However, it is well known that any excited particle naturally releases its excess of energy in the form of a photon in order to reach a more stable energy level (i.e. ionization levels). Therefore, a given plasma is characterized by a light emission at a specific wavelength, defined by the ionization levels of the present species. For example, a titanium plasma light emission is different from an aluminium discharge emission, or from a Ti-O discharge.

Plasma is not a naturally occurring state on Earth, except during weather and cosmic phenomena (e.g. lightnings and aurora). It is thanks to vacuum and electronic technologies that it is now possible to generate it artificially. Moreover, one differentiates these artificial plasmas and the natural ones by the temperature difference existing between the electrons and the ions. In a natural plasma, electronic and ionic

temperatures are similar: it is called a *hot plasma* or a *thermal equilibrium plasma* [1] [2]. In the other case, there is a temperature difference between the two species: the electron temperature is much greater than that of the ions; which are close to the ambient temperature. It is called a *cold plasma* or a *non-thermal equilibrium plasma*. A brief description of the generation and operation of the latter is given in the following sections.

I.1.2.2. Plasma physics

To artificially create a plasma, the technique consists in introducing a working gas (generally argon) at low pressure in a vacuumed chamber where a difference of electrical potentials is applied between two electrodes: the cathode (target) and the anode (substrate holder and walls of the chamber). This difference of potentials tends to accelerate the electrons towards the anode and provide them with sufficient energy to ionize the working gas. This configuration is called the *diode* configuration. The ionization by electronic impacts is described by the following reaction:

$$e^- + Ar \rightarrow 2e^- + Ar^+$$

Equation 1. Ionization of Ar by electronic impact

In here, the two electrons resulting from this collision are also accelerated by the electrical field present in the deposition chamber and can ionize two more gas atoms. This reaction is thus a *cascade reaction*. The Ar ion is accelerated in the other direction and collide with the target surface to expel metallic particles. The details of this process are explained further in this report (cf I.1.2.3) but it results in the extraction of *secondary electrons* among other particles. When the discharge stays relatively weak, the plasma in presence is called a *Townsend discharge* [3]. Along time, the previous cascade reaction for the ionization and the secondary electrons emission continue and generate more electrons and ions within the chamber. At some point, the amount of generated electrons is equivalent to the number needed to sustain the plasma. The plasma is therefore self-sustaining and the voltage drops quite significantly. This regime is called the *normal glow* regime: the plasma is now emitting light when the species are reaching their ionization levels (cf I.1.2.1). A further increase in the process power distribute the current density evenly over the entire target surface. The current increases but not the voltage. If one

keeps going, both the voltage and the current are being increased during the *abnormal glow* regime. This latter mode is the plasma used for sputtering processes and etching. However, if the voltage keeps being raised, an *arc discharge* is obtained: the voltage sharply drops to a low value while the current is very high. This conditions correspond to the arcs that can be observed during sputtering when too many charge carriers accumulate at the target surface. It is also used in cathodic arc deposition systems. An arc can partially melt the target and vaporize it. Most of the times, molten or solid parts of the target are ejected in the discharge; they are called *microdroplets*. If they reach the substrate position during deposition, they can be the origin of defects in the film structure. A presentation of these different modes is given in Figure 2.

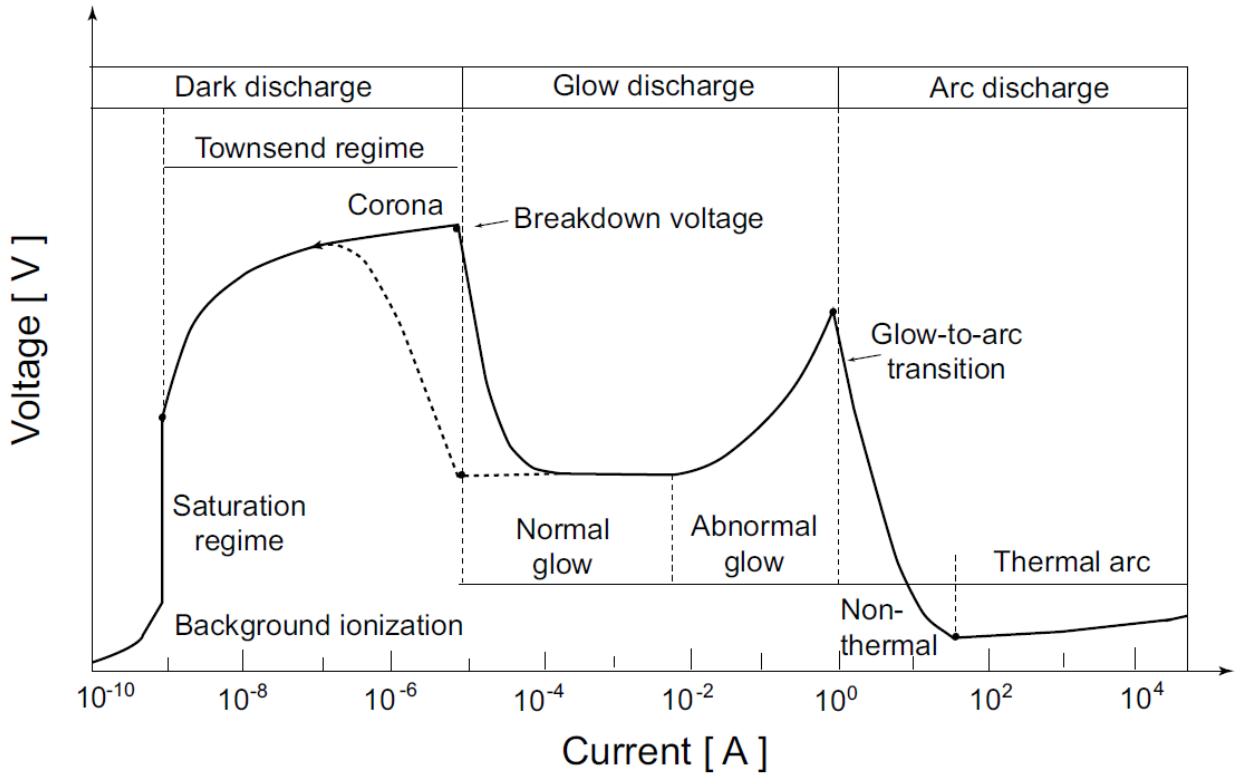

Figure 2. The different plasma discharge regimes [4]

Every state of the matter has its own specific properties. The plasma follows this rule since the cohabitation of energetic atoms/ions and electrons provides new kinetics to the plasma. These dynamics are direct consequences of the Maxwell's equations applied to a charged fluid (the plasma). It is considered a fluid because the density of charge carriers in such plasmas is generally around 10^{15} m^{-3} to 10^{19} m^{-3}. The study of all Maxwell's equations influences on the plasma behaviour would be a too specific task for

the work conducted here. However, it is quite essential to have a look at the Poisson equation (or Gauss law):

$$\nabla.\vec{\boldsymbol{D}} = \nabla.\varepsilon_0\vec{\boldsymbol{E}} = e(n_i - n_e)$$

Equation 2. Poisson equation (or Gauss law)

With n_i and n_e being respectively the positive ions and the electrons densities. When resolving this previous equation in one dimension, using the Boltzmann relation, the approximation that $n_i \approx n_0$ and the boundary condition that $\lim_{x\to\pm\infty} V(x) = 0$, the following result is obtained:

$$V = V_0 e^{-|x|/\lambda_D} \quad \text{Where:} \quad \lambda_D = \left(\frac{\varepsilon_0.T_e}{e.n_o}\right)^{1/2}$$

Equation 3. Definition and expression of the Debye length

The latter value, λ_D, is known as the Debye length and corresponds to the space scale on which charge densities can exist. For sputtering plasmas, this length is around a few µm. The existence and the value of λ_D leads to the understanding of a phenomenon specific to the discharges generated in vacuum chambers: the sheaths structure. Indeed, the knowledge of this Debye length implies that the only place where the quasi-neutrality of the plasma can be violated is in between the bulk plasma and the boundaries of the chamber (walls and target). At these positions, the electrons gather on the boundary vicinity (due to their higher velocity compared to the ions) and it results in the formation of a potential difference between the plasma and the walls. The region of the corresponding potential drop is called the *anode sheath* for the walls and the *cathode sheath* for the target. The cathodic sheath repeal electrons and attract ions and is characterized by an absence of ionization and therefore no light emission. Once a sheath has appeared, the plasma is slightly more positive than the walls and its potential (usually a few V) is called the *plasma potential* V_p. In the target vicinity, the applied voltage enhances the previous phenomenon and a larger sheath appears (a few mm in the HiPIMS configuration [5]). The existence of these sheaths is not essential for the work conducted here but is essential for the understanding of the sputtering process. If only two things had to be kept in mind, it is that the ions are accelerated towards the target's

surface through the cathodic sheath and the bulk plasma is quasi-neutral (no potential drop within it).

Another essential point to be raised is the behaviour of the electrons in the vicinity of the target in the case of magnetron sputtering. Indeed, the presence of a magnetic field coupled to the electrical field of the cathodic *dark space* (i.e. cathodic sheath) induces the appearance of the Lorentz force described as follows:

$$\vec{F} = q(\vec{E} + \vec{v}\wedge\vec{B})$$

Equation 4. Lorentz force equation

With $\vec{E}$ being the electric field in the chamber, $\vec{B}$ the magnetic field of the magnetron, q the charge of the particles and $\vec{v}$ their speed. The study of the previous equation leads to the conclusion that this force reaches a maximum when the two fields are perpendicular ($|\overrightarrow{E}|$ is considered to be constant near the target, as is $|\overrightarrow{B}|$). The only area where the two fields are perpendicular corresponds to half the distance between North and South poles of the magnetron. In this region, the electrons are trapped in the magnetic lines and their movement is described by the *Hall drift* (a representation is given in Figure 3). Normally, it would be expected to see ions being trapped as well but the calculation of the *Larmor radius* (i.e. the radius of the gyrating motion around the field lines) of both species in sputtering plasmas leads to a value of tens of cm for ions and about 1 mm for electrons. It is then evident that ions cannot be contained in the target vicinity, contrary to electrons. The electrons trapping zone described here is widely called the *preferential ionization zone* (or IR for *ionization region*) in the literature because it corresponds to the region where the electronic density is the highest and therefore where the ionizing collisions are occurring the most. This inhomogeneity in the electronic density results in the appearance of an *erosion track* between the inner and outer poles, where the sputtering of the target is enhanced. So, in practice, the symmetry of the magnetron leads to an incomplete erosion of the target (~ 30-40%) and is easily spotted on the target.

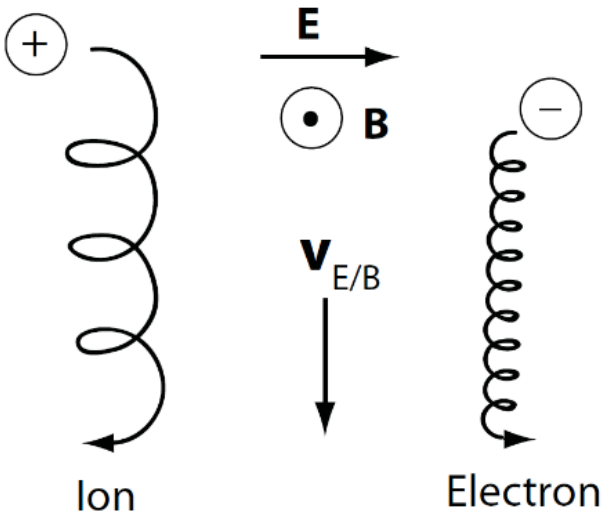

Figure 3. A schematic representation of the Hall drift in the vicinity of the target

I.1.2.3. Sputtering

Here, the actual process of sputtering is briefly described; the interest is focussed on the ions-target interaction for a metallic discharge. A further investigation of the process for HiPIMS discharges is conducted later in the thesis (cf. I.1.4). Here, only the ions-target interaction is described at its surface and vicinity. The presence of the cathodic sheath and the high electronic concentration in the magnetron field lines have previously been explained (cf. I.1.2.2) and are assumed for the following explanations.

The sputtering process describes the erosion of the target by the ions of the plasma. These ions can be either gaseous or metallic. Indeed, the gaseous ions are the first ones to be present in the plasma and therefore are the only ones sputtering the target in the first instants of the deposition but later on, they are joined by the sputtered species in the plasma. The sputtering by gaseous species is studied first. In this case, the positive ions are accelerated by the dark sheath towards the surface of the target and impact the latter. This collision results in two phenomena if the ions are energetic enough: the extraction of secondary electrons and the sputtering of atoms from the target. If the incident particle is not energetic enough to extract any particle from the target, it is reflected into the plasma by either an elastic or an inelastic collision. The latter can result in the heating of the target's surface –which sometimes results in the emission of a photon- and/or the modification of the target's topography. It can also result in the

neutralization of the incoming gaseous particle, which is then sent back towards the bulk plasma in a neutral state.

The importance of the secondary electrons emission has been explained earlier: it is essential for the sustainability of the discharge and the maintaining of its quasi-neutrality. They are expelled from the target and accelerated in the cathode sheath (if not trapped in the magnetron field lines) before entering the bulk plasma. The bulk plasma being the *neutral* plasma, filling the space in between the target and the substrate. In here, they create ion-electron pairs which keep taking part in the sputtering process. The efficiency of these electrons extraction is defined as the *secondary emission electron coefficient* γ_{se} and its value principally depends on two things: the ionization potential of incoming ions and the work function of the sputtered material [6]. A further investigation of these potentials and work functions in the sputtering case leads to another important observation: the secondary electron emission can be observed with singly ionized gas species but the incident metallic atoms need to be at least doubly ionized to perform this type of extraction. In other words, the *self-sustained self-sputtering* mode can only occur when the species had enough time to be at least doubly ionized [7]. It also explains why the self-sputtering phenomenon is intensified in HiPIMS discharges (higher ionization rates and degrees of ionization are observed in these discharges) [7].

The secondary electrons are not the only particles that the incident ions are ejecting from the target: atoms are also being sputtered. As a matter of fact, their extraction is the main purpose of this process because these atoms are depositing on the substrate and forming the thin film. Like secondary electrons emission, the efficiency of the extraction of metallic atoms can be defined by a specific value: the *sputtering yield*. It is the number of atoms sputtered per incident particle and is included between 0.5 and 2 in most cases. Even if the relationship is not direct, a higher sputtering yield corresponds to a higher deposition rate and is therefore generally preferred. This yield is mainly dependant on the materials used and the voltage applied. For the latter, the fact that its relationship with the sputtering yield is non-linear but $\sim\sqrt{V_0}$ (with V_0 the applied voltage to the cathode) should however be highlighted [8]. The evolution of the sputtering regimes with the modification of the incident ions energy is represented in the figure

below (cf Figure 4). On this figure, the three following regimes are presented: *(a)* single knock-on (low energy), *(b)* linear cascade, and *(c)* spike (high energy).

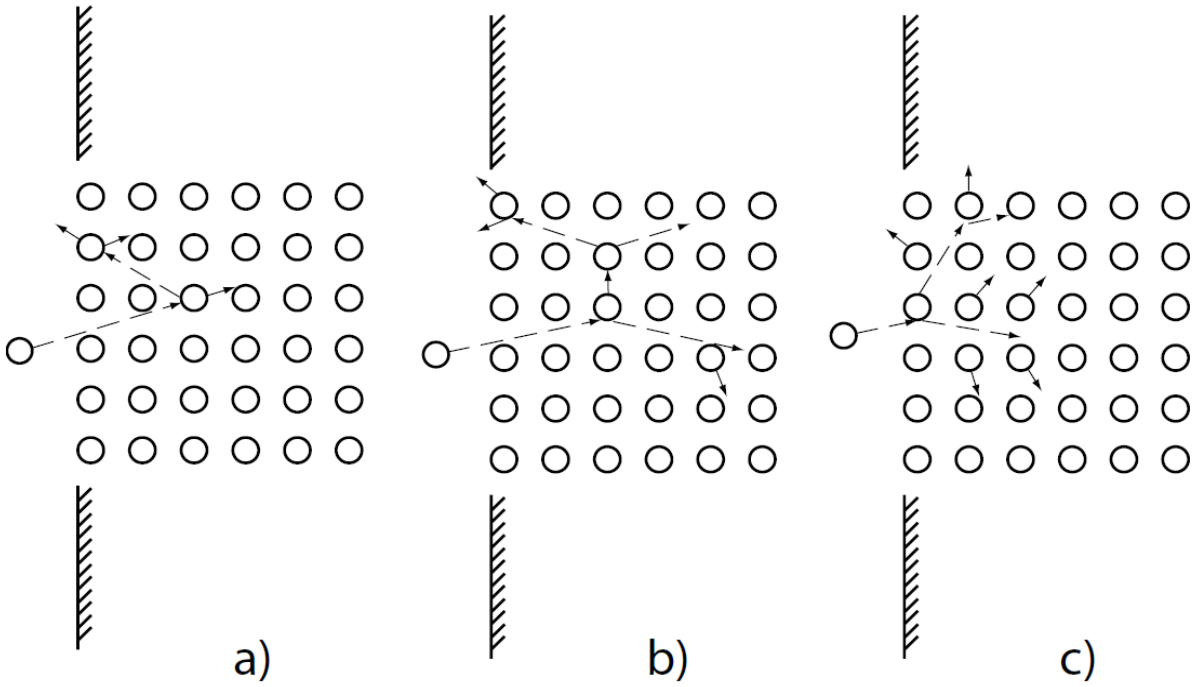

Figure 4. The different sputtering regimes ([9] from [10])

Concerning, the material used, the reality is that some metals are more easily sputtered than others and that for a given target material, the nature of the incident ions has an influence. First, the metallic ions present a lower sputtering yield than the argon ions for physical reasons and this has been proven many times in papers. After, for the gaseous species impacting the surface, the rule is simple: the heavier the incoming ions, the greater the sputtering yield. However, this is not entirely true since, for example, the argon sputters the zirconium at higher rates than xenon even if xenon atoms are heavier than argon's. It is due to the high similarity in the masses of the argon and zirconium atoms. In summary, the sputtering yield is enhanced with heavier gaseous species unless the mass of the target's atom is close to the mass of a specific inert gas atom [11] [12].

I.1.2.4. Transportation

After being sputtered from the target, the atoms are ejected towards the chamber and begin their trip towards the substrate position. The diffusion of the particles is mainly due to the density gradient in the chamber: the zones of higher density (i.e. target) diffuse

towards the zones of lower density (i.e. boundaries). This type of diffusion is a so-called *acoustic wave* and is the main transportation process occurring in the chamber. However, in a plasma, the charged particles in presence also interact with one another while diffusing and the *ambipolar diffusion* is observed. In brief, the ambipolar diffusion describes the coupled diffusion of two species with different polarities (e.g. ions and electrons) in the presence of both electric and magnetic fields. On their way towards the bulk plasma, the ejected particles can encounter other species and the consequences of these collisions are numerous. In this section, each one of the different scenarios is listed and explained. Moreover, it is also essential to understand that the ionization of the sputtered species mainly occurs near the target before they continue to *diffuse* in the chamber, around the erosion track, as it is seen in the following LIF imaging acquisitions:

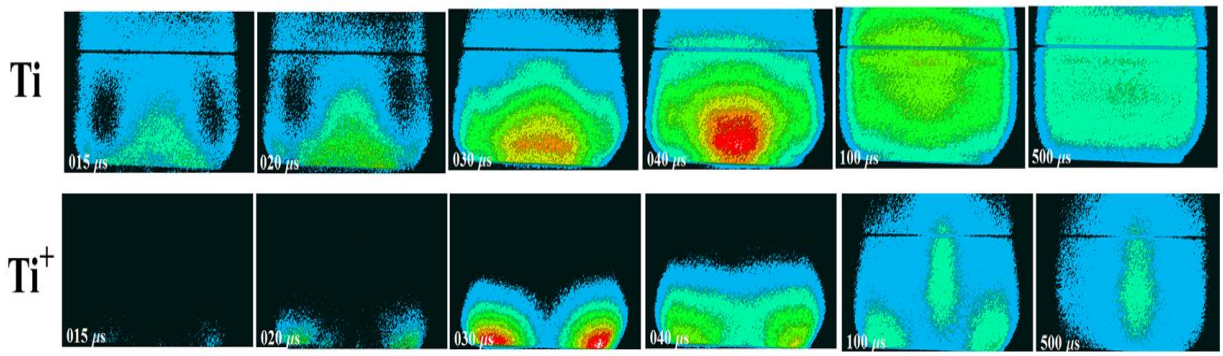

Figure 5. Two-dimensional normalized density maps of Ti and Ti^+ ions during an Ar-Ti HiPIMS discharge (from [13])

First, there are cases when the metallic atom is not energetic enough when it is leaving the surface of the target and the potential drop of the dark sheath attracts it back to the target. This phenomenon is called the *back-scattering*. Some other ions are also back-scattered because, even if they supposedly have enough energy to get out of the sheath when they leave the target, they collide with particles before to be able to reach the bulk plasma and are no longer energetic enough. The back-scattered ions are taking part in the sputtering process explained earlier.

The same inelastic collisions as the one described just before can also occur in the bulk plasma. This time, because of the quasi-neutrality of the plasma, the ions are not necessarily back-scattered but another process is occurring: the gas *rarefaction*. It corresponds to the inelastic collisions between the target's sputtered atoms and the

gaseous species around the target. These collisions induce a momentum and heat transfer from the metallic to the gaseous species and it results in a diminution of the latter's density in the vicinity of the target. However, the heat transfer is the major reason leading to this reaction: the gas expands and its density diminishes, following the thermo-dynamics principles. Therefore, less gas is available for the sputtering of the target and the metallic particles are now majorly participating in the sputtering of the target: it is the *self-sputtering* process (i.e. sputtering of the target by metallic particles of the same element). It may be necessary to specify that –due to their origins- the particles participating to self-sputtering have a lower kinetic energy than the initial noble gas atoms.

In the chamber, the species can undertake different types of collisions within the plasma. The first type of impact has been evocated in the previous paragraphs: their ionization by electronic impact. It mainly occurs in the preferential ionization zone but can also happen with the electrons from the bulk plasma. The others ionization collisions are neglected (i.e. atoms-atoms and ions-atoms). It is therefore evident that the proportion of incoming ions at substrate position is enhanced when the electron density (and thus the ionization rate) in the chamber is higher. However, the same electrons are also at the origin of the *recombination* of a certain number of ions coming from the target position. This time, the ionization rate of the plasma is lowered by this process. A third type of non-elastic collision existing in the plasma is the excitement of a given particle by another. It has been evocated earlier as the thermalization. In this case, the excited atom reaches an unstable energetic level. The direct consequence to this is the relaxation to a lower and more stable energetic level (i.e. ionized or ground level) with the emission of a photon. It has already been explained earlier that this light emission is specific to each plasma and depends on its composition.

A certain balance exists between the recombination, thermalization and ionization impacts and is specific to each setup. The probability of occurrence of each process is translated by the calculation of the corresponding *cross sections* for the species in the plasma but these calculations are not relevant -and thus not presented- here. Finally, the metallic particles coming from the bulk plasma (i.e. ions and atoms) reach to the chamber boundaries (i.e. the anode), including the substrate. The particles not reaching the substrate position are considered as lost. One last remark to do is that, if a

bias is applied to the substrate holder, the ions incoming to the substrate position are accelerated by the anode sheath, while the atoms are not; which can be an argument for reaching a plasma as ionized as possible to achieve better film growth. A phenomenological model of the different processes seen in this section has been developed in the literature and is summarized in section I.1.4.1.

I.1.2.5. Deposition and film growth

The incoming atoms and ions are depositing on the substrate after having travelled through the bulk plasma. This section focuses on the deposition process, and the different growing regimes of a thin film are presented. The incoming particles can either be atoms, ions and/or excited particles. Depending on their energies, the incoming particles are not behaving the same way. Indeed, if an atom reaches the substrate surface with no energy (or not enough), it simply links at its arriving position. The particle needs intrinsic energy to be able to move around, at the substrate's surface. The energetic flux at the substrate position is thus an important parameter to study during the deposition of thin films. However, in all cases, even once the *adatom* is linked to the film, there is always a possibility of desorption of the particle; which is going back into the chamber.

If the particle has not been re-evaporated and has enough energy, it can migrate on the substrate surface until it finds a place to stop. The place where the adatom stops depends on the work function of the surface. Indeed, the lower the work function is, the more likely the particle is to stop. The zone where the surface work function is lower corresponds to defects in the substrate most of the time, but once the first atoms have been deposited, they lower the mechanical potential of the work function at their positions and thus enhance the chances for other adatoms to join them at their position. This step is called the *nucleation*. It means that small, independent islands are growing onto the substrate surface (i.e. *nuclei*). These nuclei keep expanding until they enter in contact with one another: it is the so-called *coalescence* process. If one continues, these regions keep spreading until they form a homogeneous layer and the following adatoms deposit on the latter.

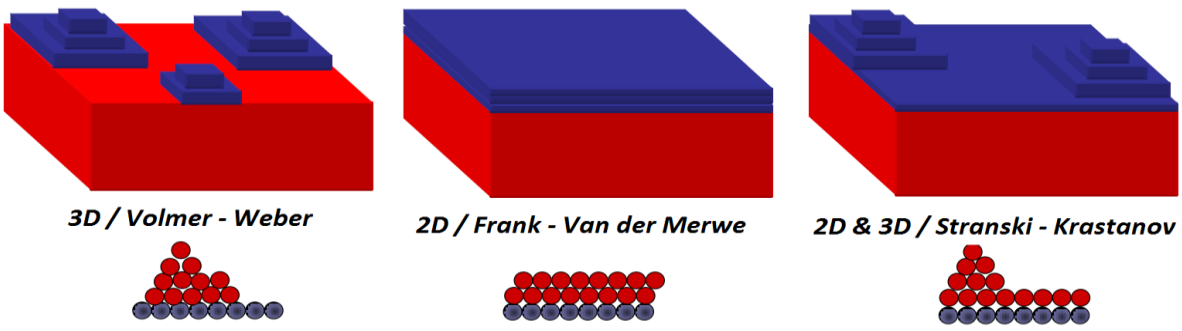

Figure 6. The three different regimes of film growth

At this point, there are three scenarios possible. First, the incoming particle is directly captured from the vapour and deposit where it lands. In this case, the formation of 3D islands is spotted: the atoms arriving at the top of the island do not have enough energy to move out of the surface and take part in the 2D growth of the nuclei. In the second scenario, the particles are growing a 2D layer following the process described above for energetic particles. In a third situation, the energy of the incoming particles is sufficient to grow a 2D layer onto the substrate surface but the work function of this latter is too high to permit the following adatoms to grow in 2D. It results in the growth of islands at the top of the first 2D layer. The three regimes are presented in Figure 6.

The existence of these three different scenarios is the origin of the different microstructures (1, T, 2 and 3) that can be observed during deposition. Although it is more precisely studied further in this report (cf. Chapter II), it is necessary to present the following graphs (Figure 7). The first one, the Thornton diagram [14], represents and classifies the different growing phases for evaporation process into several categories and shows that the pressure affects the phase transitions as much as substrate temperature. However, Anders has modified this diagram, preferring to indicate the (normalized) kinetic energy of the adatoms rather than the pressure [15]. The latter has also added the conditions corresponding to the HiPIMS case and indicated the structures in presence [15]. The two diagrams are directly related to one another.

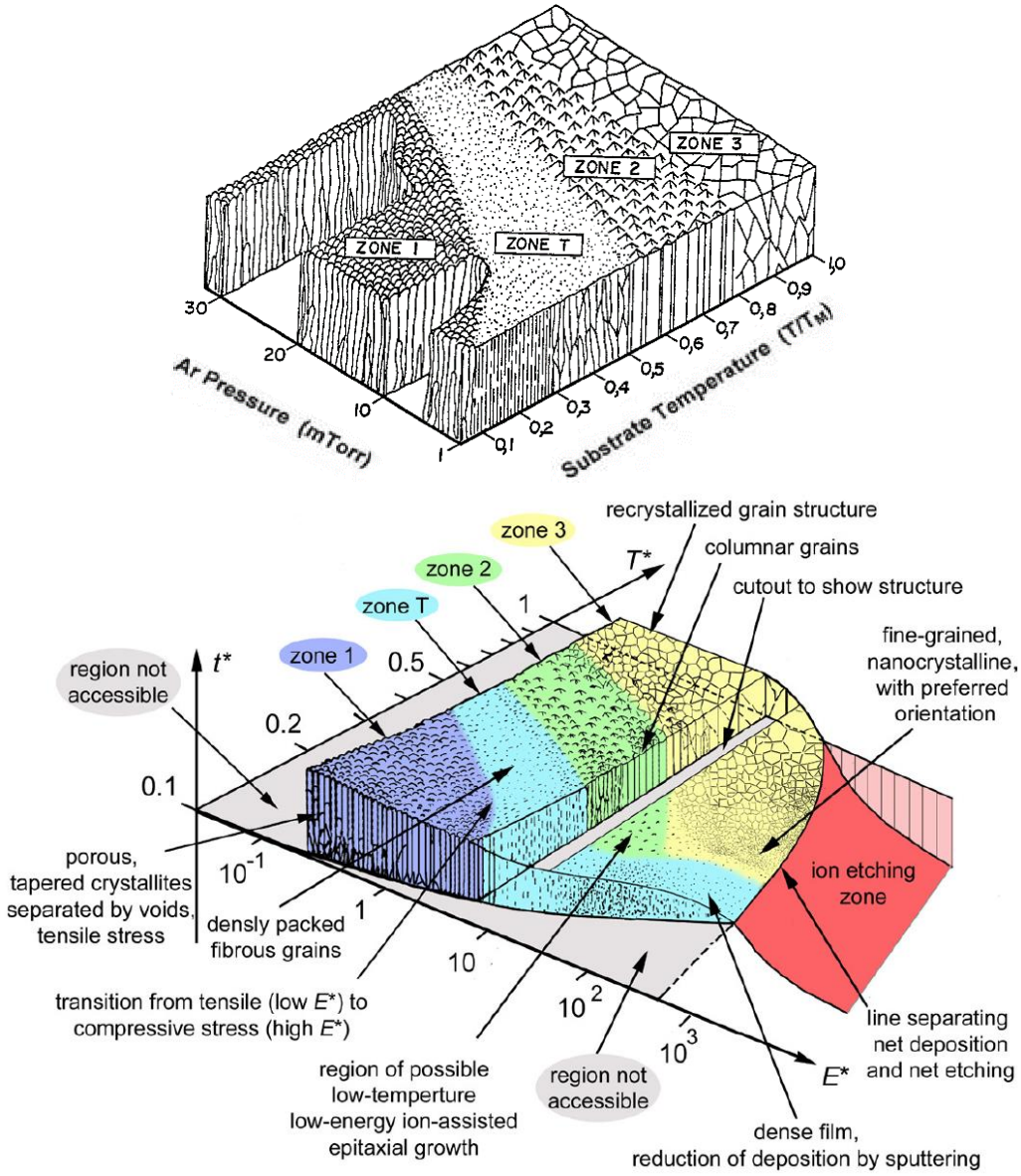

Figure 7. The Thornton (top) and Anders (bottom) diagrams [14] [16]

The first zone, corresponds to a porous growth of the film. The film has a very low density because of the gaps existing between the different inhomogeneous columns, which results in a high roughness of the thin film surface. The zone T is a transitional phase where different crystallographic plans are present at the substrate vicinity but then, on top, one predominates the others and a semi-columnar structure is observed. The gaps are widely reduced and a preferential orientation starts to be spotted. The third zone (i.e. zone 2) is the zone corresponding to perfect columnar grains growth of the film with a preferential orientation of the crystal. Finally, in the zone 3, recrystallized structures are found. Here, the grown film is identical to the bulk material. For some deposition

processes, it is only made possible by an annealing of the film either during the deposition or after.

I.1.3. A brief historical review of sputtering processes

I.1.3.1. From the DC Magnetron Sputtering

The first vacuum thin film depositions have been made thanks to the works of Grove in 1852 [17], and then Nahrwold in 1887 [18]. The latter realized the first cathodic sputtering in a glow discharge. At first, this technique was mainly used to produce reflective deposits (~ 1880-1930) but it is with the development of semiconductors technologies (~ 1950) that the process experienced a huge development. Indeed, these Physical Vapour Deposition (PVD) processes being transferable to industrial scales, thanks to their ability to combine both large surface treatment (up to metric scale) and high precision (i.e. nanometric scale), correspond to the expectations of many new industrial technologies, but also to a large number of research areas.

The most common configuration is called the *diode* configuration, and it consists in only a cathode (target) and an anode (the rest of the chamber). This type of rig allows the deposition of various thin films but because of its high operating pressure, results in defects in the layers. In 1936, Penning, to reach lower pressures, had the idea of establishing a magnetic field near the target. This field would trap the secondary electrons along its magnetic lines via the Lorentz force [19] and thus give them a helical trajectory. It extends their lifetimes and makes ionization easier. Later, it has been noticed that the field could be created through a permanent magnet, limiting the cost and complexity of the systems. The magnetron can be rectangular, circular or cylindrical, balanced or unbalanced, in a closed-field configuration or not. Every configuration is chosen to suit the aimed deposition conditions. In Figure 8 are shown schemes of the magnetic field lines for different possible settings [20].

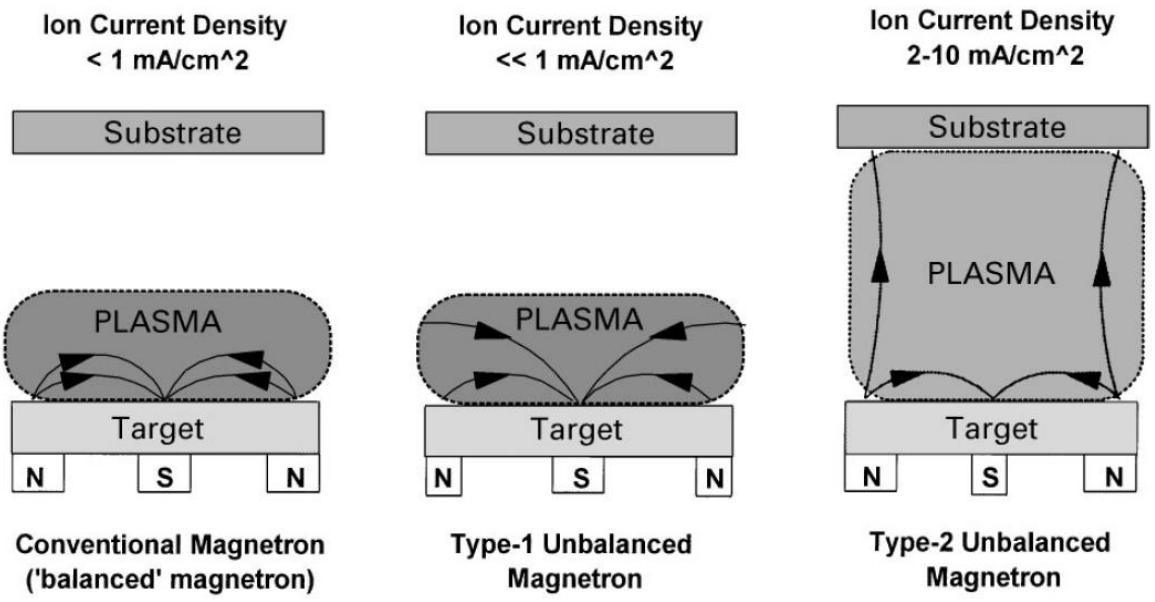

Figure 8. Magnetic field lines for the balanced, unbalanced and closed-field configurations and the corresponding cathodic ion current density [21]

The conventional magnetron, the *balanced* magnetron, consists in a balanced static magnetic field generated behind the target. This means that the South and North poles of the magnetrons present the same magnetic power. It results in a system where all (or most of) the field lines are contained within the bulk plasma between the North and South poles. The *type 1 unbalanced* configuration refers to a system where the inner pole (in the centre of the target) is stronger than the outer poles. This time, it results in more field lines going inside the plasma compared to the balanced configuration. In this configuration, the plasma tends to be intensified in the centre of the target and its ionization is enhanced. The *type 2 unbalanced* magnetron has outer poles more powerful than the inner pole. The direct consequence is the existence of some field lines linking the target surface and the substrate holder. This configuration eases the transport of the electrons and ionised species due to –among others- extending the plasma towards the target. Window and Savvides were the first persons to recognize and classify unbalances magnetrons [22].

Systems have also been developed where the field strength of the magnetron can be modified. These types of system allow the user to modify the position of the inner and outer poles, and therefore their magnetic fields strength at the target surface. By doing so, the magnetic configuration can be modified from balanced to unbalanced type-1 and

type-2 and thus modify the ion-to-atom ratio (cf I.1.2.1) reaching the substrate. This ionization rate is of a great importance in the growing process of films. If one goes further, *closed-field* configurations can be realised. In this case, two -or more- type 2 unbalanced magnetrons are placed on each side of the substrate holder so the latter is fully immersed in the bulk plasma. The polarity of the magnetrons must be the opposite of one another so their field lines can link as shown in Figure 9.

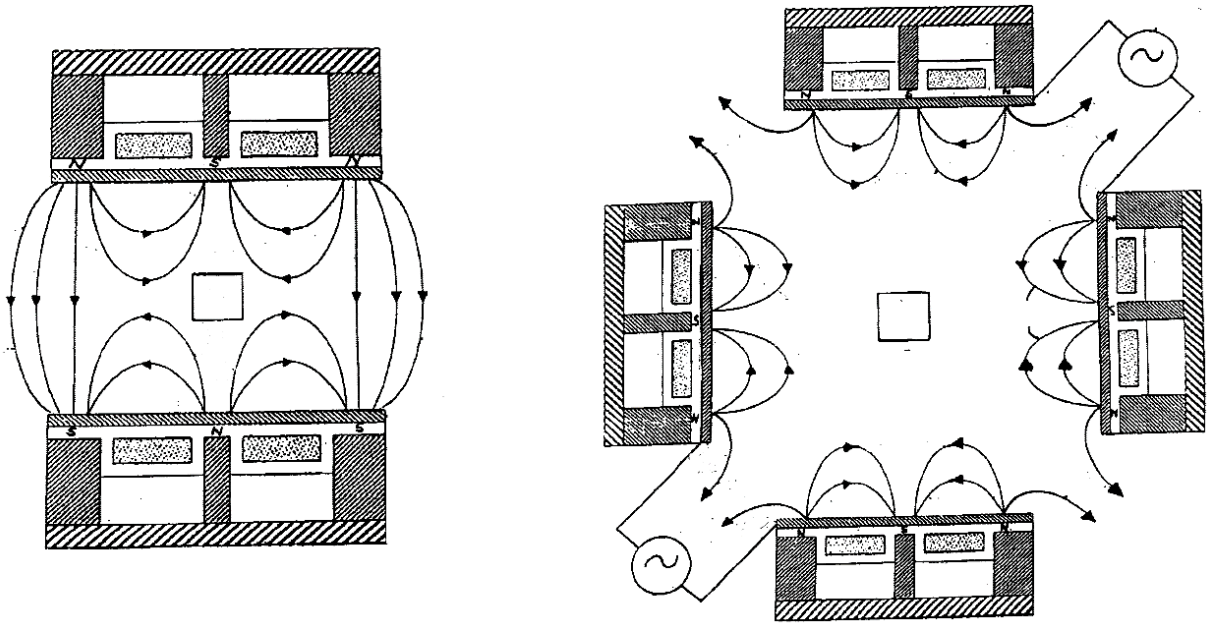

Figure 9. Closed-field configurations for a two magnetrons system on the left and four magnetrons on the right (from [21])

With these kinds of configurations, the cathode voltage values are typically between -300 and -700V and they can lead to current densities in the range of 4 to 60 mA/cm²; which results in power densities going from 1 to 10 W/cm² at the target surface. Electronic densities are in the range of 10^{15}-10^{17} cm^{-3} and deposition rates between 1 and 10 $nm.s^{-1}$ have been measured [23]. It should however be noticed that the ionization rate of the sputtered vapour ($\frac{Metallic\ ions}{Metallic\ ions+atoms}$) is only of a few percent - or even less. Previously, it has been explained why a better ionised plasma means better growing conditions and a better control on the latter, thanks to the bias for example. So, to increase this ionization rate, many other techniques have been developed [20] [24] until the emergence of the High Power Impulse Magnetron Sputtering (HiPIMS) process.

These several techniques include -along others- the radio frequency and mid-frequency sputtering processes, which are discussed in the next section (cf I.1.3.2).

Besides, another way to improve the sputtering process is by implementing a hot filament in the chamber [25] [26]. A voltage of roughly 10 to 50V (or even more) is applied to this filament so it is negatively polarized compared to the bulk plasma, and thus can eject electrons. These electrons are essential to the well-being of the plasma. The voltage applied to the filament should however stay as low as possible so the material composing the filament does not get sputtered as well; which could add impurities in the plasma composition. Again, this novel sputtering process allows users to reach lower pressures ($10^{-3}/10^{-4}$ mbar) and voltages, while keeping the deposition rate constant. A lowered pressure means that less pollutants are present within the chamber and fewer collisions are occurring. This results in a major consequence: a diminution of the number of arcs. Both consequences allow a better-quality growth of the film without necessarily reducing its speed. The reduction of the voltage needed to sustain the plasma has also a direct consequence on the temperature of the target and thus the need to cool it down (to avoid arcing or other unwanted processes).

However, it still does not correspond to some projects and applications, and another sputtering process had to be developed: the ion-beam sputtering. In this case, an ion source is place in the chamber. The ions are generated by collisions with electrons densely trapped in a magnetic field within the ion source. These ions are then accelerated through the ion gun and sent towards the target surface. However, before to get expelled from the *ion gun*, they pass through a grid that neutralises them. There are then neutral atoms striking the target surface, which allows the users to sputter either conducting or insulating targets. Instead of being the only ion source in the chamber, this process is mainly used in ion-beam assisted sputtering. In this case, a secondary ion source is operating at a lower pressure than the principal ion source and is directed towards the substrate. By enhancing the adatom mobility (i.e. energy), the *assisting beam* helps the film to grow properly by removing the impurities or sputtered particles that are not bound to the film strongly enough (i.e. crystallized).

I.1.3.2. Through the pulsed magnetron sputtering

The next step in the improvement of the sputtering processes has been the development of pulsed-DC power supplies [27]. These processes aim to reach lower target temperatures and higher ionization rates. The previous works done to reach it concerned the improvement of the rig itself (e.g. magnetron, unbalanced field, triode, ion beam) but the power supply itself still have not been improved. First, studies have shown that switching off the plasma for short times at regular intervals results in a massive reduction of the numbers of arcs along time; especially during reactive sputtering (e.g. for depositing oxides). As evocated in section I.1.2, arcs occur when there is a charge carrier accumulation at the surface of the target. It is most likely to happen when the target is a ceramic but also if operating under reactive atmosphere. In both cases, it happens because the target surface is not conductive enough to evacuate the charge carriers brought by the plasma. These charges accumulate until an arc occurs, which is the physical consequence of this release. It is not rare to see molecules and droplets being ejected when this happen. It can have unwanted consequences such as defects creation during the film growth or modification of the plasma stoichiometry. Both must be avoided so the film properties can be enhanced.

There are two main types of pulsed magnetron sputtering processes: radio frequency and mid-frequency sputtering. The first one is usually run at a 13.56 MHz frequency while the latter corresponds to frequencies going from 20 to 350 kHz. However, only the mid-frequency process is presented here because it has attracted more interest from industry thanks to its relatively high deposition rates. Indeed, some studies have shown deposition rates for ceramics and compound materials of the same range as pure metal films. This mid-frequency sputtering presents two different types of power supply management. They differentiate one from another by the voltage applied during the off-time. The voltage can either be oscillating between the negative sputtering voltage and the ground (i.e. *unipolar* mode) or it can also be set to a slightly positive voltage during the off-time (i.e. *bipolar* mode). In general, the positive bias is set in between 10 and 20% of the operating voltage due to the higher mobility of the electrons. By doing so, the neutralisation of the charge carrier from the target surface is enabled. These techniques had shown better quality film growths for common materials. It is believed to be due to

a better charge evacuation leading to fewer arcs, and an increase in the electron temperature (i.e. energy) of the plasma due to the oscillations in the bias.

I.1.3.3. To the High Power Impulse Magnetron Sputtering and Modulated Pulse Power Magnetron Sputtering systems

The first publication referring to the HiPIMS process has been written in 1999 [28] and the paper reports a very dense plasma, with a proportion of metallic ions coming to the substrate surface close to 70% for some materials. It results in more homogeneous and denser films due to a more energetic plasma (i.e. higher ionization rate and greater adatoms mobility). Indeed, one of the technical limits of PVD is to be able to control the trajectory and the energy of the (metallic) ions to enable a better homogenization of the growth speed on surfaces presenting complex geometries, as presented in Figure 10 and reported in several papers [28] [29] [30]. This is only possible by controlling the plasma's ions by applying a (negative) bias to the substrate holder and for this to have a maximum effect, the plasma had to be as ionized as possible.

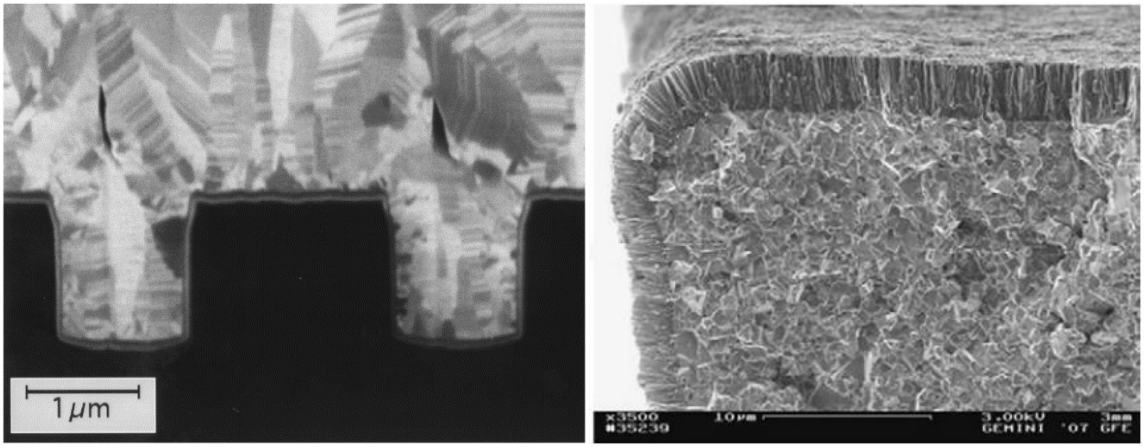

Figure 10. Films deposited on non-flat substrates from the work of Kouznetsov et al. on the left [28] and Bobzin et al. on the right [29]

The solution proposed by Kouznetsov and his team is to generate a very high power peak (~ 3 kW.cm^{-2}) to enhance ionization within the plasma [28]. However, to avoid an *overheating* of the target, this electrical input signal must be pulsed at low duty-cycles (< 10%). The high power pulsed nature of the discharge then leads to a much higher ionization rate (~ 70%) compared to the Direct Current Magnetron Sputtering DCMS

case. It also leads to much more energetic particles reaching the substrate and therefore a *supersaturation* [23] and high mobility of the adatoms on the substrate surface; resulting in new growing conditions for the films. The supersaturation of adatoms corresponds to the case where the number of atoms arriving at the surface of the substrate is too important to consider that each adatom relaxation is independent; they can collide with one another while migrating at the surface. As said above, it also permits coverage of substrates presenting complex surface geometries.

In addition, these ions have an average energy higher than in DCMS discharges (see Figure 11 below). Thus, having a highly-ionized plasma improves the quality of the film and the control over it in terms of density, hardness, adhesion, roughness, reactivity, growth phase, etc. One can also add that the role of the bias is to manage the quantity, the orientation and the energy of the ions reaching the substrate surface. It can also have an impact on other film properties such as intensity and direction of the crystallinity, grain size, deposition velocity, film density, and internal stresses.

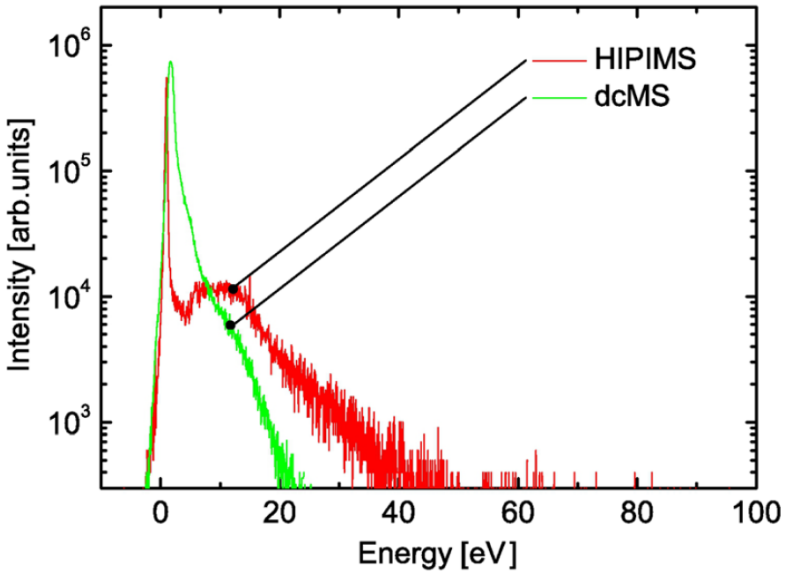

Figure 11. Comparison of temporal mean valued of ionic energy distribution for titanium sputtering [23]

Having a pulsed signal involves taking a new parameter into account: the *duty cycle* –which is kept low. The latter is defined as the on/off ratio of the signal and has a key role in explanations of the reactive plasma behaviour. For a more complete and clear approach, most of the studies separate the duty-cycle influence in both the pulse width

and frequency influences. They are responsible for several effects: the effective sputtering time, the *refill time* (i.e. time corresponding to the refill of the target vicinity in gaseous species after sputtering) and the relaxing time (i.e. period along which the ionized and energetic particles are relaxing back to their ground state). The occurrence of phenomena such as rarefaction and self-sputtering also depends on the duty cycle value.

In their 'High Power Impulse Magnetron Sputtering Discharge' review [23], the authors, relying on the already existing literature, listed the following values as being the operational range of the HiPIMS process discharges. These values lead to the Figure 12 presented below.

•Current density: 3-4 A/cm² •Peak power: 0.5 - 10 kW/cm² •Frequency: 50-5000 Hz

•Cathode voltage: 500-2000 V •Duty-cycle: 0.5 - 5%

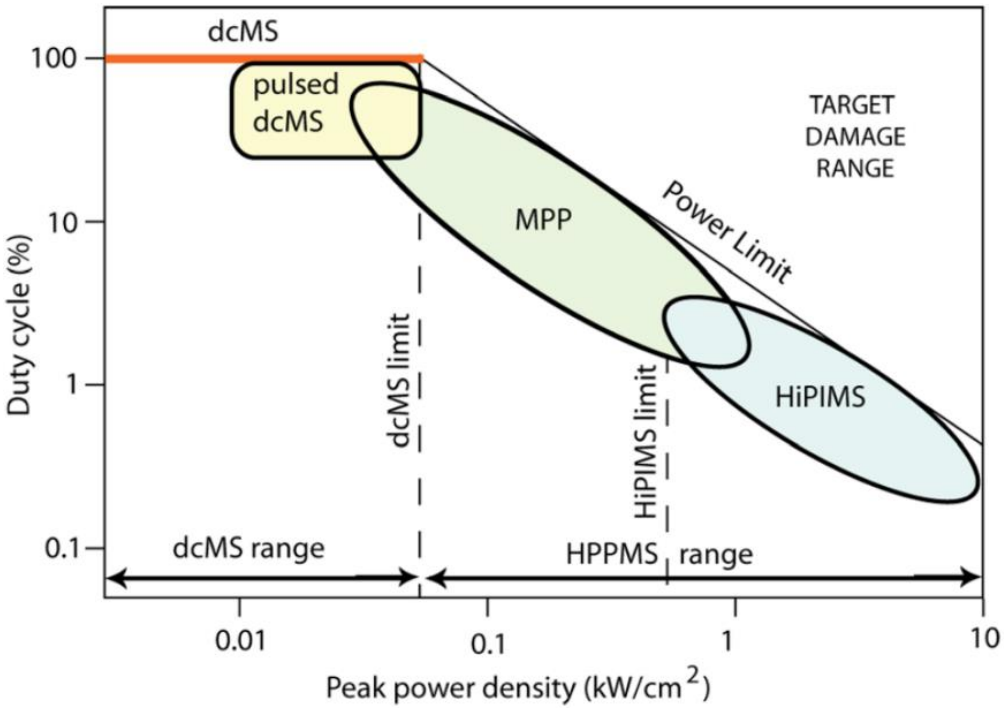

Figure 12. Representation of the HiPIMS process envelope on a peak power density against duty-cycle diagram [23]

Over the last decade, another type of sputtering system -based on the HiPIMS process- has been developed and studied: the Modulated Pulse Power Magnetron Sputtering, also known as MPP (or MPP-MS) systems. The aim of this technique is to keep (or even enhance) the high ionization rate measured during HiPIMS deposition but

widely improve the deposition rate. To do so, Christyakov and his team had the idea to increment short pulses within the major deposition pulse as follows [31] [32]:

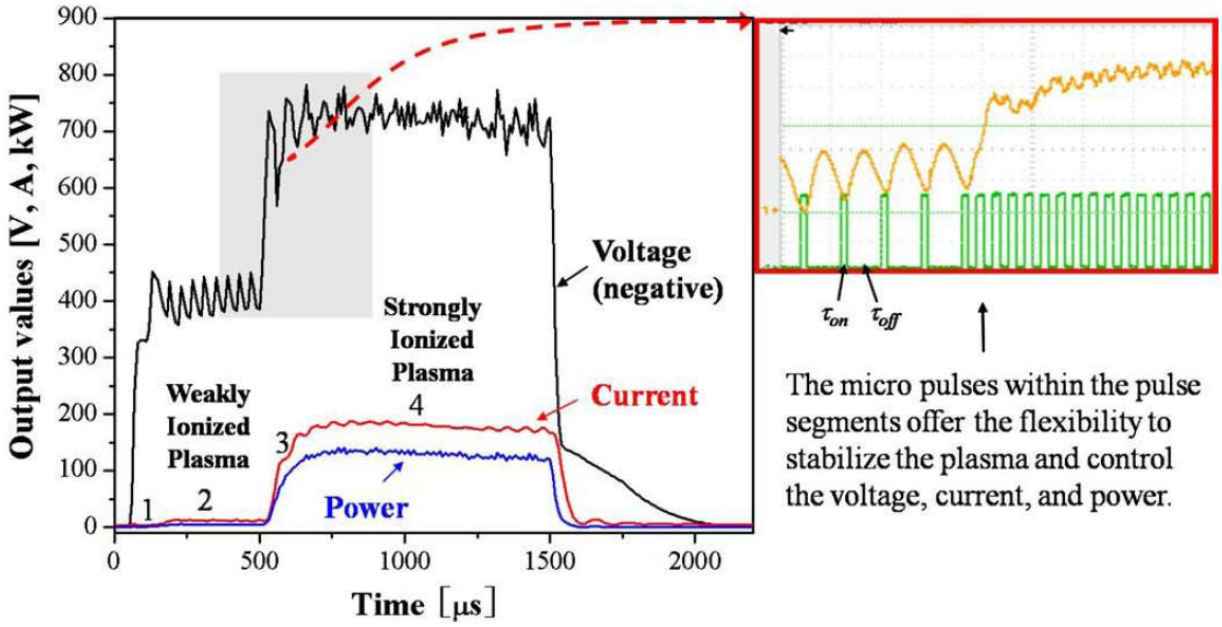

Figure 13. Representation of a typical MPP pulse with the four different steps of the process and the figure showing the micro-pulses within the pulse (from [33])

In this type of discharge, the pulse is constituted of four different steps. Frist, a weak plasma is initiated by the application of a negative voltage at the target's position. Then, a succession of short pulses with a relatively low duty-cycle is applied to maintain and stabilize this weakly ionized plasma; it is the *low power discharge*. Then, there is a transition stage during which the duty cycle of the micro-pulses is increased, resulting in cathodic voltage raising. As seen previously, an increase in cathodic voltage means a better ionization of the discharge. The plasma thus reaches his strongly ionized state, comparable to HiPIMS discharges. This *high power ionization discharge* is kept on for several hundreds of μs before being switched off. The entire MPP pulses can be as wide as 3000 μs, with a maximum duty-cycle of 28%. The frequency is maintained in between 4 and 400 Hz. Peak power density is generally measured within a 0.5 to 1.5 kW/cm² range.

This technique is very useful for the deposition of materials presenting unstable and very sensitive HiPIMS discharges; such as carbon for example. The coatings deposited using this sputtering technique present the same advantage than HiPIMS-deposited films: improvement of the microstructure and properties: density, low stress,

good adherence, etc... [34] However, the main difference with HiPIMS deposition, is the improved deposition rate. Indeed, Lin and his team have reported deposition rates for MPP deposition of Cr coatings comparable and even higher than DCMS deposition rate. However, longer pulses and higher duty-cycle also means that the heating occurring at substrate position during deposition is quite important and therefore do not correspond to the specifications of this project.

I.1.4. The HIPIMS discharge

I.1.4.1. Introduction – A phenomenological model

This section provides the reader with an overview of the different steps constituting the entire HiPIMS sputtering process and summarizes in a simplified model the information presented in the next section (cf. I.1.4.2). The necessity to develop such a model originates from the fact that the simulation methods developed for DC and RF systems are not convenient in the case of HiPIMS discharges. The HiPIMS process is more complex than DC or RF processes, mainly due to the high quantity of ions present in the chamber. Therefore, the simulations are too heavy; they need long time scales for their calculations. The first model, the so-called *target material pathways* model, has been developed by Christie [35]. It has a large impact on the explanation of the low deposition rate observed for HiPIMS discharges. The model has been modified several times: Vlček et al. in [36], Vlček and Burcalová in [37], and Lundin in [5]. The presentation given below relies on the Figure 14 and the discussion given by Lundin in [5]. The roman numerals correspond to the different processes taking place during the whole sputtering duration.

First, it has been seen before that there are two types of ions impinging on the target surface after being accelerated within the cathode sheath (cf I.1.2.2 and I.1.2.3): working gas ions G^+ (I) and metal ions M^+ (II). The metal ions are previously sputtered atoms (III) that have been ionized in the Ionization Region (IV) -with a probability α- and back-scattered towards the target (V) -with a probability β_t- because they were not energetic enough to escape from the cathodic potential drop. The collisions of energetic ions upon the surface of the target result in the ejection of target material: atoms and secondary electrons. The amount of sputtered atoms (III) is ruled by the sputtering yields Y_{tg} and Y_{ss} corresponding to, respectively, sputtering by the working gas and self-

sputtering by metal ions. The emission rate of secondary electrons is given by the secondary electron emission coefficient γ_{se}. The secondary electrons are essential for the sustainability of the discharge (more details are given in sections I.1.2.2 and I.1.2.3). The sputtered atoms can follow different scenarios after being ejected. As it has previously been mentioned, the sputtered atoms can either be ionized in the IR with a probability α. But they can also continue their ways towards the bulk plasma without undertaking any collision. Another situation for the ejected particles is the so-called *gas rarefaction* effect where the energetic sputtered atoms collide with the background species (X); it has been more deeply described in section I.1.2.4. Some of the gas ions can also take part in the thermalization/rarefaction process (XII). In addition, there also are particles neutralised at the target surface and reflected back to the plasma (XI) (in opposition to particles being evacuated through the pumping system). The neutrals that are now in the bulk plasma can still be ionized (VIII) with a probability γ (see section I.1.2.2). They increase the amount of metal ions in the bulk plasma, adding to the atoms that have been ionized in the IR but not back-attracted towards the target (VI) (with a probability 1-β_t). These metal ions, are then travelling through the chamber and are either lost on the walls of the deposition chamber or contributing to the growing process of the film (VII) (see I.1.2.5 for details). The same situation is observed for the neutrals (IX) and the probability for the ions or neutrals to take part in the film growth are respectively noted ξ_i and ξ_n.

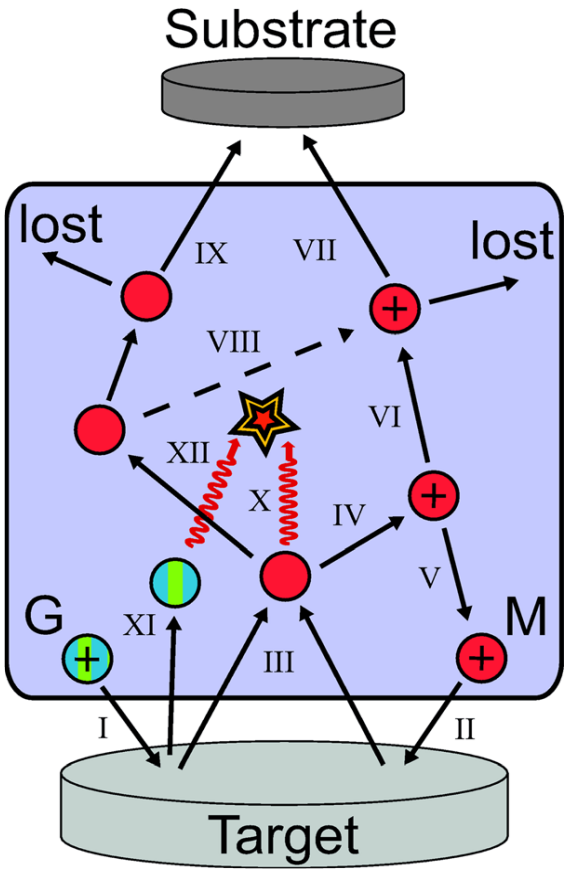

Figure 14. Schematic of the target material pathway model. The letters G and M stand for gas and metal species, respectively. [5]

I.1.4.2. Time-scaled description of a pulse in metallic mode

This section provides a better and deeper description of the plasma used in this project. To do so, the different stages composing one relatively long pulse (300 µs) in an inert atmosphere (argon) while sputtering a metallic target is described. The differences occurring in the case where a reactive gas is injected into the chamber are discussed in the following section (cf. I.1.4.3). This summary mainly relies on Figure 15 and on multiple scientific articles characterizing the HiPIMS plasma [38] [39] [40] [41] [42] and other reviews or thesis, summarizing a great part of the knowledge acquired on this subject [5] [19] [23] [43] [44] [45] [46] [47] [48] [49] [50].

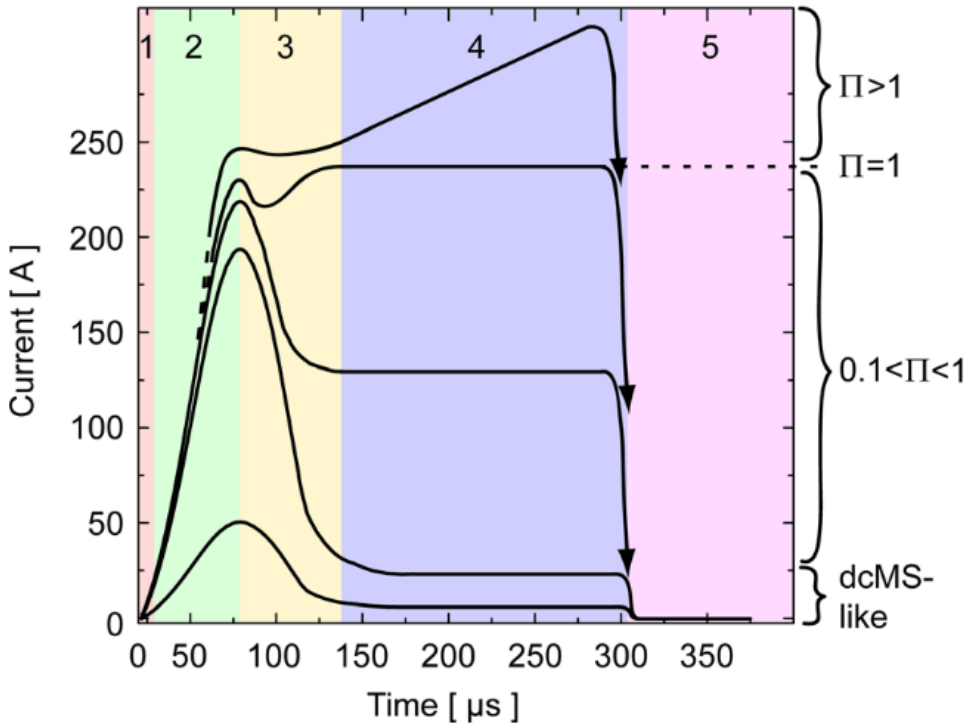

Figure 15. Schematic illustration of the current for long HiPIMS pulses [23] – with Π the sum of the sputtering and self-sputtering rates

Figure 15 is a schematic representation of the different cathodic current discharge profiles possibly observed during a pulse and it is divided into five distinct regions: the five steps of a pulse. It should be specified that the curves represented in Figure 15 are time-averaged acquisitions. It means that some atoms, ions, and electrons of low energy persist in the deposition chamber before the ignition of the represented pulse. These species can come either from the working (or reactive) gas or from the metallic target. Therefore, the profiles are reflecting an already initiated plasma state by smoothing the initial pulse.

The first phase, the ignition, corresponds to the first tens of microseconds after the application of the cathodic voltage. It corresponds to the generation of the plasma. It lasts between 20 and 50 µs and can be delayed between 0 to 30 µs after the voltage application [39] [40] [42] [51] [52]. This possible delay can appear as a consequence of the pressure and/or the composition of the atmosphere, but it can also be due to the applied voltage and the duty cycle [53]. The reasons are various. For example, the rarer the species are and the higher their ionization energies are, the more time the plasma takes to initiate. At low pressure, a longer time is needed to enable enough electrons to ionize the

gaseous species. In brief, this first period corresponds to the period when the first ions and electrons are accelerated by the electric field existing in the chamber [39] [40] [41] [54].

During the second period, there is many highly and very highly energetic electrons [55]; resulting a first warming of plasma. There is also a large number of working gas ions reaching the target, inducing a rise in the cathodic current intensity [42] [56] [57] [58]. Indeed, measurements made by optical emission spectroscopy (OES) had shown that the peak of working gas ions density (Ar^+ & Ar^{2+}) appears during this ignition stage. However, no metal species is yet detected [42]; or only a very few (cf Figure 16). It has also been pointed out that it is during this period that the electrons reach their highest density, along the magnetic field lines. Below, in Figure 16, are presented the 10 µs periods integrations of Ion Energy Distribution Function (IEDF) spectra acquired during a pulse, showing the time evolution of ions density near a Cr target. A lag of approximately 30µs between the *wave* of Ar^+ ions (incoming) and the Cr^+ ions (sputtered) can clearly be spotted.

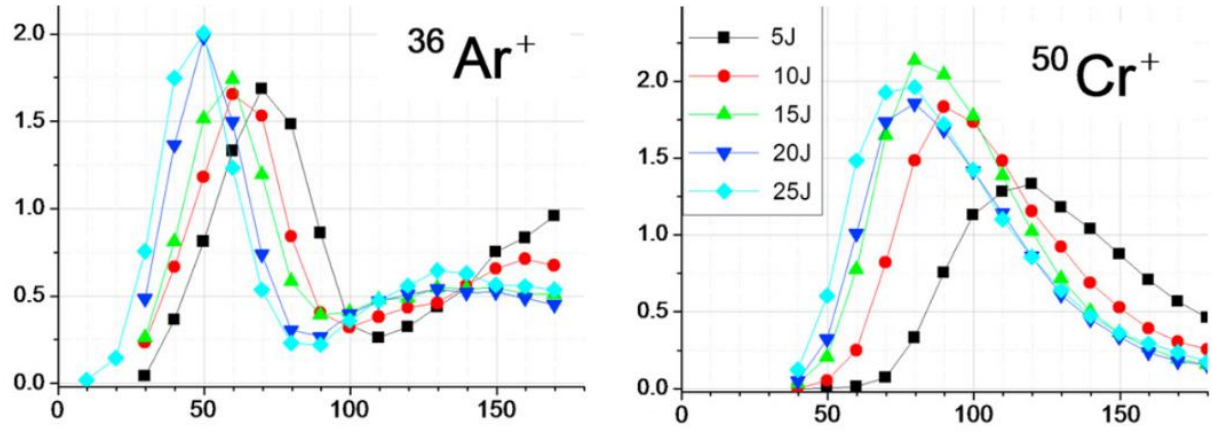

Figure 16. Time-resolved ionic presence distributions [42]

This is due to the fact that, once it has been ionized, the gas generates a strong ionic current towards the cathode (due to the cathodic sheath). Then, these energetic ions come and affect the surface of the target by extracting metallic atoms from it: the sputtering process begins (cf. I.1.2.3). These sputtered metallic atoms therefore acquire a lot of energy from the impact by momentum transfer and travel towards the bulk plasma. However, on their way, near the target, they are meeting the *barrier* of high electron density trapped in the magnetic field mentioned previously, the so-called ionization

region. From the induced collisions, the sputtered vapour is ionized by electronic impact. Moreover, because the metallic species have an ionization energy lower to that of the working gas [59], electrons are cooled down: it is the beginning of the electronic thermalization/rarefaction process explained in I.1.2.4 [60].

The third step is assimilated to the rarefaction of the working gas, a phenomenon exacerbated in a HiPIMS discharge [61] [62]. Close to the target, the multiple inelastic collisions occurring between metallic and gaseous particles (and even electrons) result in a homogenization of the species temperatures. The so-called *thermalization* of the plasma by the sputtered particles results in a plasma dilatation and thus a considerable reduction of the working gas density is observed [63]. It is the *rarefaction* effect during which the density of the sputtered metallic species is greater than the argon density in the vicinity of the target. Indeed, argon is *consumed* by the sputtering process in the same time that energetic metallic particles are ejected from the target. The latter are thus pushing away the gaseous species and, therefore, a plasma mainly composed of metal ions exists in the target vicinity. The so-called *self-sputtering* process takes place. The corresponding sputtering yield (Y_{ss}) is significantly lower than the sputtering yield of gaseous species (Y_s) as it has been seen previously. All the previous processes have already been described in sections I.1.2.3 and I.1.2.4.

At some point, a balance is established between the thermalization, the rarefaction and the self-sputtering processes, in terms of both plasma temperature and density (electronic, atomic, and ionic). It the 4^{th} step of the sputtering process. Both the self-sputtering and the argon sputtering processes are taking place in the same time and all the particles present the same energies –due to thermalization- so none of the species can supplant the other species. It is only possible because the self-sputtering rate (Π_{ss}) is lower than the argon-sputtering rate (Π_s). The Π_{ss} factor, the self-sputtering rate, is the product of the probability of ionization of the sputtered atoms (α), the probability that the thus created ions return to the target (β_t) and the self-sputtering yield of these ions (Y_{ss}) (see section I.1.4.1) [23]. Thus, even if the self-sputtering yield Y_{ss} exceeds the sputtering yield Y_s (cf. section I.1.2.3 and Equation 5), Π_{ss} is still generally inferior to Π_s, because $\alpha<1$ and $\beta_t<1$ (both are probability factors). Consequently, the metallic plasma near the target is not dense enough to prevent neutral gas to keep taking part in

sputtering of the target. There is thus an equilibrium level where $\Pi = \Pi_{ss} + \Pi_s \equiv constant$.

At this point, four different cases can be distinguished from one another. The first one, where Π<0.1, is close to the DCMS situation: the current presents a low intensity plateau shape and the vapour is not highly energetic. Then, there is an expected increase of this plateau intensity with the increase of the Π rate. An increase in the latter can be due to the nature of implied species, voltage applied, magnetic field, pressure, etc... These parameters can then be set to obtain the most stable and efficient sputtering process possible; corresponding to Π = 1. However, it should be done with care. Otherwise, an avalanche reaction could be initiated in the plasma, leading to its instability. In this case, the cathodic current shape does not show a flat profile, but a constant and continuous increase (Π is no longer a constant, the equilibrium is lost) until the extinction of the plasma. In this regime, the probability of arcing is much greater.

The voltage is finally switched off: the species lose their energy (step 5). They are not subject to the electric field anymore and stop sputtering the target. It is during this time that the entities within the plasma become less energetic but stay numerous. This has been confirmed by some mass spectroscopy studies [39] [40] [41] [42] [64]. The gas cools down and its ions return to their atomic state by recombination with the surrounding electrons. Note that some of the gas and the metal ions can persist for a few ms, even until the next pulse. In the meantime, the electrons are diffusing into the sputtering chamber even if the magnetic field is still present. This diffusion has been observed by Langmuir probe measurements and is both the product of an electronic acoustic wave [23] [58] and of the ambipolar diffusion [65] [66] (these two transportation regimes are described in section I.1.2.4). The results of Bohlmark et al. [63] are presented on Figure 17. Moreover, during this same period of diffusion, the vicinity of the target refills itself in argon: the continuous flow coming in the chamber replaces the gaseous atoms used and pushed away during the previous pulse. It is why it is important to properly manage the on/off ratio (i.e. duty cycle) of the pulse in the case of reactive gases.

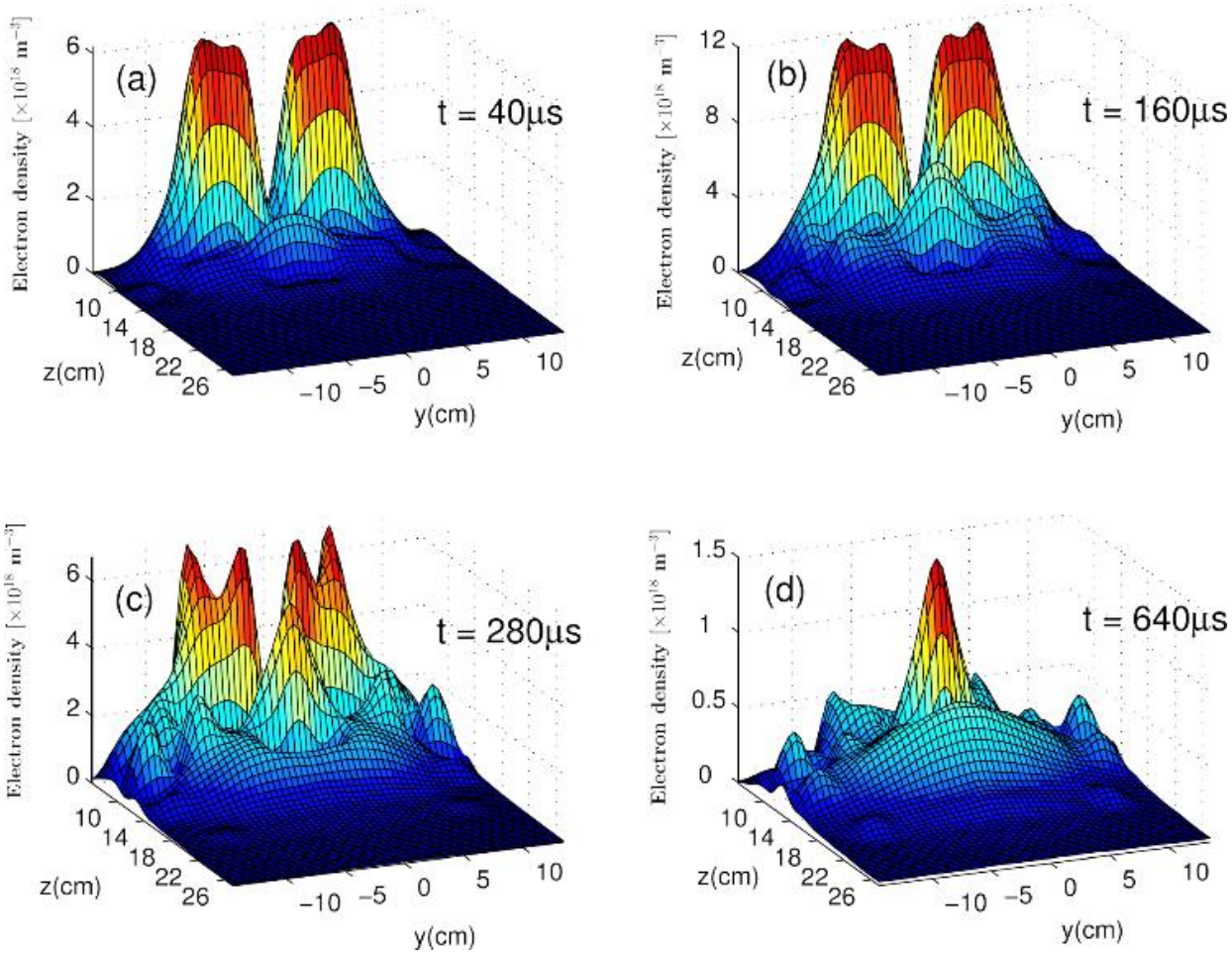

Figure 17. 3D representation of temporal and spatial electron density distributions during a HiPIMS discharge [23], from the work of Böhlmark et al. in [63] – with z the normal coordinates and y the lateral position and the origin of the graph being the middle of the target's surface.

I.1.4.3. Reactive plasma

It is possible to insert a second gas, a reactive gas (e.g. O_2 and/or N_2), within the chamber during the sputtering of the target. It is mainly used for the deposition of oxides or nitrides (e.g. TiO_2, NiO, AlN, etc…). The appearance of this new gas disturbs the plasma, or at least brings new kinetics and therefore changes its behaviour [23] [42] [52] [67] [68] [69]. This reactive process is already well known and understood for the DCMS process, but it slightly differs when it comes to consider a pulsed plasma.

The most important consequence of the insertion of a reactive gas in the deposition chamber is called the *poisoning* of the target surface. This so-called effect

corresponds to the fact that the reactive gas particles react with the target surface atoms. Therefore, the target is progressively coated by a thin film of the compound material [70] [71] [72] [73] [74]. The stoichiometry and covering proportion of this new layer is directly related to the amount of reactive gas present in the plasma. This latter amount is adjustable with several parameters: mainly the gas flow, the pumping speed and the duty-cycle of the pulse. Apart from the stoichiometric point of view, the reactive gas proportion can also modify other parameters, like the voltage for example, as presented in Figure 18.

On a practical point of view, the surface state is indeed reflected by the value of the average cathodic voltage needed to keep the current constant. In most cases, it is possible to observe a clear transition from the metallic to the poisoned mode when keeping track of the cathodic voltage while increasing the reactive gas content [23] [71] [70] [75]. This transition is due to the modification of the *secondary electron emission coefficient* (i.e. γ_{se}) with the modification of the target surface composition and most of the time, the oxidized layers on the target has a higher γ_{se} coefficient than the pure metallic specie. To illustrate the previous explanations, Figure 18 shows oxidation curves for two different materials.

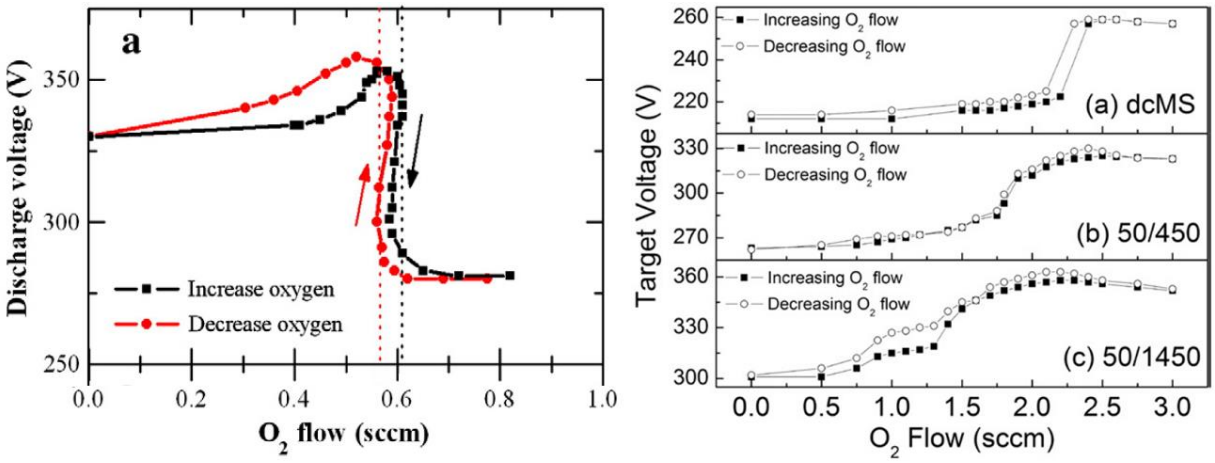

Figure 18. Oxidation curves for aluminium (left) [76] and zirconium (right) [77] targets

A *hysteresis* shape can also be spotted on each of the graphs of Figure 18, and has also been reported and studied in other papers [71] [72] [73] [75] [76] [77] [78] [79]. This hysteresis behaviour finds its explanation in the covering of the target by the reactive gas atoms and the fact that the sputtering rate is lower for compound materials. Indeed, initially, the target is not poisoned and therefore, a certain flow rate of oxygen is necessary

to cover it (i.e. *poison*). The full covering (i.e. saturation) of the target surface and the walls of the chamber by the compound material corresponds to the *fully poisoned mode* of the discharge. It is the first transition observed (from metallic to poisoned). However, if this reactive gas flow is then lowered, some poisoning atoms are already in the chamber -still bound to the walls- and they contribute to the poisoning of the atmosphere. Therefore, the injected gas flow does not correspond to the exact amount of reactive particles in the chamber. It results in a chamber more poisoned than it should be at a given gas flow, and thus a shift in the voltage needed to keep the cathodic current constant. The second transition observed (from poisoned to metallic) is therefore shifted, compared to the oxidation curve. It results in the hysteresis shape of the curve.

It should be specified that this hysteresis shape is much more pronounced in the DCMS case and can fully disappear for the HiPIMS discharge [76]. Indeed, since the HiPIMS process is more energetic, the reactiveness of the species is enhanced and thus, for a given reactive gas content, the state of the system is always the same. There is no need to send reactive gas in excess to proceed to the full oxidation of the chamber (increase of the reactive gas content), and these same entities tends to get off the walls more easily and therefore do not contribute to the sputtering at lower reactive gas content (i.e. hysteresis shift). Briefly, it means that the HiPIMS system uses and evacuates the pollutant (i.e. reactive gas atoms) off the chamber more efficiently.

Another factor of great importance must be pointed out: the geometry configuration and dimension of the deposition chamber. For a same scaled pumping system, a smaller deposition chamber is less likely to produce hysteresis shapes compared to a bigger chamber. In addition, it should also be added that the atoms of the common reactive gases present lower ionization energies than the argon's [59] and they are therefore more easily and quickly ionized: a few µs shift in the ignition delay has been reported in some papers [42] [52] [51]. They are also more easily doubly ionized; which means even more energy delivered during film growth (i.e. new growing conditions) [42].

I.1.5. Plasma diagnostic – Discharge modification through deposition parameters

The HiPIMS process is very complex, due to the long list of system parameters available and modifiable: pressure, current intensity, cathode voltage, content of reactive gas, frequency, pulse width, nature of the target and/or target-substrate distance. This complexity is hard to master but it offers a lot of control possibilities on the conditions of film deposition. It is necessary to understand every single one of the influences and how each parameter interact with one another. The existing literature on the subject is quite complete; reviews have even been written to summarize and organize these data for a global vision of the phenomena involved. For each parameter, its influence on the properties of the plasma (pulse shape, chemical composition, ionization rate, energies, etc…) is briefly presented. It should be kept in mind that these plasma modifications have an influence on the deposited thin film properties.

I.1.5.1. Cathodic voltage

The cathodic voltage is one of the main parameters. It corresponds to the negative potential applied to the target and it is responsible for the ionization of the species within the chamber (see section I.1.2). It has a direct influence on the sputtering yield and thus on the deposition rate [77] [80] [81] [82] [83] and in 1970, B. Chapman [84] was able to model the sputtering yield for ions presenting energies below 1 keV by the following equation:

$$Y_s(E_i) = \frac{4m_1m_2}{(m_1+m_2)}\frac{3\alpha}{4\pi^2}\frac{E_i}{U_0}$$

Equation 5. Empirical law for the sputtering yield [84]

Where α is a dimensionless quantity, depending on the mass ratio m_1/m_2 (with m_1 the incident ion mass and m_2 the mass of the ejected atom), U_0 is the sublimation/binding energy of the atoms at the target surface and E_i is the energy of the incident ions; which can be calculated from Equation 6.

$$E_i = E_o + q.V$$

Equation 6. Kinetic energy of a charged particle in an electrical field

Where E_o is the initial energy of the ion, q is the elementary charge, and V is the applied potential. This equation reflects the fact that the greater the electric field is, the more energetic (i.e. kinetic energy) the ions of the working gas are, and therefore the more able to extract particles off the target they are. However, it should be noticed that it is not fully under control: as mentioned earlier, the voltage is strongly correlated with the oxidation state of the target (cf. I.1.4.3); and the hysteresis behaviour presented earlier can be a factor of an uncontrollable variation for the voltage. Numerous studies have been made on the reduction of the hysteresis width [71] [75] [76]. A reduction of the hysteresis width corresponds to a better control on the plasma and thus on the deposition (e.g. plasma and film stoichiometries).

Although the voltage peak can exceed the kV during the pulse, the particles kinetic energies never exceed the kV when reaching the target's surface: they do not have enough space (time) to be fully accelerated. Therefore, the energies of the ejected ions do not exceed hundreds of eV – due to the inelasticity of the (multiple) collisions leading to the sputtering of the particle (cf. I.1.2.3). Values of sputtering rates obtained from mathematical models are presented in Figure 19 for the sputtering of Ni, by incident Ar (sputtering) or Ni (self-sputtering) ions of energy included between 100 and 1000 eV.

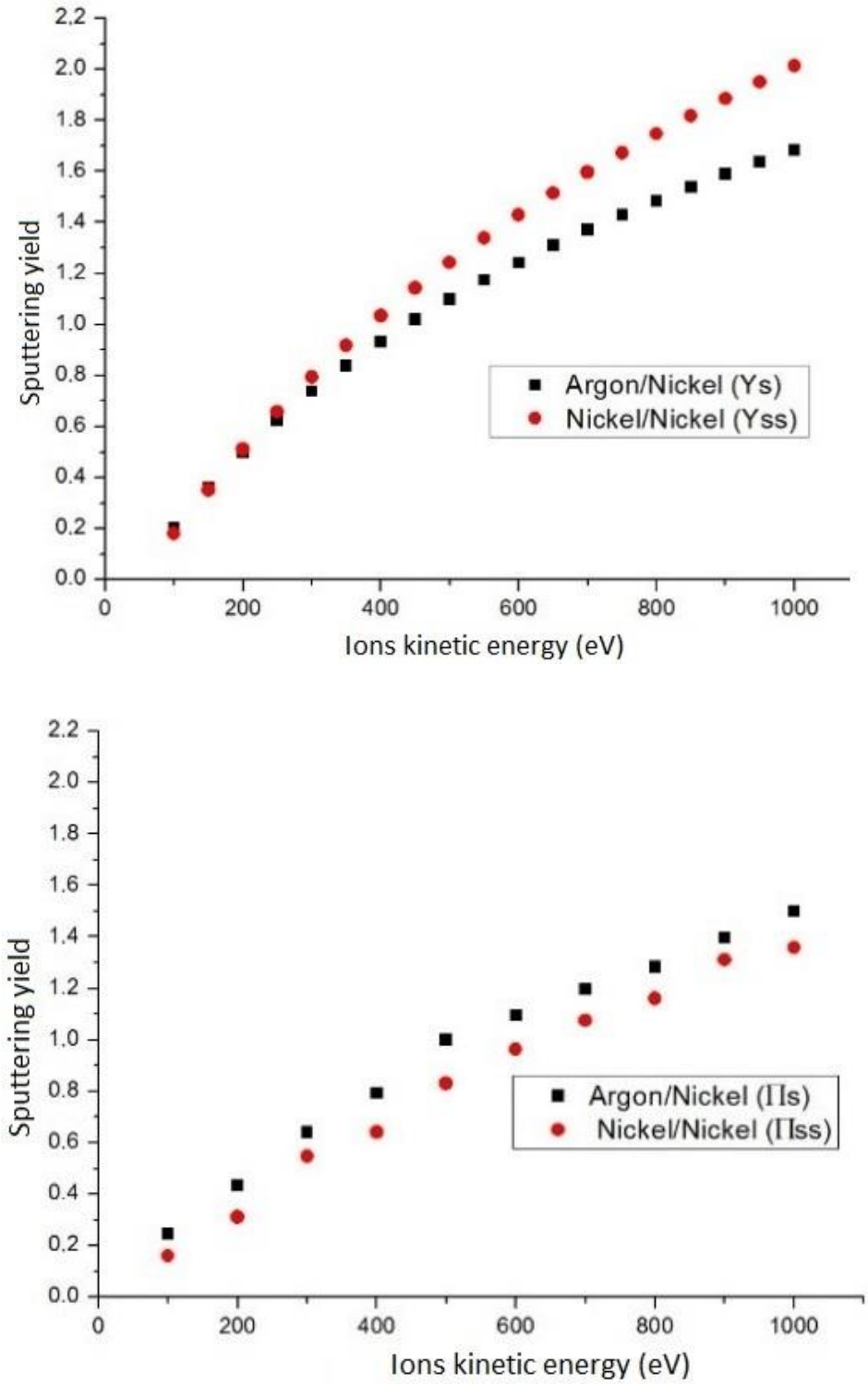

Figure 19. Sputtering yields for a nickel target under Ar or Ni atmospheres (calculated from empirical equations [85])

In comparison, a graph showing the calculated values for Π_s and Π_{ss} is added. This difference is explained as being due to various causes (e.g. insertion, ionization, back-

scattering) that can occur during sputtering. Π_s and Π_{ss} sputtering yields are therefore much more representative of the effectiveness of the sputtering process, compared to Y_s and Y_{ss} since they represent the total rate of particles being ejected from the target towards the bulk plasma.

The applied cathodic voltage is also one of the factors responsible for the proportion of ions present in the plasma and their degrees of ionisation. The HiPIMS technique has been developed in this particular objective [28]. By increasing the cathodic voltage, it has been shown that the ionic proportion is drastically changed. First, studies have shown that the metallic ions are more easily doubly ionised in HiPIMS discharges than in DCMS discharges [73]. Mass spectrometry studies also showed that the Ar/Ti proportion is modified within the plasma: the titanium population is much greater than the argon population in the case of a HiPIMS discharge but for the DCMS plasma, the ratio is inversed [73]. This can have different consequences on the deposition process, such as the enhancement of self-sputtering in HiPIMS discharges, the modification of the sputtering rate and even the modification of the plasma stoichiometry.

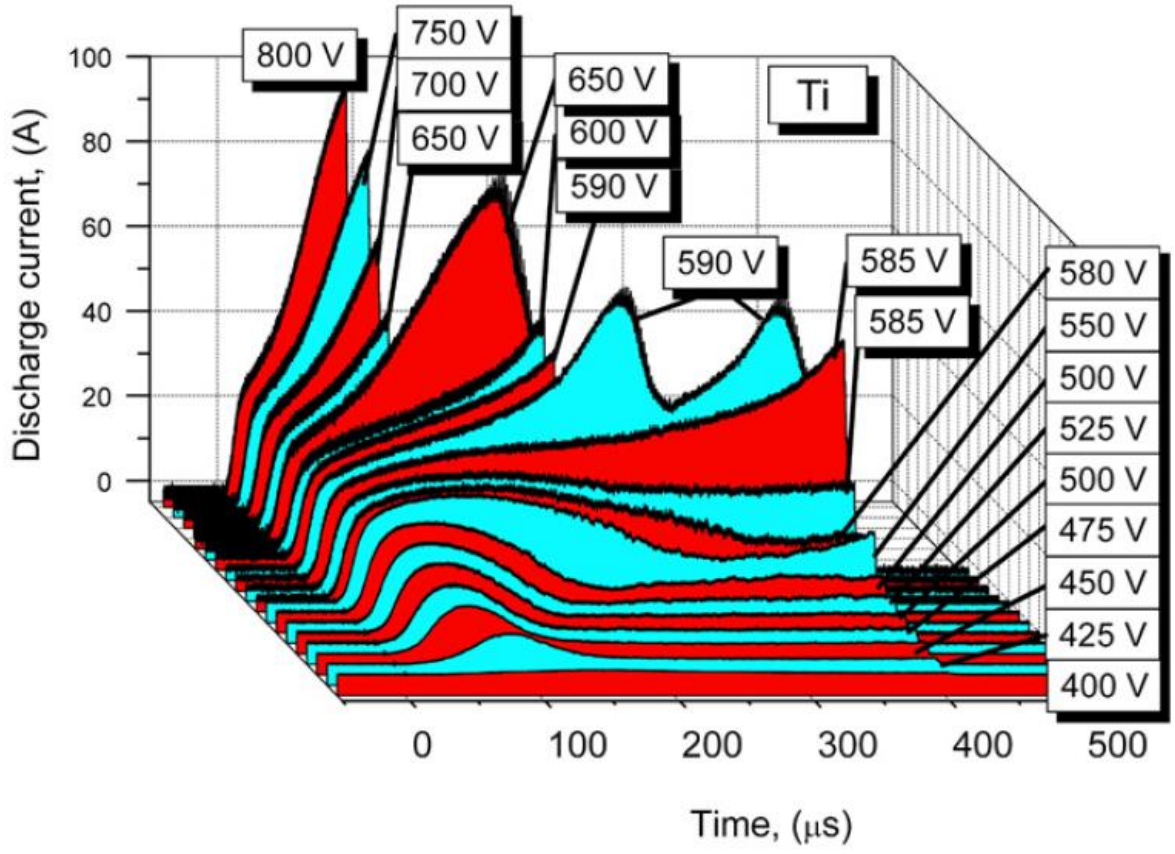

Figure 20. Current-voltage-time profiles for a Ti target from [6]

It should however be noted that this difference in the plasma's chemical composition can also be due to the specific processes occurring only in the HiPIMS discharge (e.g. rarefaction, self-sputtering, etc…) and these effects are enhanced by an increase of the applied voltage. Figure 20 illustrates this fact. With the amplification of the phenomena specific to the HiPIMS discharge, the ions energy is also diminished [47]: the ions participating to the self-sputtering process are less energetic than the initial argon ions (see sections I.1.2.3 and I.1.2.4).

In addition to the voltage applied to the cathode (i.e. target), in some apparatus, a weaker (i.e. a few tens of V) negative voltage is applied to the substrate holder. This so-called *bias* voltage can have several purposes. The first one is to give more energy to the adatoms coming onto the substrate by giving them more kinetic energy (heating). Indeed, applying a slight negative voltage (i.e. < 100V) on the substrate holder increases the anode sheath depth and thus the energy acquired by the positive ions before to reach the substrate. Moreover, since the relaxation process generates a lot of energy and is believed to be the bigger addition of energy on the substrate's surface, different growing phases can be reached/selected as seen earlier (see Figure 7). This supplementary bias can also be used to *select* parts of the substrate where the film can be thicker, for example - by being only applied on the targeted area(s) of the substrate. It is also possible to observe an enhancement of the deposition conditions for substrates with non-planar topography [28] [29]. It should not be forgotten that his substrate bias only concerns the ions, which makes even more effective for HiPIMS plasma (due to its high ionization rate).

Finally, the cathode voltage is mainly responsible for the ion energies and the plasma composition. The first consequence of its raise is the acceleration of the working gas atoms. The plasma is thus more energetic and can generate doubly ionised metallic species much more easily. The plasma composition can therefore be modified. However, an increase of the voltage can also mean (for long pulses) that rarefaction and self-sputtering effects are exacerbated and these processes are known to be responsible for a decrease in the plasma energy (i.e. thermal and kinetic). The energy of the depositing ions can finally be slightly raised thanks to the application of a bias to the substrate holder.

I.1.5.2. Current

The cathodic current is defined as being the sum of electronic and ionic currents (i.e. $I_c = I_e + I_i$). It therefore provides information on the ionic (and electronic) flow(s) arriving onto the target surface but it does not directly affect the sputtering yield. Indeed, it has been seen before that this yield is a direct function of cathodic voltage [84] [86] (cf. Equation 5). However, the sputtering and deposition rates can be functions of the number of ions in the chamber, which is proportional to the number of ions reaching the target. Indeed, the cathodic current reflects the amount of ions (and/or electrons) reaching the cathode but it should be kept in mind that the cathode current intensity depends on a lot of other parameters such as pressure, voltage, duty-cycle, etc. For this reason, it should not be considered as a *1st order* parameter (see section II.3.4).

However, a few studies have been made where both influences of the peak current intensity and the average intensity are considered as being initial parameters. Using the cathodic current intensity as a parameter is a good way to get rid of some other parameters influences but can be a good and a bad thing to do. For example, some studies vary the peak current value by modifying either the pulse width or the frequency [78] but both of these parameters have distinct consequences on the plasma behaviour and characteristics, independently to the cathodic current (cf. I.1.5.3). The discussion on the results can then get complicated because the origin of the plasma modification. For example, for some power supplies, the voltage is automatically modified to keep the current equal to a certain constant value, chosen by the user. In this case, the discharge is different than a discharge where the pulse width is changed to keep the cathodic intensity constant to the same value. Indeed, it has been seen previously that the modification of the pulse width does not have the same consequences on the plasma compared to the voltage (see section I.1.2). Voltage and pulse width are not the only parameters presenting different plasma modifications; each parameter has its own way to influence the discharge properties.

An increase in the amount of metal ions - and a change in their natures - in the plasma has been reported in several papers when the set point for the current intensity (peak or average) is modified [41] [42] [67] [87]. Indeed, the main effect observed is the improved ionization of the plasma when I_{peak} (i.e. the intensity of the current peak) is required to be higher [87] [78]. It has been explained by the authors by the enhancement

of the ionization and dissociation rates when I_{peak} is increased. Ehiasarian and his team [87] also showed an improvement of the Ti^+/Ar^+ ratio and the plasma density in the same time. It means that when I_{peak} is increased, the sputtering is more effective and generate a greater proportion of metallic ions. This modification of the ratio is mainly due to an observed increase of the energy of the ions. Indeed, Hecimovic and his team showed that the maximal energy reached by the ions is higher when I_{peak} is increased; such as their average energy when reaching the substrate [41]. As a confirmation, the same observations have been made by Greczynski and his team [42]. Moreover, Ehiasarian et al. revealed an increase of T_{eff} -the *electronic temperature*- during the pulse under the same conditions [87].

To explain the improvement of the Ti^+/Ar^+ ratio, it can also be suggested that an increase in the I_{peak} value lets the self-sputtering occur more easily. Indeed, phenomena such as rarefaction, back-scattering and self-sputtering are enhanced with the ionization rate of the plasma [72] [88] (cf I.1.2). It has been confirmed by other studies that had the same explanation and also revealed a diminution of the deposition rate with the increase of I_{peak} [78] [89] [90]. This diminution of the deposition rate has another cause: the plasma impedance and the presence of an ionic barrier within the chamber; slowing down the ion transport [78] [88]. So, contradictorily, in some cases, when the cathodic current I_{peak} is increased, fewer ions are reaching the substrate and the deposition conditions can therefore be modified [91].

Another value that has been studied is the average cathodic current, corresponding to the average value of the current along time. For example, it has been shown that when the latter is increased, the ignition delay τ of the plasma is reduced and the ion flux reaching a biased substrate is also improved [92]. Both are obviously consequences of the plasma density raise, enhancing the amount of ions within the plasma and thus helping for the ignition of the pulse and reaching the biased substrate.

Several very complete studies also allow characterization of the plasma and the phenomena occurring in it by relying on the current-voltage-time profiles. Indeed, thanks to these, the influences of several main parameters such as the pressure, the frequency or the average voltage applied [6] [93] [94] can be revealed; and the voltage required for these phenomena to appear can then be identified and quantified for some metals [6]. One can thus notice that during a transition phase, the voltage being modified, these

profiles are also modified. The study of these curves permits identification of the phenomena described in I.1.4.2.

I.1.5.3. Frequency and pulse width

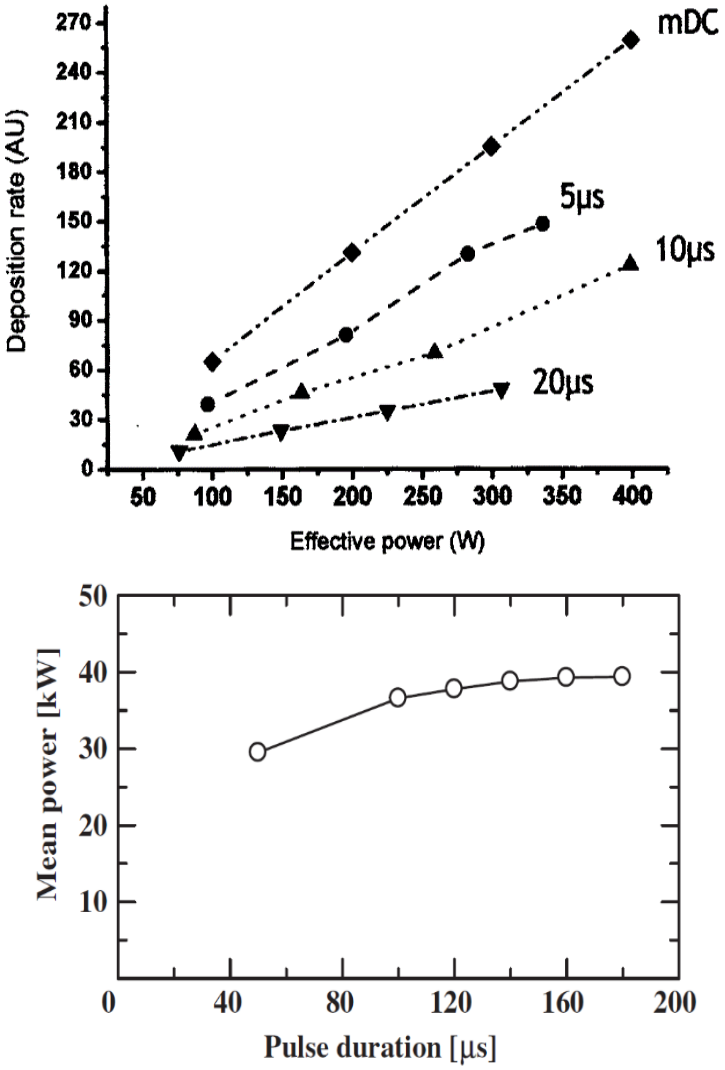

Figure 21. (a) Effective power and deposition rate as functions of the pulse duration for a constant duty cycle from [95] and (b) mean power values for different pulse lengths and constant frequency from [82]

These two parameters principally affect the deposition rate, via the ionization rate of the sputtered vapour and the modification of the duty cycle. Indeed, for the same average power, it has been shown that deposition rates could go up from 20% to 70% of the

normalized value by changing the pulse width from 20µs to 5µs [95].It is believed to be due to the necessary increase of I_{peak} to keep the power constant; which means a higher ionization rate (see section I.1.5.2). On another hand, for longer pulses, depletion takes place after a complete use of the working gas (i.e. rarefaction) and it can be prevented from occurring by not allowing enough time to the sputtering process to consume all the working gas atoms: i.e. by reducing the pulse duration. This same effect is also found with the frequency regulation [93] [94] since the common entity remains to be the *duty cycle*. However, each influence should be discussed independently at first to better identify which consequences correspond to which parameter.

The pulse width has been studied in different papers and showed fundamental changes in the plasma properties and especially concerning the occurrence of certain phenomena. The section I.1.4.3 describes the whole chronology of a pulse and it will therefore not be discussed any further in this section. However, there is a need to better understand what the consequences of the pulse duration modification are.

Mainly, a pulse duration reduction allows to avoid the presence and/or predominance of the self-sputtering and back-scattering processes [96] [47] [97] [95] [6] and thus modifies the plasma ionization rate [95]. It has previously been specified that the self-sputtering rate Π_{ss} is lower than the sputtering rate Π_s. This is why when the duty-cycle is kept constant but the pulse width is decreased, it is normal to see an improvement of the deposition rate [95] [98] (see Figure 21). However, if the frequency is not modified to keep the duty cycle constant, the effective duration of sputtering is lowered and the deposition rate follows [82] [73]. This time, it is due to the clear diminution of the average power (i.e. integrated over the whole time), even if the mean power (i.e. integrated over the pulse) modification is not as important, as shown in Figure 21(b) [82] [88]. Moreover, the ionic current reaching the substrate has been measured as being enhanced with longer pulse durations [82] [78]. It is believed to be true only for pulses where the rarefaction effect is not occurring yet. It should also be noted that the pulse duration modification also has a consequence on the Electron Energy Distribution Function (EEDF) profiles of the plasma. Indeed, the highly energetic ions are created during the pulse but they cool down –mostly by recombination with electrons- as soon as the pulse is switched off [40] [99], no matter the pulse duration. It means that by having a wider pulse, more energetic ions are created and thus, the thermal load is more

important. An illustration of the EEDF that can be measured is presented in Figure 22. Highly energetic electrons are created during the pulse but they return to lower energies once the cathodic voltage is switched off.

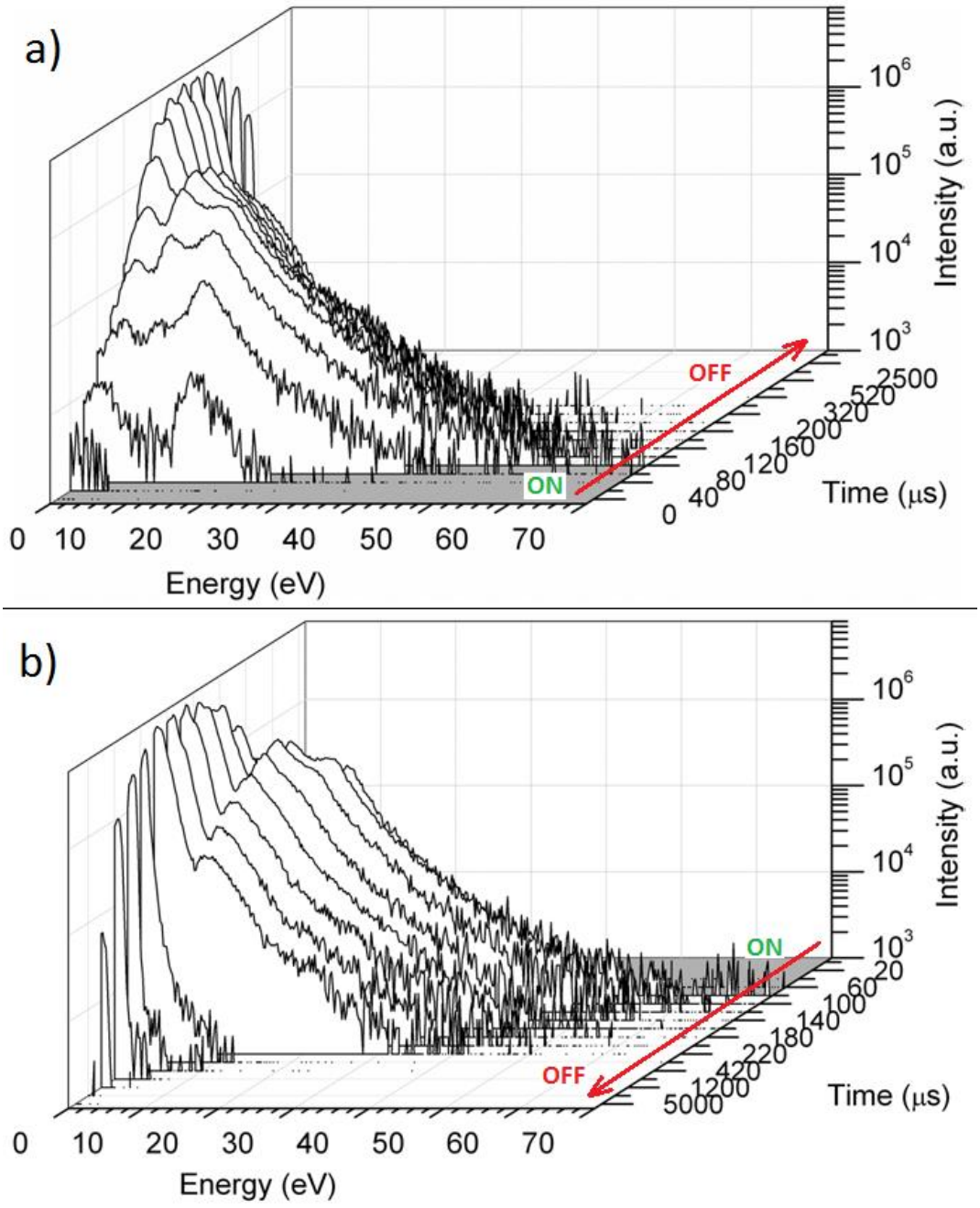

Figure 22. Time-resolved measurement of Cr^+ ions from the start of the pulse until 2.4ms from the start of the pulse. (a) shows the start of the pulse and (b) shows the post-discharge conditions and decay in the IEDF intensity [40]

Nevertheless, these low energy ions have a crucial role in the deposition process. Indeed, if enough ions remain in the chamber until the start of the next pulse, the ignition delay observed in some circumstances can be reduced or even disappear. Yushkov and Anders showed a diminution of the delay until a certain saturation value when the frequency and the pulse width are increased independently (i.e. decrease of the off-time) [53]. It is the proof that the remaining ions help the plasma to initiate when the voltage is switched on again. This off-time is also the moment when the target vicinity is refilled with working and/or reactive gases. In some cases, as a direct consequence, a diminution of the cathodic current has been observed when the frequency is further increased. This is due to the fact that the off-time is shorter than the complete refill time and thus, less entities are available to produce ions [72] [75] [93].

The frequency modification, itself, has another consequence, and it concerns the hysteresis behaviour of the oxidation (or nitridation) curve. Indeed, several studies showed that an optimal frequency can be found, where the hysteresis width can be considered as negligeable [71] [72] [78] [73]. Aiempanakit et al. also demonstrated that the oxidation curve is smoother for higher frequencies [88]. Indeed, the modification of the frequency is crucial in the reactive mode. As said above, a higher frequency corresponds to a diminished time to refill the chamber in gases, and it can explain the augmentation of the oxygen flow needed to reach the poisoning state of the target. It has been specifically observed and reported by a couple of research teams [72] [78]. However, the size of the chamber must be considered as well: a bigger chamber needs more time to refill with the same gas influx. A third fact to keep in mind is also the position of the gas inlet. In fact, if the time is reduced, the insertion flow must be increased to have enough reactant to obtain the same stoichiometry during the pulse within the chamber. Thus, Surpi and his team showed that the frequency modulation can be responsible of a modification of the plasma composition [73]. One can notice that, in the same way that frequency does, the pulse width can also influence this ratio. Indeed, with longer pulses, the target cleaning process is more efficient [75]. Finally, for the work presented in this thesis, the thermal load received at the substrate position is very important so it should be kept in mind that this latter has been reported to be increased when the frequency is raised [100].

I.1.5.4. The reactive gas content

As it has been mentioned previously, the oxygen content has a great influence on the generated plasma and therefore on the deposited material. Indeed, it mainly adjusts the stoichiometry of the deposited thin film and thus its intrinsic characteristics (e.g. optical, electrical and mechanical properties). To do so, the gas first reacts with the surface of the target and creates a compound layer, more or less stoichiometric, on its surface. The secondary electron emission coefficient of the new surface is different (lower in most cases) than that of the metallic surface. To keep a constant intensity, the voltage is generally the first parameter to be modified, and this is how an oxidation –or nitridation- curve can be obtained [101] [102]. Two separate modes generally appear: a metallic and a *poisoned* (e.g. nitrided or oxidized) mode; as seen earlier (see section I.1.4.3). However, it should be highlighted that A. Karpinski et al. [70] showed that for a constant intensity, the cathodic voltage -proportional to the oxidation rate- varies according to the percentage of oxygen in an *unnatural/abnormal* way for nickel oxide, as shown in the Figure 23.

The literature divides the *normal* curves –represented in Figure 23 (left)- in three distinct regions. The first corresponds to a sub-stoichiometric state of the target: the amount of oxygen reaching the target is immediately re-sputtered by the incident ions so the target remains in a more metallic state and the discharge voltage does not significantly change. It slightly diminishes in most cases, showing a situation closer to a difficult oxidation of the target than a steady metallic state.

After that, a transition mode appears where the oxygen reaching the target becomes sufficient to react with its surface, and create a thin layer of compound (~ 2 to 5 nm). Some authors [70] claim that this evolution of the voltage is also due to a decrease in the electron density near the target while injecting more oxygen. The voltage should then increase to offset this effect if the cathodic current is supposed to be kept constant. The third phase, corresponds to the maximum of this electronic consumption. The author, by relying on literature, attributes this stabilisation to the creation of negative ions of oxygen by electronic impacts ($1e^- + O_2 \rightarrow O + O^-$).

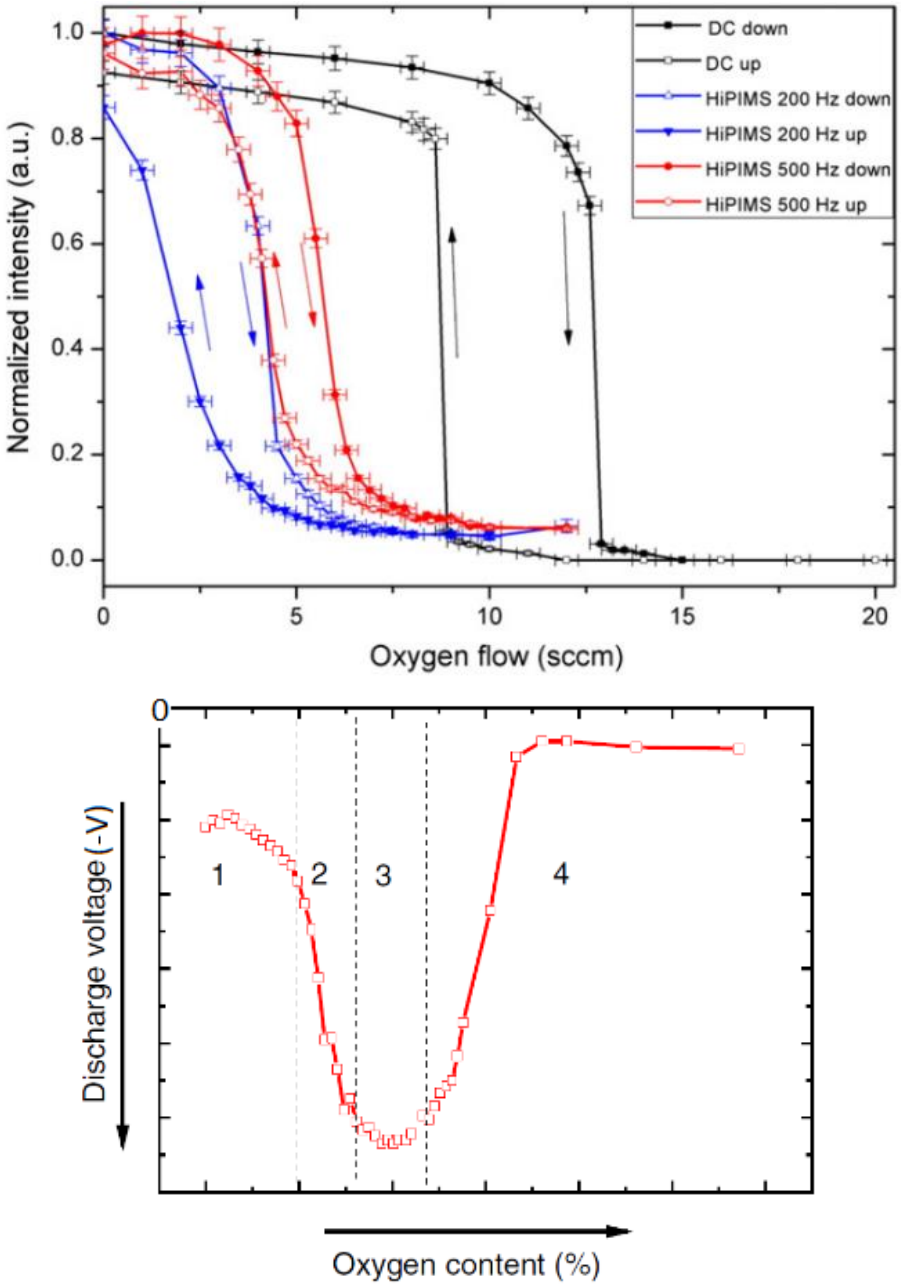

Figure 23.Oxidation curves for a titanium discharge (top) [39] with normalized intensities and for a nickel discharge (bottom) [36]

The fourth area showed on Figure 23 (bottom) has only been reported for NiO discharges and is characterized by a stabilization of the voltage to a lower (absolute) value. It is assimilated to an oxygen super-saturation on the target surface. The transition to this new voltage value would be due to an increase of the secondary electron emission coefficient. The origins of this increase of γ_{se} are not fully understood. And since I_c increases with γ_{se}, the voltage should decrease to keep the cathodic current constant –

which corresponds to a decrease in the sputtering yield. However, this fourth state is very specific to the NiO case and has been reported by no other research team. The maximum (in absolute value) that can be observed corresponds to the optimum oxidation state of the target surface in the stoichiometric sense and permits to deposit stoichiometric films. It also corresponds to the higher deposition rate, because it is characterized by a maximum value of the voltage.

I.1.5.5. The pressure

Studies have shown the influence of pressure during deposition of thin films [58] [6]. The work carried out by A. Hecimovic et al. [41] is a good example, where measurements by mass spectrometry have been carried out on HiPIMS discharges with Cr and Ti targets under Ar atmosphere for two pressures: low (3mTorr) and a high (20 mTorr). They were able to see that pressure could change the energy profiles of the plasma and reduce the current effects on the latter. Indeed, even if the electron density has been shown to be independent of the pressure in [92], the same study showed that for high pressure, the rarefaction process is more likely to occur and thus lower the plasma density in the target vicinity. This kind of consequence can change the pulse shape. The decrease of the mean free path when pressure is increased has also been reported to be responsible of the generation of more ions within the plasma by increasing the number of (inelastic) collisions [91]. This has been shown to be true only until a certain limit. Indeed, after a certain point, it lowers the electron temperature and thus reduces the ionization rate of the plasma: i.e. not enough time for particles to be fully accelerated between two collisions.

Pressure also changes the deposition rate, due to a multiplication of the collisions between the entities constituting the plasma: the more collisions there are, the less species reach the substrate [38]; especially for ions [92]. The energy of the arriving ions at the substrate surface is also decreased when pressure is raised - due to the inelastic collisions evocated before [78] [103]. A diminution of pressure is also responsible for a delayed ignition of the plasma after a certain limit [38] [92], which can also have a negative influence on the deposition rate. However, a solution to increase the deposition rate could be to modify the nature of the working gas (see section I.1.2.3). Indeed, Bowes and his team showed in their work that the deposition can be enhanced by inserting a

heavier working gas. The authors explain it by a diminution of the return effect occurrence [12]. The return effect describes the phenomenon where a fraction of the ionized sputtered material is back-attracted to the target surface [86]. In addition to change the deposition rate, pressure also has a strong influence on the film structure like it has been seen previously on this report (cf Figure 7).

I.1.5.6. Temperature

The temperature effects on deposition (and especially for metal oxide) seen for several sputtering systems shows that it helps to rearrange the crystallographic structure of the thin film during its growth and clean its impurities at the same time (cf I.1.2.5). Thus, a stoichiometric and preferentially oriented compound can be obtained from a slightly over-stoichiometric material presenting multiple crystallographic orientations [104] [105]; either by a post-deposition annealing [106] or by increasing the temperature of the substrate during the deposition time [105] [107] [108]. The properties of the metal oxide can thus be modified [109] [110] [111]; through its Anatase/Rutile ratio for example in the case of Titania. In the work presented in this thesis, it is of a huge importance to find the good equilibrium between a plasma of high enough energy so it can be easily controllable and grow the expected phase, and a temperature low enough to prevent melting of polymeric substrates. The Anders diagram shown in Figure 7 also present the evolution of the film growing phase and surface morphology when the temperature (energy) is modified.

Surprisingly, Cormier and his team have seen that for a same average power, the total energetic flux reaching the substrate for a DCMS discharge is higher in a balanced configuration compared to the unbalanced case [112]. It is due to the fact that the substrate heating has two major origins: the *recombination/relaxation* of the ionic flux reaching the substrate and the infrared contribution emitting from the hot target. The ratio between this two heat supplies may vary widely between different magnetron configurations. In the case of a DCMS discharges the IR heating coming from the target overcomes the ionic flux reaching the substrate. Then, since the balanced configuration enhances the heating of the target, it is normal to see an increase of the temperature for balanced-DCMS compared to unbalanced-DCMS. However, since the much more ions are reaching the

substrate in a HiPIMS discharge, the ratio of the influences can be inverted in the latter case.

In the project presented in this thesis, the temperature has a great importance since the final aim is to deposit a suitable film on polymeric substrates. The substrate composition thus imposes a temperature limit to the process. However, it should still be possible to deposit effective layers thanks to the ionization rates reachable in HiPIMS discharges (which eases the growth of crystals). So far, a very few studies have been conducted on the deposition of TiO_2 at low temperature with the growth of a fully multi-functional film [91] [100] [113] [114]. Also, note that the unbalanced configuration of the chamber used in this work should help to reduce the IR heating process but might increase the ionic heating process.

I.1.5.7. Target composition and substrate position

In the first part of the project, a pure titanium target is used to deposit TiO_2 but it is known from previous studies that to improve Titania properties -particularly to reach visible light applications- a dopant (metallic some of the time) must be added to the film [115] [116] [117]. There are three ways to do it: the insertion of a reactive gas (e.g. N_2 or CO_2), the utilisation of a second target made of the doping metal or the integration of a certain amount of the doping material in the original target. In this project, the second solution cannot be used because of the impossibility of using another target with the same power supply. However, M. Ratova et al. obtained good results with a compound target, doped at a specific percentage of dopant (5% of tungsten) [118] and have even improved the film properties for a HiPIMS process [100]. Moreover, experiments are carried out to study the feasibility of co-doping. For example, an already doped target could be used while still inserting a reactive gas to add C or N to the deposited film.

In addition to its composition, the distance separating the target and the substrate also has an influence on the deposited film. This influence is comparable to the pressure influence: a longer distance increases the collisions (and energy losses) that the plasma species undertake before reaching the substrate [54] [103]. Since the intrinsic properties of the plasma are not modified by the increase of the distance, the ionization rate is unmodified –or not noticeably- when the substrate is placed further from the target. The augmentation of the number of collisions thus means that the particles lose more energy

when they travel on a greater distance but do not mean that more ions are generated. The adatoms are thus less energetic when reaching the surface of a distant substrate [54] [119]. Ehiasarian and his team –as well as Vasina et al- also showed that there are less ions reaching the substrate when the distance is increased, besides the fact that they are less energetic [119] [97]. They also pointed out the fact that it mostly concerns the metallic ions (e.g. Cr and Ti) and therefore, the plasma composition changes along the distance from the target. All these facts (i.e. less ions, less energy and stoichiometric modification) mean that the growing conditions are modified and therefore the deposited film characteristics are likely to be modified by the distance from the target. On another hand, it should still be pointed out that in the case of an unbalanced magnetron configuration, the distance is less likely to be responsible for a decrease of the particles flux reaching the substrate since the plasma density is more equally spread along the chamber, because of the magnetic connecting field lines between the cathode and the anode. However, a decrease in the deposition rate with greater distances [81] [12] [80] is a phenomenon considered as being always verified in the literature.

In addition to the distance from the target, the angle is also an important parameter for the plasma properties. Indeed, several teams have realised spatial-resolved acquisitions of the plasma characteristics to highlight the fact that the magnetron and the chamber configurations have an influence on the electronic and ionic transport within the chamber. The first study ever made concerned the spatial electron density distribution and revealed a two orders of magnitude difference in the plasma density along the radial axis as shown in Figure 17 (~10^{17} to ~10^{19} m^{-3}, 160µs after pulse ignition) [63]. It means that at a given instant, there can be a two orders of magnitude difference in the plasma density, depending on location. Other papers present several angular-resolved distributions for deposition rates [80] [120], energy flux [120] [121], velocity distributions [122] and electronic densities [123]. There also are simulation models that have been developed to better understand the plasma kinetics [124]. In every case, a magnetron-like symmetry can be spotted, where the fluxes are more important above the racetrack (cf. Figure 24). The measurements presented in Figure 24 have all been conducted with circular planar magnetron targets but although the work presented in this paper uses a rectangular target, the general observations made in the literature can be assimilated to the rectangular configuration.

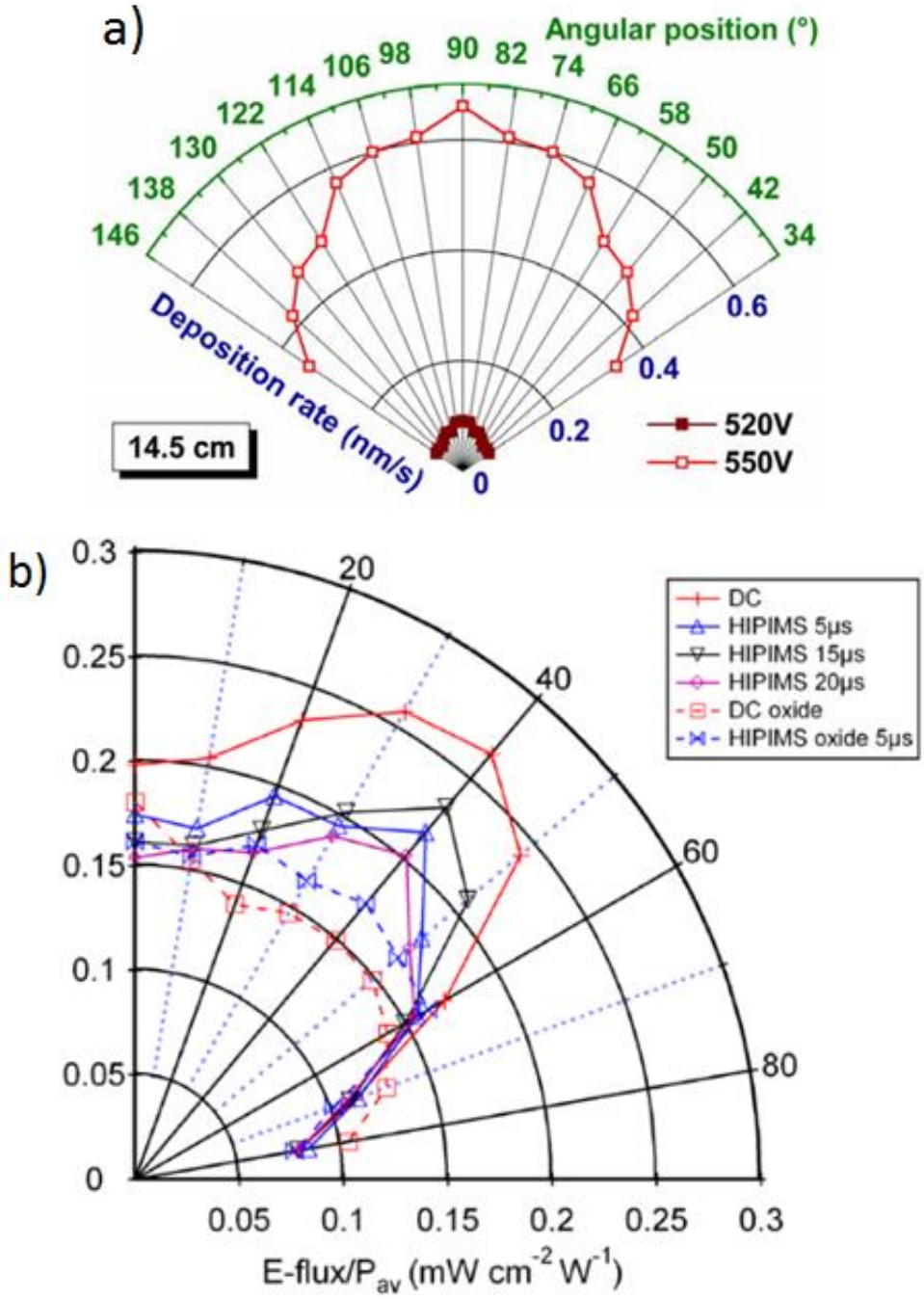

Figure 24. Different energy flux distributions from Horwart et al. (a) [80] and Leroy et al (b) [120]

As it can be seen on Figure 24(a), the first observation that can be made is that the deposition rate is always maximum when the substrate is facing the target and is placed alongside the normal axis. Even if different angles corresponding to the maximal energy flux have been reported in the literature (cf. Figure 24(b)), the differences can most likely be explained by different positioning of the probe and different chamber configurations.

For example, Leroy et al. referenced to a higher energy flux around 40° (to 60°) from the normal axis with a cylindrical magnetron and a probe always facing the centre or the racetrack [120]. It is confirmed by the velocity measurements made by Cada et al. where they find maximum energies for angles between 45° (reactive mode) and 75° (metallic mode) but this time even if the probe was also facing the racetrack centre, the target was planar (and not cylindrical) [122]. Finally, with a probe surface always parallel to the target surface, Lundin et al. found a maximum energy flux at the normal position but they revealed a maximum perpendicular flux around a 35° angle [121]. These different results are good evidences that the electrons and ions of the plasma have non-linear behaviours and are strongly dependent on the rig configuration. In conclusion, even if angle-resolved measurements are a good tool to prove expected plasma behaviours like compression and rarefaction [62], for the work presented here, the substrate holder is not always facing the centre of the racetrack and positioned along the normal axis. The substrate holder can be rotating during some depositions, if needed but since the entire range of angles are going to be covered, no preferential behaviour should be identified. Moreover, it can be added the fact that even if the values are different, the spatial repartition and proportions have been shown to be similar when HiPIMS is compared to DCMS [80] [121].

I.2. Titanium dioxide

This section reviews a great part of the present literature on titanium dioxide. A brief historical review is given on the advances made on the way to generate titanium dioxide and its applications in real life cases. A further investigation of the material itself is done after this. The objective is to better know the possibilities offered by this material. First, its known properties are presented, and for each of them an explanation is given about their functioning.

I.2.1.A brief historical review

Determining the origins of the photocatalytic process as we know it now is a difficult task. Most people report series of works and articles published in Japan around the 1960's [125] [126] [127]. However, in their 2008 review [128], Fujishima and his team determine the first observations of such processes in the 1920's/1930's, where oxidation and reduction processes were observed on illuminated oxides (e.g. TiO_2 and ZnO). In the early 1970's, an article was published in Nature, showing a water photolysis with a TiO_2 electrode [129] under near-UV light illumination (see Figure X). This article showed that water could be decomposed into oxygen and hydrogen under UV light and was published during the oil crisis of the 1970's, generating a great interest from the scientific community. In the 1980's, the TiO_2 has been widely used as powder to produce hydrogen from water but the results were not good enough so the focus shifted to the destruction of pollutants in air and water with TiO_2 suspensions.

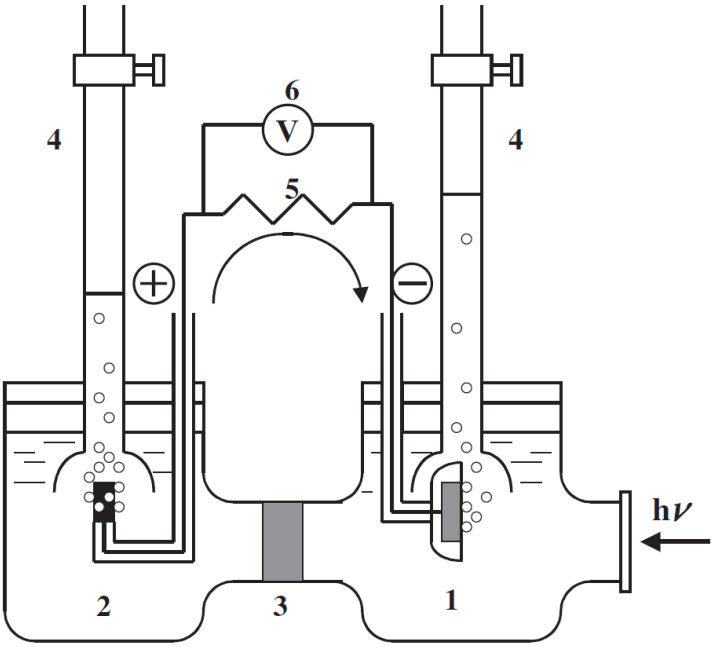

Figure 25. Schematic diagram of electrochemical photocell. (1) n-type TiO2 electrode; (2) platinum black counter electrode; (3) ionically conducting separator; (4) gas buret; (5) load resistance; and (6) voltmeter. From [130]

It is in the early 1990's that the idea appeared of using Titania as a two-dimensional system to reduce the amount of UV light needed to treat effectively the pollutants [131] [132]. The works reported a self-cleaning behaviour of coated titania films and an antibacterial behaviour of the latter (against *E. coli*, for example). Materials coated with TiO_2 would destroy the pollutants at their surfaces with only a *weak* UV illumination of around 1 mW/cm^2 [133]. This value corresponds to an approximation of the available UV light even in outdoor shade during daytime. The works conducted on titania films during this period also showed an important photo-induced super hydrophilicity, where, typically, a drop at the surface of the film would *flatter* itself under illumination. More details on the process are given in I.2.2.2.

In the 21st century, the photocatalytic process keeps attracted a lot of interest from the scientific community as the range of applications is very wide. The research focuses on the improvement of the films effectiveness. For example, for the improvement of its hydrophilicity, nano-scaled design of the film, where the crystal structure and orientation can be chosen and improved are shown to be very important [134]. Photoetching of the films to add porosity is another example [130]. In addition to the improvements of the film photocatalytic activity, researchers also reported a very high hydrophobicity of films

in darkness, with the possibility to transit to super-hydrophilicity under illumination (see Figure 30); opening a new range of possible applications, but also helping with the anti-fogging, self-cleaning and antimicrobial properties of the film.

With time, water (and air) treatment applications and systems also become more and more numerous, large and effective and as Hashimoto and his team said in their paper [130]: "*We believe that TiO2 photocatalysis is one of the best examples how, on the time scale of tens of years, basic scientific knowledge can be developed into a technological field and can produce a new industry*".

I.2.2. Titanium dioxide as a photocatalyst and more

I.2.2.1. Titanium dioxide, the material

Titanium dioxide can be present in three different phases: anatase, rutile, and brookite. The brookite phase is the orthorhombic phase of TiO_2 when both anatase and rutile are tetragonal phases. In all three cases, TiO_2[6] octahedrons are present but in a different pattern, resulting in different distortions of the octahedrons. The structures are presented in Figure 26. Rutile is the most stable at any temperature and pressure (below 60 kbar). However, the Gibbs free energy do not vary widely in between phases, meaning that the other metastable phases are close to be as stable as rutile. Brookite is a very difficult phase to produce artificially. Anatase and Rutile are the two most commonly studied phases. Especially in photocatalytic activity, since rutile is the most stable phase, as explained above and anatase appears to be the most effective photocatalytic material. As an indication, Table 2 is given below to provide essential crystallographic characteristics of the three phases.

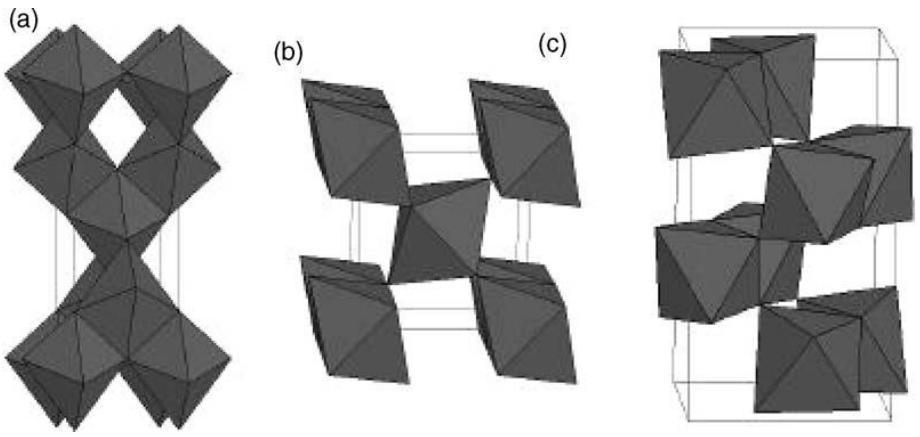

Figure 26. Crystal structures of anatase (a), rutile (b), and brookite (c). From [135]

Crystal structure	System	Space group	Lattice constants (nm)			
			a	*b*	*c*	*c*/*a*
Rutile	Tetragonal	D_{4h}^{14}-$P4_2/mmm$	0.4584	–	0.2953	0.644
Anatase	Tetragonal	D_{4h}^{19}-$I4_1/amd$	0.3733	–	0.937	2.51
Brookite	Rhombohedral	D_{2h}^{15}-Pbca	0.5436	0.9166	–	0.944
Density (kg/m^3)						
Rutile	4240					
Anatase	3830					
Brookite	4170					
Dielectric properties	Frequency (Hz)	Temperature (K)	Dielectric constant			
Rutile, perpendicular to optical *c*-axis	10^8	290–295	86			
Rutile, parallel to optical *c*-axis	–	290–295	170			
Rutile, perpendicular to optical *c*-axis	10^4	298	160			
Rutile, along *c*-axis	10^7	303	100			
Anatase, average	10^4	298	55			
Band gap (eV)						
Rutile	3.05					
Anatase	3.26					
Refractive index	n_g	n_p				
Rutile	2.9467	2.6506				
Anatase	2.5688	2.6584				
Brookite	2.809	2.677				

Table 2. Some bulk properties of the three main polymorphs of TiO2 (anatase, rutile, and brookite). From [135]

As one can spot in Table 2, the anatase shows a higher band gap value than rutile, even though it is reported to be the most efficient photocatalyst. The reasons behind this

behaviour are still subject to controversy but it seems to be mainly due to a higher Fermi level for anatase than rutile and an indirect bandgap for anatase. Both resulting in a most efficient use of the charge carriers in the lattice thanks to a longer lifetime and a better mobility of these charges.

I.2.2.2.The photo-induced properties of titanium dioxide

The photocatalytic process results from the semiconductor gap of the material. Indeed, under illumination, a photon can generate an electron-hole pair within the material. To do so, the energy of the photon needs to be greater than the band gap of TiO_2 (i.e. between 2.98 and 3.26 eV depending on the structure) so, when it transfers its energy to an electron from the valence band, the latter can migrate to the conduction band. This electron therefore migrates to the conduction band and leaves a hole in the valence band. From here, the electron/hole pair can be used in two different ways: generation of a photovoltaic current or enhancement of a photocatalytic chemical reaction. A very important aspect of such process that needs to be highlighted is that there is no consumption of the photocatalyst during the reaction.

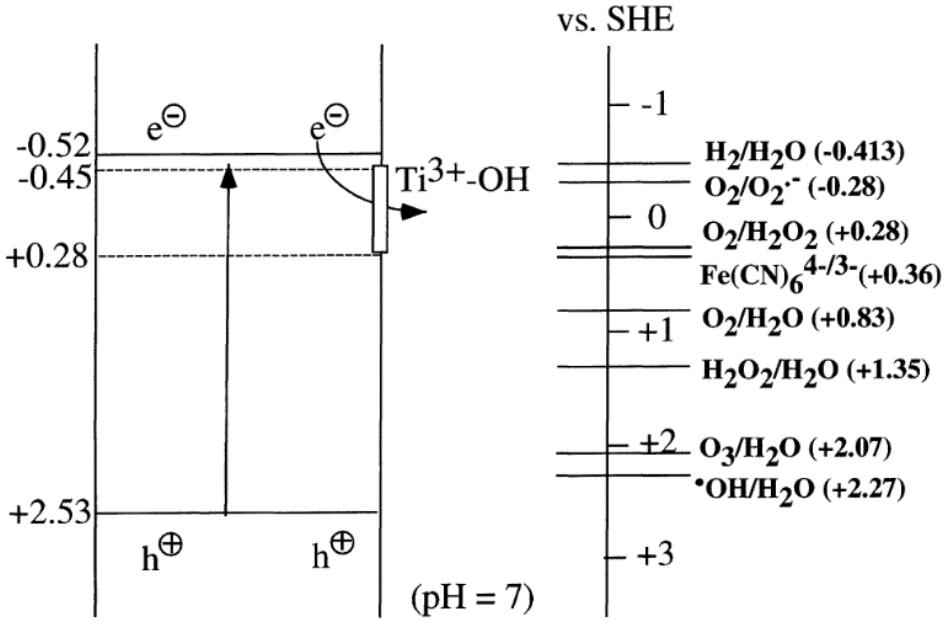

Figure 27. Schematic diagram showing the potentials for various redox processes occurring on the anatase TiO2 surface at pH=7 [136]

As shown in Figure 27, the potential of the holes generated in titania is high enough (i.e. 2.53V vs Standard Hydrogen Electrode) to produce •OH radicals from water (H_2O). These radicals can, for example, bond with Ti^{3+} and form electron holes at the surface, which is essential for superhydrophilicity, but their main purpose is the degradation of pollutants. Indeed, the holes and hydroxyl radicals are well-known to be highly oxidising and thus degrade organic and inorganic materials to less harmful substances (e.g. CO_2, H_2O, anions, etc...). On the other hand, the photo-generated electrons, with their -0.52V vs SHE redox potential, can directly produce hydrogen (H_2) from water but also be trapped in the Ti^{3+}-OH traps and still reduce water to superoxide ($O_2^{\bullet -}$) or hydrogen peroxide (H_2O_2). The combination of all these species is essential for the progression of photocatalytic reactions. Below is presented a schematic vision of the photocatalytic process:

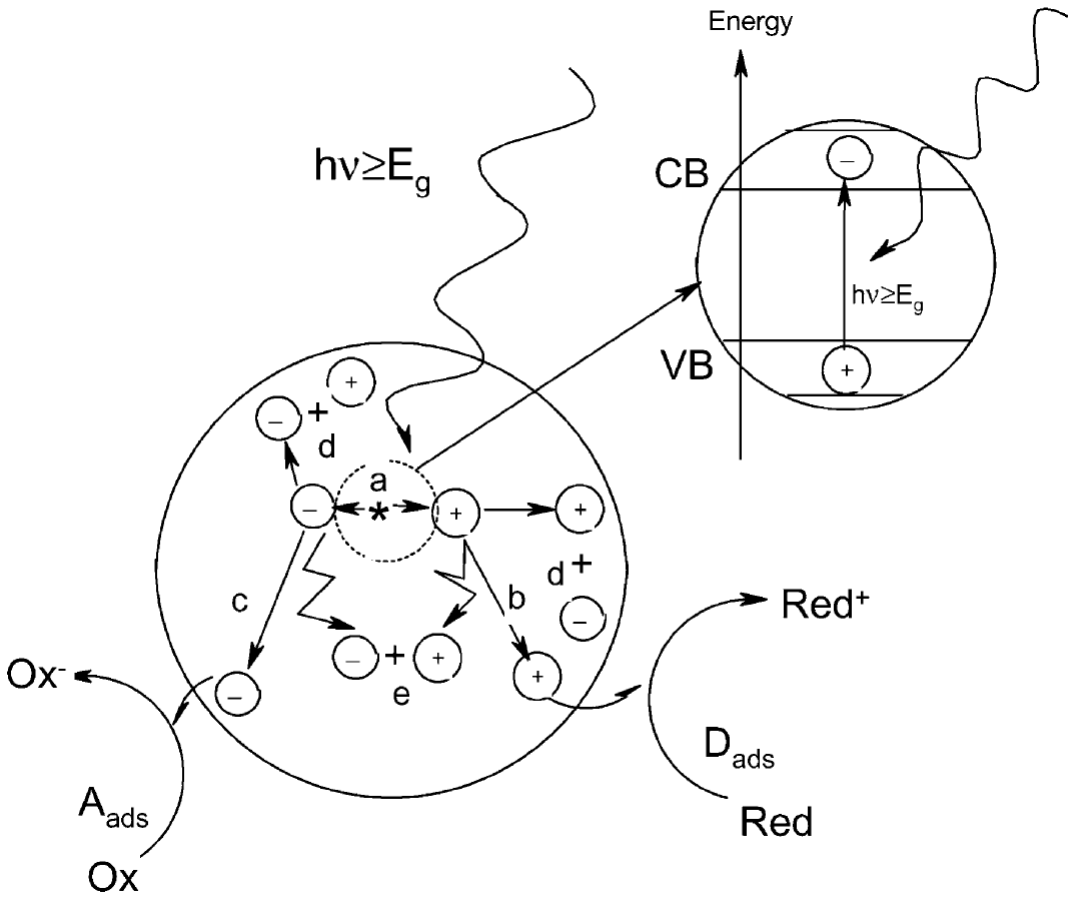

Figure 28. Main processes occurring on a semiconductor particle: (a) electron–hole generation; (b) oxidation of donor (D); (c) reduction of acceptor (A); (d) and (e) electron–hole recombination at surface and in bulk, respectively. From [137]

Not any semiconductor is ideal for photocatalytic applications. An ideal semiconductor photocatalyst should be: non-toxic to either humans or environment, cheap and easy to produce and use, chemically and biologically inert, efficiently activated by sunlight and catalysing reactions, and present a high photo-stability. It is also important to highlight that a good photocatalyst needs to offer a good mobility and lifetime to the electron-holes pairs. The TiO_2 is close to be the perfect candidate, with the exception that it does not absorb visible light but doping solutions exist to overcome this lack, as explain in the next section (i.e. I.2.2.3). However, even if it is the most widely used photocatalyst, it is far from being the only candidate: ZnO, ZrO_2, CdS, Fe_2O_3, etc… Also, the separation of electron-holes pairs gives the material the capability to destroy organic pollutants at its surface, providing it with antimicrobial properties. Several studies show its ability to fight against *E. Coli* cultures, for example (see [138] and [139] for example).

The photo-induced creation of electron-holes pairs can also result in another important property for titania films: the photo-induced superhydrophilicity (also called PSH or PIH by some). The photo-induced hydrophilicity is the result of the reduction of Ti by electrons and simultaneous trapping of holes at lattice sites or close to the surface. These holes can thus free oxygen from their associated titanium at the surface. The surrounding water can then adsorb on theses vacancies, creating -OH radicals at the surface. These radicals lead to an increase of Van der Waals forces and hydrogen bonding interactions with water, resulting in a spreading of the water at the surface. Fig x illustrates the photoinduced hydrophilicity of materials.

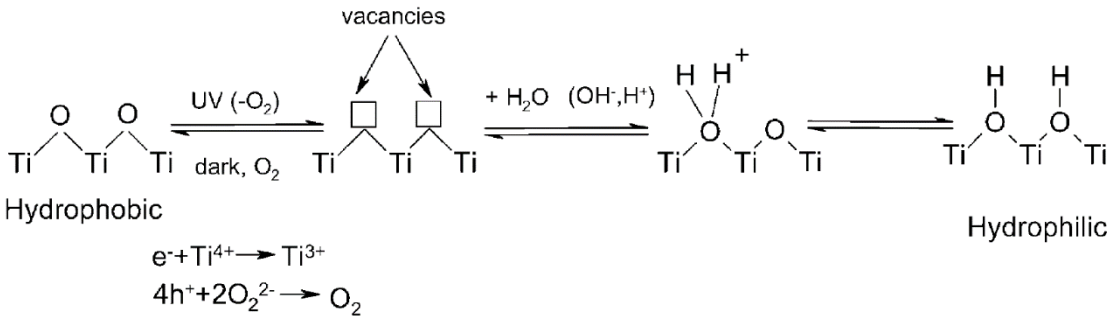

Figure 29. Mechanism of photoinduced superhydrophilicity of TiO_2. From [135]

The photoinduced hydrophilicity process is a reversible process, meaning that the reduces sites can be re-oxidized when the material is not illuminated for a certain amount of time. The film can then return to its more hydrophobic state, like shown in Figure 30. In some cases, super-hydrophobic films can be created and result in a possible transition from super-hydrophobicity to super-hydrophilicity. TiO_2 is a photocatalytic material with a phot-induced hydrophilic behaviour. One might think that both properties always come together but a material like $SrTiO_3$ is a photocatalyst but do not show low contact angles; and the opposite situation is observed for WO_3.

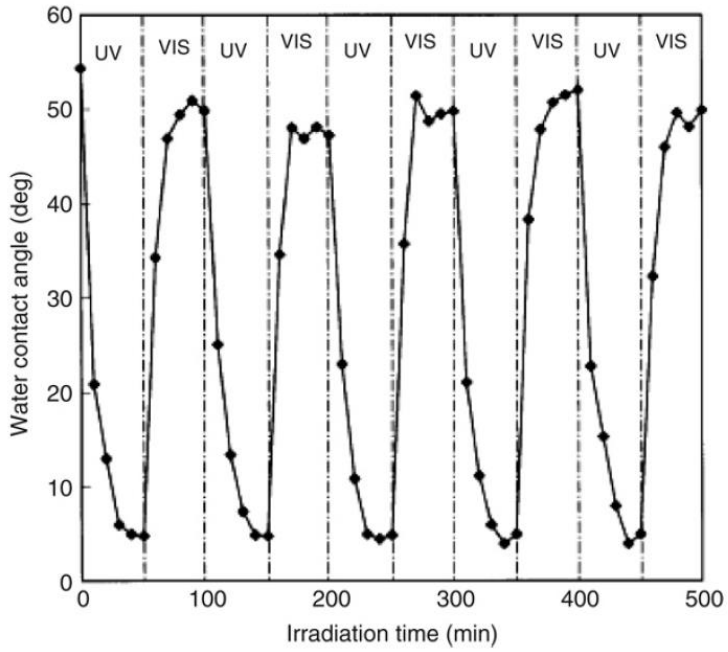

Figure 30. Trace of water contact angle (WCA) vs. time for an anatase film sample, showing reversible lowering of WCA under UV illumination and increasing WCA under visible light illumination. From [140]

I.2.2.3. Applications and limits

Historically, titanium dioxide is mainly used as a pigment for white paints, plastics, and paper. However, nowadays, it arouses a great interest from the scientific community because of its remarkable photo-induced properties [136] [141] [135] [128] [142] combined to its low-toxicity, its chemical stability and its relatively low cost. As seen previously, its band gap allows it to be used for either the generation of a photovoltaic current or its photo-induced properties. The first case is of less importance for the work presented here: the study focuses on photo-induced properties of Titania. There are two

main types of photo-induced properties for TiO_2: the degradation of organic or inorganic pollutants and the superhydrophilicity of the surface. The environmental applications are numerous but the water purification by TiO_2 powders under sunlight is one of the first applications contributing to the interest rise from the scientific community.

The range of applications is very wide for titania. Mainly, titanium dioxide is used on construction materials of various types for its self-cleaning property: glass, tiles, metal parts, traffic signs and lights, walls, etc… It can also be used for specific pieces that require to stay clean for their good use: photovoltaic panels and wind turbines, or even aeronautical parts for example. Indoor materials can also be coated with titania, such as wallpapers, paints, textiles, or even pieces of furniture. Finally, as evocated earlier, titania is also very widely used in water purification systems and air cleaners and its antimicrobial property also makes it a good candidate for food industry packaging.

From the above applications, most of them are outdoor applications, meaning that the TiO_2 needs to present certain properties, like these listed above, but also a good mechanical resistance, a good adhesion, and a good reactivity to visible light (i.e. sunlight). First, the adhesion of titania is not always good, especially for the anatase phase and that can be a problem in some situation. However, in most cases, solutions can be found to improve the adhesion of the films but these modifications can result in a deterioration of the film's photo-reactivity. Then, another limit, and the main one for titanium dioxide is the fact that it cannot use the visible light to generate electron-holes pairs in its original state, which results in a diminution of the film effectiveness. The latter can indeed be lowered by several factors, but mainly two types of solutions can be used: the doping of the film or the morphological modification of the film. The morphological modification consists in modifying the material's structure (i.e. porosity, surface area, density, etc…) to enhance its reactivity. The doping of the film consists of introducing a metal or non-metal element in the titania lattice. This doping then results in the creation of a transitive energy level, reducing the photon energy necessary to separate electrons and holes in TiO_2, meaning that the doped material can use the visible spectrum of light to produce electron-holes pairs. Also, the addition of impurities can generate carrier traps in the lattice and therefore extend the charge carriers lifetimes. Indeed, the recombination of the charge carriers within the material is one of the main limiting factors for highly effective photo-catalytic activity.

Finally, it must be highlighted that the anatase phase is well-known to be the most photo-active phase of titanium dioxide but temperatures of 400 °C or more are required in most cases to obtain an anatase crystalline phase. This thermal treatment can be brought to the material in two different ways: during deposition (i.e. substrate holder heating) or after deposition (i.e. post-annealing). The need for films to be heated at such temperatures to obtain crystals is a very limiting factor. Indeed, the industry -and especially the new technologies- shows a great interest for plastics due to their cheap production and their mechanical properties. This means that a whole development sector is closed due to the present incapacity to deposit such crystalline films onto polymers. It is then essential to be able to fully understand and master a deposition technique that could allow deposition of crystallite at temperatures typically below 100 °C. Ratova and her team showed that the HiPIMS process is an excellent candidate for the resolution of this problem as they have deposited crystalline titanium dioxide onto polymeric substrates without deteriorating the latter.

Chapter II. Experimental details and methodology

This chapter presents the project, the material and the methodology used. First, the aims of the projects are listed and explained to give the reader the full background of the study carried out is this thesis. Then, the material used also needs to be described, especially the deposition chambers and the power supplies used. Then, the plasma diagnostic procedure is explained, by listing the tools (i.e. oscilloscope, QCM, thermal probe, Speedflo) and the approach. The author's vision on the parameters classification is also given to better follow the thinking process along this thesis.

It is essential here to see that the idea is to show that deep plasma diagnostic can be carried out with a simple apparatus: an oscilloscope. This is of crucial importance for this project. The aim is to show industries they do not require complicated and expensive apparatus to efficiently manage the discharge, even for a complicated case like the reactive HiPIMS sputtering. Also, the parameters classification is essential as it is the base of the reflection given in this thesis.

II.1.Research context

This first section is here to present an overview of the project. It allows the reader to understand the general aspects of the work presented in this report. It also provides a clear description of the progression plan. The final aim is therefore explained in more details as well as the contributions to scientific knowledge. It permits the reader to understand where the project is going and how it should improve the scientific knowledge of the field. Once this is done, the different steps constituting the project are given in a chronologic order. Since each one of these steps is an essential part of the work presented here, the interests and experimental conduct plans are given. A time-scaled organization of these objectives is also presented.

II.1.1.Research aim and contribution to knowledge

The final aim of this PhD project is the low temperature deposition of functional crystalline coatings: titanium dioxide (TiO_2, or Titania) will be deposited for photocatalysis application. The aim is to obtain crystalline structure for this material while depositing it at low temperature.

In the literature, the temperature needed to deposit active photocatalytic films is generally higher than 400°C for Physical Vapour Deposition (PVD) processes. However, with such temperatures, unwanted side effects can be observed for specific applications. The most problematic of these side effects is the melting of thermally sensitive substrates such as polymers but it is also problematic when it comes to the realization of multi-layers because of the possible diffusion or mixing caused by ion bombardment. In the case of polymeric substrates, such temperatures result in a melting (complete or partial) or a degradation of the substrate and thus the impossibility of obtaining a functional coating [113]. For multi-layers' configurations, the problem is similar. The high-energy aspect of such depositions deteriorates the underlying layer and disrupts its properties. It should be specified that no matter how the increase in temperature is achieved (i.e. nature and moment of heating: infra-red or ionic bombardment, during or post-deposition annealing, etc…), the consequences remain the same.

The solution proposed in this work is the use of the High Power Impulse Magnetron Sputtering (HiPIMS) process to deposit crystalline structures at low temperature. This technique is still considered as being recent: the first paper referring to the process dates from 1999 and the first low temperature deposition has been reported in 2006 by Konstantinidis [143]. It generates a highly energetic plasma while keeping a low process temperature by pulsing the power supply signal (more details are given in I.1.3). There is an important demand from commercial and industrial sectors for low temperature deposition since it opens access to a large amount of new substrate and materials. The number of publications on TiO_2 has increased over the last few decades. The part of literature referring to PVD deposition has also increased in proportion over the years. However, so far, very few papers have reported photo-active titania films deposited by HiPIMS [144] [91] [100]. Each of these papers suggest that an optimization of deposition conditions is required to obtain more active films. However, no deep study of the HiPIMS discharge has been carried out in these papers; which results in a difficulty to explain and manage the deposition process modifications.

This project aims to develop a solid basis on how the plasma is modified by the deposition parameters and therefore what consequences these modifications have on the film growing process. This will enhance the knowledge already existing on low temperature deposition of functional films; which is arousing great interest from the scientific and industrial communities. It will result in the realization of a multi-layer coating composed of optimized multi-functional films on thermally sensitive substrates and the understanding of how the plasma modification changes the film growing conditions and properties. This will help the scientific community to complete its knowledge on HiPIMS and its applications in low temperature depositions of active crystalline films.

II.1.2. Progression plan

The work is subdivided into different objectives, each one of them constituting a step of the project progression. This section presents how the project is conducted by listing the different steps necessary to reach the final aim. The interest and necessity of these steps are explained. The point is to, overall, provide a progression plan for the project presented here.

Before starting any experimental work, a complete literature review is needed and it constitutes the first step: the redaction of the bibliographic work needs to be completed as soon as possible as this project shows that, by relying on the existing literature, the simple observation of the waveform gives important information on the plasma. Even if the information can be limited sometimes, it can always be completed with supplementary measurements but more importantly, it is believed to be sufficient for industrial applications. The literature reviewing is not time-limited: the reading of relevant articles will be kept up to date as well as their implementation in the report.

Following this preliminary work, the first step of the plasma diagnostic is taking place. This part of the project should result in a complete understanding of the rig and the power supply used for deposition during the project, and the plasma generated. The influence of each deposition parameter must be determined so the deposition process can be fully mastered. Doing so should help in accelerating and –more importantly- understanding the film optimization phase. Ti and reactive Ti-O discharges will be studied in terms of pulse-shape analysis (providing information on the plasma energy, composition, etc... [6]) completed by deposition rate and temperature measurements.

After, a basic material study will be conducted for films deposited under various conditions. The morphological aspect (i.e. SEM micrographs) and crystallinity (i.e. XRD and/or Raman) of the films are the two first aspects looked at. The point of this phase is to determine a first process envelope where a convenient stable discharge can be generated (i.e. limitation of heating and arcing, and sufficient deposition rate) for deposition of crystalline titania. The focus will also be on finding conditions where there is no arcing, as the latter imply defects in the films structure and crystallinity. The crystalline phase deposited is not yet optimized, the first objective is to show that crystalline TiO_2 can be deposited, rutile or anatase.

The TiO_2 films will then be analysed using a larger range of characterization techniques to optimize its crystallinity. The objective of this step is to understand how to optimize the properties of the film by varying the deposition parameters and conclude on optimum conditions to deposit active films. The photocatalytic activity of the films will be assessed by dye degradation, along with contact angle measurements. Each of these properties is going to be optimized and the physical reasons behind these optimizations will be explained relying on the previous plasma diagnostic. At this point,

the deposition of multi-functional TiO_2 films should be possible. The coatings should present high photocatalytic activity combined with hydrophilicity, transparency, good adherence to substrate, and anti-scratch resistance while no degradation of the polymeric substrate is observed.

Along this project, an important fact will be observed: the type of deposition chamber and power supply used can drastically change the sputtering process. It has then been decided that plasma diagnostic should be carried out for different rigs, to try and understand the origin of these changes. Two different power supplies have been used and three different chambers. The data collected here are very important and constitute an entire chapter by themselves at it shows a crucial fact: scaling-up in not a linear process for reactive HiPIMS. On the material deposition part, the importance of the type of polymer used has also been determined. It is sometimes reported in the literature that the substrate nature does not have an important influence on the growing film but it will be shown here that is does, and even for a same polymer, depending on the supplier of the latter, the film will not deposit in the same form.

This thesis goes through an understanding of the HiPIMS reactive sputtering and the familiarization with an industrial-scaled deposition chamber to deposit titanium dioxide. A deposition envelope is determined, where the discharge shows limited amount of arcs (or none, preferably), a decent deposition rate, and a stable oxide regime. This, added to the literature, leads us to deposit films in the transition window, thanks to the Speedflo system, where the deposition rate is much more important. The preliminary structural studies (i.e. SEM) also suggest a relatively high pressure*distance value. The films deposited under this type of conditions have been deposited varying any other deposition parameter, but do not show any good crystallinity, on any substrate, even orientated Silicon. When looking deeper into it, the conclusion is that the system needs to be in the poisoned mode to deposit crystalline rutile and anatase. Crystalline films have been deposited onto single-orientated silicon, glass, and some polymers, without melting the latter. No post-annealing has been used either. The films deposited in such conditions are shown to be crystalline even though there is a difficulty in duplication films: a film deposited in certain conditions does not necessarily shows the same structure and crystallinity as another film from the same conditions. However, films showing photo-activity during a dye-degradation test have been deposited. The films also show

interesting contact angles, from hydrophobic to hydrophilic. The fact that the data obtained here was quite different from the literature, the author proposed that the type of rig used could be of major influence on the plasma. Therefore, plasma diagnostics have been carried out on different rigs and using different power supplies to determine these differences, if any. The results show that, indeed, the rig dimension and arrangement along with the type of power supply used alter the oxidation process of the system; leading to totally different behaviours. However, some common points are shown and can be used as pointers to identify the oxidation state of the system and therefore identify optimal conditions for deposition. These optimal conditions do not necessarily result in the deposition of crystals but are, at least, the starting point towards their deposition, when possible. This thesis shows that using only an oscilloscope to characterize a reactive HiPIMS discharge is sufficient to find optimum conditions where crystalline anatase can be deposited in conditions where substrates do not melt. It also shows the importance of the equipment used to deposit the film: chamber, target, magnetron, power supply, substrates, etc...

II.2.Equipment – Experimental details

II.2.1. Rigs

II.2.1.1. Large rig (Nordiko rig)

The so-called large rig is represented in Figure 31. The rectangular titanium target (99.99% purity) is fitted on this water-cooled magnetron and faces a rotatable drum-shaped substrate holder. The surface of the drum is situated 27 cm away from the target's surface however, using an extension, substrates can be situated between 27 and 4.5 cm away from the target's surface. A closer position would be hazardous for the target (i.e. arcing). Both the target and the substrate holder are in vertical positions, which means the substrates need to be taped onto the substrate holder (the extension) using sellotape. The rotation speed of the substrate holder can be varied manually by the user using a potentiometer on the rig. The chamber is pumped down using a rotary vane pump (BOC Edwards 80) and a turbomolecular pump (Leybold TMP1000) to a high vacuum pressure of roughly 1.5 $.10^{-5}$ mbar before the insertion of argon (and reactive gas if needed), necessary to start the process of sputtering. The pressure inside the chamber is modified by changing the pumping speed, though the aperture of the butterfly valve.

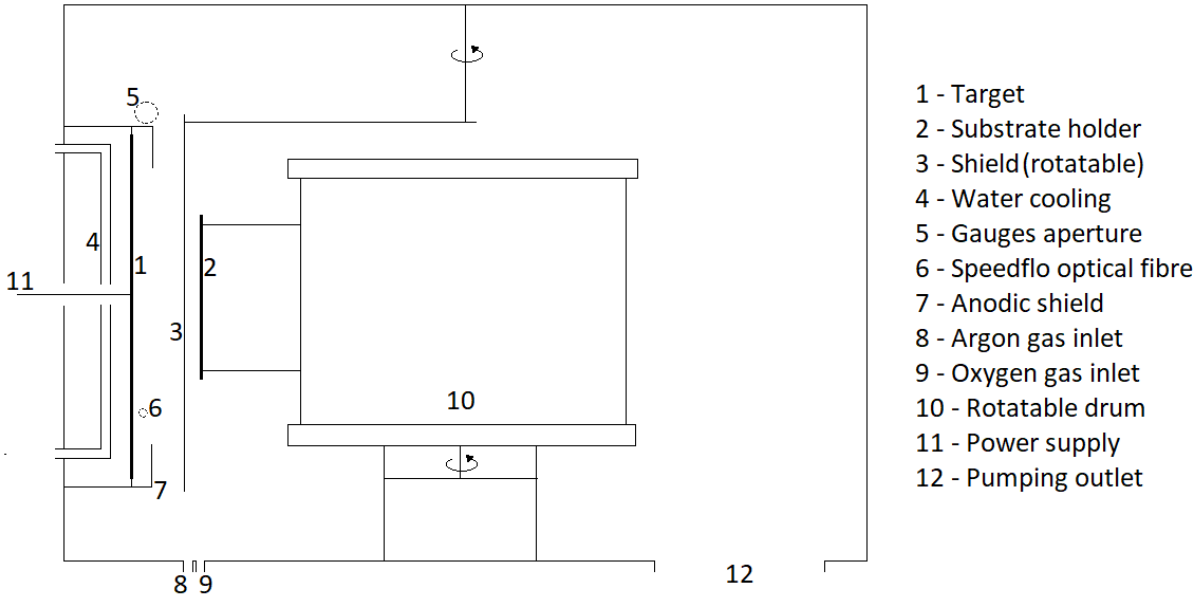

Figure 31. Scaled cross-sectional representation of the large rig. Doted circle shapes correspond to apertures at the back face of the rig.

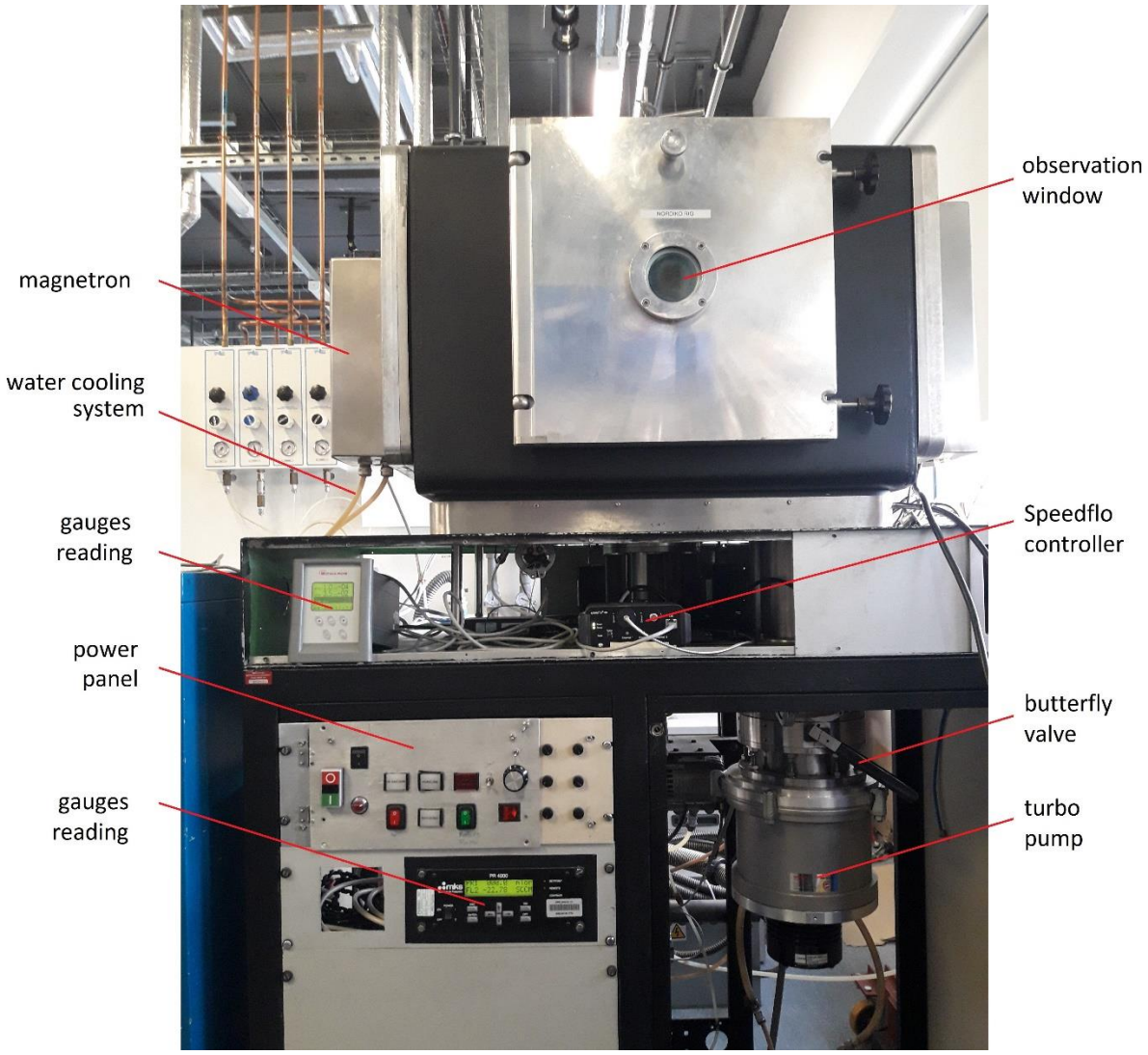

Figure 32. Photograph of the external aspect of the Nordiko rig

The pressure is measured by an ensemble of gauges: Pirani, cold cathode ionization gauge and capacitance manometer (for the process pressure) placed near the target. The pressures reached during sputtering are commonly between 4 and 20 $.10^{-3}$ mbar (3 to 15 mTorr). The gas composition is controlled using the Speedflo®™ controller system from Gencoa Ltd which regulates automatically the gas flow through Mass Flow Controllers (MFC) to keep the plasma stoichiometry constant relying on the light emission coming from the latter. The optic fibre necessary to this control is facing perpendicularly the target's vicinity as shown in Figure 31.

II.2.1.2. Small rig

The small rig is a simpler rig. It consists of a 99.99% purity titanium target with a 7.5 cm diameter, the substrates are situated on a plate facing the target situated 65 mm below the target on a horizontal axis. The magnetron is a type II unbalanced planar magnetron. The chamber is vacuumed down using a rotary pump (Leybold Trivac 16B) and then a turbo pump (Leybold Turbovac 190), to a base pressure of roughly 2.10^{-5} mbar (i.e. 2 mPa). The chamber can reach its base pressure within a few hours. Once this base pressure is reached, Argon is inserted through a MFC in the chamber to obtain a deposition pressure included in between 1.5 and 10 mTorr, approximately. The pressure is monitored using Pirani, cold cathode and diaphragm gauges, all three situated in position 4 on Figure 34.

Figure 33. Photograph of the external aspect of the small rig

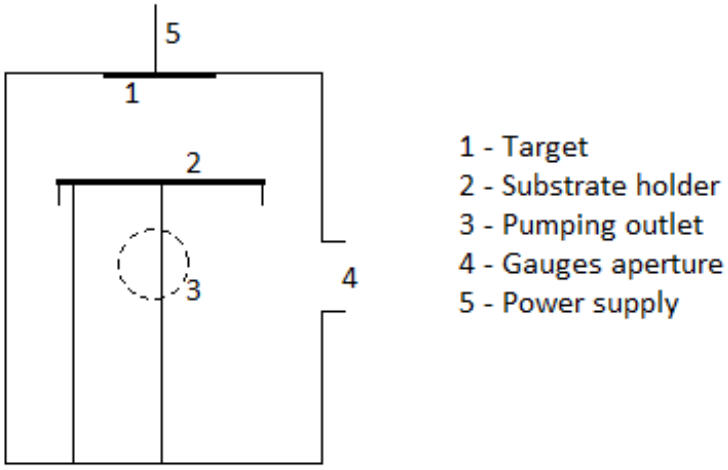

Figure 34. Scaled cross-section of the small rig. Doted circle shapes correspond to apertures at the back face of the rig.

II.2.1.3. Linköping rig

The rig used in Linköping during the collaboration project with Professor Helmersson team, at the Linköping University is described below. The so-called *Linköping rig* in this thesis is named the *HV sputtering system* in the manual – *Edward* is its shorter name. The following description is directly extracted from the user manual.

"Edward is a high vacuum sputtering system. The minimum background pressure of about 4 x 10^{-7} mTorr can be obtained with an overnight pumping. For maintaining vacuum conditions, it uses the turbo molecular pump (DN 160 DF-F by Pfeiffer vacuum, f = 833 Hz) backed by a rotary vane pump. With Edward, nitrogen, argon and oxygen gas supplies are available. For the control of these gases, available are the mass flow controllers (MFC1, MFC2 & MFC3 by MKS) that are attached with the gas outlets and the multi gas controller (MGC by MKS). Two Pirani gauges (PPir1 and PPir2, TPR 250 by Balzers), one at the foreline and the other at the chamber, one cold cathode gauge (PC.C, IKR 250 by Balzers) and one diaphragm gauge (PDiaph) are attached to the chamber for reading the pressure of the chamber. A DC power supply (MDX, 1K) for the magnetron, a DC power supply (TCR 600S1.6 by Electronic Meas. Inc.) for substrate bias and a DC power supply (SM30-100D by Delta Elektronika) for substrate heating are available for use with the system."

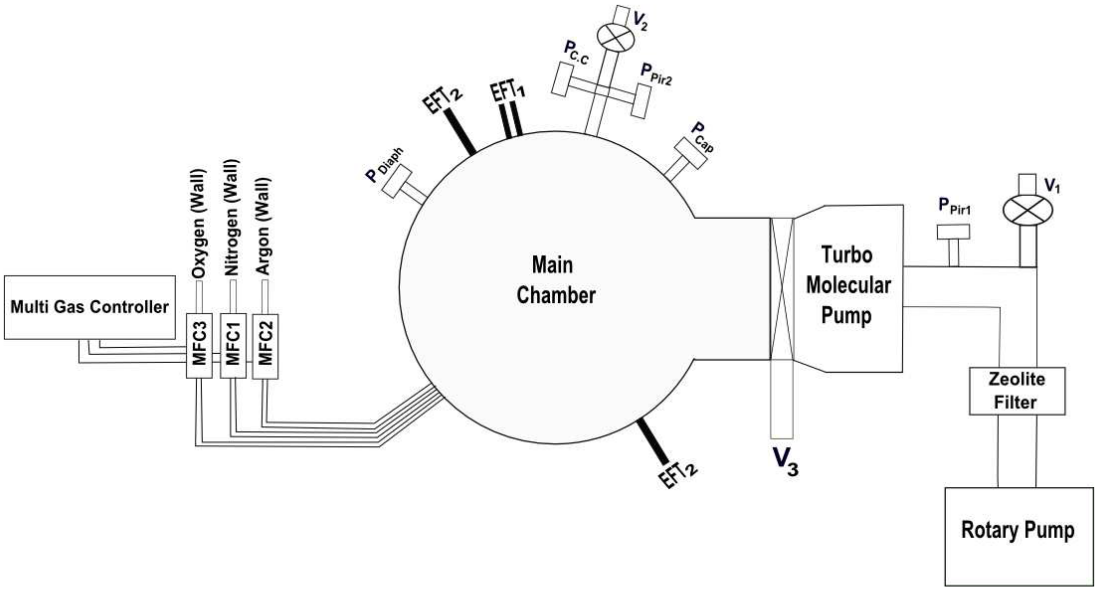

Valves

V_1 - Valve to the rotary pump
V_2 - Venting valve
V_3 - Throttle valve

Electrical feedthroughs

EFT_1 - Electrical feedthrough for the substrate bias
EFT_2 - Electrical feedthroughs for the substrate heating

Pressure Gauges

P_{Pir1} - Pirani gauge to foreline
P_{Cap} - Capicitance diaphragm gauge (Baratron gauge)
P_{Pir2} - Pirani gauge to the chamber
$P_{C.C}$ - Cold cathode gauge to the chamber
P_{Diaph} - Diaphragm gauge to the chamber

Mass flow controllers

MFC1 - Mass flow controller for Nitrogen
MFC2 - Mass flow controller for Argon
MFC3 - Mass flow controller for Oxygen

Figure 35. Schematic representation of the Linköping rig with its legend, extracted from its user manual [145]

II.2.2. Power supplies

II.2.2.1. Huettinger

The Huettinger power supply is the HiPIMS power supply mainly used during this project. It consists of a large unit that can generates a pulsed electric signal. The power supply has a set of available ranges for each power supply parameter. The ranges are as follows:

- Average power: 1500 W
- Arc control: none
- Pulse frequency: 20 - 1000 Hz
- Pulse Duration: 10 - 200 µs

- Peak Voltage: 1000 V
- Time-average current intensity: 2 A
- Regulation Modes: Voltage, Power

The main features here are both the time-averaged current intensity limitation and the absence of current regulation mode. The absence of a current intensity regulation system means that the only way to be in a current regulated is to reach the power supply limitation. However, it needs to be understood about the first limit that it does not depend on the target side, the duty-cycle or any other parameter. Meaning that when using a large target, the spatial current density is relatively low, even when reaching the power supply limit.

II.2.2.2. HiPSTER 6®

The HiPSTER 6® power supply has been generously lent by Ionautics for a total duration of 5 weeks. Using this power supply has been very important in this project as a major point of the latter is to observe the importance of order 0 parameters (see definition in II.3.4). It is then essential to use the same power supply is more than one rig, and cross-compare the results with other rigs and power supplies. The HiPSTER 6® power supply is significantly smaller than the Huettinger unit. It is a pulsing unit, that can be plugged into an existing DC system. Below are listed the available range for each parameter. The available ranges are clearly larger, compared to the Huettinger power supply limitations. This allows the user to strike discharges (if possible) in much more conditions. However, in this thesis, most of the time, the conditions are kept identical to what is done with the Huettinger power supply so data can be compared; as it is the main focus of the plasma diagnostic work conducted here.

- Average power: 6000 W
- Arc control: reaction time < 2 µs
- Pulse frequency: 1-2000 Hz
- Pulse Duration: 2.5 µs to 1000 µs
- Peak Voltage: 1000 V
- Peak Current: 600 A
- Regulation Modes: Voltage, Current, Power, Pulse current

II.2.3. Substrates

Different types of substrates have been employed for the project. As previously explained, the principal objective of this thesis is to show that crystalline and active

titania films can be obtained on polymeric substrates without deteriorating the latter. It is then then very useful for our project to study the influence of the substrate nature on the film growth. To do so, for each deposition, Si (100), glass and polyethylene terephthalate (PET) substrate were inserted on the substrate holder. In certain cases, different polymeric substrates could be inserted as well: polycarbonate (PC) films and/or poly(methyl methacrylate) (PMMA) pieces, mainly. The PEC films, very thin, were here to give an indication on the temperature reaches during deposition, since they have a lower melting point than PET substrate. The PMMA pieces, much thicker, were part of a study conducted in collaboration with Morgan Solar to obtain super-hydrophilic coatings on their photovoltaic cells. The use of silicon and glass substrate was needed to ease the characterization of the films. For example, SEM micrographs could not be acquired for polymeric substrates. Towards the end of the project, new polymers were ordered and used. There were 4 different polymers: PC, PET, PMMA and U-PVC (unplastified polyvinyl chloride). For each polymer, a film (approximatively 0.2 mm thick) and a sheet (approximatively 2.0 mm thick) were available.

All substrates are cleaned manually with methanol to eliminates surfaces pollution before being dried using pressurized air. A preliminary study showed that this simple process is found to be sufficient when done meticulously, compared to ultra-sonic baths. Also, due to the possible chemical fragility of some polymers, acetone is not used here to treat the substrates, even none polymers, to obtain a consistency in the preparation process. The substrates have not been polished at any stage. It should however be specified that the polymers ordered in the late stages of the project are polished during production and protected during transportation, resulting in a mirror-like surface.

II.3.Plasma diagnostic procedure

II.3.1. Objectives and aims

The plasma diagnostic main objective is to better control the plasma. To achieve this, the phenomena occurring within the plasma must be observed and analysed in relationship with the parameters modification. The existing literature provides descriptions and discussions about these processes, but it also reflects the fact that different observations –especially quantitative observations- have been made for different rig configurations and deposition methodologies. Therefore, there is a need to do the necessary experiments to verify and validate the plasma diagnostic knowledge available in the literature to the case of this project. This step is therefore an essential and necessary starting point before the material characterization and optimization.

This project also grants a great importance to the impact of the rig configuration (dimension, magnetron, pumps, etc…) and the type of power supply used, but also to the impact of deposition parameters such as voltage, pressure, frequency and pulse width. The interconnection in between all these parameters results in a complex approach where each condition needs to be studied individually and compared to other set of conditions. This logical approach is also a time-consuming approach but it is believed to be essential and necessary to show how important and how drastic some changes can be.

Once the discharge is fully understood, it provides explanations to the material modifications, which are going to be observed further in the project. The explanations rely on both the literature review and the experiments undertaken for the work presented here. The point is to be able to link the discharge changes to the thin film physical modifications (and therefore, to its properties) through the plasma diagnostic. It also helps to face any kind of situation. For example, if at some point, the peak intensity of the pulse needs to be reduced, the different options to reach that aim are known and understanding them permits one to choose which other parameter(s) should be modified to diminish this peak intensity, taking into accounts what would the consequences be. Thanks to this plasma diagnostic, the second part of the project is going to be accelerated and simplified.

In a more practical way, the first section (i.e. plasma diagnostic) also results in the determination of a process envelope. This envelope determines the limits after within which the discharge is stable, easily modifiable and fully mastered; but additional limits are also specific to the project aims. Indeed, the temperature is an important limiting condition, due to the objective of depositing onto polymeric substrates and sub-layers. Indeed, on both situations, the materials onto which the titania thin film is aimed to be deposited should not be deteriorated by any excess in the temperature. Thus, the first and most restrictive criteria is a low temperature process viability. In the first place, it is the reason why the HiPIMS process has been chosen. However, Professor Kelly and his team has shown that even using a HiPIMS power supply, the deposition can result in the melting of the polymeric substrate [113]. Thus, in the work presented here, the temperature must be measured for several *points* of this envelope to proceed to a first reduction of the envelope: i.e. temperature below the melting point of the substrates. It should be noted that different substrates can have different melting points and that even for the same polymer different melting temperatures can be found.

II.3.2. The Speedflo® controlling system

II.3.2.1. Principle of use

The Speedflo®™ technology has been developed by Gencoa Ltd (Liverpool) and aims to assist and facilitate the gas flow control during a magnetron sputtering process. It consists of a control box manageable by a computer interface, through the appropriate software. To help the user, that *controller* receives information on the composition and state of the plasma through the chosen sensors (Plasma Emission Monitoring (PEM), Penning PEM, PEM CCD, oxygen partial pressure gauge or voltage probe) and, thanks to its internal algorithm, respects the user's demand by sending a command to the actuators (MFC) and modifying the gas flow.

The PEM (Plasma Emission Monitoring) sensor has to be directly oriented towards the studied plasma. Since it is preferred to only see one element at a time, a filter is added between the optic fibre and the Speedflo®™ box. For this project, the oxygen and titanium contents in the plasma are of interest. The corresponding wavelengths to look at are respectively 780 and 500 nm. Moreover, this PEM sensor can also be used on the

plasma created in a 'Penning chamber', away from the bulk plasma to improve its performance. Indeed, using this procedure allows to eliminate any unexpected signal coming from substrate movements or arcing. A third method to observe the plasma consists in using a CCD camera. It allows the user to see the entire light spectrum but also to reduce the process running speed. Some systems allow the experimenter to directly measure the oxygen partial pressure instead of measuring the intensity of the light emission. Finally, the target voltage is obviously a very important parameter that must be looked at when analysing magnetron sputtering; especially in reactive sputtering because it always reflects the target state and composition and for this reason it is also a good candidate for a sensor. In the work presented in this report, an optical fibre has been installed and the light emission from the plasma in the target vicinity is used as the sensor signal.

Once the user has chosen which sensor(s) to install on the rig, all the installed sensors send information to the controller where different ways to control the plasma can be chosen. The control commands are then sent to the Mass Flow Controllers (MFC) which are then adapting their gas flows. The Speedflo®™ controller interface allows the user to choose different ways of controlling the gas stoichiometry. He can either set the flow to a *constant* value or use the *sensor mode*. For the constant mode, the user must choose a set point (expressed in % - 0%, the MFC is closed – 100%, the MFC is fully open) for a constant gas flow in sccm, no matter the data from the sensors. It is called an *open loop* process, in opposition with a *closed loop* process – which corresponds to the sensor mode. In this latter configuration, the actuator modifies its behaviour as a function of the sensor measurements and the user's demand:

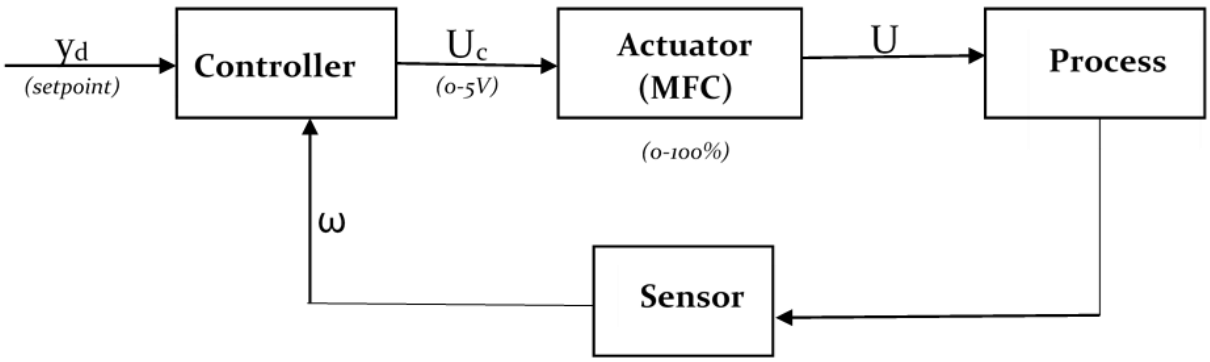

Figure 36. Schematic representation of the closed-loop functioning of the sensor mode

The experimenter also has a panel of control commands that he can use to compose more complex *recipes*, where the temporal dimension can be managed. For example, to calibrate the sensors, a sequence of increasing ramps followed by decreasing ramps is used. This mode can also set a sequence of following constant steps (open or closed loop). In addition, the slave mode is used for bigger systems and consists in *slaving* one or several actuators to another. This slavering sets the proportionality between the *slaves'* flows and the *master*'s set value through a coefficient going from 0 to 1. This kind of control is mainly used for large deposition chambers, where multiple gas inputs are used and geometric irregularities can be observed.

II.3.2.2. Details of operation of the Speedflo® controller

Before use, the closed-loop system needs to be calibrated. It means that the user needs to inform the software on what the conditions are, corresponding to the metallic mode and those corresponding to the poisoned mode. By doing this, the 0-100% scale is then set and the user can always operate at the same 'poisoning value' of the target. The system acts to keep the plasma stoichiometry constant. However, this calibration is always different for each configuration and needs to be done when any change is made to it. For example, every time a 1st order parameter is changed, the calibration has to be done again.

The calibration simply consists of setting a recipe composed of an increasing ramp and a decreasing ramp. The maximum percentage reached at the end of the increasing ramp has to be sufficient to fully poison the target but should not be excessive so the pressure remains constant. By doing so, the sensor signal (target voltage or light emission) reaches both its maximum and minimum values for the given configuration as follows:

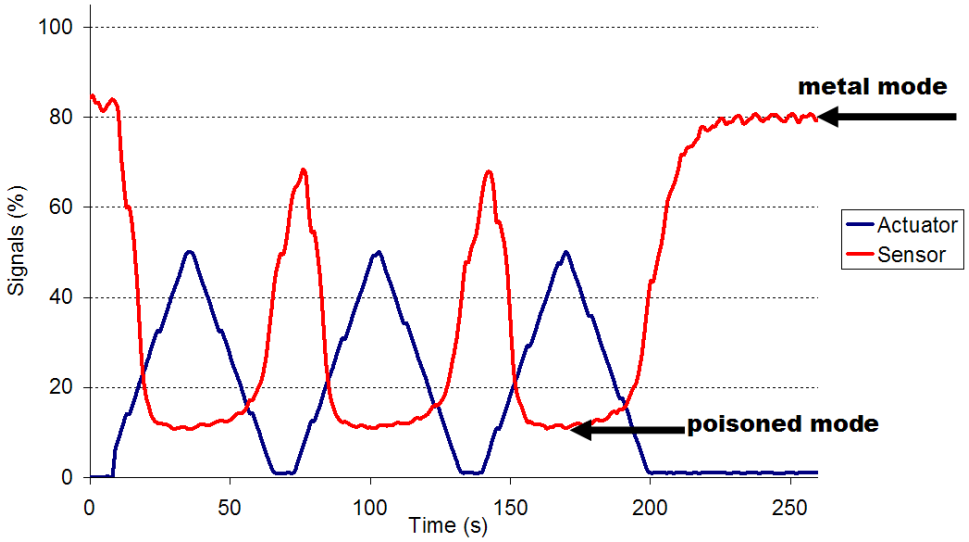

Figure 37. Calibration recipe for determination of Cal_{min} and Cal_{max}

These values are then defined as the Cal_{Min} and the Cal_{Max} (in V), which are the limit values of the poisoning scale. Once this step is done, the control precision is optimised and the user still must inform the Speedflo®™ controller if the measurement is *direct* or *inverse*. The direct mode corresponds to situations where an increase of the actuator flow results in an increase of the sensor signal and the indirect mode corresponds to the inverse behaviour. For example, if the actuator is the oxygen flow while sputtering a titanium target, the Ti^+ proportion measurement is inverse and the O^- measurement is direct.

The process can still be optimised by specifying to the software the intrinsic parameters of the system such as the chamber volume, the type of MFC used or even the gas pipe lengths. The k_1 and k_2 parameters can also be adjusted. Those parameters are directly included in the Speedflo® algorithm. The first one, k_1, reflects the *damping* of the signal. Basically, a higher k_1 coefficient permits to reduce time needed to reach the set point value but the user must be careful because if k_1 is too high, both the sensor and the actuator become unstable as it can be seen in the following images:

Figure 38. Evolution of the actuator and sensor responses when k_1 is modified

The second parameter, k_2, corresponds to the reaction speed of the Speedflo® controller. If the k_2 value is too low, the time needed to reach the set point is too long; and a too high value leads to oscillations of the signals:

Figure 39. Evolution of the actuator and sensor responses when k_2 is modified

In real terms, k_1 and k_2 should be tuned so the system is fast enough (increasing k_2) but still stable (reducing k_1). If the signal is unstable (i.e. if the curves oscillate), the inverse procedure should be applied (reduce k_2, increase k_1). The two values must be modified at the same time so the signal can be as reactive and stable as possible. The latest version of the software has an *auto-tune* option. This option automatically sets the values of k_1 and k_2 from a series of consecutive ramps running for at least one minute.

The Upper Actuation Limit (i.e. UAL) and the Lower Actuation Limit (i.e. LAL) values are respectively the maximum and minimum values sent to the MFC (in V) to set its gas flow. The UAL value is commonly left at 5.0V (higher value) but the LAL must be different to zero: typically, around 0.05. This difference avoids mechanical instabilities when opening the valve. Plus, the user can also modify the actuation time which

corresponds to the time the system is waiting between two updates of its state. It is the equivalent of the reaction time of the controller

To fully understand how the controller works, the inside of the controller can be briefly explained. The algorithm behind the controller box is a PDF (Proportional-Derivative-Feedback) type; similar to a PID (Proportional-Integrated-Derivative) control algorithm. A PID controller relies on the following schemes and equations:

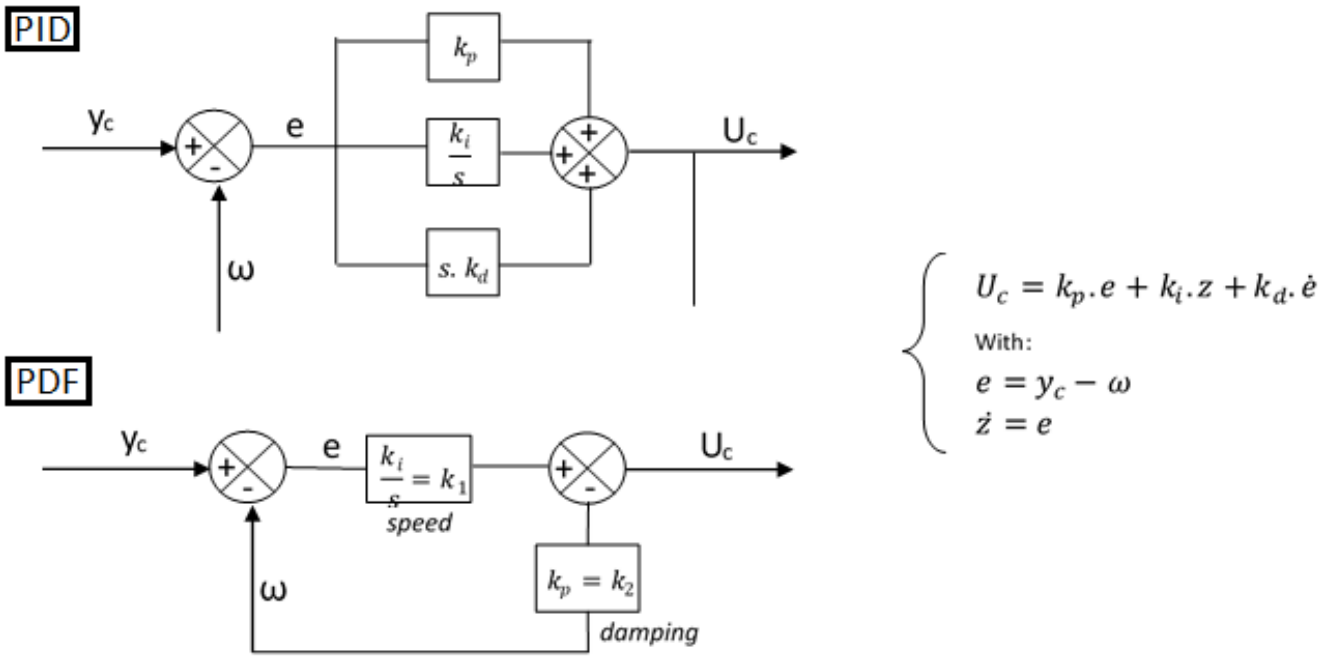

Figure 40. Schematic representation and corresponding equations for the PID and PDF algorithms

This schematic representation helps to understand where the k_1 and k_2 coefficient are coming from. They are the coefficient of the differential equation at the origin of the U_c value regulation. The difference between the PDF and PID systems is that the PID is an open-loop system when the PDF is a closed-loop. Because of this difference, the PDF algorithm needs one less coefficient than the PID algorithm since the first order derivation is no considered.

II.3.3. Plasma diagnostic instruments

II.3.3.1. The oscilloscope

For this project, most of the plasma diagnostic relies on pulse profiles acquired with an oscilloscope. The oscilloscope used for this project is a Mixed Domain Oscilloscope from Tektronix; the MDO3000 and is directly connected at the back of the target. The main point of using only an oscilloscope to study the discharge is a main aspect of this project. It aims at showing that simple and cost-effective solutions can be sufficient to carry out deep plasma diagnostic. At least at a deep enough level for industrial processes and applications. Showing that using only oscilloscope is enough to carry out reactive HiPIMS plasma diagnostic by relying on the theory found in the literature is of great importance.

II.3.3.2. The thermal probe

The thermal probe used is the calorimeter probe described in [146] and is also reported in [147]. It consists of a copper disk with a 24 mm diameter and a 2 mm thickness in which is inserted a K-type thermocouple. The unit is part of a larger probe and is thermally isolated from the rest of it with small ceramic tubes, as indicated on figure x. The thermal capacity of the probe is calculated to be of approximatively 3.1 $J.K^{-1}$. The principle of use is that, at low temperature, the losses by conduction and radiation can be neglected (cf. II.3.3.2) and therefore, the effective thermal power flux can be extracted from the heating phase of the system. Details of the theory and calculations are given in [147].

The face of the probe is situated parallel to the target's surface at different distance, as reported in III.2. Here, in the project, the main use is to determine what maximum value the temperature can reach during deposition but also observe the change in the heating coefficient (energetic flux) with the deposition parameters. This permits to determine in which conditions polymers can be coated without melting of the polymers but also determine in which conditions the energetic flux to the substrate is higher.

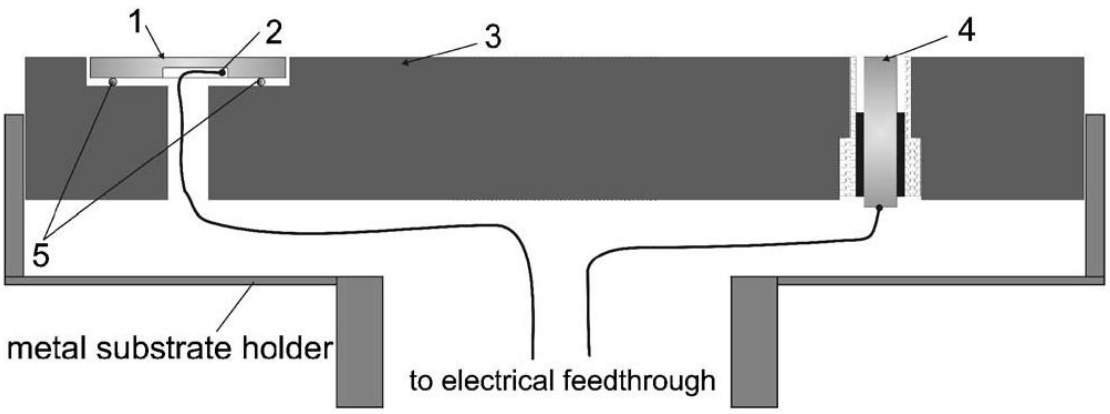

Figure 41. Schematic drawing of the calorimeter and Langmuir probes. Centres of both probes are located approximately above the racetrack. All wires are covered by alumina fish spine insulators. (1) The copper calorimeter probe, (2) the K-type thermocouple, (3) the Macor® block, (4) the planar Langmuir probe, and (5) ceramic tubes. – from [147]

II.3.3.3. The Quartz Crystal Microbalance

A Quartz Crystal Microbalance (QCM) is a specific a device allowing to measure the deposition rate in a sputtering chamber. It measures the frequency shift in an oscillator, directly connected to the quartz crystal facing the target. The shift comes from the addition (or loss) of mass at the quartz crystal. Since the resonant frequency of a quartz crystal can be precisely determined, any slight variation in this value can be spotted and inform on any mass variation. However, such a technique has to assume that the film deposited is deposited uniformly and in its solid state. For the microbalance used in this project, if the user provides an approximation of the material's density, the tool will directly indicate a deposition rate in A/s. The QCM used here also has an integrated water cooling system to avoid overheating of the crystal and deterioration of the latter.

II.3.4. Parameters classification

In the literature, the consensus is that the HiPIMS process has a long list of parameters compared to other PVD sputtering techniques: voltage, current intensity, electrical power, pressure, pulse width, frequency, gas and target composition, target size, time, temperature, substrate-target distance, rig dimensions, etc... However, no work has been found where the authors had classified these parameters, which is believed to be

essential. In this work, the plasma parameters are classified into 2 main groups: 1st and 2nd order even though a group 'zero' also emerges from the 1st order parameters.

The 1st order class unites all the parameters that are directly accessible and modifiable. These parameters can be directly modified by the experimenter and they control the plasma. They could be called the *fundamentals*, or *real* parameters. The only other parameters that could directly influence them are also 1st order parameters. The list of the 1st order parameters is as follows:

- Target voltage
- Frequency
- Pulse width
- Pressure
- Time
- Bias voltage
- Gas composition
- Distance

There are also the *order 0* parameters, listed below:

- Target dimension
- Pumping speed
- Magnetic field
- Power supply
- Chamber configuration
- Target nature
- Chamber dimensions

All the order 0 parameters are related to the rig itslef and it is the reason why they are considered as unmodified for a given experiment; although they can be modified in some specific rig configuration. For example, earlier in the report, the case of variant magnetic fields has been discussed in I.1.3.1. For the system used in this project, the only *order 0* parameter that can be modified during deposition is the pumping speed -by varying the aperture of the pump valve- which modifies the pressure within the chamber. However, the impact of changing the power supply used and even the rig itself have been studied and are reported in this thesis.

The 2nd order parameters are direct consequences of 1st order parameters modifications but do not influence the latter. It can be said that 1st order parameters rule the 2nd order parameters. The latter are a way to record the plasma, not to control it. They help the understanding of the plasma as they are consequences of the physical interactions and processes occurring within the plasma. However, they are still considered as being parameters because their modification (through the 1st order class) modify the film growing processes. These parameters constitute the link in between the modulation of the 1st order parameters and their consequences on the growing film. This class can be used as a *step* to simplify some studies but they must be used with care. In the work presented here, only three of them are measurable: the cathodic current

intensity (oscilloscope profiles), the temperature at the substrate position, and the deposition rate (cf. II.2.2 for the measurement methods).

A part of the existing literature uses a constant main or peak current intensity to compare a series of deposition. However, the way to regulate this parameter can be achieved by the modification of several different 1st order parameter (e.g. voltage, pulse width, frequency, pressure) and it creates a problem when it comes to comparing results from one paper to another. The decision of which 1st order parameter to prefer should rely on the characteristics of the equipment used, the methodology and the objectives of the project.

II.4. Film characterization instruments and methodology

II.4.1.Thin films characterization techniques

II.4.1.1. Raman spectrometer

Raman spectroscopy consists in directing a monochromatic light beam onto a material and analysing the scattered light spectrum. It is a non-destructive technique that can give information on the structure of the film and its composition. The photons from the laser are re-emitted by samples at different energies. These energies correspond to the vibrational, rotational and other modes of the material. Indeed, the photons arriving on the structure excite the molecules to higher energetic levels, corresponding to the photon energy. This level is however virtual and the molecule has to relax to a more stable energetic level (i.e. the rotational or vibrational state of the system). The difference in energy is emitted in the form of a photon, at a different energy (i.e. wavelength). There are two types of shifts observed: when the shift occurs to a higher energy state, it is called a Stokes scattering; otherwise, it is the so-called anti-Stokes scattering. It should also be specified that in some cases, there is no shift if the molecule comes back in its original state; it is known as the Rayleigh scattering and it is non-relevant to the measurement. The different scattering modes are represented in Figure 42.

The light emission from the illuminated spot is collected and, from there, the shifts can be calculated. The different shifts are measured for a given sample and a spectrum (see Figure 43) is obtained where the wavenumbers (cm^{-1}) of the different shifts are presented. The peaks on this type of graph correspond to the vibrational modes of the molecules present in the sample and therefore, are specific to certain chemical bonds and structures. Several peaks can correspond to the same crystallographic structure, each one of them for a different vibrational mode.

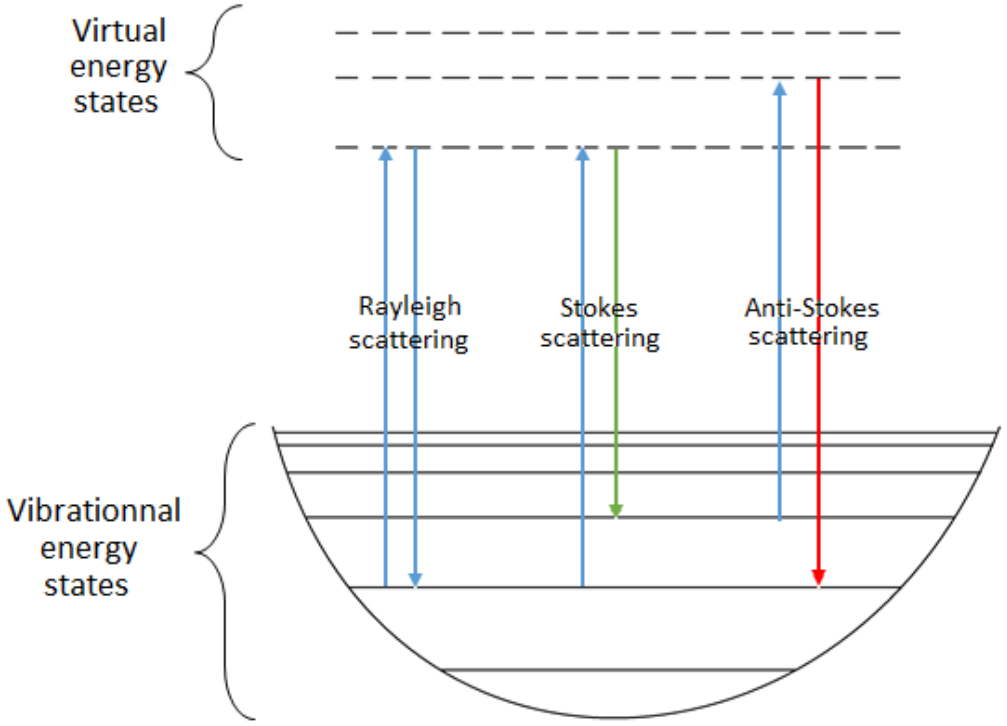

Figure 42. Different types of scattering possible observed during Raman analysis

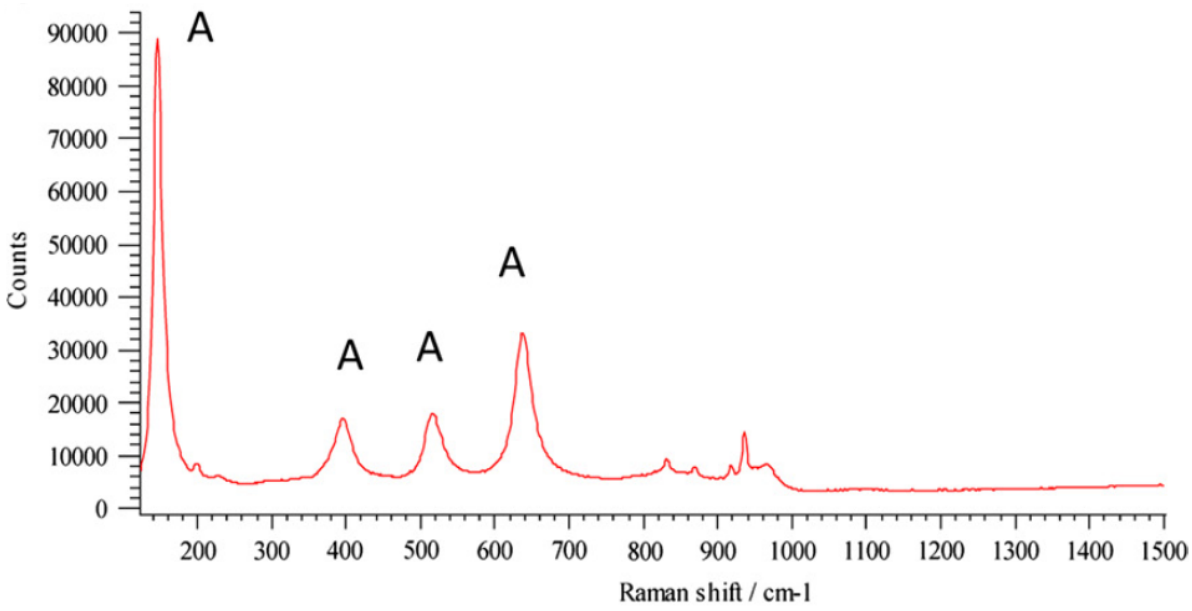

Figure 43. Raman spectra of sample with predominantly anatase structure (2.44 at. % Mo) annealed at 400 °C from [115]

II.4.1.2. Scanning Electron Microscope (SEM) & Energy Dispersive X-ray spectroscopy (EDX)

Scanning Electron Microscopy is a technique that relies on electron-matter interactions. The material surface is scanned with an electron beam and the backscattered secondary electrons are analysed. They come from a region under the surface but the thickness of this region is limited to roughly a few nm. They supply information on the position of the surface and therefore make the morphological study of the surface possible. The more secondary electrons are collected by the detector for a given point, the closer to the gun (i.e. the higher) this point is. The treatment of the data thus results in a black and white image reflecting the variations of heights between the different points of the film: a SEM micrograph can then be produced.

In the signal emitted by the sample's surface, X-rays are also found. These rays are essential for the realisation of EDX spectra. The incident electron beam ejects an electron from a deep shell of the atom and it is an electron from the external shell that replaces this lack in the structure. To do so, the electron relaxes and emits a photon of the corresponding wavelength. Thanks to this emission, the analysis of the spectrum informs us on the composition of the studied material. Indeed, the energy profile of the signal gives the chemical composition of the atom and the intensity of the peak in the spectrum indicates the number of atoms present in the sample.

The following scheme illustrates the different layers in the interaction volume of incident electrons on a surface for a better visualisation. The two previously evocated emissions are not the only one possibly emitted from a surface when interacting with an energetic electron, although the other emissions are not used in this work. They are therefore not explained here.

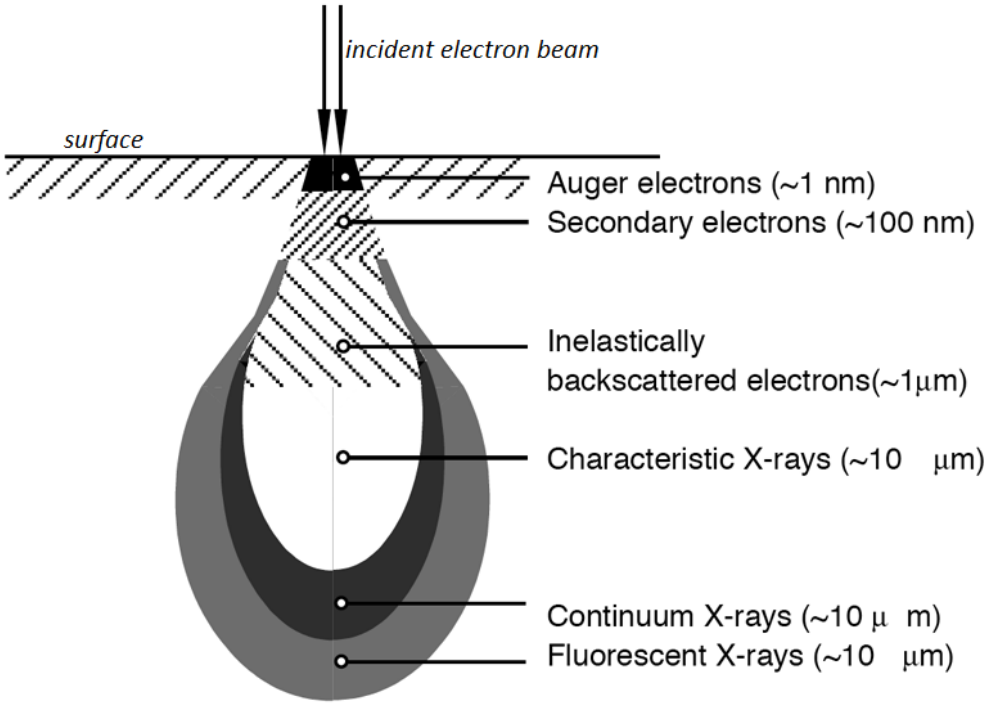

Figure 44. Schematic representation of the interaction volume

II.4.1.3. X-Ray Diffractometer (XRD)

To obtain more information on the crystallographic structure and the composition of the material, the X-Ray Diffraction process can be used. This technique consists in sending a beam of X-rays to the sample's surface and collecting the reflected rays. They are X-rays because their wavelengths are comparable to the interatomic distance and therefore make the diffraction patterns possible because the Bragg conditions are respected:

$$\sin\theta = \frac{\lambda}{2\, d_{hkl}}$$

Equation 7. Bragg conditions

•With **λ** the wavelength of the incident beam, $\mathbf{d_{hkl}}$ the inter-reticular distance of the crystal (to be determined) and **2θ** the angle measured on the instrument. A spectrum is obtained with the diffraction peak specific to the analysed sample. These peaks are compared to a database that informs the crystallographic information (structure, lattice constant, orientation, etc.) of the film. If one goes further, a quantitative comparison of

the peak intensities (if several peaks are observed for the same atomic specie) gives the user the preferential orientation of the crystal. Internal stress can also be studied by the shift of the peaks: a shift towards smaller angles corresponds to tensile stress while the compressive stress results in a shift towards higher angles. Also, the peak width gives information on the grain size. A schematic illustration of the instrument is given below in Figure 45:

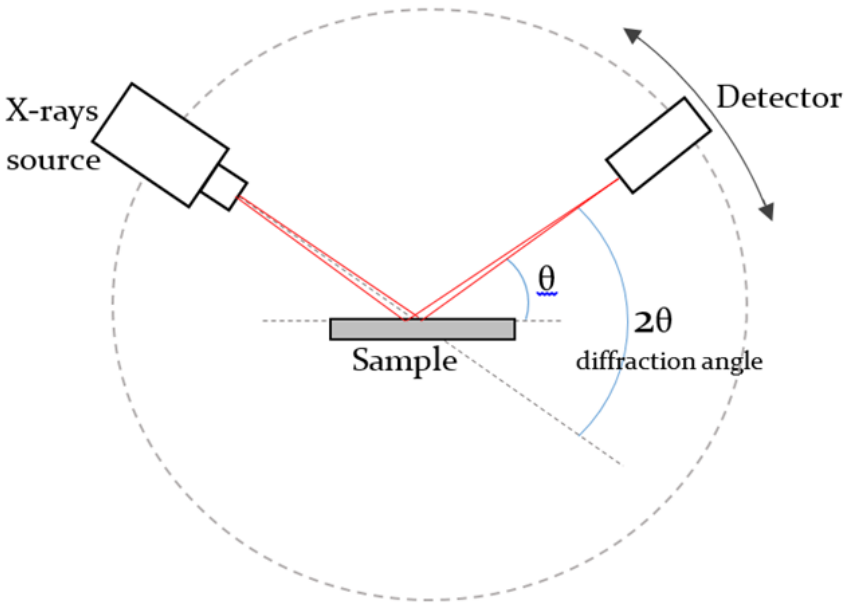

Figure 45. A diagram of an XRD measurement instrument configuration

II.4.1.4. Photocatalytic test

The photocatalytic activity of the samples is assessed by a dye degradation test in this work. These tests are known to be reliable for the calculation of photocatalytic activity. In the work presented here, Methylene Blue (i.e. MB) is used as the dye. Indeed, MB degrades under the effect of TiO_2 surface reactivity to light. Over time, in presence of a photocatalytic material and light, the concentration of MB in the solution is therefore reduced (see Figure 46). To measure this reduction, a light source is directed through the solution and the height of the MB absorption peak is measured over time using a spectrometer. This peak is situated at a wavelength of 664.11 nm. Other dyes can be used but the MB is common and relatively non-hazardous in small concentrations.

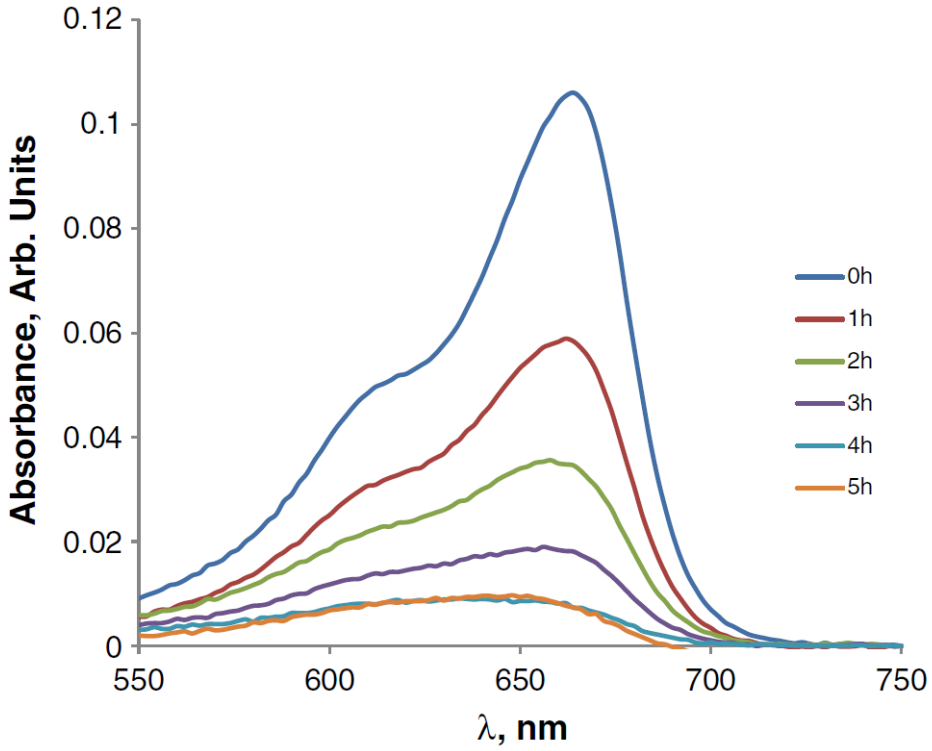

Figure 46. An example of the MB absorbance peak degradation over time during exposure to light of a photoactive material (from [118])

Prior to the testing, the samples are positioned in a methylene blue solution in the darkness to eliminate adsorption effects on the sample's surface during the measurements; which could result in wrong values (higher) of the decay rate. Indeed, in the dark, the sample's surface adsorbs some quantity of MB and thus eliminates a factor of MB degradation not due to photo-induced reactivity. All the samples present the same nominal surface area of 1.5 x 2.5 cm^2 (although the sample's roughness can modify the effective surface) and the aqueous solution is a 40 mL solution of 1.5 µmol/L MB concentration. A magnetic stirrer is continuously used during measurements to avoid static configurations and therefore permit to the entire fluid to react with the surface. The measurements can be made under different types of light emission: UV, visible and fluorescent. The peak intensity is monitored every second during the test -which is one hour long- and a decay profile is obtained at the end of the test. Since this intensity is directly proportional to the concentration of MB in the solution, it is possible to calculate the first order rate constant k_a. The latter is obtained by plotting the corresponding $\ln(A_{t=0}/A_t)$ versus time graph since the following equations (Equation 8) are verified.

$$ln\left[\frac{C_o}{C}\right] = k_a.t \quad \text{And} \quad \left(\frac{C_0}{C}\right) \approx \left(\frac{A_t}{A_{t=0}}\right)$$

Equation 8. First order rate constant calculation

Where $A_{t=0}$ and A_t are the heights of the absorption peak at respectively the beginning of the experiment and the moment the measurement is made. C_o and C are the corresponding concentration of the solution. The slope of the curve plotted is thus the first order rate constant k_a. However, it should be kept in mind that MB also slightly degrades over time even without the presence of a photocatalytic surface. The corresponding decrease rate is subtracted to the actual measurement in order to only measure the surface effect on the MB degradation.

II.4.2. Methodology and experiment details

It is necessary to remind that this project is done for industrial applications and it is the reason why parameters like the deposition rate should be optimized (or the time constancy of the plasma stoichiometry). For the same reason, this research project has been carried out by using an industrial-sized rig and it has different consequences. First, a larger scale means a modification of the particles dynamics in the chamber but also longer time needed to vacuum down the latter in between depositions. This results in a lower amount of deposited films per unit of time: after each deposition, the chamber needs to be open again to extract the covered substrates and insert new substrates in the chamber, and then needs to be vacuumed down again. However, due to the dimension of the chamber used here, the pumps need several hours before reaching a satisfying initial pressure (i.e. below $2.0 .10^{-6}$ mbar). Therefore, it is difficult to deposit more than 2 samples a day. However, for some sets of deposition, a maximum value of 6 samples a day has been reached. To do so, multiple substrate holders have been inserted in the chamber and presented one after the other to the target by rotating the substrate holder, as shown on Figure 31. A preliminary study showed that no material was deposited on the substrates facing away from the target even for a several hours long sputtering of the target.

Two different types of power supplies were available for this project but the Huettinger power supply is the one that has mainly be used. The HiPSTER 6® power supply is mostly necessary to see the importance in the choice of power supply on the deposition conditions. Both power supplies are more widely described in II.1. Here, the question is to know if, for comparable deposition conditions, similar films are obtained with different power supplies. The HiPSTER 6® power supply was lent by Ionautics and therefore only available for a limited amount of time (i.e. several weeks).

The plasma diagnostic is done by using only an oscilloscope and this same oscilloscope is used here to observe the plasma modification before and during deposition. The use of an oscilloscope only to observe the plasma is believed to be sufficient and simple enough to be applied to industrial rigs without extra additional cost needed for the implementation of a mass spectrometer, for example. One of the difficulty of this project is also to only rely on the waveforms to determine the state of the plasma within the chamber. To do so, an intense study of the literature of the past decade in terms of HiPIMS plasma diagnostic is necessary and is presented in I.1.5.

Still following this relationship to industrial configurations, the Speedflo® system is used to control the gas injection inside the chamber. The Speedflo® controller system is detailed in II.3.2 and therefore is not explained in details here. It should only be reminded that two gas control options are available: an injection at a constant sccm rate or a time-dependant injection rate, relating on the optical emission from the plasma. The deposition of crystalline Titania while using the Speedflo® controller is another essential point of the project presented in this thesis. Indeed, it is well known that using such a system increases the deposition rate of the process while keeping a plasma stoichiometry constant over time. However, this is not necessarily the most important criteria as it is primordial to obtain crystalline films for certain of the aimed applications, even if it reduces the deposition rate.

Chapter III. Plasma Diagnostic – 1st order

This chapter presents the results of the plasma diagnostic conducted during the project. This step is essential in the understanding of the processes occurring in the plasma generated in the specific rig used for this work. Because of the final objective of depositing crystalline films on polymeric substrates, an optimal set of conditions must be determined. To do so, the influences of each deposition parameter on the plasma itself and the film growth must be known. Since the discharge used here is a HiPIMS discharge, the plasma is very sensitive to the variation of conditions. In addition, the reduced number of publications –compared to DC and R-F magnetron sputtering for example- on reactive HiPIMS sputtering of Ti-O makes this chapter even more essential.

As it has been said earlier, the only three 2nd order parameters that can be measured in the work presented here are the cathodic current intensity, the heat flux at the substrate position, and the deposition rate. For each of them, their relationships with each of the 1st order parameters have been assessed. This section presents and explains these relationships. Other experimental setups allow measurement of other characteristics of the plasma, such as the ionic current at the substrate position (ionic probe, Faraday cup), the nature of the excited species present in the plasma and their ratios (Optical Emission Spectroscopy - OES), the energy of the species (Electron Energy Distribution Function Spectroscopy -EEDFS, and Ion Energy Distribution Function Spectroscopy -IEDFS), etc… However, each of these observation technics requires a specific instrument which is not available for this project.

The chapter consists of 3 main parts, one for each 2nd order parameter measured: the deposition rate, the temperature load, and the cathodic current intensity. The deposition rate data are separated in three sections. First, the effect of each 1st order

parameter is studied in the voltage regulated mode. Then, the same studies are carried out in the intensity regulated mode. And finally, the spatial homogeneity of the deposition thickness is also measured and reported in the third section. For the temperature measurements, the data are presented in only one section where the effects of the voltage and the duty-cycle on a metallic discharge are presented. There are not more data as the QCM used for this project broke down before completion of the study. However, the data is sufficient to bring the necessary knowledge for this project. Finally, the study of the pulse waveforms is divided into 4 sections: the metallic mode, the effect of the oxygen, the poisoned mode, and the effects on the transition study. In each section, the effect of every possible 1st order parameter is reported and discussed for both voltage and intensity regulated modes.

III.1.Modification of the deposition rate

III.1.1. Voltage regulation (<I> < 2.0A)

The deposition rate study mainly followed the previous worked undertaken by different teams around the world and evoked in the literature review. The first main observation that is worth being mentioned here is the fact that fairly transparent (and thus fairly stoichiometric) films have been deposited up to 15% of the fully metallic signal (cf. II.3.2) and these conditions showed deposition rate up to 3 times greater than the deposition rates for films deposited at 5% of the metallic signal as it can be seen on the following figure (Figure 47). This is the reason why the first films have been deposited at common 15% signal. Metallic signals higher than this 15% have not been reached for deposition since after this limit, the proportion of metal is too important. After this limit, the films start to be non-stoichiometric and therefore correspond to less transparent films; which is one of the principal criteria for our films. The fact that the deposition rate is lower in reactive mode is well known and referred at in the literature. However, here, there is an unusual increase of the deposition rate between 100 and 60% of signal. This increase is believed to be due to the increase of the cathodic current intensity referred at in III.3.2.1 but no further conclusions can be drawn on the matter.

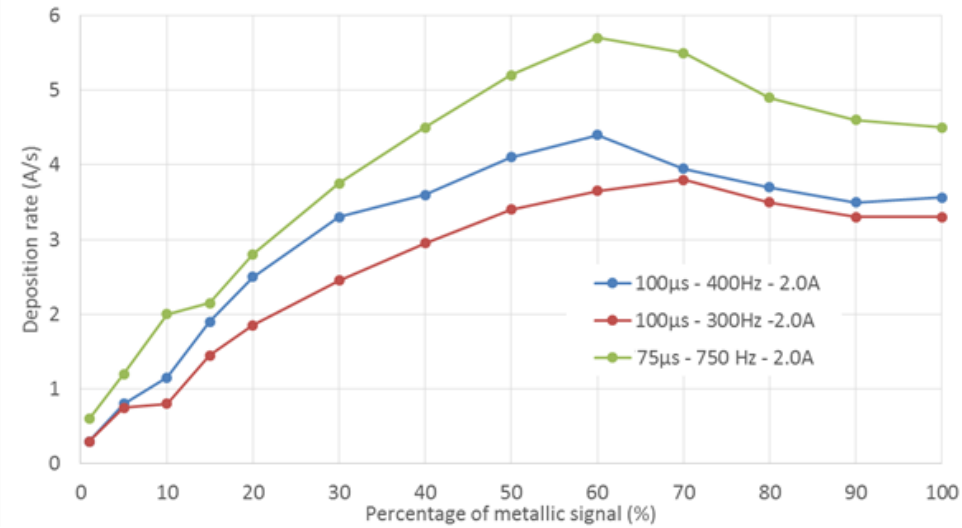

Figure 47. Deposition rate as a function of the percentage of metallic signal for different deposition conditions

In terms of deposition rate, other trends have been studied. First, parameters such as frequency and pulse width have been looked at. In both situation, a direct linear relationship with the deposition rate has been observed. It is believed to be primary due to the increase in duty-cycle (i.e. effective time of deposition). The results are shown below in Figure 48 (a) and (b).

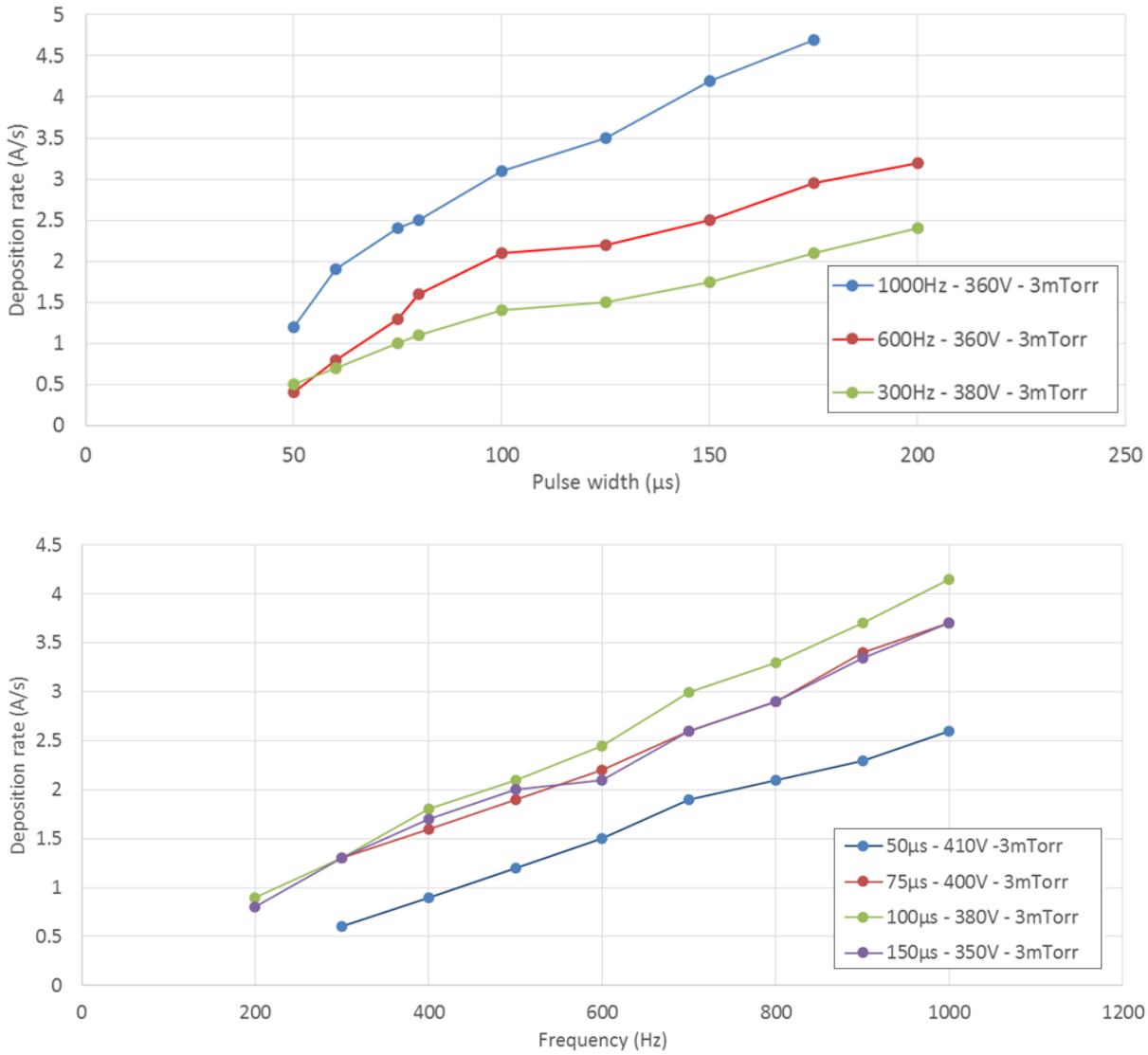

Figure 48. Pulse width (a) and frequency (b) influences on deposition rate for different conditions

However, even though the frequency dependency is very linear, an *irregularity* in the linearity can be spotted for the pulse width case. Interestingly, this irregularity seems to correspond to changes in peak current intensities. For this specific reason, the

deposition rate is represented in Figure 49 as a function of the duty-cycle to see if the relationship is indeed linear or if the peak current intensity needs to be considered.

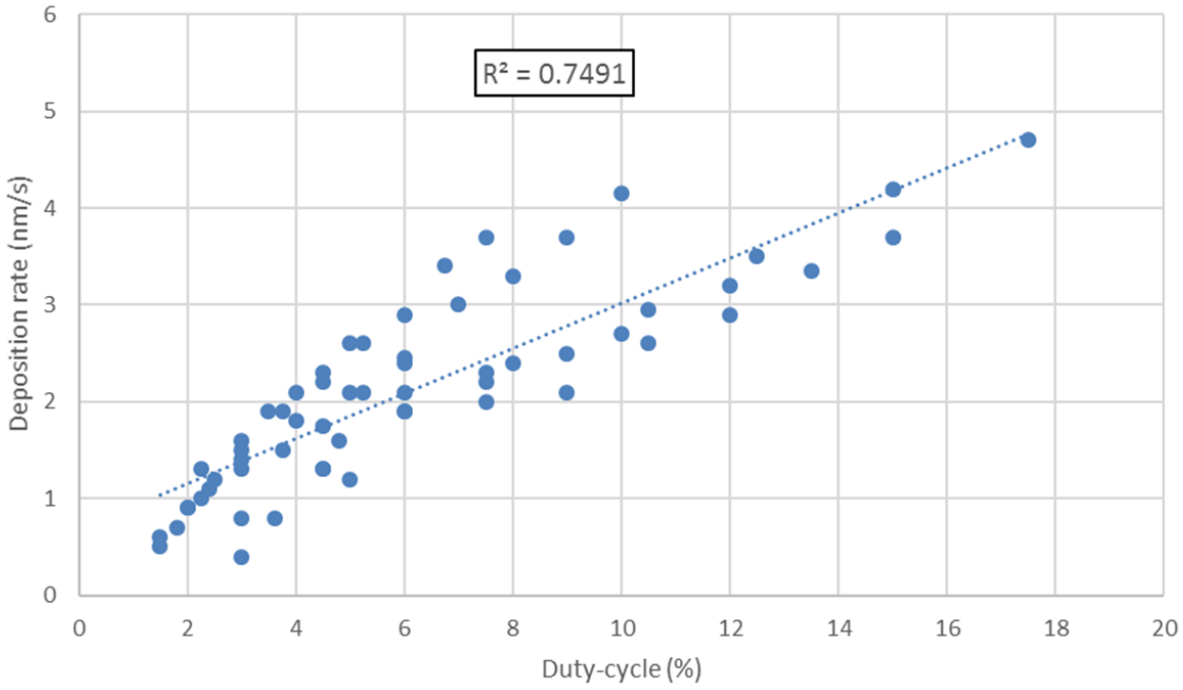

Figure 49. Deposition rate as a function of the duty-cycle for various deposition conditions

As it can be seen in Figure 49, the relationship between the two entities cannot be considered as linear since the linear approximation presents a correlation factor R^2=0.749. Indeed, a factor superior to 95% is necessary to conclude on any consistence of the approximation. This type of correlation factor is however obtained when the deposition rate is divided by the current peak intensity and represented as a function of the duty-cycle, as shown in Figure 50.

This linearity is an interesting result as it shows that the deposition rate is not only a consequence of the effective time of deposition when the pulse width and/or the frequency are modified. It shows that the quantity of entities reaching the target per pulse is also very important. In other terms, the deposition rate is function of both sputtering time and plasma intensity. And it is a very important fact to notice since the plasma intensity differs for each frequency / pulse width couple.

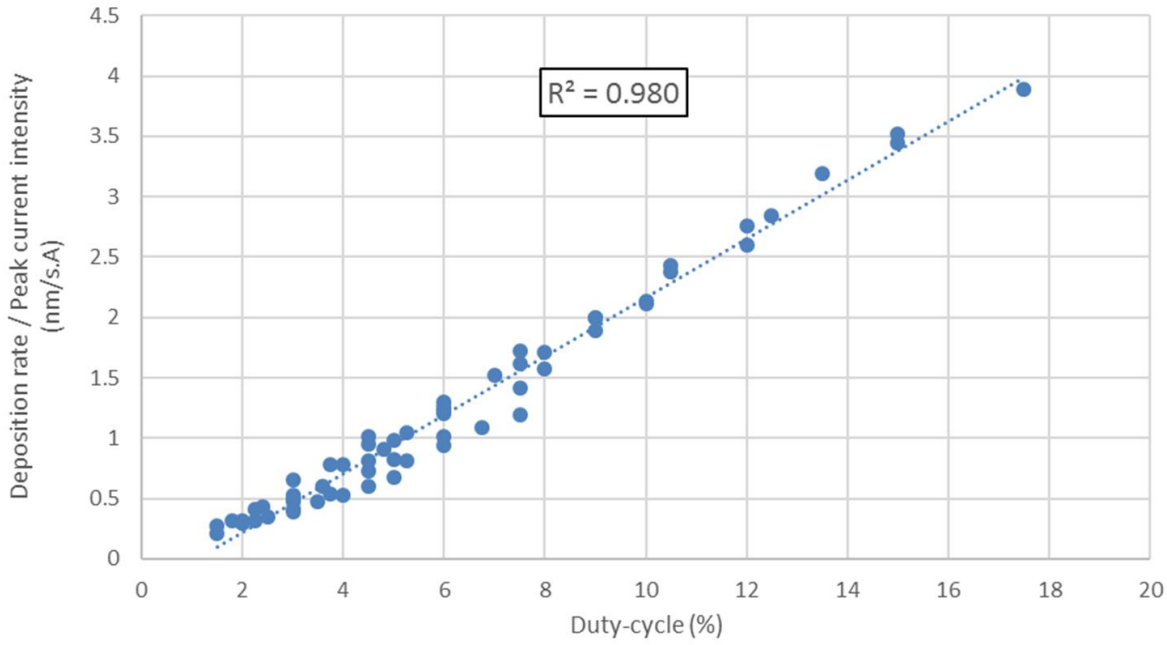

Figure 50. Deposition rate normalized by the peak current intensity as a function of the duty-cycle

It is believed that the narrowing of the linear regression could be even ameliorated if the pulse shape was taken into consideration for each configuration as well. Indeed, it has been seen previously that the pulse shape is modified as well for each configuration so the current intensity should normally be integrated along the pulse duration to precisely reflect the number of particles reaching the target per pulse. However, this result suggests that the peak current intensity is a good enough quantity to use for reflecting the waveform when comparing it to time-averaged quantities, such as the deposition rate.

It should be specified that this observation stands for the case of the work undertaken in this thesis as the pulse waveform can drastically change for different power supplies, deposition chambers and target materials, for example. Note that these parameters are *order 0* parameters (see II.3.4 for definition) and thus independent from the study conducted in this chapter, concerning the influence of 1st order parameters.

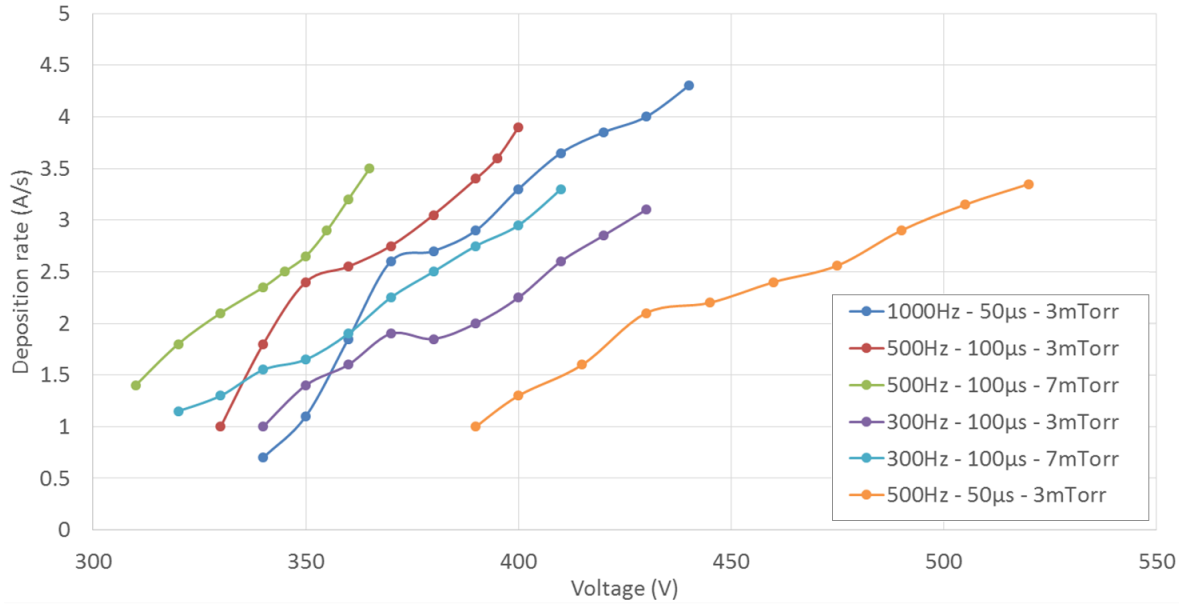

Figure 51. Voltage influence on the deposition rate

The same linear increase is observable when it comes to observe the effects of voltage as shown in Figure 51. This time, it is due to an increased sputtering rate for higher voltage. This effect is already well known and explained in the literature review.

The last influence that have been looked at is the pressure. For this one, the result is different from the 4 previous ones. Indeed, as it can be seen in Figure 52, there is an increase of the deposition rate when the pressure is increased until a Pt, from which there is a transition in the regime. From there, there are two different behaviours that have been observed: the increase in the deposition rate is reduced (i.e. linear coefficient decreases) or the deposition rate starts to decrease for higher pressures. In both cases, the existence of a 'transition' is evident. The reason behind this transition is believed to be due to the balance in between the augmentation of the number of available particles for sputtering ad the augmentation of collisions undertaken by the particles before being able to reach the substrate. We can also see that the Pt is different for different sets of deposition conditions. This confirms the statement that we just made. This observation is also the reason why we wanted to conducted work at both high pressure*distance ratios but also at low ones, to study both situations.

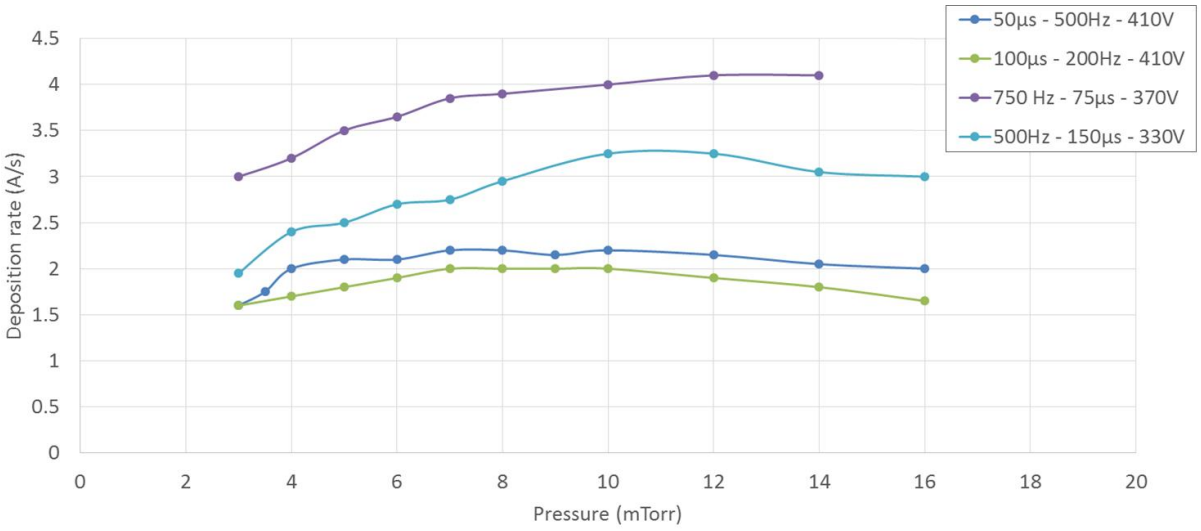

Figure 52. Influence of the pressure on deposition rate

III.1.2. Intensity regulation (<I> = 2,0A)

For the study of the deposition rate modification, a deposition rate monitor has been used during the generation of different discharges. The conditions of the discharges have been chosen so the entire envelope available with the power supply is covered. However, some conditions result in either the absence of a plasma or a plasma too weak to reach a current intensity high enough for depositing any film. Other conditions result in a plasma that is too *intense* and arc too much. In this study, the average cathodic current intensity has been kept constant to the same value for every measurement of a given series. The point of this method is to keep the same amount of ions at the target position and see what the consequences of modifying the 1st order parameters are on the plasma kinetics and dynamics between the target and the substrate.

The influence of the frequency and pulse width modification show a clear trend on Figure 53, where the deposition rate have been presented in a 3D representation in the *frequency/pulse width* referential.

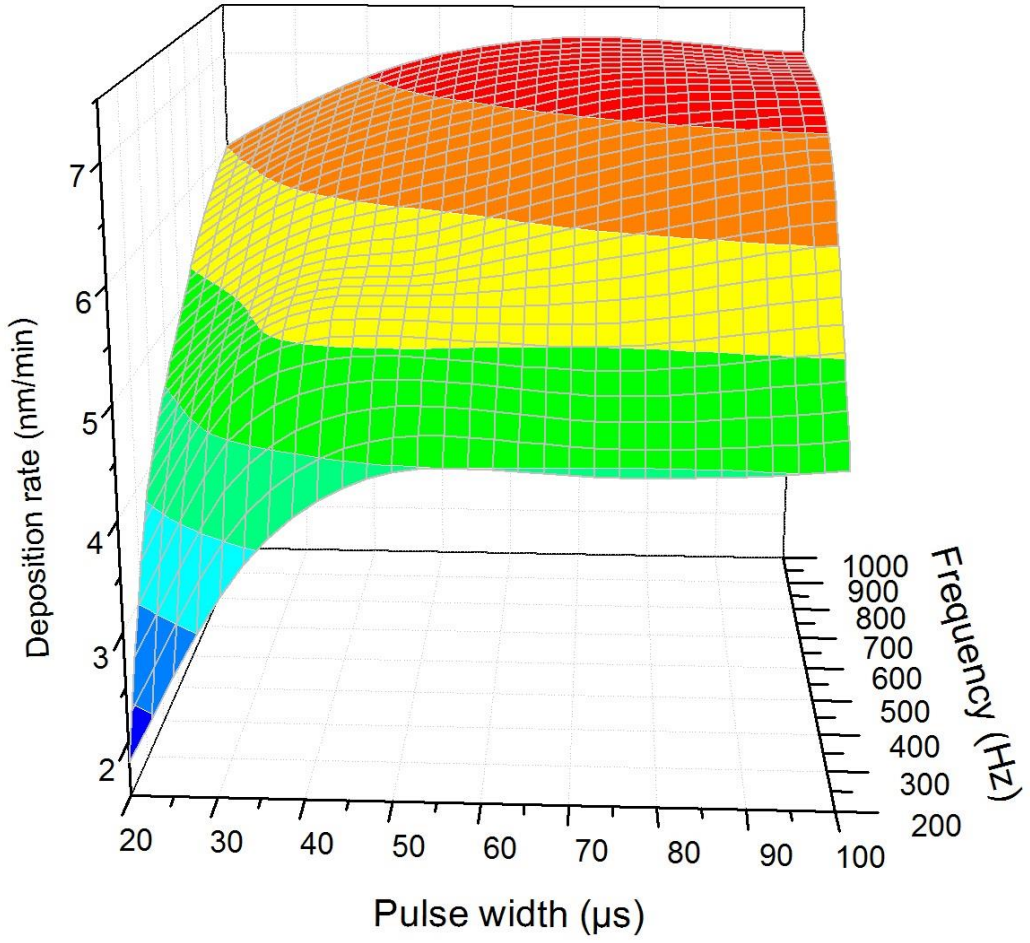

Figure 53. 3D representation of the deposition rate as a function of the frequency and the pulse width

(3 mTorr – metallic discharge – 17 cm away from the target)

This representation gives a clear understanding of what happens: the deposition rate increases with both parameters. In a more general way, it increases with the duty-cycle. It should be kept in mind that the average cathodic current intensity is kept constant on every point of this diagram (i.e. the voltage is lowered for higher duty-cycles). The behaviour observed is believed to be due to the increase of the effective sputtering duration in a given time, since the voltage is apparently not responsible for it. Indeed, it is easy to understand that for a higher duty cycle, the total on-time duration is longer than at a lower duty-cycle; which means more sputtered particles – and thus a higher deposition rate for higher duty-cycles.

However, the measurement is done using a quartz crystal microbalance that only measures the mass of deposited material. This means that there is no way to know if

different film densities are present in the envelope. The calculation of the deposition rate is made by if all thin films have the same density, no matter the frequency-pulse width couple. Another point that must be highlighted is the fact that some initial conditions should be eliminated for the further studies since the corresponding deposition rate is too low to be suitable for further investigations. In the same way, conditions where the deposition rate is very high are not necessarily suitable because they generally correspond to conditions where a lot of arcs occur (i.e. defects in the film), typically, above a 5% duty-cycle. Further in this project, one will see that even below 5%, some conditions are arcing too much to deposit films with no defects. The second envelope is presented below:

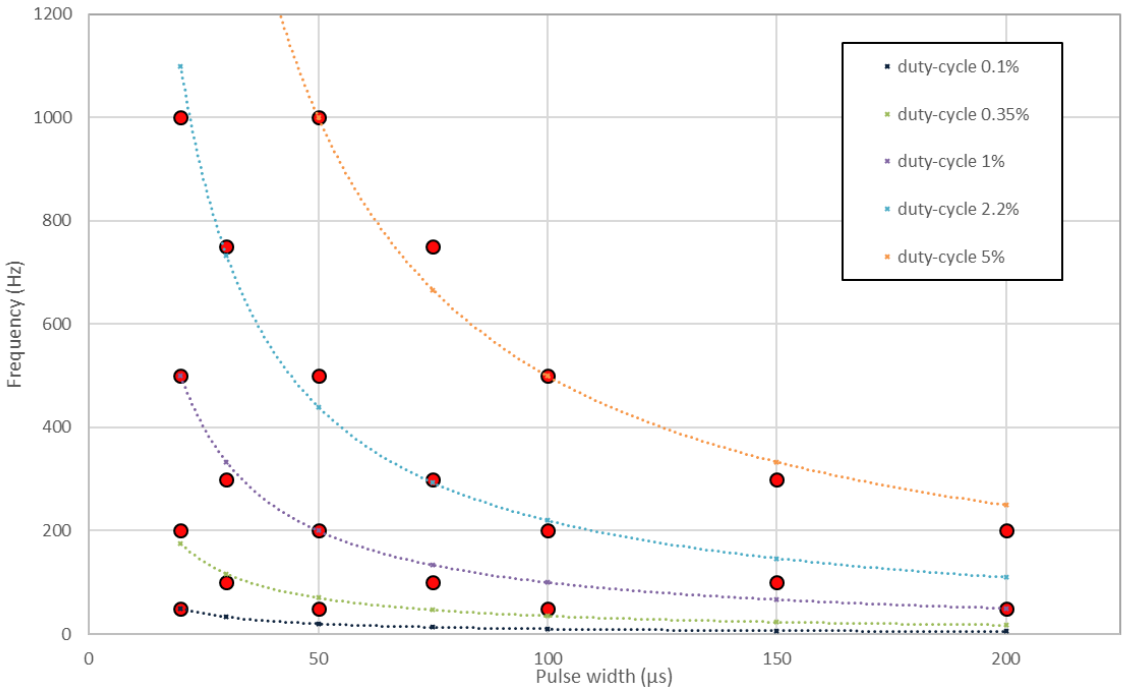

Figure 54. Representation of the deposition envelope in the frequency-pulse width space. Points have been positioned to form lines along the x-axis, the y-axis and the duty-cycle lines.

Since the measurements have been made for two different pressures (3 and 10 mTorr), conclusions on the influence of the pressure can be made (even if the data have to be confirmed by a more detailed study later on). It is seen that for lower pressure, the deposition rate is enhanced. There can be two explanations and further studies are needed before to make any conclusion. The first one is the fact that to generate the same amount of ions at the target position (i.e. constant cathodic current intensity), the voltage has to be increased at lower pressure since less particles are available. However, this rise is not very significant and it has been seen earlier that the voltage seems to have no direct

influence on the deposition rate in these conditions. The other explanation for this difference in the deposition rate is the number of collisions the particles undertake in the plasma. Indeed, at lower pressure, the particles coming from the target loose less energy and therefore, more of them can reach the substrate before to be fully relaxed. At higher pressure, a part of the ions and atoms cannot reach the 17cm distance from the target and are stopped in the bulk plasma. This trend must be verified for different target-to-substrate distances because it is possible that for shorter distances, the relationship is inversed.

No concrete study on the effect of the gas composition of the plasma has been conducted because of the large quantity of measurements needed (i.e. full envelope measurements for each oxidation state of the target). Nevertheless, a diminution of the deposition rate has been spotted between the metallic and the fully oxidized mode as it is reported in Figure 47.

III.1.3. Spatial homogeneity at substrate position

Before depositing any film, the user needs to make sure that the deposition rate is homogeneous over the whole surface of the substrate holder. To do so, metallic films have been deposited in different pulse width / frequency conditions and the thickness of the deposited films measured on different spots of the substrate holder. By doing so, a mapping of the substrate holder can be realized and is represented in Figure 55. This figure shows that the thickness is relatively homogeneous over the substrate holder, even though the films deposited in the centre of the latter are slightly thicker than those deposited on the extremity. The measurements are conducted in the metal mode to obtain thicker films in a shorter amount of time and ease the study. Indeed, the spatial homogeneity must be the same for metal and reactive mode. The values are just lower in reactive mode. The figure is very useful for later as it means that substrates can be positioned anywhere on the substrate holder with only slight and therefore negligible variations of thickness : below 5% variation within 5 cm from centre.

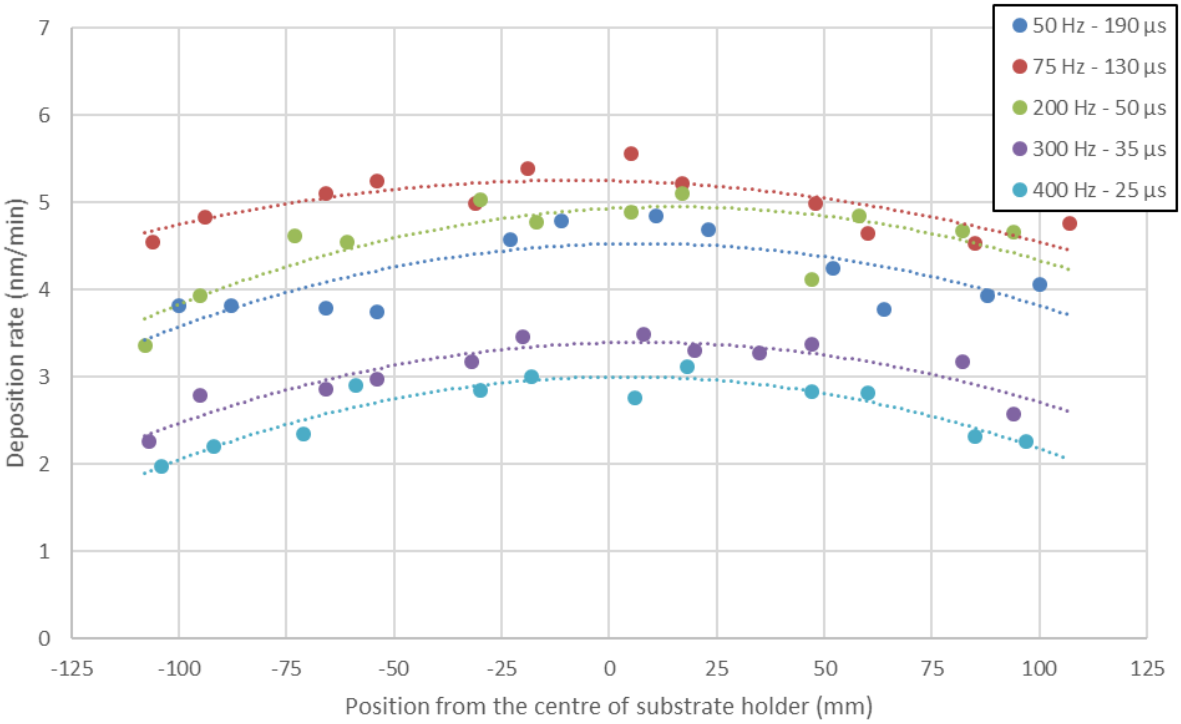

Figure 55. Mapping of the deposition rate over the substrate position along the vertical axis

III.2. Modification of the energetic flux at substrate position

The energy flux has been measured with a thermal probe following the process used by Cada et al. [147] and other teams [146] [121]. The temperature rise has been measured during the first moments after the plasma ignition. The system is considered to be at its thermal equilibrium before the discharge is initiated and since the measurement duration is short, the cooling down process of the system is considered as negligeable. Thus, the heating process during this period is only ruled by the energetic particles reaching the substrate position. The temperature rises linearly for the first 0.5°C (i.e. typically the first tens of s, up to a min) from the initial temperature is quasi-linear and a slope coefficient can be calculated in $mK.s^{-1}$. The graphs showing the temperature rise at the substrate position as a function of the cathodic voltage and peak current intensity have been plotted and are shown in Figure 56:

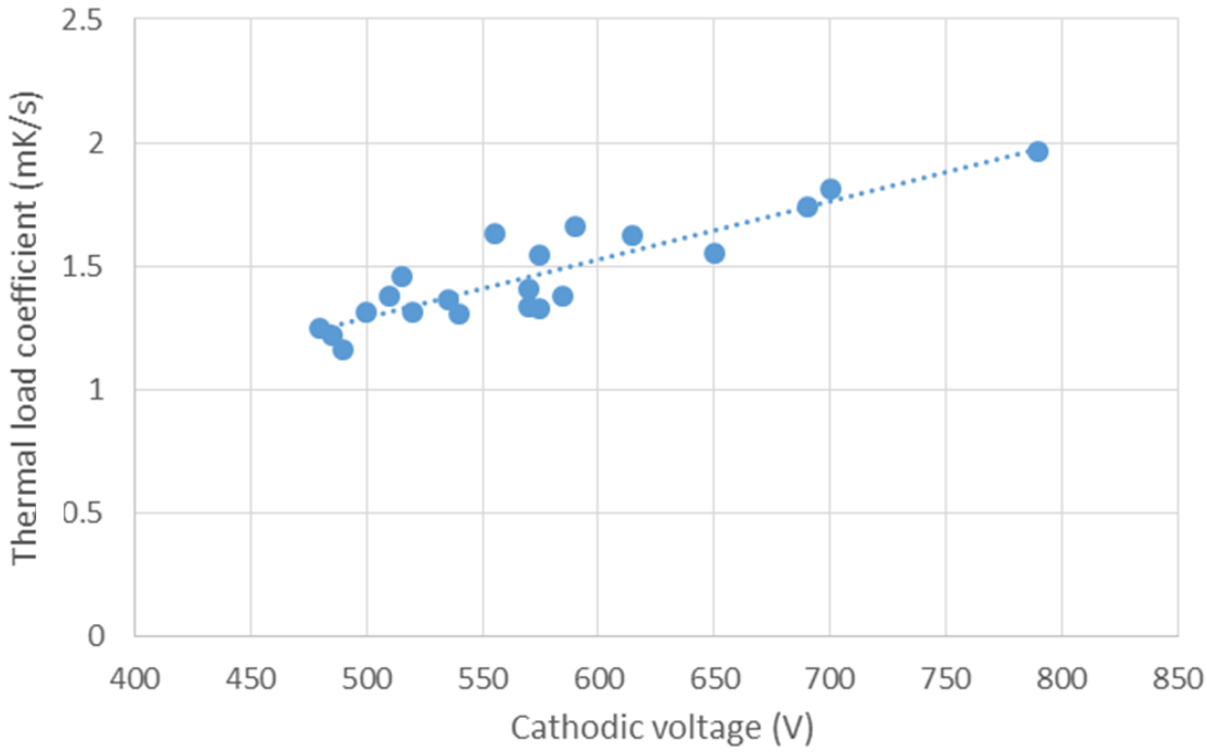

Figure 56. The thermal load coefficient at the substrate position as a function of the cathodic voltage for various frequencies and pulse widths (3mTorr, <I>=2.0A)

The relationship can be considered as being linear between the two entities. However, since the peak current intensity is a consequence of the target voltage and is also directly proportional to the latter, it is hard to define if the augmentation in the energy flux is essentially due to the kinetic energy of the particles provided by the applied voltage or due to the quantity of particles hitting the substrate at the same time (i.e. proportional to peak current intensity at constant pressure). However, the fact that the average current intensity has been kept constant suggests that the kinetic energy of the particles is more likely to be responsible for the quantity of energy received at the substrate position since the time-averages amount of particles reaching the substrate is constant. It is believed that this kinetic energy is the major fact responsible for this heating process due to the adatoms relaxation and recombination at the surface of the substrate [148] [146] [121] [147]. Also, a higher energy of the particles means that more of them will reach the substrate for a given pressure.

As a complement, the modification of this coefficient by modifying frequency and pulse width has been assessed. In both situations, the temperature rise is lowered for higher values; which results in a quasi-linear diminution of the coefficient (i.e. energy flux) with the duty-cycle as follows:

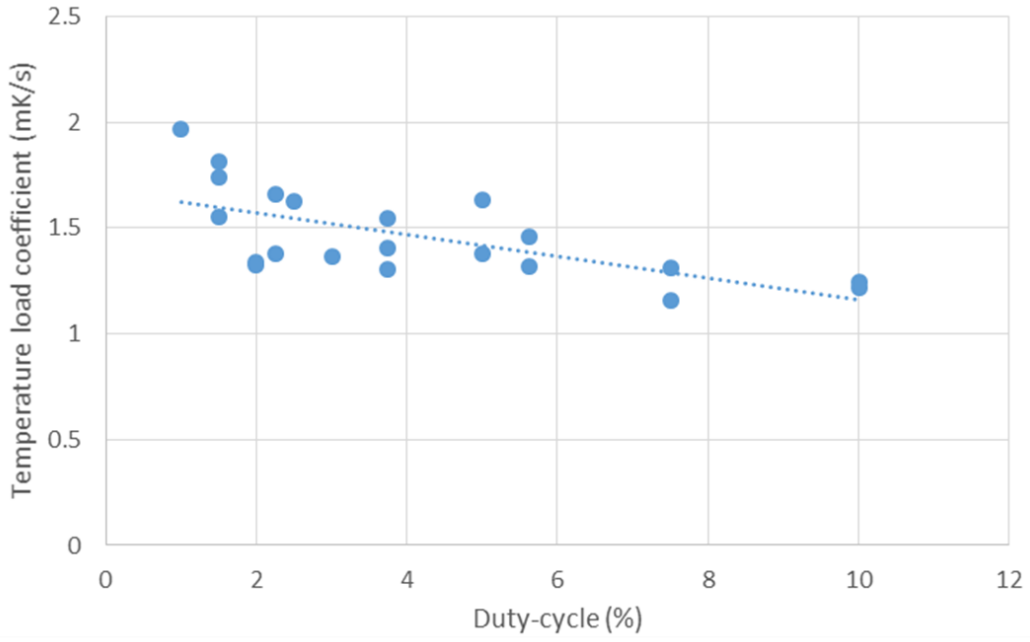

Figure 57. Modification of the temperature rise coefficient as a function of the duty-cycle of the voltage signal

This graph confirms the previous observation. Indeed, it is known that for lower duty-cycles, the voltage must be raised to keep the time average current intensity constant and since the previous data (cf. Figure 57) showed a direct relationship between the voltage and the temperature rise, it is normal to see a diminution of the coefficient for greater duty-cycles. This time, the fact that the effective sputtering time is enhanced at higher duty-cycle is insignificant compared to the voltage consequences. It confirms the idea that the energy of the ions and energetic neutrals is most likely to be responsible for the heating at the substrate position. In consequence, pulse width and frequency do not directly influence on the thermal load; they do it through the voltage.

III.3. Modification of the cathodic current intensity and waveform by the first order parameters

This section sums up the result obtained when modifying the discharge through the first order parameters of our study, in terms of cathodic (i.e. target) current intensity. This specific part of the study is very important for various reasons. The main reason is that, as previously said repeatedly, the deposition of thin films using PVD relies on a complete understanding of the discharge if the results want to be fully understood, controlled, and duplicated in other conditions. It is important to understand what are the physical discharge processes changes leading to the improvement of the deposited material. If the discharge is understood in its details, the experimenter can face any situation, by its understanding. If we go further, it is even possible to say that he needs to fully know what each parameter will do in the specific configuration used for its project before being able to improve the characteristics of the material he is trying to deposit. It is also by understanding what each parameter modification brings to the discharge characteristics that results can be duplicated. Indeed, the scaling-up or, in a more general way, the transition from one deposition configuration to another (e.g. rig, power supply, pump, target, etc…) can only be fully effective (and most of time simplified) by looking at the plasma itself, and not just the deposition parameters.

Studying the metallic mode before anything else is of great importance as it will permit to differentiate the effects of metal, argon, and oxygen particles during deposition and ease the analyses of the oxide mode. The objective is to clearly differentiate the two modes (i.e. metallic and oxide) and thus reduce the amount of information necessary for the *theoretical* explanations and the optimization phase of the deposition process.

The cathodic current intensity is a complex entity. Indeed, it is a consequence of the 1st order parameters but it is used as a basic parameter quite often in the literature. However, the variation of the intensity always implies the variation of a 1st order parameter and since each 1st order parameter has a different influence on the plasma, caution should be taken on which parameter is used and what are the other implied consequences.

III.3.1. Metallic mode

III.3.1.1. Voltage

III.3.1.1.1. On the current intensity

The first and more intuitive parameter that has a direct consequence on the cathodic intensity is the voltage applied to the target. It has been seen earlier in the literature review that an increased voltage is responsible for a rise in the ionic content and therefore the cathodic current intensity (cf I.1.5.1). Indeed, it is known that an increased voltage raises the ionization rate of the plasma and thus the sputtering rate. Since the cathodic current intensity reflects the number of ions reaching the target surface, it is expected to observe a rise in the current intensity at higher voltages. Figure 58 represents the time-averaged current intensity as a function of the target voltage for different conditions (but constant duty-cycle). It should be specified that the time-averaged current intensity is used here as the waveform changes with the pulse width and therefore, the latter do not make much sense here. Also, the power supply limit is a time-averaged current intensity limit, not a peak value limit.

The first observation that can be made is that the cathodic current intensity is directly proportional to the voltage applied. Limits are however observed at both extremities of the time-averaged intensity representation. They are due to plasma stability for low voltages and power supply limits for high intensities. Indeed, for low voltages, a discharge can be created but some of the ions cannot acquire enough kinetic energy to sputter the substrate; just enough to sustain the plasma at the target vicinity (0,0/0,1 A). Indeed, if the applied voltage is not sufficient, the ions are not energetic enough to escape the *electric trap* of the magnetron (i.e. cathodic sheath) and a weak plasma is created in the preferential ionization zone but the bulk plasma is not fully created. The plasma appears to be purple instead of blue for a relatively long range of voltage until it reaches its critical voltage (i.e. complete ignition of the discharge, sputtering possible). Then, once the critical value is reached, the current intensity is directly proportional to the target voltage since it can be considered that most of the

ionized particles of argon are reaching the cathode and the only thing the voltage is modifying is the ionization rate within the plasma.

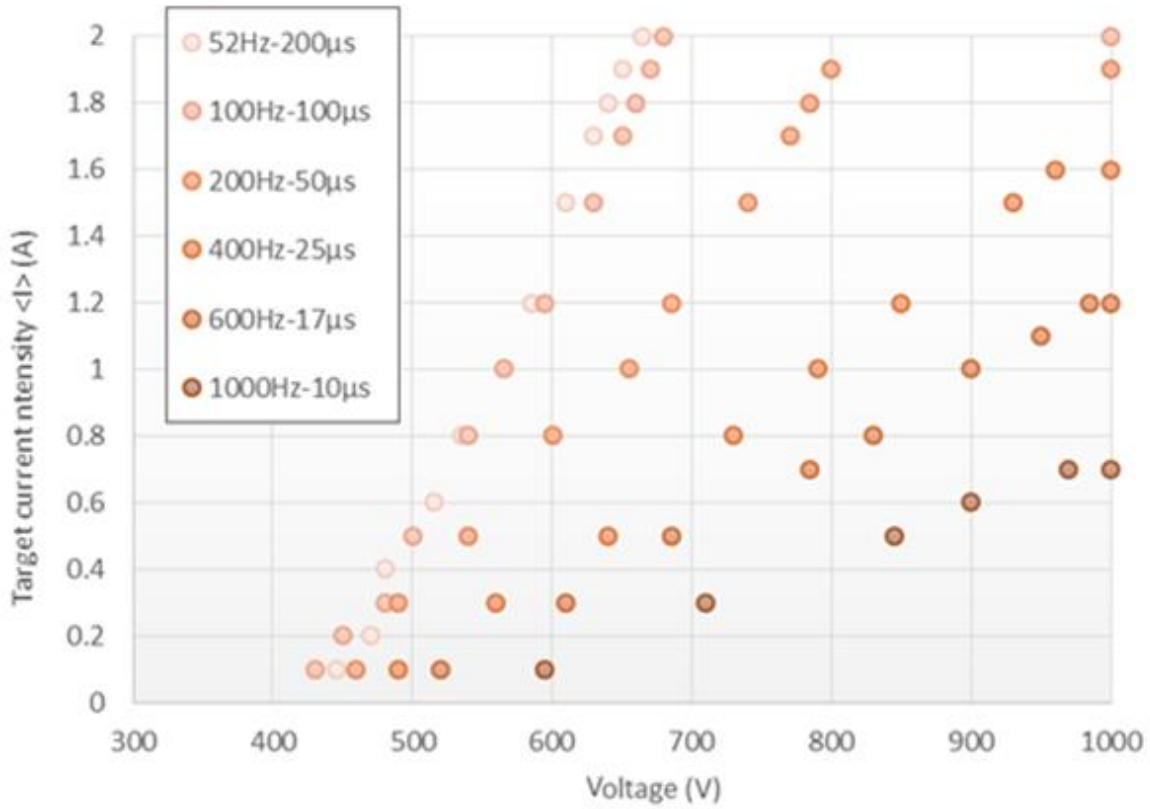

Figure 58. Influence of the frequency and the pulse width on the <I>=f(U_{max}) curves (duty cycle: 1% / Pressure: 2mTorr)

For higher voltages, the time-averaged intensity sometimes saturates at a value of 2 Amperes. The reason for this specific value is due to a physical limit of the power supply (i.e. probably its internal capacity). Therefore, this saturation is an artefact coming from the power supply: it does not accept average intensity superior to 2 Amperes. The voltage is then kept constant to the value corresponding to the 2 Amperes current intensity limit even if higher voltages are required by the user. In some other cases, the current is saturating to a lower intensity value. The reason why is explained further in this report (limitation of ionization rate [i.e. slope of the pulse] reduces the possible amount of ions created during short pulses) (cf III.3.1.2).

Concerning Ipeak, the relationship is direct: at given pulse width and frequency, the relationship is linear as seen on the following graph (Figure 59). Again, this is due to

the fact that a higher voltage corresponds to a higher ratio of ionized particles and thus a higher quantity on ions reaching the target (before rarefaction occurs). The frequency and pulse width values have been set in a way that the plasma stays stable at low and high intensities (no arcing).

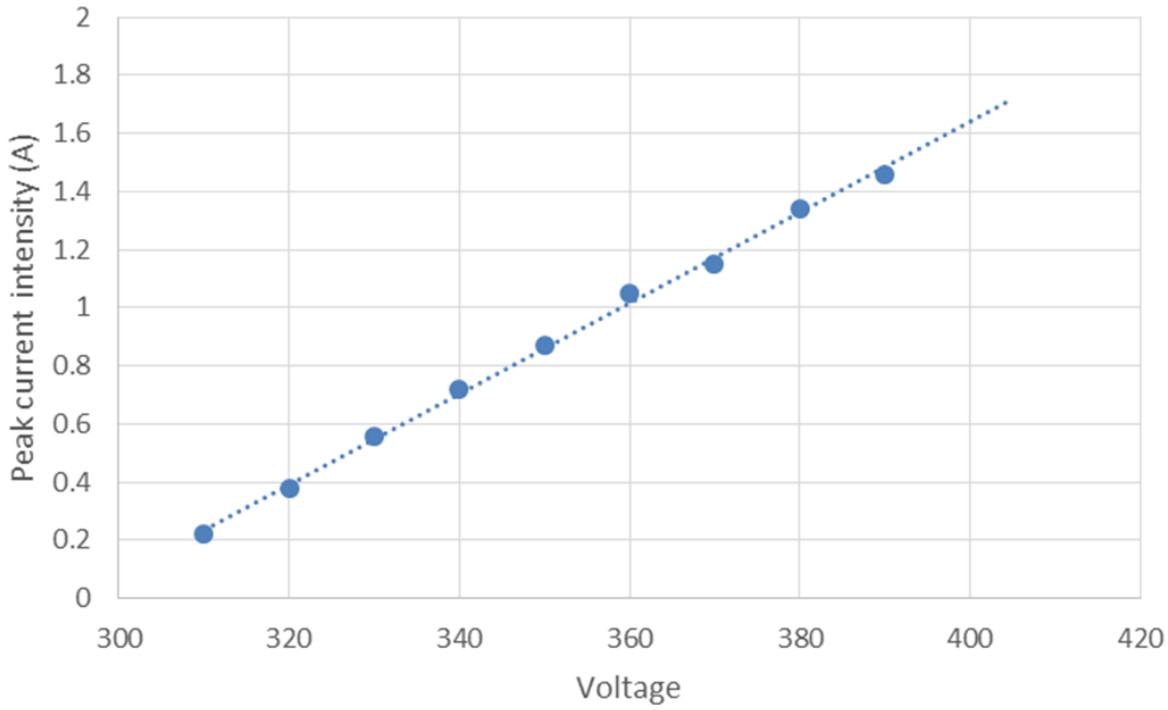

Figure 59. Cathodic current peak intensity as a function of the applied voltage (150µs – 500Hz – 3mTorr)

III.3.1.1.2. On the pulse waveform

When looking at one parameter's influence on the discharge, or more specifically on the cathodic current intensity here, the sole value of the time-averaged or peak current intensity are not sufficient. This is very important. In the work presented in this thesis, it is strongly believed that the only peak current intensity and the time-averaged values are not sufficient to lead to any conclusion, except in some cases. Indeed, for some situations, these values are sufficient to reflect the changes of the discharge but most of the time, it hides the fact that the pulse profile is modified along with the parameter modification. This needs to be kept in mind for all parameter's influence studies carried in this chapter: the waveform must be studied, not only the peak current intensity (nor the time-averaged

current intensity). The latter can however be an easier indicator in some cases. The remarks made in this paragraph are even more important when studying reactive plasma.

In this section, the effect the voltage can have on the metallic discharge is observed and analysed. The voltage has been increased from its minimal value to its maximal value in a given set of conditions. Below the minimal value, the plasma switches off and the maximum value correspond to the power supply limit (i.e. <I> = 2.0 A). The evolution of the waveform has been repeated for 3 different wavelengths: 50, 100 and 200 µs. The frequency is the same in all three cases and thus needs to remain low so the duty-cycle do not reach too high values. The chamber pressure is also the same for the three figures; it was kept low (i.e. 3 mTorr) to allow a larger range of applied voltage between the two limits and ease the observations. The results are shown in Figure 60, Figure 61 and Figure 62.

In each figure, the lowest voltages are represented by lighter blue while the higher voltages are represented by darker blue. The precise identification of each profile with its corresponding (absolute) voltage value is more difficult but is also not necessary as the importance here is to determine what the increase of the voltage does to the waveform: a qualitative work, not quantitative. It is not relevant to say that to a given voltage corresponds a given waveform (and the characteristics coming with it) as it would not be a constant observation: the slightest change in any of the 1st order (or the order 0) parameters would change this specific value. Again, the remarks done here are also very important and should be kept in mind in any of the waveform evolutions presented in this chapter.

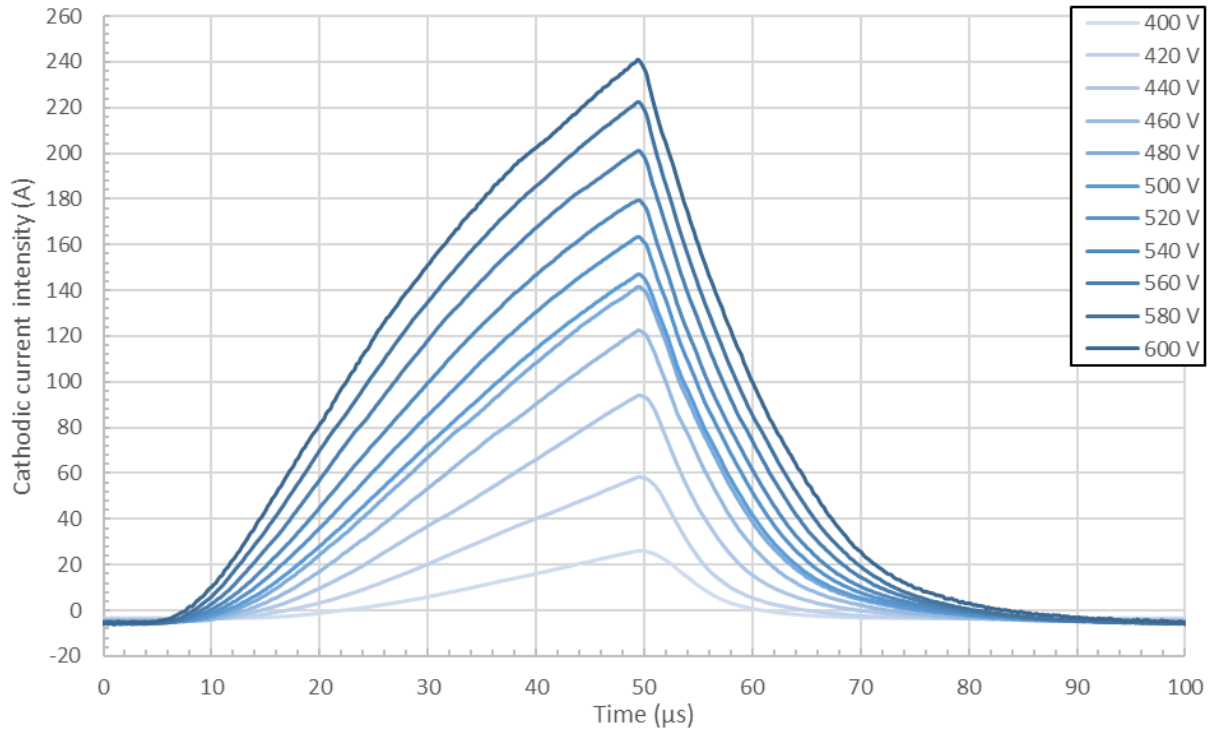

Figure 60. Evolution of the metallic pulse waveform with the increase of the applied voltage for a 50 µs pulse width (3 mTorr – 300 Hz – 50 µs – 0.0 sccm)

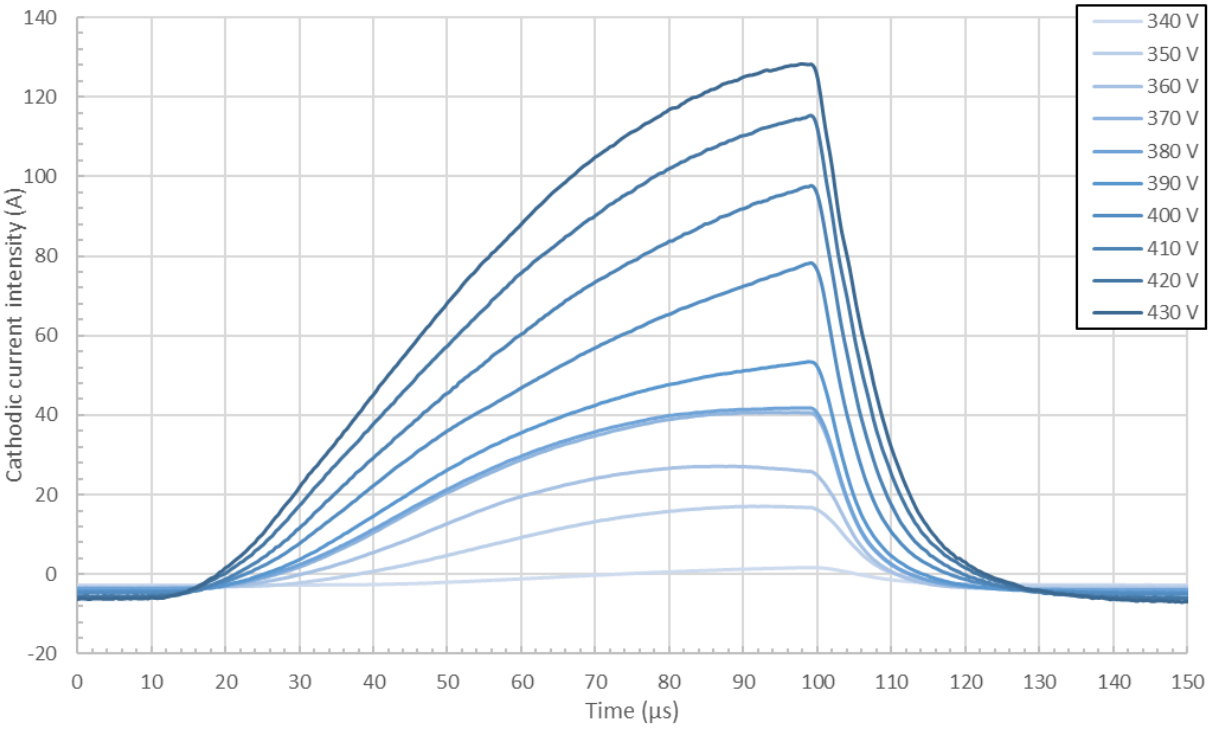

Figure 61. Evolution of the metallic pulse waveform with the increase of the applied voltage for a 100 µs pulse width (3 mTorr – 300 Hz – 100 µs – 0.0 sccm)

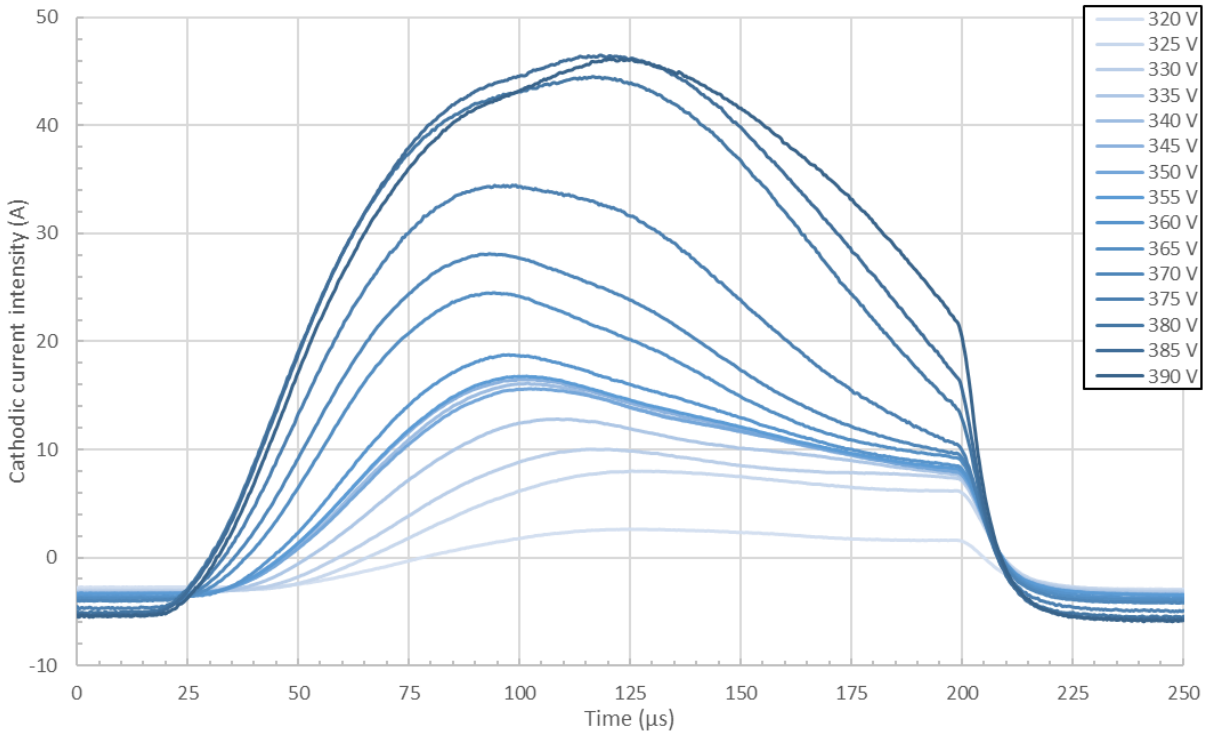

Figure 62. Evolution of the metallic pulse waveform with the increase of the applied voltage for a 200 µs pulse width (3 mTorr – 300 Hz – 200 µs – 0.0 sccm)

The observations from the three figures should be separated has they all correspond to a different state of the plasma but two observations are common to all three figures: the overall pulse intensity increases with the increase of the applied voltage, while the ignition delay decreases for each increase of the applied voltage. Indeed, for the first observation, at each step of the voltage increase, the slope of the profile increases due to an easier ionization of the species and a higher sputtering rate, resulting in a higher current intensity. For the second observation, the increase of the ignition delay with the diminution of the voltage is a result of the diminution of the ionization cross-section when the applied voltage is diminished. Indeed, if the applied voltage is more important, the ionization of the argon atoms is more likely to be happening sooner after the application of the cathodic voltage. These species then start the cascade reaction resulting in the (partial) ionization of the gas in the chamber and thus the ignition of the discharge. Also, after the end of the pulse, the current intensity decreases sharply as the sputtering stops and the charged species recombine in the chamber. It is clear to see that the more intense the pulse is, the longer it takes for the species to recombine in the chamber.

Concerning the evolution of the waveform itself, the observations are different for *short* and *long* pulses width. Indeed, for the short pulses (i.e. 50 µs and 100 µs), Figure 60 and Figure 61, show that the changes in the profile are close to be negligeable in these cases. Indeed, for each voltage, there is only a monotonic increase of the current intensity until the end of the pulse, with no *rarefaction point* observed. The rarefaction point refers to the moment when the pulse current intensity reaches its maximum value and starts decreasing until the end of the pulse. It is possible to see this rarefaction point on Figure 62.

The appearance of the rarefaction process changes the analysis. Now, the increase of the voltage also changes the pulse profile, in opposition to what has been observed previously for short pulses. Indeed, the evolution of the pulse shape with the voltage can be separated in two. First, the rarefaction point occurs sooner with the increase of the voltage. It reflects the fact that at lower voltage, the quantity of ions reaching the target is lower and thus, it takes more time to saturate the target vicinity in metal ions and *push away* the argon ions. The details of the rarefaction process are given in I.1.4 and should not be discussed any further here. The second evolution is the appearance of a second *bump* on the profile. This second peak is believed to be the self-sputtering phase, where a large amount of metal ions sputter the target, along with some argon ions as well. However, the absence of a mass spectrometer here leads to the impossibility of confirming this hypothesis. What should be reminded from this study is the fact that the voltage can lead to a change in the discharge characteristics, and especially for long pulses.

III.3.1.2. Pulse width

It has been shown previously that the maximum reachable time averaged cathodic current intensity ($<I>_{max}$) is sometimes lower than the machine limit (cf Figure 58). In these cases, the causes are believed to be both pulse width and ionization rate limitations, meaning that the plasma is the limiting factor, not the power supply.

The hypothesis is that the ionization rate is limited for each set of deposition conditions (i.e. constant frequency, voltage and pressure) and therefore is the *slope* of the current rise; which limits I_{peak} for a given pulse width. Indeed, it is logical that the

ionization rate is limited for given conditions. Several works have been conducted to show its modification by other parameters (see I.1.5) and even if the ionization rate has been shown to be modified by the deposition conditions, there is always a limit. This limit is due to the energy and the quantity of particles contained within the plasma (mainly consequences of pressure and voltage). Moreover, on the oscilloscope, the number of ions generated per unit of time (ionization rate) is reflected by the slope of the pulse shape (region 2 of Figure 15). Therefore, this slope has a limit, consequence of the plasma properties, which explains the limited <I> for shorter pulse widths.

The following graph (Figure 63) shows how the pulse width modifies the pulse shape and I_{peak}. Contrary to what could be expected, the peak intensity diminishes after a certain critical pulse width. Normally, it is expected to stay constant and to correspond to the maximum intensity reached before the rarefaction appears, around 100 µs. Since all the other parameters are kept constant (pressure, voltage, frequency, etc…), there should be no reason to see this maximum value changing although the pulse is longer than this critical width. This diminution of the pulse intensity for longer pulses can be due to either a power supply artefact or the augmentation of the duty-cycle. The second reason would be explained by the fact that at higher duty-cycle, the *refill time*/*sputtering* ratio is lowered and there is a lack of available particles during the on-time of the pulse. It is therefore impossible to determine which of these two options is true; and it could also be a combination of both.

Firstly, there is a possibility that the power supply reduces the intensity independently from the experimenter control. In this case, it would be an artefact from the power supply due to its internal capacity limit: the power supply would not be able to receive these many electrons at the same time. To reduce the number of electrons, the power supply would either slightly reduce the voltage or evacuate the electrons in the form of heating due to the Joule effect –in which case it cannot be confirmed with the rig configuration used here.

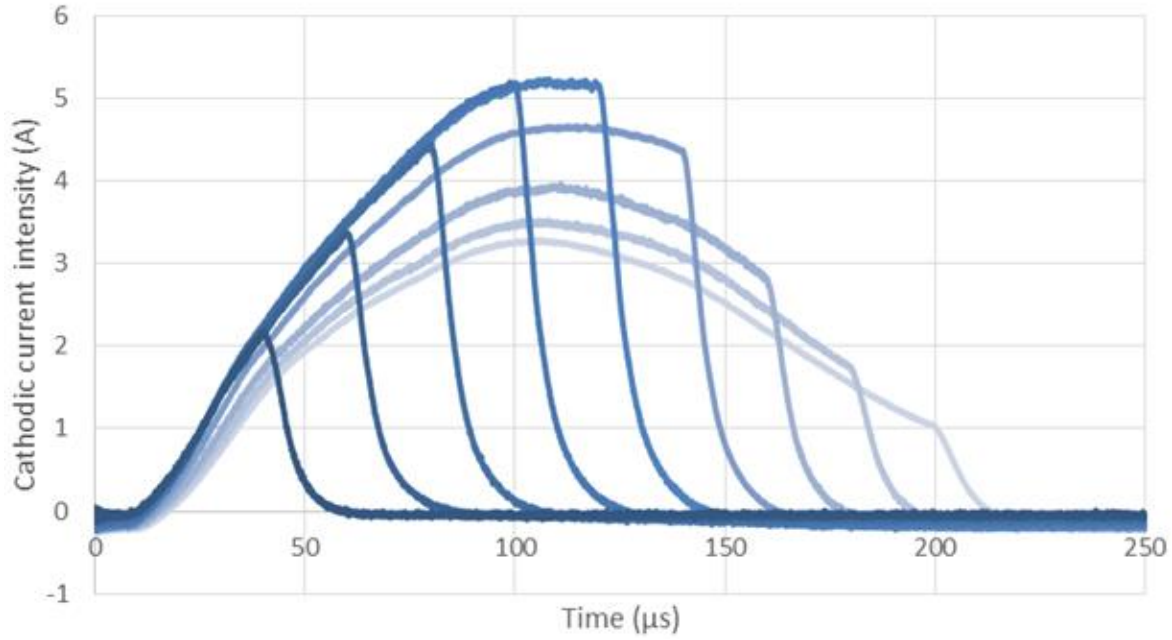

Figure 63. Influence of the pulse width modification on the current-time profile of the pulse (300Hz - 3mTorr – 435V)

Otherwise, if the power supply is not responsible for it, another explanation can be proposed. It could be because when the pulse width is increased, the duty-cycle follows; which means that the refill time is lowered. If the refill time is too short, fewer particles are available for ionization when the voltage is applied again for the next pulse and thus, the ionization rate of the plasma is diminished (cf I.1.2.2). Indeed, for longer pulses, more ions are used in the sputtering of the target and the rarefaction effect pushes the argon ions away from the target. These ions are then more likely to recombine and lose their energy during the off-time. It results in less Ar^+ available for the next pulse, and therefore difficulties in the ionization/sputtering process. It can then explain a slower rise of the cathodic current intensity (i.e. less positive ions reaching the substrate). The fact that there are less ions reaching the target and that their ionization rate is lowered can explain a diminution of the maximum current intensity reachable for a given time (before rarefaction occurs), as explained earlier. Plus, the fact that this phenomenon seems to start occurring when the pulse is long enough to see the rarefaction occurs means that it appears when the argon particles have already mostly been used to sputter the target; which could confirm the idea.

III.3.1.3. Frequency

This section concentrates on the effect of the frequency of the metallic discharge and more specifically on the modification of the pulse profile. Here, the observations are different to the other parameters: no clear evolution trend can be identified. It does not mean this influence is not important; it is the opposite.

All three figures show constant evolutions, even though one might spot a slight overall diminution of the signal with the increase of the frequency. However, the frequency range is very large, from 200 to 1000 Hz, corresponding to a factor 5 between the lower and the higher frequency, and the change in the (peak) current intensity remains below a 0.2 factor in each case. This makes it a very negligeable diminution, as compared to the other parameters influences (e.g. voltage and pressure). It means the frequency modification does not consequently modify the discharge physics and the processes occurring, in opposition to parameters like the oxygen content, the voltage, or even the pulse width. It changes the duty-cycle of the process, but barely the pulses themselves. The only observable effect on the pulse shape itself is the ignition delay for low frequency on Figure 66. It is due to the recombination process of charged species in the chamber, already evoked previously in this thesis (cf. I.1.2). The slight diminution of the signal with the increase of the frequency is believed to be due to the remaining electronegativity of the system increasing with the duty-cycle. Indeed, a population of negative charges in the chamber would result in a diminution of the signal and here, on all three figures, even the off-time signal is lower (in the negative) when the frequency is higher. It means that at higher frequencies, more electrons remain trapped in the target vicinity.

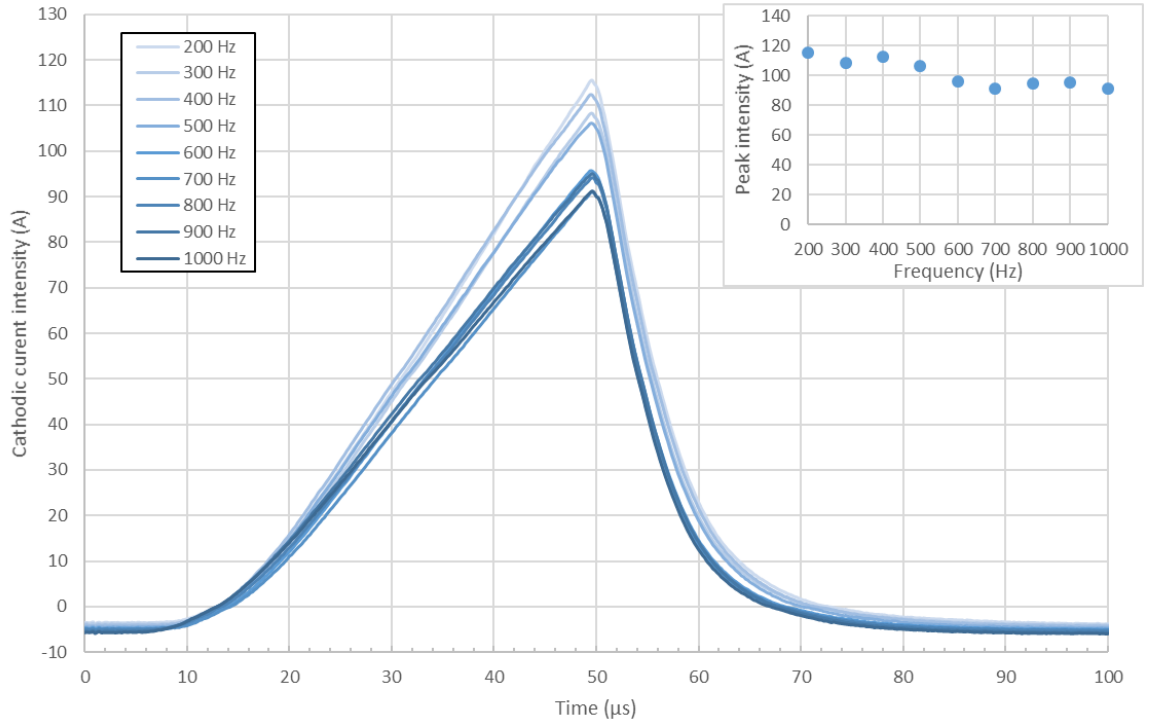

Figure 64. Evolution of the pulse shape and the peak current intensity by modifying the pulsing frequency of the system for 50 µs long pulses (3m Torr – 50 µs – 430 V – 0.0 sccm)

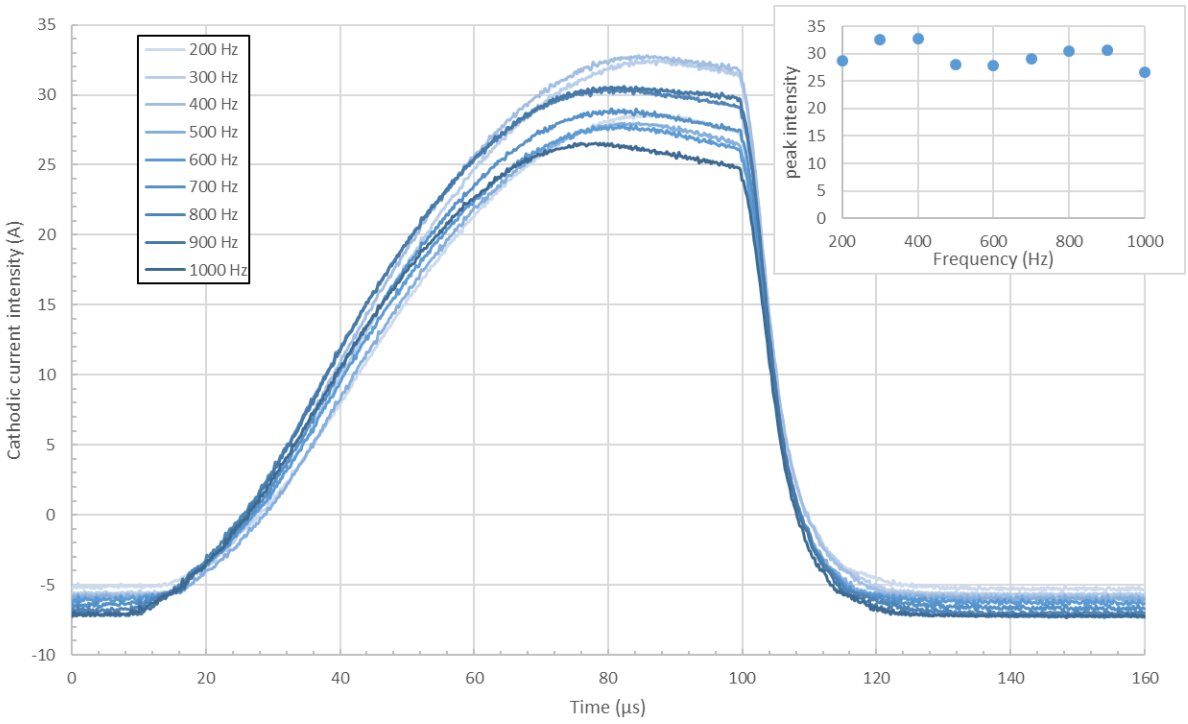

Figure 65. Evolution of the pulse shape and the peak current intensity by modifying the pulsing frequency of the system for 100 µs long pulses (3m Torr – 100 µs – 380V – 0.0 sccm)

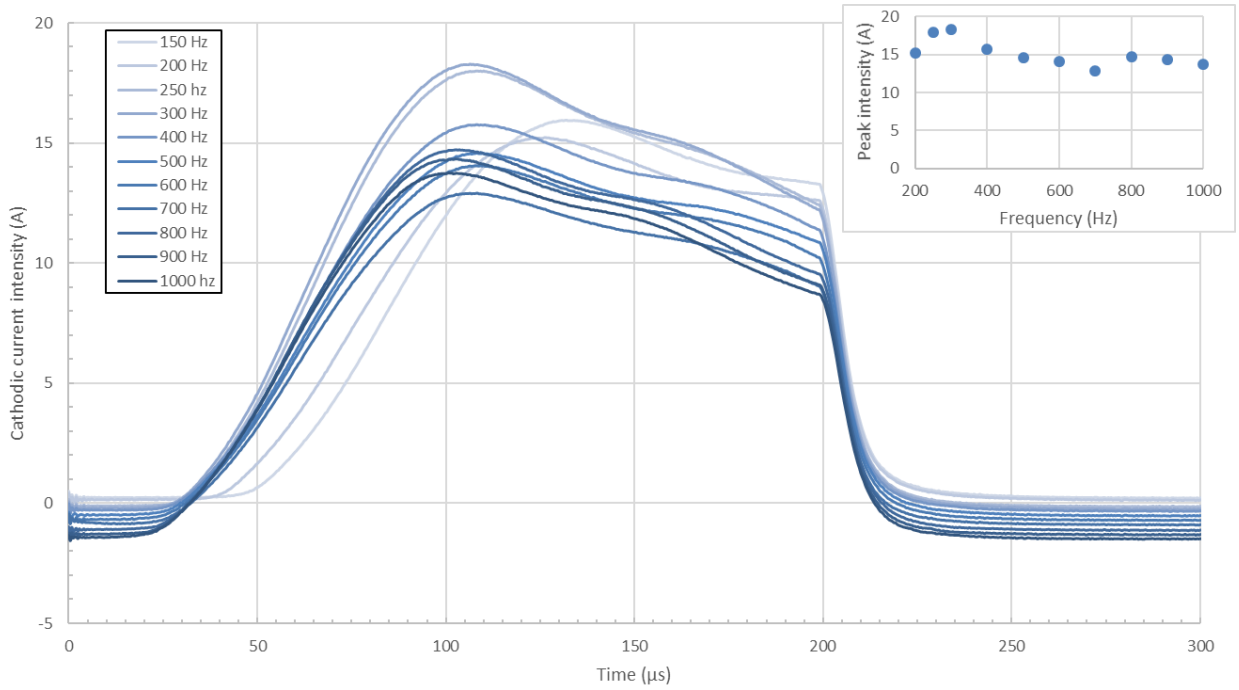

Figure 66. Evolution of the pulse shape and the peak current intensity by modifying the pulsing frequency of the system for 200 µs long pulses (3m Torr – 200 µs – 330 V – 0.0 sccm)

III.3.1.4. Pressure

An augmentation in the pressure within the chamber during the deposition time is well-known to be responsible for the cathodic current rise. Indeed, a higher pressure means that more particles are present in the chamber and are available to generate ions and take part in the sputtering process. It is then normal to see the target current intensity rising for higher pressures. Since the ions are mainly generated in the target vicinity, the mean free path stays the same order of magnitude as the distance separating the ionization region and the target's surface; it explains why no effect of too high pressures (i.e. loss of energy too important by inelastic collisions) can be spotted for the cathodic current intensity and why the peak intensity to pressure relationship is linear as shown in Figure 67.

It should also be specified that atoms do not count in the target current intensity since they are neutrals. It means that even if the amount of ions reaching the target is changed, it does not necessarily imply that the total amount of particles (i.e. including neutrals) follows.

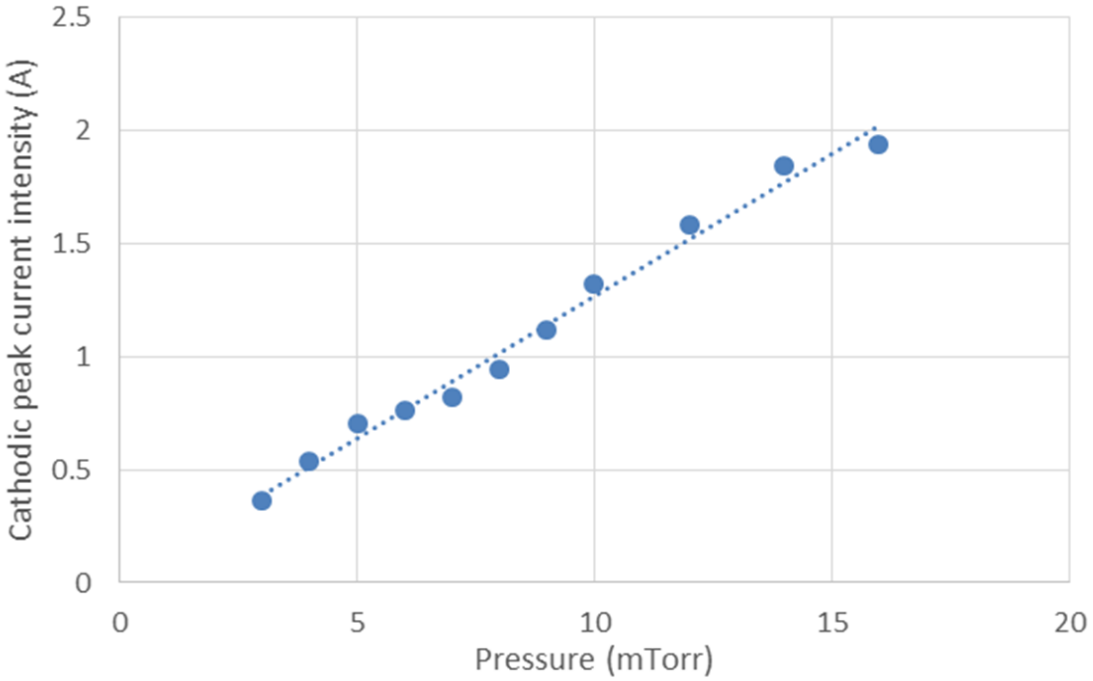

Figure 67. The relationship between the peak current intensity and the atmospheric pressure in the chamber (150µs – 500Hz – 320V)

III.3.1.5.Target-to-substrate distance

A study has been conducted to determine if the gap width between the substrate holder and the target has any influence on the plasma. The only way available to do it in this project is the measurement of the cathodic current intensity profiles on the oscilloscope. This means that the only effect that could be observed when the substrate holder position is changed is the appearance –or not- of an acoustic wave. However, since the substrate holder dimensions are negligeable compared to the deposition chamber, no clear acoustic wave has been identified from the oscilloscopes profiles. The only configuration where the current intensity is drastically changed is when the shutter is positioned in front of the target (d = 25mm). In this case, it is due to the proximity between the two surfaces of the same dimension, which results in a virtual reduction of the chamber dimension. It leads to a densification of the plasma and thus an acceleration of the processes occurring within this latter. It is not yet possible to extract precise values of these variations but an augmentation of roughly 25% of the maximum current intensity

and a reduction of roughly 20% of the time needed to reach the maximum intensity have been observed in some cases.

III.3.2. Reactive gas content

The insertion of a reactive gas (nitrogen, oxygen, etc…) modifies the plasma composition and thus its characteristics. The direct effect is the change of the ions created within the chamber, their number, their ionization levels and their kinetic energies. The second effect is the creation of a compound layer at the target's surface. The coverage proportion of this layer and its composition are responsible for modifying of the plasma. A simple way to observe these changes is through the shift in the light emission of the plasma. Indeed, since the new -reactive- species have different ionization energies, their relaxation emits at a different wavelength, resulting in a change of the discharge colour. It can be observed with the naked eye but also through an optical fibre, using the Speedflo® system described in II.3.2.

The changes in terms of gas composition during sputtering can be observed on another simple way: the modification of the pulse waveform. First, it should be reminded that for Ti-O discharges, the secondary electron emission of the compound layer is lower than that of the metallic surface. It implies that the plasma faces more difficulties to sustain itself. It is then normal to see a drop of the average and peak cathodic current intensities when the target is fully oxidised and all the other deposition parameters are kept constant. More details on the modification of the sputtering process when injecting reactive gas can be found in section I.1.5.4.

III.3.2.1. Preliminary study

A first oxidation study, shown on Figure 68, presents the modification of the cathodic peak current intensity and the pressure along with the modification of the oxygen flux. However, it needs to be specified that this oxidation curve is the one obtained in one configuration, where the target has been fully *cleaned* in pure Argon atmosphere. The oxidation curves presented further in this chapter do not all have the same shape. Indeed, the sub-stoichiometric part can differ.

Here, at low oxygen flux, the oxygen atoms set in the chamber are not sufficient to create the oxide layer on the target. They are either not depositing on the surface because there are too many titanium ions in the latter's vicinity or either re-sputtered as soon as they are on the target's surface. However, these species generate more negative charges in the chamber which eases the ionization by inelastic collisions and this results in a cathodic peak intensity increasing (from 0.0 to 2.0 sccm on Figure 68). The pressure doesn't raise since most of added oxygen atoms are reacting with the target surface (but not necessarily changing its stoichiometry) and the chamber walls. Only the percentage of ions is changed, not the overall quantity of entities in the plasma; which explains why the current intensity rises, but not the pressure.

It could also explain why this slight increase of the current intensity at low oxygen flux is not always observed and seem to disappear when the chamber walls are not *cleaned* for long enough. Indeed, for a shorter pre-sputtering time (metal mode), more oxygen ions remain in the chamber (walls), even if they left the target's surface. Therefore, as soon as the user inject oxygen ions, even in very low quantity, the latter cannot react with the walls anymore and thus start to change the target's stoichiometry (i.e. lower the current intensity). Also, it should be specified that the scale of the cathodic current intensity in Figure 68 is different to the scale of figures in III.3.5. Indeed, here, the axis starts at a higher value, to *zoom in* the curve when, in III.3.5, the axis start at zero and therefore the curves appear flatter. This can contribute to the fact that some curves can appear flat when, in fact, they also show a 10-20% increase in the sub-stoichiometric region.

After a certain point, the oxygen flux is sufficient and the nucleation at the target surface begins: oxygen atoms bond with the surface atoms of the target to create a Ti-O compound. It corresponds to the sharp diminution in the peak intensity observed on Figure 68 until a minimum intensity is reached. The pressure in the chamber starts to increase in the same time. This transition is analysed in more details in Figure 70.

From there, the graph shows that the peak intensity starts to raise again, slowly, with the increase of the oxygen content. This raise of the peak intensity is due to the augmentation of the pulse curve's slope. This means that ions are generated more efficiently. The explanation behind this behaviour is that once this layer is created, the

additional atoms of oxygen are contributing to an over-saturation of the surface. These additional atoms injected in the chamber therefore slightly raise the secondary electrons emission (O^{2-}) and thus the electronegativity of the plasma. Also, the augmentation of the intensity with the amount of oxygen is slow and could be explained by the fact that this over-saturation is not easy, from an energetic point of view, and would thus confirm this hypothesis.

The change in pressure confirms it: the excess of oxygen beyond the fully oxidised mode raises the pressure in the chamber, as all the walls are saturated and they cannot react with the saturated target anymore. This excess results in a denser bulk plasma, and therefore an increase of the peak current intensity after the transition (i.e. 2.4 sccm and more).

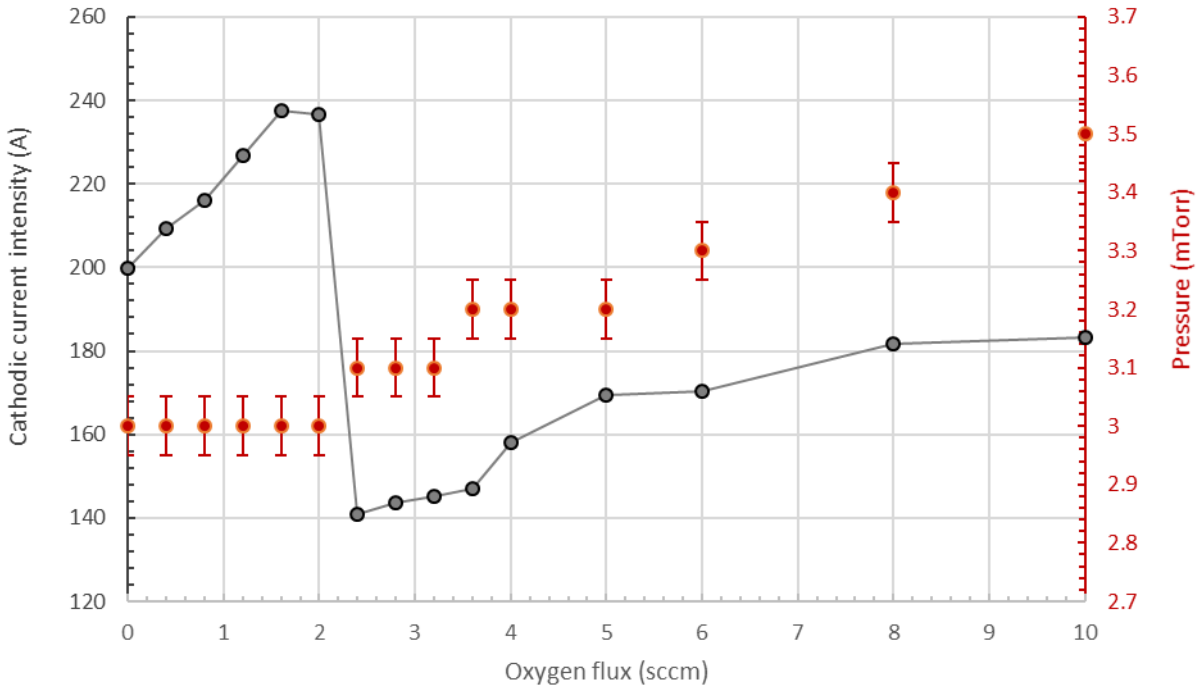

Figure 68. Oxidation curve presenting the evolution of the peak intensity and the pressure with the increase of the oxygen content in the chamber for a short pulse (480V – 1000Hz – 50µs)

III.3.2.2. Transition study

In this section, the objective is to observe this sharp transition in more details and to see how each one of the other deposition parameters could influence the latter. To

observe the transition in more details, different techniques have been used: a more precise increase of the oxygen content, a time evolution at constant oxygen flux or even a combination of both. This way of proceeding is very useful to observe the transition from the metallic to the poisoned mode in more details. First, the study has been carried out for short pulses. For the results shown in Figure 69, the voltage, the frequency, the pulse width and the pumping speed have been kept constant along the whole transition to observe the only effect of the oxygen content and nothing else.

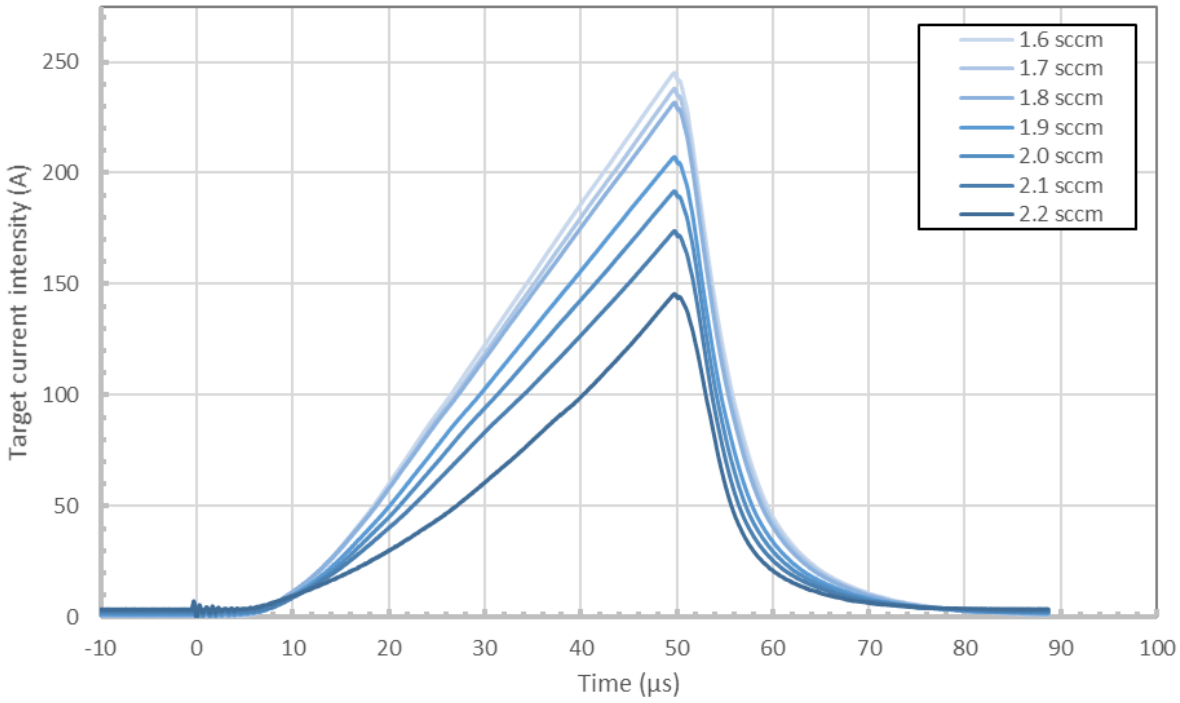

Figure 69. The transition from the metallic to the poisoned mode observed in more details for short pulses (480V – 1000Hz – 50µs – approx. 3 mTorr)

Figure 69 shows that transition from the metallic to the oxidised mode in more details by showing the evolution of the waveform for slight increases in the oxygen flux. It does not show the sub- and over-stoichiometric evolutions. For each step, the system has been given around 1 minute to stabilize, which is sufficient, according to the plasma light emissions. This figure shows that the transition can be smoothed, by a precise control of the oxygen flux in the chamber. The observed transition shows an overall diminution on the discharge intensity and when looked at it in more details, it reveals a change from a convex pulse shape (metal mode) to a concave pulse shape (oxide mode). The details of the physical reasons behind this change are not known and cannot be

confirmed with certainty due to a lack of analysing material available for this project. However, the diminution of the discharge intensity is a well-known process observed in the literature as reported in I.1.5.4.

The change in the pulse shape could however be explained by the presence of oxygen in excess in the chamber. In the early stages of the pulse, the sputtering process is slowed down, due to the presence of these additional oxygen atoms in the chamber. Later during the pulse, the generation of ions and electrons (and thus the sputtering rate) are eased by the presence of the oxygen ions (not atoms anymore). In summary, it can be said that the presence of oxygen in excess in the chamber makes the discharge ionization *delayed* but once all the species are ionised, the sputtering of the target and the generation of secondary electrons is enhanced.

Again, this explanation cannot be confirmed here as it would require the study of the discharge with a mass spectrometer; which would provide information on the species in presence during the pulse, and more importantly, the timing of their ionizations. Some papers can be found in literature on this subject and they all seem to confirm the hypothesis made above.

Also, it needs to be specified (or remembered) that the pumping speed is kept constant, not the overall pressure. Therefore, the pressure can change in the chamber when the gas content is increased. In fact, Figure 68 shows that for lower gas content, the pressure stays constant until the transition point is reached, after which, the pressure slightly increases with the augmentation of the reactive atoms flux.

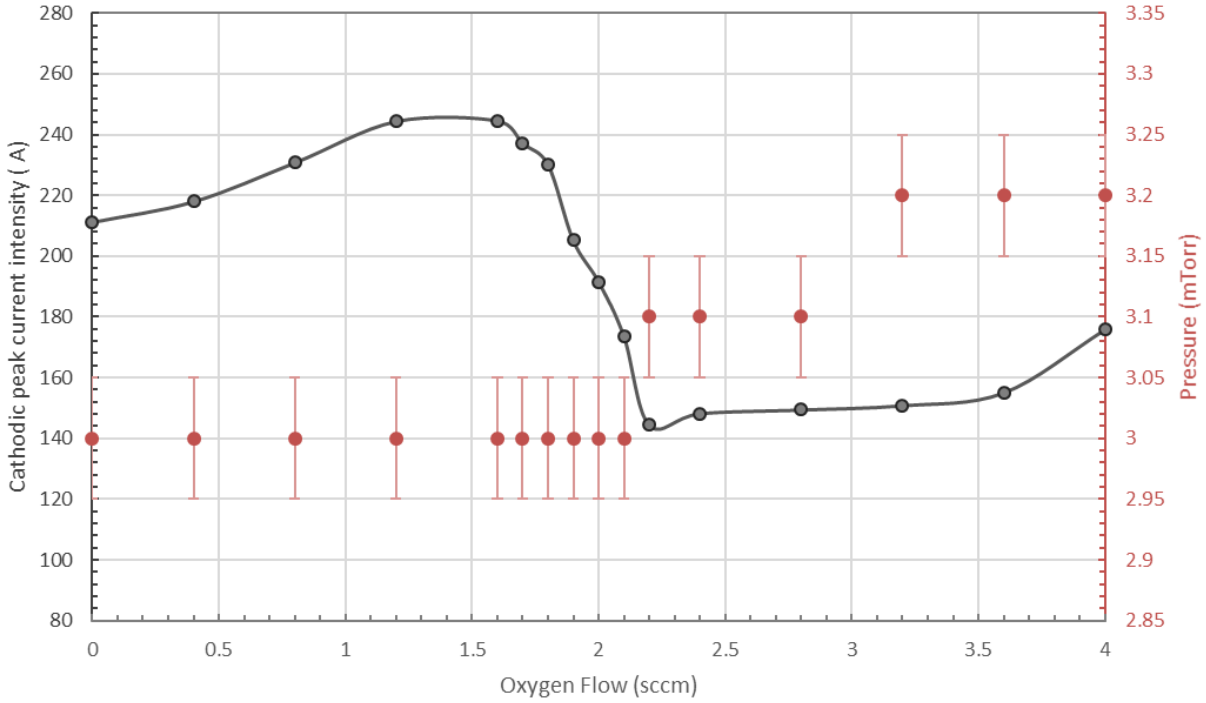

Figure 70. Transition study of the discharge with more precise oxygen content management presenting the evolution of the peak intensity and the pressure with the increase of the oxygen content in the chamber for a short pulse (480V – 1000Hz – 50µs)

When looking at Figure 70, where the details of the transition are magnified, even if the pressure measurement is not very accurate, it suggests that the pressure starts increasing once the poisoned mode is reached, and not during the transition itself. This additional information goes along with the hypothesis made in III.3.2.1. Indeed, this behaviour means that the injected atoms are all *used* in the creation of the compound layer. From 1.6 sccm of oxygen (in this case), the oxygen is sufficient to start the nucleation process on the target but it is only once the whole target is covered that the pressure starts to increase (slightly), reflecting the fact that the oxygen added from that point contributes in the increase of the chamber pressure and the electronegativity of the discharge.

III.3.2.3. Long pulse study

Studying long pulses is much more complicated with the installation used in this project. The reasons are multiple. First, and mainly, the fact that the power supply has a relatively low current limitation (for such a large target) is very disruptive as, for long

pulses, it means the voltage needs to be kept low to allow a larger range of study. Indeed, for longer pulse widths, the duty-cycle increases and therefore a change in the pulse profile (e.g. peak intensity, ignition delay, overall aspect, etc…) has a greater impact on the time-averaged current intensity (i.e. the limiting factor). This leads faster to either the lower (i.e. discharge extinction) or the higher limit (i.e. power supply limitation) of the system. For the same reason, the frequency must be reduced as much as possible to be able to carry out the study.

The second reason why longer pulses are more delicate to study is the change of the pulse shape for longer pulses, as shown in III.3.1.2. Indeed, when the pulse widths go above ~100 µs, the rarefaction effect is observable on the waveform. This means there are new processes occurring in the discharge, and it has different consequences: the plasma is less stable, the sputtering time per pulse is increased, the peak current intensity does not necessarily correspond to the end of the pulse (and this is of great importance), etc… For these reasons, parallels with shorter pulses should be avoided as much as possible.

Following, on Figure 71 and Figure 72, oxidation evolutions of the waveforms for long pulses (both 100 and 200 µs) are shown. It illustrates what has been said above as the behaviour is completely different to the one observed for short pulses of 50 µs. On the figures, are also presented the evolution of the pulse peak surface to ease the spotting of the transition. The peak surface is calculated as the integration of the peak intensity over its duration.

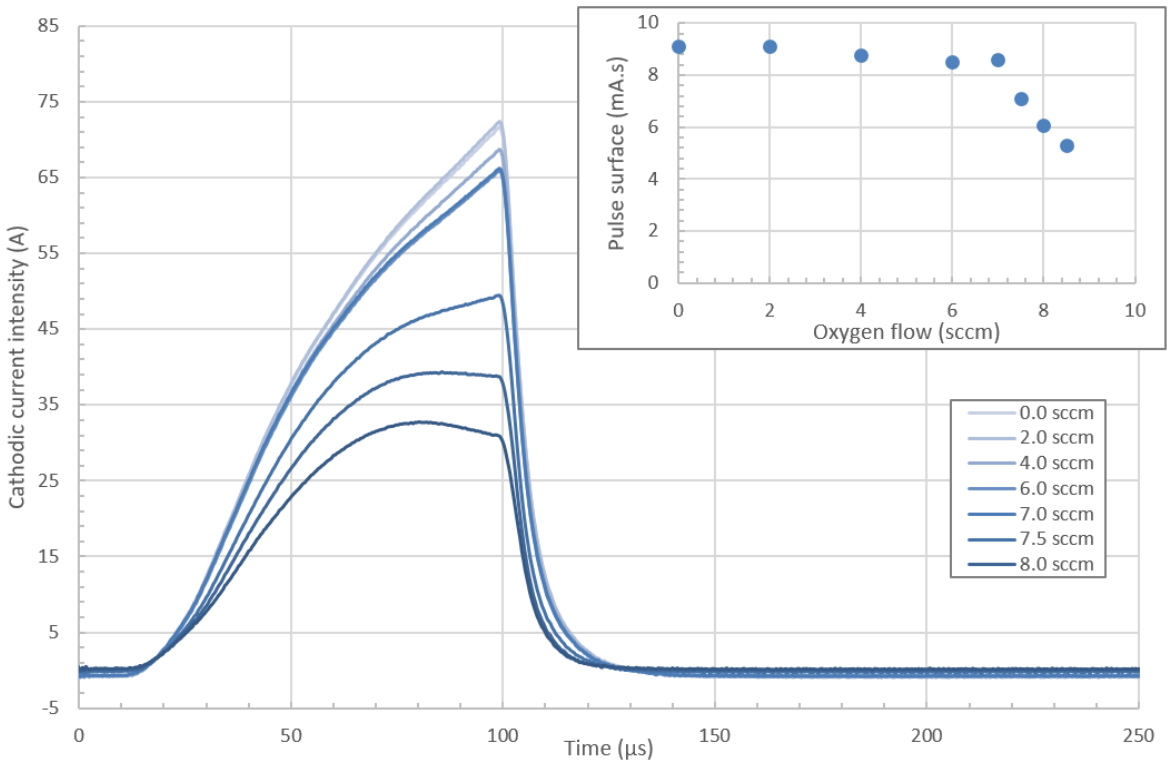

Figure 71. Evolution of the pulse waveform with the increase of the oxygen flow in the chamber for a 100 µs pulse width (3 mTorr – 500 Hz – 100 µs – 405 V)

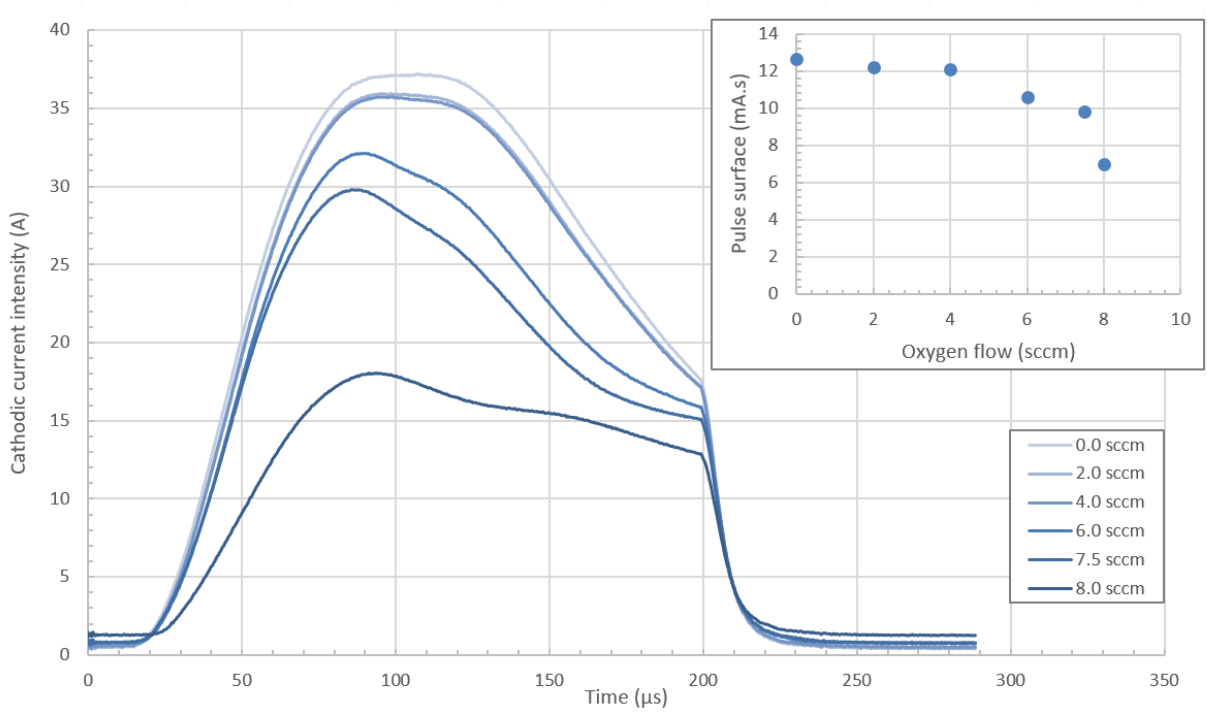

Figure 72. Evolution of the pulse waveform with the increase of the oxygen flow in the chamber for a 200 µs pulse width (3mTorr – 300Hz – 200µs – 390V)

The first observation that should be made is that pulses in the poisoned mode are not shown in the figures due to a diminution of the pulse intensity too important to keep the discharge on. Again, it should be reminded that all other parameters are kept constant for an integrity of the study, which means that voltage, pressure and frequency cannot be changed to maintain the discharge as it would change other aspects of the system, and not only the reactive gas content. However, what can be done, is to switch towards a current regulation: see III.3.2.4.

The second observation from Figure 71 and Figure 72 is a change in the early stages of the oxidation, when compared to short pulses. Indeed, Figure 68 and Figure 70 show an increase of the pulse intensity before reaching the transition point. Here, the slightest injection of oxygen atoms in the chamber results in a diminution (even if it is a small one) of the overall waveform intensity (in both cases). After a certain point, the diminution is more brutal and results in the switching off of the discharge, as previously stated. This time, it is not believed to be due to a difference in pre-sputtering time but mostly to the fact that longer pulses result in an enhanced reactivity of the gases with the target material. Indeed, at each pulse, all gas ions are used during the pulse.

III.3.2.4. Time-averaged current intensity regulation <I> = 2 A

Here, the oxidation study is carried out with a time-averaged cathodic current intensity regulation. What needs to be understood about this limit - and has already been explained in II.2.1 – is that it reduces the range of study for the observations made in most parameters influences studies. This means that the power supply imposes a limit in terms of time-averaged cathodic current intensity. For the generator used here, the value of this limit cannot be modified/chosen and is always equal to 2,0 A.

The mechanism is quite simple: if the voltage required by the user corresponds to a time-averaged current intensity above the 2 Amperes limit (measure by the power supply), the power supply automatically reduces the applied voltage to get to this limit. In other words, to work in current intensity regulation, a very high voltage is input (i.e. typically 800A or more) and thus, even though another parameter is changed, the power supply always applies a value lower than the one input to keep a constant intensity. It can be an increase or a reduction of the voltage. The study at constant current intensity is

very different to what is done at constant voltage and it is why, in this work, it is highlighted that both situations must be separated. The subject is discussed in more details in II.3.4

Figure 73 shows the evolution of the pulse profile when the oxygen content in the chamber is increased. As previously stated, this graph shows how different the *voltage regulated* and the *intensity regulated* cases really are. Here, the modifications the oxygen content can bring to the waveform are far from being as obvious as what has been observed on Figure 69. Indeed, since the duty-cycle remains constant as well as the average intensity, the pulse surface also keeps a constant value. It explains why it is quite hard to spot the evolution, because all the waveforms overlay each other on the first graph.

The second graph of Figure 73 shows only two waveforms: one from the metallic mode and the other one from the poisoned mode (when only these two waveforms are represented) it is easier to spot the difference in the shape. The transition is similar to the one observed on Figure 69: going from a convex curvature towards a concave curvature. Also, the voltage applied by the power supply to keep the intensity constant is higher (in absolute value) in the oxide mode (cf. Figure 74). It means the system needs a higher voltage to produce the same amount of charged species. This also goes along with the observation previously made: the system struggles more in the oxide mode.

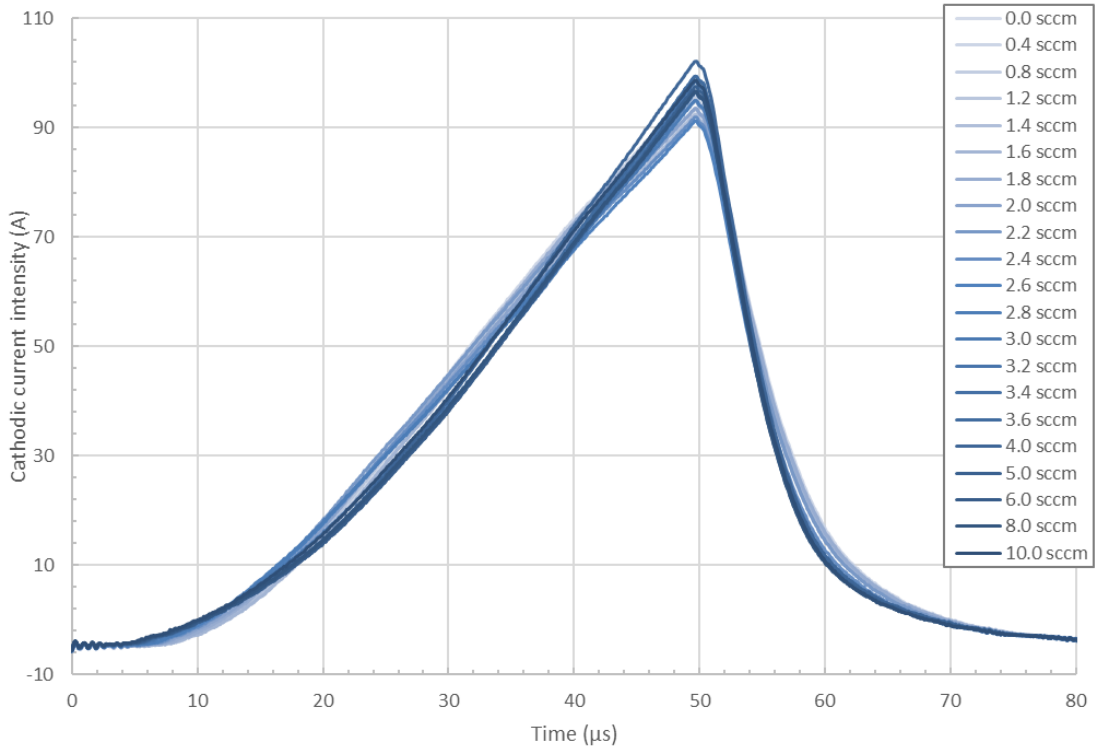

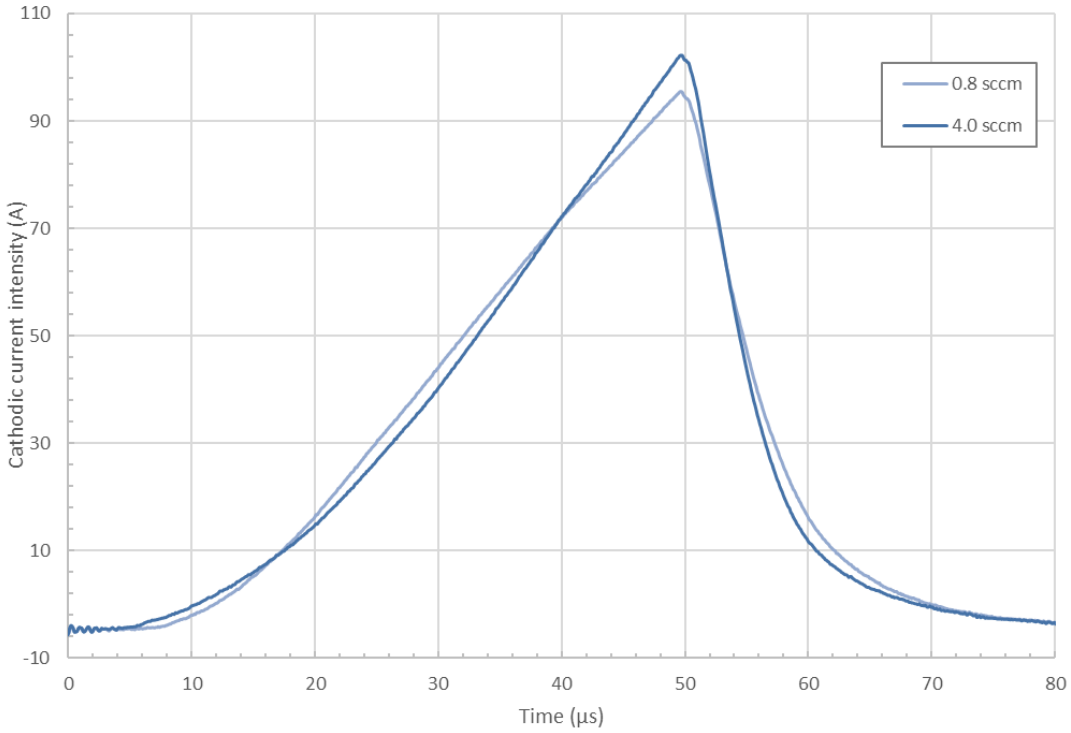

Figure 73. a. Evolution of the pulse waveform with the increase of the oxygen flow in the chamber for a 50 µs pulse width and in the current regulation mode (3mTorr – 300Hz – 50µs – 390V)

b. Isolation of two waveforms for an easier comparison

For illustration, Figure 74 represents a second type of oxidation curve (in opposition to the one proposed in Figure 68). This time, the change in voltage is reported as a function of the oxygen content as the pulse intensity is not supposed to change at a given duty-cycle (see Figure 73).

The first reactive atoms inserted in the chamber are reacting with the walls and the target's surface to create nucleation centres of a compound material. However, for low oxygen atoms concentration (i.e. flux), there is not enough reactive atoms to start the nucleation process of the compound layer. Indeed, the few species reacting with the surface are immediately re-sputtered. The target remains fully metallic, which is reflected by the flattering of the oxidation curve below this critical point, observable in Figure 74.

Behind this point, the nucleation starts at the target's surface and, for the reasons explained earlier (cf III.3.2.2) the generation of ionized species is reduced and thus, the voltage increases. However, at higher voltages, a higher amount of oxygen is needed to reach a given intensity (due to a more efficient sputtering) and it results in a smoothing of the transition.

Indeed, now the transition is significantly less sharp It means the transition is smoothed because the voltage increases along the oxidation. Another way to see it is a transition from a system with an absolute voltage of approximately 460V to a system at approximately 530V, with all the in between stages: the discharge needs 1.2 sccm of oxygen at 460V to start the oxidation but needs 3.4 sccm at 530V to finish the oxidation and every state in between these two flux – and these two voltages – corresponds to an incompletely oxidised but stable state of the plasma.

In summary, the system is transiting from the metal mode to the oxide mode but also from a lower voltage to a higher voltage, and the addition of both evolutions result in an increased difficulty for the system to get fully oxidised at each step (as each parameter is *fighting* against the other one) and thus the system can be stabilized at transitive points more easily.

This difference of oxidation curves between the voltage and the intensity regulations is an essential argument on how important it is to differentiate these two modes and how it is very difficult to compare them. It shows how explanations – and

observations – become more complex when using the average intensity limit since the modification of the voltage by the power supply adds up a level of complexity. Indeed, it makes it impossible to isolate a parameter's influence (here, the oxygen content) when the voltage is also modified by this same parameter, as it creates a *vicious circle* between them: the voltage is increased because the oxygen flux is raised, a higher voltage means a need for higher oxygen content to oxidised the target, more oxygen in the chamber results in an increase in the voltage, et cetera… This *vicious circle* results in the impossibility to affirm with certainty what phenomena are occurring and what are their origins (i.e. voltage or studied parameter). It should also be noticed that each parameter has a different consequence on the voltage evolution - as explained in their respective sections - which, again, adds up in complexity.

However, the smoothing of the curve cannot be ignored and can be very useful for a precise control of the plasma stoichiometry. It should also be specified that the range of oxygen flux is larger in this mode: higher quantities of ions are needed to fully poison the target. This helps controlling the stoichiometry of the process.

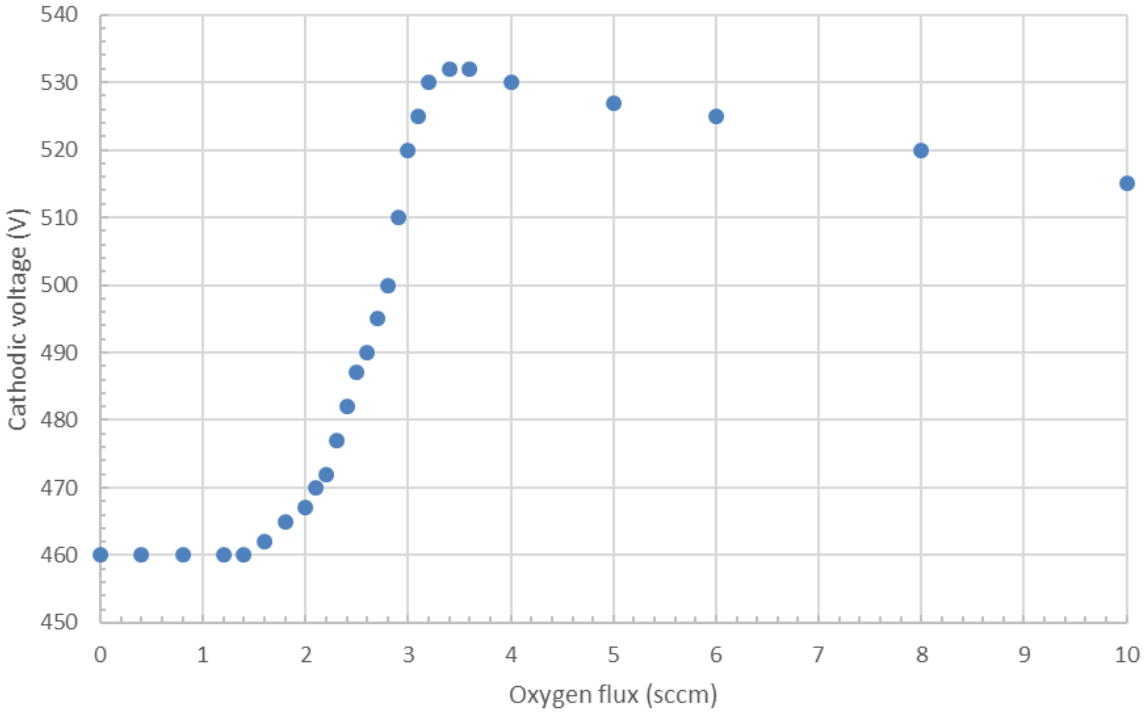

Figure 74. The evolution of the voltage applied by the power supply to keep a constant time-averaged cathodic current intensity with the increase of the oxygen flux in the chamber (1000Hz – 50µs)

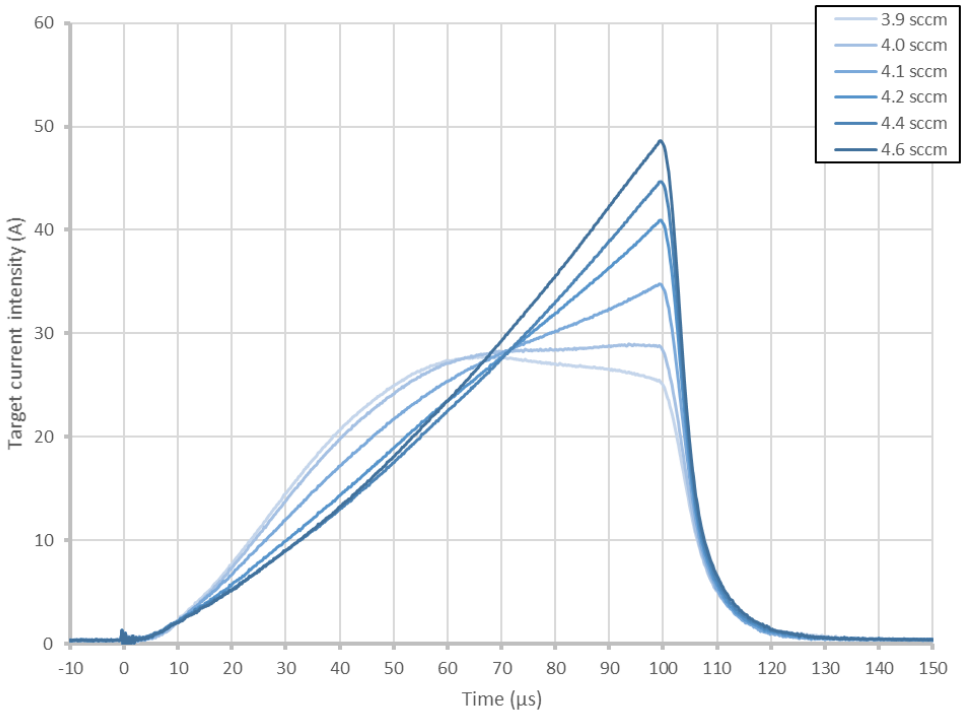

Figure 75. Cathodic current intensity waveforms at different oxygen fluxes, corresponding to the transition phase, with a pulse width of 100 µs and maximal time-averaged current intensity (2.0 A) (3 mTorr – 100 µs – 300Hz)

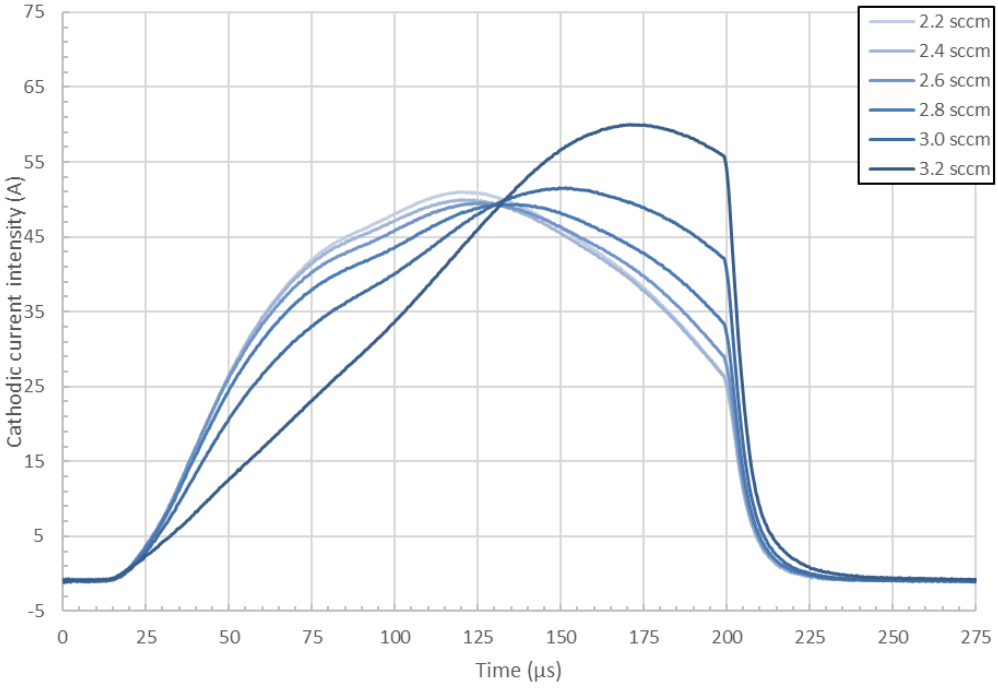

Figure 76. Cathodic current intensity waveforms at different oxygen fluxes, corresponding to the transition phase, with the maximal pulse width (200 µs) and maximal time-averaged current intensity (2.0 A) (3 mTorr – 200 µs – 300Hz)

Figure 75 and Figure 76 show the same type of data as the one on Figure 73 but for longer pulses. The frequency has been kept constant for comparison purpose. However, the poisoned mode with such pulse widths is very unstable and the arcing restrains the user from going further than 4.6 and 3.2 sccm of oxygen for respectively 100 and 200 µs pulses. Beyond these points, the arcing is too intense and could damage the target permanently (i.e. cracks). It is also why a complete voltage oxidation curve (like Figure 74) could not be obtained but a partial one is shown in Figure 77.

Having longer pulses makes a major difference. The change in the waveform during the transition can be seen much more easily since the profiles are not just positive slopes until the end of the pulse (like short pulses) but more complex shapes. Indeed, even if, along the transition, the pulse surface remains unchanged, there is a reduction of the slope in the first half of the pulse, resulting in two things: a delay in the appearance of the rarefaction point (see Figure 75 and Figure 76) and a compensation by an increase in the applied voltage (see Figure 77).

The reason behind the reduction of the slope is thought to be the same as the one behind the reduction of the slope for short pulses cases. Again, it cannot be fully confirmed as there is no mass spectrometer available for this study. Moreover, no mass spectrometry for oxidised titanium HIPIMS discharge can be found on the literature to fully explain the processes occurring.

On Figure 76, it can be observed that the *first bump* of the metallic peak disappears at higher oxygen pressures. This first *bump* is referred in the literature as being constituted of argon (and metallic) ions sputtering the target. However, when oxygen is covering the target, these argon (and metallic) ions are less likely to reach and sputter the target through the compound. It results in the observable diminution of the pulse slope in the first microseconds. The same transition has been observed in the long pulse voltage regulated case. However, here, this situation is different since reaching the oxide mode does not correspond to the disappearance of the discharge: the voltage is increased in consequence and allow to keep the discharge on.

Also, in the intensity regulated situation, the poisoning of the target is observed for a higher content of oxygen in the chamber. The hypothesis is that the number of ionized species reaching the target is much more important and results in an increased

need of oxygen atoms to fully cover the target. However, no conclusion can be drawn as other parameters have been changed in between the two figures (such as the frequency and the pulse width.

Even though the clear physical explanation cannot be found for this atypical situation, a very useful conclusion can be made: the oxide mode cannot be reached for long pulses, in either the voltage regulated mode nor the intensity regulated mode. In the first situation, the plasma is switched off and in the second situation, the plasma is too unstable. It is then supposed that in-between methods can be found: either voltage regulation with a higher voltage value or an intensity regulation with a lower time-averaged intensity limit. However, only the first solutions can be done with the system used here; but it does mean the sub-stoichiometric state of the discharge is over the intensity limit of the power supply.

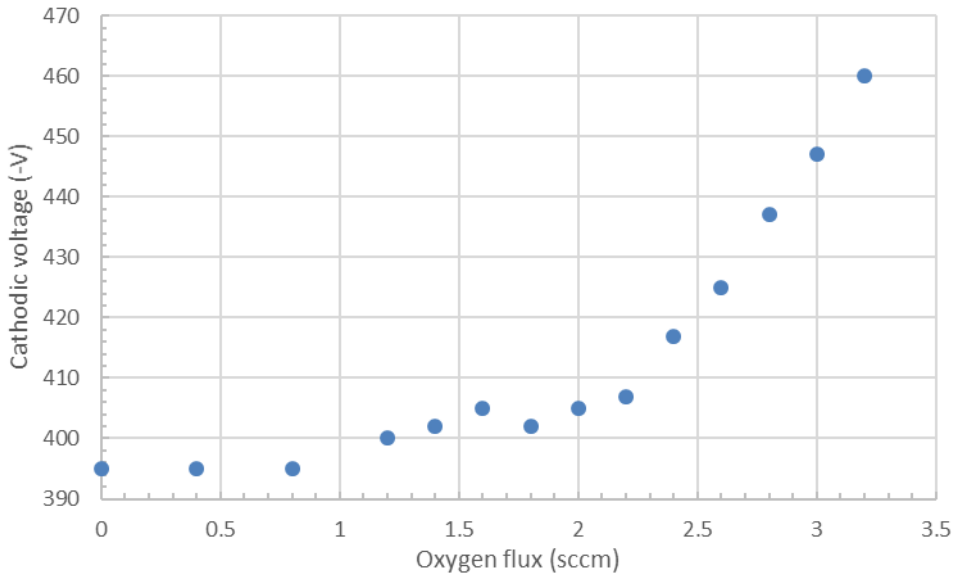

Figure 77. Partial evolution of the voltage applied by the power supply to keep a constant time-averaged cathodic current intensity with the increase of the oxygen flux in the (3mTorr - 300Hz –200 µs)

III.3.3. Poisoned mode

III.3.3.1.Voltage

This section presents the effect of the applied voltage on the poisoned mode waveform. The evolution has been observed for 3 different pulse width: 50, 100 and 200 µs. The pressure was kept constant to 3 mTorr and the frequency is 300 Hz for all three figures as well. The gas flux in the chamber is also the same for the three different situations (3.0 sccm), as it corresponds to a full poisoning (i.e. over-stoichiometric state) of the target, no matter the pulse width modification.

The observations made here are quite different to the observations from III.3.1.1.2; besides the fact that the increase of the applied voltages increases the pulse intensity. The reasons behind this behaviour are not explained further here, as it has already been explained previously in this thesis (cf. I.1.5.1 and III.3.1.1). The major difference is that, here, even for the 200 µs pulse width, the rarefaction peak does not appear. The disappearance of this peak is a consequence of the poisoning of the target: the sputtering yield in the poisoned mode is lower than that of the metal mode and the sputtered species are not only metallic. The first point explains why the target struggles more to sputter ions and therefore why the slope of the curve (i.e. sputtering yield) is lower in Figure 80 than it is in Figure 62 in the early stages of the pulse. Also, the second point highlights the fact that there are also oxygen atoms sputtered from the target and these atoms do not participate in the self-sputtering process as much as the metal ions. Both reasons have already been discussed in I.1.4.3 and I.1.5.4.

Another well-known consequence of the voltage is the appearance of an ignition delay for low voltages. Again, the explanation behind this phenomenon (clearly observable in Figure 80) have already been discussed in III.3.1.1.2 and should not be repeated here. Indeed, the discussion is the same, even though it is now a poisoned discharge: there are less ions (and electrons) in the chamber at the end of the pulse and therefore, there are also less charged species available for the next pulse ignition.

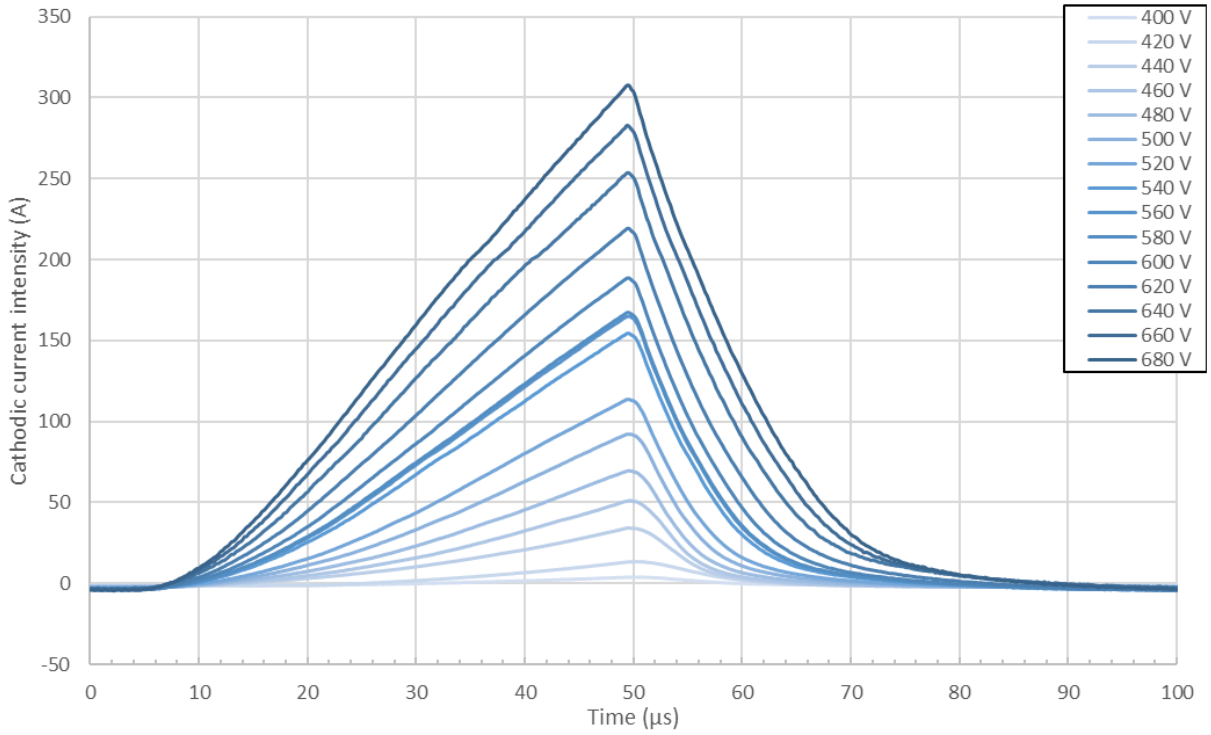

Figure 78. Evolution of the poisoned pulse waveform with the increase of the applied voltage for a 50 µs pulse width (3 mTorr – 300 Hz – 50 µs - 3.0 sccm)

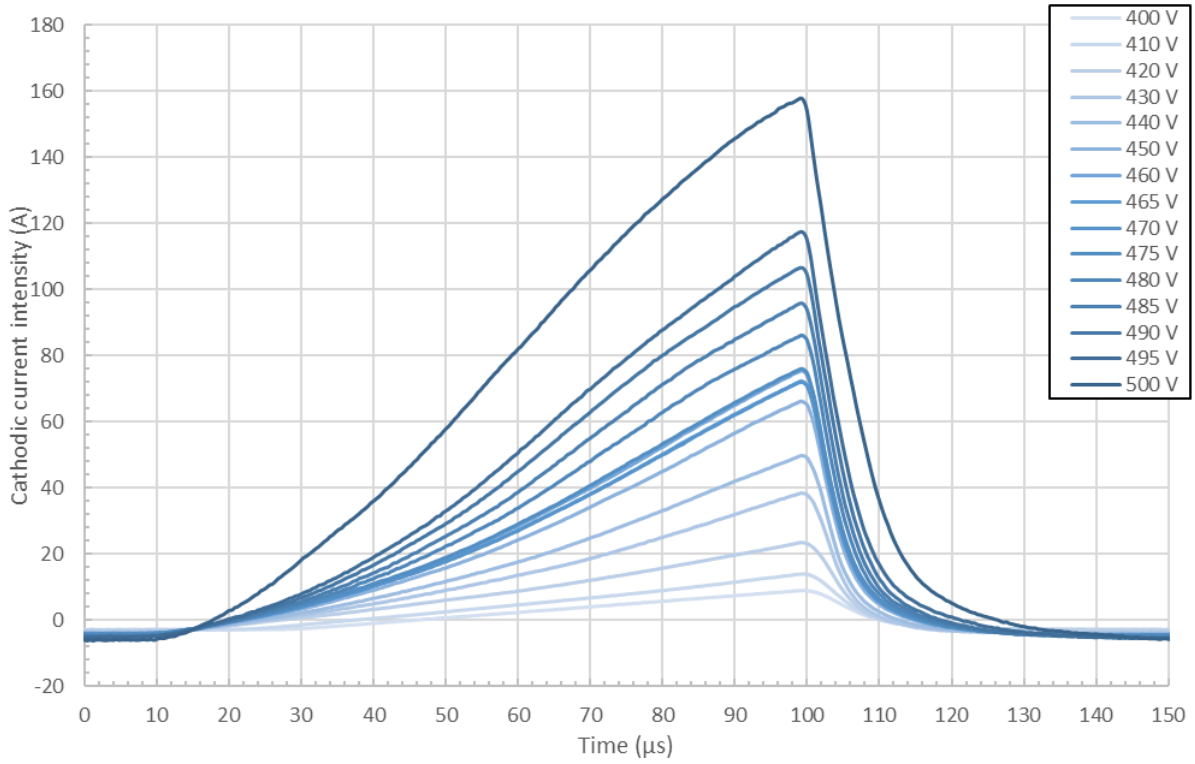

Figure 79. Evolution of the metallic pulse waveform with the increase of the applied voltage for a 100 µs pulse width (3 mTorr – 300 Hz – 100 µs – 3.0 sccm)

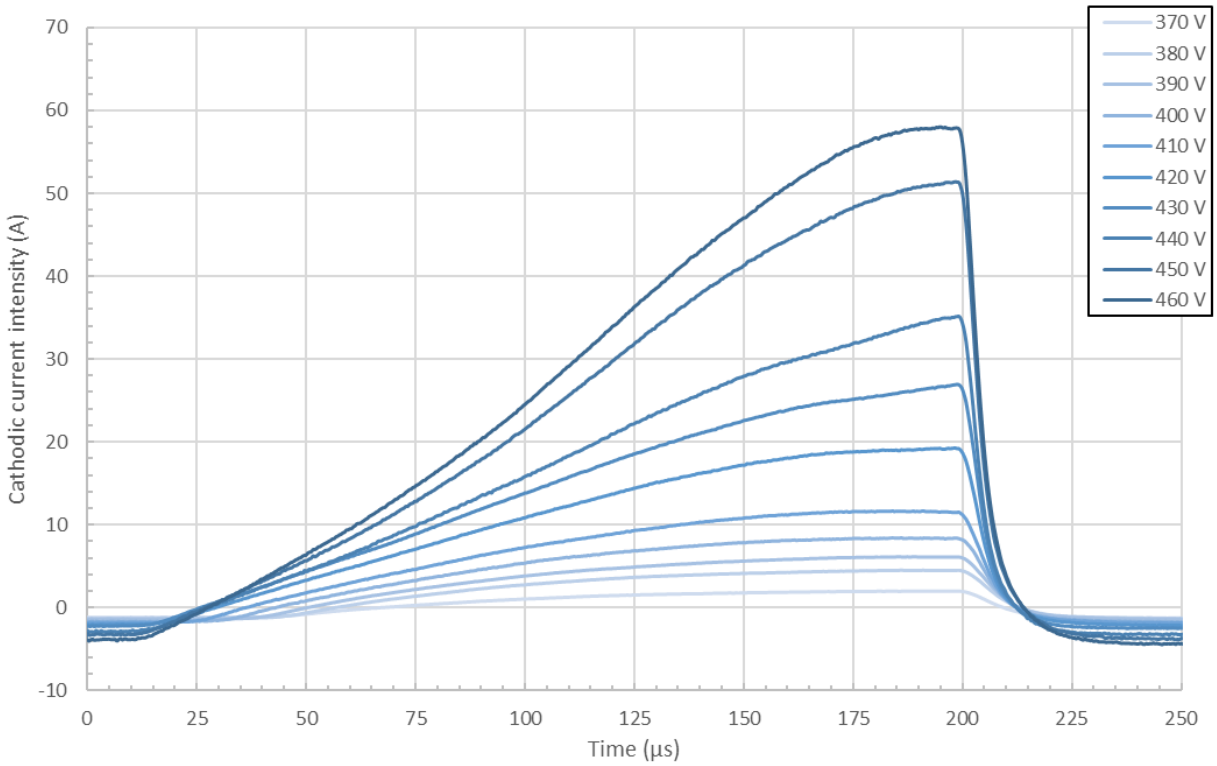

Figure 80. Evolution of the metallic pulse waveform with the increase of the applied voltage for a 200 µs pulse width (3 mTorr – 300 Hz – 200 µs – 3.0 sccm)

III.3.3.2. Pressure

When looking at the pressure, section III.3.1.4 shows that in the metallic mode the pressure only has an influence on the intensity of the pulse, but does not change the pulse shape itself. Here, Figure 81 shows that in the fully poisoned mode, the behaviour is the same: only the slope of the pulse is modified, which results in an overall increase of the pulse intensity.

It should also be noted that for lower pressure (in the case presented here, 3mTorr and lower), the pulse shape is modified. A delay in the plasma ignition can be spotted. In such case, the origin cannot be determined with certainty but it is thought to be due to the lack of species within the chamber. As a matter of fact, below 3 mTorr, the plasma switches off in such conditions (i.e. frequency, pulse width and voltage kept constant); which also explains why the pulse shapes for lower pressures are not shown in Figure 81. It is specified that the Argon/oxygen ratio is not changed with the pressure, as only the pumping speed is reduced to raise the pressure.

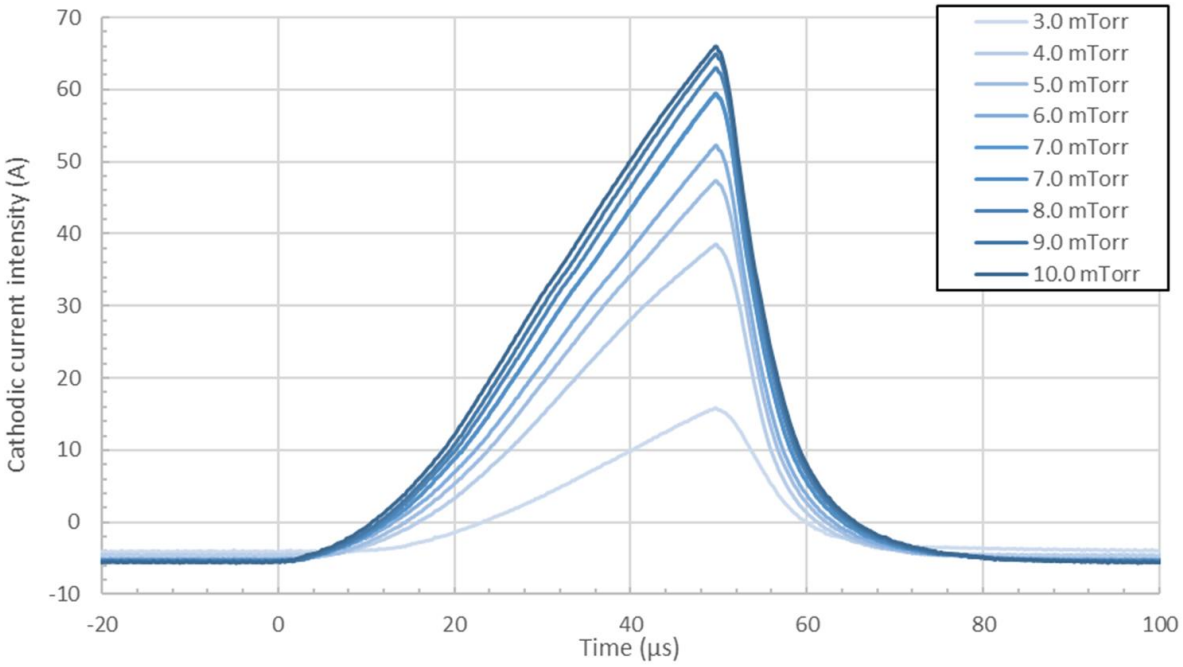

Figure 81. Evolution of the pulse shape with an increase of the pressure in the deposition chamber (1000 Hz – 50 µs – 510 V – oxide mode)

There is a transition to a *nearly-switched-off* discharge due to the lack ionized species in the chamber. However, there are no means to confirm the hypothesis with the current system. It should also be pointed out that the pressure has been reduced by augmenting the pumping speed (i.e. valve aperture), and not by reducing the argon and/or oxygen flows. Thus, the partial pressures of the gases are left unchanged in the chamber: this means that the overall plasma stoichiometry is left unchanged.

III.3.3.3.Frequency

This section contains the results on the frequency dependency of the pulse waveforms. Again, for this study, the cases of short and long pulses are differentiated. The cases of poisoned mode and transition modes are also to be differentiated as explained further.

First is studied the fully poisoned mode for different pulse widths: 50, 100, and 200 µs. For each pulse width, a constant gas flux of 3 sccm of oxygen is inserted in the chamber. This flux corresponds to a fully poisoned mode of the target in all set of

conditions. The voltage is kept constant for each evolution (but different for each pulse width) to isolate the only effect of the frequency.

In each situation (Figure 82, Figure 83, and Figure 84), the intensity of the waveform is diminished when the frequency is increased. Also, in all figures, no drastic change of the pulse waveform can be spotted, other than this diminution. The origin of the slight changes in the profile is believed to be due to the change in intensity, similar to the pressure and the voltage observations (cf III.3.3 and III.3.3.2). Again, it should be kept in mind that the system is still fully poisoned in all configuration and there is no transition towards a metal mode. This can be observed in two ways: by a visual observation of the plasma colour – meant to be *violet-ish* – but also thanks to the optical fibre of the Speedflo®® controller (cf II.3.2).

A quick observation, already made for the metallic mode, is the appearance of an ignition delay for lower frequencies. This behaviour is due to the difficulties faced by the system to keep charged species (i.e. ions and electrons) in the chamber in between pulses. These persistent species, even in relatively low number, help the ionization cascade leading to the ignition of the discharge at each start of a pulse. For long off-times, the quasi-totality of these ions and electrons recombine and become neutral again. This phenomenon is showed in Figure 22. The system then needs a short delay to re-ionize some of the atoms in the chamber and start the cascade ionization reaction leading to the ignition of the plasma. It should be highlighted that in the case of 200 µs pulses, very low frequency could be reached, where the ignition delay is quite important (i.e. ~50 µs); which explains why such conditions are not possible for shorter pulse widths

The diminution in the pulse intensity observed in each situation (see Figure 85) at higher frequencies is unclear. Indeed, as previously explained, the amount of plasma diagnostic tools is limited (on purpose) for this project and therefore, no absolute proof of the following hypothesises can be presented. These hypothesises rely only on the oscilloscope profiles and the literature review work. However, no literature on the subject could be found. Frequency studies have been carried out but not for poisoned Ti-O sputtering.

The increase of the pulses intensity is believed to be linked to the refill time. Indeed, for longer refill times, more atoms are available for sputtering. This observation

has been done and confirmed for metallic processes (see I.1.5.3). The idea is that the chamber needs to be refilled in reactive gas and working gas after each pulse. These atoms being *consumed* by the sputtering process, they become unavailable for sputtering. Then, new atoms need to be added in the chamber to compensate. During the off-time, the gas inlet sends new gaseous species in the chamber but if the refill time is too short (i.e. high frequency), the pulse intensity is limited by the amount of available atoms available for ionization/sputtering.

In summary, there is a balance to find. The refill time is responsible for two things: the ignition delay and the pulse intensity diminution. For the first one, the frequency should not be too low, as the atoms in the chamber lose their energy during a longer refill time. For the second, the frequency should not be too high, as the chamber do not have enough time to be fully refilled. However, both impacts are not *absolute* limitations: the discharge can still be used for deposition but it might have an impact on the deposited film.

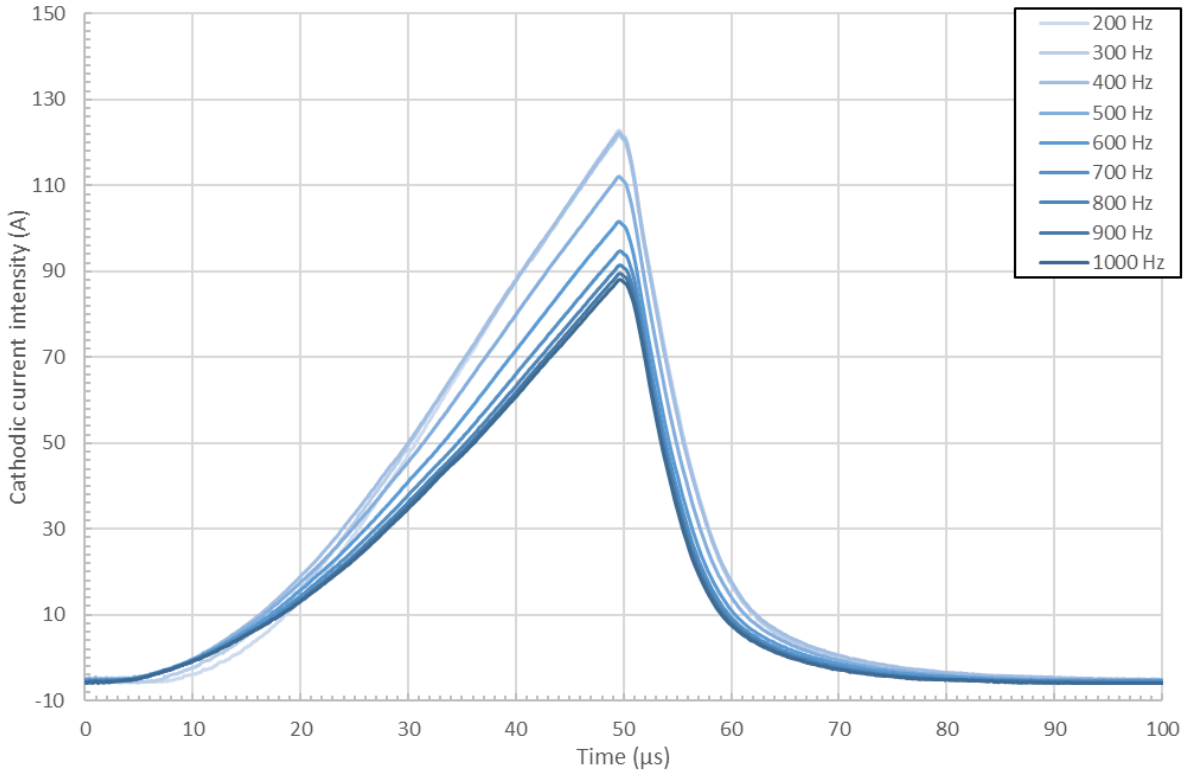

Figure 82. The evolution of the pulse waveform when the frequency is increased for a 50 µs long pulse in the poisoned mode (3 mTorr – 520V – 3.0 sccm)

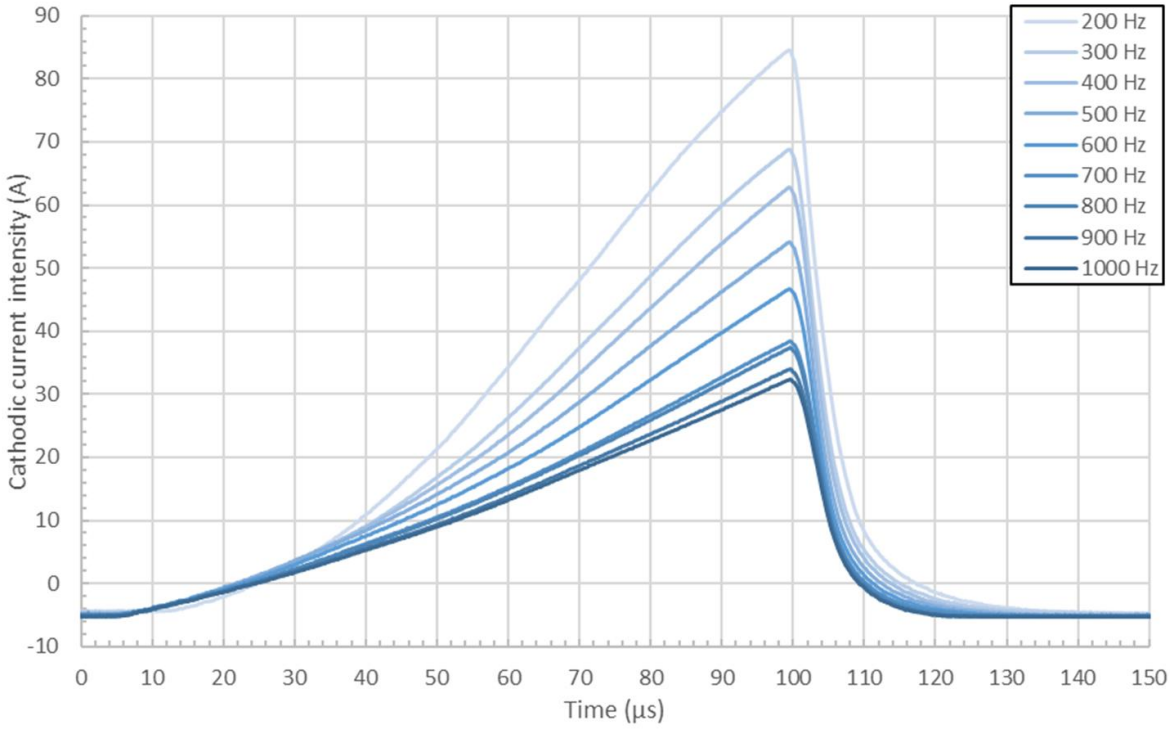

Figure 83. The evolution of the pulse waveform when the frequency is increased for a 100 µs long pulse in the poisoned mode (3 mTorr – 450V – 3.0 sccm)

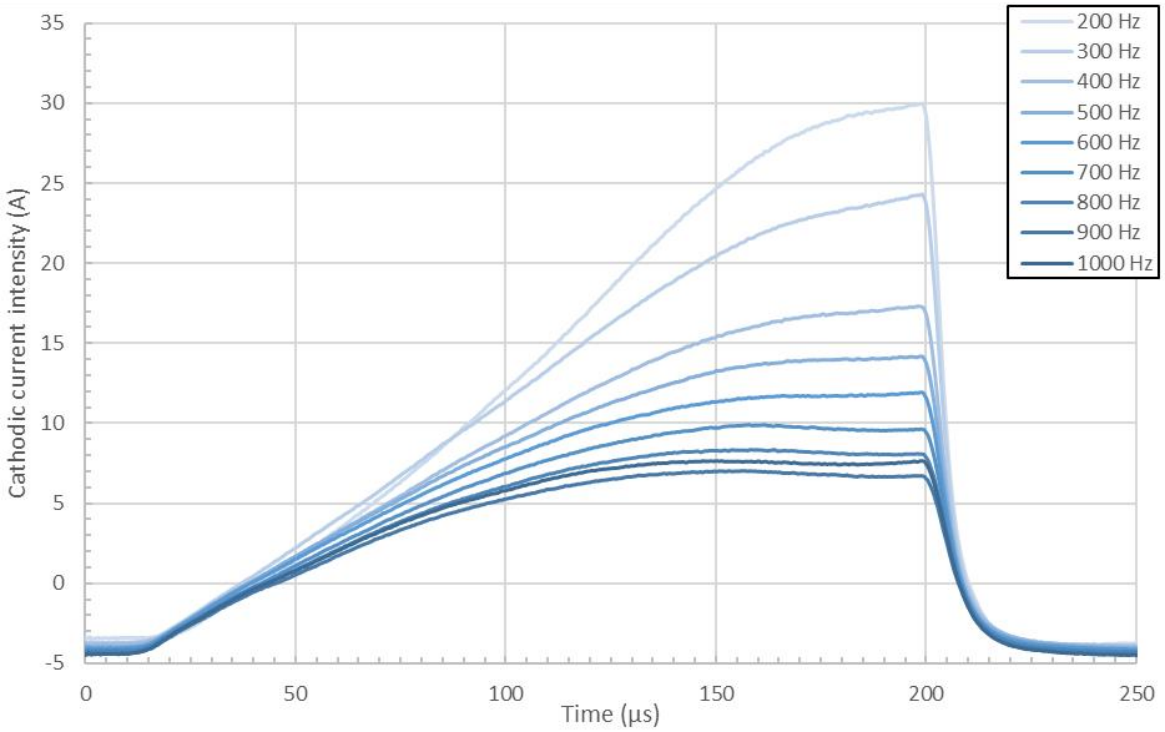

Figure 84. The evolution of the pulse waveform when the frequency is increased for a 200 µs long pulse in the poisoned mode (3 mTorr – 390 V – 5.0 sccm)

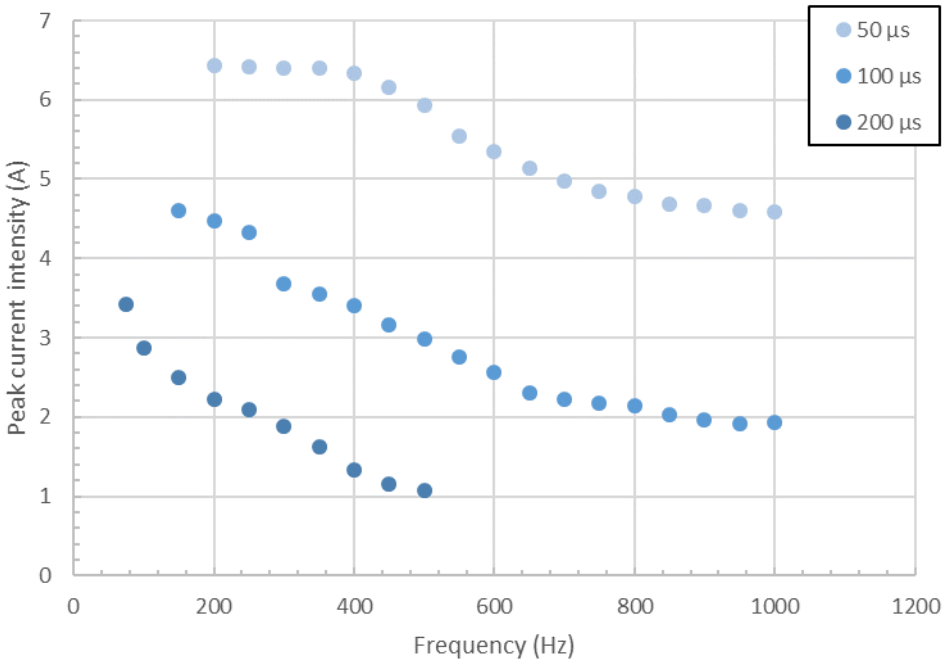

Figure 85. The combined evolutions of the peak current intensity for each pulse width as functions of the frequency (3 mTorr – 3.0 sccm)

III.3.3.4. Pulse width

In the case of the pulse width influence for a poisoned discharge, the window where the full range of pulse width is available is very narrow but the data obtained in this narrow window are presented in Figure 86. It shows a maximum peak intensity for a 100 µs width. The reasons behind this behaviour are not clearly identified but are believed to be a combination of both plasma properties and power supply limitations so it is difficult to identify what is happening. Therefore, no analytical conclusions will be drawn. However, in an empirical approach, it is useful to know that, beyond a certain pulse width, even in the fully-poisoned mode, the ionization rate reduces and therefore a longer pulse does not necessarily result in a higher number of ions deposited per pulse. It should however be kept in mind that an increase of the pulse width corresponds to an increase of the duty-cycle (i.e. effective time of deposition).

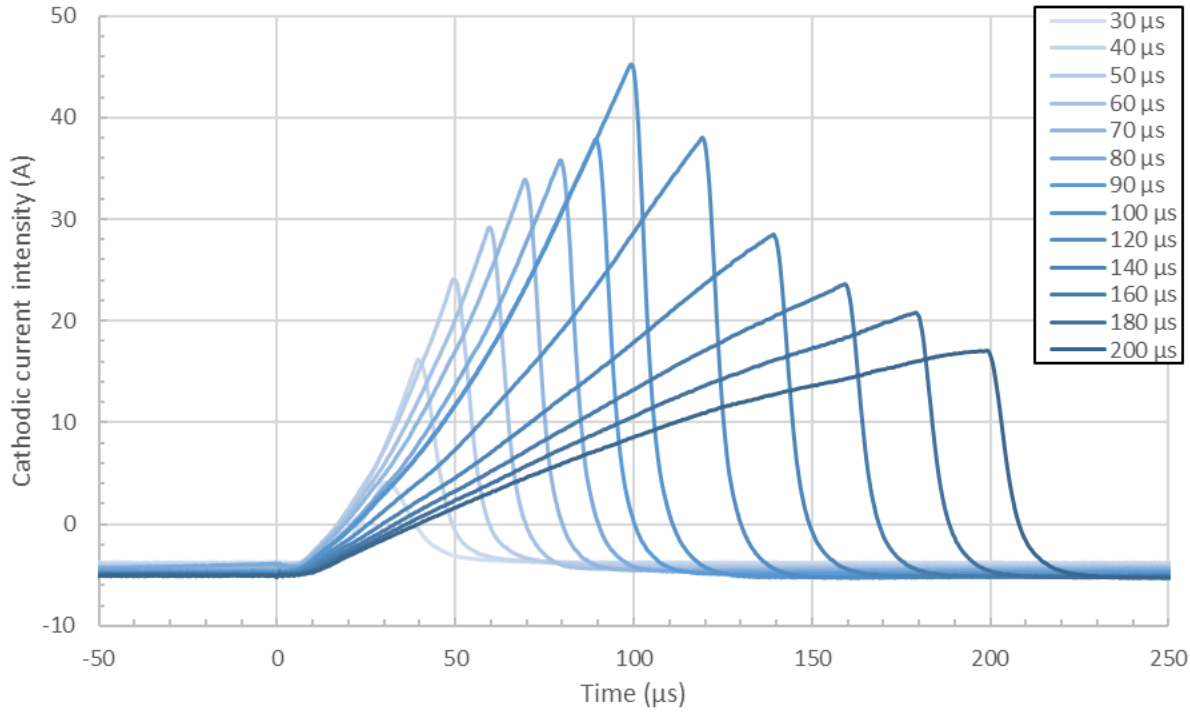

Figure 86. Modification of the poisoned pulse waveform when modifying the pulse width in the voltage regulated mode. (3 mTorr – 500 Hz – 425 V – 5.0 sccm O2)

III.3.4. Using the frequency to change the stoichiometry

III.3.4.1.1.Applied cathodic voltage regulation

Concerning the transition study, presented in Figure 87, the observation is quite different. It is, as a matter of fact, the opposite when looking at the peak current intensity evolution: in Figure 87, the latter is decreasing when the frequency is increased while, in Figure 82, the intensity is increasing in the same situation.

Earlier, in Figure 82, the system was in a fully poisoned mode: the oxygen was present in excess in the chamber. However, for the case presented in Figure 87, the amount of oxygen injected in the chamber is chosen to correspond to a state close to the stoichiometry, on the over-stoichiometry side, at 500 Hz. The frequency is increased and it results in two things: the increase of the peak current intensity evoked above and the change in the slope's curvature from concave to convex.

The combination of both observations is reported in the oxygen study (cf. Figure 69) when the oxygen amount is reduced. It is the proof that there is a change of

stoichiometry from poisoned to metal mode when increasing the frequency. The physical explanation is identical what has been described for the poisoned mode: the change in duty-cycle is the origin of the transition. Yet, the modification of the oxygen content inverts the trend here. The increase of the frequency means that the effective time of sputtering (i.e. duty-cycle) is increased and thus, more particles are impacting the target surface. More particles impacting the target implies that more of the surface compound material is sputtered away. The compound material (nucleation sites) is thus sputtered off from the target and the system switches back to a metal mode. This results in the various observations made and explained in III.3.2.2 for lower oxygen content (see Figure 69).

In summary, it can be said that the frequency has an opposite influence on the system than that of the oxygen content: an augmentation of the frequency has the same effect as a reduction of the oxygen content on the pulse width. This parallel is evident for transitive oxygen content, as explained above, but one could say that it also works for the fully oxidized mode. Indeed, for the latter, the oxidation study revealed an augmentation of the peak intensity when the oxygen flux is increased, beyond the poisoning point, and the frequency study showed a diminution of the same peak intensity when the frequency is increased; corresponding to an opposite influence.

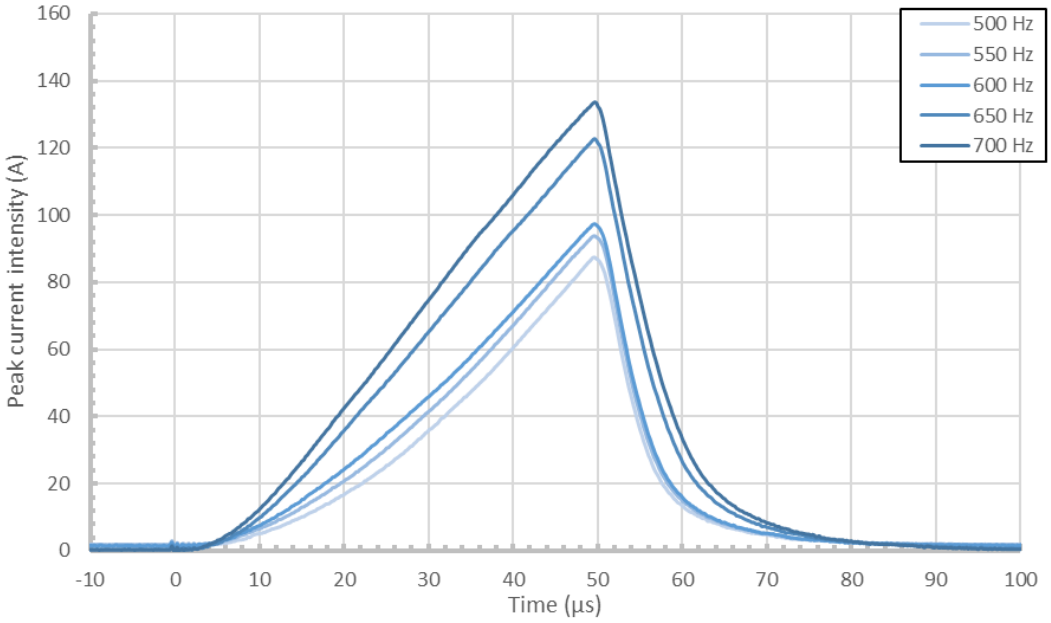

Figure 87. Study of the transition from the oxide to the metal mode by increasing the frequency for a 50 µs long pulse (3 mTorr – 500 V – 3.0 sccm)

For longer pulses, the transition study by the frequency must be carried with caution for the same reasons than the oxidation process. Indeed, it was shown that the consequences of the pulse are similar to the oxidation process: diminution of the peak intensity and modification of the slope curvature. It implies that the limitations are the same, as well: the peak switches off before reaching a fully poisoned state. For this reason, the transitions are not shown here.

III.3.4.1.2. Time-averaged current intensity regulation <I> = 2 A

Since the process has limitation at constant voltage, the long pulse studies have also been carried out in the intensity limited mode, where the voltage is modified by the power supply in each condition to keep a constant time-averaged current intensity. However, in the scenario of a frequency modification, the duty-cycle is changed and this has an important consequence: the peak surface corresponding to a constant time-averaged current intensity is different for each frequency, which was not the case for the intensity regulated oxidation study, where the duty cycle remained constant all along the evolution. To counter-balance this effect and ease comparison with the oxidation study presented in III.3.2.4, each pulse waveform has been multiplied by its corresponding duty-cycle. The results are shown in Figure 88 and Figure 89.

When compared to Figure 75 and Figure 76, the similarities cannot be ignored. First, for the 100 µs case, the evolution of the waveform is quasi-identical between the situation where the frequency is increased and the one where the oxygen content is decreased. This means that there is a change in the system's stoichiometry when modifying the frequency, again. The evolution is the same as the one observed for intensity regulated cases in the previous section (see Figure 75) and will not be discussed any further here, except by reminding that an increase of the frequency results in a transition towards the metallic mode. Of course, the waveforms are not absolutely identical between both cases but these slight differences should not be the source of too much attention. Indeed, it is normal that there are quantitative differences between two different evolution but the most important part is the qualitative observation made above: the duty-cycle change in one case but not for the other one.

This reasoning is proven by Figure 89, where the waveforms of metallic (i.e. high frequency) are quite different to the ones shown in Figure 76 but there is no denying of the fact that both situations are metallic-typed discharges, however. The differences in the waveform are due to the change in the duty-cycle, nothing else. The differences are as follow: in the oxygen flux modification scenario (Figure 76), the first *bump* is weaker and there is no plateau at the end of the pulse. The first difference is due to a longer off-time for Figure 76, resulting in a depletion of entities contributing in the sputtering and the second is due to the effective sputtering time being lower and thus, the refill time is sufficient for not reaching the on-time depletion, also called rarefaction. These observations are reported in III.3.1.3 and will not be discussed any further here. Nevertheless, the same transition for a metallic-type discharge to a poisoned-typed discharge can still be observed for 200µs pulses when the frequency is decreased.

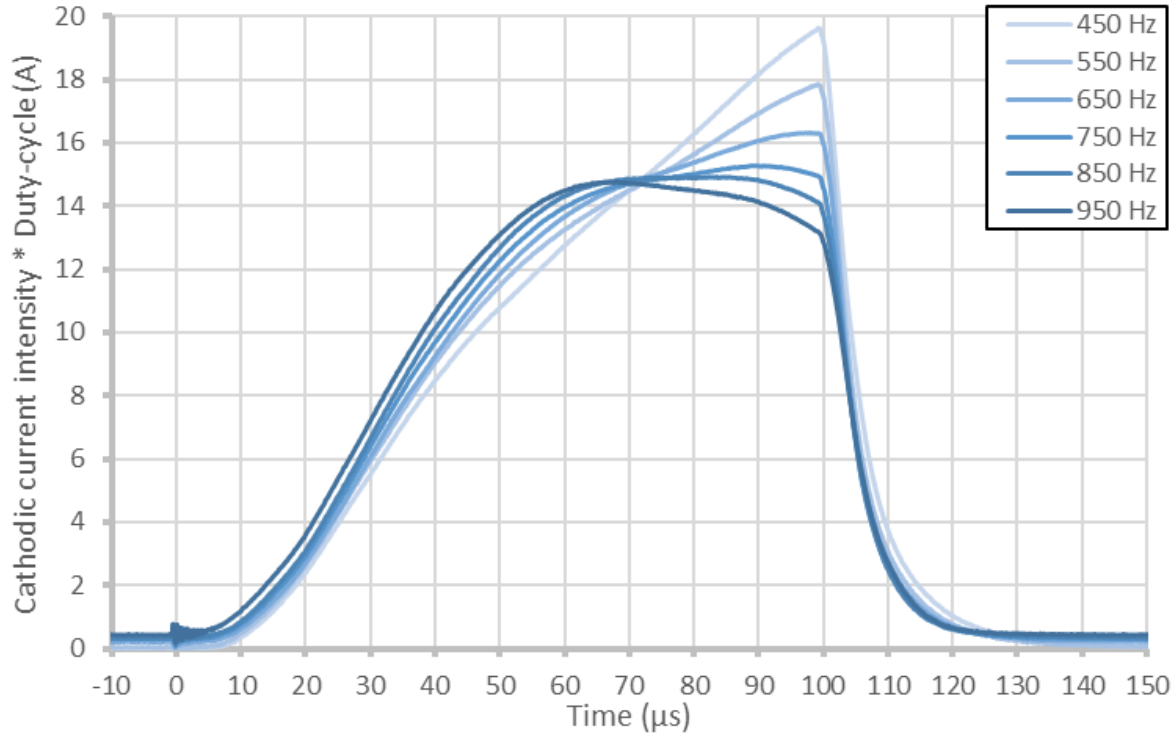

Figure 88. Modification of the pulse waveform when modifying the frequency in the intensity regulated mode. Each pulse intensity has been multiplied by its duty-cycle (3 mTorr – 100 µs – 2.0 sccm O2)

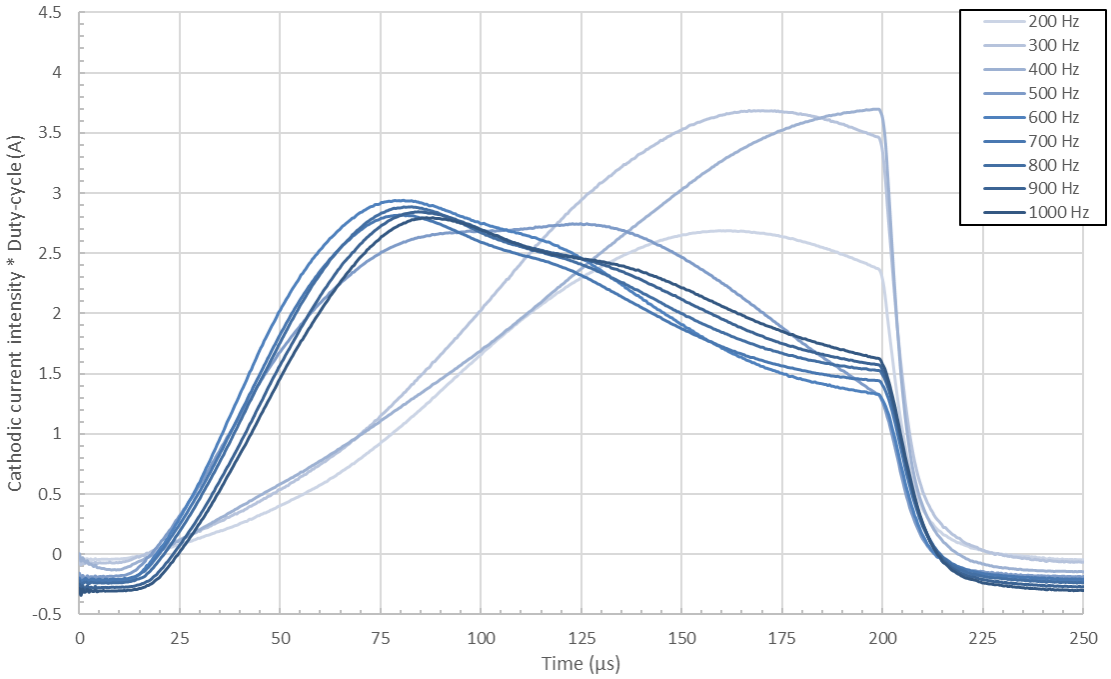

Figure 89. Modification of the pulse waveform when modifying the frequency in the intensity regulated mode. Each pulse intensity has been multiplied by its duty-cycle (3 mTorr – 200 µs – 2.0 sccm O2)

III.3.5.Study of the oxidation curves in the voltage regulated mode

In this section, the oxidation curves in the voltage regulated mode are studied, and more specifically, the effect of the deposition parameters on the curve. However, in this mode, the window of conditions possible is narrow as the voltage is not modified all along the transition and it has been seen earlier that the drop in cathodic current intensity during the transition is too important and starting (i.e. at 0 sccm of oxygen) from below the <I> = 2.0 A limitation leads to an extinction of the discharge when poisoning the target for most conditions.

III.3.5.1. Pressure

The first effect analysed is the pressure influence. Again, it should be reminded that the pressure in the chamber is modified through the pumping speed. The system keeps the same set of conditions, with the pressure as the only difference in between the four curves (see Figure 90). This means that the voltage, the frequency, and the pulse

width remain unchanged. Also, the fact that it is done in the voltage regulated mode means the range of fully observable evolution is very limited. Indeed, if the pressure is too low, the discharge switches off when transiting to the poisoned mode and if the pressure is too high, the intensity limitation is reached in the metal mode. This very narrow window only allowed the study to be carried for 4 different pressures without changing the other parameters. The results are shown in Figure 90.

There are two main observations to make from Figure 90. First, as previously seen, the increase in pressure results in an increase of the overall peak current intensity in both metallic and poisoned mode from 3 to 5 mTorr. No further explanation is given here, as it has already been discussed in III.3.1.4 and III.3.3.2. However, what should be highlighted from this graph is the shift of the *transition window* from one pressure to another. The so-called *transition window* is the range of oxygen fluxes corresponding to the transitive states in between the metallic and the poisoned phases of the discharge. Indeed, at 3 mTorr, the transition from metal to poisoned mode occurs between 0.4 and 0.8 sccm of oxygen when for 5 mTorr, it occurs between 0.6 and 1.0 sccm of oxygen. The second observation is the steadiness of the curve once past 5 mTorr. This is an unexpected behaviour as the increase of the signal between 3 and 5 mTorr should also be observed for higher pressures. It is believed to be a power supply artefact for the conditions chosen here as there is no reason for this stabilization when relying on the data presented before (see Figure 67 and Figure 81). The reasons behind this saturation are believed to be consequences of the power supply current limit. Even though it did not show any saturation on the power itself, it could be the below-2A saturation discussed in III.3.1.1.1.

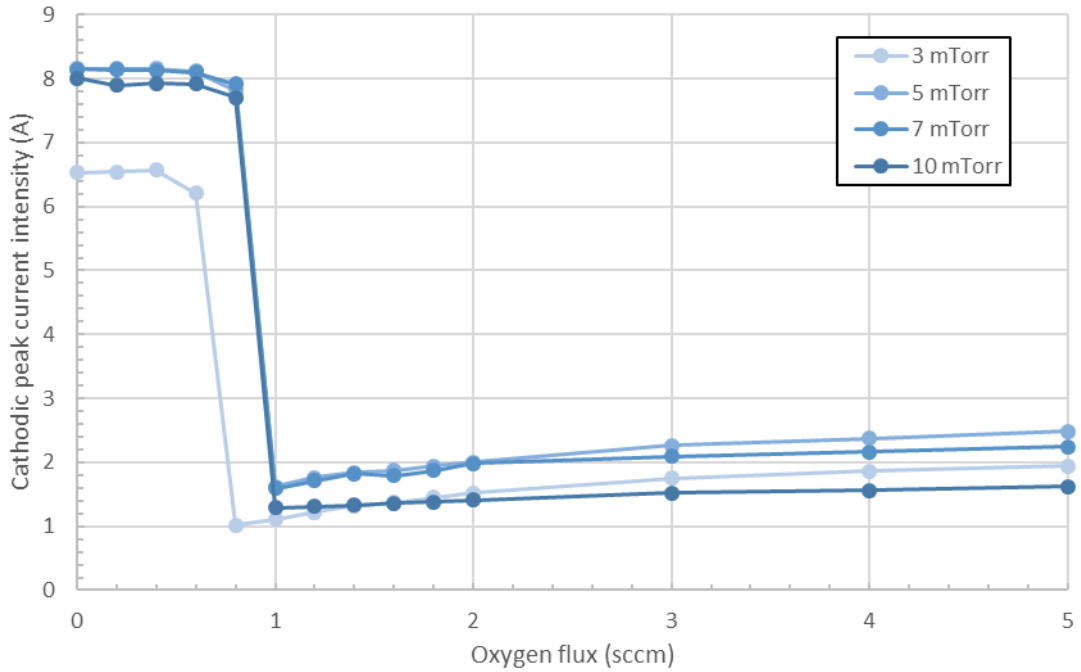

Figure 90. Modification of the voltage regulated oxidation curve with the pressure

Even if the shift observed between 3 and 5 mTorr could seem to be minor, it is in fact of great importance as an oxygen flux corresponding to a poisoned mode at a certain pressure could correspond to a sub-stoichiometric discharge at a higher pressure. At higher pressure, there are more ions generated and sputtering the target. Therefore, the nucleation at the target's surface is more difficult and therefore, more oxygen is needed for the same nucleation state. It should be added that the energy of the ions is not increased with the pressure so it seems that it is mainly the number of ions impacting the target that matters, not their energy. However, it does not mean that it is the only reason. It may just be that the impact of the number of ions is more important than the impact of their energy. This hypothesis should be completed with other studies, such as IEDFS. The observations made here mean that, in a practical point of view, the oxygen flux should be managed if the pressure is changed for the stoichiometry of the discharge to remain unchanged as there is a possible change of the stoichiometry.

III.3.5.2. Voltage

In this section, the voltage influence is studied. The system has been kept at constant pressure, frequency and pulse width but the applied cathodic voltage was

modified so its influence on the oxidation curve of the target could be observed. The results are shown in Figure 91. On the graph, the change in the cathodic peak current intensity is represented as a function of the oxygen flux injected in the chamber for different applied voltages.

The data is showing the same type of oxidation already discussed in Figure 74 (see III.3.2.4) therefore, it will not be discussed any further here. Again, the focus here is put on the change in the *transition window* with the applied voltage. Here, the increase in the cathodic voltage results in an increase in the required oxygen flux to poison the target. Here, the reasoning is slightly different to the previous section. Indeed, not only the number of ions reaching the target is increased, but also their energy and both are making the compound nucleation more difficult on the target. Therefore, they both result in an increase of the required amount of oxygen to poison the target and there is no counter-balancing of one effect on the other. It also means that it is still impossible to differentiate the effect of the amounts of ions and their energy. The next section will help determining which one is predominant.

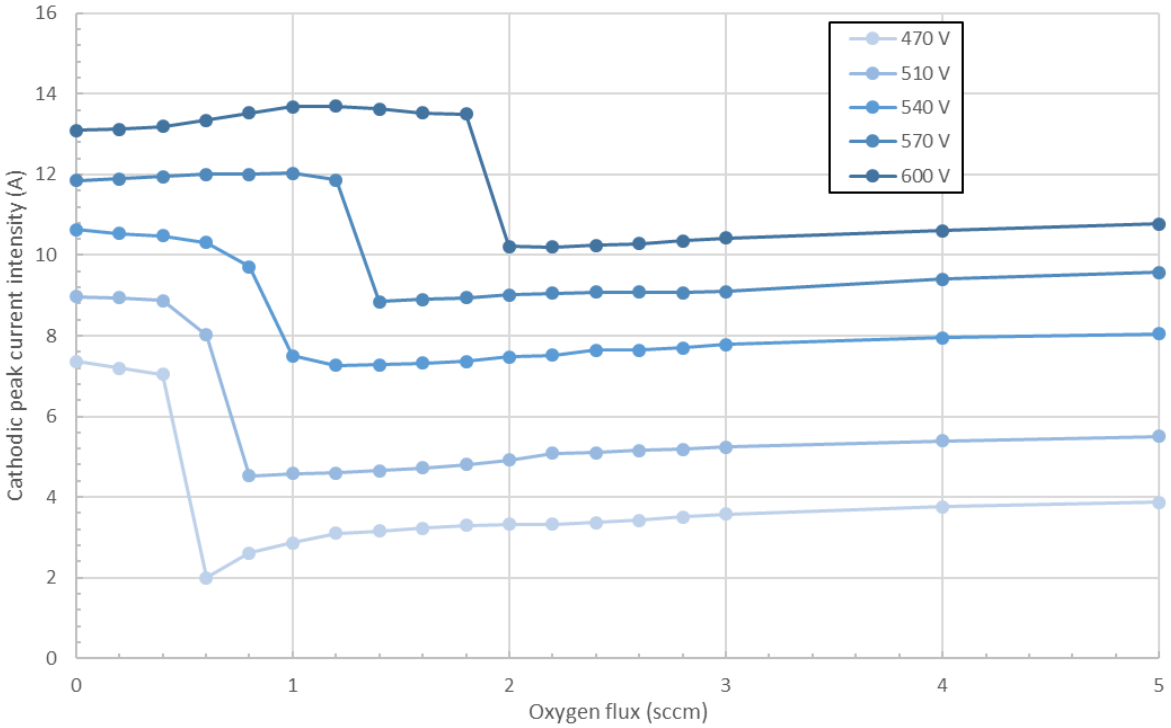

Figure 91. Modification of the voltage regulated oxidation curve for different voltages

III.3.5.3. Frequency

This section investigates the effect of the pulsing frequency on the voltage regulated oxidation curve reported in Figure 92. This figure is interesting as it permits to determine which of the ions quantity or the ions energy is the main parameter responsible for the shift in the *oxidation window*. Indeed, when keeping the same voltage, pressure and pulse width (and only varying the frequency) the energy of the atom remains unchanged in opposition to both pressure and voltage variations. The quantity of ions is the only change. Again, here, the variation could not be assessed on the full range of frequencies due to the power supply's limitations explained earlier. In fact, a full oxidation curve could only be obtained with the maximal frequency. For lower frequencies, the discharge would switch off in the poisoned mode as the ionizing process is too weak and increasing the voltage would result in a <I> = 2.0 A limit.

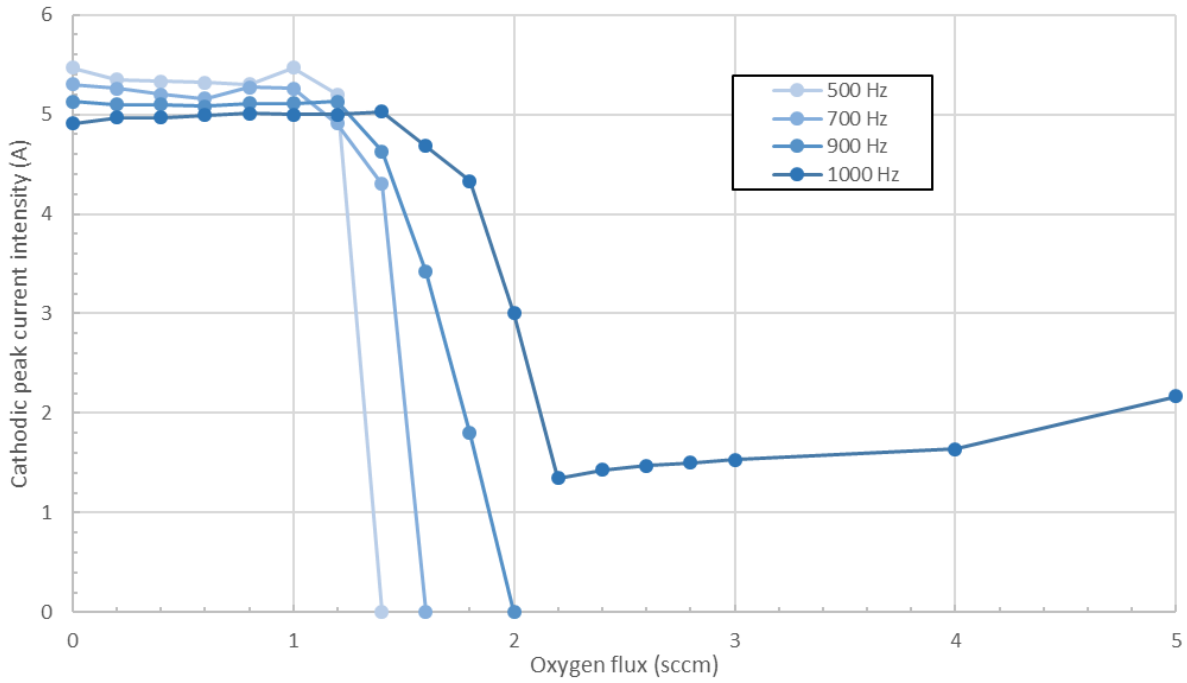

Figure 92. Modification of the voltage regulated oxidation curve for different frequencies

However, for the range observed (i.e. from 500 to 1000 Hz), a singular behaviour can be identified. Indeed, for each frequency, the metallic mode remains pretty much unchanged in terms of cathodic peak current intensity as it has previously been reported (cf. III.3.1.3). However, the shift in the *poisoning window* is still present. When increasing the frequency in this range (i.e. avoiding the ignition delay), the energy of the ions and

their quantity for each pulse remains unchanged; the sub-stoichiometric region is a witness of it. Indeed, for each frequency, the cathodic peak current intensity is similar; there is only a slight diminution with the augmentation of the frequency. However, since the duty-cycle is increased as well, the overall quantity of ions reaching the target per unit of time rises. It results in a target being sputtered with more ions with the same average energy.

The fact that for higher frequencies, a higher amount of oxygen atoms in the chamber is needed to poison the target is the proof that the number of sputtered atoms alone has a (negative) consequence on the nucleation process. Indeed, a higher amount of ions reaching the target results in a higher difficulty to poison the target. This observation shows that the peak current intensity is not necessarily a relevant entity as what really matters when studying the oxidative process of the system is the amount of ions sputtered per unit of time (i.e. time-averaged current intensity). It reminds the user that the poisoning of a system is a macro-scaled process, not a micro-scaled one and, as such, should not be expressed as a function of any instantaneous entity such as the peak current intensity.

It should be specified that it does not change the fact that the energy of these ions can also have a consequence on the poisoning process. Indeed, this case shows how the discharge is behaving when the energy of the atoms remains unchanged but their quantity evolves. To complete this study, the system should be analysed for situations where the quantity remains constant over the transition (i.e. constant time-averaged current intensity) and observe how the oxidation curve evolves when only changing the energy of the ions (i.e. cathodic voltage) between different oxidation curves. However, the only way to observe this scenario is with a modification of the duty-cycle of the signal by modifying the frequency in the intensity regulated mode. This way, the peaks and the discharge itself would not be drastically modified, the time-averaged quantity of ions reaching the target would remain unchanged, but the power supply would need to reach different ranges of voltage for each frequency, to keep <I> constant. The results of this study are reported and discussed in III.3.6.2.

III.3.5.4. Pulse width

The pulse width is a very sensitive parameter to modify as its consequences are multiple. However, a pulse width's influence study has been carried out and the results are shown in Figure 93. Once again, the reader should be reminded that the range of available conditions allowing to observe a transition without changing either the pressure, the voltage nor the frequency is very narrow and it is why the pulse width's influence could only be carried out at a low frequency and only between 75 and 150 µs. Shorter and longer pulses resulted in respectively an extinction of the discharge due to a non-sufficient voltage and an unstable discharge (reaching the power supply limitation) due to a too important applied voltage.

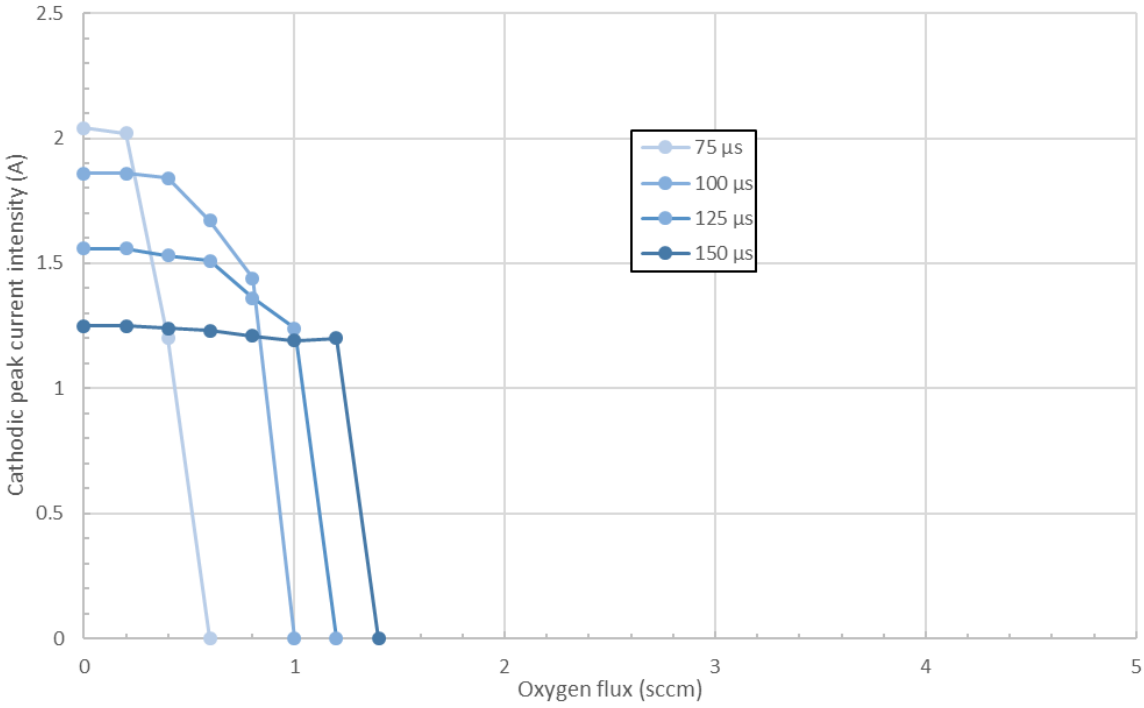

Figure 93. Modification of the voltage regulated oxidation curve for different pulse widths

Increasing the pulse widths over 75µs in these conditions resulted in a decrease of the peak current intensity in the sub-stoichiometric mode and an increase of the required oxygen flux for poisoning the system. The shift in the *poisoning window* is still believed to be mainly due to the increase in the duty-cycle, resulting in an increase of the time-averaged current intensity. However, a modification of the pulse width over these value is also known to have an influence on the species energy, as the rarefaction and

thermalization effects appear around 100 µs in metal mode. However, this effect on their energy remains unclear in this study as there is no mean to investigate the energy and the composition of the ions fully and therefore, no conclusions can be made at this point.

III.3.6. Study of the oxidation curves in the intensity regulated mode

This section is here to present the results obtained in the intensity regulated mode. In fact, as expressed earlier in this thesis, the power supply used in this project as a limitation in terms of time-averaged cathodic current intensity. This means that if the requested voltage is too high, the power supply itself limits the applied voltage so the time-averaged current intensity stays under the 2.0 A limit. This allows the user to run the system in a way that the time-averaged current intensity stays constant, even if conditions are changed, by requesting an applied voltage that would always stay above the limit (i.e. typically 800V or above). This way, the voltage is modified along with the modification of the system. The oxidation curves become evolutions of the cathodic voltage, and not of the cathodic current intensity.

Having a constant time-averaged current intensity means that, in all conditions, the amounts of ions reaching the target is always the same. More exactly, the ions-to-electrons ratio remains constant. However, their energy can vary, as well as their stoichiometry. It allows us to complete the observations made in the previous part (i.e. III.3.4).

III.3.6.1. Pressure

To copy the previous part (III.3.4), the first parameter's influence studied is the pressure. The pressure in the chamber is modified by modifying the pumping speed of the turbo pump. This means that the argon flux remains the same for all pressures, thus, the oxygen partial pressure corresponding to a given oxygen flux is the same in all conditions. This is true for all oxidation curves done in this chapter.

For this study, the pulse width is kept short so the changes in the pulse shape due to the poisoning remain minor and do not complicate the exploitation of the data. Having

longer pulses is impossible anyway as a range of pressure large enough to be relevant would result in system's limitations. The results of the study are presented in Figure 94.

From Figure 94, several observations can be made. First, as expected, in the metal mode, the applied voltage decreases when the pressure is increased. It reflects an effect previously observed: at higher pressure, there are more Argon atoms available for ionization and therefore, less energy is needed to obtain the same amount of positive argon ions reaching the target (cf. III.3.1.4). However, the figure shows that this statement is not necessarily true in the poisoned mode. Indeed, the poisoned mode part of the graph is close to being identical for each pressure, no clear trend can be identified. This should mean that, no matter the pumping speed, the poisoned mode is always similar (at least at a given frequency and pulse width).

The fact that, no matter the pressure in the chamber, the applied voltage for the poisoned mode remains the same is a surprising fact that has not been previously reported. In any case, it reflects the fact that the pressure does not seem to change the poisoned state in the intensity regulated mode, or only slightly. The physical explanation behind this could reside in a balance between different things: the loss of ion energy at higher pressure, the increase of the number of ions in the chamber, and the reduction of the pumping speed. So far, no explanation could be found to fully explain this behaviour and therefore and, again, with only an oscilloscope, it is impossible to make any conclusion.

The last observation to be made concerns the oxygen flux corresponding to the fully poisoned mode of the system. Even though the oxidation seems to be starting earlier as the pressure increases, the maximum voltage is obtained for a flux between 2.8 and 3.0 sccm for each curve. It is believed the system makes no major difference with the energy of the ions in the chamber, and their number seems to be the most important factor, regarding the poisoning of the target; supporting the hypothesis made in the previous sections. However, even if the effect is not important, it does seem that higher pressure poisoning is *easier* (i.e. it means less oxygen). It is most likely to be due to the fact that, at higher pressure, there are more inelastic collisions, and therefore, the kinetic energy of the impacting ions is lower; making poisoning easier.

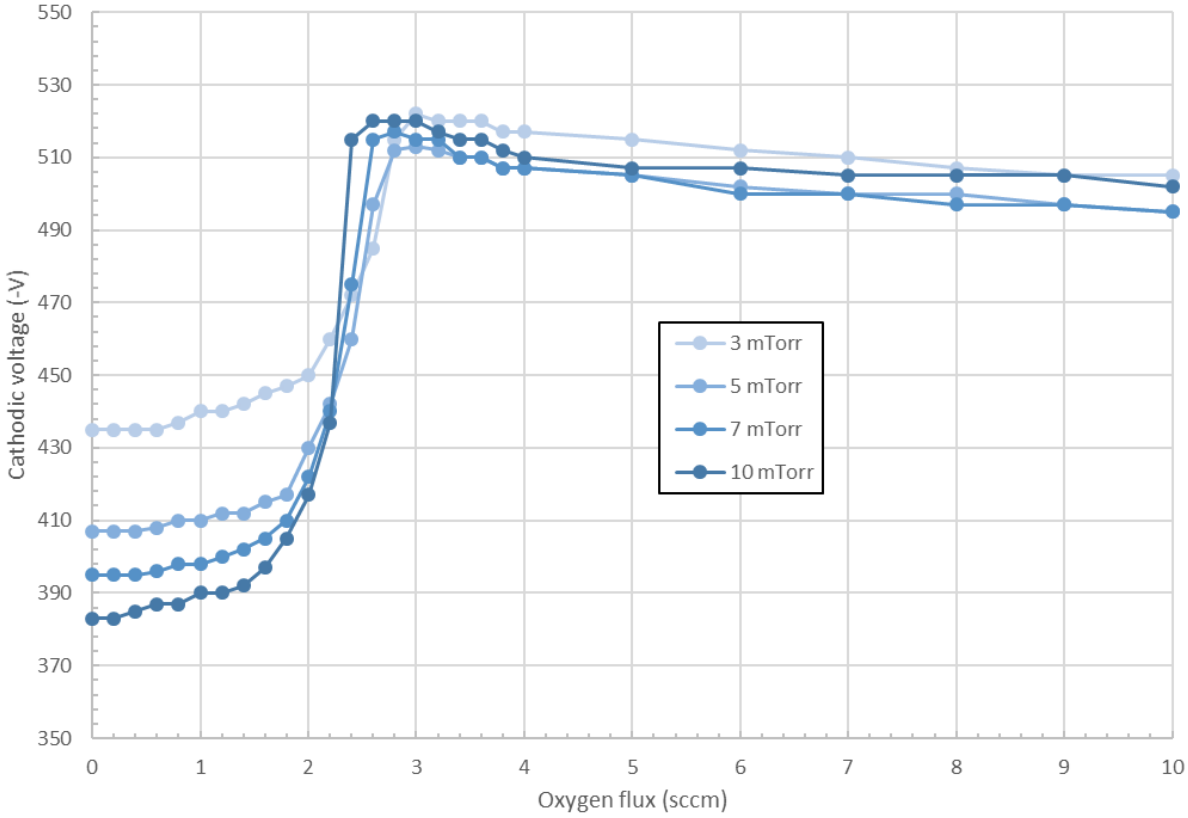

Figure 94. Modification of the intensity regulated oxidation curve for different pressures

It should also be highlighted that the amount of oxygen needed to poison the target is higher than in the voltage regulated mode. This behaviour has been explained earlier in III.3.2.4.

III.3.6.2. Frequency

This section presents and explains the oxidation curves obtained in the intensity regulated mode for different frequencies of Figure 95. The pulse width is kept at 50 µs so the frequency can be varied in the larger range possible without reaching the system's limits (i.e. duty-cycle too high). Having a short pulse also means that the waveform is only slightly modified throughout the process and therefore, no major modification of the discharge's stoichiometry other than the poisoning of the target is observed (e.g. rarefaction). These results complete the results from III.3.5.3 as explained in the latter section. Indeed, the objective, when modifying the frequency but keeping the same time-averaged cathodic current intensity, is to keep the quantity of positive ions impacting the

target constant but increasing their energy (i.e. the applied voltage). This way, it is possible to isolate the effect of the ions energy on the oxidation of the target.

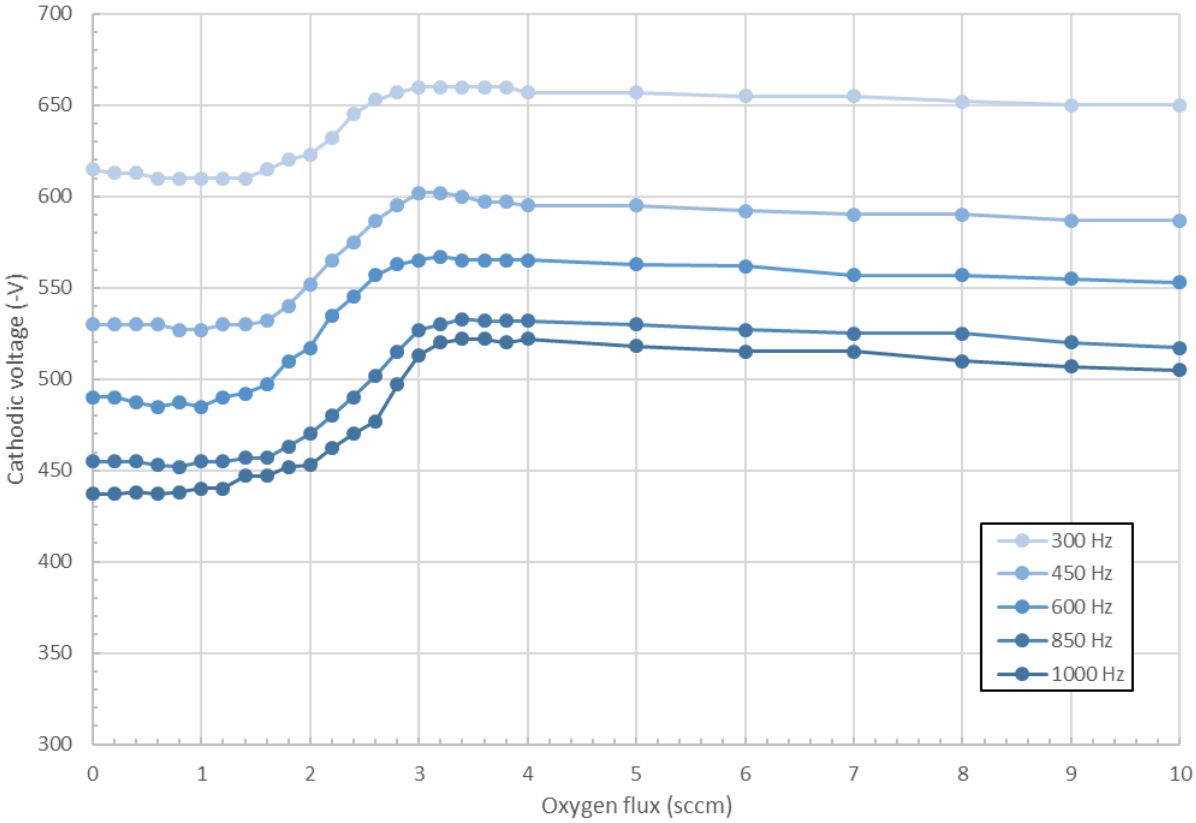

Figure 95. Modification of the intensity regulated oxidation curve for different frequencies

The results in Figure 95 show that the frequency modification has no major consequence on the range of oxygen flux corresponding to the poisoning of the target. Indeed, it shows that for each oxidation curve, the poisoned mode (i.e. maximum voltage) is obtained for an oxygen flux contained in between 3.0 and 3.2 sccm; which is a very narrow change, compared to the frequency study done in the voltage regulated mode (cf Figure 93). This behaviour means that, when the quantity of ions reaching the target is maintained constant, no matter the applied voltage, the necessary flux of oxygen to poison the target remains the same. This should mean that the quantity of positive ions reaching the target is predominating their energy when it comes to the effect on the nucleation of oxidative sites on the target surface. However, it does not mean that the (kinetic) energy of the impacting ions do not have an influence on the process, but its impact is much slighter than the impact of the number of ions impacting the target.

This behaviour is most likely due to the energy of impacting ions in such cases always being sufficient to sputter the nucleation point. This means that the sputtering rate is only slightly modified by the applied voltage (in such conditions) and therefore the balance in between the addition of oxygen atoms and the sputtering of the nucleation sites remains unchanged. In other words, the applied voltage modification may change the ionization rate of the discharge (i.e. increase of the number of ions intensity) but do not drastically change the capacity that a given positive ion has for sputtering a nucleation site. It should be noted that it seems that higher frequencies tend to need more oxygen to reach U_{mas}. It is probably because the <I> is not exactly the same for each frequency, as the power supply is more *forced* by the discharge at high frequencies

III.3.6.3. Pulse width

The last parameter to be analysed, regarding its influence on the oxidation curve of the target in the intensity regulated mode, is the pulse width. To do so, and similarly to the previous section, the frequency needs to be kept low so the duty-cycle do not reach too high values and result in a very unstable plasma. The pressure is also kept constant at a 3.0 mTorr value and the pulse width is modified between 50 and 200 µs. The results of the study are shown in Figure 96.

The observations made here are very similar to the observations made for Figure 95. Indeed, the modification of the pulse width does not impact the required amount of oxygen injected in the chamber to reach the maximum voltage of the target (i.e. fully poisoned mode), even though the range of applied voltage decreases with the pulse width.

Again, the conclusions are also very similar: the number of positive ions reaching the substrate remaining unchanged in all conditions, the poisoning of the target is not drastically modified by the applied voltage (i.e. the change in the kinetic energy of the ions). However, for the case presented here, the analysis goes even further. Indeed, changing the pulse width is also known to change the plasma composition, with the appearance of the rarefaction process. However, this also seems to have no (or a non-observable) impact on the ionizing process of the target in the intensity regulated mode. At least, it does not change the transitive range of oxygen flux. It is believed to be due to

the rarefaction peak not being present for long pulses in the fully poisoned mode (see Figure 83 and Figure 84)

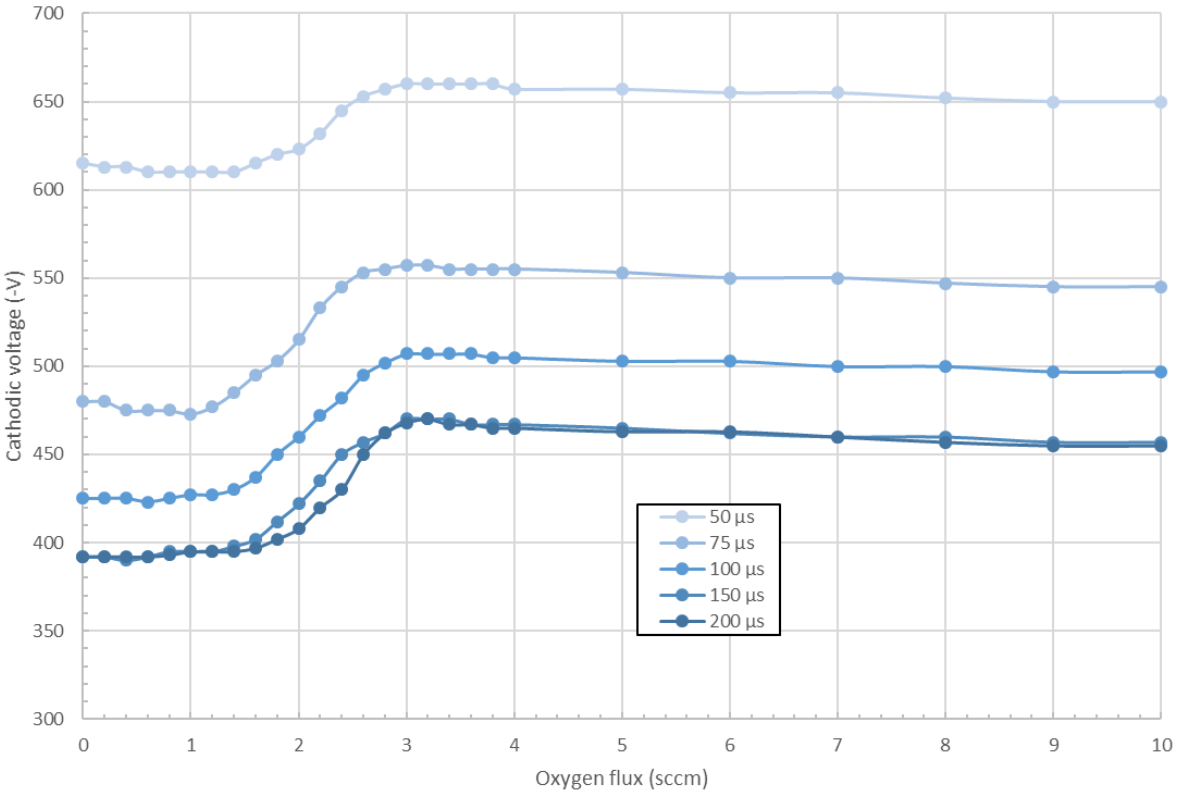

Figure 96. Modification of the intensity regulated oxidation curve for different pulse widths

III.4.Summary

III.4.1.Deposition rate

The modification of the deposition rate by the 1st order parameters has been studied and showed that the latter would increase linearly with the duty-cycle if normalized by the peak current intensity, meaning that the deposition rate is influenced by the overall deposition time but also the ionization rate of the discharge. It has also been determined that the voltage also linearly increases the deposition when all other parameters are kept constant. Finally, the pressure does not seem to majorly have an influence on the deposition rate even though it seems to show a critical pressure, where the deposition rate is maximal but a lower or higher pressure diminishes the deposition rate. In the intensity regulated mode, the influence of the duty-cycle (i.e. pulse width and frequency) has been confirmed. At the end of this first section, the microbalance has been used to determine the homogeneity of deposition on the substrate holder. It showed that the deposition is not totally homogeneous but the variations are very weak. The substrate will then be positioned in the centre of the substrate holder to result in homogeneous films. Also, a quick study showed that the deposition significantly drops when the oxygen part is increased in the chamber.

III.4.2. Energetic flux

The energetic flux at the substrate position was found to be modified by the two same main parameters: the voltage and the duty-cycle. The voltage linearly increases the thermal load coefficient while the increase of the duty-cycle seems to lead to a decrease of the coefficient, when other parameters are kept constant. The pressure showed no influence on the temperature rise in the chamber.

III.4.3.Cathodic current modification

First, in the metal mode, the time-averaged cathodic current intensity was found to be increasing linearly with the applied voltage unless it reaches the power supply limit of 2.0 A, after which the power supply does not increase the voltage anymore and keeps

it constant. When looking at the peak current intensity, the evolution is identical. When looking at the pulse waveforms in more details, the latter do not change for short pulses (i.e. without a rarefaction point) but, for long pulses, it seems that the increase of the voltage makes the rarefaction effect appear faster up to a certain point after which a second peak appears and get stronger with the increase of the voltage. This second peak is believed to be an acoustic wave of charged species. The voltage seems to be responsible for an increase of the ionization rate of the discharge when increased. Changing the pulse width seems to have no other influence on the discharge than following the pulse shape before the rarefaction point but past that point, the signal appears to be dropping as the pulse gets wider. This phenomenon can be either a power supply artefact or a consequence of the diminution of the refill time. The frequency, however, showed no major modification of the discharge, except a slight overall diminution of the latter's intensity, probably due to a diminution of the refill time as well. Finally, the pressure has a direct linear influence on the signal's intensity because of the increase of species in the chamber, leading to a more important number of ions.

After familiarizing with the metallic discharge, it was essential to study the oxidation process of the system. By adding oxygen in the chamber, it was possible to obtain oxidation curves. These oxidation curves can be divided into three main regions: sub-stoichiometric, transition window, over-stoichiometric. The sub-stoichiometric phase is characterized by either a stable or a (slight) increase of the peak current intensity due to the insertion of oxygen, covering the target's surface and generating more secondary electrons, resulting in a higher ionization rate. The transition occurs when the system reaches the stoichiometry and it results in a drop of the pulse intensity along with a modification of its shape, due to a different sputtering process taking place, where the target is fully covered by a Ti-O compound layer and oxygen participates in the discharge. Finally, the over-stoichiometric phase is reflected by an increase of the signal due to an increase of the chamber pressure. This increase of the pressure is due to the saturation of the target by oxygen atoms at the transition point, after which the excess of oxygen contributes in increasing the pressure. All the above observations were carried out for short pulse as it was impossible to do the same with long pulse while keeping a constant voltage; it would reach the power supply limits. Therefore, oxidation curves have also been realized in the intensity regulated mode to permit the observation of the long pulse

scenario. In the intensity regulated mode, the oxidation curve (voltage versus oxygen flux, here) shows an identical behaviour, with the three previous regions. The voltage diminishes where the intensity was increasing, in order to keep a constant intensity. The only and main difference between the two cases is the smothering of the curve, where the system needs more oxygen to be fully ionized: the transition window get wider. It is simply due to the voltage changing along the curve, which modifies the discharge by providing it more energy. As stated above, the intensity regulated mode should allow us to observe an oxidation process with longer pulses but the fact that the intensity limitation of the power supply cannot be hanged from 2.0 A results in a plasma being too intense, past the transition. A high voltage and a high duty-cycle result in a lot of arcs occurring in the chamber, making it impossible to acquire data (the signal keeps oscillating because of the arcs).

The effects of the deposition parameters have also been determined for the poisoned (i.e. over-stoichiometric) regime. In this regime, the voltage still has the same consequences on the discharge as it increases the signal without modifying the pulse shape itself. However, here, it also works for long pulses. It could be due to the absence of rarefaction point when poisoning the discharge. The pressure influence shows an increase of the signal again, but in a non-linear way. It shows an asymptotic behaviour, as the signal seems to stabilize its intensity at higher pressures. The frequency, however, leads to a diminution of the signal as it is increased. The pulse width modification, on its end, results in a surprizing evolution of the peak intensity as the latter increased, up to a 100 µs width, after which it decreases. The frequency has also been found to be an easy way to change the stoichiometry of the discharge while keeping a constant oxygen content in the chamber. It seems that every other deposition parameter can change the stoichiometry of the system but not sufficiently to be observed directly.

An interesting study consists in looking at this change indirectly. As a change in the stoichiometry of the system results in a slide of the transition window, it is easier to obtain oxidation curves for different values of each parameter and see how the transition window is affected. The results shown a very slight change when the pressure is increase: there is a critical pressure for which the oxygen content necessary to the transition is maximum. The voltage, however, showed a greater effect on the transition window. Increasing the voltage means that the system needs more oxygen to fully oxidize the

system. It is due to the augmented number of ions and sputtered species in the chamber. Increasing the duty-cycle by either the frequency or the pulse width results in a higher need in oxygen to poison the discharge even though, for the frequency, it does not change the amount of sputtered entities.

In the intensity regulated mode, the transition windows do not change when the frequency or the pulse width are changed, even though the initial voltage is different for each case. This behaviour shows that the time-averaged current intensity (i.e. the number of sputtered atom) is more important than their energy when looking at the necessary amount of oxygen to poison the system; and that is an important point to be reminded. For the case of the pressure modification, the data showed a slight difference in the transition. There are still no slide of it, but it widens. In other words, the transition gets smother as the pressure decreases.

III.5. Conclusion

This chapter reviewed the effect of each 1st order deposition parameter on the discharge for the rig used to deposit the films presented in Chapter V. It is essential to understand how each 1st order parameter affects the discharge and especially its oxidation process. First, the deposition rate and the thermal load at the substrate position were studied in the whole envelope available by the power supply. The results showed that the deposition rate is increased by both duty-cycle and voltage when the pressure did not seem to have a significant impact on it. The thermal load seemed to be only increased by the voltage but diminished by the duty-cycle. Ten centimetres away from the target, the temperatures reached even after 1 hour of sputtering are all below 60°C and even below 40°C for the second envelope (i.e. below 5% of duty-cycle). It is an essential point: it means that any film deposited in these conditions will be deposited at temperature where polymers are not meant to melt. It means that this power supply allows depositing onto polymeric substrate.

The pulse waveforms have been studied deeply to show that even when using only the waveforms provided by an oscilloscope, a deep understanding of the discharge is possible. This is only possible thanks to the knowledge already available in the literature and reviewed in **Erreur ! Source du renvoi introuvable.**. All the influences described i n this chapter (i.e. pressure, frequency, pulse width, and voltage) are identifiable to the data presented in I.1.5: the voltage increased the ionization rate and therefore the current signal, the pressure increases the inelastic collisions and therefore the ions created, the frequency and the pulse width modifies the duty-cycle (and the refill time), leading to diminutions of the ionization rate. The ionization process is also to the oxidation processes shown in Figure 18 and Figure 23, where there are three separate regions: a *constant* sub-stoichiometric region (or slight increase, depending on the conditions), an important drop at the transition window, and a slight increase for the over-stoichiometric region. The effects of each 1st order parameter on the oxidation curves haves also been determined. However, the following chapter will show that oxidation curves can differ from a rig to another (order 0), even when reactively sputtering Titanium in an oxidized atmosphere using HiPIMS.

This chapter suggests that the higher ionization rate is obtained for short pulses, low frequencies, high voltage, and higher pressure; and that any condition seems to be deposited at low temperature, supposedly not melting polymeric substrates. It will be the starting point for the material study.

Chapter IV. Plasma diagnostic – order 0

This chapter aims at observing and analyse the effect the modification of order 0 parameters can have on the system. The point is to analyse the effect of the power supply used and the effect size of the rig/target. First, the results obtained with a different supply on the same rig are presented to show the changes it can have on the discharge. Next, this same power supply is used on a smaller rig to determine the effect of the deposition chamber size. Finally, the same power supply, again, is used on a third (small) rig in Linköping. Chronologically, the third set of data was obtained first but is presented last because it shows a clearer evolution and thought process. In each scenario, the influence of each first order parameter was observed on the metallic and poisoned plasma, as well as the influence of the oxygen injected. Also, the modification of the oxidation process by the deposition parameters has also been determined when possible.

IV.1. Data from HiPSTER 6® on large rig

Here are presented the results in terms of plasma diagnostic obtained with the HiPSTER 6® power supply connected to the large (Nordiko) rig. The aim is to compare the data to the data from previous chapter to determine the importance of the power supply on the discharge.

IV.1.1. Metal mode

IV.1.1.1. Voltage

In metal mode, the effect of the voltage is very much like that of the Huettinger power supply for both short and long pulses. Indeed, when comparing to Figure 60 and Figure 62, it is clear to see that the effect of voltage increase of the waveforms are overall similar. The increase of the voltage results in an increase of the pulse intensity with only minor changes on the short pulse waveform and similar changes for the 200 µs pulse. Indeed, for short pulses, there is only an overall increase of the pulse intensity, through an increase of the shape's slope in the early stages of the pulse, mainly. The effect has already been explained several times and is not discussed any further here.

For the 200 µs pulse, the observations are also the same, in a quantitative way: the pulse presents two peaks, that both appear sooner during the pulse as the voltage increases. Moreover, the second peak's evolution is faster than the first one, which results in a narrowing of the delay in between these two peaks. Also, the second peak always remain lower than the first one, except for the maximum voltages. The nature of these peaks is believed to be as follows: the first peak is the sputtering of the Argon ions on the target and the second peak is the mixed metal and gas sputtering of the target, which is why the intensity reduces after that second peak (the self-sputtering yield is lower than the sputtering yield).

However, it should be noted that there is a difference between the HiPSTER 6® and the Huettinger shapes: the post-pulse. Indeed, in the case of the HiPSTER 6® power supply, the post-pulse decease of the current intensity occurs faster. It is believed to be due to a faster switching off of the applied voltage, resulting in a faster evacuation of the

charges away from the target, as the only change in the apparatus is the power supply, i.e. the applied voltage.

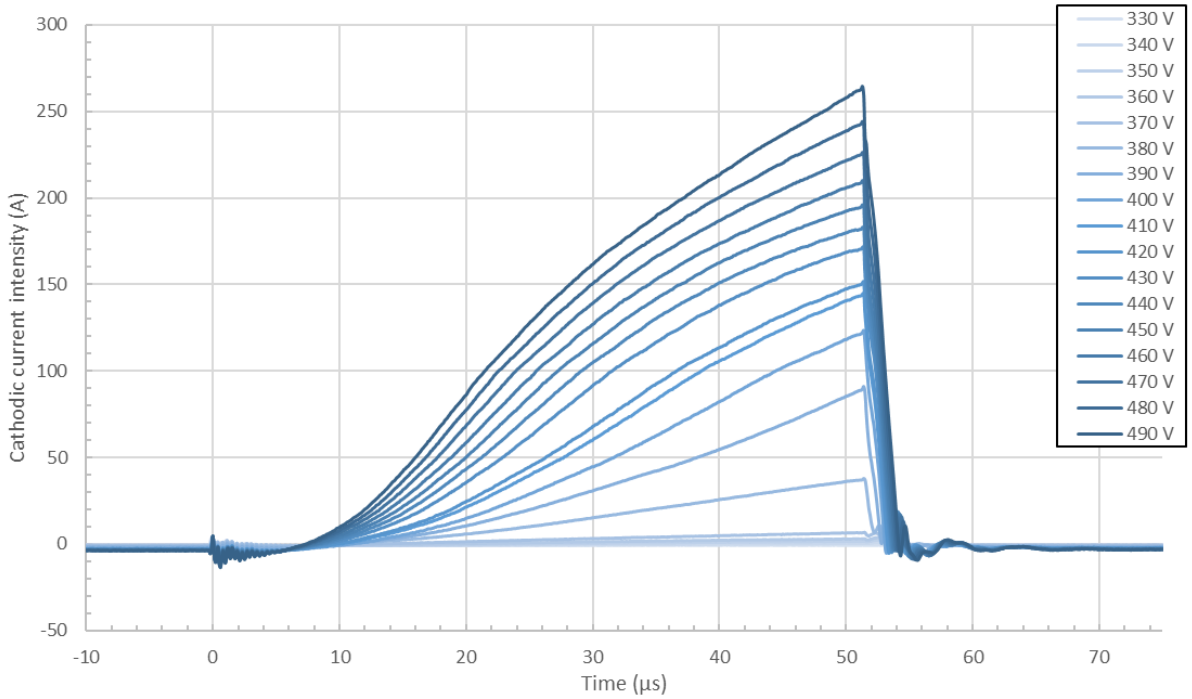

Figure 97. Modification of the metallic pulse waveform when increasing the applied voltage for 50 µs long pulses (3 mTorr – 300 Hz – 50 µs – 0.0 sccm)

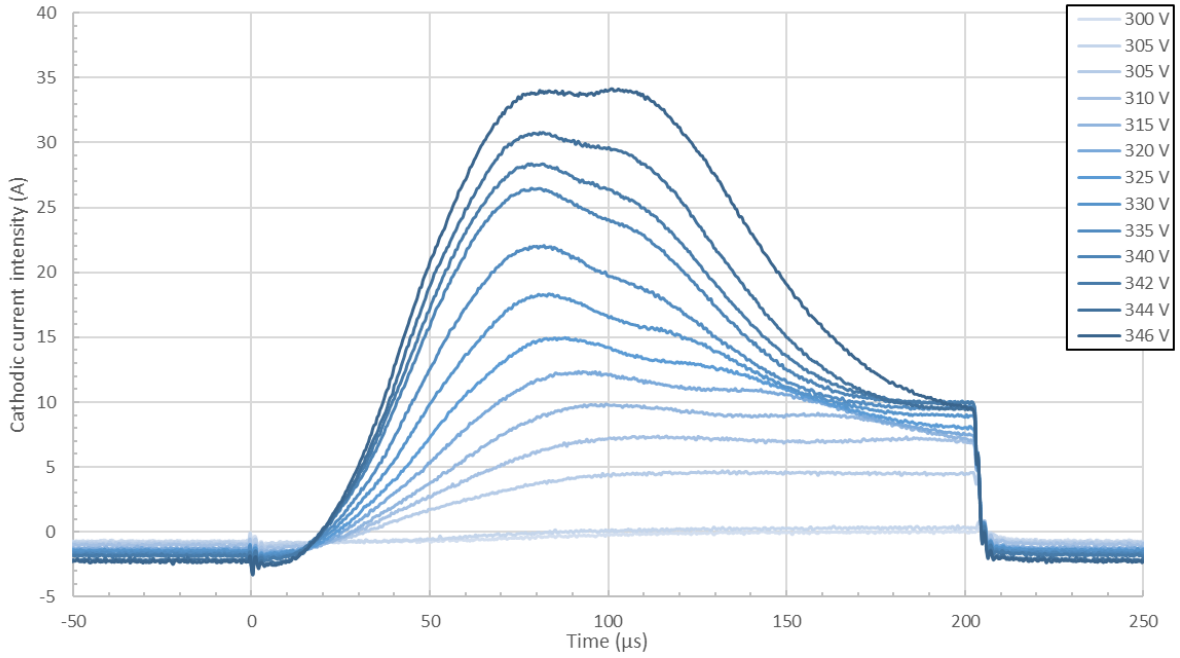

Figure 98. Modification of the metallic pulse waveform when increasing the applied voltage for 200 µs long pulses (3 mTorr – 300 Hz – 200 µs – 0.0 sccm)

IV.1.1.2. Pressure

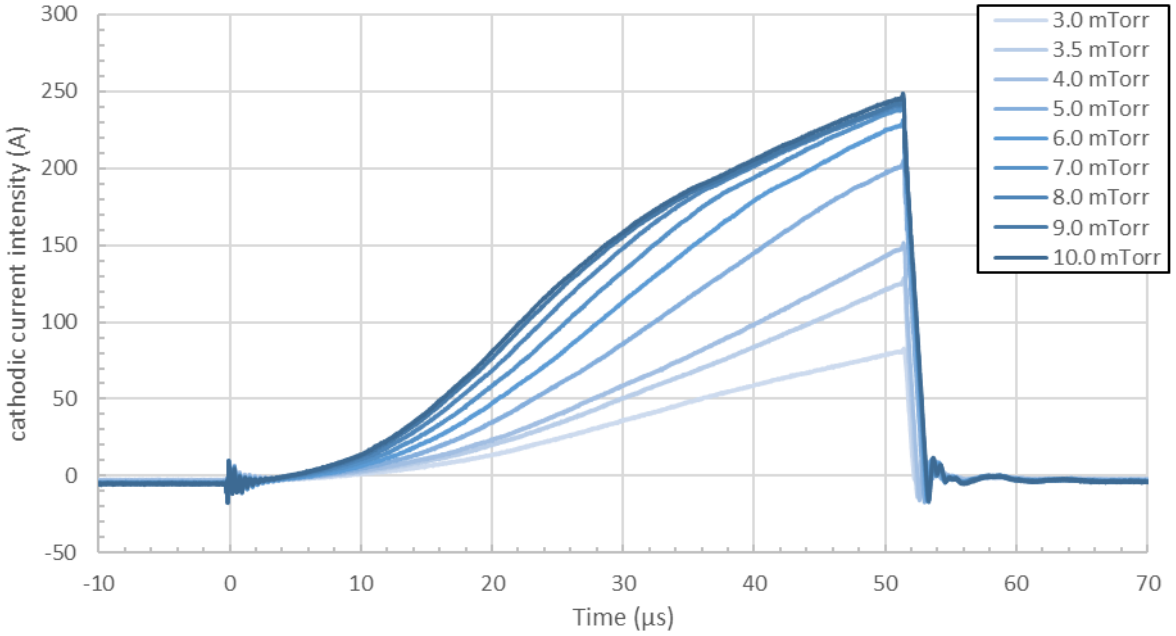

Figure 99. Modification of the metallic pulse waveform when increasing the pressure for 50 µs long pulses (50 µs – 500 Hz – 410 V – 0.0 sccm)

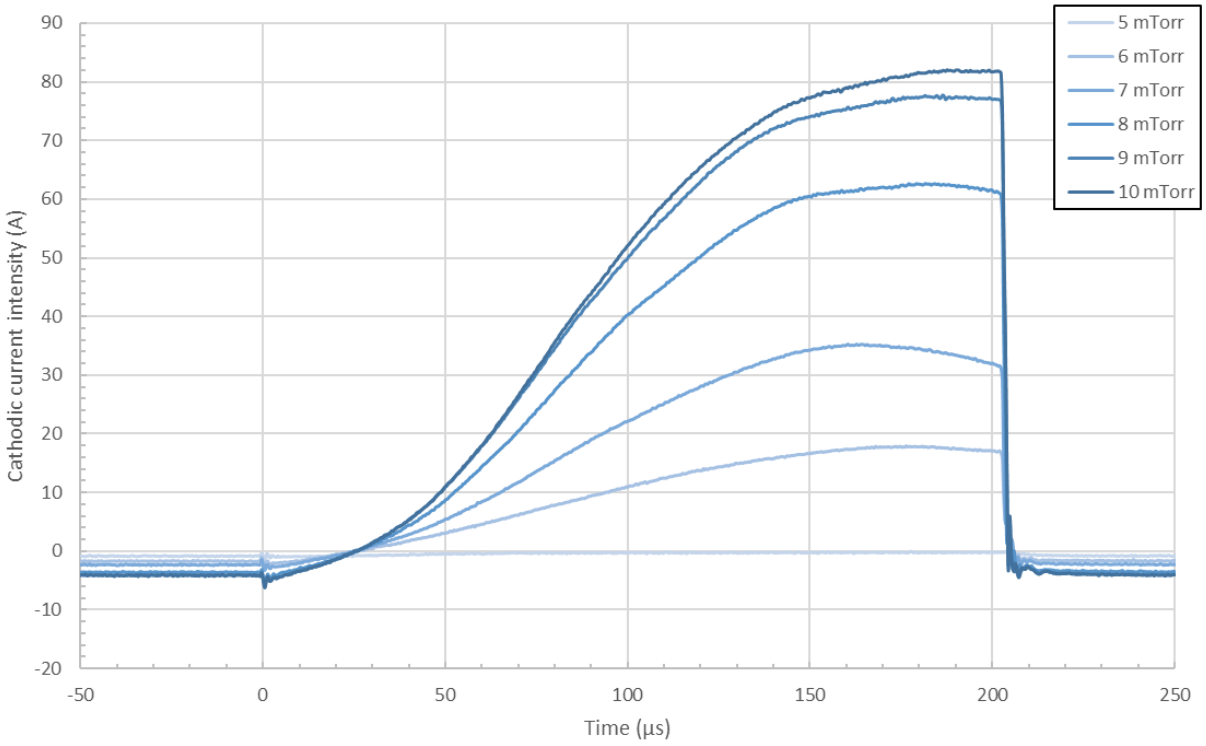

Figure 100. Modification of the metallic pulse waveform when increasing the pressure for 200 µs long pulses (200 µs – 300 Hz – 285 V – 0.0 sccm)

Both Figure 99 and Figure 100 show the same consequences for the pressure increase. Indeed, in both situations, the increase of the chamber pressure results in an increase of the peak intensity. This increase is relatively important but seems to slow down after a certain point.

The fact that the pulse intensity increases reminds of the voltage effect, especially for short pulses. For longer pulses, the situation is different: there is a clearer change in the evolution. Indeed, when comparing Figure 100 and Figure 98, it is clear to see that even if the maximum pulse intensity reached by increasing the pressure is higher than the maximum reached using the voltage, the rarefaction effect does not appear in the first case. The fact that the rarefaction effect does not occur faster with increase of the intensity means that the quantity of ions in the chamber is greater, but not their energy, in opposition to what was observe in Figure 98. This observation can be of great importance as it shows that higher pressure brings more ions but the energy of these ions is most likely to be reduced, or at least remain the same.

IV.1.1.3. Frequency

The pulse intensity increases up to a certain frequency, after which it stabilizes to a constant value. It is believed that at such short pulses, the duty-cycle is too low at low frequencies and it results in difficulties for the process to keep ionized species in the chamber. These difficulties are believed to be the reason here since, after a certain point, the intensity does not increase anymore and remains constant, showing that there is a maximum intensity reachable at a given voltage, pressure and pulse width (in this rig). This has already been evoked in previous chapter (see Chapter III).

For the 200 µs long pulses case, presented in Figure 102, the situation is similar for low frequencies: the signal decreases due to the recombination of the ions/electrons pairs in the chamber during the off-time. The longer the off-time is, the more recombination there are, the harder it is to ionize the gas at each pulse. Again, this process has already been evoked previously and has been shown in Figure 22.For longer pulses, this time, a decrease of the intensity is observed. This phenomenon is most likely to be due to the other end of the spectra: an off-time being too short. Indeed, the pulses being this long lead to the apparition of self-sputtering, meaning a majority of metal ions in the target vicinity during the pulse. At low frequency, these ions are recombined and/or replaced

by argon atoms/ions but at higher frequencies, these metal species are believed to remained in the chamber long enough to still be present for the next pulse. This results in a lowered sputtering rate at the plasma is not constituted of argon ions alone anymore; there are also metal ions, with a lower sputtering yield.

In previous chapter, the effect of frequency on the pulse intensity was far from being this evident in the metal mode. It was mainly due to a more unstable plasma and the fact that the power supply had a power limit that could have influenced the plasma at high duty-cycle. This shows that, clearly, using a different power supply can change the plasma physics in the chamber. However, it should be highlighted that this effect is observed in the metal mode.

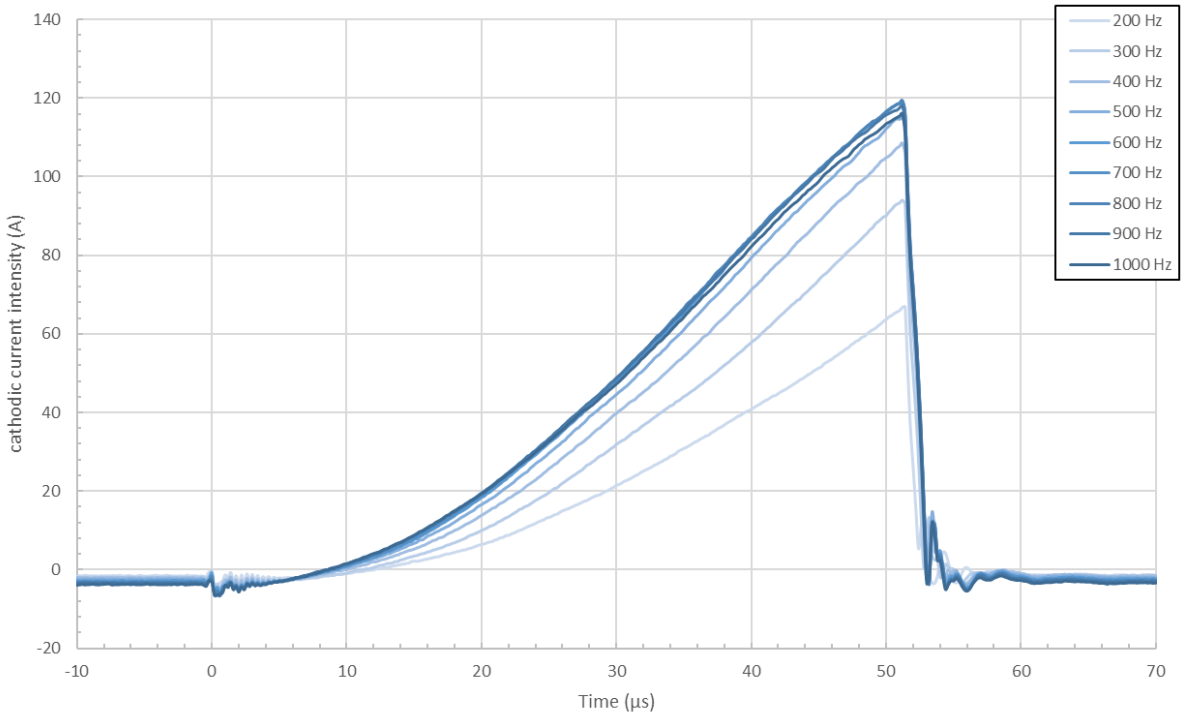

Figure 101. Modification of the metallic pulse waveform when increasing the frequency for 50 µs long pulses (3 mTorr – 50 µs – 390 V – 0.0 sccm)

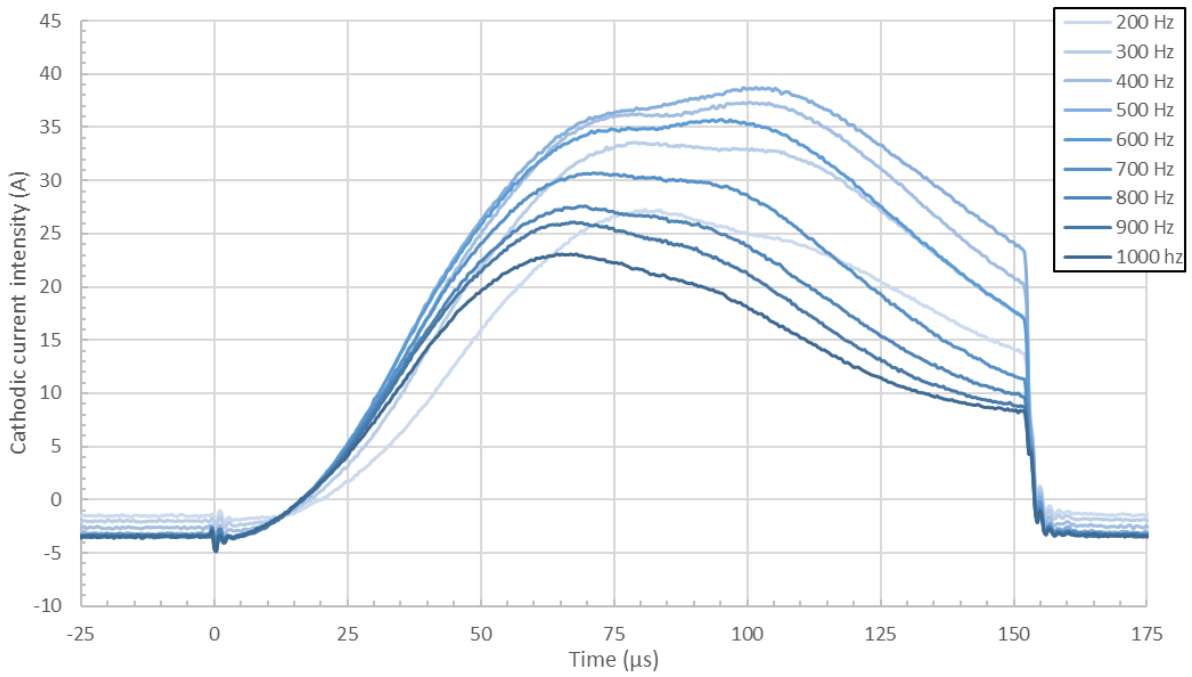

Figure 102. Modification of the metallic pulse waveform when increasing the frequency for 150 µs long pulses (3 mTorr – 150 µs – 350 V – 0.0 sccm)

IV.1.1.4.Pulse width

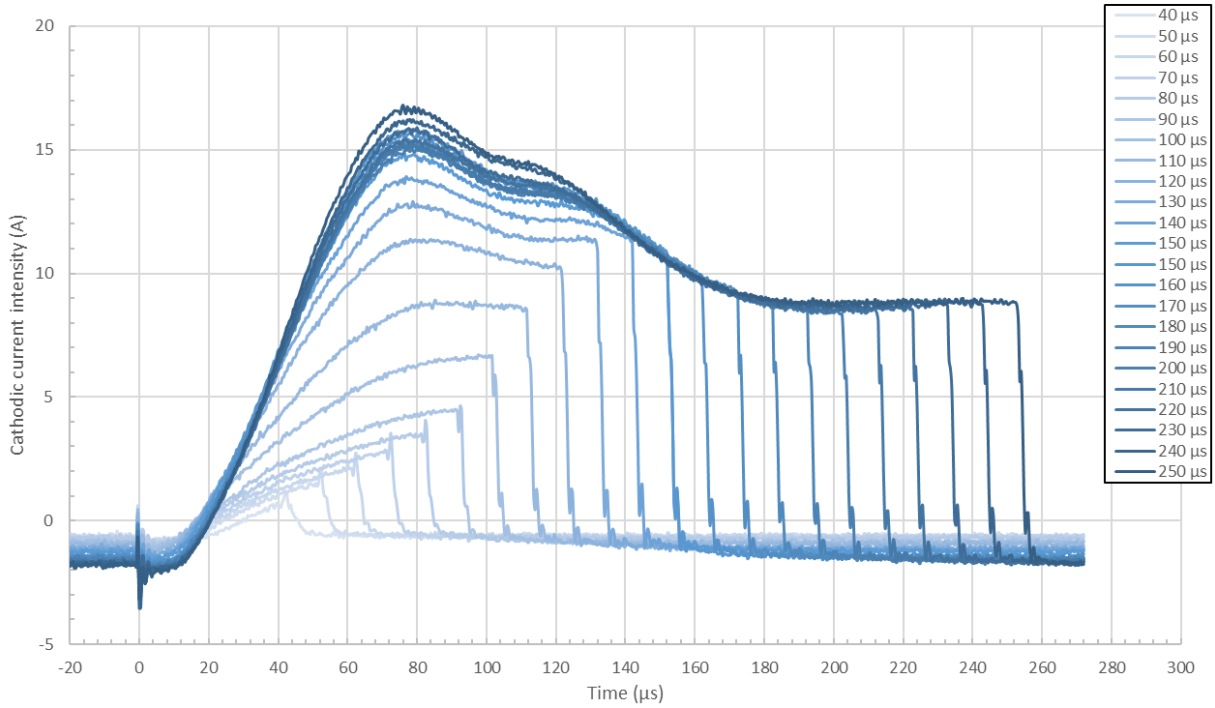

Figure 103. Modification of the metallic pulse waveform when increasing the pulse width (3mTorr – 300 Hz – 350 V – 0.0 sccm)

The data presented in Figure 103 shows a different evolution of the pulse shape when increasing the pulse width than what has previously been observed. It seems that increasing the pulse width tends to increase the peak current intensity, up to a certain limit. It would mean that increasing the time of sputtering increases the amount of ions possibly created in the chamber. The only hypothesis that can be provided here would relying on an augmented duty-cycle, leading to a persistence of charged species in the chamber, easing the ionization of the atoms in the chamber. However, no conclusion can be made and these results would need complementary studies, focusing on identifying if the difference between the pulse width evolutions originates from the power supply or from a specific physical phenomenon.

IV.1.2. Reactive gas content

IV.1.2.1. Voltage regulated

In this section, the effect of inserting oxygen in the chamber is studied. For both sets of data presented in Figure 104 and Figure 105, all parameters remain unchanged, even the voltage. This way, the effect of oxygen insertion in the chamber can be isolated and studied independently from the other parameters.

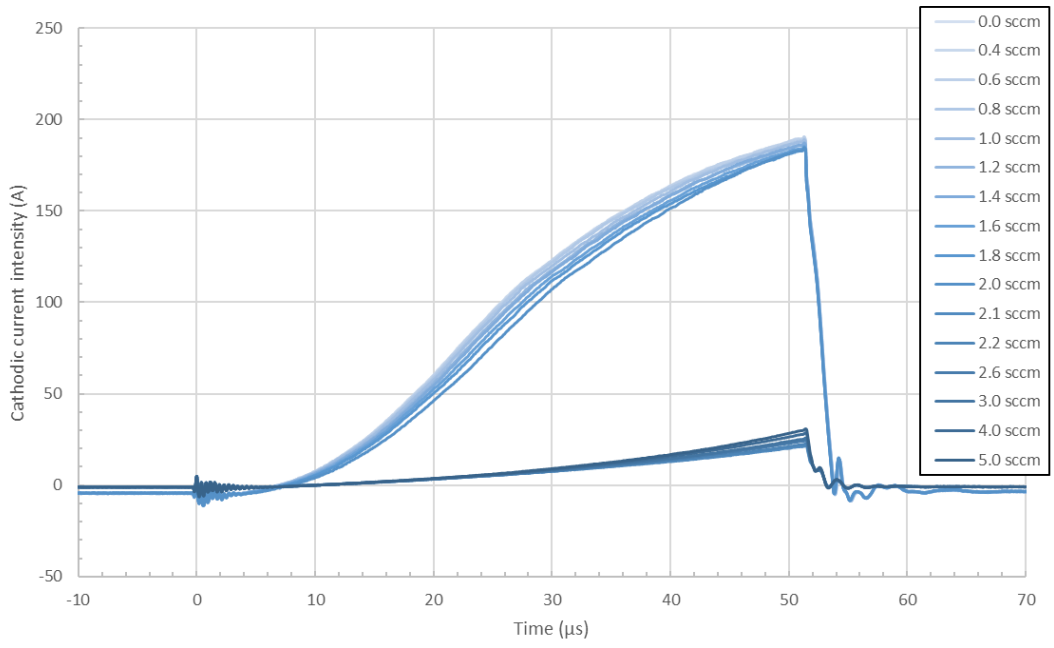

Figure 104. Modification of the pulse waveform when increasing the oxygen content in the chamber (3 mTorr – 500 Hz – 50 µs – 420 V)

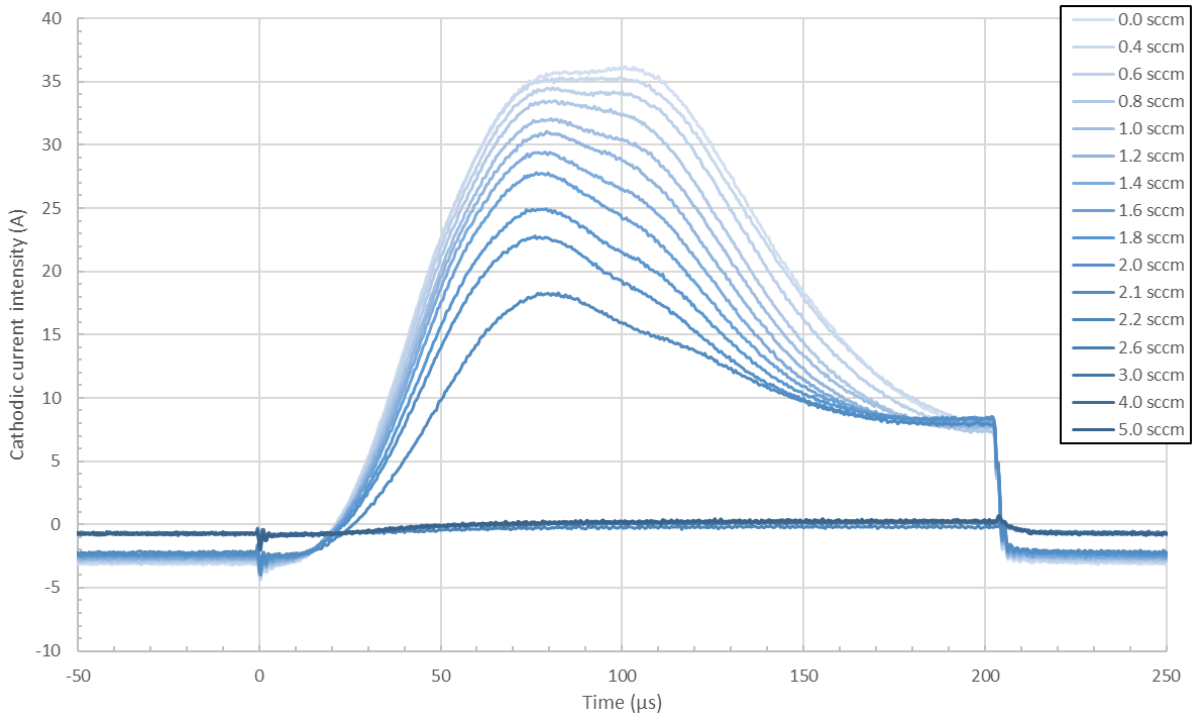

Figure 105. Modification of the pulse waveform when increasing the oxygen content in the chamber (3 mTorr – 500 Hz – 200 µs – 330 V)

Here, both evolutions show the same trend: a *slow* diminution of the peak intensity with the increase of the oxygen flow sent in the chamber until a critical point (so-called transition window) where the intensity drops to a much lower value and from which the signal then increases with the oxygen content. Again, as evoked in the previous chapter, the sub-stoichiometric part of this evolution can change, depending on the set of conditions chosen. More oxidation curves and discussion on the topic are found in IV.1.5 and follows the discussion already made in III.3.2 and are therefore not discussed in detail here. It is only reminded that the two scenarios in sub-stoichiometric mode are either a slight decrease of the pulse current intensity due to a coverage of the target by oxygen atoms or a slight increase in the peak intensity due to the appearance of negative oxygen ions in the chamber, easing the ionization process in the chamber.

The transition phase is a well-known process now: the target is fully covered with the Ti-O compound material and therefore diminishes the amount of ions in the chamber. The details on this process can be found in I.1.5.4. Briefly, it is due to the diminution of the secondary electrons emission factor when the target is fully covered,

resulting in a diminution of the plasma intensity: the ionization process is more difficult as less charged species are *released* from the target.

The third regimes, so-called over-stoichiometric regime, corresponds to any increase of the oxygen content beyond that point. Here, the pulse intensity is rising when the oxygen content keeps increasing. This phenomenon appears because any additional oxygen atom beyond this point is adding to the bulk plasma, and not the target's surface anymore and this leads to two different things: mainly an increase in the chamber pressure but also probably a higher ionization rate in the bulk plasma due to the excess in negative oxygen ions.

The oxidation process presented here is very much like the oxidation process presented in III.3.2, which shows that using a different power supply does not drastically change the oxidation process of the target. This observation is of great importance for reactive HiPIMS. Indeed, it shows that when changing the power supply used on a given deposition chamber is not likely to change the oxidation process and therefore the possibility to deposit oxide layers in this given chamber. This observation is even more important when completed by the results obtained in the next sections, where the oxidation process is shown for the same power supply used on different deposition chambers and should therefore be discussed further.

The only noticeable difference between this oxidation process and the one shown in III.3.2 is the amplitude of the stoichiometric drop in the intensity. Indeed, in Figure 104 and Figure 105, the drop is much greater than that of Figure 69 and Figure 70. To this, no explanation could be found but it is not essential in this project as it is not a change in the process physics in a qualitative way but only in a quantitative way. The observation of a greater drops also leads to another observation. Indeed, with the Huettinger power supply, there were difficulties to find sets of parameters where the plasma would not switch off when getting oxidized when, with the HiPSTER 6® power supply, the plasma remains on, even at very low pulse intensities (illustrated by the long pulse case). Even if, again, no explanation can be given, it still shows that the quantitative changes brought by using a different power supply can lead to an easier running of the process (here, with the HiPSTER 6® power supply).

IV.1.2.2. Intensity regulated

Here are presented the oxidation curves in the cathodic current intensity regulated mode. Again, the transition is shown for 50 µs and 200 µs long pulses with the pressure and the frequency remaining unchanged in between the two cases. The results are presented in Figure 106 and Figure 107. When comparing these results with the results obtained with the Huettinger power supply (i.e. Figure 73 and Figure 76), the transitions are very similar but *clearer* and more stable.

First, for 50µs long pulses, the difference between the sub-stoichiometric pulse shapes and the over-stoichiometric pulse shapes is much more easily spotted. The difference in the curvature is more important, which results in a greater difference in the shapes. The reasons behind this greater difference in the curvature is, again, not a qualitative difference of the processes occurring during the discharge; it is only quantitative.

For 200 µs long pulses, it is also a quantitative difference but this time, it is much more significant. Indeed, in the poisoned mode, the pulse changes from a self-sputtering mode in the sub-stoichiometric mode to a sputtering mode in the over-stoichiometric mode. It is clear here since the sub-stoichiometric pulse shapes present a peak intensity before the end of the pulse, which has been identified as the rarefaction point in the literature, which disappears when reaching the poisoned mode. In the poisoned mode (i.e. over-stoichiometric), the pulse intensity has a monotonic rise until the end of the pulse, which means that no self-sputtering by metal atoms occurs, a sit would result in a lowering of the sputtering rate and therefore the current intensity. This observation could only be suggested in previous chapter as the plasma became very unstable when reaching poisoned mode for long pulses. Here, the plasma is much more stable in such conditions and allows to observe the full transition, in opposition to the data presented in Figure 76. It can be said that the oxidation process seems much more stable when using the HiPSTER 6® power supply but it does not seem to change the process itself.

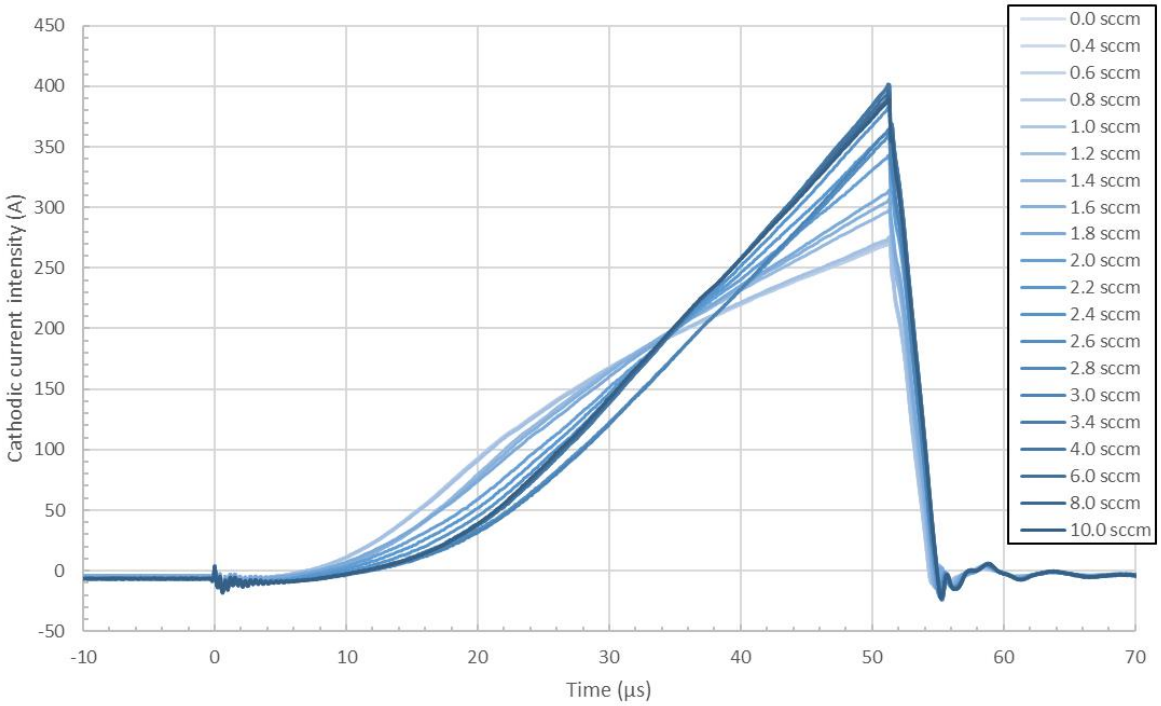

Figure 106. Modification of the pulse waveform when increasing the oxygen content in the chamber, in the intensity regulated mode (3 mTorr – 300 Hz – 50 µs – 2000 mA)

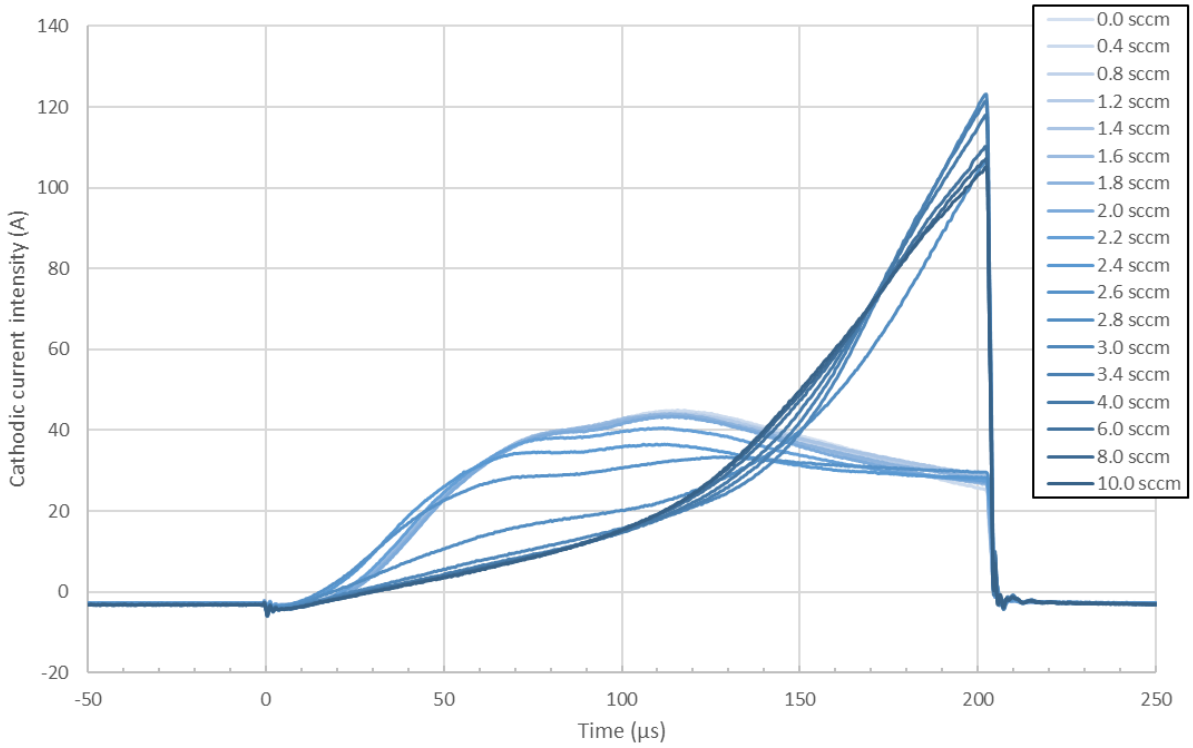

Figure 107. Modification of the pulse waveform when increasing the oxygen content in the chamber, in the intensity regulated mode (3 mTorr – 300 Hz – 200 µs – 2000 mA)

IV.1.3.Poisoned mode

This section presents the results obtained when the system is fully poisoned with oxygen. It is close to reflect the deposition conditions. The main objective is to, once again, compare these results with those presented in the previous chapter to determine the effect that a change in power supply can have on the system.

IV.1.3.1.Voltage

IV.1.3.1.1. Voltage regulated

In Figure 108, the pulse shape is recorded for a 50 µs long pulse and low frequency (to allow a larger range of study) while the voltage is increase by 10 Volts steps. The waveforms are presented together and show the evolution of the pulse when increasing the voltage. It shows an identical trend that that of Figure 78: the pulse intensity rises, without changing the overall form of the pulse shape. Also, using this power supply results in a faster decay of the intensity once the applied voltage is switched off at the end of the pulse, as evoked in previous section. Other than that, the waveforms are very similar.

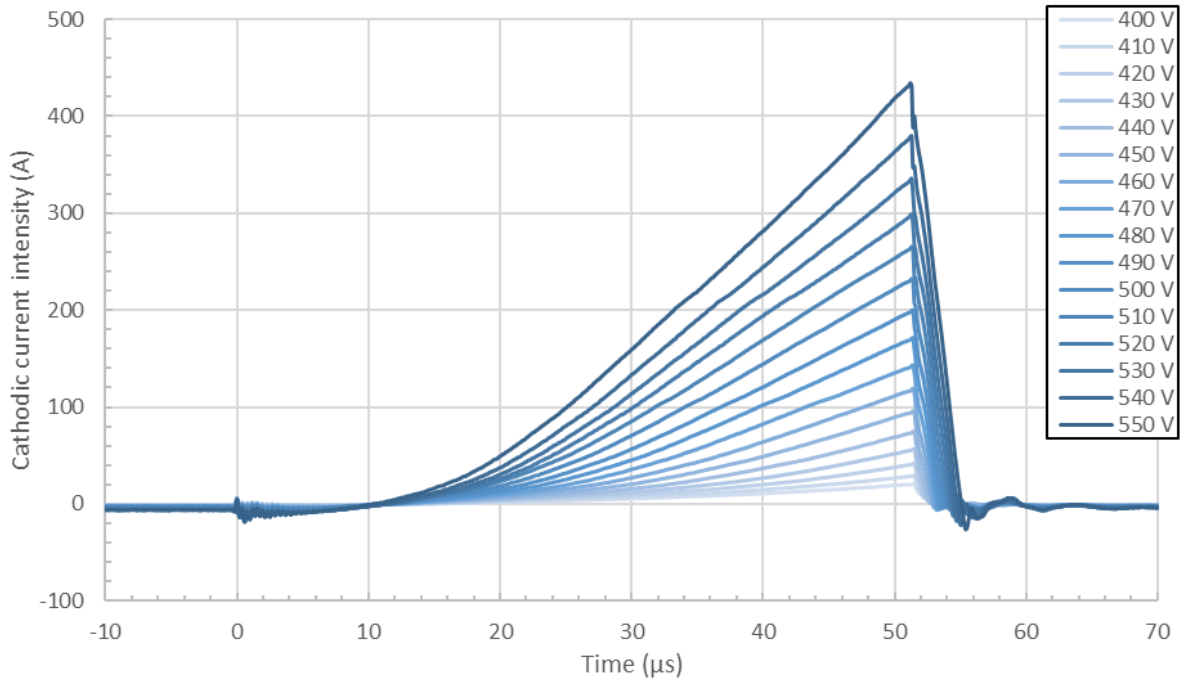

Figure 108. Modification of the poisoned pulse waveform when increasing the voltage for 50 µs long pulses (3 mTorr – 300 Hz – 50 µs – 4.0 sccm)

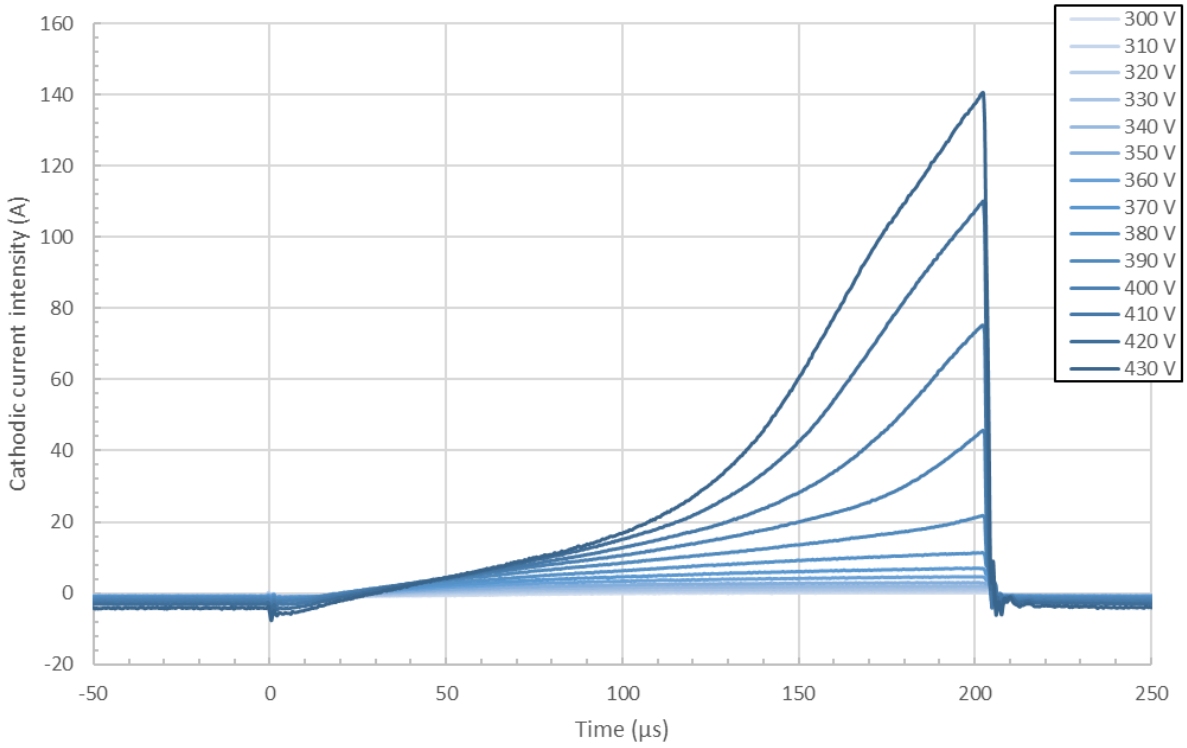

Figure 109. Modification of the poisoned pulse waveform when increasing the voltage for 200 µs long pulses (3 mTorr – 300 Hz – 200 µs – 4.0 sccm)

Things are different when looking at long pulses. For long pulses, the comparison between Figure 109 and Figure 80 leads to a simple observation: the waveform is quite different at high voltages in the poisoned mode. Indeed, with the Huettinger power supply, poisoned mode shapes still show a diminution of the slope towards the end of the pulse, showing that there is still some self-sputtering, even though it does not reach the rarefaction point, past which it is only driven by self-sputtering. Here, in Figure 109,the slope never comes to a null value during the on-time of the pulse, showing that more ions are created all along the pulse, this is a proof that the ionization process is quite different. Using the HiPSTER 6® power supply seems to be more efficient in terms of ions production at a given voltage. When looking at the pulse peak current intensity in Figure 80, it does not go higher than 30 A at 430 V, when Figure 109 shows that for the same voltage, the peaks current intensity is around 140 A with the HiPSTER 6® power supply. This major is believed to be due to the difference is power supplies limits, resulting in a much more accurate representation of the process. It is believed that the Huettinger slightly limits the amount of electrons it can receive per unit of time, which is why, important slopes like these presented in Figure 109 cannot be observed with the Huettinger power supply. The HiPSTER 6® power supply allows the user to choose the

maximum value for that slope, so if this parameter is set to a high enough value, the power supply does not limit the discharge.

IV.1.3.2. Pressure

IV.1.3.2.1. Voltage regulated

Here, the observation is very surprising. Indeed, the behaviour is opposite to what was observed with Huettinger: the signal decreases with the pressure being raised. The exact reason behind this behaviour remains unconfirmed but the author suggests a more ionized plasma here, for which any increase of the pressure would only lead to a loss of energy by inelastic collisions. However, this hypothesis is far from being confirmed, it is only a suggestion by the author. IEDFS studies would help determining the processes occurring here when the pressure is increased.

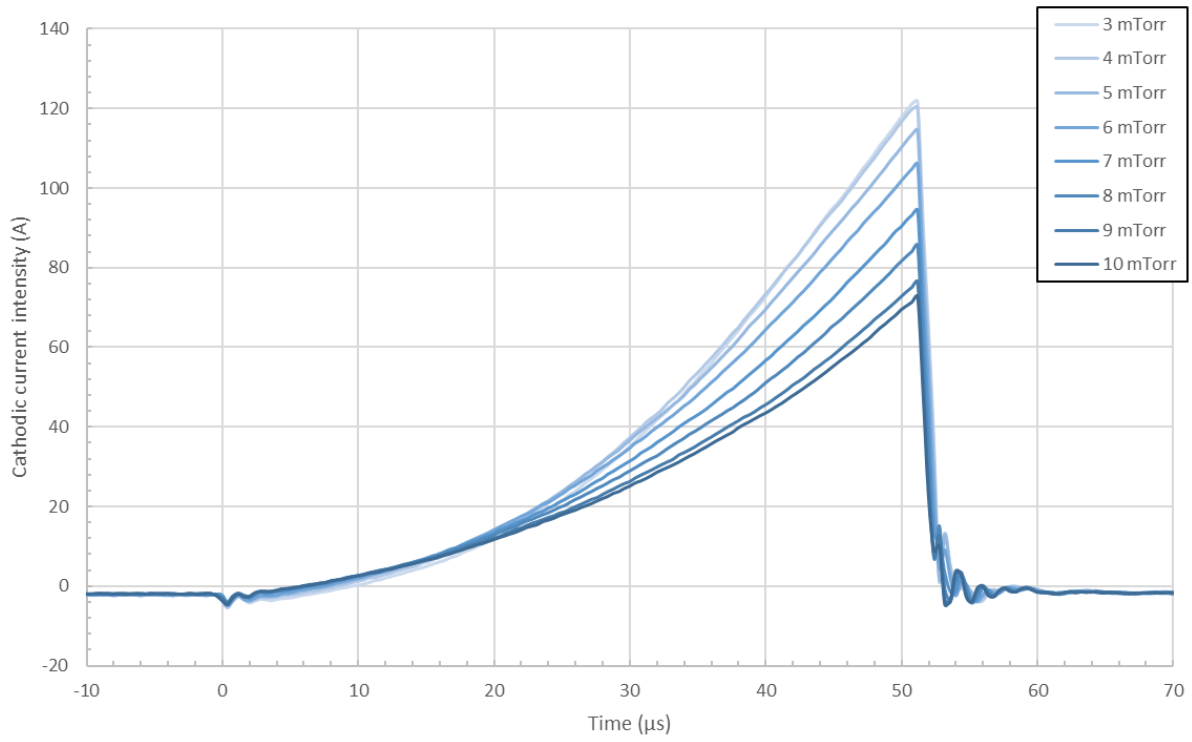

Figure 110. Modification of the poisoned pulse waveform when increasing the pressure for 50 µs long pulses (50 µs – 500 Hz – 460 V – 5.0 sccm)

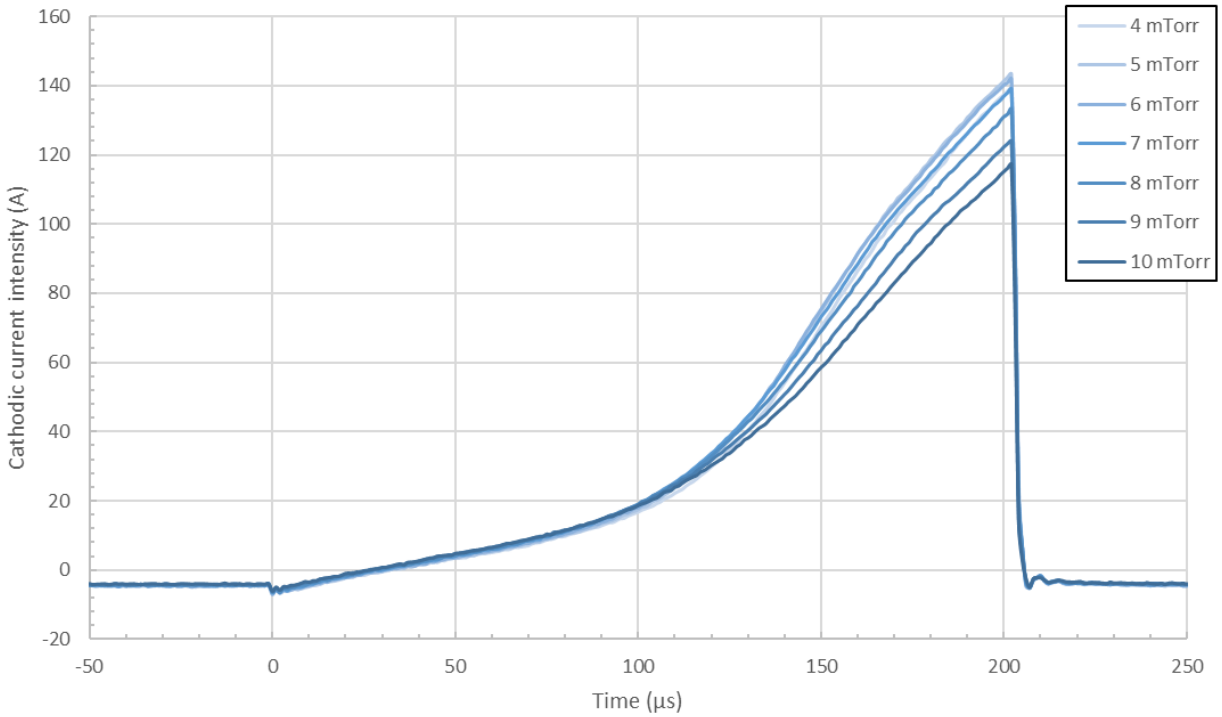

Figure 111. Modification of the poisoned pulse waveform when increasing the pressure for 200 µs long pulses (200 µs – 300 Hz – 420 V – 5.0 sccm)

IV.1.3.2.2. Intensity regulated

Here, the waveforms are presented but since the latter are not changing majorly with the increase of the pressure in the oxide mode (i.e. they only change in terms of intensity, not in terms of shape), the pulse shapes appear to be unmodified by the increase of the pressure in the oxide mode. The applied voltage is increased by the power supply to overcome the loss of intensity originating from the pressure raise. These evolutions therefore do not need any further discussion. The change in the voltage, however, remains low – under 10 Volts - and thus do not influence the waveform.

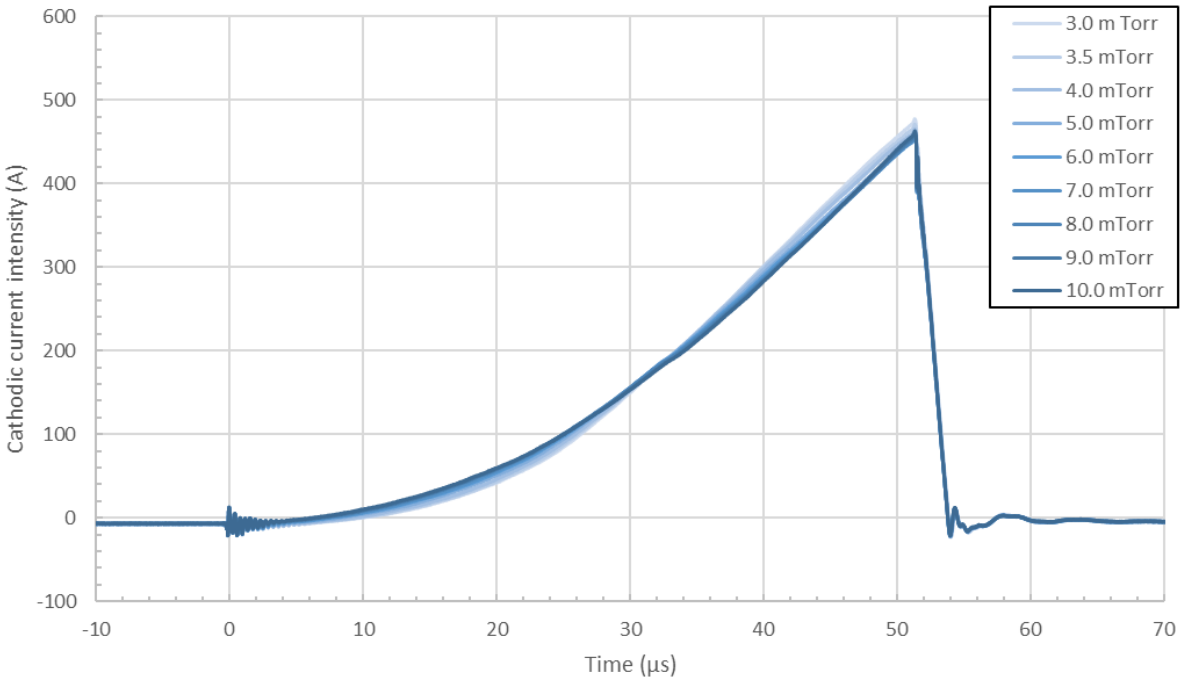

Figure 112. Modification of the poisoned pulse waveform when increasing the pressure for 50 µs long pulses in the current intensity regulated mode (500 Hz – 50 µs – 2000 mA – 5.0 sccm)

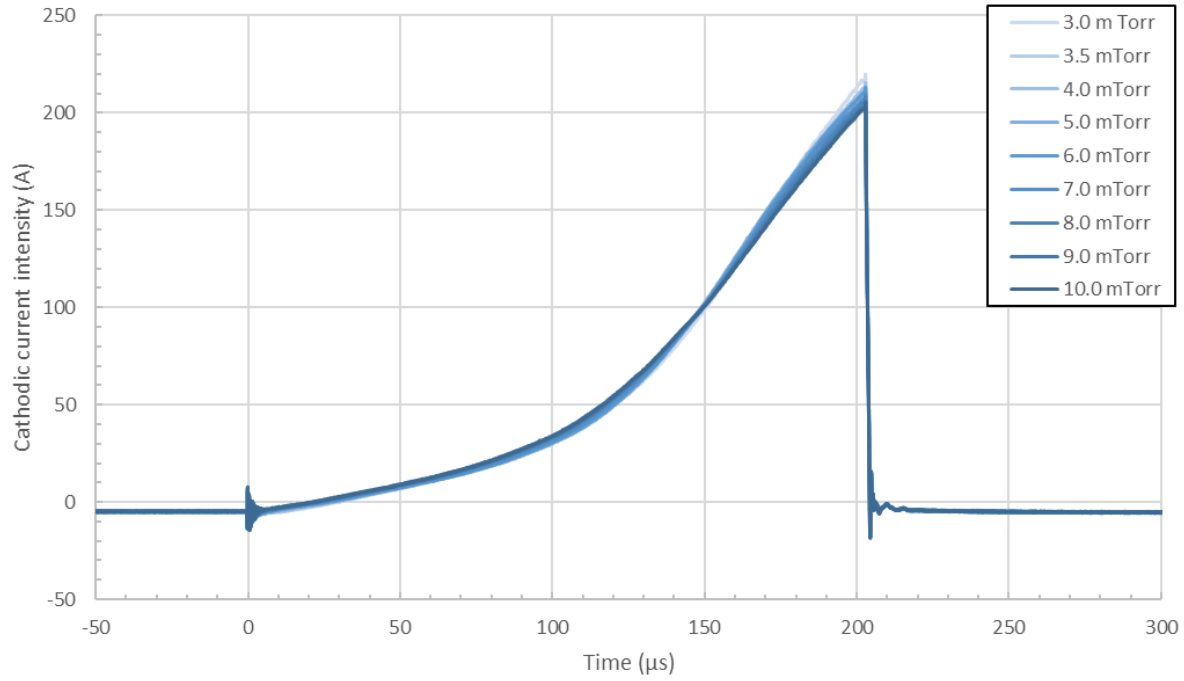

Figure 113. Modification of the poisoned pulse waveform when increasing the pressure for 200 µs long pulses in the current intensity regulated mode (300 Hz – 200 µs – 2000 mA – 5.0 sccm)

IV.1.3.3.Frequency

IV.1.3.3.1. Voltage regulated

The results shown in Figure 114 and Figure 115 show a very similar behaviour to what was observed in III.3.3.3. The pulse intensity diminishes when the frequency is increased. It has already been explained that, even though there are no proof of it, the hypothesis is the diminution of the refill time when increasing the frequency, leading to a lack of *new* species in the chamber. It seems that the phenomenon is only observed in the long pulses case in the metal mode but, here, in the poisoned mode, it also appears to be true for short pulses. The reasons behind it are still unclear but it clearly shows that at higher frequencies, the system tends to generate less ions for a given voltage. The fact that the effect it much more important in the 200 µs pulse case could indicate that the change in duty-cycle is indeed the determining factor leading to this decrease of the signal. To be able to fully identify the physical processes leading to this diminution, EEDFS and mass spectrometer should be used to trace the presence of the electrons and the different ions in the chamber.

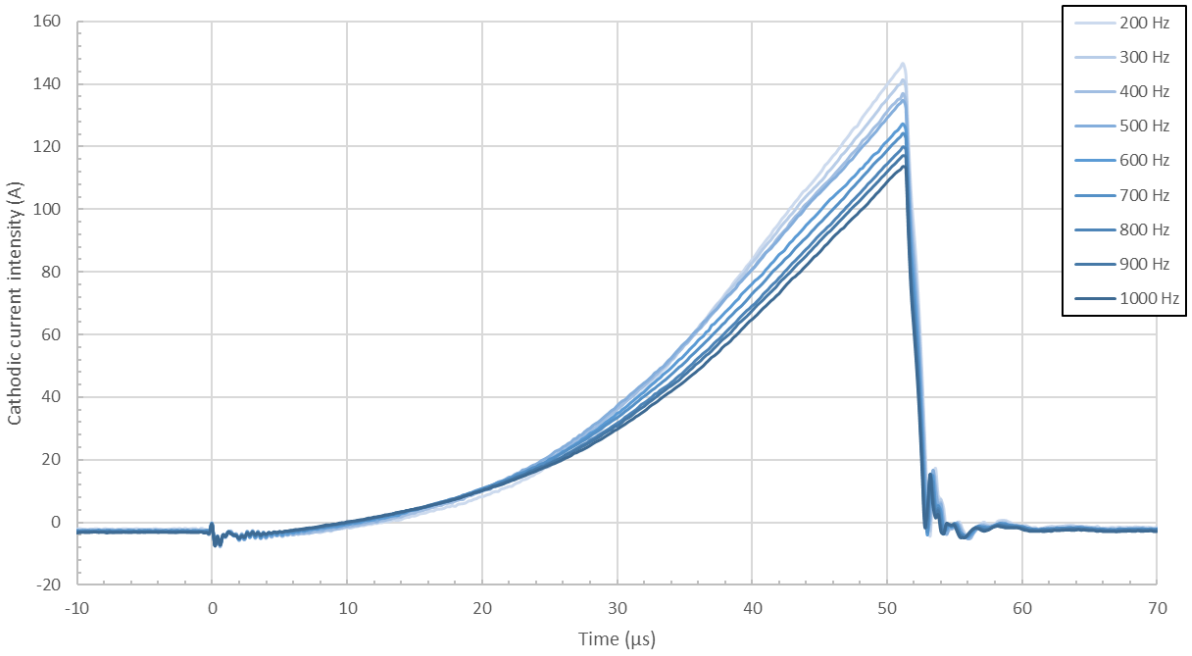

Figure 114. Modification of the poisoned pulse waveform when increasing the frequency for 50 µs long pulses (3 mTorr – 50 µs - 470 V – 5.0 sccm)

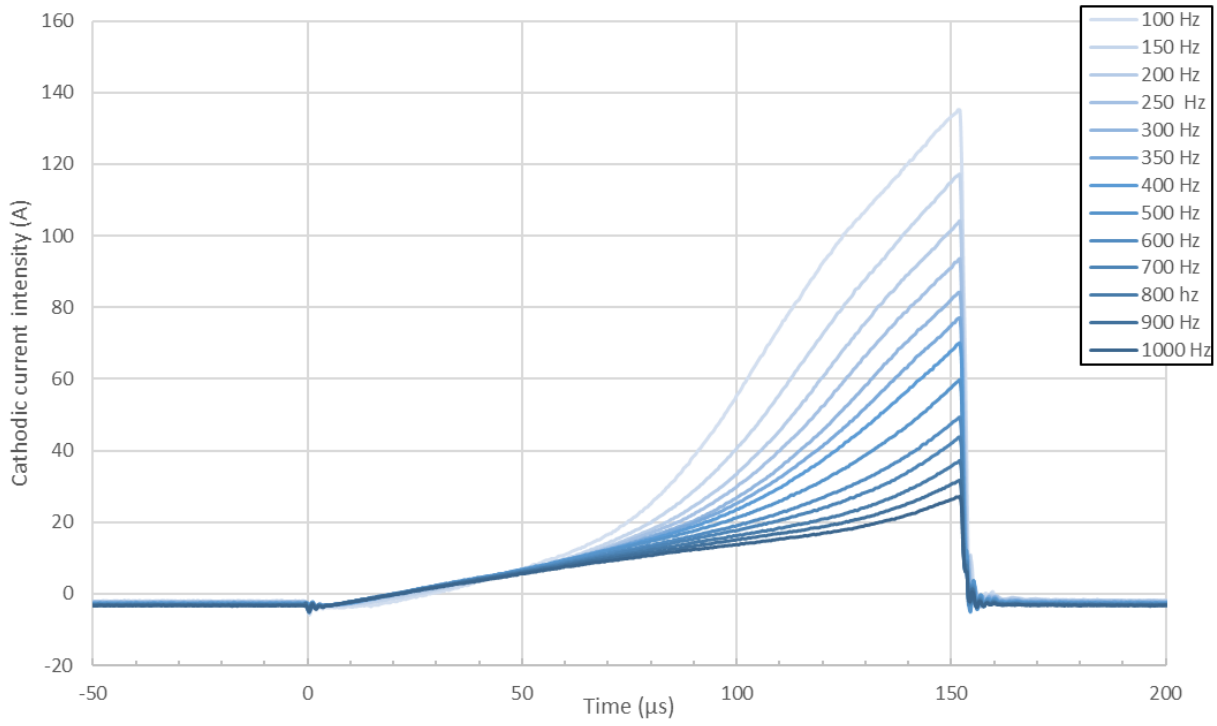

Figure 115. Modification of the poisoned pulse waveform when increasing the frequency for 150 µs long pulses (3 mTorr – 150 µs – 415 V – 4.0 sccm)

IV.1.3.3.2. Intensity regulated

In the intensity regulated mode, the signal is reducing when the frequency is increased but we know that this is an artifact from the power supply, as it is modifying the voltage to compensate the duty-cycle modification. The solution is to multiply each pulse by its own corresponding duty-cycle and obtain an evolution where each pulse has the same surface (in theory). Both types of graphs are presented for short and long pulses. It becomes easier to observe the changes in the pulse waveform. It must be kept in mind that the voltage is increase when the frequency is decreased: need of a more important pulse at low duty-cycles.

The 50 µs long pulse evolution shows a slight change in the shape of the pulse when increasing the frequency (and diminishing the voltage): the slope becomes more concave. This concavity has already been identified as being due to the presence of oxygen in excess in the chamber: the reactive gas makes the sputtering by Ar^+ ions more difficult in the early stages of the pulses but once the oxygen species in the bulk plasma

gets ionized, there is a rapid raise of the slope, reflecting a large amount of O^+ ions generated in the chamber. However, at higher duty-cycle, we could expect a less effective poisoning of the target as the effective time of sputtering is increased but here, the voltage diminution with the increase of the frequency makes the poisoning easier for oxygen species; resulting in the evolution observed. That is why it is very important to keep in mind what other 1st order parameter is modified when studying the effect of another 1st order parameter while keeping a 2nd order parameter constant because in such cases, there is always a balance between the two parameters modifications. Here, the voltage diminution overcomes the augmentation of the duty-cycle. The number of positive ions reaching the target (i.e. <I>) remains the same for each pulse but their composition/energy changes (slightly, here).

The long pulse scenario shows a much more important change in the shape. The balance is still tipping on the voltage side: the voltage being diminished at higher frequencies, the capacity for the system to generate positive oxygen ions is also diminished. It appears more clearly in Figure 118, where the early stages of the pulse (i.e. first 70 µs) is identical for all frequencies, the major differences appear in the second part of the pulse. Also, when comparing Figure 119 and the over-stoichiometric shapes of Figure 107, the hypothesis that increasing the frequency results in a higher *poisoning* (i.e. excess of oxygen ions in the chamber) is clear: the evolution between 3.0 and 10.0 sccm in Figure 107 is quasi-similar to the evolution reported in Figure 119.

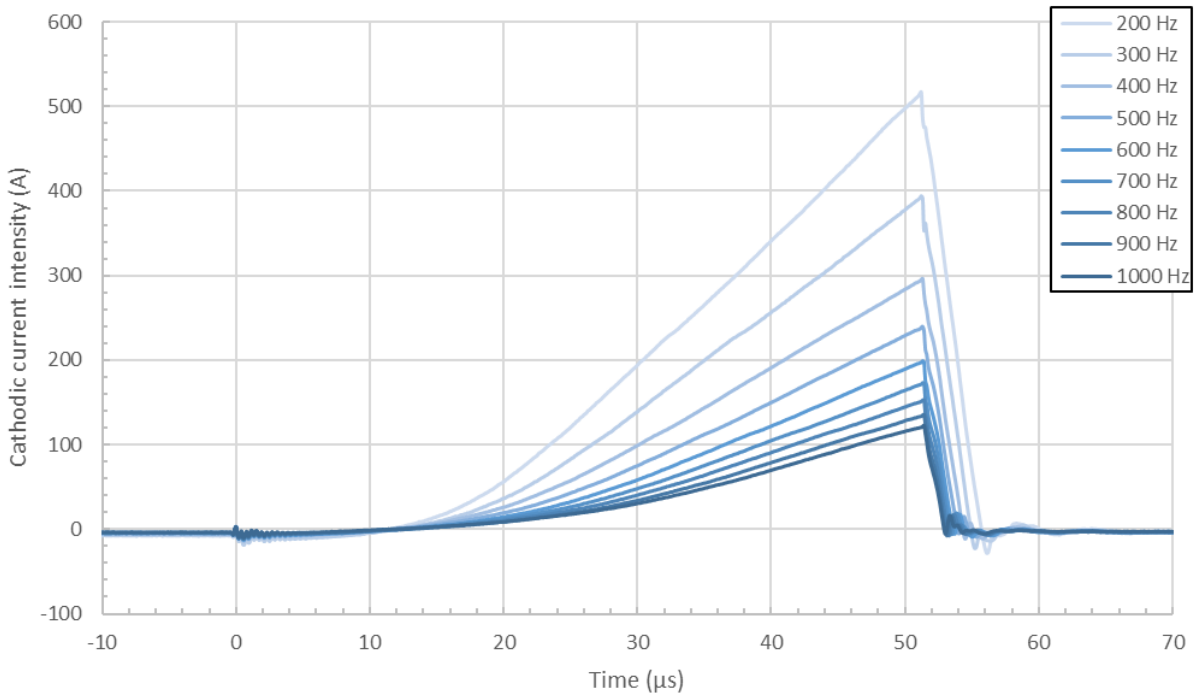

Figure 116. Modification of the poisoned pulse waveform when increasing the frequency for 50 µs long pulses in the current intensity regulated mode (3 mTorr – 50 µs – 2000 mA – 5.0 sccm)

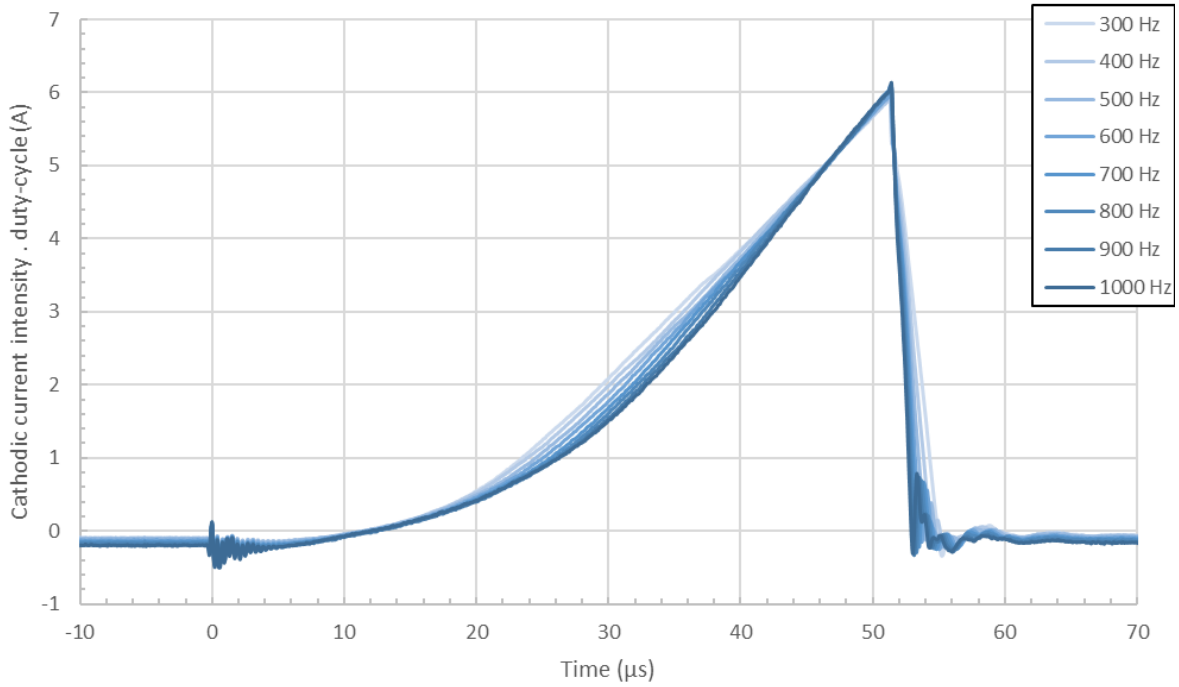

Figure 117. Modification of the poisoned pulse waveform when increasing the frequency for 50 µs long pulses in the current intensity regulated mode (3 mTorr – 50 µs – 2000 mA – 5.0 sccm). Each pulse has been multiplied by its own duty-cycle

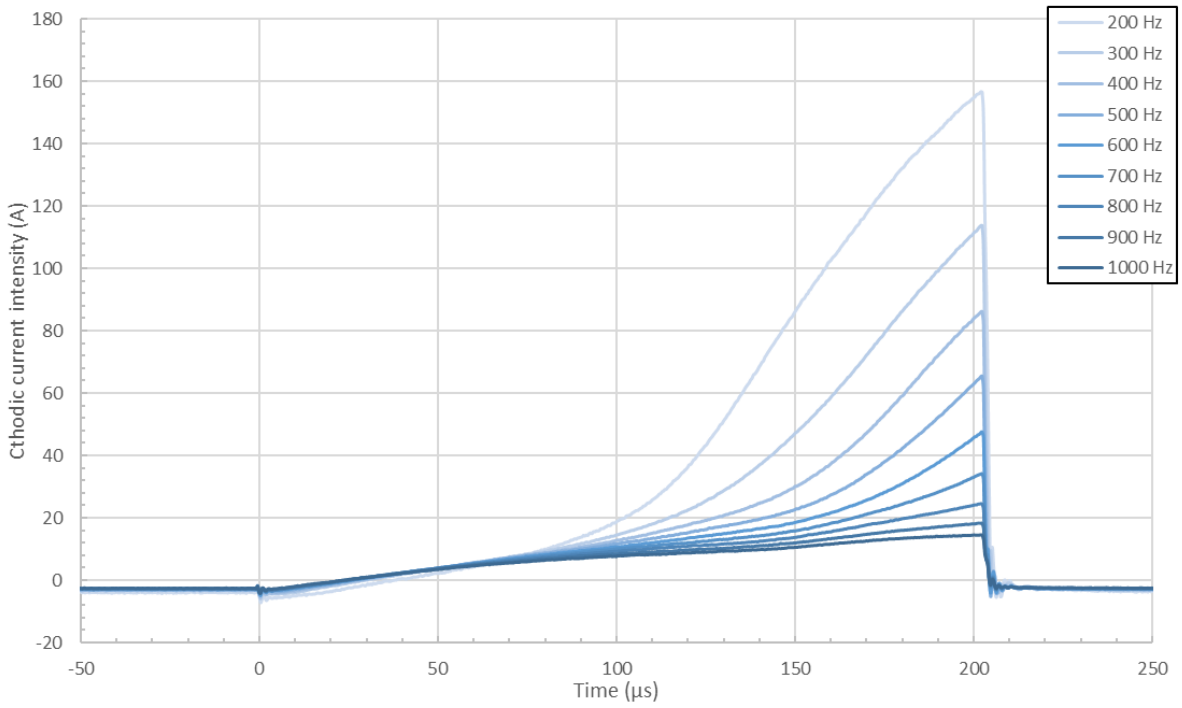

Figure 118. Modification of the poisoned pulse waveform when increasing the frequency for 200 µs long pulses in the current intensity regulated mode (3 mTorr – 200 µs – 2000 mA – 5.0 sccm)

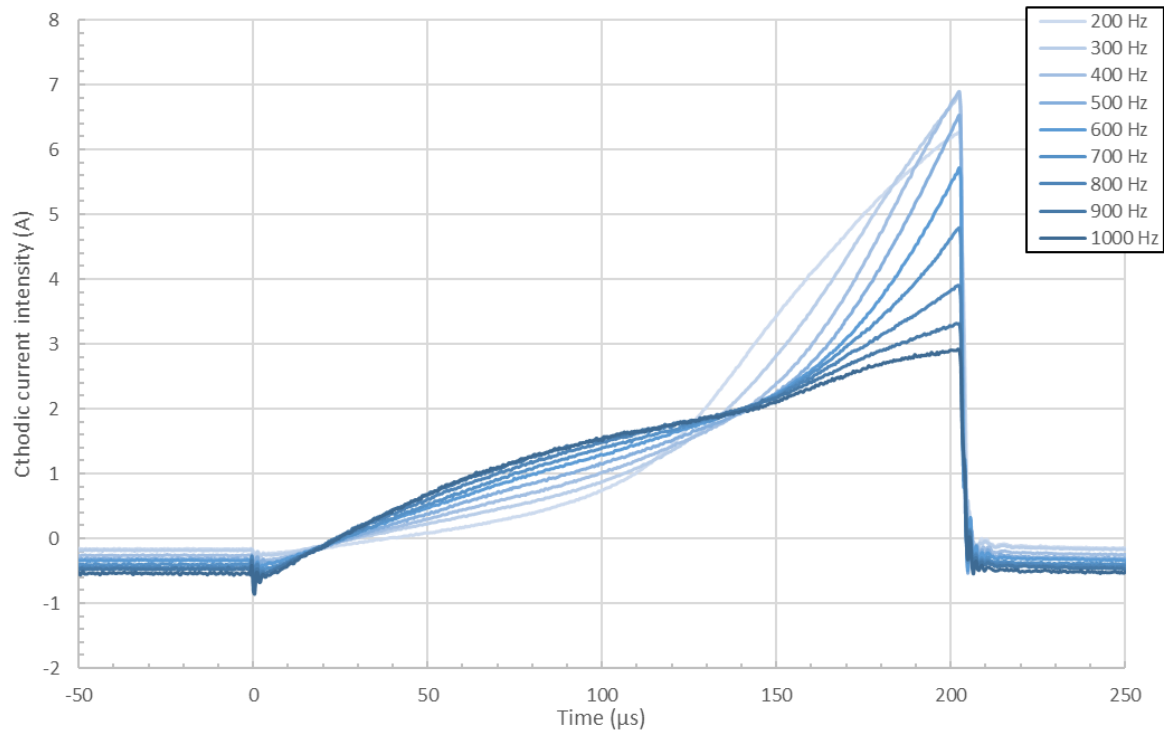

Figure 119. Modification of the poisoned pulse waveform when increasing the frequency for 200 µs long pulses in the current intensity regulated mode (3 mTorr – 200 µs – 2000 mA – 5.0 sccm). Each pulse has been multiplied by its own duty-cycle

IV.1.3.4.Pulse width

IV.1.3.4.1. Voltage regulated

Here is presented the evolution of the pulse waveform with the increase of the pulse width in the poisoned mode. The observations are quite simple: the pulse intensity increases at each pulse. The fact that it continuously increases until the longest pulse width is different to what was observed with the Huettinger power supply. With the latter, the peak current intensity would start decreasing after a critical pulse width of about 100 µs. As it has been explained earlier for the Huettinger use, the reasons behind this behaviour could not be identified as it could be due to either a power supply limitation or plasma physics. Since this *saturation* is not observed with a different power supply, it is a good indication that it was power supply limit that was responsible for the diminution of the peak current after a certain point. Here, the peak current keeps increasing along time even though the slope of the curve reduces with the pulse width. The latter phenomenon cannot be clearly identified but it is most likely to be due to the augmentation of the duty cycle with time and therefore the diminution of the refill-time.

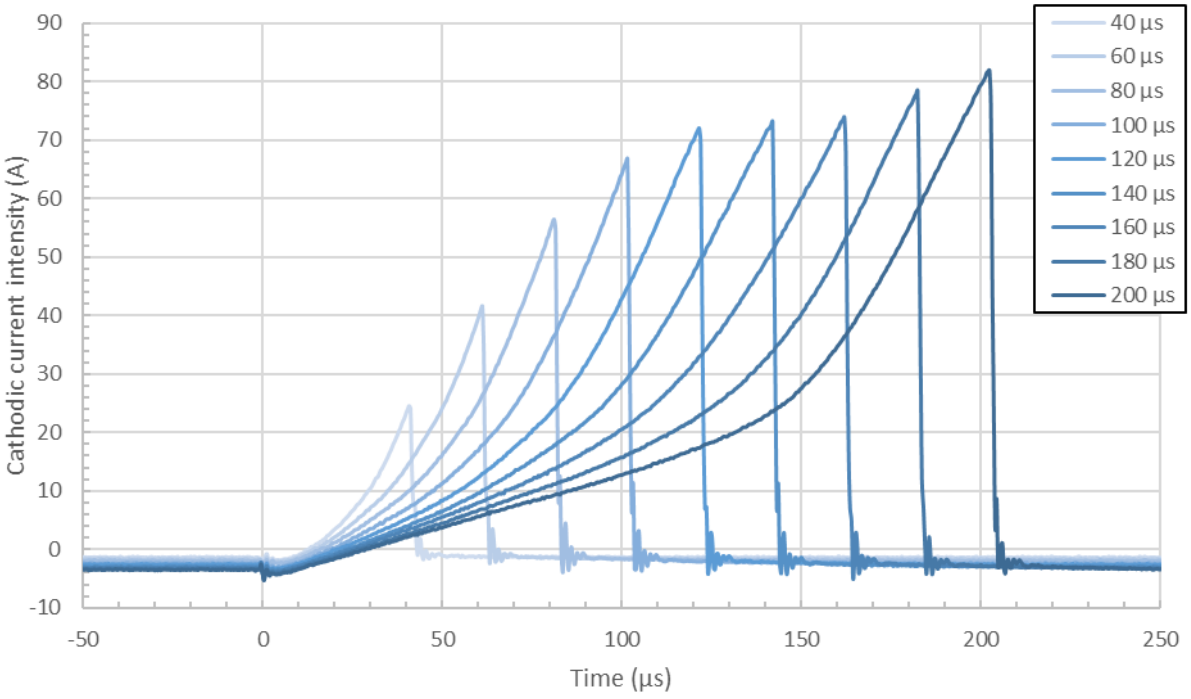

Figure 120. Modification of the poisoned pulse waveform when increasing the pulse width (3 mTorr – 500 Hz – 410 V – 5.0 sccm)

IV.1.3.4.2.Intensity regulated

In the intensity regulated mode, the first observation is the same as for frequency dependency: the duty-cycle is greatly modified so the voltage needs to be as well. Here, when the pulse width is increase, the voltage needs to be reduced to keep a constant average current intensity. The solution proposed earlier is to multiply each pulse by its own duty-cycle to compensate this effect. However, it should be reminded that this is only an artifice and that the voltage is still different for each pulse width.

It seems that the power supply struggles identifying the mean current intensity here as the peak surface appears to remains constant when the duty-cycle is changed, resulting in a higher time-averaged current intensity. Normally, it should be the peak surface multiplied by its own duty-cycle.

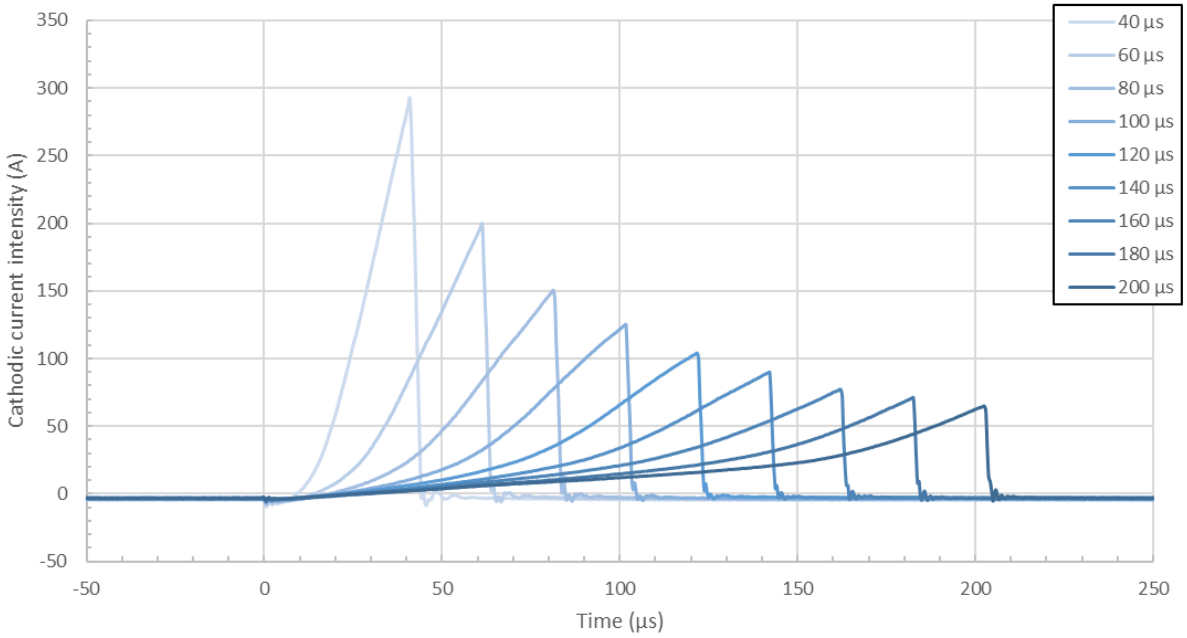

Figure 121. Modification of the poisoned pulse waveform when increasing the pulse width in the current intensity regulated mode (3 mTorr – 500 Hz – 2000 mA – 5.0 sccm)

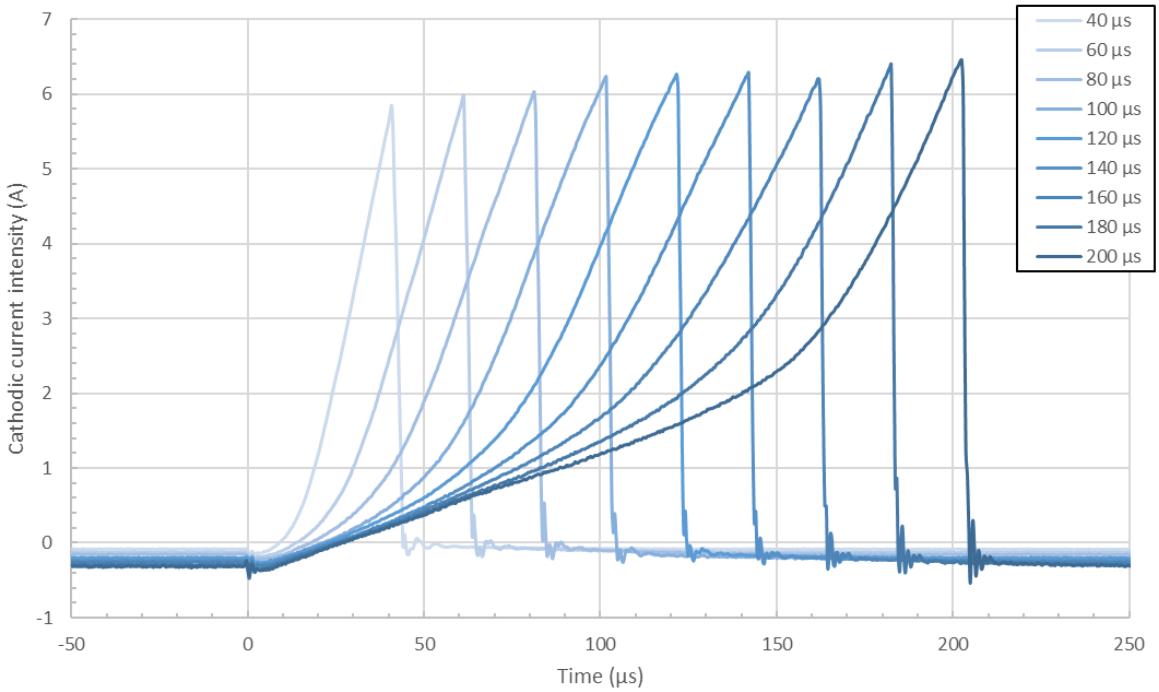

Figure 122. Modification of the poisoned pulse waveform when increasing the pulse width in the current intensity regulated mode (3 mTorr – 500 Hz – 2000 mA – 5.0 sccm). Each pulse has been multiplied by its own duty-cycle

IV.1.4. Transition window

This section is here to show that, if carefully chosen, each 1st order parameter can change the poisoning state of the target as it will *shift* the system to another, where the transition window is different. This results in a change of the discharge stoichiometry, even though the oxygen flow remains unchanged. All the date presented here are also reflected by the data shown in IV.1.5. However, in IV.1.5, the full oxidation curve could not always be acquired. Here, the fact that the transition can be observed by modifying any 1st order parameter show that each one of them results in a drift of the oxidation curve. Each first order parameter modifies the oxidation process.

The transitions could be observed in any scenario here: voltage and frequency regulated modes and for each of the four parameters. The aim here is not to necessarily discuss the physics behind each transition as it has been discussed in previous chapter. Here, the curves are mainly here to show that these transitions can still be observed even when using a different power supply and they are quasi-identical to what has been reported in previous chapter.

IV.1.4.1.Voltage

First, the voltage. Diminishing the voltage results in a transition from sub-stoichiometric to over-stoichiometric mode. This transition is due to the overall loss of energy in the plasma when the voltage is decreased. Here, the loss of energy is due to the diminution of the potential drop in the chamber, resulting in an easier poisoning of the target, as the sputtering is less efficient. Indeed, the sputtering yield diminishes when the voltage is reduced, and if less atoms/ions are sputtered from the target it means that the oxygen species can react more efficiently with the target surface without being re-sputtered.

The evolutions shown here show a very important drop in the intensity. Indeed, when the target starts being poisoned in a voltage regulated mode, the signal drops, as shown in IV.1.2.1. Here, there even is the addition of the voltage diminution that leads to a sharpening of this transition. The phenomenon is even more pronounced when looking at longer pulses (i.e. Figure 124), because the peak current intensity is much smaller (i.e. easier oxidation). Again, when comparing Figure 123 and Figure 124 to Figure 104 and Figure 105, it appears clearly that the transitions are very similar. The effect of reducing the applied voltage at a constant oxygen rate and the effect of increasing the oxygen rate at a constant voltage are identical: they both shift the process from the sub-stoichiometric region to the over-stoichiometric region.

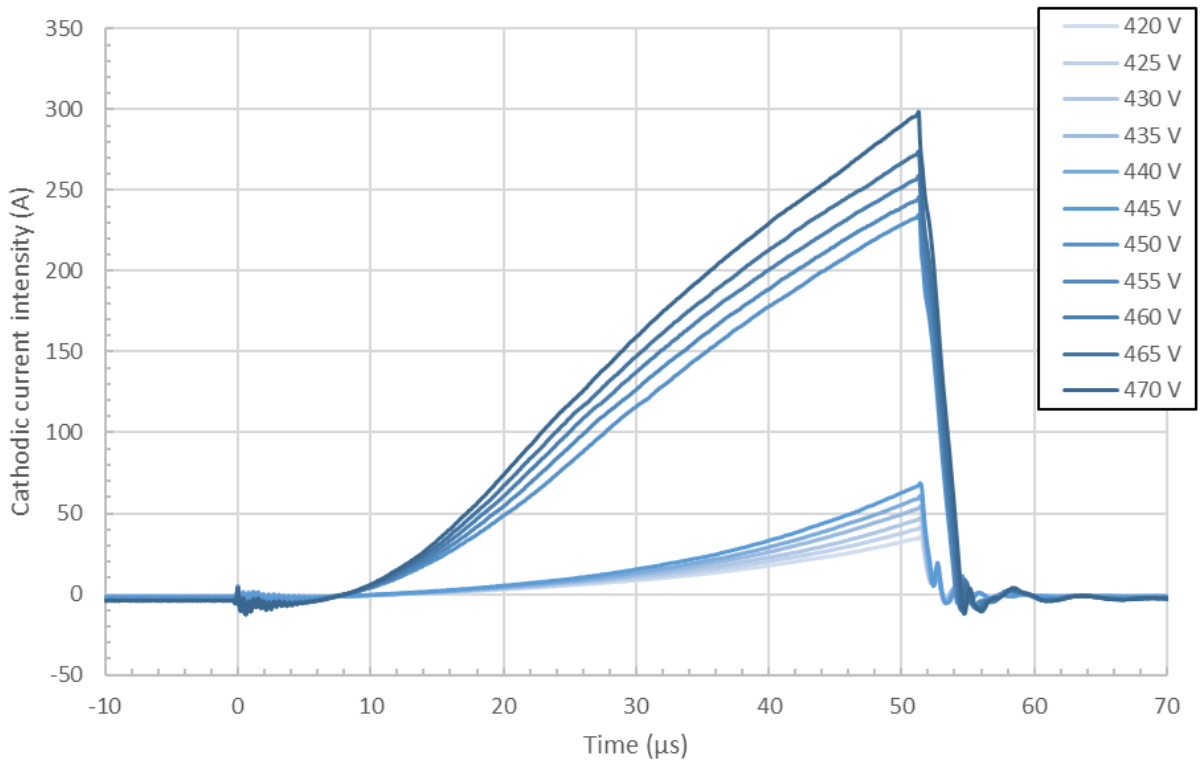

Figure 123. Modification of the pulse waveform in the transition window when increasing the voltage for 50 µs long pulses (3 mTorr – 50 µs – 300 Hz – 1.0 sccm)

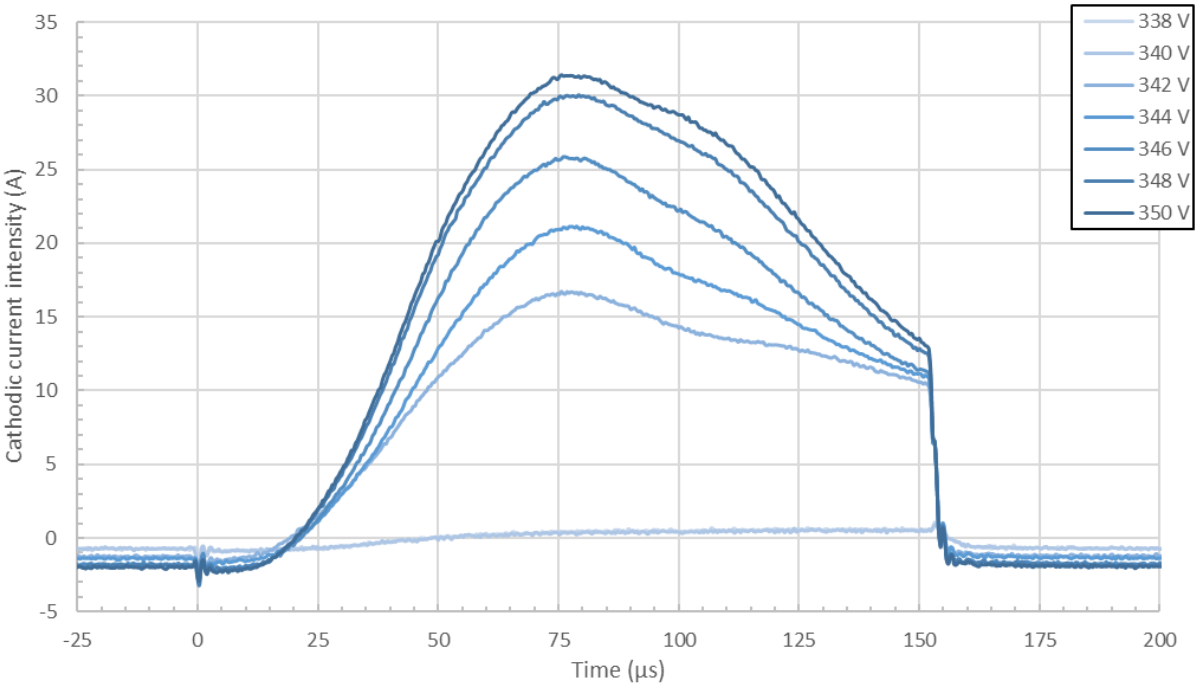

Figure 124. Modification of the pulse waveform in the transition window when increasing the voltage for 150 µs long pulses (3 mTorr – 150 µs – 300 Hz – 0.75 sccm)

IV.1.4.2.Pressure

IV.1.4.2.1. Voltage regulated

The pressure also shows the same type of transition. This time, it appears that when increasing the pressure, the systems shifts to the sub-stoichiometric mode. Here, the explanation is different to the voltage situation: it is not the mean energy of the species in the chamber that is changed, but their quantity. Indeed, increasing the pressure only means three things: there are more species in the chamber, these species can lose kinetic energy due to too many collisions in the plasma (after a certain critical pressure), or these same collisions can also result in an increase of the ionization rate, again, after a certain critical point. Here, it seems that increasing the pressure leads to more difficulties for the system to get oxidized which means that here, the sputtering is more intense at higher pressure. The quantity of species in the chamber increases with the pressure, but also the relative proportion of ions, resulting in more ions impacting the target, and therefore an improved sputtering rate. It should be highlighted that, here, the sputtering rate is increased, not the sputtering yield; or only slightly. Also, the transition could not be observed for long pulses as the plasma would totally switch off after the transition point.

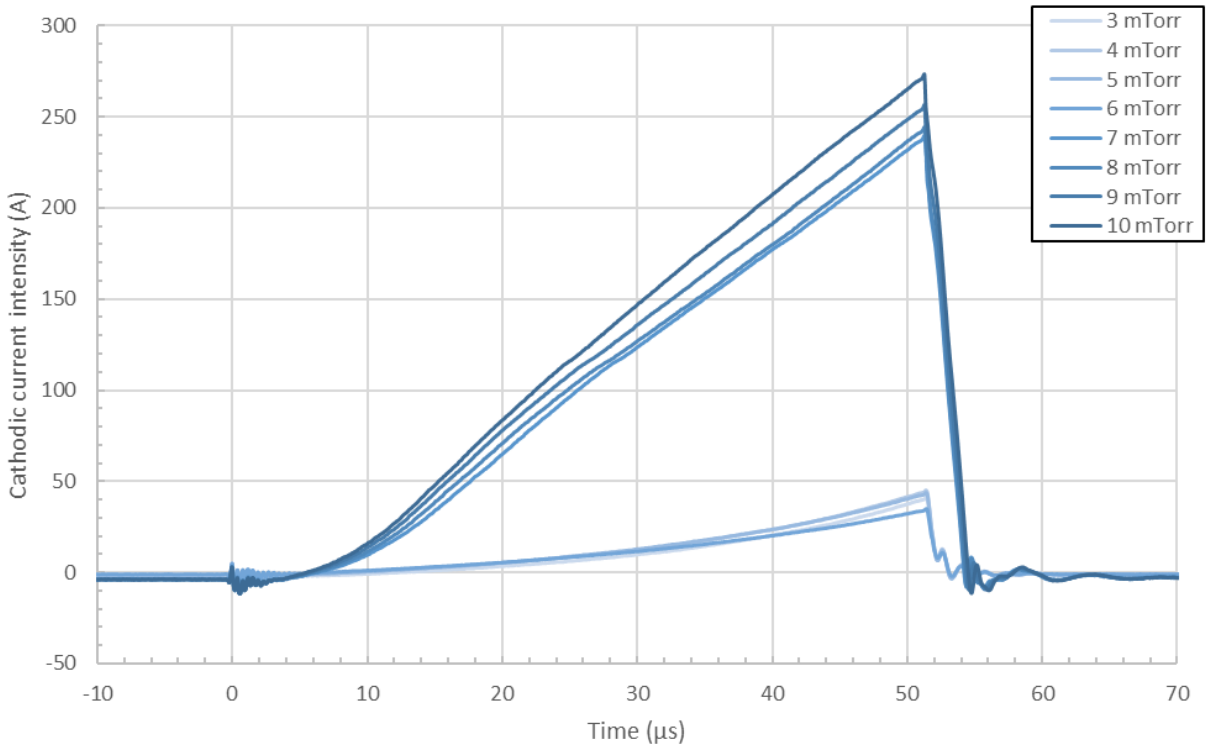

Figure 125. Modification of the pulse waveform in the transition window when increasing the pressure for 50 µs long pulses (300 Hz – 50 µs – 510 V – 1.0 sccm)

IV.1.4.2.2.Intensity regulated

In the intensity regulated mode, both 50 and 200 µs transitions are observed. are observed. However, here, something surprising can be observed: the behaviour is inverted: the system switches to the poisoned mode when the pressure is increased.

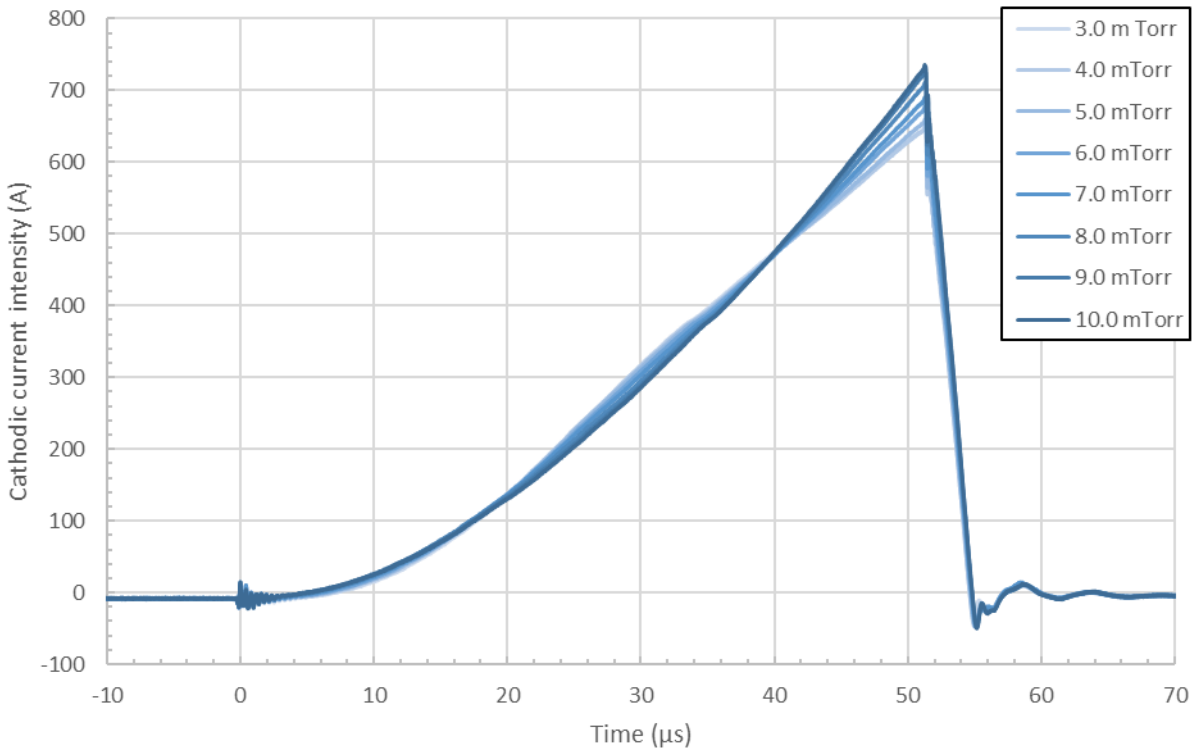

Figure 126. Modification of the pulse waveform in the transition window when increasing the pressure for 50 µs long pulses operated in the intensity regulated mode (300 Hz – 50 µs – 2000 mA – 0.9 sccm)

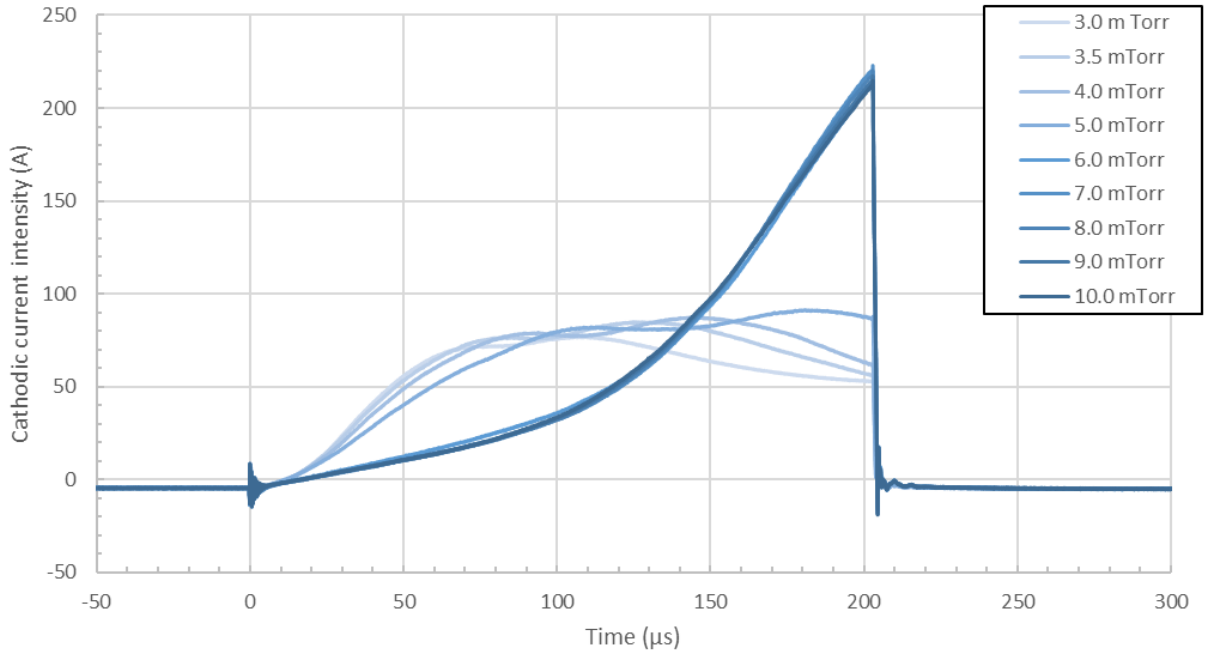

Figure 127. Modification of the pulse waveform in the transition window when increasing the pressure for 200 µs long pulses operated in the intensity regulated mode (300 Hz – 200 µs – 2000 mA – 2.0 sccm)

IV.1.4.3. Frequency

IV.1.4.3.1. Voltage regulated

For the frequency, the system shifts to the poisoned mode when the frequency is diminished. This behaviour has already been explained several times in this thesis: the change in the duty-cycle is responsible for it. A lower frequency means a shorter amount of sputtering time per second, which means a shorter amount of sputtered species. Moreover, in such cases, it has also been explained that the oxidation state for a given reactive gas flux is mainly linked to the sputtering rate. Here, since the sputtering duration per unit of time is reduced, the sputtering rate follows - it is a time-averaged value, by definition. This leads to the transition observed here: the target is more easily poisoned at lower frequencies. Again, it should be highlighted that, here, the full transition is observed for both short and long pulses.

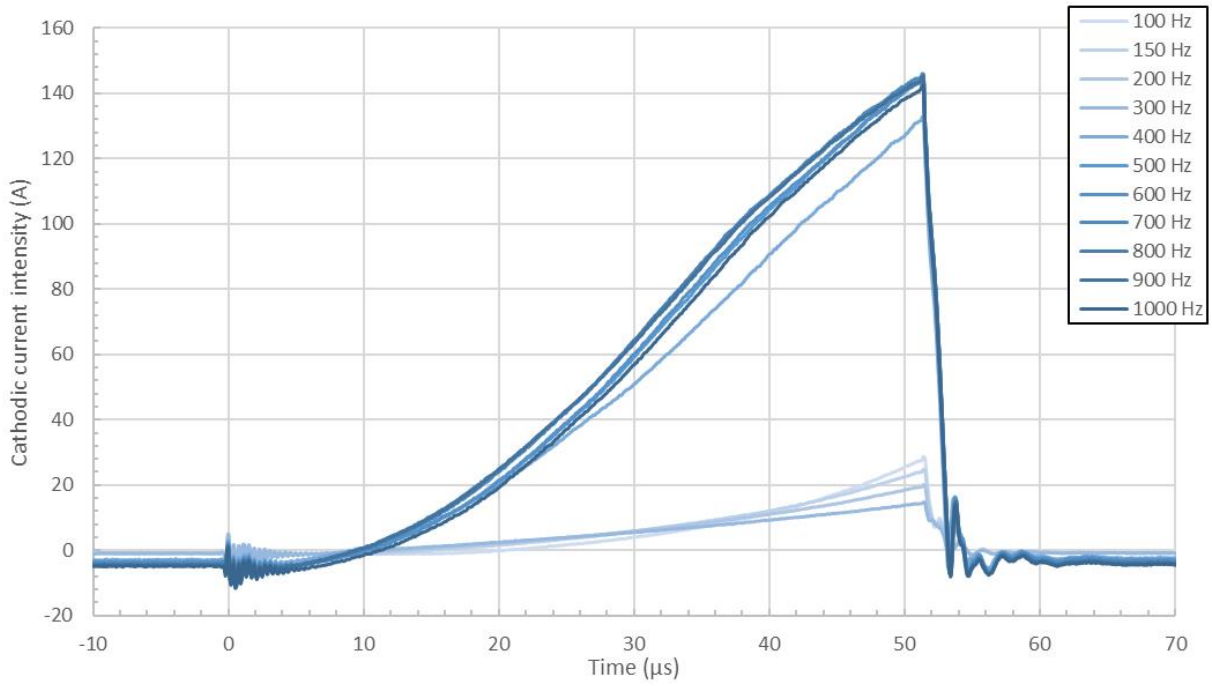

Figure 128. Modification of the pulse waveform in the transition window when increasing the frequency for 50 µs long pulses (3 mTorr – 50 µs – 415 V – 1.0 sccm)

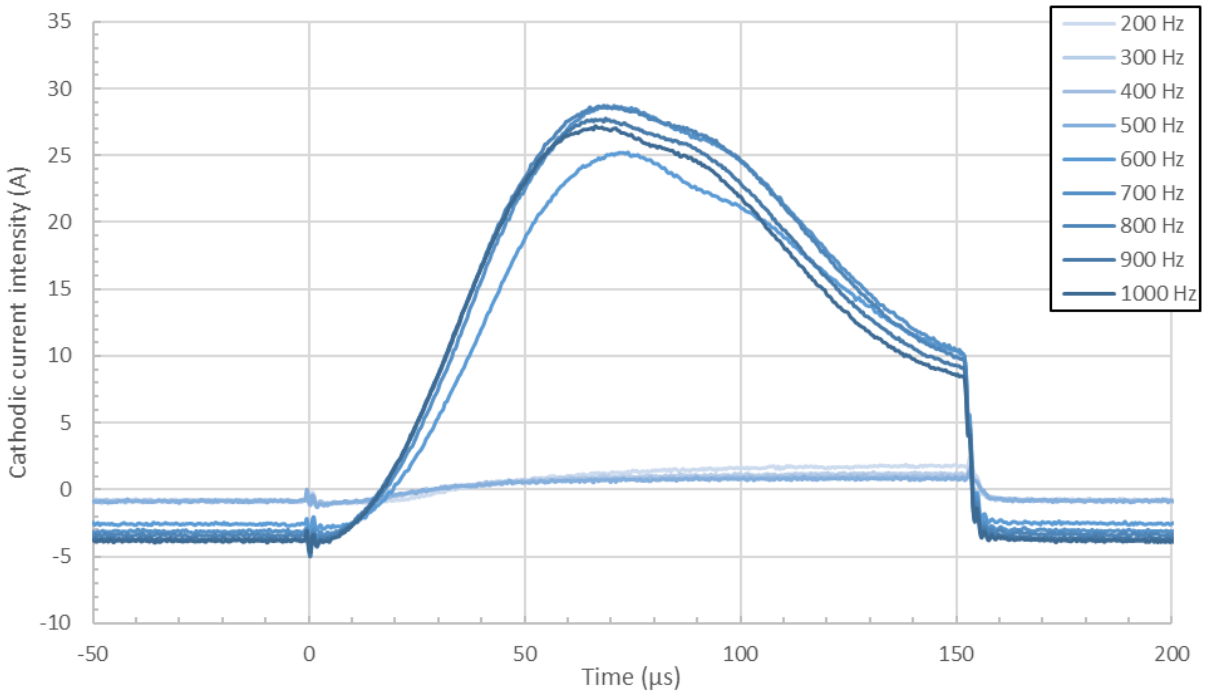

Figure 129. Modification of the pulse waveform in the transition window when increasing the frequency for 150 µs long pulses (3 mTorr – 150 µs – 355 V – 1.25 sccm)

IV.1.4.3.2. Intensity regulated

Here are presented the results for the cathodic current intensity regulated mode. This time, the transition is similar between voltage and current regulated modes: the target gets poisoned when decreasing the frequency. Again, for the data presented in Figure 130 and Figure 132, each pulse has been multiplied by its own duty-cycle to help observing the transitions. And it appears clearly in both cases that the pulse shape changes from sub-stoichiometric at high frequency to over-stoichiometric at low frequency.

Even if the transition seems to be simple, as it is identical to what has been observed in the voltage regulated mode. However, one should not forget that when decreasing the frequency, the voltage is increased to keep a constant time-averaged cathodic current intensity. However, section IV.1.4.1 showed that increasing the voltage is supposed to bring the target too its sub-stoichiometric for a constant oxygen flux. There are then two opposite effects occurring but the frequency effect overcomes that of the voltage.

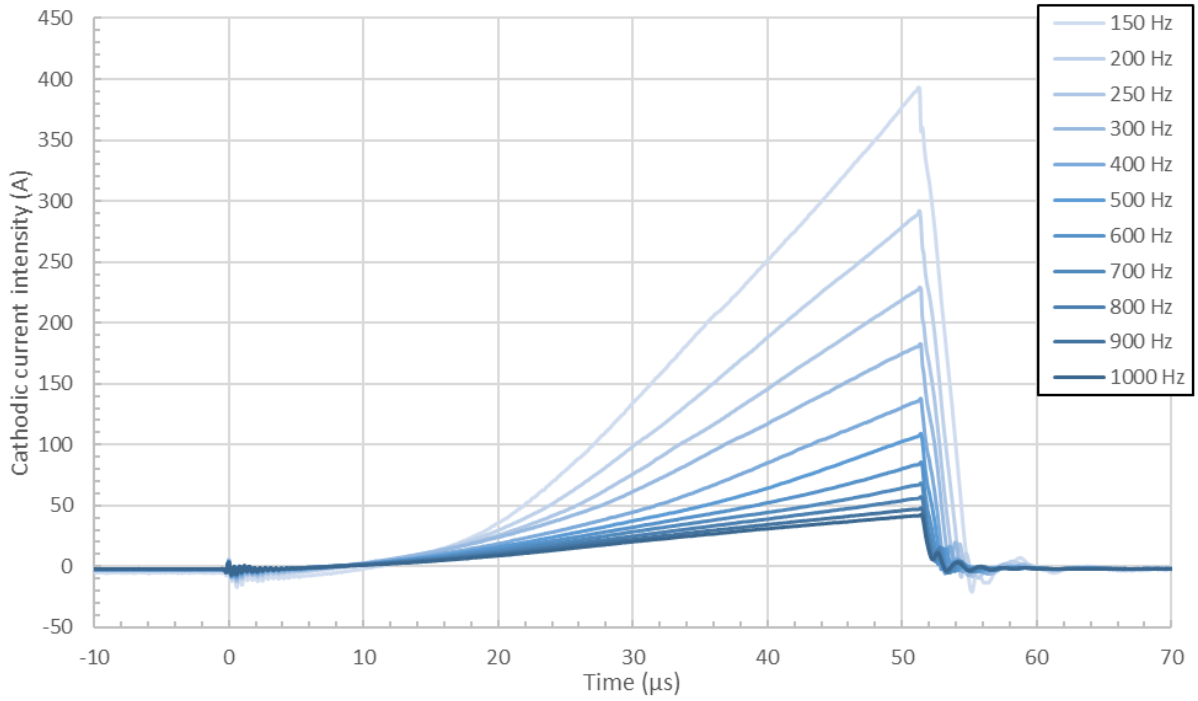

Figure 130. Modification of the pulse waveform in the transition window when increasing the frequency for 50 µs long pulses operated in the intensity regulated mode (3 mTorr – 50 µs – 1000 mA – 1.3 sccm)

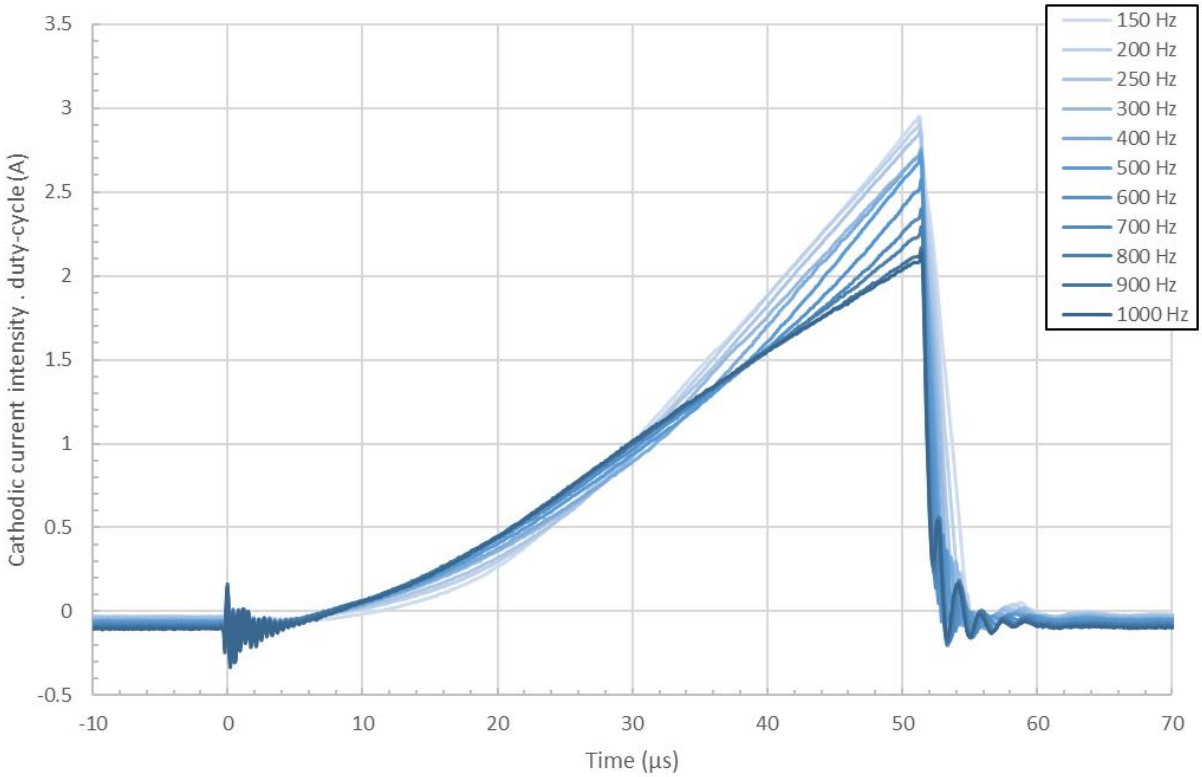

Figure 131. Modification of the pulse waveform in the transition window when increasing the frequency for 50 µs long pulses operated in the intensity regulated mode (3 mTorr – 50 µs – 1000 mA – 1.3 sccm). Each pulse has been multiplied by its own duty-cycle

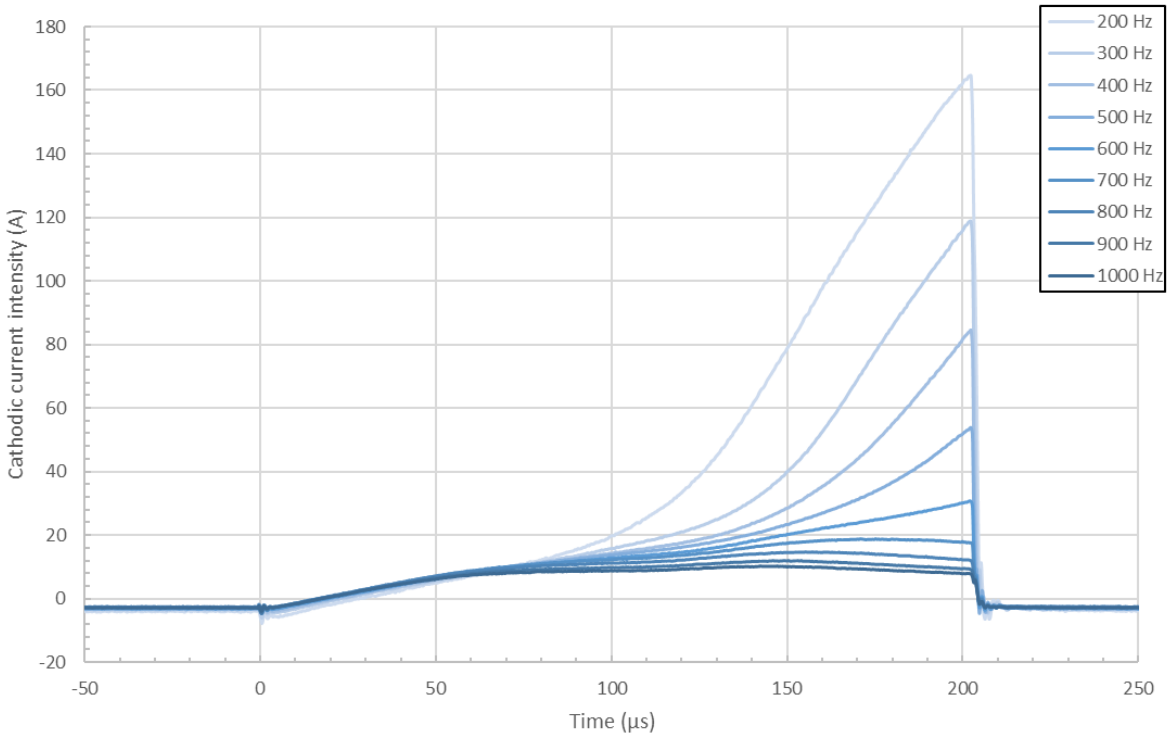

Figure 132 Modification of the pulse waveform in the transition window when increasing the frequency for 200 µs long pulses operated in the 2000 mA intensity regulated mode (3 mTorr – 200 µs – 2000 mA – 2.5 sccm)

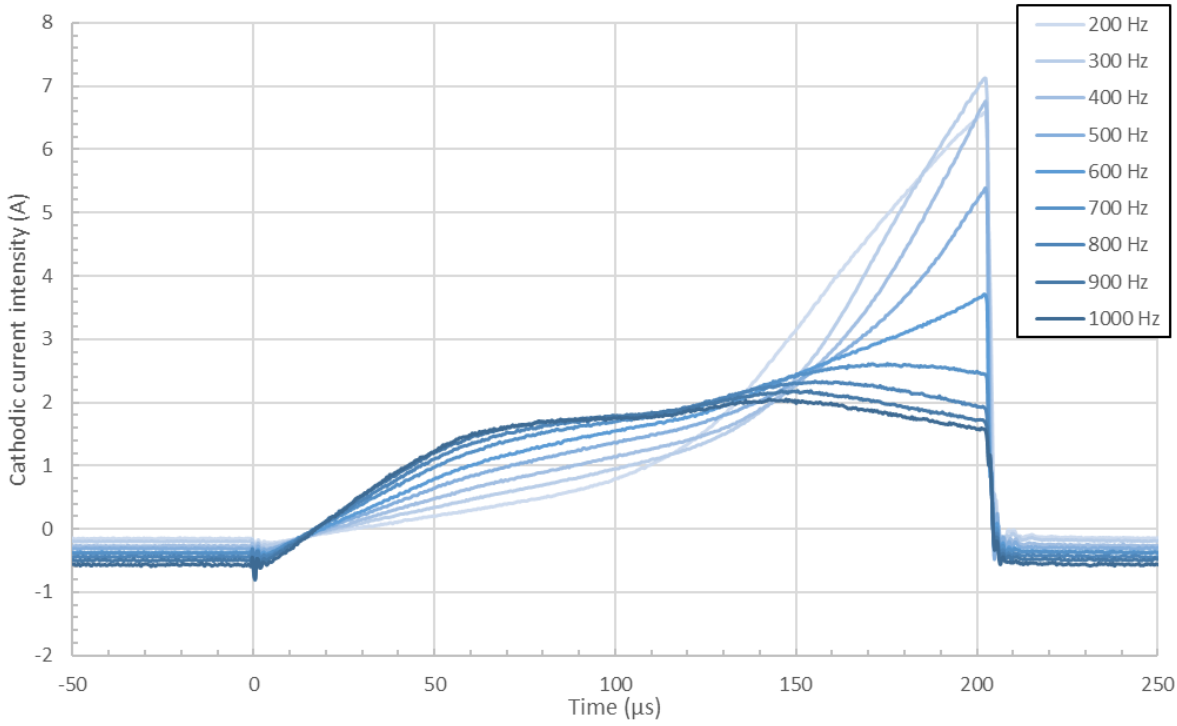

Figure 133. Modification of the pulse waveform in the transition window when increasing the frequency for 200 µs long pulses operated in the 2000 mA intensity regulated mode (3 mTorr – 200 µs – 2000 mA – 2.5 sccm). Each pulse intensity has been multiplied by its own duty-cycle

IV.1.4.4. Pulse width

IV.1.4.4.1. Voltage regulated

The effect of increasing the pulse width is shown in Figure 134. Here, the same effect that that observed for the frequency is observed: the system shifts to the sub-stoichiometric mode when the duty-cycle is increased. It shows an incomplete transition, however. It is believed to be because the current intensity had to remain low to make the measurement possible. No further comment is brought here as the only objective is to show that it is possible to do it with this power supply (i.e. HiPSTER 6®) when it is not with the Huettinger power supply.

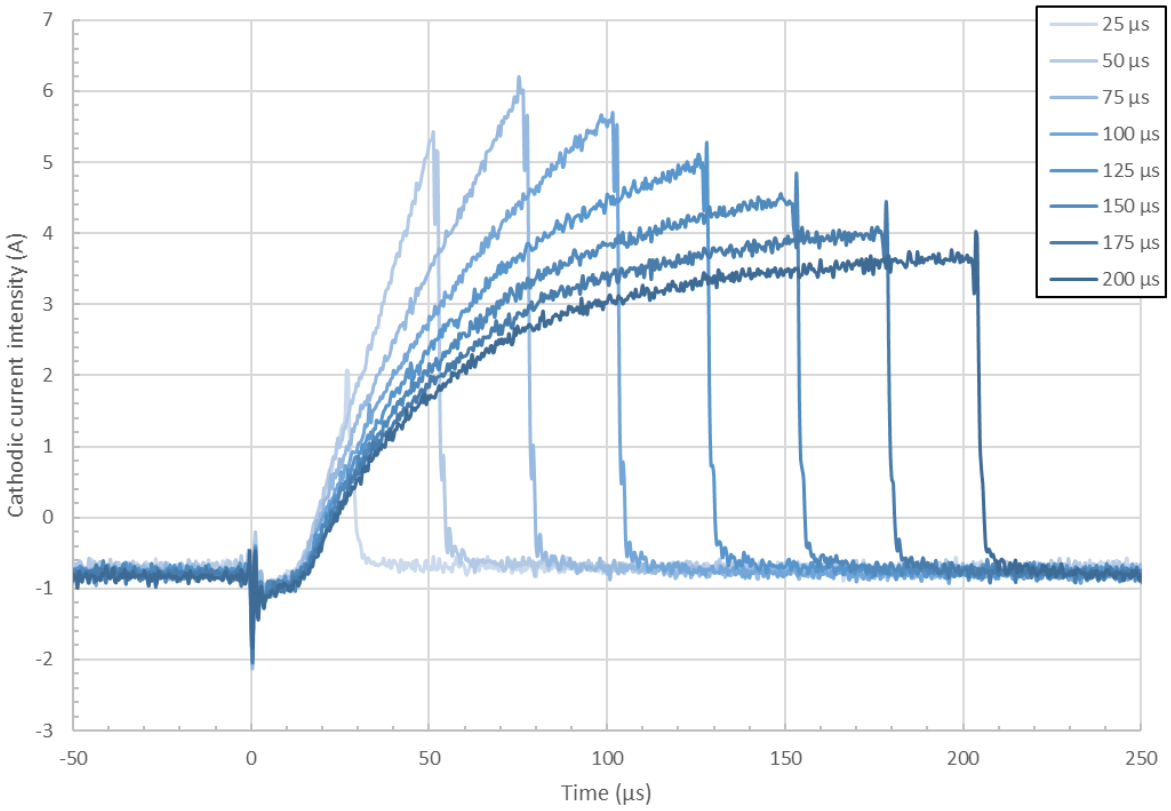

Figure 134. Modification of the pulse waveform in the transition window when increasing the pulse width (3 mTorr – 300 Hz – 370 V – 1.0 sccm)

IV.1.4.4.2.Intensity regulated

Here, the effect remains identical to the frequency effect and the voltage does not overcome the consequences of increasing the duty-cycle. Again, no more comment is given here at it has already been explained in the previous sections.

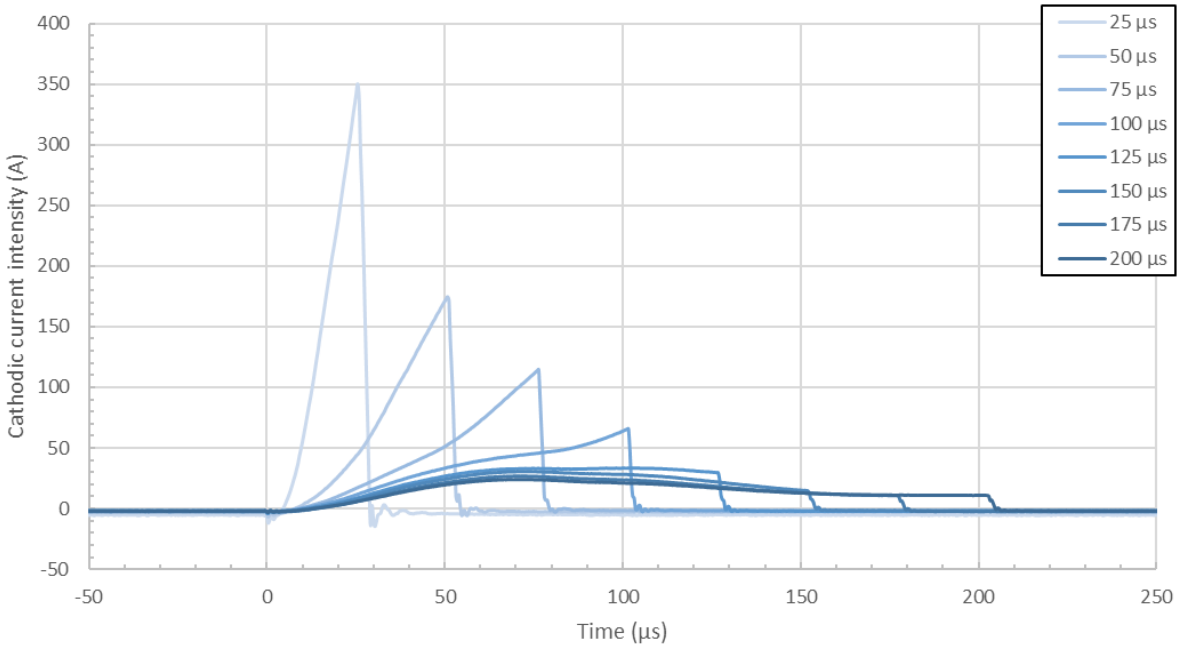

Figure 135. Modification of the pulse waveform in the transition window when increasing the pulse width in the intensity regulated mode (3 mTorr – 300 Hz – 1000 mA – 1.0 sccm)

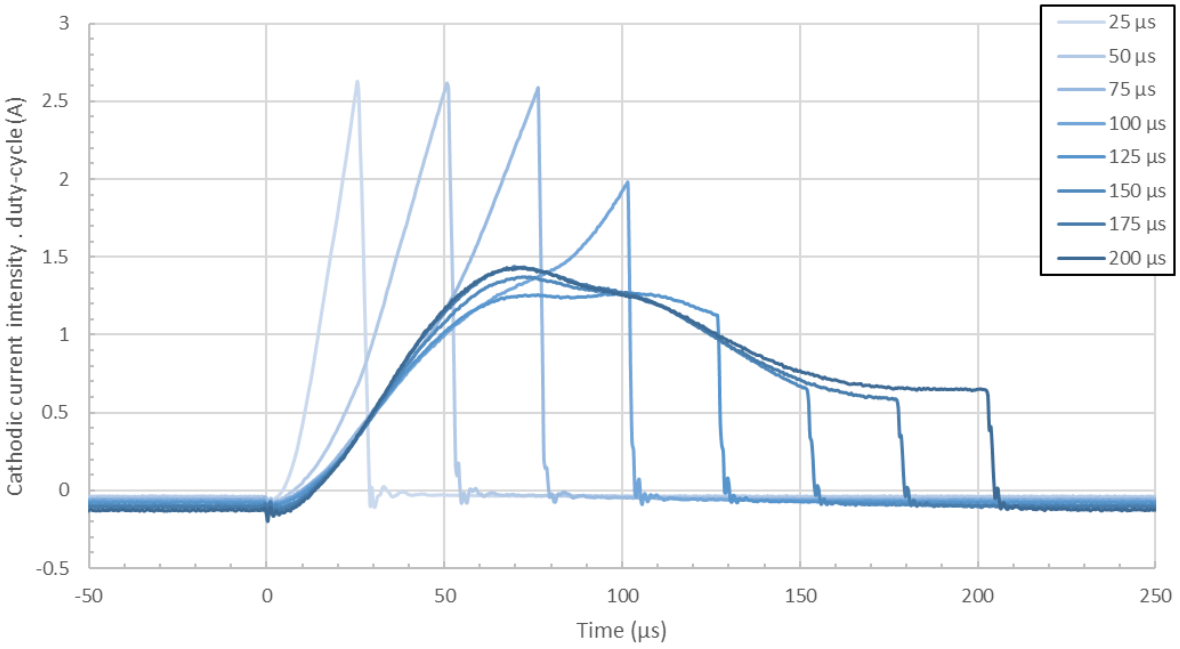

Figure 136. Modification of the pulse waveform in the transition window when increasing the pulse width in the intensity regulated mode (3 mTorr – 300 Hz – 1000 mA – 1.0 sccm). Each pulse intensity has been multiplied by its own duty-cycle

IV.1.5. Modification of the oxidation curve in the voltage regulated mode

IV.1.5.1. Voltage

The oxidation curves shown here are only here to confirm what has been said in the section above. Here, one can see that the transition window switched to higher oxygen content when the voltage is increased, showing an increased difficulty for the system to poison the target when the voltage is increased (i.e. more efficient sputtering).

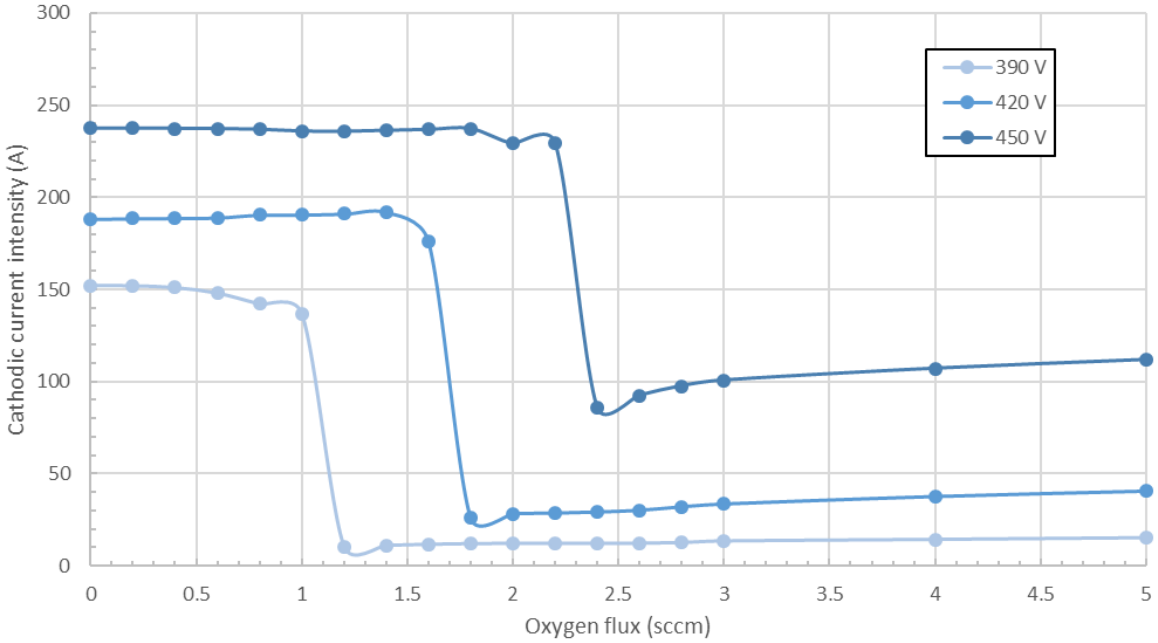

Figure 137. Modification of the oxidation curve in the voltage regulated mode for different voltages (3 mTorr – 50 µs – 500 Hz)

IV.1.5.2. Pressure

The transition curves study shows that the effect of the pressure is uncertain as it does seem to influence the oxidation process but nothing linear. Duplication work of these curves showed that there is no clear trend in the effect of the pressure. A trend comparable to what is presented in Figure 138, where the transition window seems to be delayed when the pressure is increased, up to a certain point, after which it seems to either reduce or stabilize. However, it is preferred to make no conclusion on the data here as it still remains unclear.

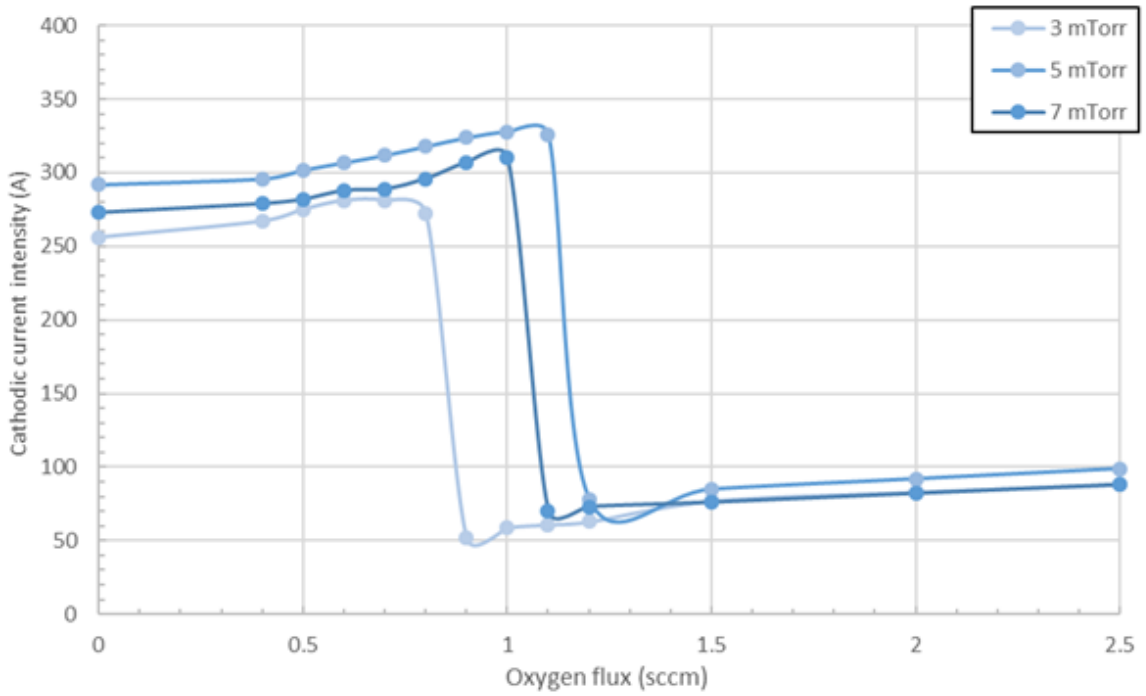

Figure 138. Modification of the oxidation curve in the voltage regulated mode for different pressures (410 V – 50 µs – 500 Hz)

IV.1.5.3. Frequency and pulse width

It is impossible to obtain a metal signal that is neither too intense (power limit) nor too weak (switched off) with the same voltage and along the whole range of frequencies. Therefore, these oxidation curves where not acquired due to the limited amount of time

IV.1.6. Modification of the oxidation curve in the intensity regulated mode

IV.1.6.1. Voltage

Using the HiPSTER 6® power supply makes it possible to choose the value of the time-averaged cathodic current intensity used as a limiting factor in the intensity regulated mode. It means that the amount of ions reaching the target per unit of time and/or the voltage range can be chosen. The graphs in Figure 139 demonstrate that if the time-averaged current intensity is lowered, the transition window flows. It completes the

previous data acquired when modifying pressure, frequency and pulse width to confirm the fact that the transition window is a direct function of the time-averaged cathodic current intensity.

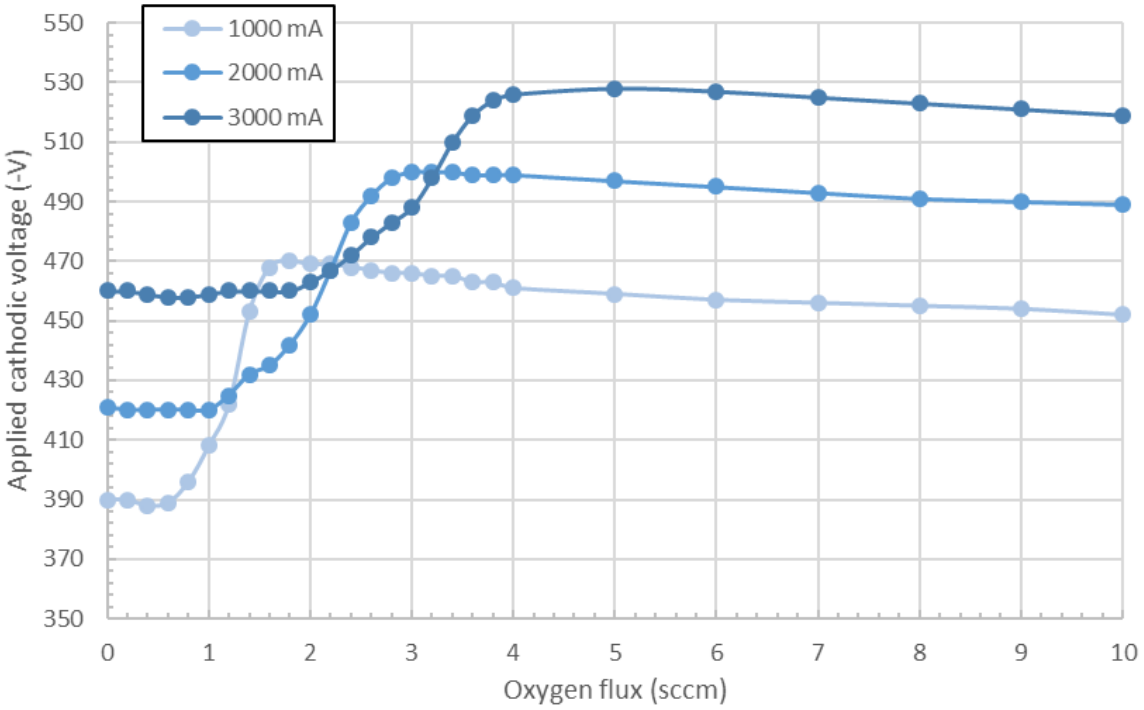

Figure 139. Modification of the oxidation curve in the intensity regulated mode for different current intensities (3 mTorr – 50 µs – 500 Hz)

IV.1.6.2. Pressure, Frequency and pulse width

Figure 140, Figure 141 and Figure 142 show identical results than, respectively, Figure 94, Figure 95, and Figure 96. This means that changing the power supply does not change the fact that at constant time-averaged current intensity, changing the pressure still only widens the transition window while the frequency and the pulse width do not change that transition window even though the voltage range changes. The details about these evolutions are not discussed again as they have already been in III.3.6.1, III.3.6.2 and III.3.6.3.

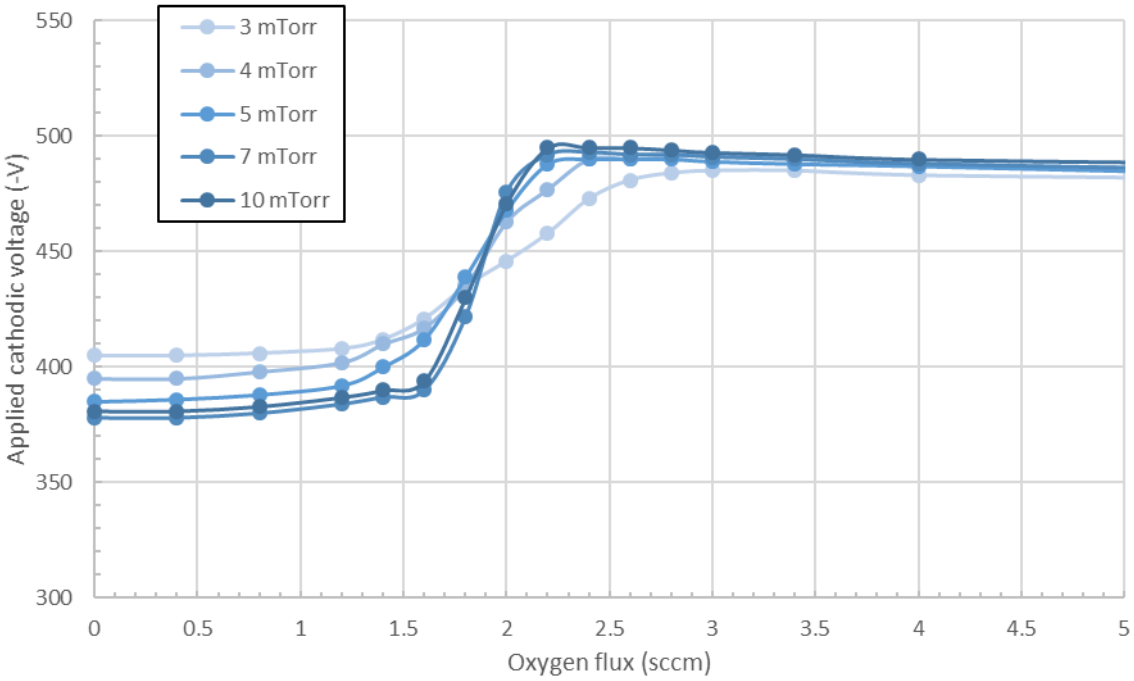

Figure 140. Modification of the oxidation curve in the intensity regulated mode for different pressures (2000 mA – 50 µs – 500 Hz)

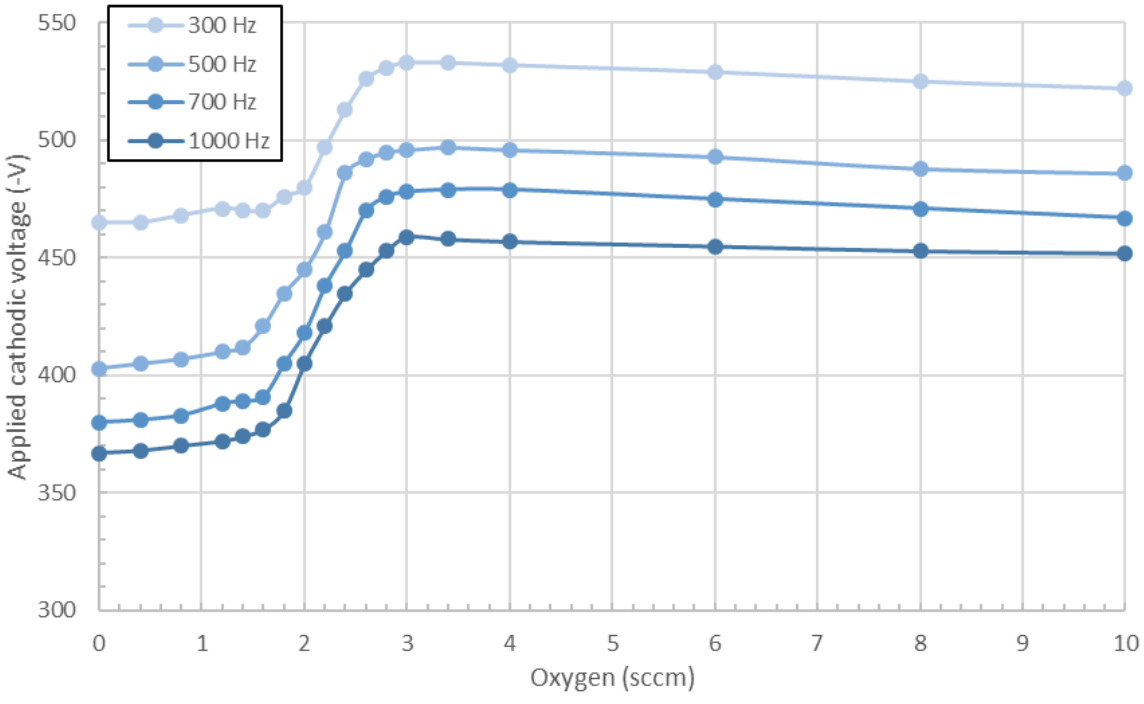

Figure 141. Modification of the oxidation curve in the intensity regulated mode for different frequencies (3 mTorr – 50 µs – 2000 mA)

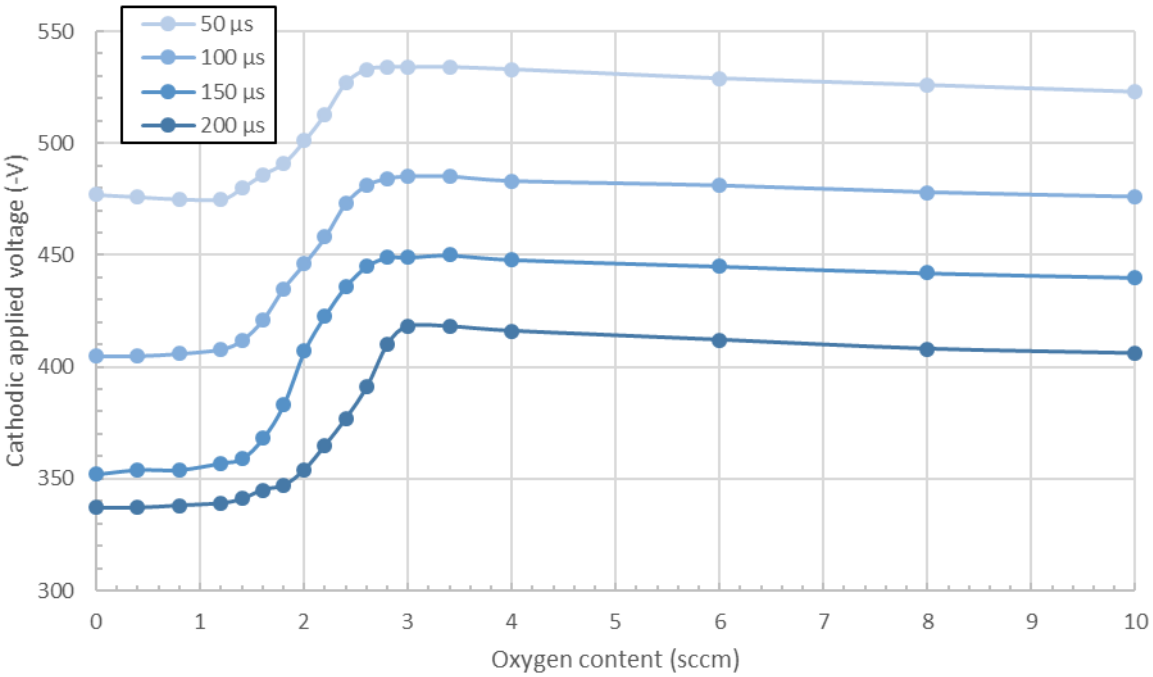

Figure 142. Modification of the oxidation curve in the intensity regulated mode for different frequencies (3 mTorr – 300 Hz – 2000 mA)

IV.2. Data from HiPSTER 6® on small rig

This section completes the previous one as now the HiPSTER 6® power supply is mounted on a smaller rig. The rig details are given in II.2.1.2. The point in changing the rig is to determine whether the rig configuration is important or not. As a matter of fact, it appears to be very important here. To isolate the effect of the rig configuration, the data presented here needs to be compared with the data from the previous section IV.1 (and the next one, IV.3), but not the previous chapter (i.e. Chapter III) as the power supply needs to be the same.

IV.2.1. Metal

IV.2.1.1. Voltage

The first study, as per usual, is the voltage influence on a metallic discharge, as its effects are already well-known. The main point of these studies is to determine the pulse shapes for short and long pulses in metal mode. Here, the observations are very interesting. First, for short pulses, the shape is drastically different to what has been observed in the case of the large rig. If one compares Figure 97 and Figure 143, the change is clear. When using the Nordiko rig, the pulse intensity shows a relatively rapid increase of the current after ~10 µs and this increase would slightly slow down until the end of the pulse. Here, the current intensity does not start to increase significantly before 20-30 µs in the pulse and the slope keeps increasing until the end of the pulse. The shape described in Figure 143 can be associated with difficulties for the system to ionize the species in the chamber, but, once these species are in sufficient number, the ionization process increases exponentially. For 200 µs long pulses (i.e. Figure 144), again, the pulse shape is slightly different to what is found in Figure 98. Indeed, in the previous case, the shape also showed a critical value around 100 µs, after which the current intensity drops down to a *plateau* value until the pulse is switched off. However, in the large rig, the profiles show two convoluted peaks during the *increase* phase. The fact that this doubling of the peak disappears when changing rig and that even short pulses differ show a first important fact: a different rig means a different sputtering regime; a different process, with new kinetics.

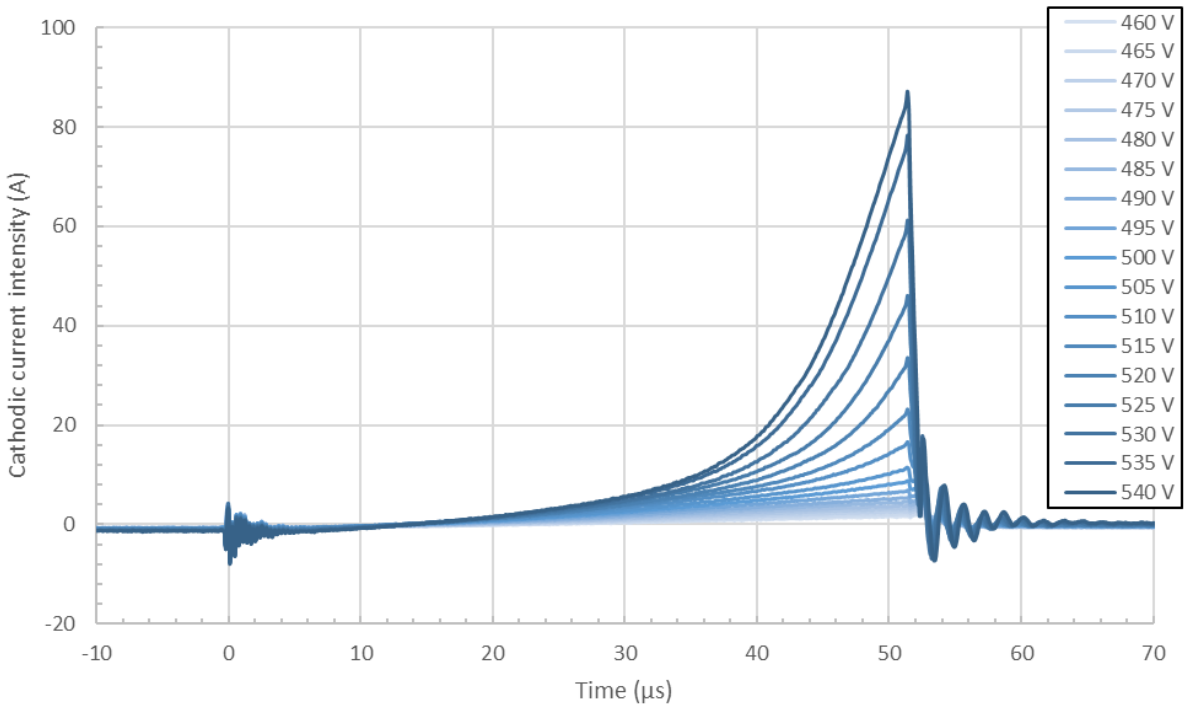

Figure 143. Evolution of the 50 µs metallic pulse waveform when increasing the applied voltage using the HiPSTER 6® power supply on the small rig (3 mTorr – 500 Hz – 50 µs – 0.0 sccm)

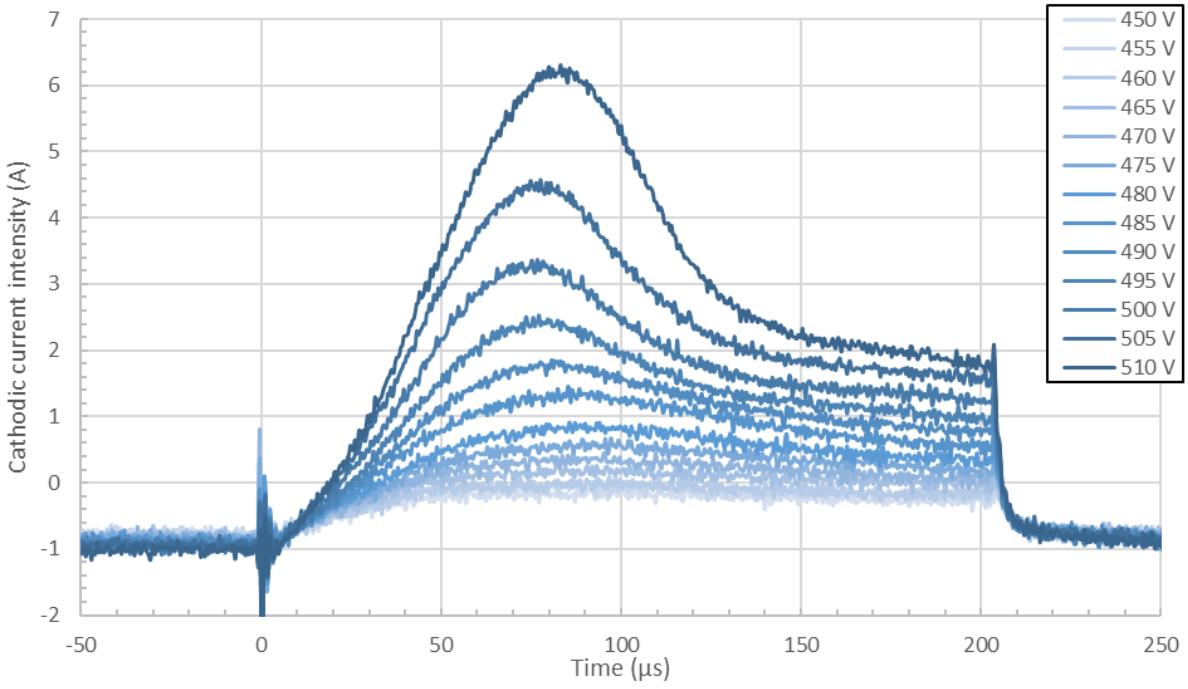

Figure 144. Evolution of the 200 µs metallic pulse waveform when increasing the applied voltage using the HiPSTER 6® power supply on the small rig (3 mTorr – 500 Hz – 200 µs – 0.0 sccm)

IV.2.1.2. Pressure

This section shows an important result. Indeed, here, the pulse signal does not monotonically increase with the pressure. It only does it until a pressure of around 2-3 mTorr, after which the pressure reduces the signal. This behaviour shows the importance of the mean free path of the particles. In such a small rig, if the pressure is too high, the shortening of the mean free path added to the close walls result in a loss of the overall energy within the chamber, due to too many inelastic collisions.

Inelastic collisions are the origin of ions in the discharge but if the atoms do not have sufficient kinetic energy (i.e. high pressure), the inelastic collisions may be more numerous but they do not result in ionization processes, due to the lack of energy. For long pulses, the observation is quite similar, but with a high critical pressure: the signal increases up to a pressure of around 7 mTorr to then decrease. What we also see is that the rarefaction point is delayed with the increase of the pressure. This delay is most likely due to the loss of energy in the ions, as already explained in this thesis.

The fact that, for longer pulses, the critical pressure is higher is certainly due to the lower peak current intensity of the pulse, meaning that since the ions are already less numerous, it requires a higher pressure to have an influence on them: the ions cross-sections being smaller, the mean free path needs to be even shorter before influencing the balance on the other side.

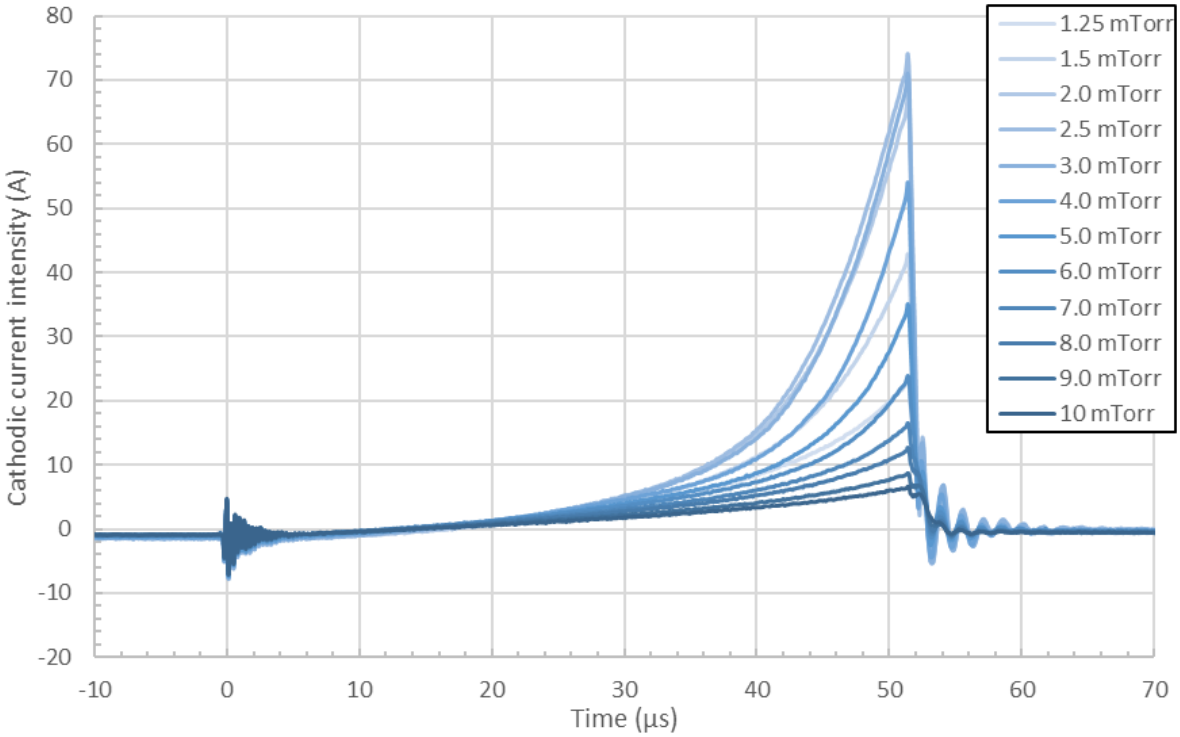

Figure 145. Evolution of the 50 µs metallic pulse waveform when increasing the pressure using the HiPSTER 6® power supply on the small rig in the voltage regulated mode (530 V – 500 Hz – 50 µs – 0.0 sccm)

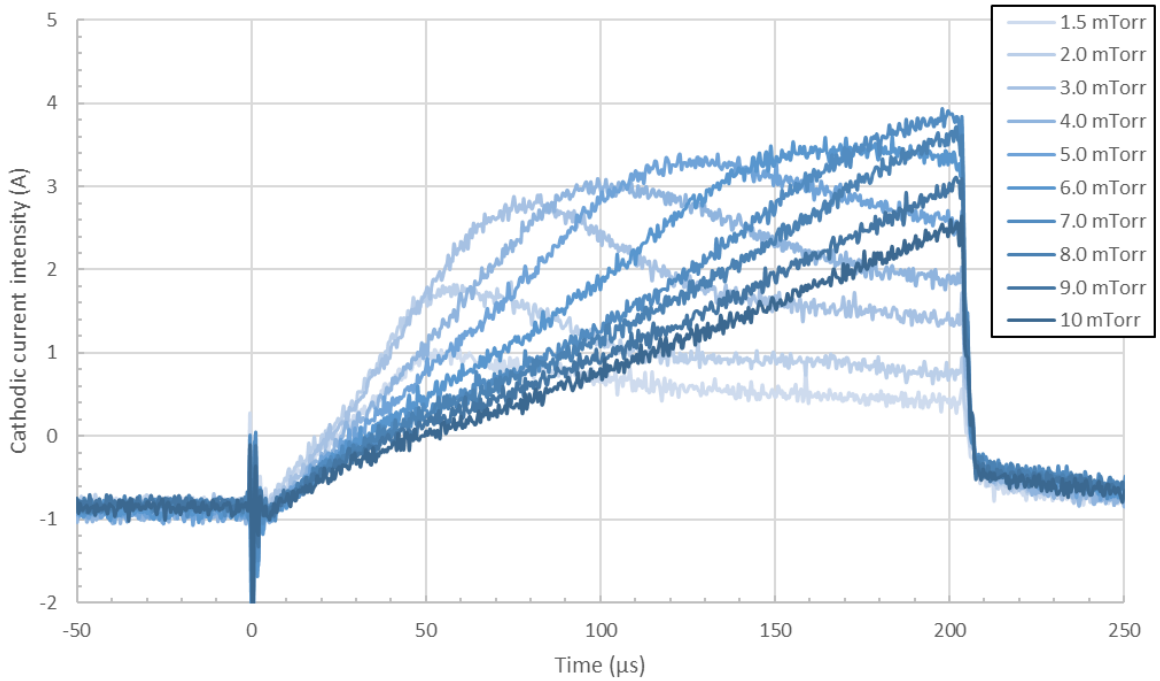

Figure 146. Evolution of the 200 µs metallic pulse waveform when increasing the pressure using the HiPSTER 6® power supply on the small rig in the voltage regulated mode (500 V – 500 Hz – 200 µs – 0.0 sccm)

IV.2.1.3. Frequency

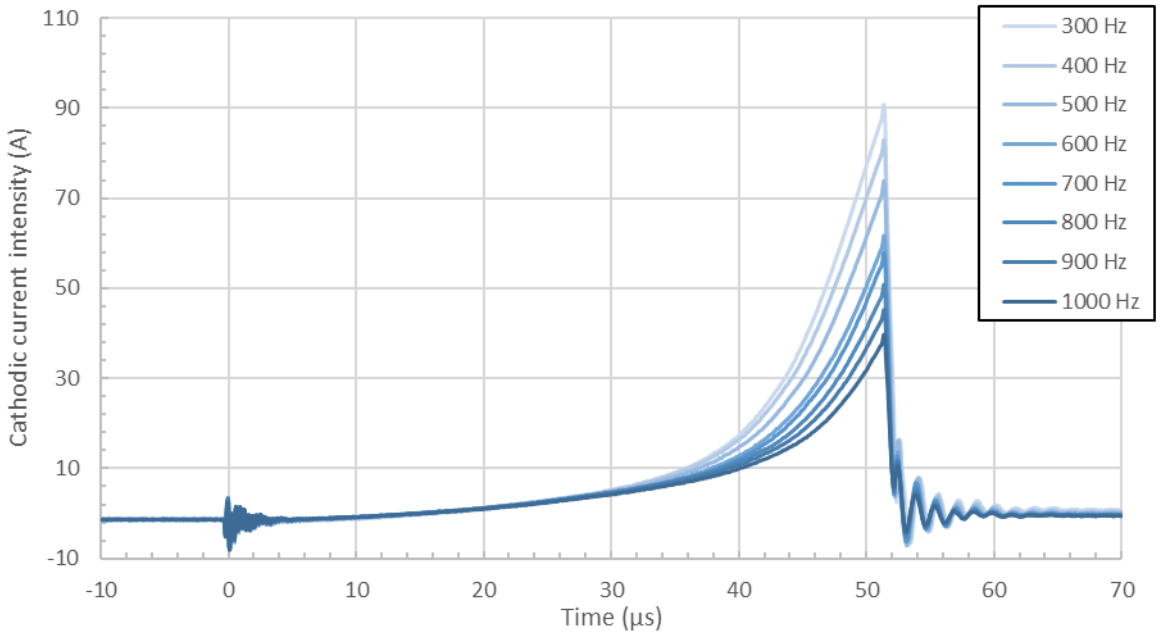

Figure 147. Evolution of the 50 µs metallic pulse waveform when increasing the frequency using the HiPSTER 6® power supply on the small rig in the voltage regulated mode (3 mTorr – 540 V – 50 µs – 0.0 sccm)

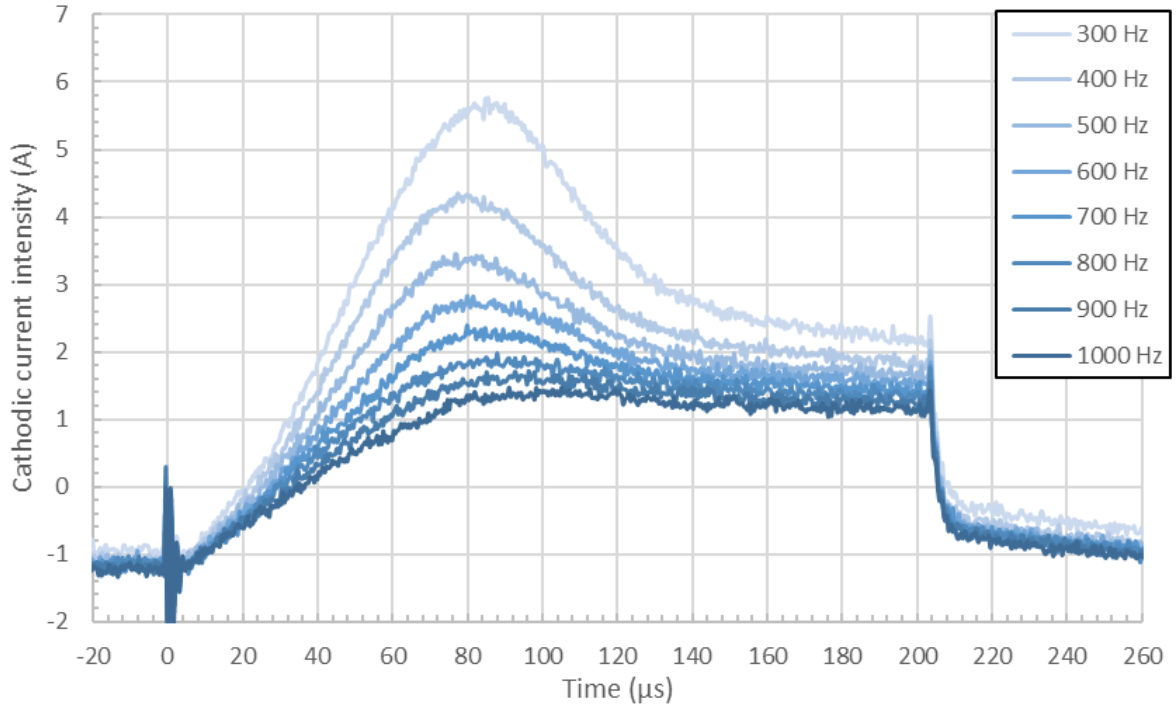

Figure 148. Evolution of the 200 µs metallic pulse waveform when increasing the frequency using the HiPSTER 6® power supply on the small rig in the voltage regulated mode (3 mTorr – 510 V – 50 µs – 0.0 sccm)

Here, the frequency reduces the signal in both cases, which is the phenomenon already observed in the other cases. This is due to the increase of the duty cycle and is not furtherly discussed here. Refer to III.3.1.3 and IV.1.1.3 for more details.

IV.2.1.4.Pulse width

In metal mode, the modification of the pulse width shows a very unexpected behaviour, shown in Figure 149. It shows an intense drop of the signal past the rarefaction point, implying a discharge dependency of the evolution, where the appearance of the rarefaction process leads to an important reduction of the signal. However, this behaviour has not been observed on the other configuration and is impossible to clarify here due to the lack of data in the literature. For short pulses (i.e. without a rarefaction point), the behaviour is also different to what has been observed earlier in this project (see III.3.1.2 and IV.1.1.4).

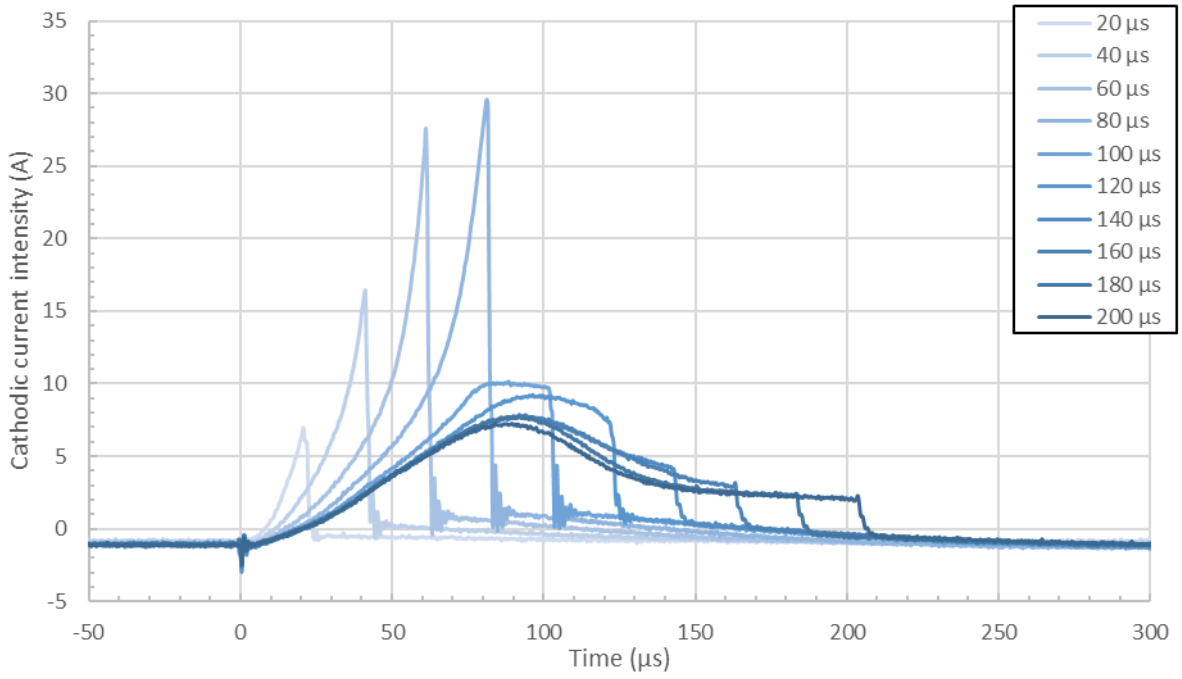

Figure 149. Evolution of the metallic pulse waveform when increasing the pulse width using the HiPSTER 6® power supply on the small rig in the voltage regulated mode (3 mTorr – 500 Hz – 510 V – 0.0 sccm)

To these behaviours, no explanation could be found as it is deeply believed to be a power supply dependent evolution. As this hypothesis cannot be either proved or denied here, it is preferred to make no further comment on the situation other than

highlighting that modifying the pulse width and using it as a modifiable deposition parameter is a risky thing to do as it seems to involve the power supply and the rig in the equation, and not only the plasma physics itself.

IV.2.1.4.1.Intensity regulated

The intensity regulated mode also gives surprising results as it barely shows any difference between with the voltage regulated mode. Again, no conclusion is made here apart from the fact that it shows a different behaviour, showing that the pulse width modification implies different data if the power supply and/or the deposition rig are changed.

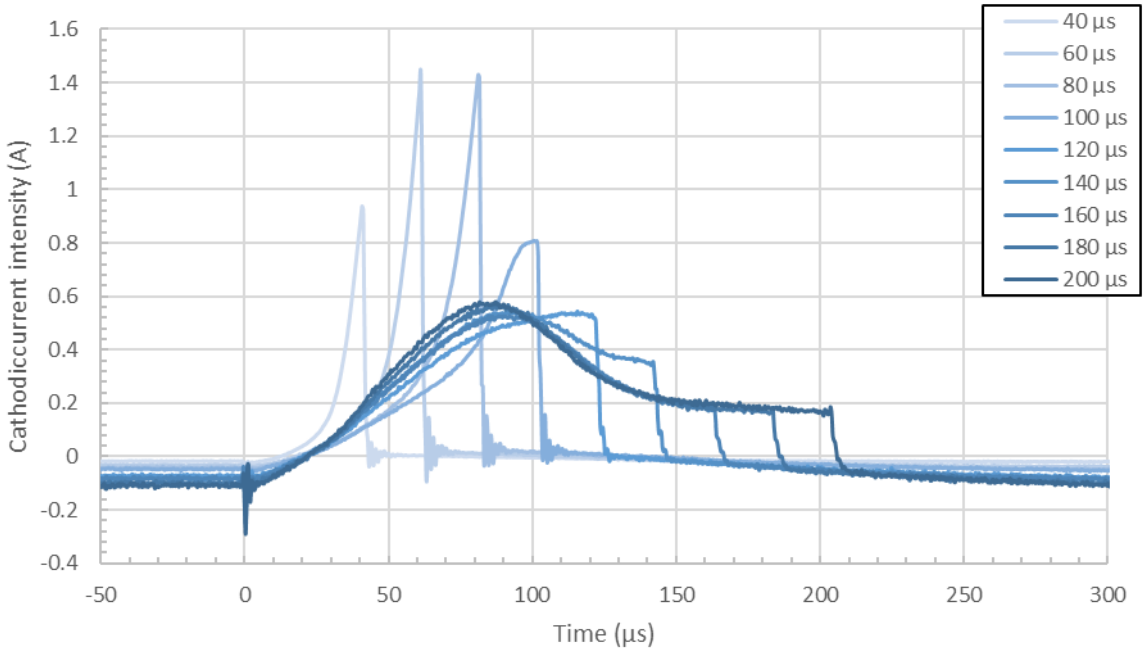

Figure 150. Evolution of the pulse waveform when increasing the pulse width using the HiPSTER 6® power supply on the small rig in the intensity regulated mode (3 mTorr – 500 Hz – 400 mA – 0.0 sccm)

IV.2.2. Oxygen content

IV.2.2.1. Voltage regulated

The oxidation process is very particular in this rig. The result shown in Figure 151 and Figure 152 are very different to what has been measured and showed in the previous parts. For both cases, the signal decreases continuously as soon as oxygen is injected in

the chamber but at no point any sharp transition is observed, where the intensity of the pulse drops or the latter's shape significantly changes. This is a very important observation as it shows that in some cases, even with significantly high oxygen contents, the transition window cannot be identified, even though there is a transition from the metal to the oxide mode, relying on the optical emission of the discharge. The long pulse shows that there is indeed a change of the shape that was previously identified as the poisoning of the target (see Figure 75 and Figure 76). It is therefore clear that the oxidation process is totally different when the rig is changed. This is of a great importance as it means that reactive studies carried out in one rig may be totally different to these carried out in another rig. It then becomes very difficult (or even impossible) to compare this kind of works and duplicate the results.

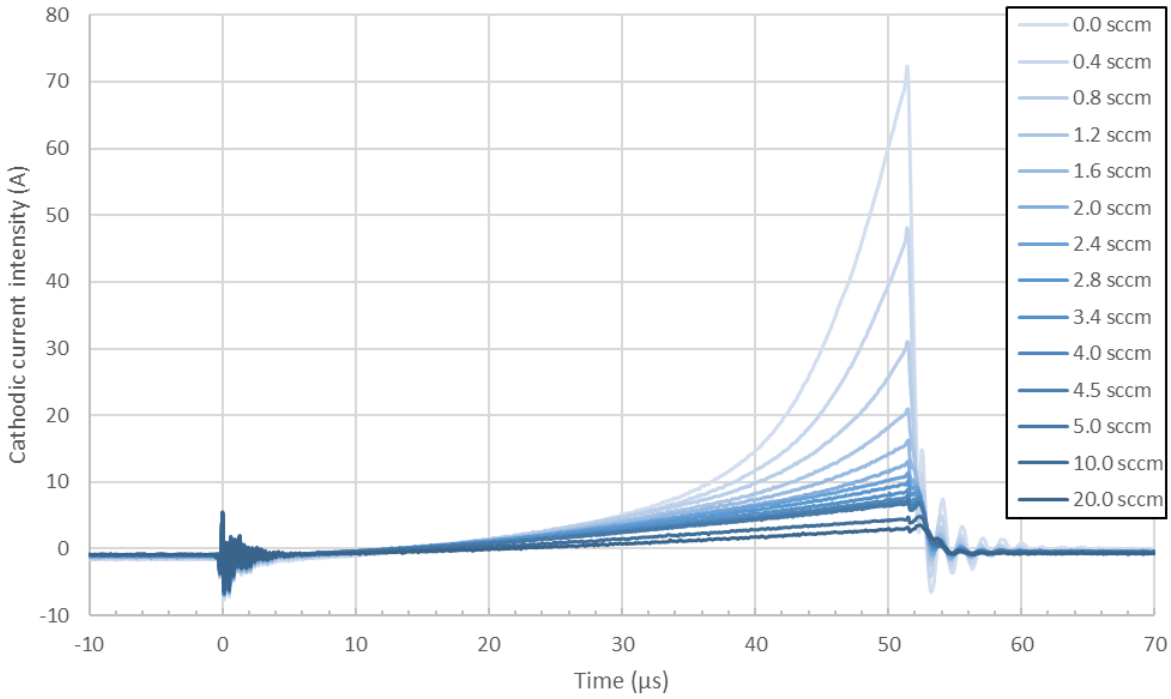

Figure 151. Evolution of the 50 µs pulse waveform when increasing the oxygen content using the HiPSTER 6® power supply on the small rig in the voltage regulated mode (3 mTorr – 500 Hz – 50 µs – 530 V)

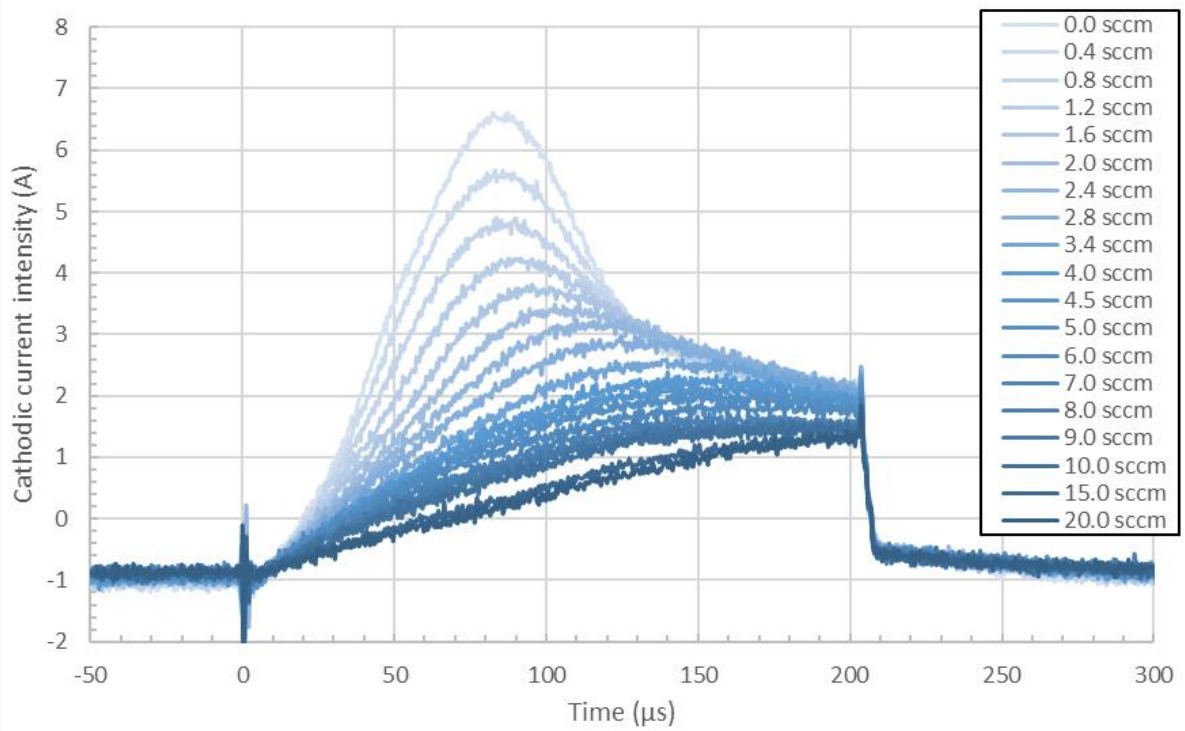

Figure 152. Evolution of the 200 µs pulse waveform when increasing the oxygen content using the HiPSTER 6® power supply on the small rig in the voltage regulated mode (3 mTorr – 500 Hz – 200 µs – 510 V)

IV.2.2.2. Intensity regulated

In the intensity regulated mode, the oxidation process is also very different to what has been observed previously. It is an opposite behaviour for short pulses, compared to the large rig studies. For longer pulses, we observed a similar trend even though in the previous configuration the oxidation seemed to be more complete as it reached a very unstable and arcing regime at high oxygen content.

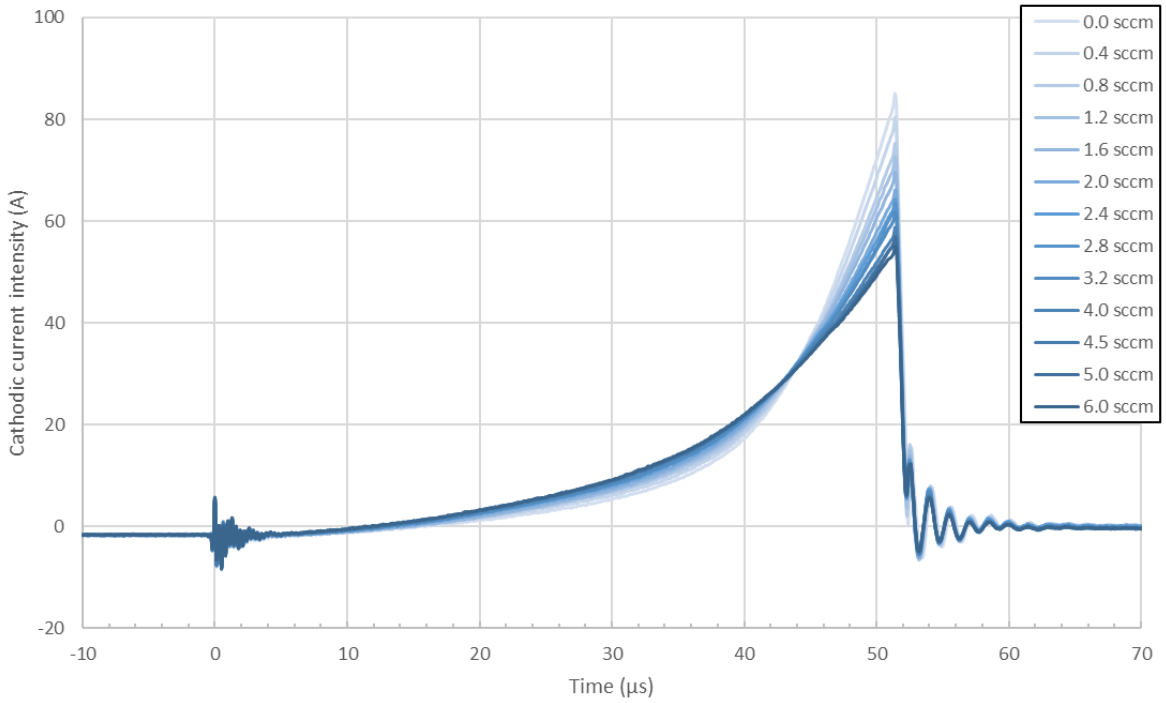

Figure 153. Evolution of the 50 µs pulse waveform when increasing the oxygen content using the HiPSTER 6® power supply on the small rig in the intensity regulated mode (3 mTorr – 500 Hz – 50 µs – 400 mA)

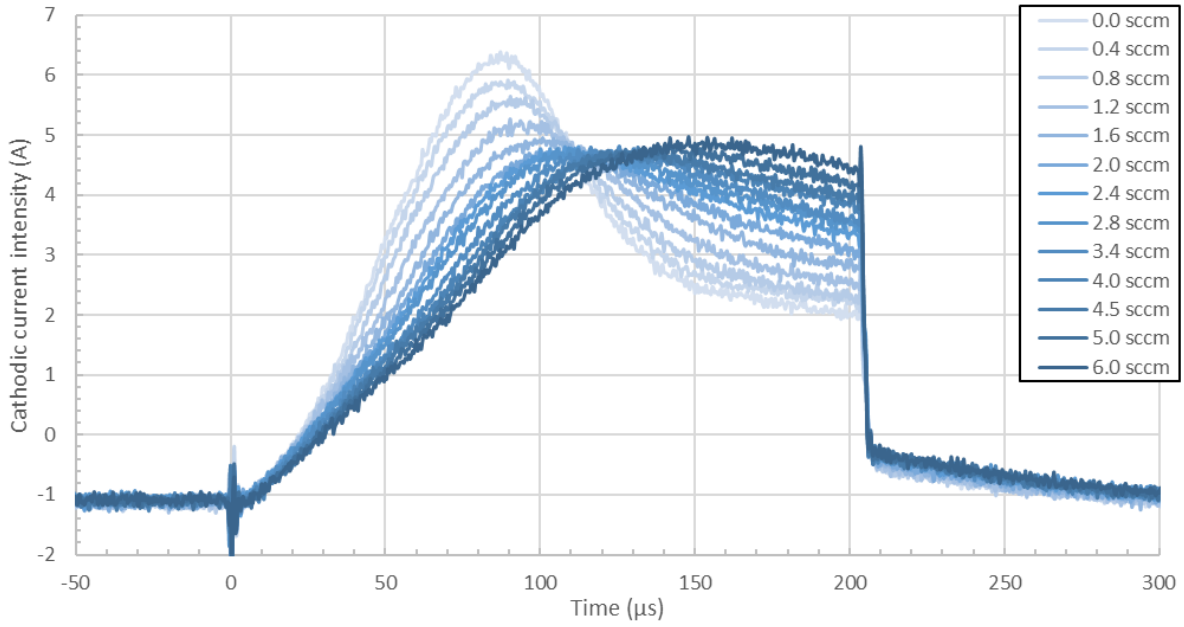

Figure 154. Evolution of the 200 µs pulse waveform when increasing the oxygen content using the HiPSTER 6® power supply on the small rig in the intensity regulated mode (3 mTorr – 500 Hz – 200 µs – 400 mA)

IV.2.3. Poisoned mode

Here are presented results where first order parameters are modified and a constant oxygen flux is inserted in the chamber. Even though the section should correspond to the fully poisoned mode of the discharge, it does not, here, as it has been shown previously (see IV.2.2) that it is impossible to reach a fully-poisoned discharge identical what could be achieved in the previous rig.

IV.2.3.1.Voltage

IV.2.3.1.1. Voltage regulated

Once again, the effect of the voltage is identical to what has been reported previously in this thesis: the signal increases with the applied voltage in both short and long pulses cases without changing the overall pulse shape.

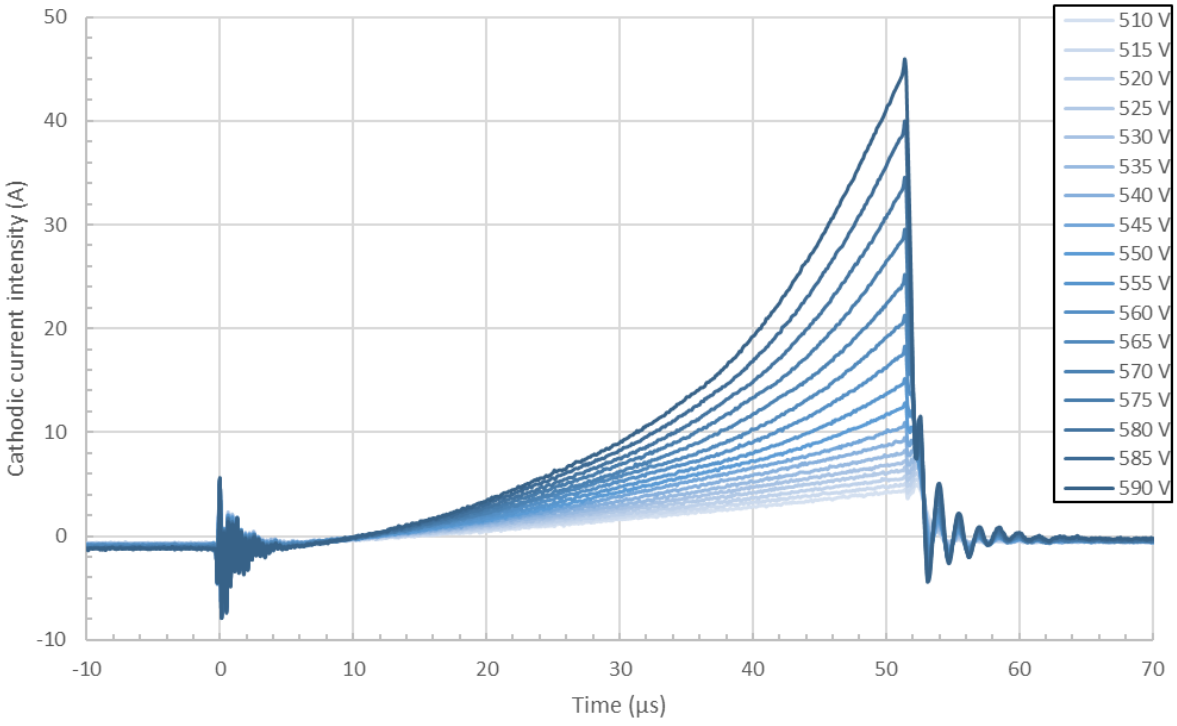

Figure 155. Evolution of the 50 µs poisoned pulse waveform when increasing the voltage using the HiPSTER 6® power supply on the small rig (3 mTorr – 500 Hz – 50 µs – 5.0 sccm)

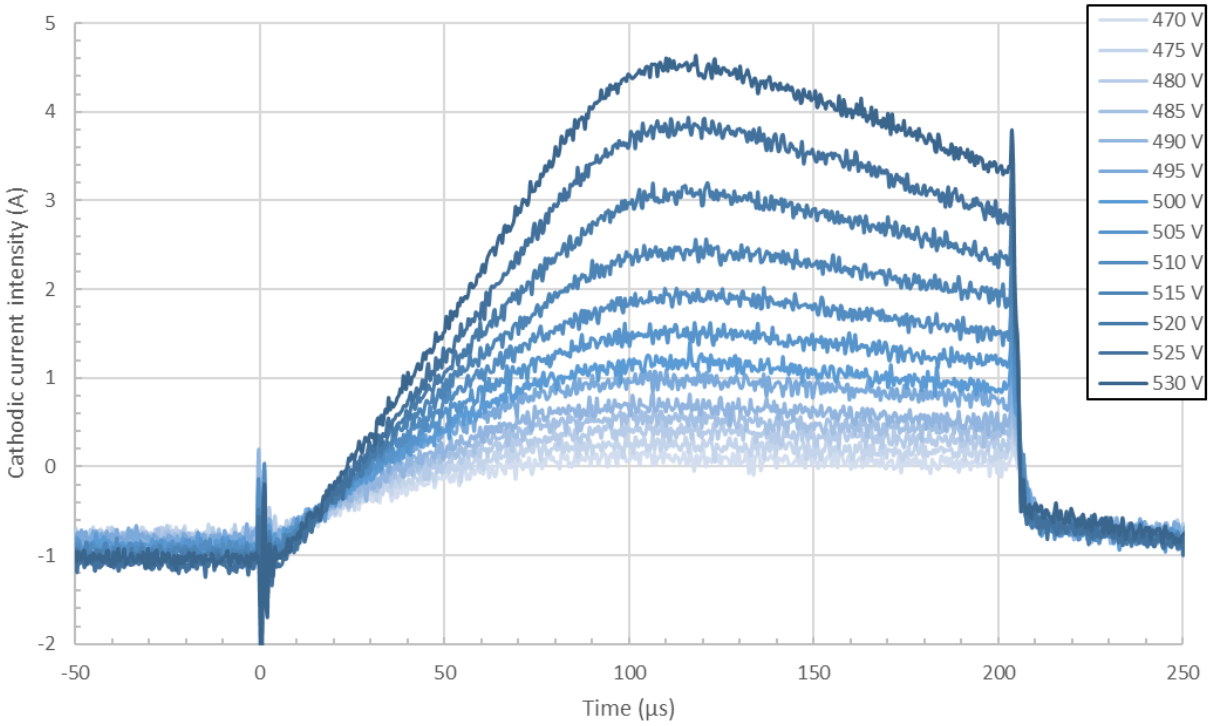

Figure 156. Evolution of the 200 µs poisoned pulse waveform when increasing the voltage using the HiPSTER 6® power supply on the small rig (3 mTorr – 500 Hz – 200 µs – 5.0 sccm)

IV.2.3.2. Pressure

IV.2.3.2.1. Voltage regulated

Here, the results are really similar to the metal mode. When comparing Figure 145/Figure 146 and Figure 157/Figure 158, the same evolutions can be observed. It shows that in this configuration, the addition of oxygen species in the chamber do not change the consequences of increasing the pressure in such a rig: the species in the chamber lose their energy and it results in a diminution of the signal.

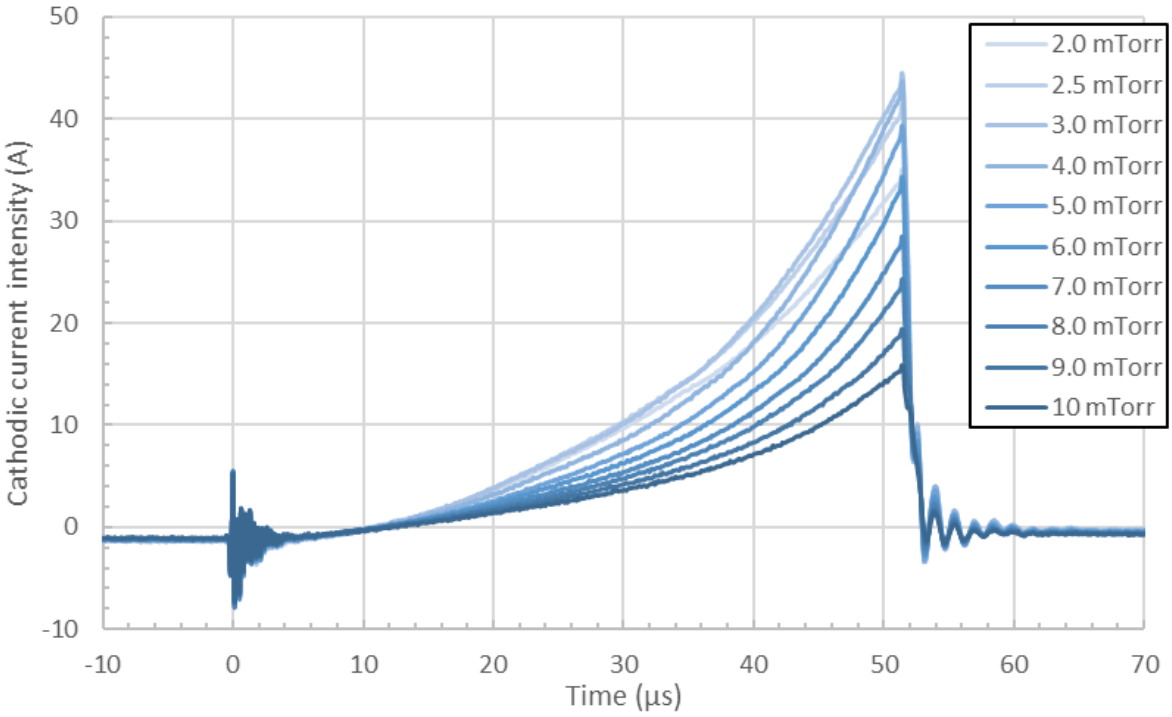

Figure 157. Evolution of the 50 µs poisoned pulse waveform when increasing the pressure using the HiPSTER 6® power supply on the small rig in the voltage regulated mode (585 V – 500 Hz – 50 µs – 5.0 sccm)

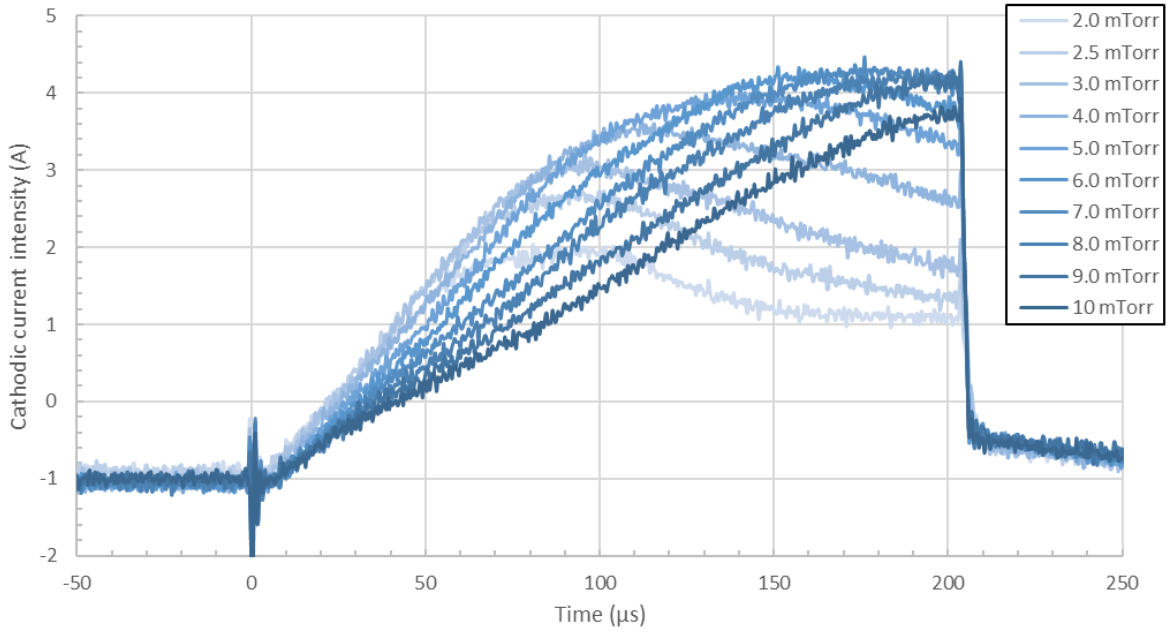

Figure 158. Evolution of the 200 µs poisoned pulse waveform when increasing the pressure using the HiPSTER 6® power supply on the small rig in the voltage regulated mode (530 V – 500 Hz – 200 µs – 5.0 sccm)

IV.2.3.3. Frequency

IV.2.3.3.1. Voltage regulated

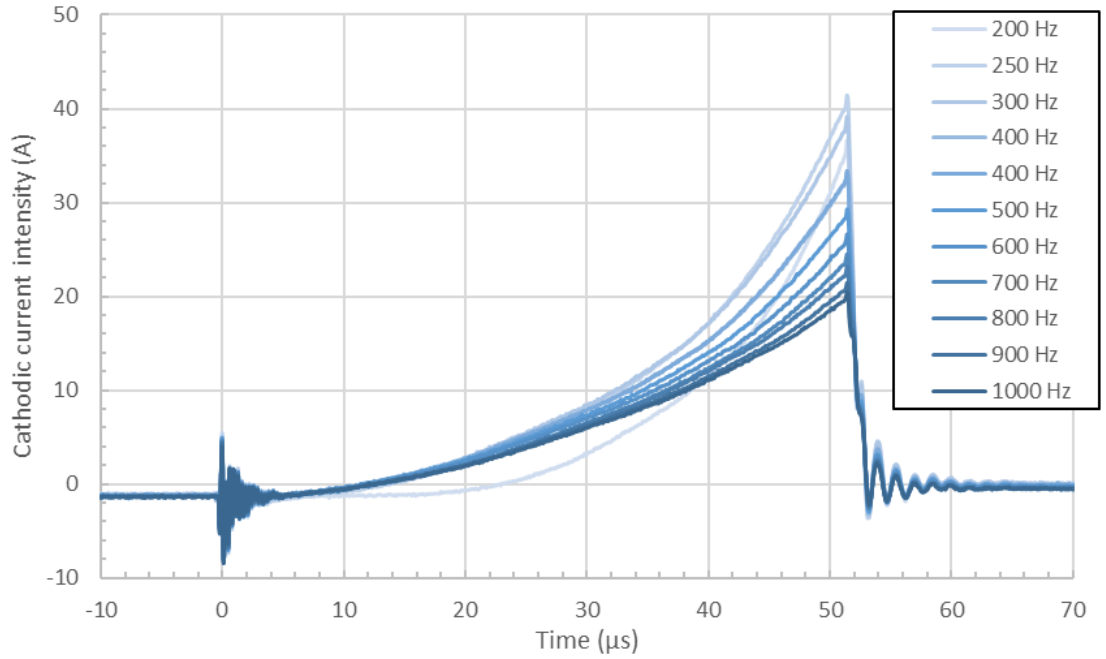

Figure 159. Evolution of the 50 µs poisoned pulse waveform when increasing the frequency using the HiPSTER 6® power supply on the small rig in the voltage regulated mode (3 mTorr – 575 V – 50 µs – 5.0 sccm)

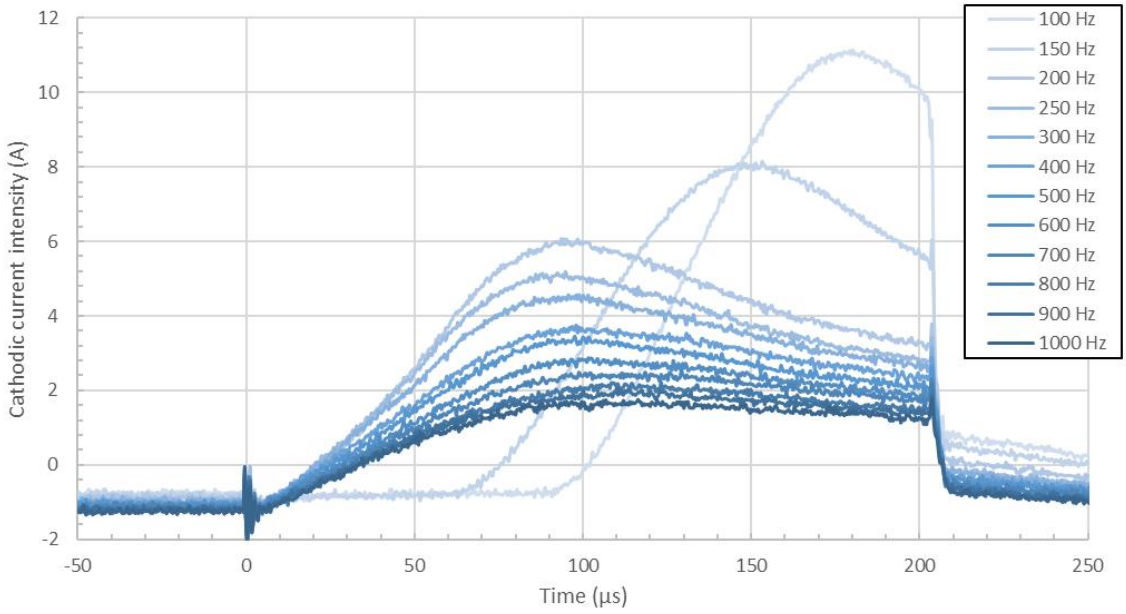

Figure 160. Evolution of the 200 µs poisoned pulse waveform when increasing the frequency using the HiPSTER 6® power supply on the small rig in the voltage regulated mode (3 mTorr – 525 V – 200 µs – 5.0 sccm)

The frequency effect is identical the effects observed in the previous configurations: the signal diminishes with the increase of the frequency. Also, for very low frequency, the ignition delay appears, showing an up to 90 µs delay for long pulses

IV.2.3.4. Pulse width

IV.2.3.4.1. Voltage regulated

Here, surprisingly, the drop observed in metal mode disappears. Instead, the situation is alike what has been observed for previous discharges, with a signal staying relatively constant with the increase of the pulse width. Here, there is still a change in the peak intensity but the latter remains low. Once again, this set of data shows that the modification of the pulse width is a very sensitive thing to do as it remains generally unknown as it seems to be quite rare for the signal to just *follow* the long pulse contour as its width is changed; like it is the case for the Huettinger power supply on the large rig (see Chapter III)

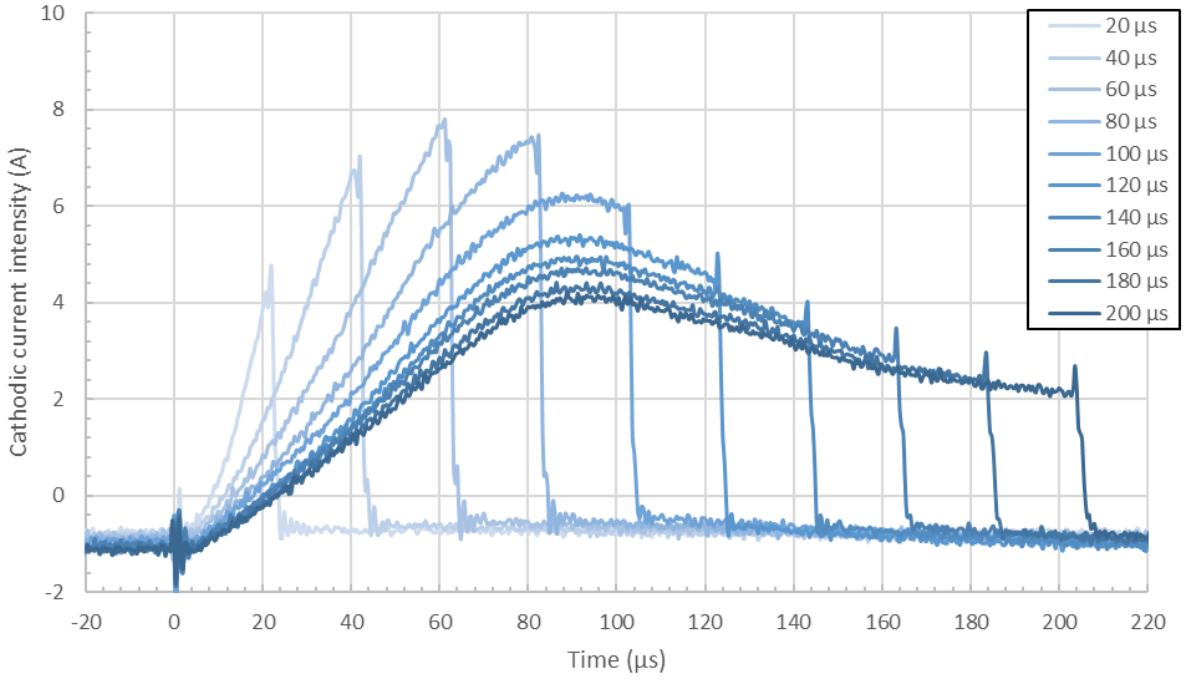

Figure 161. Evolution of the poisoned pulse waveform when increasing the pulse width using the HiPSTER 6® power supply on the small rig in the voltage regulated mode (3 mTorr – 530 V – 500 Hz – 5.0 sccm)

IV.2.3.4.2. Intensity regulated

In the intensity regulated mode, on can also observe a situation much more like the previous configuration, where the peak surface remains approximatively constant when the pulse width is increased. But a very important point here is that this phenomenon is meant to be observable when the pulse intensity has been multiplied by its corresponding duty-cycle because only in this case it means that the average current intensity is kept constant: $< I > \propto I_A * dc_{\%}$, with <I> the time average current intensity, I_A the peak surface, and $dc_{\%}$, the duty-cycle. Therefore, this set of data shows that the intensity regulated mode can be not operating the same way from one power supply to another.

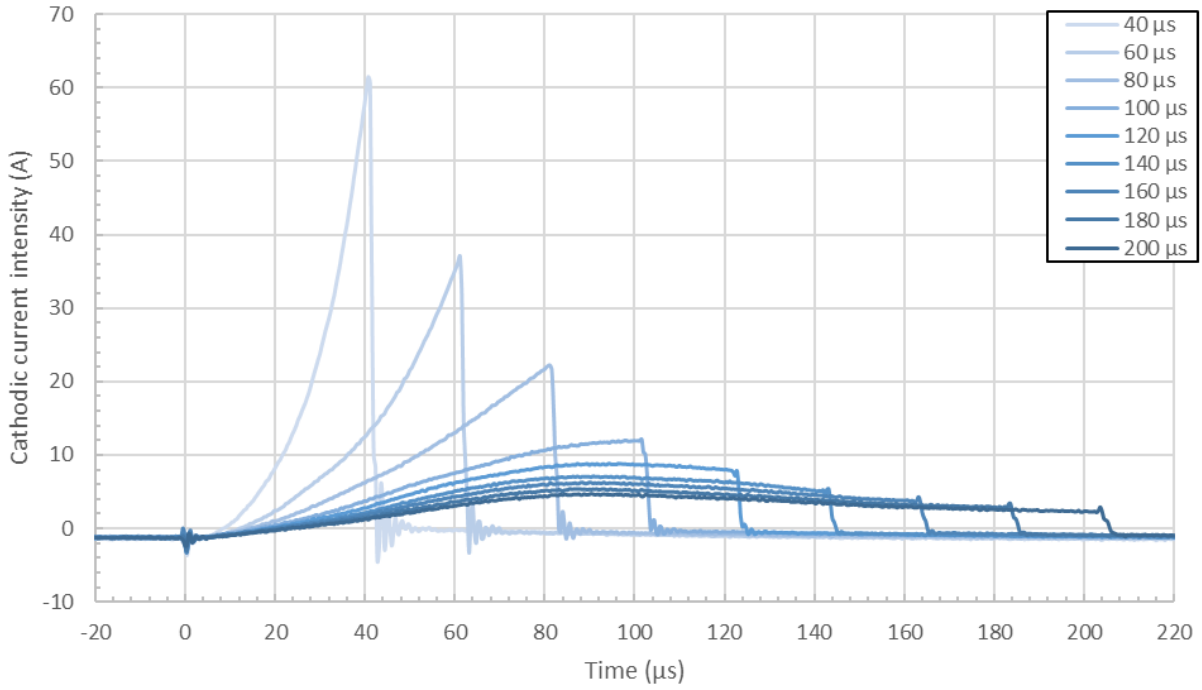

Figure 162. Evolution of the poisoned pulse waveform when increasing the pulse width using the HiPSTER 6® power supply on the small rig in the intensity regulated mode (3 mTorr – 400 mA – 500 Hz – 5.0 sccm)

IV.3. Data from Linköping

This was done in a short period of time during an exchange with Linköping University so the results are not as complete as they are in the other parts but they also show how a different rig can again results in a totally different physics. Indeed, even if the power supply used is the HiPSTER 6® and the rig dimensions are very close to the ones of the small rig used in Manchester, the waveforms and the oxidation process is clearly different.

The study focuses on the oxidation process in the chamber. The systematic approach for each parameters influence could not be carried out in such a short time so here, the approach consisted in acquiring different oxidation curves with their corresponding waveforms modifications in a few different conditions. In all cases, the voltage and frequency are the same, respectively 600V and 700 Hz. The pulse width has been changed to 20 and 40 µs the pressure to 3 and 5 mTorr. For each set of parameters, both oxidation and deoxidation evolutions have been observed and compared. In the meantime, thin films have been deposited and characterized, to mainly determine the stoichiometry of the films; the results are shown in Chapter V.

IV.3.1. Discharge diagnostic in the voltage regulated mode for different pulse widths (3 mTorr – 700 Hz – 600 V)

IV.3.1.1. Short pulse – 20 µs

The first conditions observed were chosen to correspond to the short pulse scenario. Indeed, the previous studies showed that it is necessary to differ short and long pulses from one another with long pulses being pulses showing a rarefaction point. Here, the pulse needs to be below 30 µs wide so the rarefaction point does not appear. The width of 20 µs was then chosen to keep a margin of error. For longer pulses, two widths were chosen because the oxidation curve were still different in such configurations.

Figure 163 shows the evolution of the pulse shape when increasing the amount of oxygen inserted in the chamber. The system was found to be *sensitive* as the shape would start changing for low oxygen flux (typically 0.5 sccm). This seems to be due to the low

duty cycle here and the small size of the chamber. The change in the shape is similar to the change observed in Manchester: at the transition point, the signal drops and the profile curvature changes from convex to concave. However, here, an important observation to be made is the increase in the pulse intensity past the transition window is more important than the transition drop itself. This results in a current intensity that can be higher in the poisoned mode than the metal mode, even with a constant voltage. This observation is quite important as it shows another type of transition curve. Indeed, when comparing Figure 164 and Figure 68, one can see that the oxidation curves are different but when comparing profiles, one can see that the oxidation process is the same; it is only a matter of proportions.

In Figure 164 is also presented the evolution of the lambda factor with the amount of oxygen. The lambda factor is in fact the voltage measured by the chemical gauge situated in the rig (away from the target), measuring the content of oxygen in the chamber. The voltage diminishing when the oxygen is detected. A 13V value (approximatively) reflects a purely metallic regime and a 5V value corresponds to the detection of oxygen. Its evolution shows that both the pulse (peak) intensity and the lambda factor drops at the same oxygen content. It is the expected behaviour, as it is normal to expect the signal to drop as soon as the part of ionized titanium in the chamber drops. However, section IV.3.1.2 and IV.3.1.3 shows a different behaviour that is discussed deeper in the same section.

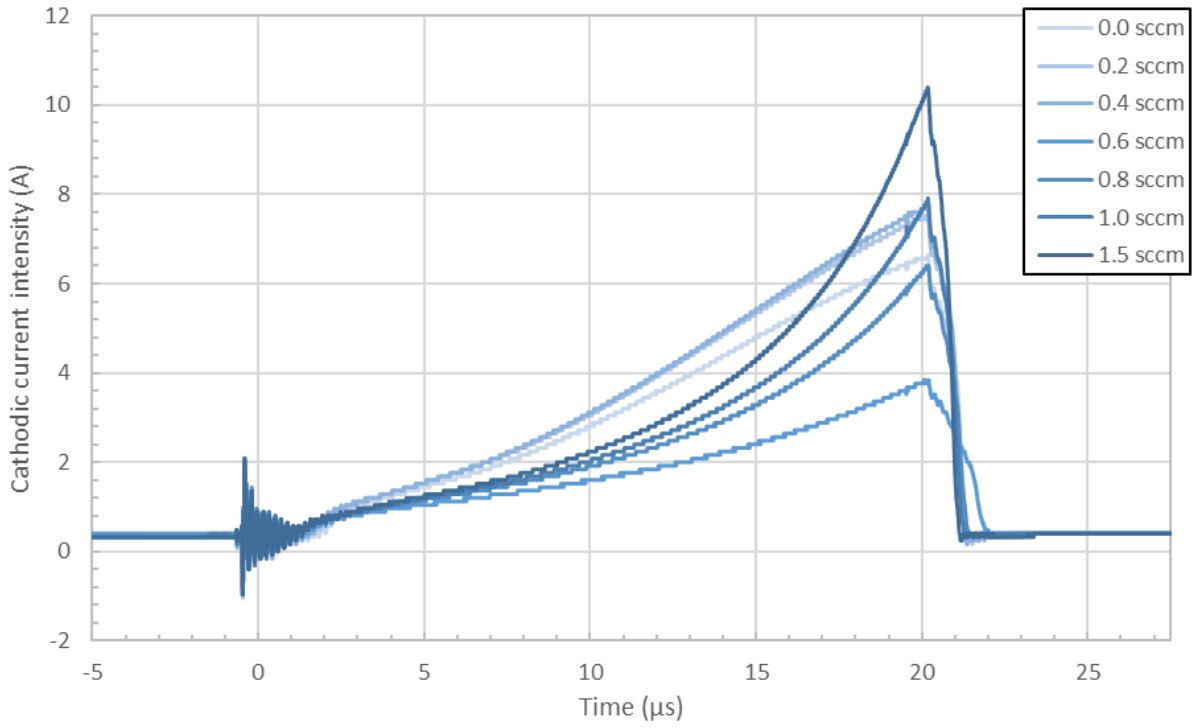

Figure 163. Evolution of the 20 µs pulse waveform when increasing the oxygen content using the HiPSTER 6® power supply on Linköping rig in the voltage regulated mode (3 mTorr – 700 Hz – 20 µs – 600 V)

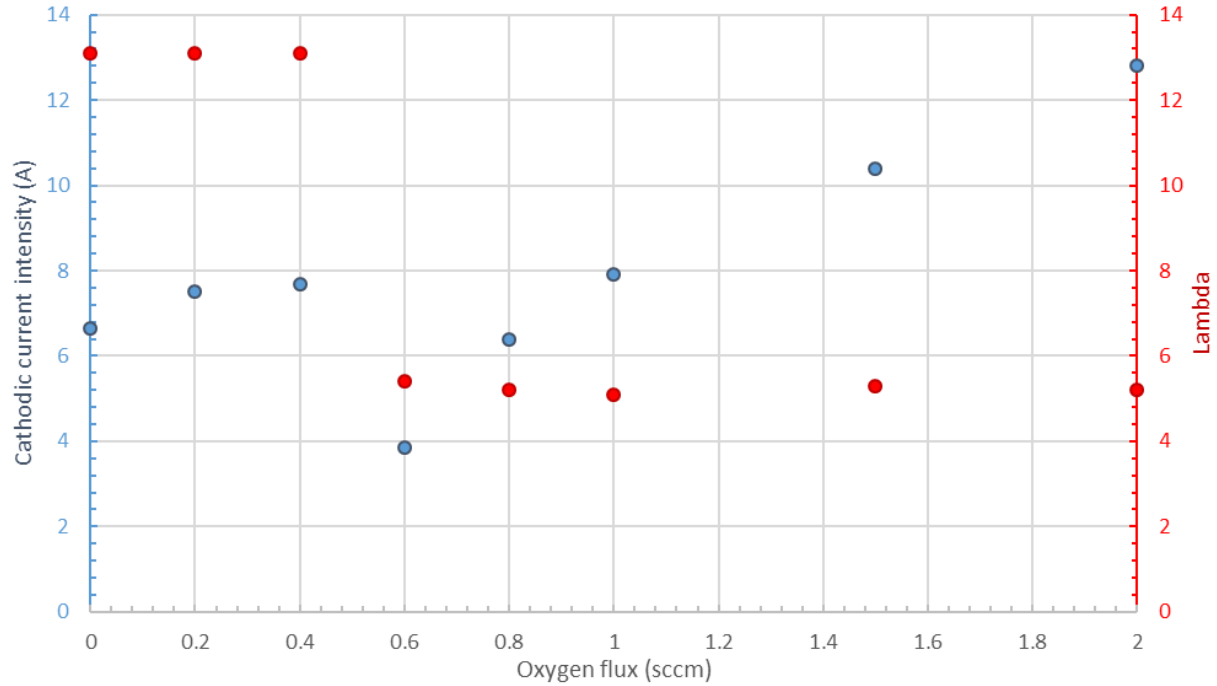

Figure 164. Combined evolutions of the cathodic peak current intensity and the lambda factor when increasing the oxygen content using the HiPSTER 6® power supply on Linköping rig in the voltage regulated mode (3 mTorr – 700 Hz – 20 µs – 600 V)

IV.3.1.2. Average pulse – 40 µs

Here, the shapes change. The pulse shape but also the shape of the oxidation curves. First, the pulse shape in metal mode is quite different as there is now a rarefaction point, around 25µs (see Figure 165), which results in a different evolution of the pulse shape during the oxidation of the system. Indeed, here the oxidation of the system is quite different to what has been reported previously in this thesis. Indeed, here, the sub-stoichiometric mode is very different. Previously, sub-stoichiometric evolutions showed either no major changes or only a relatively slight overall increase of the pulse signal, with no changes of the shape itself (see III.3.2, IV.1.2 and IV.2.2). However, here, the sub-stoichiometric mode shows important changes in the pulse shape. These changes only concern the post-rarefaction point. Indeed, the first half of the pulse does not seem to be changing much when the oxygen content is increased but the second half keeps increasing, going from a metal mode where the signal decreases to a mode where the current intensity keeps increasing until the end of the pulse. Typically, any point beyond the rarefaction point is a balanced mode between sputtering, self-sputtering, rarefaction effect and thermalization. These phenomena are discussed much further in I.1.2.4. The hypothesis to explain this behaviour lays on the target material pathway coefficients. It is believed that the coefficients are modified by the insertion of oxygen in the discharge (α and β_t), which result in an increase of the Π_{ss} coefficient. In I.1.4.2, it was discussed that the increase of the Π_{ss} coefficient is responsible for an increase of the post-rarefaction signal. However, the details of the physics behind this change of coefficients remain unknown as it requires more plasma characterization tools that were not available for this project.

However, the rig had a chemical gauge to measure the oxygen part in the chamber. The gauge is situated away from the target surface and measures a lambda coefficient, measure in volts that represents the quantity of oxygen in the chamber. The lower the signal is, the more oxygen there is in the chamber. The evolution of this coefficient is presented in Figure 166, along with the evolution of the peak current intensity. The lambda coefficient evolution shows to states: the metal mode, with a value of around 13V, and an oxidised mode with a value of around 5V. The lambda transition is very sharp and occurs before the peak current transition. This means that the oxygen inserted in the chamber does not have an influence on the plasma before it fully fills the chamber,

around 0.3 sccm here. Once it has, the transition presented in the previous paragraph starts, until the transition drop around 2.0 sccm.

This second transition consists of a sharp drop of the current intensity, accompanied with a complete change of the shape, where the waveform becomes concave. This transition is very similar to the transition observed in the Manchester large rig and is therefore believed to be the poisoning stage of the discharge, where the latter can deposit TiO_2. This conclusion also relies on materials deposition and characterization, presented in Chapter V, where it seems that the films deposited before this *second* transition are TiO films and the films deposited below that point are made of titanium dioxide.

The comprehension of this oxidation process remains partially uncertain, as it was only a quick analysis of the system, done a relatively short amount of time (around a week). However, the author believes that the explanations given above are correct, relying on both plasma and films characterizations. At the very least, the data presented here show another different oxidation process when sputtering a Titanium target with a HiPIMS discharge. This, it self, is a capital point that needs to be highlighted and deeply understood: The reactive HiPIMS sputtering of a given metal shows various oxidation profiles, depending on the rig used, but also depending on the pulse width. The following section confirms this vision. Also, it should be noticed that the power supply did not show any sign of interaction/control at any point so none of the observation should result from a power supply artefact.

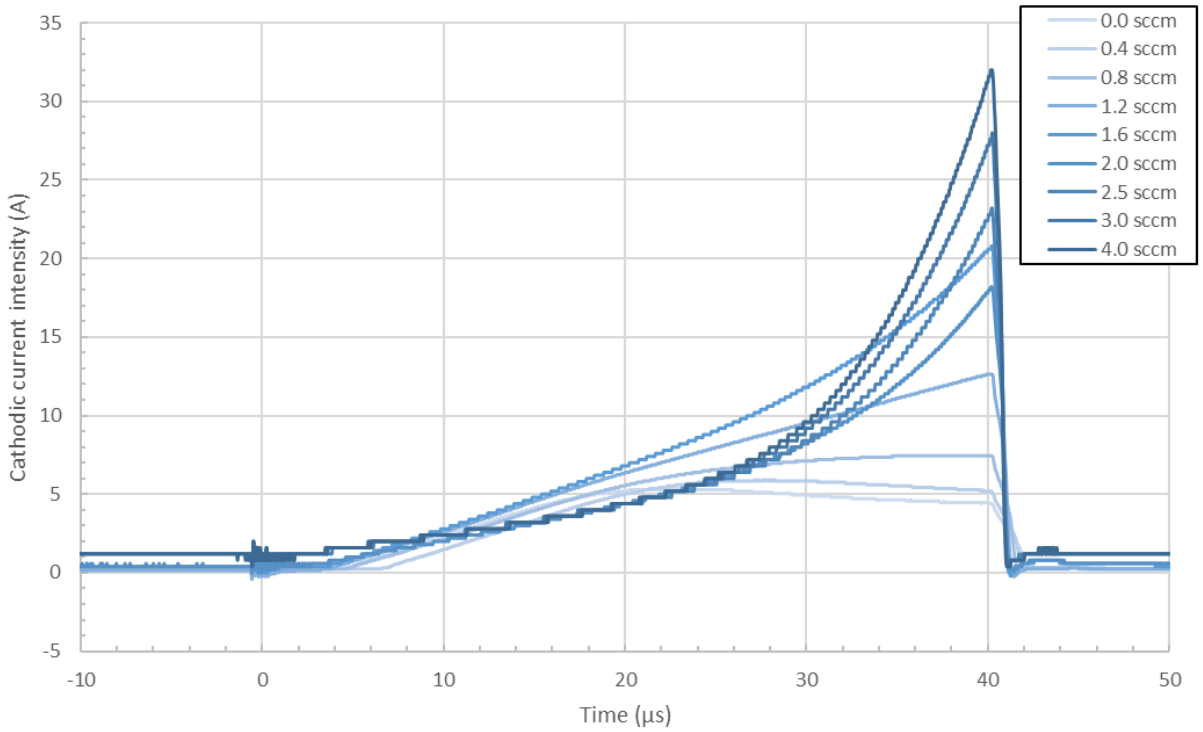

Figure 165. Evolution of the 40 µs pulse waveform when increasing the oxygen content using the HiPSTER 6® power supply on Linköping rig in the voltage regulated mode (3 mTorr – 700 Hz – 40 µs – 600 V)

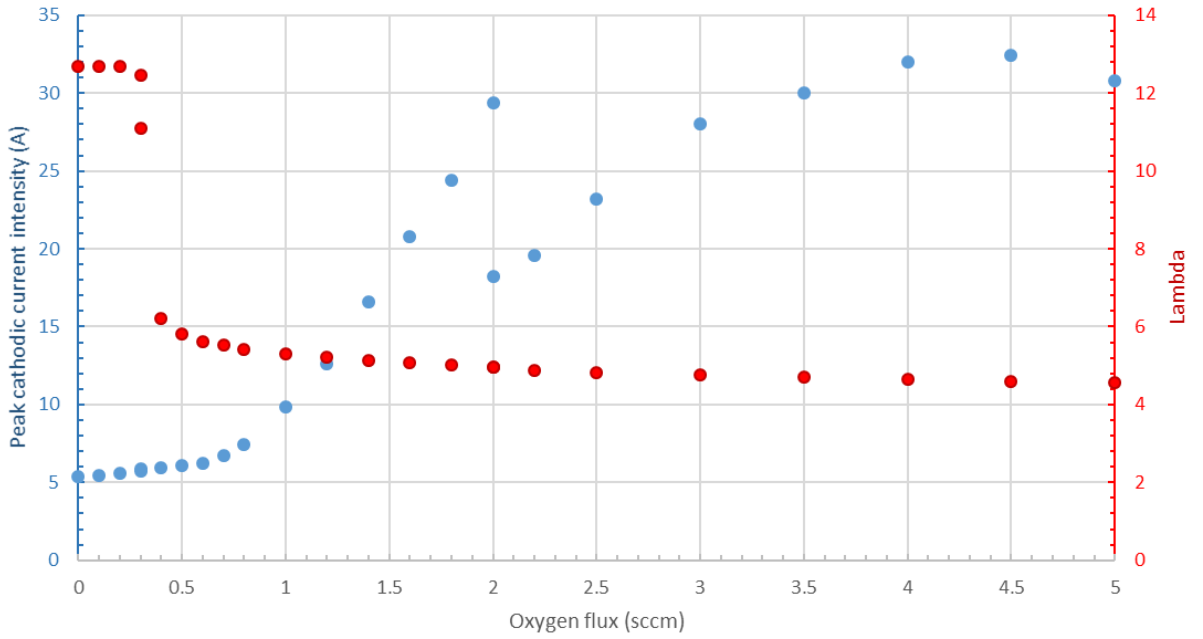

Figure 166. Combined evolutions of the cathodic peak current intensity and the lambda factor when increasing the oxygen content using the HiPSTER 6® power supply on Linköping rig in the voltage regulated mode (3 mTorr – 700 Hz – 40 µs – 600 V)

IV.3.1.3. Long pulse – 65 µs

This section is here to show another case, where the pulse width is much longer, and where the post-rarefaction plateau can be observed. The interest is to observe if, even after the rarefaction point is passed, the pulse width can have an influence on the discharge behaviour. The results presented in Figure 167 and Figure 168 show that there is, indeed, a change in the oxidation process. It shows a third case of oxidation, different from both situations presented above: there is no sharp drop of the signal. This absence of signal drop is surprising as it shows a completely different type of oxidation, where the signal only increases, with no diminution. This oxidation process is identical to the small rig oxidation process, where the system does not present the current drop either. Again, this absence of transition is believed to be due to an insufficient amount of oxygen inserted in the chamber but the curves of Figure 168 show a certain saturation of the current intensity, which would reflect a stabilization of the system, which could be due to its saturation in oxygen, corresponding to a poisoned mode. In which case, it would show an oxidation process where the signal increases with the addition of oxygen, with no decrease. However, the first scenario, where the oxygen content is not sufficient to reach the transition, even though there is a stabilization of the intensity is believed to be the accurate explanation as Figure 170 shows a set of conditions where the current intensity starts stabilizing before dropping to a lower value. The rig used could not send an oxygen flux superior to 5 sccm in the chamber and there was not enough time to deposit films at various oxygen flux to verify their stoichiometries, so this hypothesis could not be verified.

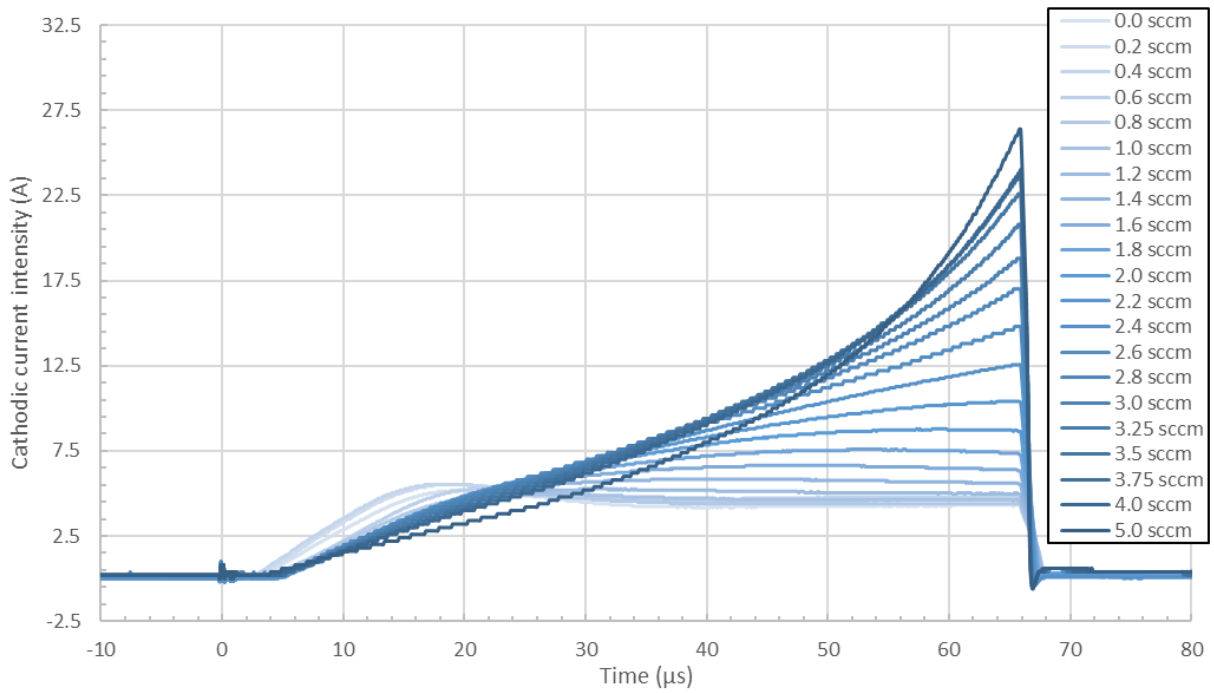

Figure 167. Evolution of the 65 µs pulse waveform when increasing the oxygen content using the HiPSTER 6® power supply on Linköping rig in the voltage regulated mode (3 mTorr – 700 Hz – 65 µs – 600 V)

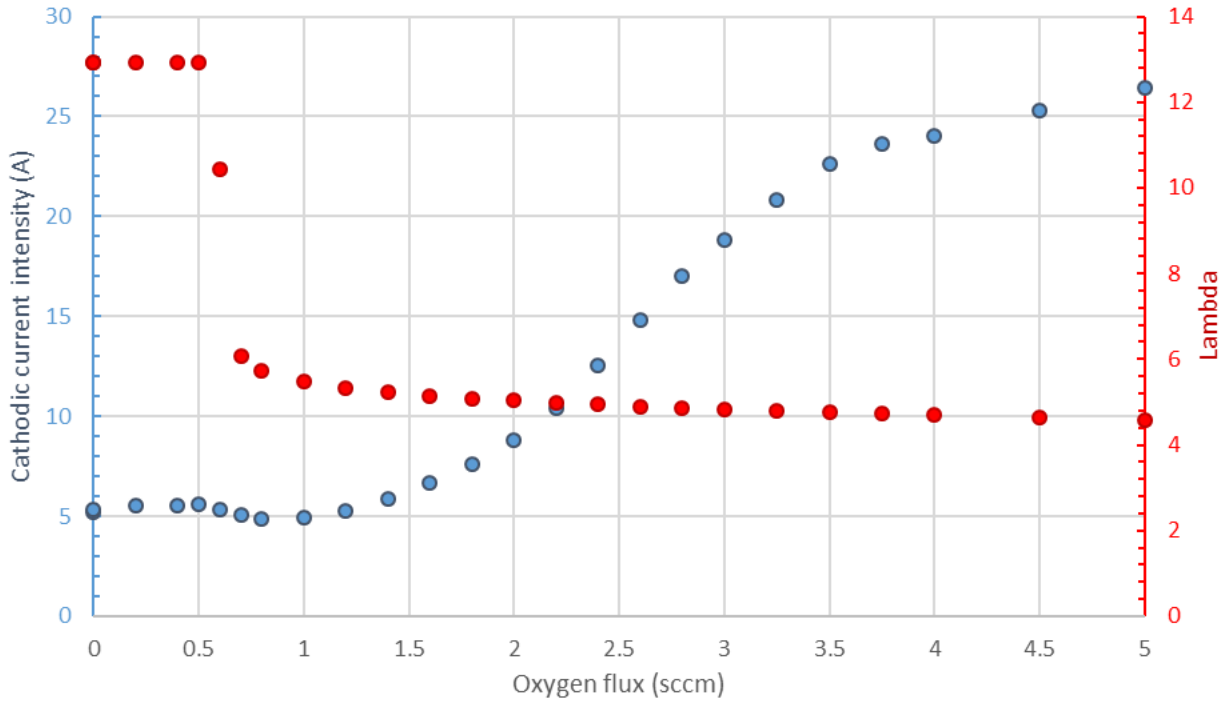

Figure 168. Combined evolutions of the cathodic peak current intensity and the lambda factor when increasing the oxygen content using the HiPSTER 6® power supply on Linköping rig in the voltage regulated mode (3 mTorr – 700 Hz – 65 µs – 600 V)

IV.3.2. Higher pressure – 5 mTorr

For the short pulse scenario (i.e. Figure 169), again, another type of oxidation curve, where the post-transition phase shows a current intensity that does not increase again and where, in opposition, the sub-stoichiometric mode presents a very intense raise of the current. For the longer pulse, the oxidation curve also shows an important rise of the pulse signal in the sub-stoichiometric mode but, here, it starts stabilizing its value before the transition drop, showing that the hypothesis in which there is not sufficient oxygen sent in the case of a 3 mTorr pressure could very well be verified.

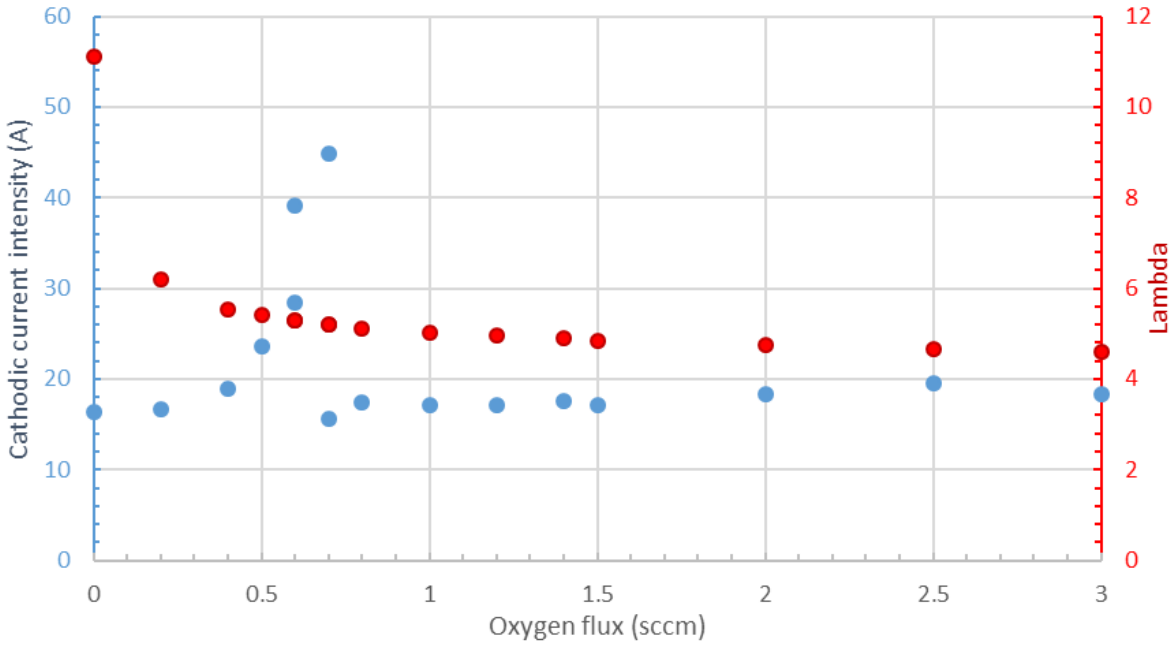

Figure 169. Combined evolutions of the cathodic peak current intensity and the lambda factor when increasing the oxygen content using the HiPSTER 6® power supply on Linköping rig in the voltage regulated mode (5 mTorr – 700 Hz – 20 µs – 600 V)

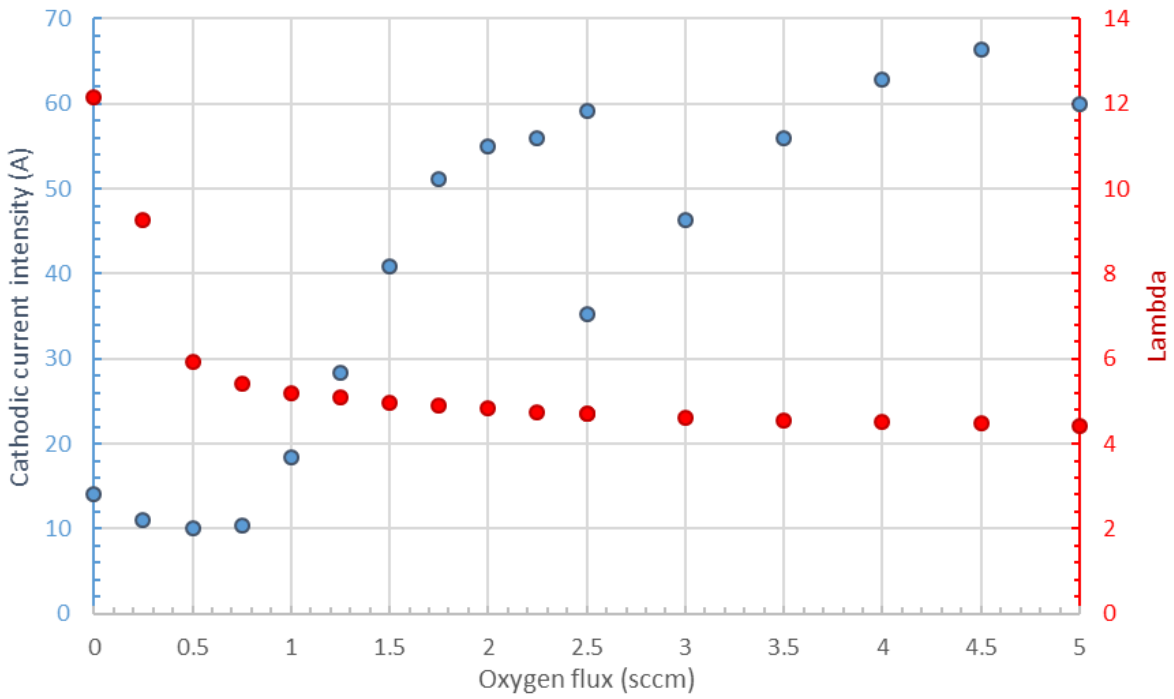

Figure 170. Combined evolutions of the cathodic peak current intensity and the lambda factor when increasing the oxygen content using the HiPSTER 6® power supply on Linköping rig in the voltage regulated mode (5 mTorr – 700 Hz – 40 µs – 600 V)

Even though every oxidation curve showed here seems to be different, the overall aspects of the latter remain identical to the lower pressure scenarios (apart from the 65µs long pulse at 3 mTorr), with a metal mode, finishing when the lambda coefficient drops. Then, the sub-stoichiometric regime starts, where the current intensity increases until the transition sharp drop, finally leading to the poisoned regime.

Again, the details behind these evolutions cannot be determined with certitude due to the lack of means and time for this project but the main point of showing the data acquired at higher pressure is to show that, once again, a change in only one of the deposition parameters can bring major modifications to the oxidation process of the system.

IV.3.3. Hysteresis

As the oxidation process observed on the Linköping rig is unusual, it is also important to see if there is any hysteresis behaviour of the latter. The following sets of data have therefore been recorded. Figure 171 shows the evolution of the peak current

intensity during the increase and then the decrease of the oxygen content in the chamber while Figure 172 shows the same evolution for the lambda coefficient. Both figures show relatively clearly that, in such conditions, there is no hysteresis. The absence of hysteresis is believed to be due to the very low volume of the chamber, in which case the energetic particles interact directly with the totality of the deposition chamber, leaving no residual oxide on the walls, responsible for hysteresis shapes. The fact that there is no hysteresis also show another aspect of this transition as it confirms that the lambda factor decreases before the transition occurs. It also confirms that the transition drop is a stoichiometric change of the discharge as it occurs to the same oxygen content. Figure 171 also shows the instability of the transition window, where, for a given oxygen content, the system fluctuates between a sub-stoichiometric state (i.e. high intensity) and a poisoned state (i.e. lower intensity). For each oxygen flux where this fluctuation is observed, the system seems to be oscillating for up to a few minutes before favouriting one or the other option and stabilizing.

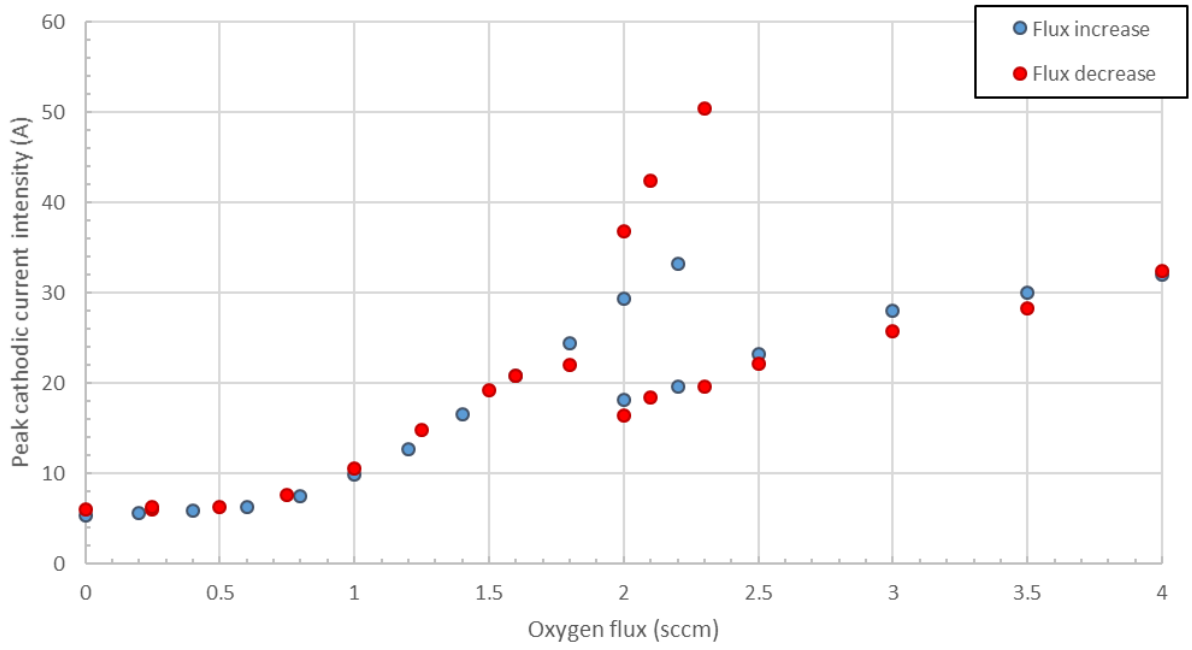

Figure 171. The evolution of the cathodic peak current intensity when increasing and then deceasing the oxygen flux when using the HiPSTER 6® power supply on Linköping rig in the voltage regulated mode to show the quasi-absence of hysteresis (3 mTorr – 700 Hz – 40 µs – 600 V)

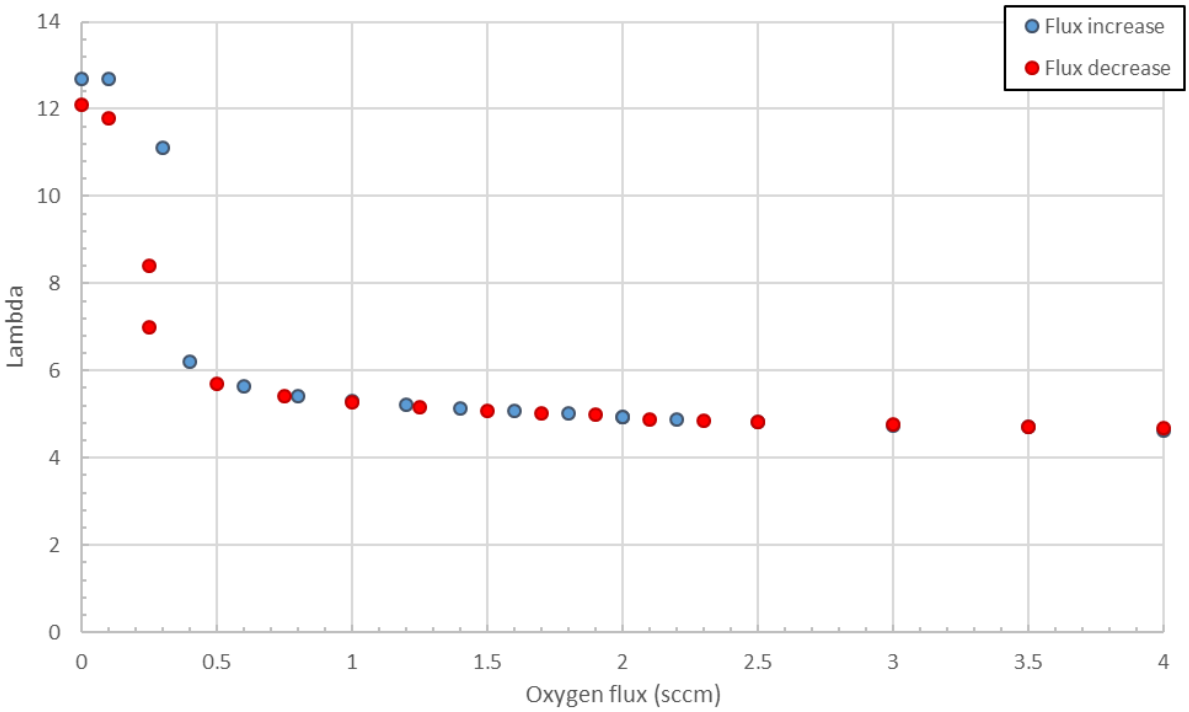

Figure 172. The evolution of the lambda factor when increasing and then deceasing the oxygen flux when using the HiPSTER 6® power supply on Linköping rig in the voltage regulated mode to show the quasi-absence of hysteresis (3 mTorr – 700 Hz – 40 µs – 600 V)

IV.4. Summary

IV.4.1. HiPSTER 6® on large rig

For the discharge stroke by the HiPSTER 6® power supply, the metal discharge pulse shapes are identical to the pulses observed with the Huettinger power supply. The only major difference being the post-pulse signal decay: it is a much sharper decay with the HiPSTER 6® power supply, showing that the power supply can change the how the charged species behave. The voltage has the same consequences on the metallic discharge: it increases the pulse signal, with a reduction of the delay between the two convoluted peaks, for long pulses. The pressure, even though it also shows an increase of the pulse intensity, do not show a linear rise, as the Huettinger did. The frequency shows an increase of the signal at low pulse widths, and a decrease of the signal at longer pulse widths. Changing the pulse width has different consequences than it had in the previous chapter.

The oxidation process is also identical to previously: the signal is slightly decreasing or slightly increasing in the sub-stoichiometric mode, then follows a sharp signal drop at which follows an over stoichiometric phase where the signal increases. However, the intensity drop is much greater with the HiPSTER 6® power supply.

In the poisoned mode, all parameters have the same consequences on the pulse evolution, except the pressure. The pressure shows an inverted influence: it decreases the poisoned signal when raised. Using the Hipster power supply made it possible to use the first order parameters to change the stoichiometry of the discharge; thing impossible with the Huettinger power supply because of its limitations. However, here, obtaining of oxidation curves for different frequency and power supplies for example, was impossible due to the important transition gap. The transition studies showed that the stoichiometry of the system can be increased by either diminishing the voltage, the pressure, the frequency and/or the pulse width.

IV.4.2. HiPSTER 6® on small rig

Here, the rig dimension is changed to see how it can influence the discharge. First, the metallic waveforms are very different to the previous waveforms in both cases. For the short pulses, the waveform has an unexpected shape, where the curvature is concave, which was previously assimilated to the poisoned mode. For longer pulses, the second 'acoustic' peak disappears and the waveform consists of only one peak. The voltage still increases the pulse intensity without changing its shape. The pressure, however, does not show the linear increase observed in the large rig: here, there is an optimal pressure for which the signal is maximum. It also changes the shape of longer pulses. Increasing the frequency decreases the signal, which is what was observed for longer pulses (only) in the larger rig, using the HiPSTER 6®. The pulse width modification shows, once again, a different behaviour, where the short pulses have very high peak intensity whereas the long pulse have much smaller peak intensity.

The oxidation process is much more different here as there is no sharp transition. Indeed, the system only shows a slow transition when the oxygen is inserted in the chamber. In the voltage regulated mode, the signal drops, but it seems like there is not 3 different regions as presented before but more a unique transition phase as soon as oxygen is inserted.

Therefore, for the so-called *poisoned mode*, the system is not really in a poisoned mode, but only an oxidized mode. In this mode, the voltage still, as usual, changes the pulse intensity without changing its shape. The pressure, here, decreases the pulse signal, similarly to the case of the large rig but only for short pulses. Again, for longer pulses, the shape of the pulse changes. Increasing the frequency decreases the pulse intensity as well, with the exception of very low frequencies where a pulse ignition delay. Increasing the pulse width shows a more consistent evolution, closer to what has been observed in the larger rig.

IV.4.3. Linköping rig

For the Linköping rig, the effects of 1st order parameters on the discharge in metallic and poisoned mode have not been analysed due to a lack of time. However, the

oxidation process has been observed in different conditions to observe how the latter behaves. The oxidation process has been shown to have the similarities with the oxidation processes observed in the large rig: the three distinct regions. However, the sub- and over-stoichiometric regimes show much more important increases of the signal. Also, the 1st order parameters such as the pulse width and the pressure have been shown to drastically change the shape of the oxidation curve, not only the transition window. Another difference is the rarefaction timing. Indeed, the rarefaction seems to be already observed for pulse as long as 40 µs.

IV.5. Conclusion

From this chapter, the main conclusions are that changing either power supply or the deposition chamber influences the discharge, and especially its oxidation process. Indeed, the 1st order parameters do not influence the pulse waveform identically if the rig configuration is modified. The only exception is the voltage as it always increases the pulse intensity without modifying the shape of the pulse itself; or at least not in a major way. The pressure however, has shown to have a different effect on smaller rigs, where its increase tends to diminish the signal when the behaviour is opposite for the large rig. The frequency also proved itself to not always influence the discharge the same way. Finally, the pulse width seems to be a very complicated case, as it is very difficult to identify the changes occurring; some results suggest possible the power supply to be responsible for the evolution. More importantly, the oxidation process has shown to be very dependent on the rig configuration.

The major conclusion on the data presented in this chapter is that scaling up and duplication results from one rig to the other is far from being a simple process. First, the HiPIMS power supply used can bring important changes to the way the discharge reacts to the modification of 1st order parameters; which can influence the optimization process for the film deposition. It does not seem to change the way the particles behave in a drastic way, however, as the pulse shapes do not change importantly. The oxidation process is also only slightly modified as it seems that the most important change is the amplitude of the transition gap, which remains a minor change: it does not change the oxidation process itself. Using a power supply such as the HiPSTER 6®, compared to the Huettinger can however bring important changes in the ease of use and the liberty of the user. It has been experienced that the HiPSTER 6® provides much more liberty since its limitation are much wider than that of the Huettinger. It is also easier to use as it allows the user to choose between the voltage regulated and the intensity regulated modes, where you can hose the limiting intensity in the latter.

Now, when changing the rig, things get more complicated. The rig dimension and configuration are very important, they can drastically change the way the discharge and how the plasma reacts to any changes. In total, three different rigs have been used for this study and they all show a different sputtering process, even though the power supply

is always the same. This is of critical importance as it shows that the data/conclusions found in the literature for small lab rigs (i.e. typically a few dm^3 or less) are not necessarily applicable for the deposition in larger rigs (i.e. typically around 1 m^3 or more). It is therefore essential, when depositing, to identify the oxidation process as it is also (at least slightly) different for each rig. This is at least true for titanium dioxide deposition using the HiPIMs process. The literature on HiPIMs and reactive HiPIMS is quasi-totally constituted of deep physical characterizations of the discharge but the plasma physics in small rigs is different to industrial rig. It is then becoming essential to the research community in the field to adapt their research to larger rigs, so the industrial world can directly use their observation. It should be remembered that thin films deposition, and especially reactive HiPIMS, aims at direct state-of-the-art industrial applications to bring the new technologies forward and therefore, the plasma should be studied at scales closer to the industrial scale as it is clearly shown in this thesis that the plasma does not act the same way in large rigs (e.g. possible acoustic wave and hysteresis) but more importantly it does not get oxidized the same way at all.

Chapter V. TiO_2 films characterization

This section presents the results of the ongoing work and is therefore incomplete. However, some measurements are consequent enough to be presented here. In most cases, the quantity of data is limited and cannot really lead to any conclusions.

This section follows the previous chapter on plasma diagnostic. During the latter part, each deposition condition has been studied, and their individual influences on the plasma have been described. As a result, a *stable process* envelope has been defined and the following deposition will be realised in such conditions. This envelope corresponds to the limit of the system used for this project. The major limits of this envelope are as follows:

- Pulse width: 50 – 200 µs
- Frequency: 300 - 1000Hz
- Duty-cycle: 5%
- Pressure: 3 – 10 mTorr
- Distance: 45 – 170 mm

The studying process is identical to what has been done in the previous chapter: each deposition parameter is looked at, to determine its individual influence on the deposited film. This time, the objective is to determine their optimal values where it was impossible in terms of plasma diagnostic. For certain conditions, there are absolutely no indication so far of possible limitationso: e.g. oxygen content or distance. However, for these optimizations, it is essential to define criteria to fulfil. In the case of the project presented here, the criteria are multiple as a long list of properties are aimed to be observed and optimized: transparency, photocatalytic activity, mechanical resistance, anti-microbial behaviour, hydrophilicity and hydrophobicity.

To obtain these properties, the major criteria is to deposit a crystalline thin film. This is therefore the first and principal objective while depositing the films. For each one of them, a Raman spectrum is acquired and for the films showing the clearest peaks on Raman, an XRD spectra is also acquired to study the crystallinity of the film is a more effective way. The structure of the film is also essential and determining for the latter's

efficiency in terms of photocatalytic activity and wettability. For this particular reason, all films are also observed by SEM for surface and cross-section micrographs. In parallel, certain films are tested for transparency, contact angles and photocatalytic activity to determine which deposition condition corresponds to which film property.

This chapter is also essential to link plasma diagnostic and film properties. Indeed, this part is essential to fully explain the process of optimization. Each deposition parameters influence can be observed on the film but it is necessary to understand the reasons behind these modifications of the material, relating on the plasma diagnostic previously done. This way, the work conducted here is more likely to be useful while disseminated to other research teams. Indeed, the plasma diagnostic is the common entity to every system and eases the comparison between different works and results.

V.1. Methodology / Progession plan

Characterizing the structure of the films is one of the first steps of the project, when determining the deposition envelope as it essential to identify the regions where defects are too important on the film, due to arcing or other. Alongside these measurements, the crystallinity of the films is also assessed, using both XRD and Raman techniques. Again, the objective of the first crystallographic studies is to find deposition conditions allowing the deposition of crystalline phases, but in no case trying to already optimize the phases in presence and even less their orientations.

At the end of this first step, the process envelope has been reduced, by limiting the range of some parameters, even limiting it to one given value (e.g. pressure and deposition time). Following this, can start the optimization process of the crystallinity of the film, where the main objective is to find conditions in which crystalline anatase can be deposited. One might suggest XRD to study the crystallinity of the films but the idea here is not to determine the orientation of the phase, but only the phases in presence (i.e. Anatase or Rutile). With this objective, the Raman is the most efficient technique to use. Indeed, for each deposition condition, there are four different substrates, added to the fact that HiPIMS presents a longer list of 1st order parameters than other techniques., it results in a very large quantity of samples to characterize. Also, the fact that there are a lot of sample results in a slower process. But more importantly, the material study presented in this thesis is a very slow process because the maximum films possibly deposited per day is three, but generally of one or two. the chamber needs to be venting and vacuumed back down between each deposition and with a chamber of this size, it takes about 5 to 6 hours to reach the base pressure. Also, the deposition time to obtain films thick enough to be observable correctly by SEM and Raman is of about an hour. However, the XRD is a technique that requires long runs (up to several hours) to obtain XRD patterns of good quality, with acceptable peaks definition when a Raman run only last around 1 min to obtain the same quality of peaks, and even better. Therefore, every single film deposited has been analysed with the Raman spectrometer to try and find optimal conditions to deposit crystalline anatase.

In addition to the crystallinity, it is also essential to determine if the samples deposited are photo-active, as it is the main objective here. To do so, the MB test

described in II.4.1.4 has been used to determine the k_a coefficient for some samples, with different levels of crystallinity. The results are mainly here to confirm the direct relationship between the anatase crystallinity and the material's photocatalytic activity and therefore, no measurements of the samples roughness and surface area have been conducted has it is believed to be too early to focus on these. To complete the photocatalytic properties, contact angle measurements have also been carried out to determine what type of contact angle the films presented and if the latter could be modified under illumination.

It also needs to be specified that a collaboration project with Morgan Solar, a company building transparent photovoltaic cells, has resulted in an extra set of data, presented in this chapter. The objective, for the company, was to obtain a thin transparent film showing photocatalytic activity to coat on complex shaped PMMA substrates. The results are shown in a separate section. A more recent collaboration with the Department of Sanitary and Environmental Engineering at the Federal University of Minas Gerais in Brazil consisted in depositing photo-active titanium dioxide on large pieces of PET. These types of project are the perfect examples of applications for the work conducted here. They consist in being able to deposit crystalline films onto polymers but also in industrial scale. A photovoltaic panel consists of tens or even hundreds of smaller units, and the PET pieces deposited for Brazil were one meter long, which is only possible coat in an industrial scaled rig. The results for both projects have been shown to be quite interesting.

V.2. Results and discussion

V.2.1. SEM micrographs

V.2.1.1.Dependence on the substrate nature

For SEM observations, the nature of the substrate has shown to be crucial to make the observation possible. Only the samples deposited onto Si have been analysed using the SEM and the results are presented in the next section (see V.2.1.2). However, no clear micrograph has been obtained in the case of polymeric substrates, due to the mechanical stability of the substrate itself, as it is impossible to cut the samples in a clean way that allows a good observation of the cross-section without deteriorating the film itself. The samples of the latest stage of the project (PEC, PET, PMMA and UPVC) are not characterized here either for the same reasons. The observation of the samples deposited onto glass is also impossible and not reliable because of the important charges accumulation effects, compromising the micrographs, as shown in Figure 173.

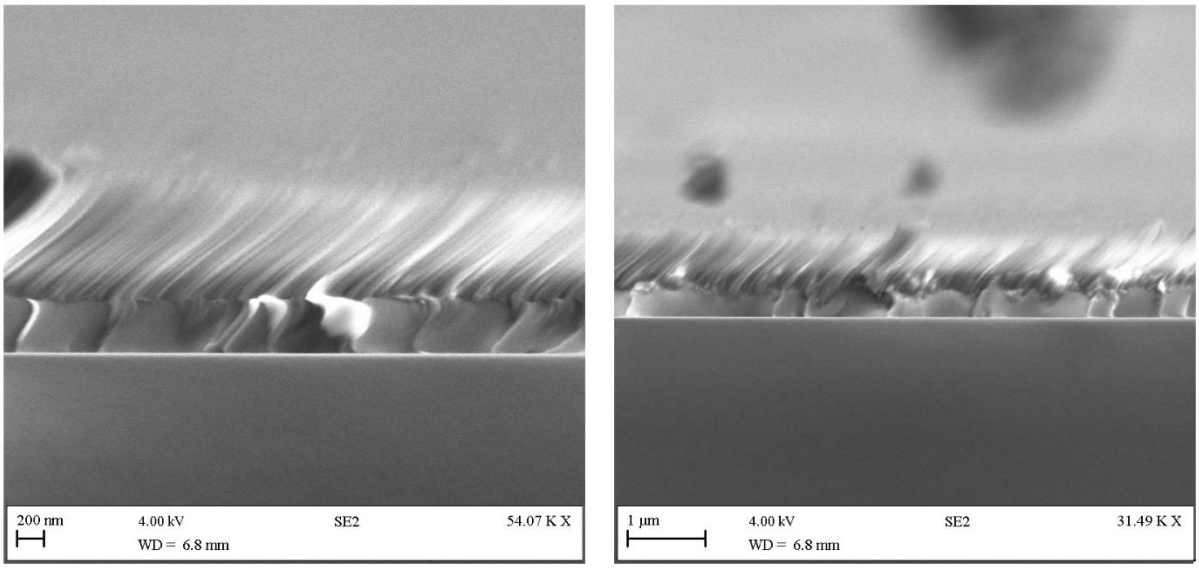

Figure 173. Typical SEM micrographs for two different films deposited on glass substrates where the effect of the charge accumulation can be observed

Certain films deposited onto polymers have been observed as presented in Figure 174 but as it can be seen, the cross sections are pretty much impossible to observe in a

clear fashion and thus their study cannot occur. Unfortunately, one knows the type of substrate used influence the structure of the film, and its crystallinity.

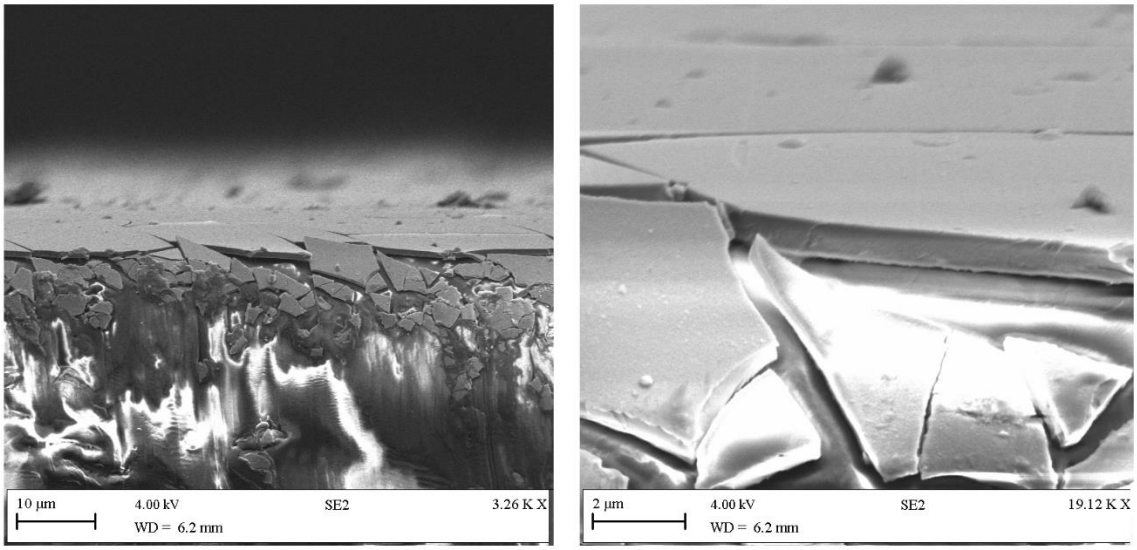

Figure 174. Typical micrographs for a sample deposited onto a PET substrate for two different magnifications

V.2.1.2. Deposition parameters influences – 1st step

V.2.1.2.1. Results

The study of the SEM micrographs has been useful to determine the growing structures of the films deposited in different deposition conditions. Concerning the films deposited onto Si substrates, the first step of the experiment consisted in keeping a constant frequency-pulse width couple and modifying the pressure*distance product. Indeed, it has been referred several times in the literature as being a very important factor when it comes to study the films structure. The first films that have been deposited have been deposited for high pressure*distance products. The objective is to reduce even more the temperature and the kinetic energy of the ions reaching the substrate, by increasing the amount of collisions within the chamber. The idea is to determine if any kind of crystal can be deposited in these extreme conditions and, if not, if it is possible to obtain columnar structures (i.e. corresponding to higher surface area).

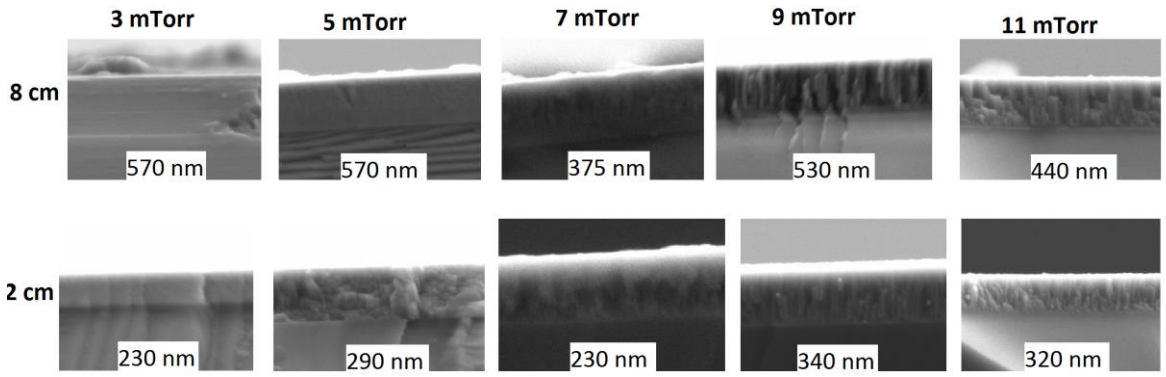

*Figure 175. Cross-sectional micrographs for Titania samples deposited onto Silicon for high pressure*distance couples (75µs-750Hz-500V-15%-30min)*

The first observation made is a decrease of the columnar structure when the pressure is reduced, going towards a bulk structure. Thus, it is possible to obtain films with columnar structures at high pressure and/or distance from the target. However, obtaining such structures is a delicate process and is not achieved in every situation: other parameters influenced the structure such has the voltage and the oxygen content for example. Indeed, any variation of these parameters could drastically change the morphology of the film. As a matter of fact, most of the films deposited at such pressure*distance products shown bulk morphologies. Also, at higher pressure*distance products, the films show (very) poor crystallinity. Therefore, it is decided for the rest of the project to keep the pressure at a low value of 3 mTorr and position the substrate holder close to the target, at about 6.5 cm, facing it.

The arcing ratio of the discharge is also very important in terms of film morphology. For different frequency-pulse width couples, the discharge can either present a lot of arcing or no major arcs at all and this parameters couple thus constitute a good way of reducing the arcing of the discharge (see Figure 180). The pressure is also an effective parameter to manage the arcing of the discharge. In Figure 176 are presented surface micrographs of samples deposited at different (low) pressures. For better comparison, the acquisitions have been done with the same magnification (30K). It needs to be highlighted that the frequency-pulse width couple is high, here and therefore to ease the observation of the phenomenon studied. The micrographs are as shown in Figure 176. Below each micrograph is put an infographic level of arcing during deposition.

Indeed, there was no way of counting arcs during deposition but a manual assessment of the latter is used here. The classification goes as follows:

- 0: No arcing at all during deposition
- 1: A few arcs during deposition (30-60 min)
- 2: Arcing occurs every minute or so
- 3: A major arcs every 20-30 seconds or so
- 4: Constant arcing of the plasma, about an arc every couple of seconds

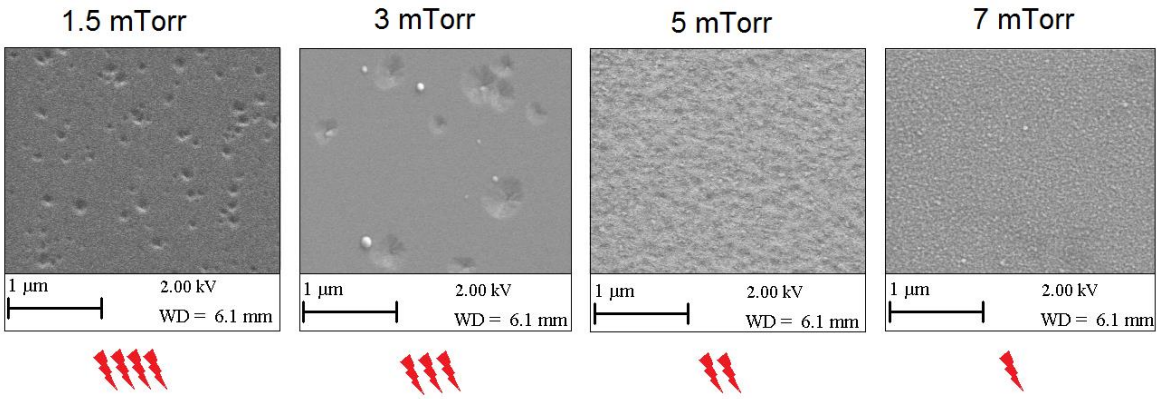

Figure 176. Comparison study of surface micrographs to observe the pressure (arcing) effect on the films morphology (8cm-75µs-750Hz)

These micrographs show a clear trend where the apparition of massive defects at lower pressure can be observed. It is believed to be directly correlated to the arcing ratio more than the pressure itself. Indeed, since it is operated in the intensity regulated mode (to obtain identical films thicknesses) it seems that more arcs occur at low pressures, due to higher voltage (see Chapter III). Therefore, lower pressures do not imply more defects in the film by itself, but a higher voltage does. It is believed that the defects observed at high voltage. These defects are believed to originate from the macromolecules (or droplets) reaching the substrate's surface. A *defective* bulk then grows from there, with no bond –or weak bond- to the bulk film (matrix) and it eventually detaches from the thin film later on; leaving a specific type of hole behind. A schematic view of the process is presented in Figure 177.

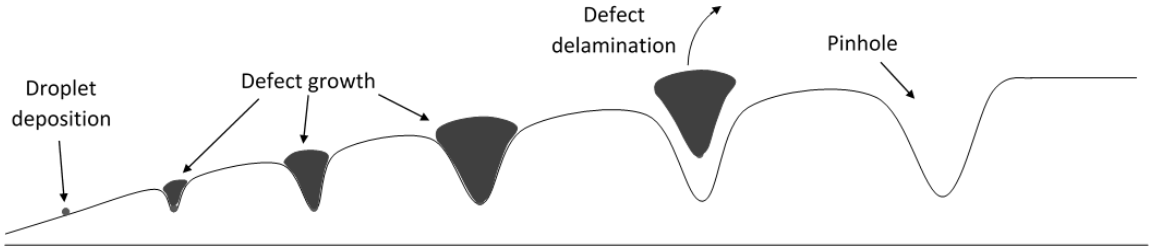

Figure 177. Schematic representation of a pinhole defect creation in a thin film

Another main observation from Figure 176 is the apparition of *small white dots* at higher pressures (i.e. 5 - 7 mTorr). These small bumps at the film's surface are believed to be the top of the columns previously observed for such films (see Figure 175). This type of surface morphology is responsible for an augmentation of the surface area, which is an important parameter for the applications aimed at in our project and should therefore be kept in mind.

V.2.1.2.2. Conclusions

This first SEM study resulted in interesting results: different types of film morphologies can be obtained by modifying the sputtering conditions. For example, the pulse width can modify the film density, the pressure can modify the columnar aspect of the films, arcs could generate defects of various sizes on the film surface, etc…

However, for this first part of the experimentation, the oxygen content sent into the chamber has been managed by using the Speedflo® controller, where the optical signal was kept at a constant 15% of its metallic mode (see II.3.2) for higher deposition rate but this oxygen content was later shown to not be the optimum oxygen flow to deposit anatase films. However, here, again, the objective was to determine conditions with limited arcing and defects in the films.

Raman spectroscopy results (cf. V.2.2) show that the crystallinity of the films was not sufficient in such conditions so the next objective of the experimental work consisted in obtaining more crystalline films. Thus, the point of the second SEM study step is to obtain films showing no defects - and optimally columnar structures - at low pressures. It is believed to be possible by modifying the system of oxygen management during deposition. It should also be kept in mind that arcing should be avoided as much as possible. As supplemental work, a complete study in terms of 1st order parameters (i.e.

frequency, pulse width and voltage) influences could be carried out for lower pressure. The aim would be to confirm that the previous observations are also true when the oxygen flow is increased and the pressure constantly kept low (involving higher voltages in the intensity regulated mode).

V.2.1.3.Deposition parameters influences –2nd step

For this second study, the work is conducted at lower pressure to determine if crystalline anatase can be obtained. However, before looking into the structures of the films, an intermediate step has been carried out, where the focus was on how to obtain a better crystallinity of the film. This study (cf. V.2.2 and V.2.3) has confirmed that the method used so far for the gas regulation during deposition (i.e. 15% of the metallic signal) is not the optimal oxygen flux regulation. Instead, the discharge is now run in the fully poisoned mode. This regime corresponds to a drop in the deposition rate and should be avoided for industrial applications but it is the regime showing the best anatase crystallinities.

Finally, the distance between the target and the substrate has also been reduced to 6,5 cm (or less). This last modification takes place because it is believed that in order to reduce the number of collision and therefore increase the ions energy, the diminution in the pressure may not be sufficient. Indeed, chronologically speaking, the temperature measurements have been carried out after the first step of film characterization and has shown that none of the deposition condition should result in the melting of the polymeric substrates. Therefore, the energy of the ions can be optimized to the higher value possible to ease the adatoms mobility and their capacity to crystalize at the substrate's surface. The addition of all these modifications results in a first amelioration of the films in terms of crystallinity, as aimed (cf. V.2.2 and V.2.3) but it is also of great interest to investigate how the structure of the films evolves. In this section, the results in terms of morphology modification are presented.

First, the influence of the frequency-pulse width couple on the film structure is studied. The main objective is to see if there is any trend that could help knowing which region of the envelope would correspond to which structure. Cross-sectional acquisitions have been realised by SEM analysis for numerous samples, deposited at various frequencies and pulse widths. The results are presented in Figure 178. The upper-right

section of the graph (high frequency and high pulse width) is not filled and this is due to a duty-cycle too high and thus a limitation in terms of plasma stability, due to the power supply and system used in this work.

What can be seen on this figure is that most of the films present columnar structures. This result is in slight contradiction with the first study that had been carried out, where there was a disappearance of the columnar structure when the pressure*distance product was reduced (see Figure 175). Therefore, it is believed that the reason behind this structural modification is mainly due to the modification of the gas flow during deposition, more than being due to the reduction of the pressure*distance factor. It is believed to be a consequence of the change in the sputtering mode from within the transition window to the poisoned mode. The hypothesis, for now, is that the modifications induced by the slight increase in reactive gas flux (cf. I.1.5.4) in terms of the species in presence in the target vicinity and their energies are crucial for the determination of the growing morphologies and phases. More precisely, it is believed that only a fully covered target can result in depositing a stoichiometric film in such a rig and that a stoichiometric deposition leads to an easier crystallisation of the deposited adatoms, as there is no excess of any of the species, which could lead in defect centres in the crystallographic structure. By operating in the poisoned mode, the effects of the pressure*distance product diminution observed earlier are counter-balanced and columnar films can be obtained at 3mTorr and 6cm away from the target's surface. This shows that the oxidation state of the system is the most essential parameter to manage if crystalline films are aimed to be deposited.

When having a closer look to the micrographs, additional explanations can be given on the growth process for such films. Indeed, on most micrographs where a columnar structure can be observed, one can also observe an *intermediate* bulk layer between the substrate and the columns. This transitional bulk structure is building up but the growing process continues with columns. This transition can have various explanations. One of the hypothesis developed to explain this type of structures is that the surface energy of the substrate and that of the film are different and result in a change of the growing structure. The deposition of nanometric defects onto the bulk structure could also imply a columnar growth from the latter. However, it is believed that the first hypothesis is the most likely to be true.

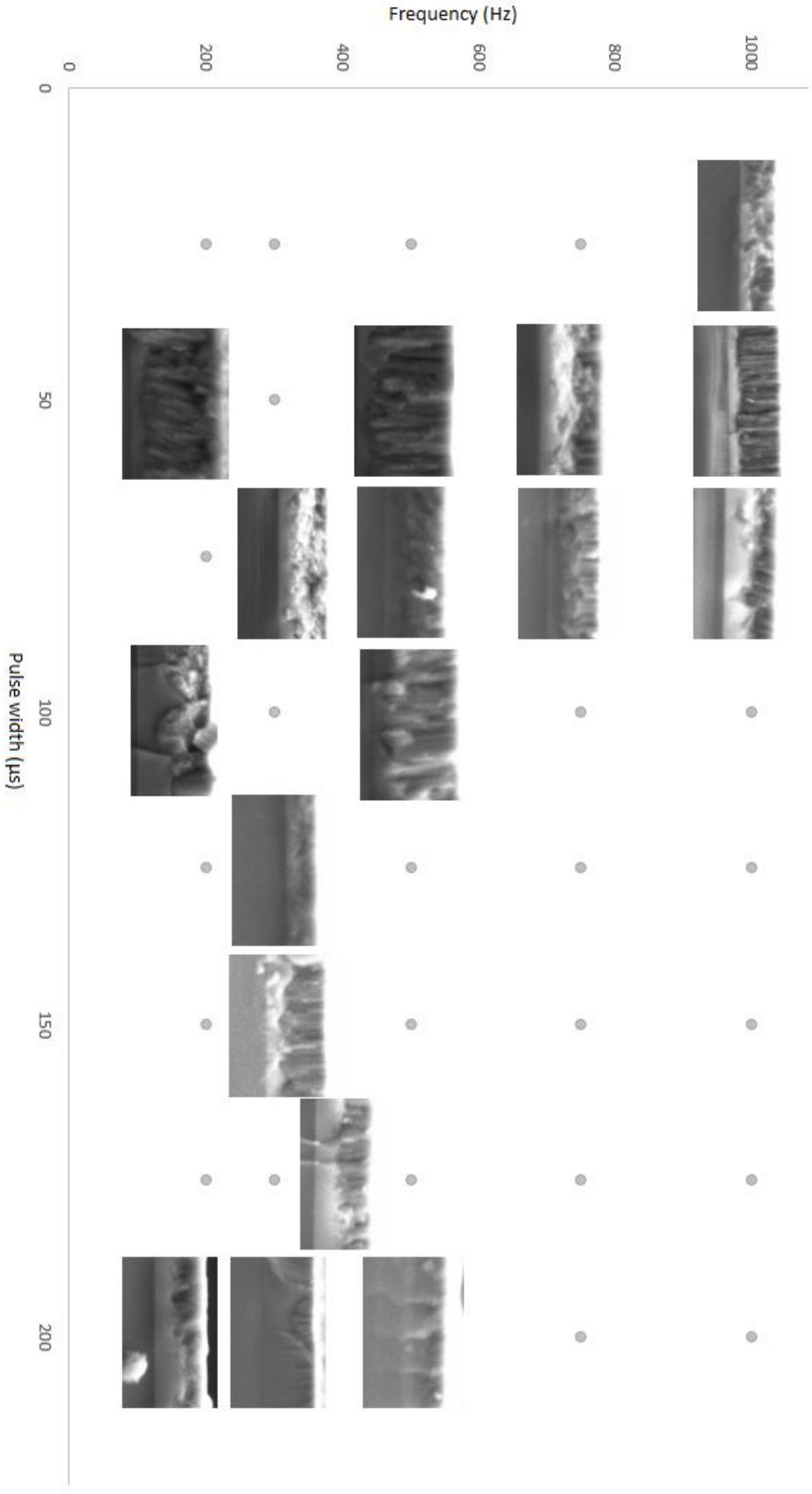

Figure 178. SEM cross-sectional views of the thin films, represented in the frequency-pulse width space

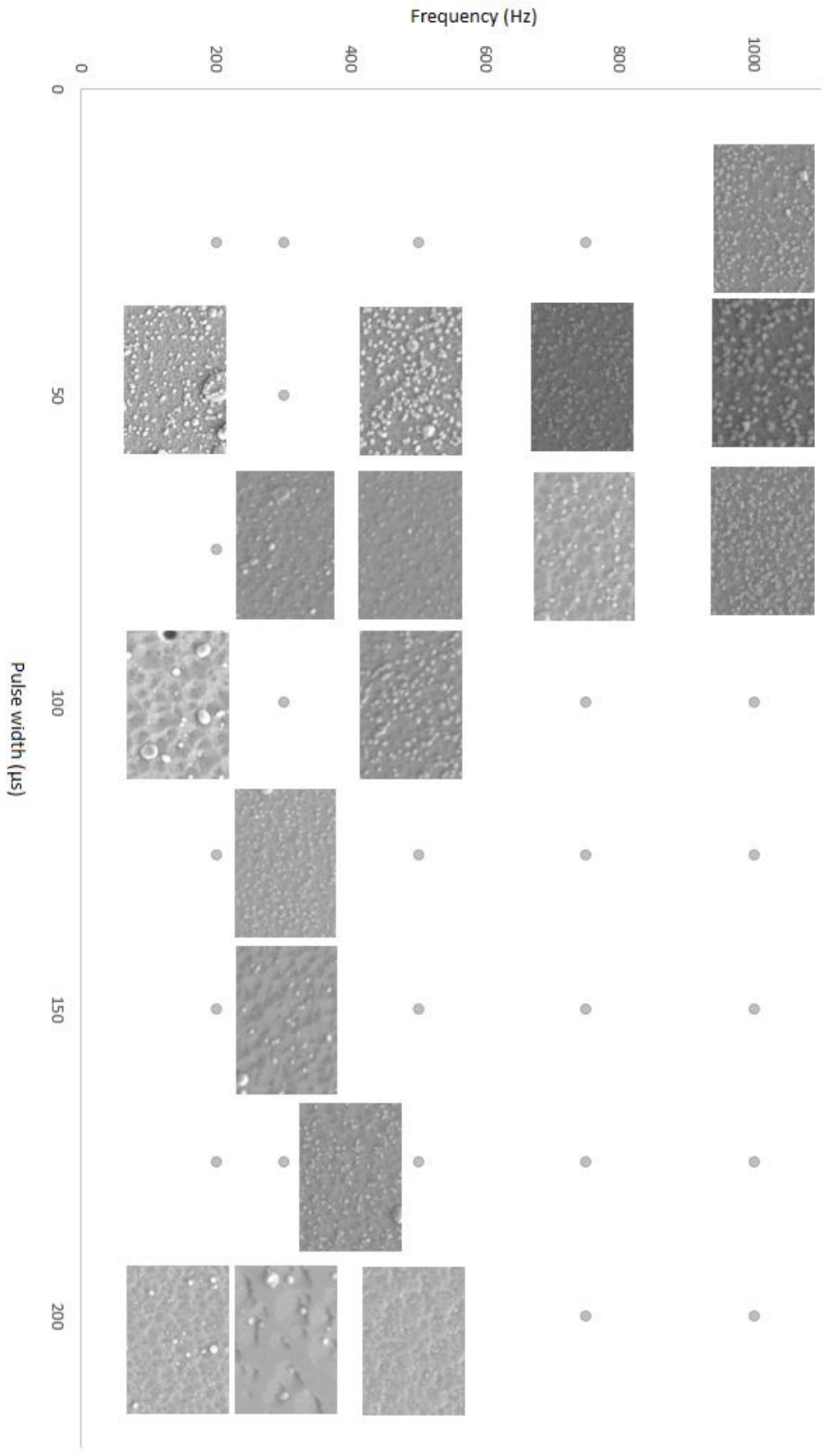

Figure 179. SEM surface views of the thin films, represented in the frequency-pulse width space

In addition to the cross-sections, the films surfaces have also been studied for the same process envelope. The results are shown in Figure 179. These micrographs are essentially here to corroborate the results previously obtained, where *white dots* and pinholes were seen (cf. Figure 176). One can observe the same particularities here and when these micrographs are compared with the cross-sections, it appears that the more columnar the film is, the more dots are observed. It is then safe to conclude that they are indeed the top of the columns in the film. In a general way, there are more dots for shorter pulses and higher frequencies and more pinholes for long pulses and low frequencies. Again, if one compares these acquisitions to the arcing ratio during deposition, the direct correlation is evident. The arcing ratios are represented in Figure 180 in an infographic fashion as there was no precise way to measure the arcing of the system otherwise than by visual assessment. Another correlation seems to emerge from Figure 179 and Figure 180: the more pinholes there are, the less *white dots* are seen at the surface of the film. It means that arcing is most likely to be preventing the columnar growth because of too important droplets reaching the film and disrupting the columnar growth.

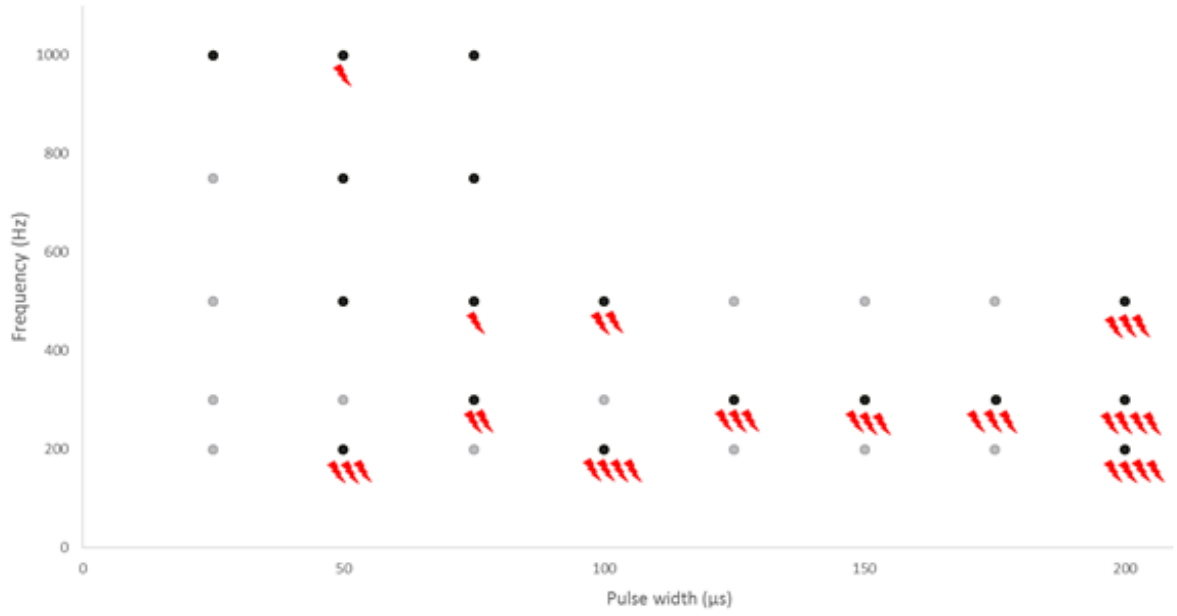

Figure 180. Arcing infographic representation in the frequency-pulse width space

The films deposited for crystallographic enhancement should be deposited with a short pulse and a high frequency as the columnar growth is preferred to the bulk morphology: a columnar structure enhances the surface area of the sample and thus its surface reactivity for the applications aimed at (i.e. photocatalytic activity) [149] [150].

Moreover, defects in the film structure lead to a reduction of the film's capacity to transport charge carriers. This transportation is essential for enhanced photocatalytic activity.

A study to see what happens to the structure when the oxygen flux is changed beyond the transition mode has been carried out and showed no further effect on the structure of the film: all films deposited in the poisoned mode present columns. Also, EDX analysis of these samples deposited in the *over-stoichiometric* regime of the discharge. However, the EDX analysis is not fully reliable because of the difficulty for the machine to provide good quantifications of the films stoichiometries if the films are too thin. Typically, the films need to be at least 1 µm thick for the substrate to be *invisible* and not alter the quantification (see II.4.1.2). However, such a thickness would imply 2 hours long deposition, or even more. Therefore, it has only been done for some films, and the results showed a slight excess of oxygen in each case, but this excess does not seem to majorly change beyond the transition window.

V.2.2. Raman spectra

*V.2.2.1. High pressure*distance products*

The first set of thin films, deposited at high pressure*distance products, have been tested for every type of substrate: Si, glass, PET and PEC (when not melted during deposition) but the Raman spectra did not show any crystallinity of the films. However, as it can be seen in Figure 181, a nano-crystallinity of the films is suspected because of the bumps observed for wavelength corresponding to Titania phases. Figure 181 does not attend to identify which films show a better (nano-) crystallinity. Its only purpose is to show that every sample show very similar spectra, with only a few exceptions, showing possible peaks. Therefore, the curves are not labelled, as it is not necessary. However, even if *bumps* appear, the (nano-) crystalline phases of the latter are unclear as some peaks do not correspond to the values reported in the literature as being those of anatase and rutile. For Silicon wafers substrates, the situation is different, the films show more evident peaks, for both rutile and anatase. This better crystallisation is a consequence of the nature of the substrate: the silicon wafers are single orientated crystals of Si, and such a surface is favouriting the crystalline growth of films, due to the high level of order in

the structure. Again, the objective here is to only show that in such conditions, a certain crystallinity can be found, but no specific trend in the deposition parameter can be identified.

It should be reminded that these sets of data have been deposited in the very early stages of the project, where, no optimization of any kind had been carried out and the objective is to determine if crystals can be deposited at high pressure*distance products, where films seem to be more columnar. The high number of curves in the two previous figures is due to the high range of parameters modified (i.e. frequency, pulse width, pressure, distance, time, etc…)

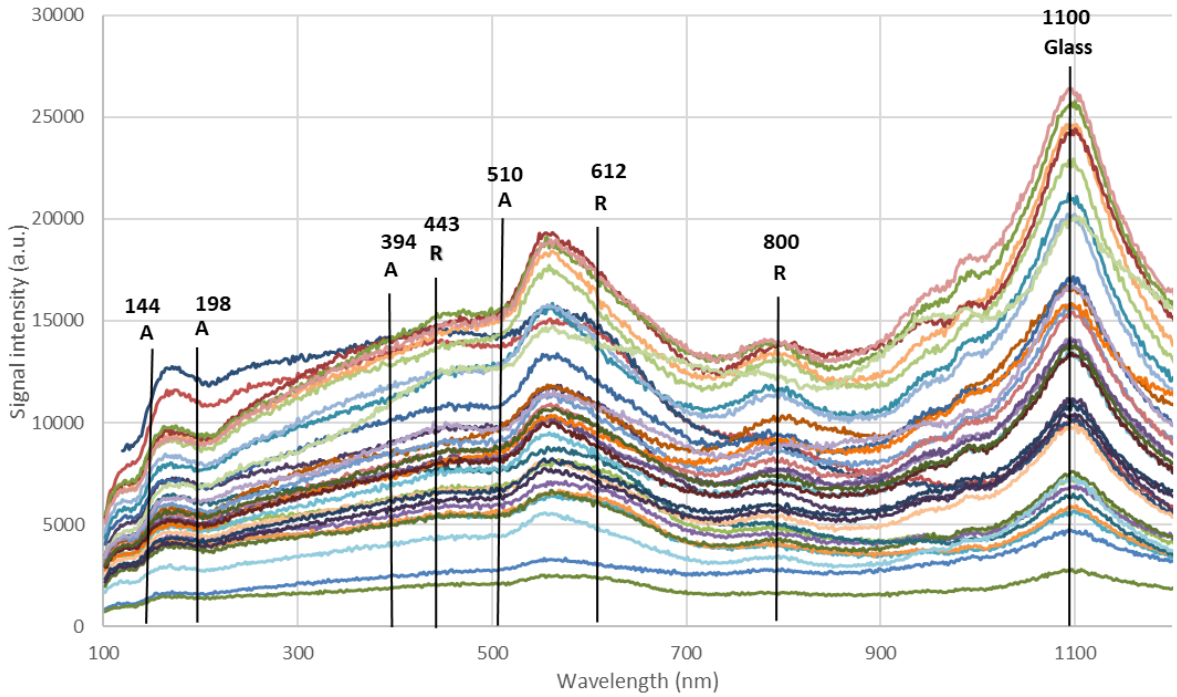

*Figure 181. Raman spectra for films deposited onto glass at high pressure*distance products (<I> = 2.0 A / Frequency : 200-1000 Hz / pulse width : 50-200 µs / Pressure : 7-10 mTorr / target to substrate distance : 17 cm)*

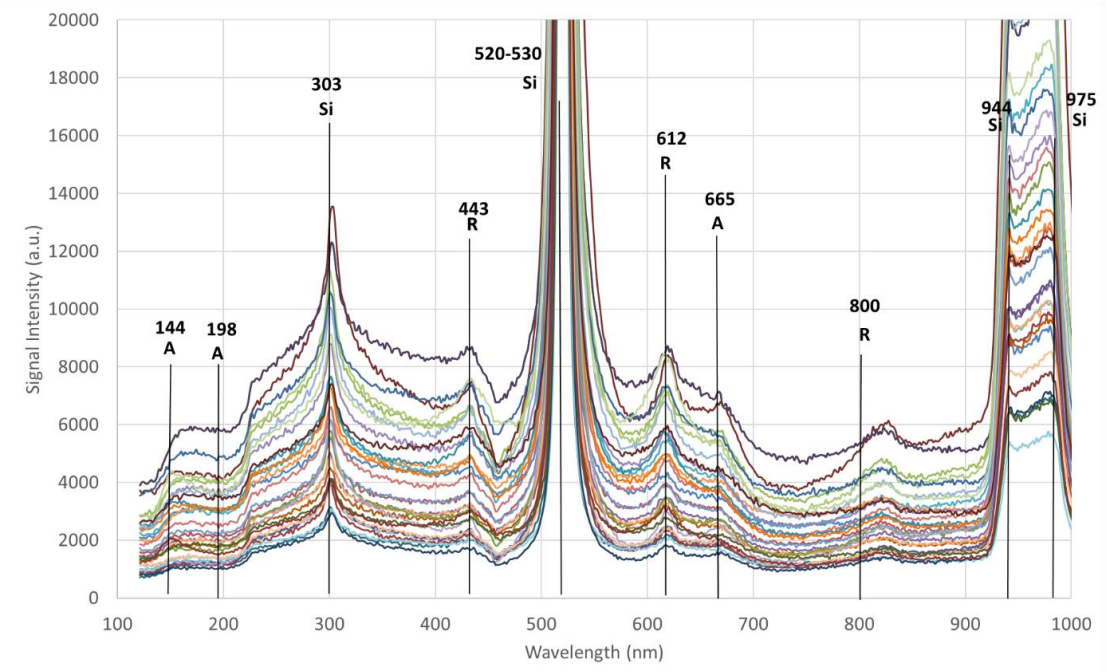

*Figure 182. Raman spectra for films deposited onto silicon at high pressure*distance products (<I> = 2.0 A / Frequency : 200-1000 Hz / pulse width : 50-200 µs / Pressure : 7-10 mTorr / target to substrate distance : 17 cm)*

V.2.2.2.Optimization of the crystallinity

As previously said, the main objective of the second set of films deposited is to deposit crystalline anatase as it is well known to improve the photocatalytic activity of the film. For this reason, films have been analysed by Raman spectroscopy (as well as XRD) to conclude on any way to improve the films crystallinity. Each 1st order parameter has been varied independently, while keeping all other parameters constant, to identify their specific consequences on the film.

Films deposited onto Si substrates for a various range of frequency – pulse width couples have been characterized to identify if the latter could have an influence on the films deposited. Only films deposited onto Silicon have been analysed as they seemed to show better crystallinities. Films have been deposited in the intensity regulated mode, as it eases the poisoning process of the target and maximizes the deposition rate. Figure 183 shows the results in an infographic way, as it remains the clearest way to present such data. It also makes the conclusion much easier to draw: the arcing degrades the crystallinity of the films. Again, this is a general trend but no clear linear trend could be

identified. It does not mean that the trend does not exist: shorter pulses along with higher frequencies lead to an easier growth of crystals, and especially anatase, due to the absence of arcing during deposition. The absence of arcing is a combination of 3 different things:

- A lower voltage, meaning less energy given to the ions so they don't reach the substrate with too much kinetic energy
- A lower pulse width, meaning no thermalization, nor rarefaction, where the plasma can become unstable
- A higher frequency, meaning a short off-time and therefore a consistency of charged species in the chamber.

At the end, the most important observation that came out of this set of thin films characterizations is that arcing deteriorates the crystalline growth in a very clear fashion. For this reason, it has been determined that pulses 75 µs long or shorter and frequencies of 400Hz or higher are suitable conditions where crystalline growth is possible. A 50µs – 1000Hz couple has been selected as a first choice to study the effect of the other deposition parameters: pressure and reactive gas content.

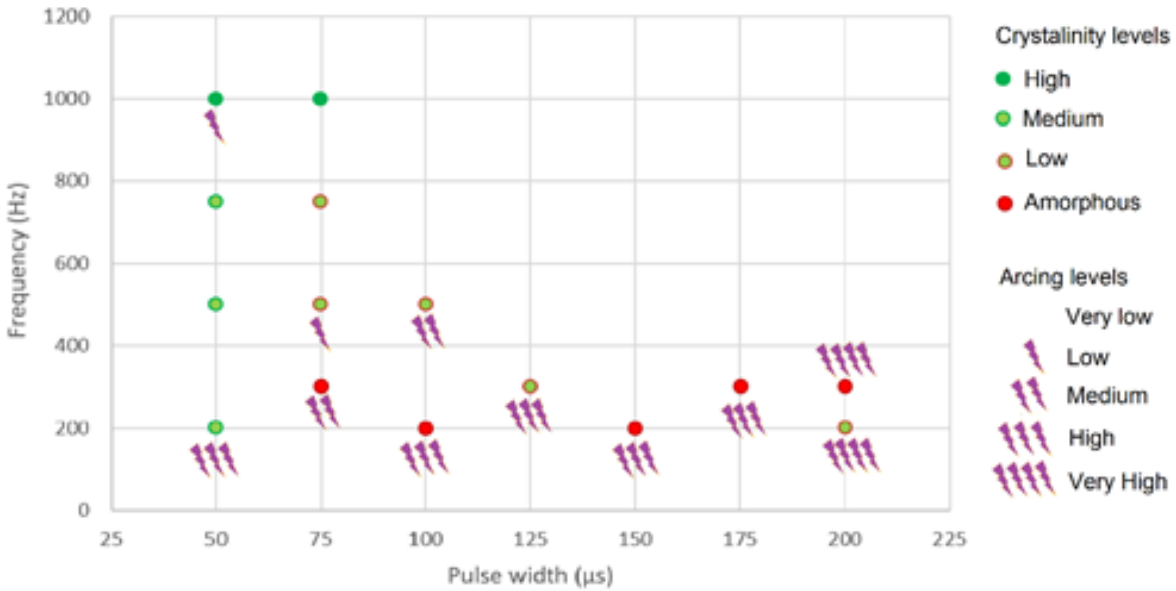

Figure 183. Comparative mapping of arcing and crystallinity of the films deposited onto Silicon

While the pressure did not show some clear evidence of film modification in term of crystallinity, the oxygen content however demonstrated to be of a crucial importance as shown in Figure 184 for example. Indeed, replacing the Speedflo® controlling system

relying on the optical emission of the plasma by the more classic constant sccm option (still using the Speedflo® unit) showed a clear improvement of the films crystallinity as it allows to reach *over-stoichiometric* states of the discharge and this type of discharge seems to be favourable to deposit anatase. Results in Figure 184 show that for a 2 sccm difference in the oxygen flow (i.e. ~5% of partial pressure), one can drastically improve the crystallinity of the film.

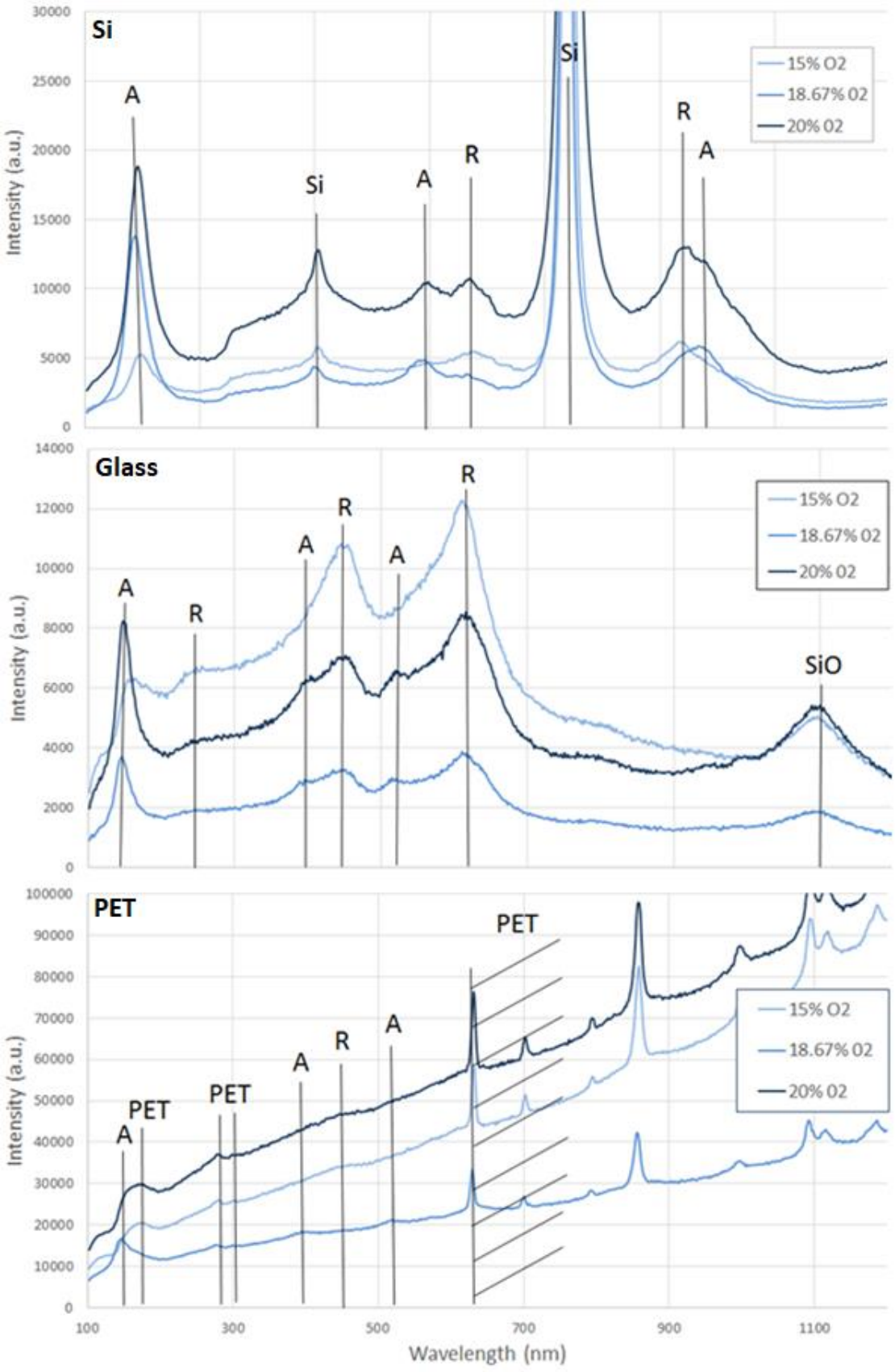

Figure 184. Raman spectra showing the oxygen content influence on the crystallinity of the films deposited onto various substrates (3 mTorr – 700 Hz – 50 µs – 2.0 A)

When one compares this 2 sccm difference to the range of 5-6 sccm used by the Speedflo® controller to keep the optical signal to a constant value over time, it becomes clear that the use of the Speedflo® optical controlling system can have a negative effect on the crystallinity of the film. It does not mean that it necessarily does, only that it could. More importantly, the oxygen flux optimization phase showed that the films are more likely to grow anatase if deposited in the poisoned mode of the discharge. This means the Speedflo® optical controlling system cannot be used and the signal do need to be run in a constant flux mode.

Indeed, the Speedflo® controller allows us to keep a very precise stoichiometry of the plasma during the deposition of films, even when using HiPIMS process that requires a long deposition time but it can only operate correctly in between the metallic and the fully-poisoned mode. In the case of over-stoichiometric plasmas, the control of the signal level is impossible to achieve in the precision range that we require to deposit anatase crystals. The Speedflo® optical controlling system is not adequate for the project presented here and using it to prevent from having too low deposition rates might have been the reason behind the absence of crystallinity since the beginning of the study. It can be concluded that it is impossible here to deposit anatase while keeping a relatively high deposition rate.

The results obtained after this first optimization are very promising as they show that crystalline anatase can be deposited onto all the substrates available at this stage of the project: Si, glass, PC and PET. In fact, Figure 185 shows the example of a set of films deposited together and where all substrates have anatase on. However, conditions in which anatase crystals would be deposited onto a certain type of substrate would not necessarily deposit anatase onto other substrates. The example given in Figure 185 is an exception, this situation shows that it is indeed possible to have a discharge that would deposit anatase onto any substrate but these results have been impossible to duplication; at least one substrate would show an absence of anatase.

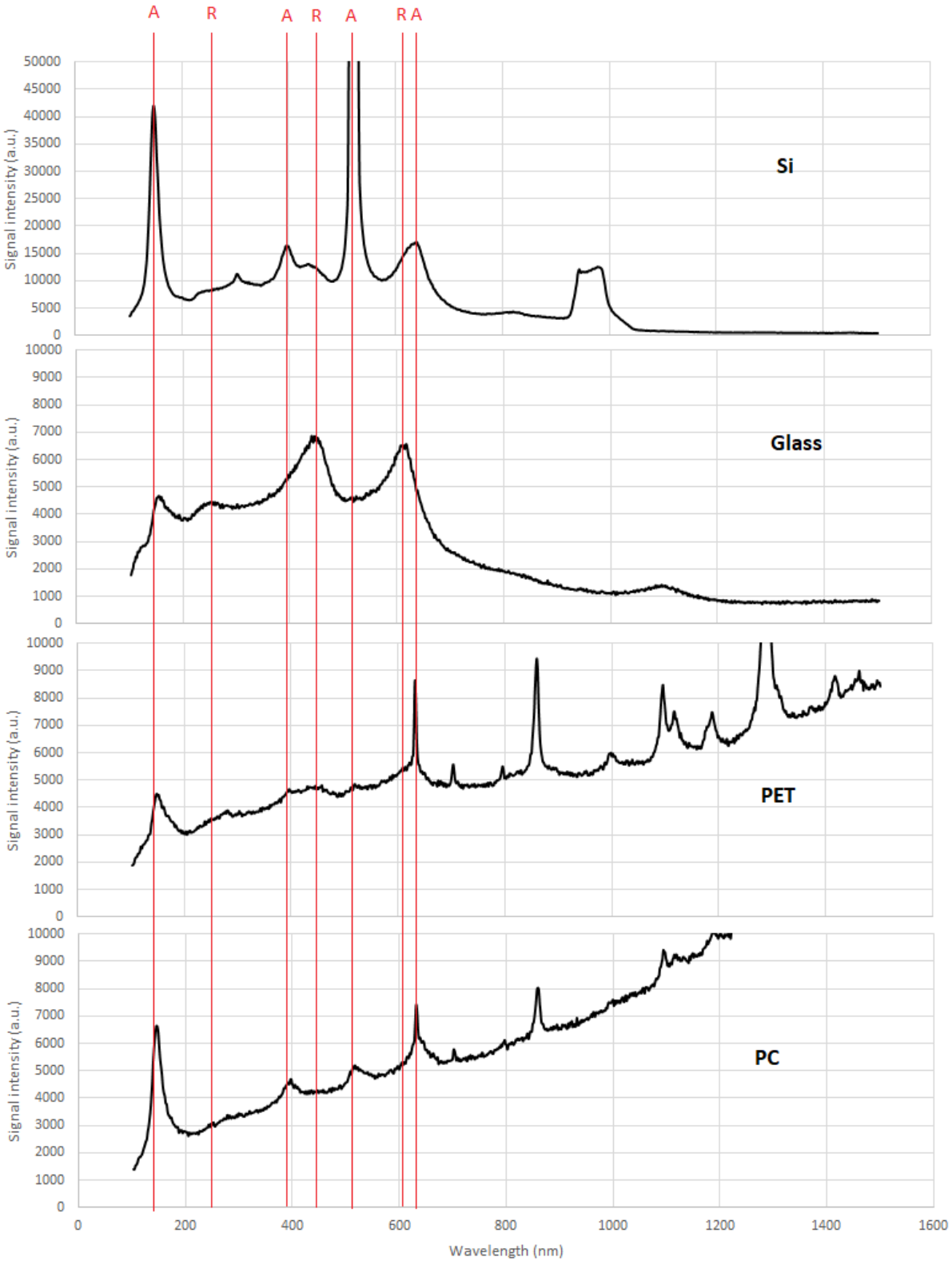

Figure 185. Raman spectra of samples deposited under the same conditions and showing Anatase on each substrate

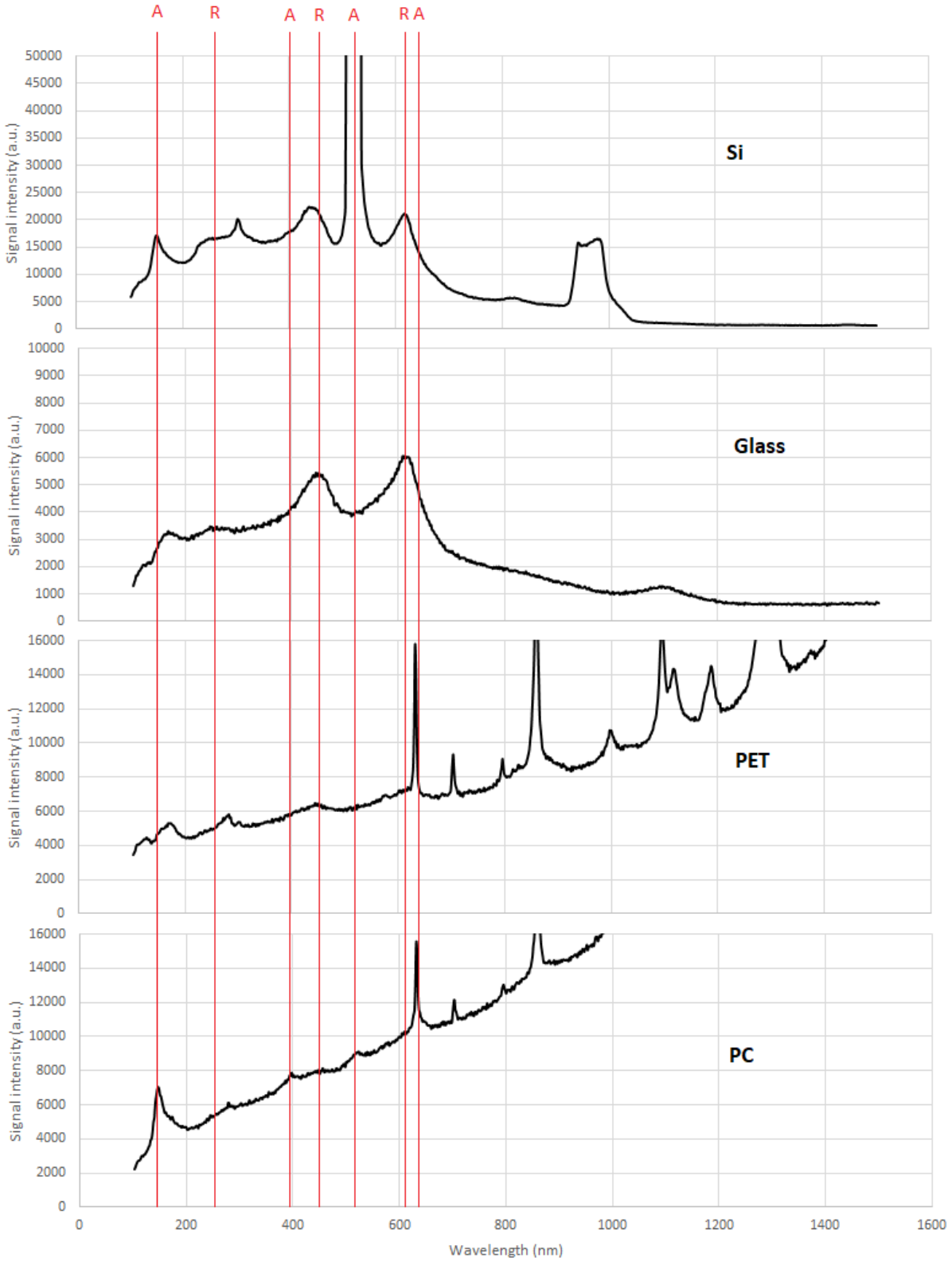

Figure 186. Raman spectra of samples deposited under the same conditions and showing Anatase only on Si and PC

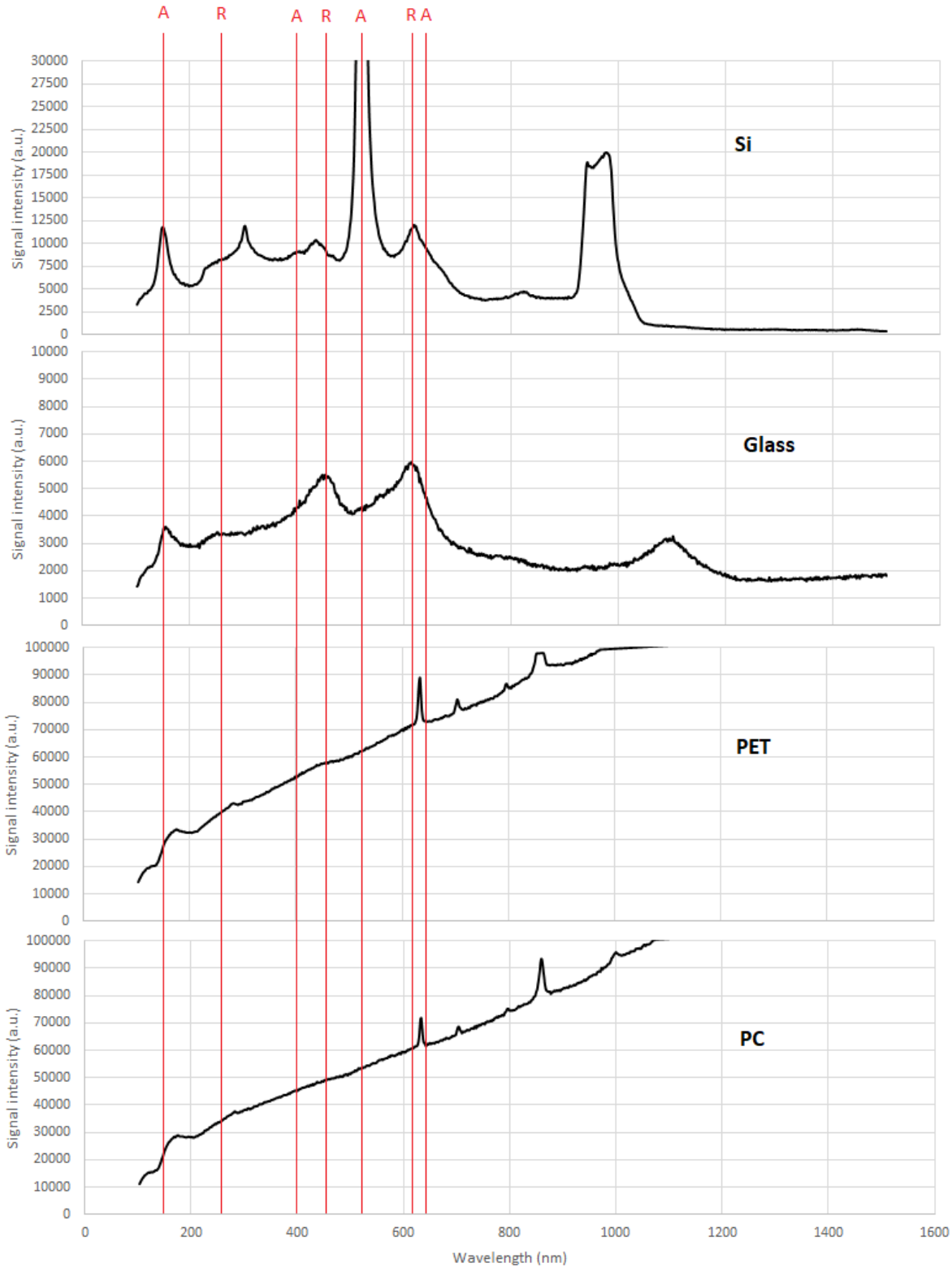

Figure 187. Raman spectra of samples deposited under the same conditions and showing Anatase only on Si and glass

For example, Figure 186 shows the case where one could deposit anatase (and rutile) on Silicon and PC, but the same conditions would not deposit any anatase crystal onto either glass or PET. Figure 187 shows the same type of situation but this time Anatase is seen on Silicon and glass, but not on either PET or PC. Again, the reasons behind this behaviour are believed to be the inconsistency of the discharge in such a rig and the fact that the polymeric samples are unpolished samples. Indeed, the films deposited onto Silicon are the most crystalline, in a general prospect, because is it a single-orientated crystal and it makes it the most likely to grow anatase crystals when the PET and PC samples are unpolished plastic samples, cleaned manually, as explained in II.2.3.

V.2.2.3. Duplication work

The duplication work of this type of film is very difficult indeed. For the conditions in which films of good crystallinity have been deposited, the deposition has been reiterated several times, with absolutely no change of the deposition conditions. The duplication films rarely showed the same levels of crystallinity, or even the same phases in presence. This is an important fact, as it implies that the process is quite unstable. This instability probably originates from the apparatus used here. Indeed, the chamber being opened in between each deposition, the state of the chamber's walls (including the substrate holder and the substrates) can vary. This is assumed to be the most important factor at the origin of the difficulty to obtain a repetitive process for which all films are identical.

Also, due to the large volume of the chamber, the plasma seems to be less stable, and influenced by the rest of the chamber (i.e. non-sputtering species). The configuration of the chamber given in II.2.1.1 shows that the plasma is not confined. This means that the sputtered species can travel long distances in the chamber, without necessarily meeting the substrate holder. This phenomenon happens in any type of rig but here, due to the amount of non-sputtering species in the chamber and the large volume of the latter, it is believed to make the discharge less stable, and less consistent. In small lab rigs, the plasma generally takes the totality of the space available in the chamber, reacting with all walls; it is filling up the chamber. For larger rigs, the bulk plasma is only a portion of the entire available volume, leading to instabilities.

In the latest stage of the project, polished polymeric substrates have been ordered. The films would be in either a film or a sheet form, with thicknesses of respectively ~0.2 mm and ~2.0 mm. the aim is to obtain better reproducibility of the crystalline films on polymers. Four different polymerics have been ordered: PET, PC, PMMA and UPVC. However, surprisingly, the results are disappointing: none of the coated polymer showed any type of crystallinity. This behaviour needs more investigation as it shows that crystalline titanium dioxide can be deposited on one type of PET for example, but not on another one. This time, it is not believed to be a rig dependency, but more a samples production dependency.

V.2.3. XRD patterns

The result showed in Figure 188 proves that the films deposited at lower pressure*distance products can show both Anatase (JCPDS: 21-1272) and Rutile (JCPDS: 21-1276) phases with good peak definition on Si substrate; implying good level of crystallinity. However, on glass substrate, only Rutile could be observed, which confirms the importance of the substrate nature on the growing phases of the film. The films deposited on the PC and PET sheets could not be analysed as they are not flat enough. As previously stated, this higher crystallinity for films deposited onto Si is associated to the similarity in lattice parameters between Si and TiO2. It is not necessary to present more data than what is presented here as previously explained: the Raman study is sufficient for a project like this one as it is a fast way to determine the phases in presence. Figure 189 shows that, in some cases, both anatase and rutile phases could be found on silicon and glass for the same deposition conditions. However, in these conditions, the overall crystallinity of the film is much lower. It should be highlighted that no conditions have been found where only anatase is deposited on the substrates, it is always either mixture of anatase and rutile or only rutile.

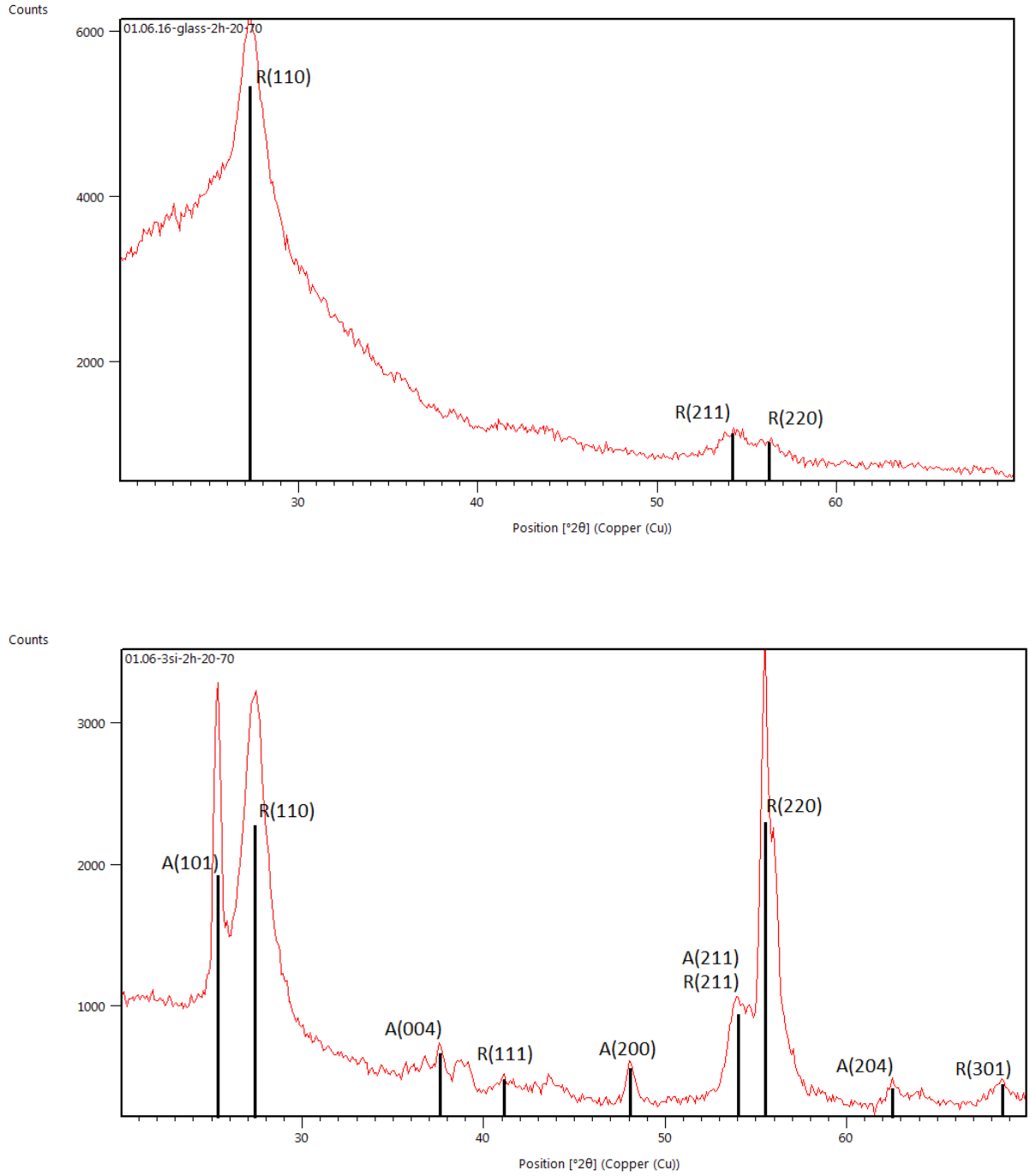

Figure 188. XRD patterns for a crystalline film deposited onto glass (top) and Si wafer (bottom) obtained during the second set of depositions

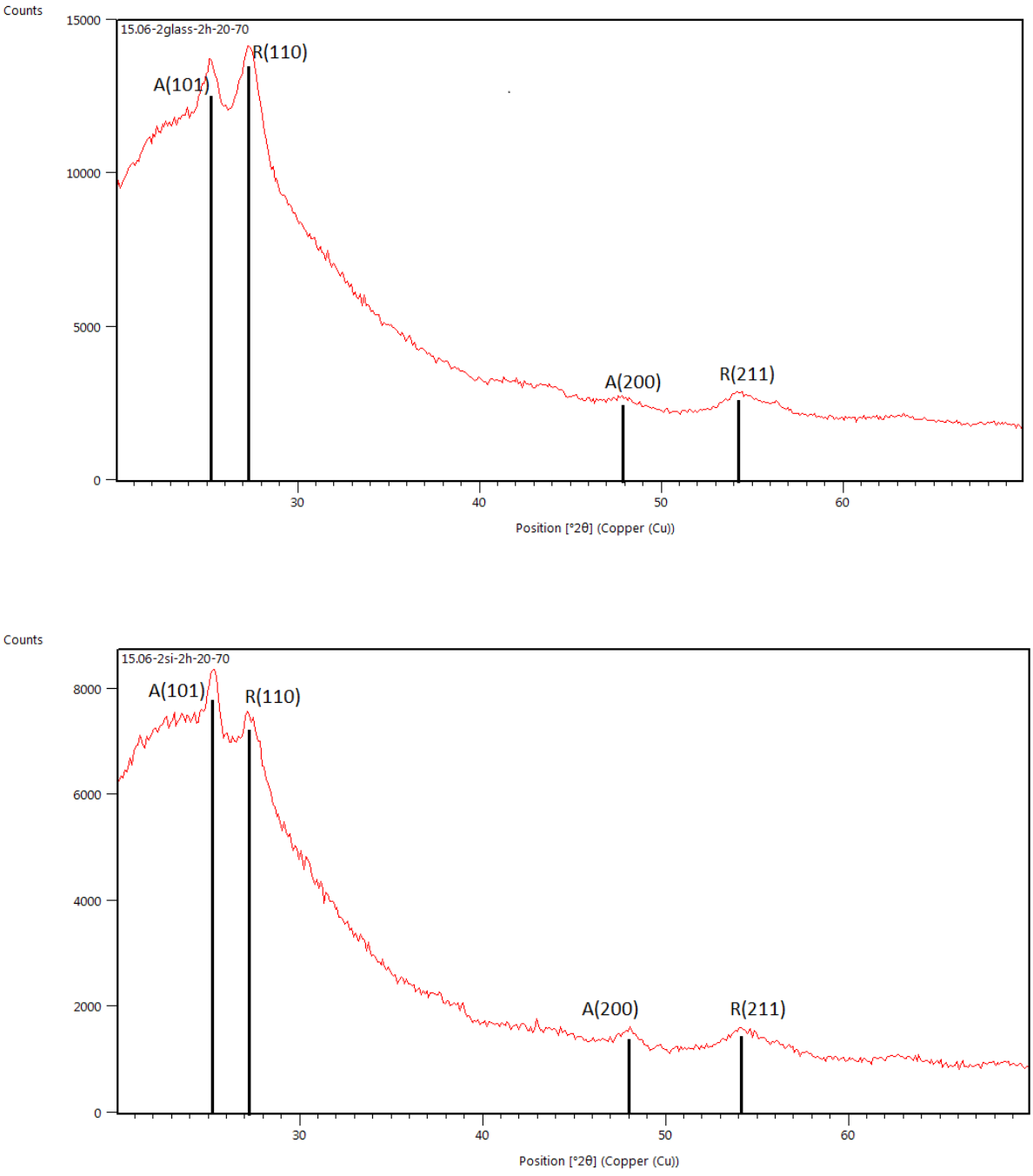

Figure 189. XRD patterns obtained for TiO2 films deposited onto both glass (top) and Si wafers (bottom) and showing Anatase and Rutile phases in both cases

A final XRD pattern is showed in Figure 190. This spectrum has been acquired on a film showing one of the strongest anatase peak on the Raman analysis. This crystalline film has been obtained after an optimization phase only based on Raman spectra, where no XRD patterns have been acquired.

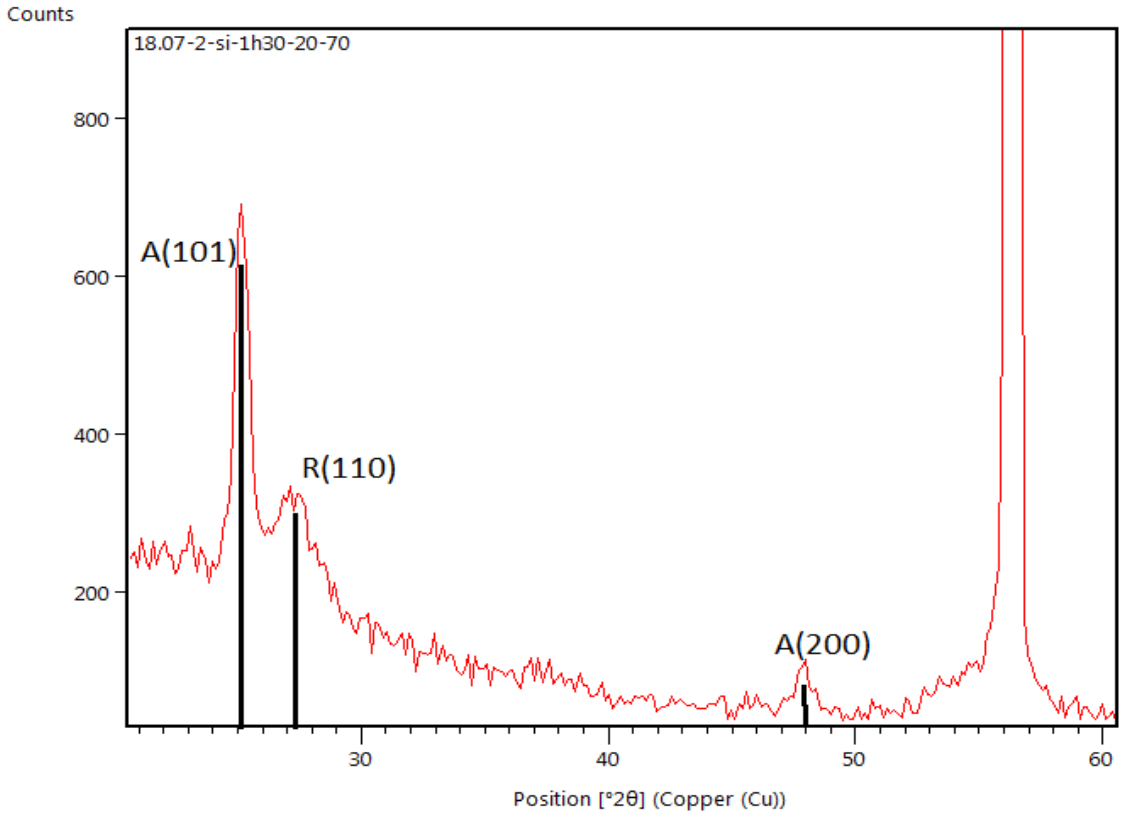

Figure 190. XRD spectrum for a TiO2 film deposited onto Si after optimization of the deposition conditions

V.2.4.Photocatalytic activity

The films showing the best crystallinity have also been tested for their photocatalytic activity as it is the objective of this project. There is no use in depositing crystals if the latter are not photo-active. The data presented in Figure 191 are the results of the MB tests for 4 different samples depositing onto glass and all showing an anatase peak. The difference between these samples is the anatase/rutile ratio and the quality of crystallinity. The corresponding spectra are joined in Figure 192. The deposition conditions of each film are not indicated as it is not relevant here. Indeed, the samples

presented here have vary various deposition conditions. Thus, they do not show any optimization of the activity by a given parameter. Again, here, it is not the aim. The aim is to confirm that the photo-catalytic activity is directly linked to the part of anatase in the film and the combination of both figures do lead to this conclusion. The samples have been organised from #A to #D, according to their photo-catalytic activity but when looking into the Raman spectra, it appears that sample #A shows the weakest anatase-to-rutile ratio and #D shows the highest ratio. It is therefore evident that the part of anatase in the deposited film increases the photo-activity of the film.

The data presented here need to be analysed with caution. It is only here to show a general trend observed along the large quantity of samples deposited. In fact, some samples showing very weak anatase peaks but better rutile peaks have proven to also be capable to have high photocatalytic activity. The opposite has also been seen sometimes: films with anatase phases could show very low, or even inexistent photocatalytic activity. However, these cases are exceptional and are assimilated to problems during the MB test. They should therefore not be taking into consideration. Also, although only four samples are presented here, much more samples have been tested but no conclusion can be withdrawn from them.

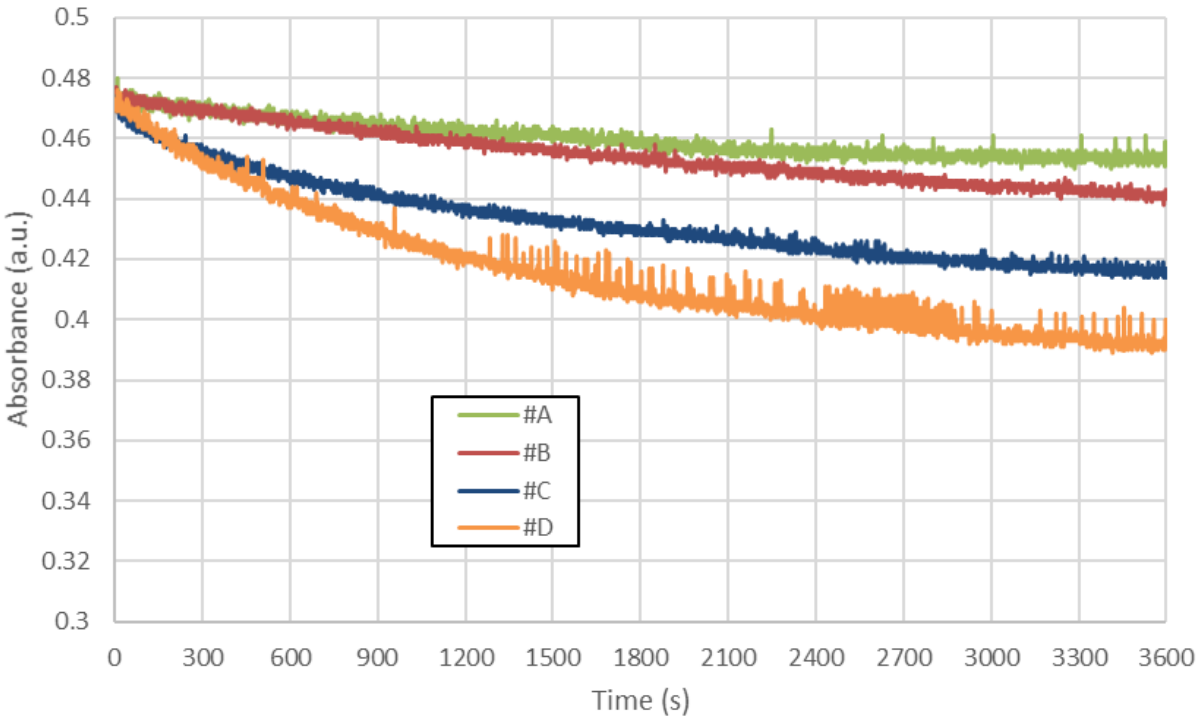

Figure 191. Absorbance profiles for photo-active films

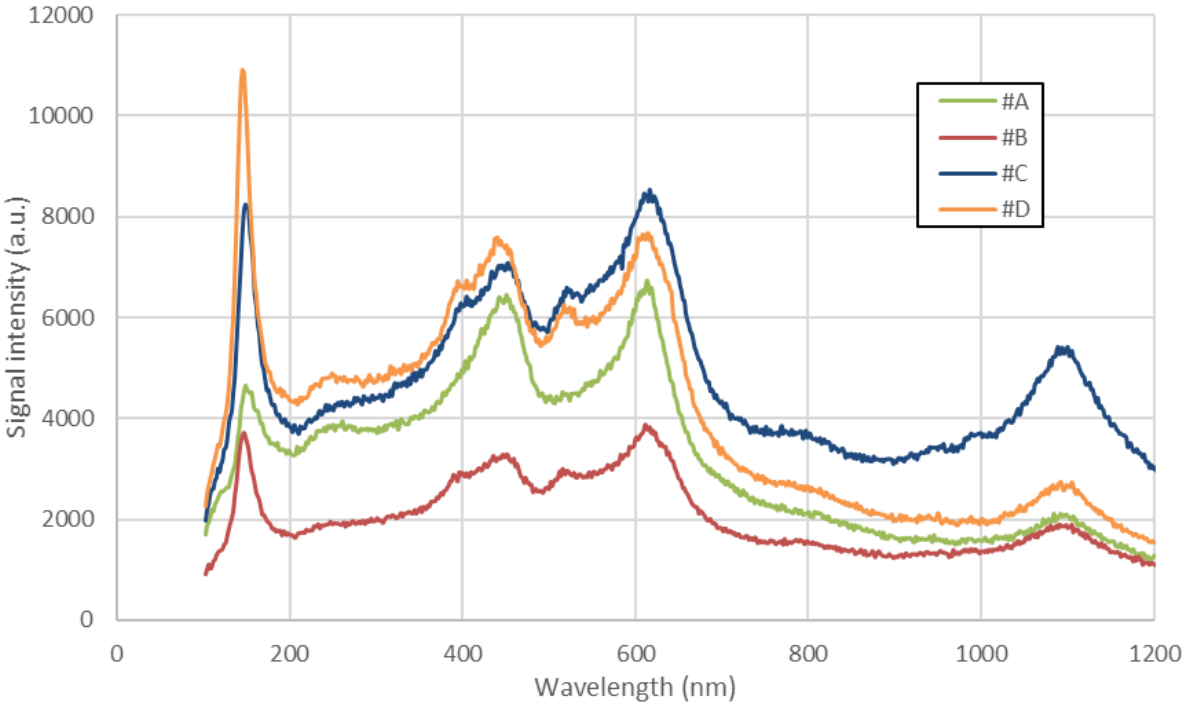

Figure 192. The Raman spectra of the samples tested

V.2.5. Contact angles

A first observation made and worth mentioning is the time-evolution of the contact angle after being taken out of the deposition chamber. In fact, every film deposited shows (very) low contact angle right after deposition but this contact angle increases with time until stabilization after about 24 hours. This evolution reflects the fact that a thin film like TiO_2 needs to wait for at least a day before being characterized; This delay seems to be sufficient for these sample to relax their internal stress and react fully with the atmosphere. No further conclusion is looked after here, the data is uniquely here to show that every sample is stored at least 24 hours before being tested in any way.

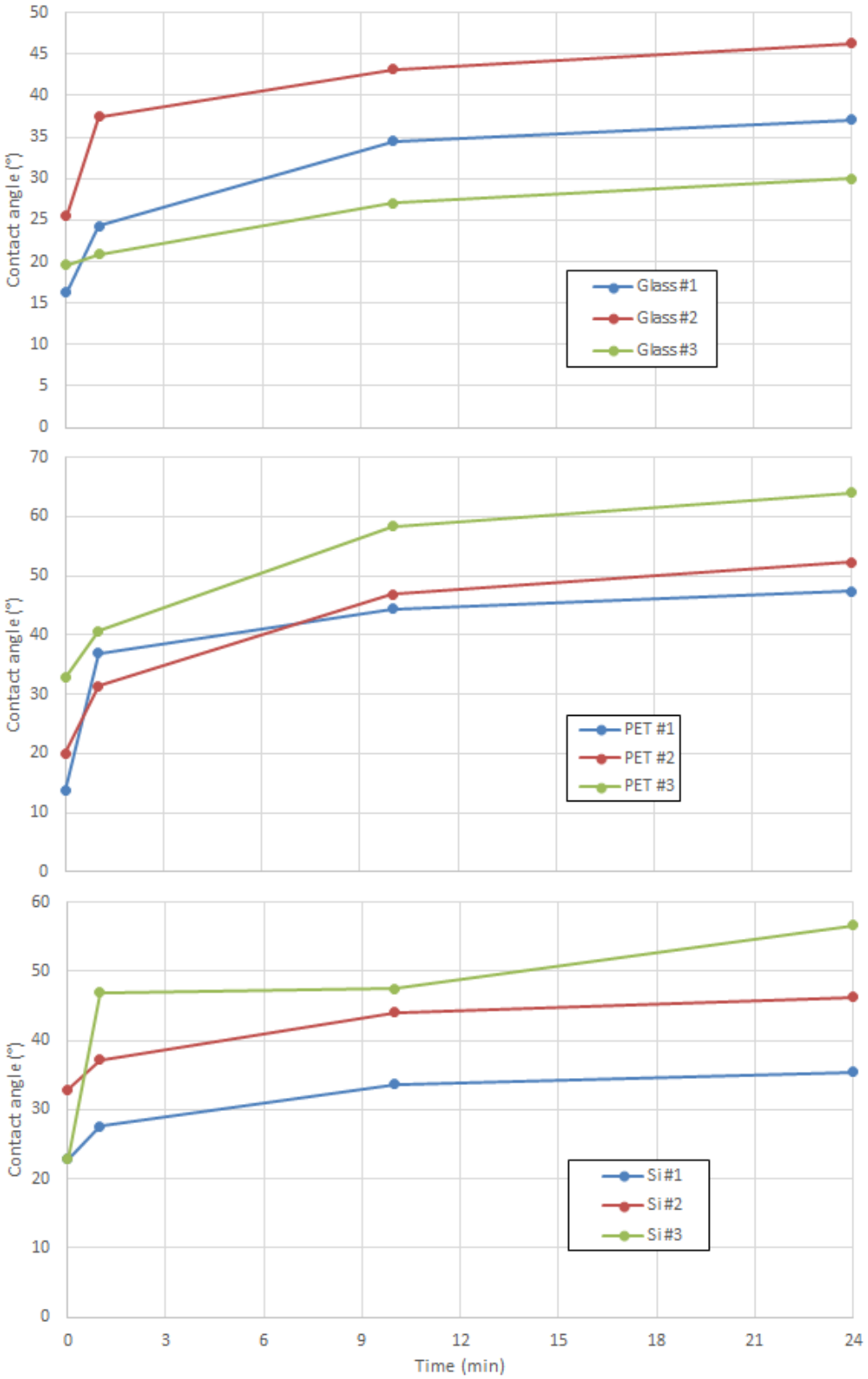

Figure 193. Evolution of the contact angle after deposition for different coatings, deposited on three different substrates

The contact angles have been measured for some films to assess whether the films show a photo-induced hydrophilicity or not. The objective here is to show the type of contact angles obtained with the films deposited previously and show how this contact angle can evolve along time and under illumination. First, the crystalline films do show a reduction of their contact angle when illuminated under UV light. Figure 194 shows the results obtained for films showing good crystallinity deposited onto glass, PET and Si.

The contact angles are measured once under ambient light in the lab before the film to be illuminated for 30 minutes under UV light and re-tested straight away. For glass and PET, the contact angle drops from about 55° to about 20° after illumination. On Si, the film is super-hydrophobic under ambient light but the contact angle also drops after illumination, resulting in a hydrophilic film. Evolutions are shown for only three coatings but the diminution of the contact angle is always observed for crystalline films. Films showing the highest reduction of the contact angle are not necessarily the best photo-active films but, according to literature, it is not necessarily a direct relationship.

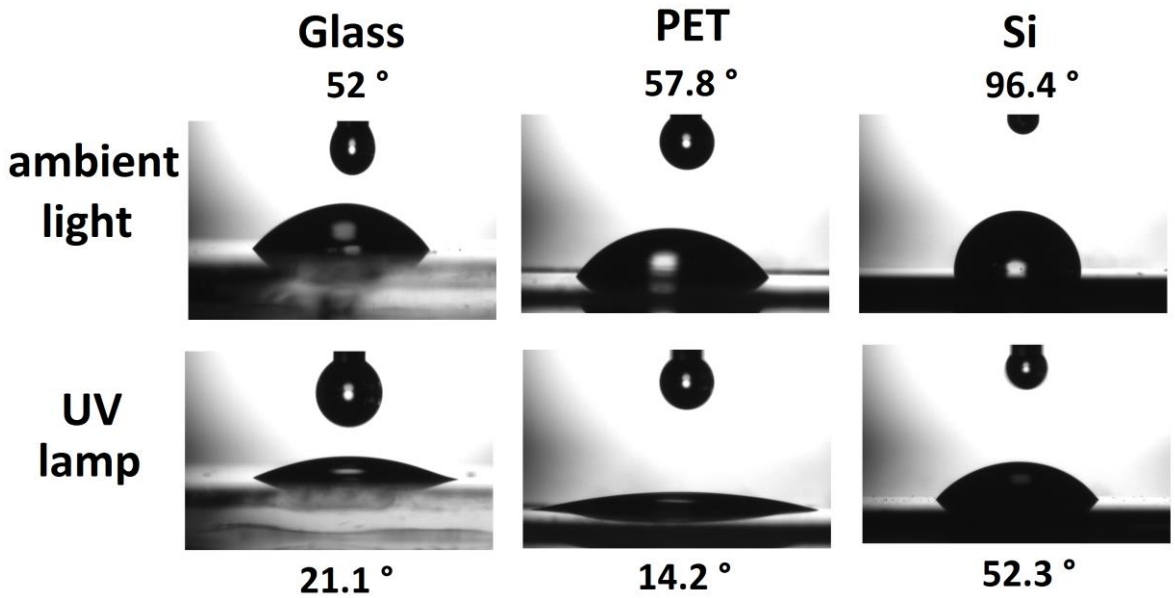

Figure 194. Evolution of the contact angle before and after UV illumination for different substrates.

V.2.6. Films deposited on PMMA

Some films have been deposited onto PMMA substrates, provided by an external company. These films showed very interesting results. In Figure 195, only the films

showing the best crystallinity but most of deposited films showed anatase peaks, and rutile in some cases. That is the main change with previous coating on polymers: films deposited on this substrate showed very high anatase crystallinity and a very low rutile content. The samples can however not be characterized by XRD due to the complicated surface profile of the latter and SEM is impossible as well due to the reasons explained above for polymeric substrate preparation.

The point of showing these results is to show that quasi-pure anatase films can be deposited onto polymeric substrates. It thus confirms the substrate dependency of the deposition and show how important it can be. Here, the high crystallinity can be a consequence of either the fact that the substrates are polished and protected or the crystallography of the films. In fact, the PET and PC films used above are films stored in the lab and subject to micro-scratches when manipulated when the PMMA samples are polished samples, sent with protective films to prevent scratching. Also, even though there is no confirmation of it, it is supposed that these films are semi-crystalline. This assumption is made on the fact that polished and protected amorphous PMMA sheets have also been deposited and the latter showed no crystallinity of any kind. It is specified to the reader that a non-disclosure agreement has been signed with the company providing the PMMA samples and the Raman spectra are the only data that has been produced by the author. Complementary tests have been carried out by the company but cannot be presented here.

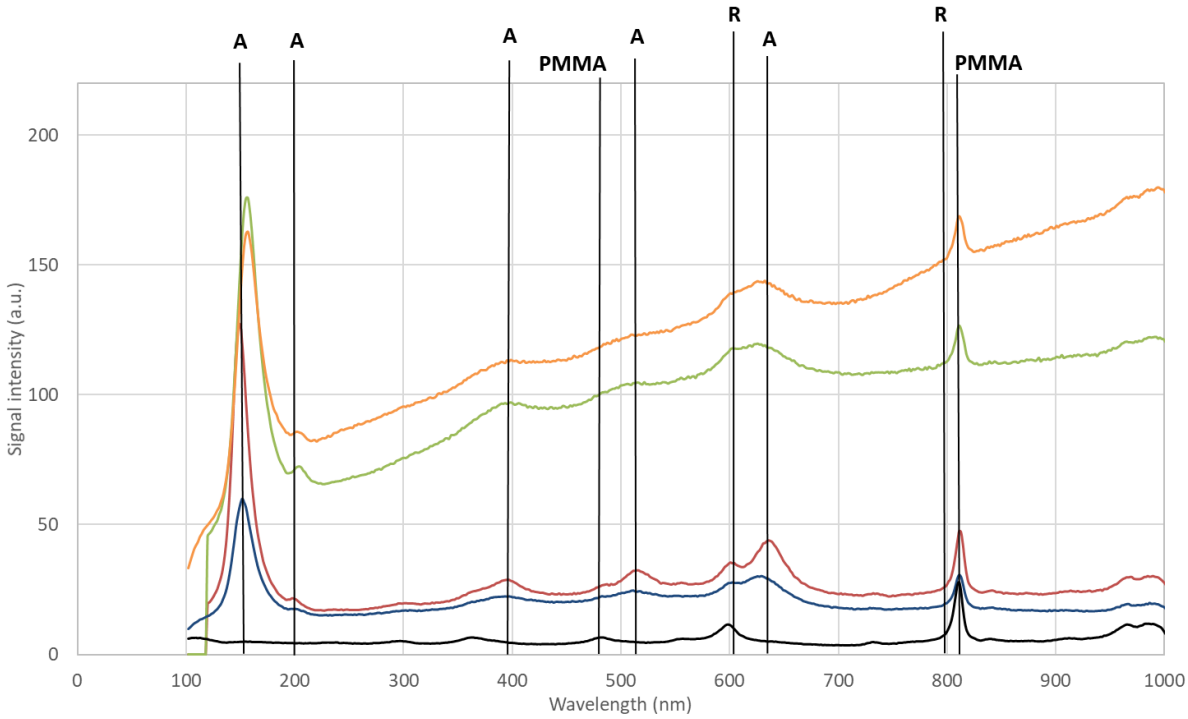

Figure 195. Raman spectroscopy for various titanium dioxide films deposited onto PMMA substrates

V.3. Summary and conclusion

In summary, this chapter has shown the type of thin films that have been deposited during this project. First, the SEM micrographs have suggested that higher pressure*distance products would help depositing columnar structures, and thus increase the surface area but these films showed very low crystallinity. Studies showed that if the voltage is too high, the films presents pinholes, due to droplet or macroparticles expelled from the target. However, after a first step of film optimization in terms of crystallinity, the oxygen regulation in the chamber has been changed along with the substrate holder position: closer to the target. The pressure has also been reduced in these conditions. The effect of the frequency and the pulse width on the film's structure has been determined in such conditions. Here, even if no pinholes could be observed at the films surface, arcing is still responsible for disrupting the columnar growth of the film. At low pressure*distance and in the intensity regulated mode, the discharge is arcing more when frequency is decreased and pulse width increased. These conditions are less stable because of the rarefaction/thermalization coupled with a long off-time duration.

The Raman spectroscopy demonstrated that the films deposited in the early stages of the project only showed weak or inexistent crystallinity; even on single-orientated Silicon wafers. However, the optimization deposition condition lead to the deposition of crystals in the process envelope. The process envelope has been defined as follows: a low pressure, a high frequency, a short pulse width, and an over-stoichiometric discharge. The oxygen content in the chamber is the factor that proved to be the most determining for the crystalline growth of the film but is a very sensitive parameter, even in the intensity regulated mode. The Raman spectroscopy of the films has also shown a difficulty in duplicating results. The configuration of the rig is suggested to be responsible for the difficulty in duplicating even though no specific reason could be identified. The substrate nature has an influence on the films structure as it has been even more difficult to find conditions where all four substrates are coated with anatase. Si always shows better anatase crystals, when glass seems to favourite the rutile growth. Polymers would struggle growing crystals at their surfaces but grow anatase when they do.

XRD studies confirmed that the Raman analysis of the films was sufficient to determine if the films were crystalline and what phases were in presence. However, the technique is too slow for our project. It would be interesting if the orientation of the crystals was to be determined but here the objective is to know which phase is in presence, no more.

Methylene blue degradation tests confirmed that the more intense the anatase peak appears to be on Raman spectra, the more photo-active the film is, which justifies the fact that the films optimization consists in improving the quantity of anatase crystals in the film. Contact angle measurements demonstrated two main facts: the contact angle increases during the first 24 hours of exposure to ambient atmosphere and the contact angle decreases under UV illumination. Films have been tested right after deposition and all showed low contact angles but the latter increased until a certain stabilization after 24 hours at higher values. This shows that films need at least 24 hours of relaxing time before being tested in any way as it needs to stabilize chemically and mechanically.

Finally, films have been deposited on high-quality PMMA substrate and the results showed high anatase crystallinity of the films deposited, and smaller rutile peaks. These results confirm the importance of the substrate nature and its quality (i.e. polished, semi-crystalline)

Conclusions and future work

V.4. Conclusions

This project has shown that the HiPIMS discharge varies with the apparatus used for deposition. Each different deposition chamber and each different power supply changes the discharge and how it behaves. In each rig, the pulse waveform is different and is modified by the 1st order parameters differently. Each coating system has its own process envelope with its own particularities, especially when it comes to reactive sputtering. Therefore, results obtained in one given rig do not seem to be transferable to another rig. For example, conditions showing good quality deposition in research-scaled rigs do not necessarily correspond to good quality growth in an industrial-scaled rig.

For the deposition rig used for deposition in this project, the system has been optimized to deposit crystalline anatase on polymeric substrates. It was found that such films could be deposited at a low pressure (3 mTorr), with a high frequency (500-1000 Hz), a short pulse width (30-75 µs), a short target-to-substrate distance (~6.5 cm), and more importantly, with an oxygen content corresponding to an over-stoichiometric state of the discharge. Arcs have also been designated as being responsible for difficulty for the process to grow crystals. Operating the system in the intensity regulated mode has proven to be easier as it smothers the oxidation curve and allows the user to be more precise when flowing oxygen in the chamber.

This project has also demonstrated that using only an oscilloscope is enough to do sufficient plasma diagnostic for films optimization. Relying on the state-of-the-art literature, the study of the pulse waveform is sufficient to identify the process occurring in the plasma and how they evolve when any 1st order parameter is modified. Even if the details of the physical phenomena occurring cannot yet be identified, the information from these waveforms is sufficient to optimize the deposition conditions for the aimed application. It offers the industries a simple and cheap way to optimize the reactive HiPIMS deposition they aim at.

Here, the objective was to deposit crystalline photo-active titanium dioxide onto polymers and has been reached. It opens a large range of new industrial applications for reactive HiPIMS but industries should be careful when using data from the literature as the scaling-up process is more complicated than a simple proportionality problem.

V.5.Future work

As future work suggestions, the author suggests

• The complete study of the scaling-up process for reactive HiPIMS discharges. This could start with answering the questions about a few parameters influences. This way, uncertain hypotheses given in the plasma diagnostic chapters of this thesis could be confirmed or not. The complementary work should mainly consist of Mass spectrometry, EEDFS and IEDFS

• Determining with exactitude the influence of the substrate condition on the growing properties. For polymers, it seems that the surface state of the film and its level of crystallinity can impact the quality of the growing film.

• The optimization of the films at a deeper level. Now that it has been demonstrated that high-level anatase crystals can be deposited at such temperatures that the polymeric substrates do not melt, the films can still be improved for specific applications by refining the deposition parameters to have an impact on the surface roughness for example, or even the crystallographic orientations. However, it is recommended that such optimization should be carried out directly on the industrial rig used for the production.

• Deep investigation of the scaling-up problems faced when comparing HiPIMS discharges in small research rigs and large industrial rigs. Industrial rigs have much bigger volumes, sometimes movement within it (e.g. rolling processes), and that can change the plasma but identifying how exactly and why would ease the development of industrial applications. It could even result in modifications of the industrial deposition chambers to ease the stability of the process. A first suggestion by the author would be confinement walls in between the target and the substrate holder to help obtaining a more stable plasma while making it possible to deposit large areas of substrates.

References

[1] K. S. Sree Harsha, Principles of Physical Vapor Deposition of thin films, Oxford: Elsevier Science, 2006.

[2] M. A. Lieberman and A. Lichtenberg, Principles of plasma discharges and material processing, 2nd edition, New Jersey: John Wiley & sons, 2005.

[3] M. Ohring, Materials science of thin films, San Diego: Academic Press, 2002.

[4] J. Roth, Industrial plasma engineering volume I: principles, Bristol: Institute of Physics Publishing, 1995.

[5] D. Lundin, The HiPIMS process, Linköping University, 2010.

[6] A. Anders, J. Andersson and A. Ehiasarian, "High power impulse magnetron sputtering: Current-voltage-time characteristics indicate the onset of sustaines self-sputtering," *Journal of applied Physics 102,* p. 113303, 2007.

[7] A. Anders, "Self-sputtering runaway in high power impulse magnetron sputtering: The role of secondary electrons and multiply charged metal ions," *Applied Physics Letters 92,* 2008.

[8] J. Emmerlich, S. Mraz, R. Snyders, K. Jiang and J. Schneider, "The physical reason for the apparently low deposition rate during high-power pulsed magnetron sputtering," *Vacuum 82,* pp. 867-870, 2008.

[9] D. Lundin, Plasma properties in high power impulse magnetron sputtering, Linköping University, 2008.

[10] P. Sigmund, "Theory of Sputtering. I. Sputtering Yield of Amorphous and Polycrystalline Targets," *Phys. Rev. 184,* 1969.

[11] P. Puckett, S. Michel and W. Hughes, Thin Film Processes II, New York: Academic Press, 1991.

[12] M. Bowes and J. Bradley, "Inert gas effects on the deposition rate of TiO2 during reactive HiPIMS," *Surface & Coatings Technology 250,* pp. 2-6, 2014.

[13] N. Britun, S. Konstantinidis and R. Snyders, "Plasma diagnostics for understanding the plasma-surface interaction in HiPIMS discharges: a review," *Journal of Physics D Applied Physics 47,* 2014.

[14] J. Thornton, "Influence of apparatus geometry and deposition conditions on the structure and topography of thick sputtered coatings," *Journal of Vacuum Science & Technology,* p. 666, 1974.

[15] A. Anders, "A structure zone diagram including plasma based deposition and ion etching," *Thin Solid Films 518,* 2010.

[16] A. Anders, "A structure zone diagram including plasma based deposition and ion etching," *Thin Solid Films,* 2010.

[17] W. R. Grove, *Trans. R. Soc.,* vol. 1, no. 142, p. 87, 1852.

[18] R. Nahrwold, *Ann. Physik.,* no. 31 , p. 467, 1887.

[19] A. Anders, J. Andersson, D. Horwat and A. Ehiasarian, "Physics of High Impulse Magnetron Sputtering".

[20] P. Kelly and R. Arnell, "Magnetron sputtering: a review of recent developments and applications," *Vaccum 56,* pp. 159-172, 2000.

[21] D. A. Glocker and M. Romach, "System for unbalanced magnetron sputtering with AC power". Patent US6733642 B2, 2004.

[22] B. Window and N. Savvides, *Journal of Vaccum Science and Technologies,* vol. A4(2), p. 196, 1986.

[23] J. Gudmundsson, N. Brenning, D. Lundin and U. Helmersson, "High power impulse magnetron sputtering discharge," *Journal of Vacuum Science & Technology,* 2012.

[24] R. Arnell and P. Kelly, "Recent advances in magnetron sputtering," *Surface and Coatings Technology 112,* pp. 170-176, 1999.

[25] L. C. Fontana and J. L. R. Muzart, "Characteristics of triode magnetron sputtering: The morphology of deposited titanium films," *Surface and Coatings Technology,* vol. 1, no. 107, pp. 24-30, 1998.

[26] L. Fontana and J. Muzart, "Triode magnetron sputtering TiN film deposition," *Surface and Coatings Tehcnology,* vol. 1, no. 114, pp. 7-12, 1999.

[27] S. Schiller and K. Gedicke, "Pulsed magnetron sputter technology," *Surface coatings technologies,* no. 61, pp. 331-337, 1993.

[28] V. Kouznetsov, K. Macák, J. M. Schneider, U. Helmersson and I. Petrov, "A novel pulsed magnetron sputter technique utilizing very high target power densities," *Surface and coatings Technology 122,* pp. 290-293, 1999.

[29] K. Bobzin, N. Bagcivan, P. Immich, S. Bolz, J. Alami and R. Cremer, "Advantages of nanocomposite coatings deposited by high power pulse magnetron sputtering technology," *Journal of Materials processing technology 209,* pp. 165-170, 2009.

[30] J. Alami, P. Persson, D. Music, J. Gudmundsson, J. Bohlmark and U. Helmersson, "Ion-assisted physical vapor deposition for enhanced film properties on nonflat surfaces," *Journal of Vacuum Science Technologies A 23(2),* pp. 278-280, 2005.

[31] R. Chistyakov, B. Abraham and W. Sproul, "Advances in High Power Pulse Reactive Magnetron Sputtering," in *Proceedings of the 49th annual SVC Technical Conference*, Washington DC, 2006.

[32] R. Chistyakov, B. Abraham, W. Spoul, J. Moore and J. Lin, "Modulated pulse power technology and deposition for protective and tribological coatings," in *Proceedings of the 50th annual SVC technical conference*, Louisville, 2007.

[33] J. Lin, J. Moore, W. Sproul, B. Mishra, J. Rees, Z. Wu, R. Christyakov and B. Abraham, "Ion energy and mass distributions of the plasma during modulated pulse power magnetron sputtering," *Surface & coatings Technology 203,* pp. 3676-3685, 2009.

[34] J. Lin, W. Sproul, J. Moore, Z. Wu, S. Lee, R. Chistyakov and B. Abraham, "Recent advances in Modulated pulsed power magnetron sputtering for surface engineering," *Structural, Functional, and Biological thin films,* pp. 48-58, 2011.

[35] D. J. Christie, "Trget material pathways model for high power pulsed magnetron sputtering," *Journal of Vacuum Science & Technology A 23,* pp. 330-335, 2005.

[36] J. Vlček, P. Kudláček, K. Burcalová and J. Musil, "High-power pulsed sputtering using magnetron with enhanced plasma confinement," *Journal of Vacuum Science & technology A,* pp. 42-47, 2007.

[37] J. Vlček and K. Burcalová, "A phenomenological equilibrium model applicable to high-power pulsed magnetron sputtering," *Plasma Sources Science and Technology,* vol. 19, no. 6, 2010.

[38] J. Gudmundsson, P. Sigurjonsson, P. Larsson, D. Lundin and U. Helmersson, "On the electron energy in the high power impulse magnetron sputtering discharge," *Journal of Applied Physics 105,* 2009.

[39] J. Bohlmark, M. Latteman, J. Gudmundsson, A. Ehiasarian, Y. Aranda Gonzalvo, N. Brenning and U. Helmersson, "The ion energy distributions and ion flux composition from a high power impulse magnetron sputtering discharge," *Thin solid films 515,* pp. 1522-1526, 2006.

[40] A. Hecimovic and A. P. Ehiasarian, "Time evolution of ion energies in HIPIMS of chronium plasma discharge," *Journal of Physics D: Applied Physics,* 2009.

[41] A. Hecimovic, K. Burcalova and A. P. Ehiasarian, "Origins of ion energy distribution function (IEDF) in high power impulse magnetron sputtering (HIPIMS) plasma discharge," *Journal of Physics D: Applied Physics 41,* 2008.

[42] G. Greczynski and L. Hultman, "Time and energy resolved ion mass spectroscopy studies of the ion flux during high power pulsed manetron sputtering of Cr in Ar and Ar/N2 atmospheres," *Vacuum 84,* pp. 1159-1170, 2010.

[43] A. Anders, "Discharge physics of high power impulse magnetron sputtering," *Surface and Coatings Technology 205,* pp. S1-S9, 2011.

[44] K. Sarakinos , J. Alami and S. Konstantinidis, "High power pulsed magnetron sputtering: A review on scientific and engineering state of art," *Surface & Coatings Technology 204,* pp. 1661-1684, 2010.

[45] K. Sarakinos and D. Lundin, "An introduction to thin film proessing using high-power impulse magnetron sputtering," *Journal of Materials Research,* pp. 780-792, 2012.

[46] J. Alami, S. Bolz and K. Sarakinos, "High power pulsed magnetron sputtering: Fundamentals and applications," *Journal of alloys and Compounds 483,* pp. 530-534, 2009.

[47] C. Huo, D. Lundin, M. R. Raadu, A. Anders, J. T. Gudmundsson and N. Breening, "On the road to self-sputtering in high power impulse magnetron sputtering: particle balance and discharge characteristics," *Plasma Sources Sci. Technol. 23,* 2014.

[48] V. Stranak, On high power impulse magnetron sputtering, Greifswald, 2011.

[49] M. Aiempanakit, Reactive high power impulse magnetron sputtering of metal oxides, Linköping, 2013.

[50] A. Ferrec, J. Kéraudy and P.-Y. Jouan, "Mass spectrometry analyzes to highlight differences between short and long HiPIMS discharges," *Applied surface Science,* no. 390, pp. 497-505, 2016.

[51] M. Aiempanakit, A. Aijaz, D. Lundin, U. Helmersson and T. Kubart, "Understanding the discharge current behavior in reactive high power impulse magnetron sputtering of oxides," *Journal of Applied Physics 113,* p. 133302, 2013.

[52] M. Hala, N. Viau, O. Zabeida, J. Klemberg-Sapieha and L. Martinu, "Dynamics of reactive high-power impulse magnetron sputtering discharge studied by time- and space-resolved optical emission spectroscopy and fast imaging," *Journal of Applied Physics 107,* 2010.

[53] G. Y. Yushkov and A. Anders, "Origin of the delayed current onset in High Power Impulse Magnetron Sputtering," *IEEE Transactions on Plasma Science 38,* pp. 3028-3034, 2010.

[54] A. Hecimovic and A. P. Ehiasarian, "Spatial and temporal evolution of ion energies in high power impulse magnetron sputtering plasma discharge," *Journal of Applied Physics 108,* 2010.

[55] P. Poolcharuansin and J. W. Bradley, "Short- and long-term plasma phenomena in a HiPIMS discharge," *Plasma Sources Science and Technology 19,* 2010.

[56] A. Ferrec, J. Keraudy, S. Jacq, F. Schuster, P.-Y. Jouan and M. Djouadi, "Correlation between mass-spectrometer measurements and thin film characteristics using dcMS and HiPIMS discharges," *Surface & Coating Technology 250,* pp. 52-56, 2014.

[57] J. T. Gudmundsson, J. Alami and U. Helmersson, "Evolution of the electron energy distribution and plasma parameters in a pulsed magnetron discharge," *Applied Physics Letters, vol.78, n°22,* pp. 3427-3429, 28 mars 2001.

[58] J. Gudmundsson, J. Alami and U. Helmersson, "Spatial and temporal behavior of the plasma parameters in apulsed magnetron discharge," *Surface and Coatings Technology,* pp. 246-256, 2002.

[59] CRC Press, CRC Handbook of Chemistry and Physics, 85th edition, Boca Raton, FL, USA, 2004-2005.

[60] R. E. Somekh, "The thermalization of energetic atoms during the sputtering process," *Journal of Vacuum Science and Technology A,* pp. 1285-1291, 1984.

[61] S. M. Rossnagel, "Gas density reduction effects in magnetrons," *J. Vac. Sci. Technol. A 6,* pp. 19-24, 1988.

[62] D. Horwat and A. Anders, "Compression and strong rarefaction in high power impulse magnetron sputtering dischrges," *Journal of Apllied Physics,* 2011.

[63] J. Bohlmark, J. T. Gudmundsson, J. Alami, M. Latteman and U. Helmersson, "Spatial Electron Density Distribution in a High-Power Pulsed Magnetron Discharge," *IEEE Transactions on Plasma Science, vol. 33, n°2,* pp. 346-347, Avril 2005.

[64] M. Palmucci, N. Britun, T. Silva, R. Snyders and S. Konstantinidis, "Mass spectroscopy diagnostics of short-pulsed HiPIMS discharges," *Journal of Physics D: Applied Physics,* 2013.

[65] A. R. Hochstim, Kinetic processes in gases and plasmas, New York and London: Academic Press, 1969.

[66] C. Koch and G. Matthieussent, "Diffusion ambipolaire d'un plasma collisionnel à travers un champ magnétique inhomogène. Application à une décharge multipolaire," *J. Physique 43,* pp. 67-75, 1982.

[67] V. Vancoppenolle, P.-Y. Jouan, A. Ricard, M. Wautelet, J.-P. Dauchot and M. Hecq, "Oxygen active species in an Ar-O2 magnetron discharge for titanium oxide deposition," *Applied Surface Science 205,* pp. 249-255, 2003.

[68] M. Cada, D. Lundin and Z. Hubicka, "Measurement and modeling of plasma parameters in reactive high-power impulse magnetron sputtering of Ti in Ar/O2 mixtures," *Journal of Applied physics,* no. 121, 2017.

[69] D. Lundin, J. Gudmundsson, N. Brenning, M. Raadu and T. Minea, "A study of the oxygen dynamics in a reactive Ar/O2 high power impulse magnetron sputtering

discharge using an ionization region model," *Journal of applied physics,* no. 121, 2017.

[70] A. Karpinski, A. Ferrec, M. Richard-Plouet, L. Cattin, L. Brohan, M. Djouadi and P.-Y. Jouan, "Deposition of nickel oxide by direct current reactive sputtering - effect of oxygen partial pressure," *Thin Solid films 520,* pp. 3609-3613, 2012.

[71] M. Aiempanakit, T. Kubart, P. Larsson, K. Sarakinos, J. Jensen and U. Helmersson, "Hysteresis and process stability in reactive high power impulse magnetron sputtering of metal oxides," *Thin Solid Films 519,* pp. 7779-7784, 2011.

[72] T. Kubart, M. Aiempanakit, J. Andersson, T. Nyberg, S. Berg and U. Helmersson, "Studies of hysteresis effect in reactive HiPIMS deposition of oxides," *Surface & Coatings Technology 205,* pp. S303-S306, 2011.

[73] A. Surpi, T. Kubart, D. Giordani, M. Tosello, G. Mattei, M. Colasuonno and A. Patelli, "HiPIMS deposition of TiOx in an industrial-scale appartus: effects of target size and deposition geometry on hysteresis," *Surface & Coatings Technology 235,* pp. 714-719, 2013.

[74] T. Kubart and A. Aijaz, "Evolution of sputtering target surface composition in reactive high power impulse magnetron sputtering," *Journal of applied physics,* no. 121, 2017.

[75] M. Hala, J. Čapek, O. Zabeida, J. Klemberg-Sapieha and L. Martinu, "Hysteresis-free deposition of niobium oxide films by HiPIMS using different pulse management strategies," *Journal of Physics D: Applied Physics 45(5),* 2012.

[76] E. Wallin and U. Helmersson, "Hysteresis-free reactive high power impulse magnetron sputtering," *Thin Solid Films 516,* 2008.

[77] K. Sarakinos, J. Alami, C. Klever and M. Wuttig, "Process stabilization and enhancement of deposition rate during reactive high power pulsed magnetron sputtering of zirconium oxide," *Surface and Coatings Technology 202,* 2008.

[78] C. Nouvellon, M. Michiels, J. Dauchot, C. Archambeau, F. Laffineur, E. Silberberg, S. Delvaux, R. Cloots, S. Konstantinidis and R. Snyders, "Deposition of titanium oxide films by reactive High Power Impulse Magnetron Sputtering (HiPIMS): Influence of the peak current value on the transition from metallic to poisoned regimes," *Surface & Coatings Technology 206,* pp. 3542-3549, 2012.

[79] N. Britun, S. Konstantinidis, A. Belosludtsev, T. Silva and R. Snyders, "Quantification of the hysteresis and related phenomena in reactive HiPIMS discharges," *Journal of Applied physics,* no. 121, 2017.

[80] D. Horwat and A. Anders, "Spatial distribution of average charge state and deposition rate in high power impulse magnetron sputtering of copper," *Journal of Physics D: Applied Physics 41,* 2008.

[81] F. Jing, K. Yukimura, H. Kato, Y. Lei, T. You, Y. Leng and N. Huang, "Film characterization of titanium oxide films prepared by high-power impulse magnetron sputtering," *Surface & Coatings 206,* pp. 967-971, 2011.

[82] F. Jing, T. Yin, K. Yukimura, H. Sun, Y. Leng and N. Huang, "Titanium film deposition by high-power impulse magnetron sputtering: Influence of pulse duration," *Vacuum 86,* pp. 2114-2119, 2012.

[83] G. Greczynski and L. Hultman, "Peak amplitude of target current determines deposition rate loss during high power pulsed magnetron sputtering," *Vacuum,* no. 124, 2016.

[84] B. Chapman, Glow discharge processes - Sputtering and plasma etching, John Wiley & Sons, 1980.

[85] N. Matsunami, Y. Yamamura, Y. Itikawa, N. Itoh, Y. Kazumata, S. Miyagawa, K. Morita, R. Shimizu and H. Tawara, "Energy dependence of the Yields of Ion-induced Sputtering on Monoatomic Solids," *IPPJ-AM-32 (Institute of plasma physics, Nagoya University, Japan, 1983).*

[86] D. Christie, "Target material pathways model for high power pulsed magnetron sputtering," *Journal of Vacuum Sciences & Technology A,* 2005.

[87] A. Ehiasarian, A. Vetushka, A. Hecimovic and S. Konstantinidis, "Ion composition produced by high power impulse magnetron sputtering discharges near the substrate," *Journal of Applied Physics 104,* 2008.

[88] M. Aiempanakit, U. Helmersson, A. Aijaz, P. Larsson, R. Magnusson, J. Jensen and T. Kubart, "Effect of peak power in reactive high power impulse magnetron sputtering of titanium dioxide," *Surface & Coating technology 205,* pp. 4828-4831, 2011.

[89] M. Samuelsson, D. Lundin, K. Sarakinos, F. Björefors, B. Wälivaara, H. Ljungcrantz and U. Helmersson, "Influence of ionization degree on film properties when using high power impulse magnetron sputtering," *J. Vac. Sci. Technol. A 30(3),* pp. 1-5, 2012.

[90] Q. Wang, S.-H. Kwon, K. Hui, D.-I. Kim, K. Hui and K. Kim, "Synthesis and properties of crystalline TiO2 films deposited by a HIPIMS+ technique," *Vaccum 89,* pp. 90-95, 2013.

[91] M. Ratova, G. West and P. Kelly, "Optimisation of HiPIMS photocatalytic titania coatings for low temperature deposition," *Surface and Coatings Technology 250,* pp. 7-13, 2014.

[92] M. Cada, Z. Hubicka, P. Adamek, J. Kluson and L. Jastrabik, "Time-resolved plasma parameters in the HiPIMS discharge with Ti target in Ar/O2 atmosphere," *Surface & Coatings Technology 205,* pp. S317-S321, 2011.

[93] F. Magnus, O. B. Sviensson, S. Olafsson and J. T. Gudmundsson, "Current-voltage-time characteristics of the reactive Ar/N2 high power impulse magnetron sputtering discharge," *Journal of applied Physics 110,* p. 083306, 2011.

[94] F. Magnus, T. K. Tryggvason, S. Olafsson and J. T. Gudmundsson, "Current-voltage-time characteristics of the reactive Ar/O2 high power impulse magnetron sputtering discharge," *Journal of Vacuum Science and Technology A 30,* p. 050601, 2012.

[95] S. Konstantinidis, J. Dauchot, M. Ganciu, A. Ricard and M. Hecq, "Influence of pulse duration on the plasma characteristics in high-power pulsed magnetron discharges," *Journal of Applied Physics 99,* 2006.

[96] C. Huo, M. Raadu, D. Lundin, J. Gudmundsson, A. Anders and N. Brenning, "Gas rarefaction and the time evolution of long high-power impulse magnetron sputtering pulses," *Plasma Sources Science and Technology 21,* p. 12pp, 2012.

[97] P. Vasina, M. Mrazkova, M. Mesko, J. Imbert, M. Ganciu, C. Boisse-Laporte, L. de Poucques, M. Touzeau, D. Pagnon and J. Bretagne, "Influence of the pulse duration of fast high power magnetron discharge on the amount of ion collected on the substrate".

[98] M. Samuelsson, D. Lundin, J. Jensen, M. Raadu, J. Gudmundsson and U. Helmersson, "On the film density using high power impulse magnetron sputtering," *Surface & Coatings Technology 205,* pp. 591-596, 2010.

[99] A. Pajdarova, J. Vleck, P. Kudlacek and J. Lukas, "Electron energy distributions and plasma parameters in high-power pulsed magnetron sputtering discharges," *Plasma Sources Science and Technology 18,* pp. 025008 1-7, 2009.

[100] M. Ratova, G. West and P. Kelly, "HiPIMS deposition of tungsten-doped titania coatings for photocatalytic applications," *Vacuum 102,* pp. 48-50, 2014.

[101] D. Depla, G. Buyle, J. Haemers and R. De Gryse, "Discharge voltage measurements during magnetron sputtering," *Surface & Coatings Technology 200,* pp. 4329-4338, 2006.

[102] D. Depla, S. Mahieu and R. De Gryse, "Magnetron sputter deposition : Linking discharge voltage with target properties," *Thin Solid Films 517,* pp. 2825-2839, 2009.

[103] V. Stranak, A.-P. Herrendorf, H. Wulff, S. Drache, M. Cada, Z. Hubicka, M. Tichy and R. Hippler, "Deposition of rutile (TiO2) with preferred orientation by assisted high power impulse magnetron sputtering," *Surface & Coatings Technology 222,* pp. 112-117, 2013.

[104] H.-L. Chen, Y.-M. Lu and W.-S. Hwang, "Characterization of sputtered NiO thin films," *Surface & coatings Technology 198,* pp. 138-142, 2005.

[105] L. Ai, G. Fang, L. Yuan, N. Liu, M. Wang, C. Li, Q. Zhang, J. Li and X. Zhao, "Influence of substrate temperature on electrical and optical properties of p-type semitransparent conductive nickel oxide thin films deposited by radio frequency sputtering," *Applied Surface Science 254,* pp. 2401-2405, 2008.

[106] J.-L. Yang, Y.-S. Lai and J. Chen, "Effect of heat treatment on the properties of non-stoichiometric p-type nickel oxide films deposited by reactive sputtering," *Thin Solid Films 488,* pp. 242-246, 2005.

[107] B. Agnarsson, F. Magnus, T. Tryggvason, A. Ingason, K. Leosson, S. Olafsson and J. Gudmundsson, "Rutile TiO2 thin films grown by reactive high power impulse magnetron sputtering," *Thin Solid Films 545,* pp. 445-450, 2013.

[108] W. Feng, X. Wang, F. Chen, W. Liu, H. Zhou, S. Wang and H. Li, "Influence of substrate temperature on structural, morphological and electrical properties of PbSe film deposited by radio frequency sputtering," *Thin Solid films 578,* pp. 25-30, 2015.

[109] G. Gonçalves, E. Elangovan, P. Barquinha, L. Pereira, R. Marins and E. Fortunato, "Influence of post-annealing temperature on the properties exhibited by ITO, IZO and GZO thin films," *Thin Solid Films 515,* pp. 8562-8566, 2007.

[110] F. Cao, Y.-D. Wang, J.-Z. Yin, M.-L. Cong and L.-Y. Han, "Influence of post-annealing temperature on properties of Ta-doped ZnO transparent conductive films," *Chinese Physics Letters 26(11),* p. 114203, 2009.

[111] S. Ahmad, N. Sin, M. Berhan and M. Rusop, "Influence of post annealing temperature on the properties of ZnO films prepared by RF magnetron sputtering," *Advanced Materials Research 10,* pp. 602-606, 2012.

[112] P.-A. Cormier, A. Balhamri, A.-L. Thomann, R. Dussart, N. Semmar, T. Lecas, R. Snyders and S. Konstantinidis, "Titanium oxide thin film growth by magnetron sputtering: Total energy flux and its relationship with the phase constitution," *Surface & Coatings Technology 254,* pp. 291-297, 2014.

[113] P. Kelly, P. Barker, S. Ostovarpour, M. Ratova, G. West, I. Iordanova and J. Bradley, "Deposition of photocatalytic titania coatings on polymeric substrates by HiPIMS," *Vacuum 86,* pp. 1880-1882, 2012.

[114] S. Latthe, S. Liu, C. Terashima, K. Nakata and A. Fujishima, "Transparent, adherent, and photocatalytic SiO2-TiO2 coating on polycarbonate for self-cleaning applications," *Coatings,* no. 4, pp. 497-507, 2014.

[115] M. Ratova, P. Kelly, G. West and I. Iordanova, "Enhanced properties of magnetron sputtered photocatalytic coatings via transition metal doping," *Surface & Coatings Technology 228,* pp. S544-S549, 2013.

[116] S. Sathasivam, D. Bachu, Y. Lu, N. Chadwick, S. Althabaiti, A. Alyoubi, S. Basahel, C. Carmalt and I. Parkin, "Tungsten Doped TiO2 with Enhanced Photocatalytic and Optoelectrical Properties via Aerosol Assisted Chemical Vapor Deposition," *Nature: scientific reports,* 2015.

[117] L. Zhang, P. Tan, C. Lim, X. Guo, M. Tse, O. Tan and V. Chang, "N–TiO2-coated polyester filters for visible light—Photocatalytic removal of gaseous toluene under static and dynamic flow conditions," *Journal of Environmental Chemical Engineering,* no. 4, pp. 357-364, 2016.

[118] M. Ratova, Enhanced properties of photocatalytic titania thin films via doping during magnetron sputter deposition, Manchester, 2013.

[119] A. P. Ehiasarian, J. Andersson and A. Anders, "Distance-dependent plasma composition and ion energy in high power impulse magnetron sputtering," *Journal of Physics D: Applied Physics 42,* 2010.

[120] W. Leroy, S. Konstantinidis, S. Mahieu, R. Snyders and D. Depla, "Angular-Resolved Energy Flux Measurements of a DC- and HIPIMS- powered rotating cylindrical magnetron in reactive and non-reactive atmosphere".

[121] D. Lundin, M. Stahl, H. Kersten and U. Helmersson, "Energy flux measurements in high power impulse magnetron sputtering," *Journal of Physics D: Apllied Physics 42,* 2009.

[122] M. Cada, P. Adamek, V. Stranak, S. Kment, J. Olejnicek, Z. Hubicka and R. Hippler, "Angle-resolved investigation of ion dynamics in high power impulse magnetron sputtering deposition system," *Thin Solid Films 549,* pp. 177-183, 2013.

[123] R. Hippler, Z. Hubicka, M. Cada, P. Ksirova, H. Wulff, C. Helm and V. Stranak, "Angular dependence of plasma parameters and film properties during high power impulse magnetron sputtering for deposition of Ti and TiO2 layers," *Journal of applied physics,* no. 121, 2017.

[124] T. Minea, C. Costin, A. Revel, D. Lundin and L. Caillault, "Kinetics of plasma species and their ionization in short-HiPIMS by particle modeling," *Surface & Coatings Technology 255,* pp. 52-61, 2014.

[125] K. S. and M. F., "Abtr. Book Annu. Meet. Chemical society of Japan," p. 223, 1959.

[126] K. S. and M. F., *Kogyo Kagaku Zasshi,* no. 67, p. 1136, 1964.

[127] A. Fujishima, K. Honda and S. Kikushi, "Photosensitized electrolytic oxidation on semiconducting n-type TiO2 electrode," *Kogyo Kagaku Zasshi,* vol. 72, pp. 108-113, 1969.

[128] A. Fujishima, X. Zhang and D. Tryk, "TiO2 photocatalysis and related surface phenomena," *Surface science reports 63,* pp. 515-582, 2008.

[129] A. Fujishima and K. Honda, "Electrochemical photolysis of water at a semiconductor electrode," *Nature,* no. 238, pp. 37-38, 1972.

[130] K. Hashimoto, H. Irie and A. Fujishima, "TiO2 photocatalysis: A historical overview and future prospects," *Japanese Journal of Applied Physics 44-12,* pp. 8269-8285, 2005.

[131] T. Watanabe, K. Hashimoto and A. Fujishima, Photocatalytic purification and treatment of water and air, Amsterdam: Elsevier, 1993.

[132] A. Fujishima, K. Hashimoto and T. Watanabe, TiO2 Photocatalysis: fundamentals and Applications, Tokyo: BKC, 1999.

[133] K. Sunada, Y. Kikuchi, K. Hashimoto and A. Fujishima, "Bactericidal and Detoxification Effects of TiO2 Thin Film Photocatalysts," *Environmental Science and Technology,* vol. 32, no. 5, pp. 726-728, 1998.

[134] R. Wang, N. Sakai, A. Fujishima, T. Watanabe and K. Hashimoto, "Studies of Surface Wettability Conversion on TiO2 Single-Crystal Surfaces," *The journal of physical chemistry B,* vol. 12, no. 103, pp. 2188-2194, 1999.

[135] O. Carp, C. Huisman and A. Reller, "Photoinduced reactivity of titanium dioxide," *Progress in Solid State Chemistry 32,* pp. 33-177, 2004.

[136] A. Fujishima, T. Rao and D. Tryk, "Titanium dioxide photocatalysis," *Journal of photochemistry and photobiology C: Photochemistry reviews 1,* pp. 1-21, 2000.

[137] A. Mills and S. Le Hunte, "An overview of semiconductor photocatalysis," *Journal of Photochemistry and Photobiology A: Chemistry,* vol. 108, pp. 1-35, 1997.

[138] L. Caballero, K. Whitehead, N. Allen and J. Verran, "Inactivation of Escherichia coli on immobilized TiO2 using fluorescent light," *Journal of photochemistry and photobiology A: Chemistry 202,* pp. 92-98, 2009.

[139] L. Caballero, K. Whitehead, N. Allen and J. Verran, "Photocatalytic inactivation of Escherichia coli using doped titanium dioxide under fluorescent irridiation," *Journal of photochemistry and photobiology A: Chemistry 276,* pp. 50-57, 2013.

[140] M. Miyauchi, N. Kieda, S. Hishita, T. Mitsuhashi, A. Nakajima, T. Watanabe and K. Hashimoto, *Surface Science,* vol. 511, pp. 401-407, 2002.

[141] U. Diebold, "The surface science of titanium dioxide," *Surface Science Reports 48,* pp. 53-229, 2003.

[142] S. Girish Kumar and L. Gomathi Devi, "Review on modified TiO2 photocatalysis under UV/Visible light: Selected results and related machanisms on interfacial charge carrier transfer dynamics," *The Journal of Physical Chemistry A 115,* pp. 13211-13241, 2011.

[143] S. Konstantinidis, J. Dauchot and M. Hecq, "Titanium oxide thin films deposited by high-power impulse magnetron sputtering," *Thin Solid films 515,* pp. 1182-1186, 2006.

[144] M. Twu, A. Chiou, C. Hu, C. Hsu and C. Kuo, "Properties of TiO2 films deposited on flexible substrates using direct current magnetron sputtering and using high

power impulse magnetron sputtering," *Plymer degradation and Stability 117,* pp. 1-7, 2015.

[145] A. Aijaz, "A User's guide for High Vacuum Sputtering System Edward," 2009.

[146] G. West, P. Kelly, P. Barker, A. Mishra and J. Bradley, "Measurements of deposition rate and substrate heating in a HiPIMS discharge," *Plasma processes and polymers,* 2009.

[147] M. Cada, J. Bradley, G. Clarke and P. Kelly, "Measurements of energy transfer at an isolated substrate in a pulsed DC magnetron discharge," *Journal of Applied Physics 102,* 2007.

[148] N. Britun, M. Palmucci, S. Konstantinidis, M. Gaillard and R. Snyders, "Time-resolved temperature study in a high-power impulse magnetron sputtering discharge," *Journal of Applied Physics 114,* 2013.

[149] G. Tian, H. Fu, L. Jing, B. Xin and K. Pan, "Preparation and Characterization of stable biphase TiO2 photocatalyst with high crystallinity, large surface area, and enhanced photoactivity," *The Journal of Physical Chemistry C,* no. 112, pp. 3038-3039, 2008.

[150] N. Xu, Z. Shi, Y. Fan, J. Dong, J. Shi and M.-C. Hu, "Effects of particle size of TiO2 on photocatalytic degradation of methylene blue in aqueous suspensions," *Industrial and Engineering Chemistry Research,* no. 38, p. 373, 1999.

[151] D. Nguyen, A. Ferrec, J. Keraudy, M. Richard-Plouet, A. Goullet, L. Cattin, L. Brohan and P.-Y. Jouan, "Ellipsometric and XPS characterization of transparent nickel oxide thin films deposited by reactive HiPIMS," *Surface & Coatings Technology 250,* pp. 21-25, 2014.

[152] O. Kohmoto, H. Nakagawa, Y. Isagaw and A. Chayahara, "Effect of heat treatment on the oxygen content and resistivity in sputtered NiO films," *Journal of Magnetism and Magnetic Materials,* pp. 1629-1630, 2001.

[153] A. Karpinski, N. Ouldhamadouche, A. Ferrec, L. Cattin, M. Richard-Plouet and L. Brohan, "Optical characterization of transparent nickel oixde films deposited by DC current reactive sputtering," *Thin Solid Films,* pp. 5767-5770, 2011.

[154] J. Olejnicek, Z. Hubicka, S. Kment, M. Cada, P. Ksirova, P. Adamek and I. Gregora, "Investigation of reactive HiPIMS + MF sputtering of TiO2 crystalline thin films," *Surface & coatings Technology 232,* pp. 376-383, 2013.

[155] S. Chen, B. Wu, D. Xie, F. Jiang, J. Liu, H. Sun, S. Zhu, B. Bai, Y. Leng, N. Huang and H. Sun, "The adhesion and corrosion resistance of Ti-O films on CoCrMo alloy fabricated by high power pulsed magnetron sputtering (HPPMS)," *Surface & Coatings 252,* pp. 8-14, 2014.

[156] P. Barker, S. Konstantinidis, E. Lewin, N. Britun and J. Patscheider, "An investigation of c-HiPIMS discharges during titanium deposition," *Surface and Coatings Technology,* 2014.

[157] P. Kelly, G. West, M. Ratova, L. Fisher, S. Ostovarpour and J. Verran, "Structural formation and photocatalytic activity of magnetron sputtered titania and doped-titania coatings," *Molecules 19,* pp. 1-24, 2014.

[158] N. Farahani, P. Kelly, G. West, M. Ratova, C. Hill and V. Vishnyakov, "Photocatalytic activity of reactively sputtered and directly sputtered titania coatings," *Thin Solid Films 520,* pp. 1464-1469, 2011.

[159] M. Ratova, G. West and P. Kelly, "Optimisation of HiPIMS photocatalytic titania coatings for low temperature deposition," *Surface & Coatings Technology 250,* pp. 7-13, 2014.

[160] S. Pradhan, S. Sahoo and S. Pradhan, "Influence of annealing temperature on the structural, mechanical and wetting property of TiO_2 films deposited by RF magnetron sputtering," *Thin Solid Films 518,* pp. 6904-6908, 2010.

[161] A. Haseeb, M. Hasan and H. Masjuki, "Structural and mechanical properties of nanostructured TiO_2 thin films deposited by RF sputtering," *Surface & Coatings Technology 205,* pp. 338-344, 2010.

[162] T. Obee and R. Brown, "TiO_2 photocatalysis for indoor air applications: Effects of humidity and trace contaminant levels on the oxidation rates of Formaldehyde, Toluene, and 1,3-Butadiene," *Environ. Sci. Technol. 29,* pp. 1223-1231, 1995.

[163] J. Kim, J. Lee and W. Choi, "Synergic effect of simultaneous fluorination and platinization of TiO_2 surface on anoxic photocatalytic degradation of organic compounds," *Chem. Commun.,* pp. 756-758, 2008.

[164] J. Kiwi, S. Rtimi and C. Pulgarin, "Cu, Cu/TiO_2 thin films sputtered by up to date methods on non-thermal thin resistant substrates leading to bacterial inactivation," 2014.

[165] M. Setvin, U. Aschauer, P. Scheiber, Y.-F. Li, W. Hou, M. Schmid, A. Selloni and U. Diebold, "Reaction of O2 with subsurface oxygen vacancies on TiO2 anatase (101)," *Science 341,* pp. 988-990, 2013.

[166] J. Dervaux, P.-A. Cormier, S. Konstantinidis, R. Di Ciuccio, O. Coulembier, P. Dubois and R. Snyders, "Deposition of porous titanium oxide thin films as anode material for dye sensitized solar cells," *Vacuum 114,* pp. 213-220, 2015.

[167] E. Burunkaya, Ö. Kesmez, N. Kiraz, H. Çamurlu, M. Asiltürk and E. Arpaç, "Sn4+ or Ce3+ doped TiO2 photocatalytic nanometric films on antireflective nano-SiO2 coated glass," *Materials Chemistry and Physics 120,* pp. 272-276, 2010.

[168] D. Hurum, A. Agrios, K. Gray, T. Rajh and M. Thurnauer, "Explaining the enhanced photocatalytic activity of Degussa P25 mixed-phase TiO2 using EPR," *J. Phys Chem. B 107,* pp. 4545-4549, 2003.

[169] D. Hurum, A. Agrios, S. Crist, K. Gray, T. Rajh and M. Thurnauer, "Probing reaction mechanisms in mixed phase TiO2 by EPR," *Journal of Electron Spectroscopy and related Phenomena 150,* pp. 155-163, 2006.

[170] B. Liu, Q. Wen and X. Zhao, "The effect of sputtering power on the structure and photocatalytic activity of TiO2 films prepared by magnetron sputtering," *Thin Solid Films 517,* pp. 6569-6575, 2009.

[171] M.-L. Kaariainen, T. Kaariainen and D. Cameron, "Titanium dioxide thin films, their structure and its effect on their photoactivity and photocatalytic properties," *Thin Solid films 517,* pp. 6666-6670, 2009.

[172] N. Mathews, E. Morales, M. Cortes-Jacome and J. Toledo Antonio, "TiO2 thin films - Infleunce of annealing temperature on structural, optical and photocatalytic properties," *Solar Energy 83,* pp. 1499-1508, 2009.

[173] B. Abdollahi Nejand, S. Sanjabi and V. Ahmadi, "The effect of sputtering gas pressure on structure and photocatalytic properties of nanostructured titanium oxide self-cleaning thin film," *Vacuum 85,* pp. 400-405, 2010.

[174] E. Moser, S. Chappuis and J. Olleros, "Production of photocatalitically active titania layers: A comparison of plasma processes and coatings properties," *Surface & coatings 227,* pp. 2-9, 2013.

[175] P. Navabpour, S. Ostovarpour, J. Hampshire, P. Kelly, J. Verran and K. Cooke, "The effect of process parameters on the structure, photocatalytic and self-cleaning

properties of TiO_2 and Ag-TiO_2 coatings deposited using reactive magnetron sputtering," *Thin solid Films 571,* pp. 75-83, 2014.

[176] J. Krysa, M. Zlamal, S. Kment, M. Brunclikova and Z. Hubicka, "TiO_2 and Fe_2O_3 films for photoelectrochemical water splitting," *Molecules 20,* pp. 1046-1058, 2015.

[177] C. McCullagh, J. Robertson, D. Bahnemann and P. Robertson, "The application of TiO_2 photoctalysis for desinfection of water contaminated with pathogenic micro-organisms: a review," *Res. Chem. Intermed. 33,* pp. 359-375, 2007.

[178] T. Luttrell, S. Halpegamage, J. Tao, A. Kramer, E. Sutter and M. Batzill, "Why is anatase a better photocatalyst than rutile? - Model studies on epitaxial TiO_2 films," *Scientific reports 4,* pp. 1-7, 2014.

[179] G. Li and K. Gray, "The solid-solid interface: Explaining the high and unique photocatalytic reactivity of TiO_2-based nanocomposite materials," *Chemical Physics 339,* pp. 173-187, 2007.

[180] V. Stranak, M. Cada, M. Quass, S. Block, R. Bogdanowicz, S. Kment, H. Wulff, Z. Hubicka, C. Helm, M. Tichy and R. Hippler, "Physical properties of homogeneous TiO_2 films prepared by high power impulse magnetron sputtering as a function of crystallographic phase and nanostructure," *J. Phys. D: Appl. Phys. 42,* p. 12pp, 2009.

[181] A. Amin, D. Köhl and M. Wuttig, "The role of energetic ion bombardment during growth of TiO_2 thin films by reactive sputtering," *J. Phys. D: Appl. Phys. 43,* p. 12pp, 2010.

[182] E. Lecoq, J. Guillot, D. Duday, J.-B. Chemin and P. Choquet, "Elaboration of a wide range of TiO_2 micro-nanostructures by high power impulse inverted cylindrical magnetron sputtering," *J. Phys. D: Appl. Phys. 47,* p. 12pp, 2014.

[183] C. Maszl, W. Breilmann, J. Benedikt and A. von Keudell, "Origin of the energetic ions at the subtrate generated during high power pulsed magnetron sputtering of titanium," 2014.

[184] L. Caballero, K. Whitehead, N. Allen and J. Verran, "Photoinactivation of Escherichia coli on acrylic paint formulations using fluorescent light," *Dyes and pigments 86,* pp. 56-62, 2010.

[185] M. Raadu, I. Axnäs, J. Gudmundsson, C. Huo and N. Brenning, "An ionization region model for high-power impulse magnetron sputtering discharges," *Plasma Sources Science and Technology 20,* p. 10pp, 2011.

[186] S. Konstantinidis, J. Dauchot, M. Ganciu and M. Hecq, "Transport of ionized metal atoms in high-power pulsed magnetron discharges assisted by inductively couples plasma," *Applied Physics Letters 88,* pp. 021501 1-3, 2006.

[187] D. Lundin, U. Helmersson, S. Kirkpatrick, S. Rohde and N. Brenning, "Anomalous electron transport in high power impulse magnetron sputtering," 2008.

[188] D. Lundin, N. Brenning, D. Jädernäs, P. Larsson, E. Wallin, M. Lattemann, M. Raadu and U. Helmersson, "Transition between the discharge regimes of high power impulse magnetron sputtering and conventionnal direct current magnetron sputtering," *Plasma Sources Science and Technology 18,* 2009.

[189] A. Anders, "High power impulse magnetron sputtering and related discharges: Scalable plasma sources for plasma-based ion implantation and deposition," *Surface & Coatings Technology 204,* pp. 2864-2868, 2010.

[190] J. Gudmundsson, "The high power impulse magnetron sputtering discharge an an ionized physical vapor deposition tool," *Vacuum 84,* pp. 1360-1364, 2010.

[191] D. Lundin, S. Al Sahab, N. Brenning, C. Huo and U. Helmersson, "Internal current measurements in high power impulse magnetron sputtering," *Plasma Sources Science and Technology 20,* 2011.

[192] S. Drache, V. Stranak, A.-P. Herrendorf, M. Cada, Z. Hubicka, M. Tichy and R. Hippler, "Time-resolved Langmuir probe investigation of hybrid high power impulse magnetron sputtering discharges," *Vacuum 90,* pp. 176-181, 2013.

[193] M. Liao, H. Niu and G. Chen, "Effect of sputtering pressure and post-annealing on hydrophilicity of TiO_2 thin films deposited by reactive magnetron sputtering," *Thin solid films 518,* pp. 7258-7262, 2010.

[194] CSM Instruments - Advanced Mechanical Surface Test, "Applications of the ConScan Surface Profilometer," 2010.